Perylene Bisimide Atropisomers: Synthesis and Optical and Chiroptical Properties

Dissertation zur Erlangung des
naturwissenschaftlichen Doktorgrades
der Julius-Maximilians-Universität Würzburg

vorgelegt von
Peter Uwe Osswald
aus Laupheim

Würzburg 2007

Eingereicht am: 30.03.2007
bei der Fakultät für Chemie und Pharmazie

1. Gutachter: Prof. Dr. Frank Würthner
2. Gutachter: Prof. Dr. Manfred Christl
der Dissertation

1. Prüfer: Prof. Dr. Frank Würthner
2. Prüfer: Prof. Dr. Manfred Christl
3. Prüfer: Prof. Dr. Christoph Lambert
des Öffentlichen Promotionskolloquiums

Tag des Öffentlichen Promotionskolloquiums: 14.06.2007

Doktorurkunde ausgehändigt am: .....

für Ariane

Acknowledgement / Danksagung

Ich bedanke mich bei allen, die zum Gelingen dieser Arbeit beigetragen haben. Mein besonderer Dank gilt:

Herrn Prof. Dr. Frank Würthner für die Überlassung des sehr interessanten und vielseitigen Themas und zahlreiche Anregungen und Diskussionen, sowie das in mich gesetzte Vertrauen, die mir gewährten Freiräume und seine uneingeschränkte Unterstützung.

Herrn Dr. Chantu Saha-Möller für die Unterstützung während der Anfangsphase, sowie seine stets zuverlässige und exzellente Überarbeitung der Manuskripte und die aufgebrachte endlose Geduld.

Herrn Dr. Rainer Dobrawa für die Einführung in alle Aspekte der Perylenbisimidchemie, sowie die unzähligen hilfreichen Diskussionen und so manche Fahrt nach Ulm!

Allen Mitarbeitern des Perylenlabors 412 für die gute Zusammenarbeit und das stets sehr gute Arbeitsklima.

Den Mitarbeitern der Arbeitskreise Adam und Ihmels für die freundliche Aufnahme im 4. Stock des Institutes für Organische Chemie der Universität Würzburg, ihre Unterstützung in der Aufbauphase, sowie für die Einladung zum Holzberghof.

Herrn Dr. Matthias Grüne und Frau Elfriede Ruckdeschel sowie Herrn Dr. Rüdiger Bertermann und Frau Marie-Luise Schäfer für die motivierte und sorgfältige Messung der temperaturabhängigen NMR-Spektren, sowie der DOSY NMR-Messungen (Kapitel 3, 4 und 6 dieser Arbeit).

Herrn Dr. Dirk Leusser und Herrn Prof. Dr. Dietmar Stalke sowie Herrn. Dr. Krystof Radacki und Herrn Prof. Dr. Holger Braunschweig für die Messung der Röntgenstrukturanalysen (Kapitel 3 und Kapitel 5).

Herrn Dr. Matthias Reichert und Herrn Prof. Dr. Gerhard Bringmann für die Berechung von CD-Spektren (Kapitel 4) und zahlreiche hilfreiche Diskussionen über axiale Chiralität.

Herrn Dipl.-Ing. Vladimir Stepanenko für die Durchführung der AFM-Messungen (Kapitel 7 und 8).

Herrn Joachim Bialas und Frau Manuela Deppisch für die tatkräftige Unterstützung im Labor und ihre immerwährende gute Laune.

Frau Ana-Maria Krause für die Durchführung der Cyclovoltammetriemessungen (Kapitel 3 und 5) und Frau Dipl.-Chem. Dörte Novak und dem Arbeitskreis Lambert für spektroelektrochemische Messungen (Kapitel 3).

Herrn Dr. Erwin Lang und Herrn Prof. Dr. Jürgen Köhler für die Einführung in die Einzelmolekülspektroskopie und die eingehende Charakterisierung einiger meiner Verbindungen.

Den Kooperationspartnern Frau Dr. Elisabetta Iengo und Herrn Prof. Dr. Enzo Alessio von der Universität Triest (Italien) für die gute Zusammenarbeit.

Dr. Masayku Takeuchi und Herrn Prof. Dr. Shenji Shinkai für das zur Verfügungsstellen von 1,4-Bis(*N*-Methylaminomethyl)-2,5-diiodbenzol sowie des amino-funktionalisierten π-conjugierten Polymers (Kapitel 8).

Meiner Praktikantin Katja Hertlein und Marina Safonte-Sempere sowie den Auszubildenden André Schuster und Peggy Seibt für die engagierte und zuverlässige Arbeit.

Allen früheren und aktuellen Mitarbeitern des Arbeitskreises Würthner für die schöne Zeit und so manchen lustigen Abend.

Allen meinen Kommilitonen aus der Ulmer Studienzeit, insbesondere Tobias Urban, Rainer Leppelt, Anke Wörz und Marc Holz.

Frau Valerie Huber für ihre Unterstützung und Herrn Andreas Lohr für die unzähligen Diskussionen und die Wochenend-Fahrgemeinschaft ins schwäbische Hinterland.

Meinen Eltern und meiner Familie danke ich für ihre unschätzbare Unterstützung.

Und zuletzt danke ich Dir, Ariane, für die unermessliche Unterstützung, für dein Verständnis und die viele Zeit, die Du mich entbehren musstest, und deiner Geduld vor allem während des Zusammenschreiben.

List of Abbreviations:

AFM	Atomic force microscopy
APBI	1,6,7,12-Tetraaryloxy-substituted perylene bisimide
APCI	Atmospheric pressure chemical ionisation
Boc	*tert*-Butyloxycarbonyl
1-BuOH	1-Butanol
CD	Circular dichroism
CV	Cyclic voltammetry
DABCO	Diazabicyclo-[2.2.2]-undecan
DAPBI	1,7-Diaryloxy-substituted perylene bisimide
DCTB	2-[(2*E*)-3-(4-*tert*-Butylphenyl)-2-methylprop-2-enylidene]malononitrile
DMSO	Dimethylsulfoxide
DNMR	Dynamic nuclear magnetic resonance
DOSY	Diffusion ordered spectroscopy
ESI-TOF	Electron spray ionisation-time of flight
EtOAc	Ethylacetate
FDCD	Fluorescence detected circular dichroism
HOMO	Highest occupied molecular orbital
HOPG	Highly ordered pyrolitic graphite
HPLC	High performance liquid chromatography
LED/OLED	Light emitting diode/Organic light emitting diode
LUMO	Lowest unoccupied molecular orbital
NMP	*N*-Methylpyrrolidon
MALDI-TOF	Matrix-assisted laser desorption ionisation-time of flight
MeOH	Methanol
OFETs	Organic field effect transistors
PBI	Perylene bisimide
TBAHFP	Tetrabutylammonium hexafluorophosphate
THF	Tetrahydrofuran
TMS	Tetramethylsilane
Tos	para-Toluene sulfonate
UV/Vis	Ultraviolet/Visible
VCD	Vibrational circular dichroism

Table of Content

Introduction and Aim of this Thesis

Chirality is of significant importance in nature, in particular for the control of the three-dimensional structure of biopolymers and their self-assembly into larger architectures, e.g. DNA and collagen, as well as for the enantioselective recognition of substrates by well-defined chiral cavities.[1] The importance of supramolecular chirality in nature substantiated scientists to investigate extensively the influence of chirality on the structure of artificial self-assembled systems[2] and the experimental evidence for chiral amplification by "the sergeants and soldiers" and "majority rules" principles have contributed to our understanding of the origin of homochirality in nature.[3] Apart from this more academic interest in chirality, chiral molecules are widely applied in numerous other fields such as enantioselective recognition (with particular importance in drug research),[4] enantioselective catalysis[5] and in non-linear optics[6] as well as molecular switches.[7] Furthermore, chiral polymeric emitters or chiral dopants in nematic liquid crystals show potential for application in photo- and electroluminescence devices owing to their circular polarized emission which should enable stereo-imaging.[8]

Conformational chiral molecules based on inherently chiral chromophores have been demonstrated to be especially useful for the above mentioned applications. Prominent examples are biphenyl[9] and binaphthyl[10] derivatives as well as helicenes and helicene-like systems[11] for which the chirality arises from a distortion of the π-system. The significance of these inherently chiral chromophores in chiral recognition, enantioselective catalysis and as chiral molecular switches have been amply demonstrated.[10-12] However, these chiral systems are mostly colorless UV/Vis absorbers and, therefore, further functionalization is required to extent the scope of such conformational chiral molecules. Basic requirements for novel conformational chiral molecules for applications mentioned above, particular as efficient sensors, are

high fluorescent quantum yield and/or an absorption in the visible region of the solar spectrum which, on one hand should allow an efficient screening (“naked eye detection”) and, on the other hand, improve the sensitivity at a single molecular level.[12] Thus, the synthesis of novel conformational chiral molecules based on functional dyes such as cyanines or acenes have been reported in literature.[13]

A class of chromophores which properly fulfill the criteria mentioned above are perylene bisimides as they possess excellent optical properties and are highly persistent against environmental influences.[14] At bay area (1,6,7,12-positions) substituted perylene bisimides exhibit a twisted π-system due to repulsive interactions of the substituents. The twisted nature of the perylene core gives rise to two conformations which behave as image and mirror-image and, thus, bay-substituted perylene bisimides exhibit conformational chirality. However, the resolution of atropo-isomers (*P*- and *M*-conformers) of perylene bisimides has not been reported prior to this work. The high luminescence of perylene bisimides in combination with the conformational chirality would add a highly attractive chromophore to the class of functional chiral molecules.

Therefore, the aim of this thesis is the synthesis and isolation of enantiopure perylene bisimide fluorophores. For this purpose the formation of macrocycles by covalent and non-covalent approaches seems to be a promising strategy because a macrocyclization of perylene bisimides by bridging the bay substituents by appropriate linkages (1,7- and 6,12-linkage, see Figure 1A) will prevent the interconversion between the enantiomers. Therefore, di- and tetra(3-hydroxyphenoxy)-functionalized perylene bisimides (Figure 1A) are chosen as building block for macrocyclization by etherification of the resorcin units.

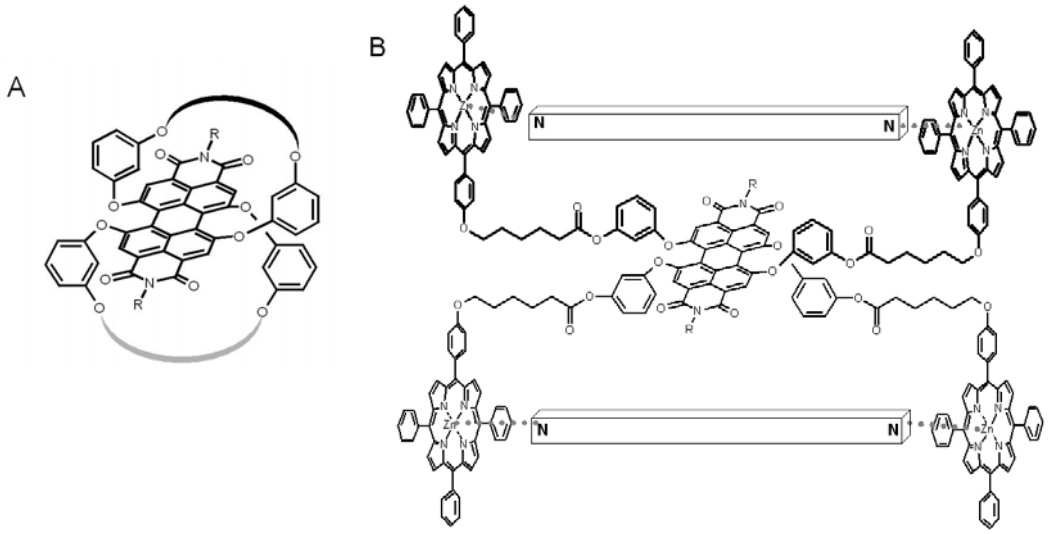

Figure 1. Concepts for the synthesis of stable atropisomeric perylene bisimides through macrocyclisation by etherification (A) and by non-covalent interactions (B).

For the self-assembly approach, the interaction of zinc porphyrin with nitrogen-containing ligands seems to be very promising as it is a well-understood, non-covalent binding process providing high binding constants.[15] Thus, the porphyrin-functionalized perylene bisimides shown in Figure 1B have been designed for this purpose.

As a further approach toward enantiopure perylene bisimides (Figure 2), the influence of the bulkiness of bay substituents on interconversion (*M* ⇌ *P*) barriers of atropo-isomers of perylene bisimides has been explored to identify substituents which lead to isomerization barriers facilitating resolution of atropisomeric perylene bisimides.

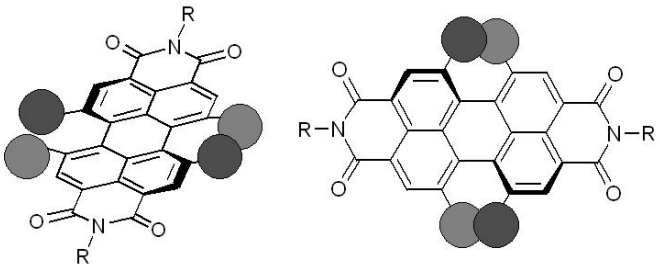

Figure 2. Concept for the synthesis of stable atropisomeric perylene bisimides by introduction of large bay-substituents. Shown are the view along the *N*,*N* axis and the top view of bay-substituted perylene bisimides.

In Chapter 1, an overview of known conformational chiral molecules is given. The definition of conformational chirality and basic concepts concerning the interconversion process are outlined on selected examples. Applications of conformational chiral molecules are presented which include those related to stable enantiomers but also those based on the dynamic properties of conformational chiral molecules.

In Chapter 2, the structural properties of bay-substituted perylene bisimides are discussed on the base of molecular modeling investigations as well as literature known X-ray structures. The symmetry of several bay-substituted perylene bisimides is derived, the stereochemistry of these dyes is defined, and the interconversion process of conformational isomers is demonstrated.

The synthesis of macrocycles based on 1,6,7,12-tetraaryloxy-substituted perylene bisimides is described in Chapter 3. The optical and electrochemical properties of macrocycles are investigated and a relationship between the optical and conformational properties of tetraaryloxy-substituted perylene bisimides is shown.

In Chapter 4, the synthesis and the resolution of atropo-diastereomeric perylene bisimides are presented. The chiroptical properties of the epimers are described and the assignment of the stereochemistry of the enantiomers is determined by CD spectroscopy in combination with quantum chemical calculations.

The concept of chiral macrocycles is extended to 1,7-diaryloxy-substituted perylene bisimides in Chapter 5. The isolation of perylene bisimide enantiomers is presented and their optical and chiroptical as well as electrochemical properties are discussed.

In Chapter 6, the dynamic properties of bay-substituted perylene bisimides are investigated for a series of halogen-substituted perylene bisimides. The separation of the enantiomers of tetrabromo-substituted derivative is demonstrated and a concept for the synthesis of conformationally stable enantiomers of perylene bisimides is provided.

A self-assembly approach toward the synthesis of macrocycles by using the non-covalent interaction between zinc porphyrin and nitrogen-containing ligands is shown in Chapter 7. The synthesis of a zinc porphyrin-functionalized perylene bisimide is described and the self-assembly with aza-ligands is investigated by ^{1}H NMR and UV/Vis titrations and DOSY NMR spectroscopy. The deposition of the well-defined macrocycles on graphite is elucidated by atomic force microscopy (AFM).

In Chapter 8, the use of the tetra(zinc porphyrin)-substituted perylene bisimide for the alignment of an amino-functionalized linear π-conjugated polymer is described.

The thesis concludes with summaries in English (Chapter 9) and German (Chapter 10).

References and Notes

1 J. W. Steed, J. L. Atwood, *Supramolecular Chemistry*; John Wiley & Sons, Chichester, **2000**; (b) A. D. Mesecar, D. E. Koshland, Jr., *Nature* **2000**, *403*, 614-615; (c) V. Sundaresan, R. Abrol, *Chirality* **2005**, *17*, S30-S39.

2 (a) M. A. Mateos-Tomoneda, M. Crego-Calama, D. N. Reinhoudt, *Chem. Soc. Rev.* **2004**, *33*, 363-372; (b) *Supramolecular Chirality* (Eds. M. Crega-Calamara, D. N. Reinhoudt), *Top. Curr. Chem*.; Vol. 256, Springer Verlag, Berlin, **2006**.

3 A. R. A. Palmans, J. A. J. M. Vekemans, E. E. Havinga, E. W. Meijer, *Angew. Chem.* **1997**, *109*, 2763-2765; *Angew. Chem. Int. Ed.* **1997**, *36*, 2648-2651; (b) J. van Gestel, A. R. A. Palmans, B. Titulear, J. A. J. M. Vekemans, E. W. Meijer, *J. Am. Chem. Soc.* **2005**, *127*, 5490-5494; (c) A. J. Wilson, J. van Gestel, R. P. Sijbesma, E. W. Meijer, *Chem. Commun.* **2006**, 4404-4406.

4 Recent reviews: (a) T. W. Bell, N. M. Hext, *Chem. Soc. Rev.* **2004**, *33*, 589-598; (b) L. Pu, *Chem. Rev.* **2004**, *104*, 1687-1716.

5 Recent reviews: (a) J. Ding, D. W. Armstrong, *Chirality* **2005**, *17*, 281-292; (b) K. Muniz, *Chem. Unserer Zeit* **2006**, *40*, 122-124; (c) P. Wessig, *Angew. Chem.* **2006**, *118*, 2224-2227; *Angew. Chem. Int. Ed.* **2006**, *45*, 2168-2171.

6 For a review, see: B. L. Feringa, R. A. van Delden, N. Koumura, E. M. Geertsma, *Chem. Rev.* **2000**, *100*, 1789-1816.

7 For reviews, see: (a) E. W. Meijer, B. L. Ferringa, *Mol. Cryst. Liq. Cryst.* **1993**, *235*, 169-180; (b) P. Fischer, F. Haché, *Chirality* **2005**, *17*, 421-437.

8 (a) J. P. Riehl, F. S. Richardson, *Chem. Rev.* **1986**, *86*, 1-16; (b) B. M. W. Langeveld-Voss, R. A. J. Janssen, M. P. T. Christiaans, S. C. J. Meskers, H. P. J. M. Dekkers, E. W. Meijer, *J. Am. Chem. Soc.* **1996**, *118*, 4908-4909; (c) E. Peeters, M. P. T. Christiaans, R. A. J. Janssen, H. F. M. Schoo, H. P. J. M. Dekkers, E. W. Meijer, *J. Am. Chem. Soc.* **1997**, *119*, 9909-9910; (d) R. P. Lemieux, *Acc. Chem. Res.* **2001**, *34*, 845-853.

9 For recent examples, see: (a) F. Ceccacci, G. Mancini, A. Sferrazza, C. Villani, *J. Am. Chem. Soc.* **2005**, *127*, 13762-13763; (b) M. Omote, Y. Nishimura, K. Sato, A. Ando, I. Kumadaki, *Tetrahedron* **2006**, *62*, 1886-1894; for a current review, see: (c) G. Bringmann, A. J. Price Mortimer, P. A. Keller, M. J. Gresser, J. Garner, M. Breuning, *Angew. Chem.* **2005**, *117*, 5518-5563; *Angew. Chem. Int. Ed.* **2005**, *44*, 5384-5427.

10 For recent examples, see: (a) E. Ishow, A. Credi, V. Balzani, F. Spadola, L. Mandolini, *Chem. Eur. J.* **1999**, *5*, 984-989; (b) R. A. van Delden, T. Mecca, C. Rosini, B. L. Feringa, *Chem. Eur. J.* **2004**, *10*, 61-70; (c) Y. Zhou, D. Zhang, Y. Zhang, Y. Tang, D. Zhu, *J. Org. Chem.* **2005**, *70*, 6164-6170; (d) Z.-B. Li, J. Lin, Y.-C. Qin, L. Pu, *Org. Lett.* **2005**, *7*, 3441-3444; for a review, see: (e) L. Pu, *Chem. Rev.* **1998**, *98*, 2405-2494.

11 For recent examples, see: (a) M. T. Reetz, S. Sostmann, *Tetrahedron* **2001**, *57*, 2515-2520; (b) K. E. S. Phillips, T. J. Katz, S. Jockusch, A. J. Lovinger, N. J. Turro, *J. Am. Chem. Soc.* **2001**, *123*, 11899-11907; (c) A. Rajca, M. Miyasaka, M. Pink, H. Wang, S. Rajca, *J. Am. Chem. Soc.* **2004**, *126*, 15211-15222; (d) T. J. Wigglesworth, D. Sud, T. B. Norsten, V. S. Lekhi, N. R. Branda, *J. Am. Chem. Soc.* **2005**, *127*, 7272-7273; (e) E. Botek, J.-M. André, B. Champagne, T. Verbiest, A. Persoons, *J. Chem. Phys.* **2005**, *122*, 234713, 1-6; (f) R. Fasel, M. Parschau, K.-H. Ernst, *Nature* **2006**, *439*, 449-452; for reviews, see: (g) W. H. Laarhoven, W. J. C. Prinsen, *Top. Curr. Chem.* **1984**, *125*, 63-130; (h) S.

Grimme, J. Harren, A. Sobanski, F. Vögtle, *Eur. J. Org. Chem.* **1998**, 1491-1509; (i) C. Schmuck, *Angew. Chem.* **2003**, *115*, 2552-2556; *Angew. Chem. Int. Ed.* **2003**, *42*, 2448-2452.

12 A. P. da Silva, H. Q. N. Gunaratne, T. Gunnlaugsson, A. J. M. Huxley, C. P. McCoy, J. T. Rademacher, T. E. Rice, *Chem. Rev.* **1997**, *97*, 1515-1566.

13 (a) R. A. Pascal, Jr., D. van Engen, B. Kahr, W. D. McMillan, *J. Org. Chem.* **1988**, *53*, 1687-1689; (b) V. Buss, S. Falzewski, K. Kolster, *J. Org. Chem.* **1999**, *64*, 1071-1073; (c) J. Lu, D. M. Ho, N. J. Vogelaar, C. M. Kraml, R. A. Pascal, Jr. *J. Am. Chem. Soc.* **2004**, *126*, 11168-11169; (d) D. J. Morrison, T. K. Trefz, W. E. Piers, R. McDonald, M. Parvez, *J. Org. Chem.* **2005**, *70*, 5309-5312.

14 (a) F. Würthner, *Chem. Commun.* **2004**, 1564-1579; (b) F. Würthner, *Pure Appl. Chem.* **2006**, *78*, 2341-2350 .

15 A. Satake, Y. Kobuke, *Tetrahedron* **2005**, *61*, 13-41.

Chapter 1

Conformational Chirality
– Principles and Applications –

Abstract: In order to emphasize the importance of conformational chirality for my thesis, the first introductory chapter gives an overview and presents the special structural features of biphenyl, binaphthyl and helicene derivatives. In the first part, the effect of the structural modification on the activation parameters of the interconversion between the atropo-enantiomeric conformers as well as on the chiroptical properties have been illustrated by means of selected examples. To demonstrate the technological potential of conformational chiral molecules, a survey of different applications for conformational chiral molecules in chemistry, materials and life sciences has been presented in the second part, and the differences compared with applications of configurational chiral molecules have been underlined by representative examples. In the last part, some recent examples for self-assembled chiral π-systems and π-conjugated foldamers have been discussed as well.

1.1 Introdcution

Chirality is among the most interesting and important topics in chemistry and biology. Since the pioniering work of Pasteur in the early 19th century,[1] scientists of different disciplines have contributed tremendously to our today's detailed picture of chirality and thus to our understanding of nature. Chirality is present in large variety in nature and can be found on any scale from a molecular level as, e.g., amino acids and DNA, to a macroscopic scale like human hands or sea shells. Examples for chirality in macroscopic world are shown in Figure 1. Lord Kelvin gave a general definition of chirality: "*I call any geometrical figure, and say it has chirality if its image in a plane mirror, ideally realized, cannot be brought to coincident with itself.*"[2] Thus, any object is chiral if it neither has a plane of symmetry nor a center of inversion nor a mirror reflection axis which would provide the similarity of image and mirror image. Objects are classified according to their symmetry in symmetry point groups which can be obtained by summation of all symmetry elements of an object. At least 41 different symmetry point groups can be derived for molecules by varying combination of symmetry elements and 11 of these groups neither have an inversion center nor a mirror plane nor a rotatory reflection axis and objects of these symmetry groups are therefore chiral.[3] Thus, it is apparent that the chirality is strongly related to symmetry or, more precisely, to the dissymmetry of an object or molecule.

Figure 1. Photographs of some examples (a spiral, left and sea shells, right) for chirality in the macroscopic world.

There are several ways in which chirality can be expressed in a molecule, e.g., asymmetric carbon atoms, axial, helical or topological chirality. In this chapter the focus is set on conformational chiral molecules as they are of main interest for this work. A detailed account of the chiroptical and dynamic properties of conformational chiral molecules is given on the examples of biphenyl and binaphthyl derivatives as well as different helicene-like compounds and perylene quinone. In these systems, the chirality arises from a "molecular distortion" which can be directly influenced by proper

functionalization of the molecules. Several excellent reviews on the different conformational chiral compounds were published,[4] thus selected examples are discussed here.

1.2. Definition of Conformational Chirality

Chiral molecules are classified based on their stereochemical origin of chirality. Like achiral stereoisomers, chiral molecules can also be classified as conformational and configurational isomers. Conformational and configurational chirality are umbrella terms comprising all other classes of chirality (e.g., axial and helical chirality). Configurational chirality results from different configurations of a molecule, for example asymmetric carbon atoms, which behave as image and mirror image. In contrast, conformational chirality is given if the molecules exhibit at least two different conformations which show mirror-image relation and represent the two enantiomers. The fact that the enantiomers herein are defined by different conformations implies that an equilibrium between the conformers should be present and the extent of the energy barrier of this equilibrium (racemisation process) determines the stability of the chiral conformers. The classical examples of conformational chirality are given by biphenyl **1** and spiro-[5.5]-undecanes **2** (Figure 2).[1] Conformational chirality is often related to axial chirality or helical chirality, thus, helicenes and also a large variety of functional molecules are conformational chiral. Different acene derivatives[5] and some cyanine dyes, which are frequently applied in non-linear optics, were reported to exhibit conformational chirality.[6] Another important class of dyes with excellent functional properties are bay-substituted perylene bisimides, which also exhibit conformational chirality.[7]

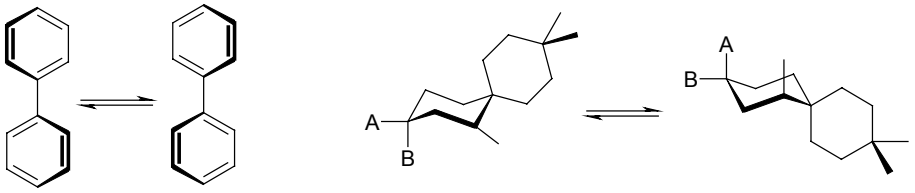

1 **2**

Figure 2. Equilibrium between two conformational enantiomers of biphenyl (left) and spiro-[5.5]-undecane (right).

Conformational chiral molecules are not a serendipity of synthetic organic chemistry, as different types of conformational chiral molecules, e.g., axial chiral biaryl compounds can be found in a large variety in nature.[8] One of the most prominent examples of natural conformational chiral molecules is given by the oligopeptide vancomycine, which exhibits remarkable bioactivity.[4d,9] Bilirubin dyes,[10] in which the conformational

enantiomers are stabilized by hydrogen bonds, are formed in the metabolism of hemoglobin and perylene quinones such as hypericin,[11] which mainly function as pigments or toxins in plants and some beetles, are further examples of naturally occurring π-systems with conformational chirality.

Since functional chromophores are of main interest of this work, the chirality of chromophores is considered here. In this context, chromophores are molecules which have an electronic transition in the UV (250-400 nm) and/or visible region (400-650 nm) of the solar light spectrum. Moffit and Moscowitz classified chromophores in inherent chiral and inherent achiral chromophores.[12] For inherent achiral chromophores, the chromophore itself is not chiral, but it is embedded in a chiral environment leading to chirality of its electronic transition. Examples for such inherently achiral chromophores are the carbonyl groups in steroids. In contrast, inherent chiral chromophores are molecules, in which the chromophore itself is chiral, for example in helicenes. Furthermore, interaction (by excitonic coupling) of two or more chromophores can result in exciton chirality. The use of exciton chirality for the determination of absolute configuration of various molecules such as cyclohexane-1,2-diols was reported in literature.[13]

1.3 Stereochemical Properties, Chiroptical Properties and Assignment of Stereochemistry of Conformational Chiral Chromophores.

The characteristics of conformational chirality are the presence of two conformations which behave as image and mirror image and the existence of an equilibrium between these conformers. In this section, inherently chiral dyes with conformational chirality are considered (Figure 3) and the relation between the structure and the chirality is discussed.

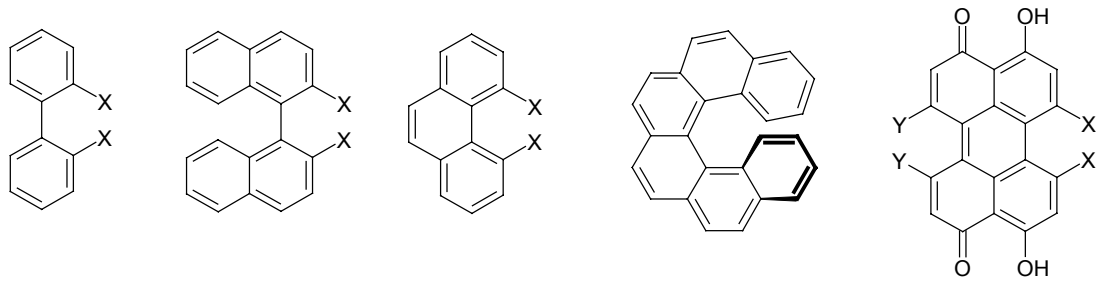

3 4 5 6 7

Figure 3. Structures of chiral dyes used for the discussion of dynamic properties of conformational chiral molecules.

For axial chiral molecules such as biphenyls **3** and binaphthyls **4**, the energetically little demanding rotation around a C_{sp2}-C_{sp2} single bond (as shown in Figure 2) leads to

chiral conformations. For phenanthrenes **5**, and helicenes **6** and perylene quinones **7**, the chirality is induced by a more sever competition between π-conjugation and steric repulsions and is expressed in a deviation from planarity of the π-system. For supramolecular rotaxanes such as **8** (Figure 4), the conformational chirality results from the topology of the knotted molecule.[14] Prezlan **8** is able to adopt only two stable conformations, each corresponds to one enantiomer (Figure 4, right).

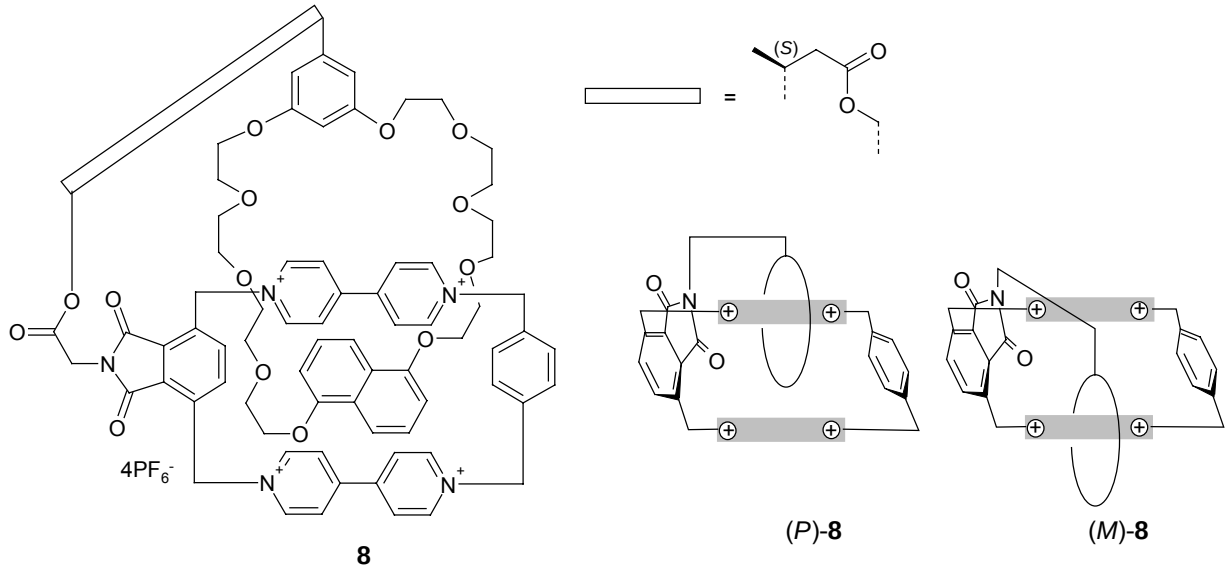

Figure 4. Structure of conformational chiral prezlan **8** (left) and schematic representation of the conformational diastereomers (*P*)-**8** and (*M*)-**8** (right).[14]

As mentioned in the introduction, the chirality can be related to the dissymmetry of a molecule. Thus, the chirality for the aromatic molecules considered in this overview arises from the deviation from an ideal planar conformation (with the highest π-conjugation). The quantitative measure for the extent of deviation from planarity is given by the dihedral angle θ (see Figure 5). For biphenyl and binaphthyl derivatives, the deviation is given by the torsion of the two benzene or naphthalene units along the chiral axis (Figure 5), and the available dihedral angles are not restricted and can thus vary from –180° to 180°. For phenanthrenes, perylene bisimides or perylene quinones, the torsion is related to the twist of the two aromatic halves of the molecule against each other. The dihedral angle for phenanthrenes varies from 5° for the parent compound up to 63° for the 1,10-diiodo derivative (X = I).[15] In the case of perylene bisimides, this angle θ varies from 4° to 36° as X-ray crystallographic analysis revealed (see Chapter 2). For helicenes, the deviation from planarity is related to the pitch of the helix present in these molecules as outlined in a recent overview.[16]

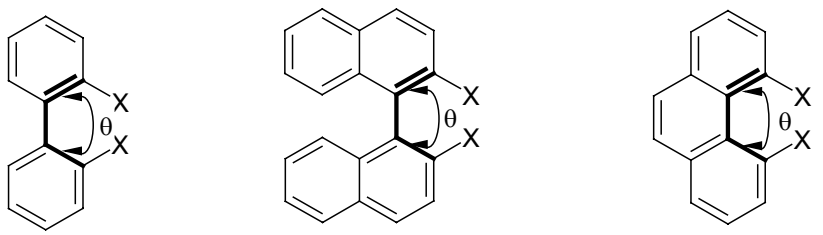

Figure 5. Definition of the dihedral angle θ for biphenyl, binaphthyl and phenanthrene.

The relationship of chirality with symmetry was pointed out by Lord Kelvin and can be used to quantitatively assess the chirality content of a molecule.[17] This was applied by Katzenlenson and co-workers to develop the *Continuous Chirality Measure*.[18] Herein, the dissymmetry of the respective twisted enantiomers in comparison to the closest symmetric counterpart available (which corresponds to a planar structure in the present cases) was used for the calculation of the chirality content of a molecule by quantum chemical methods.[18,19] The application of this *Continuous Chirality Measure* method for expressing the differences in chirality of helicenes revealed a clear correlation of the absolute chirality content, expressed by the dissymmetry, and the experimentally determined chiroptical properties, e.g., optical rotation.[18] These results demonstrated that the factors, which are responsible for the symmetry breaking (the dihedral angle θ or the pitch of the helix), are also responsible for the extent of the chiroptical properties.

The correlation of structural and chiroptical properties was already proposed by Mislow in 1957.[20] The theoretically calculated distribution (based on similar symmetry assumptions as described before) of the optical rotation for biphenyl derivatives showed maxima at dihedral angles of 45° and 135°, yet with opposite signs, indicating that these two conformations exhibit the largest chirality content. This relation is also valid for all other compounds presented in this chapter, except helicenes. This structure-property relationship was further confirmed by comparing the optical rotation values with the structures of the molecules obtained from X-ray crystallography or quantum chemical calculations.[21]

The data presented in Figure 6 clearly show that the optical rotation values are further dependent on the extent of the conjugated π-system involved in the chiral structure. This is reasonable, although the value for **13** has to be taken with care as this molecule exhibits an absorption maximum in close proximity of the detection wavelength. Accordingly, a significant dispersion enhancement of the α^D-value can be expected. The dependence of the chirality on the extent of the π-conjugated systems for a series of helicenes was further confirmed by quantum chemical calculations.[22]

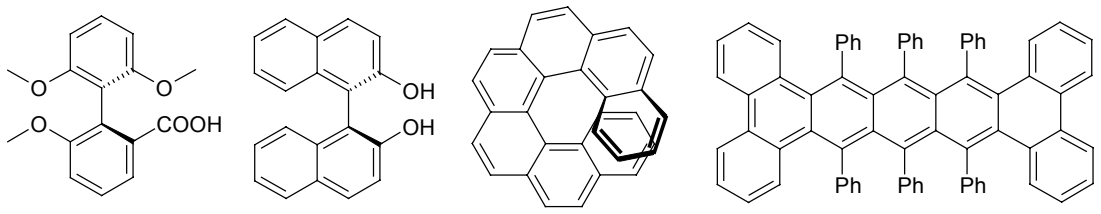

10: $[\alpha]_{589}^{15}$ = -12 **11**: $[\alpha]_{578}^{25}$ = -38 **12**: $[\alpha]_{579}^{25}$ = -5900 **13**: $[\alpha]_{589}^{25}$ = +7440

Figure 6. Structures and specific optical rotation values [α] of conformational chiral molecules **10**-**13**.[5c,23]

The relation of the optical rotation [α] to the twist angle θ presented by Mislow allows the determination of the absolute stereochemistry of biphenyl derivatives by the sign of the optical rotation. As a direct method for the determination of dihedral angle (in turn, the stereochemistry) of biphenyl derivatives, NMR spectroscopic measurements in combination with quantum chemical calculations were reported by Bates et al.[24] Furthermore, the sign of the CD signals of appropriate transitions was applied for the determination of the absolute configuration for biphenyls by Mislow and co-workers already in 1962.[25] In recent years, the relation of the experimental CD, vibrational CD (VCD) or fluorescence detected CD (FDCD) spectra to absolute configuration of the enantiomers has been evolved to the most important tools for the determination of the configuration of chiral UV/Vis absorbers. For the assignment of the absolute configuration by such spectroscopic methods, further information are required. For twisted aromatic molecules, the exciton coupling method as well as other empirical methods such as the Hug-Wagniére rule for C_2-symmetrical molecules were successfully applied for the assignment of the stereochemistry.[26] Quantum chemical calculations of optical spectra (CD, FDCD, VDC) have become most powerful tools for the assignment of absolute stereochemistry of chiral molecules. In a recent review article, Grimme, Vögtle and co-workers have presented a large number of examples for the stereochemical assignment by CD spectroscopy in combination with quantum chemical calculation of the CD spectra.[16]

The examples given here demonstrate that the chiroptical properties can be related to the origin and extent of the chirality for the respective stereoisomers. In general the intensity of the chiroptical response increases with increasing extension of the chiral structure (e.g., helicene) and the deviation from an ideal planar structure. For the determination of the absolute configuration, CD spectroscopy in combination with empirical rules and theoretical calculations is particularly suited.

1.4 Dynamic Properties of Conformational Chiral Molecules

The most important molecular property of conformational chiral compounds is given by the activation barrier for the interconversion between the enantiomers (or diastereomers), since the dynamic properties of such molecules determine the stability of the chiral conformers. The magnitude of the activation barrier provides a quantitative measure for the stability which in turn, provides a clue whether the respective enantiomers can be resolved or not. A simple estimation based on the Eyring equation suggest that an activation energy $\Delta G^{\ddagger}$ of 113 kJ/mol for the interconversion process leads to a half-life time $\tau_{1/2}$ of 1 year at 295 K. For a $\Delta G^{\ddagger}$-value of 119 kJ/mol the half life time increases to 10 years, providing sufficient stability of the respective enantiomers for any desirable application. For the resolution of enantiomers it was reported in literature that the barrier for the interconversion process has to be in the order of 93 kJ/mol at ambient conditions for the chromatographic separation of chiral conformers by high performance liquid chromatography (HPLC).[27]

For the elucidation of dynamic properties of conformational enantiomers, a large variety of techniques are available. For racemic mixtures, low-temperature HPLC (>40 kJ/mol) or dynamic NMR spectroscopy (DNMR; 20-100 kJ/mol) was used and spectroscopic methods such as CD and optical rotation were applied for the investigation of the racemisation process of pure or enriched enantiomers.[28]

Because of the relationship between the activation parameter and the stability of the chiral conformers the characterization of the dynamic properties of conformational enantiomers is an important aspect. Of special significance for the design of at room temperature stable enantiomers is the influence of structural modifications on the dynamic properties. The relevant substitution positions for controlling the activation parameter can be assessed from the structure of the molecule if the geometry of the twisted conformer as well as the mechanism and the transition state of the interconversion process are known.

Biphenyl derivatives represent the simplest and most extensively studied system among the compounds presented here.[4d] Activation parameters for a large variety of diversely substituted biphenyl compounds are available from literature, thus, this class of conformational chiral compounds is taken as model to outline some general principles. For the unsubstituted 1,1´-biphenyl, an activation enthalpy $\Delta H^{\ddagger}$ of 4.5 kJ/mol was determined by raman spectroscopy and the activation barrier was estimated to be 8 kJ/mol,[1,29] demonstrating an essentially free rotation around the central C_{sp2}-C_{sp2} bond. The racemisation for biphenyl derivatives is given by the rotation around the central

single bond connecting the two benzene ring as shown in Figure 7, and the transition state was demonstrated to be a planar structure in the majority of cases.

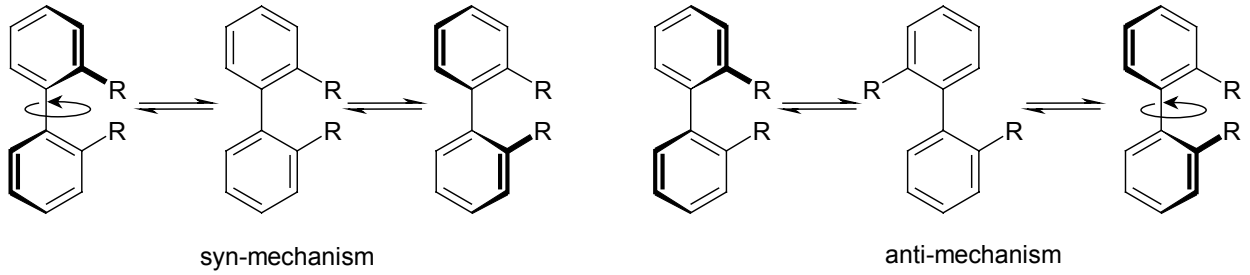

Figure 7. Mechanism for the racemisation of 2,2´-substituted biphenyls. A similar mechanism is also valid for binaphthyl derivatives. The arrows indicate the rotational direction of the upper benzene ring.

Thus, it can be assumed that the introduction of substituents in the proximity to the chiral axis should significantly influence the activation parameter. This influence of the size of the substituents in 2, 2´, 6 and 6´ positions of biphenyls (Figure 8) was demonstrated by Sternhell and co-workers through determination of the activation parameters for the anti-racemisation (Figure 7) of a large variety of diversely 2,2´-disubstituted biphenyls using dynamic NMR spectroscopy. In the series of halogen-substituted biphenyls **14**-**18** (Figure 9) an increase of the free enthalpy of activation from 59.6 kJ/mol (**14**) to 97.0 kJ/mol (**18**) was observed.[30] These results reveal a strong influence of the size of the substituent in these positions on the activation parameters of the interconversion process of biphenyls.

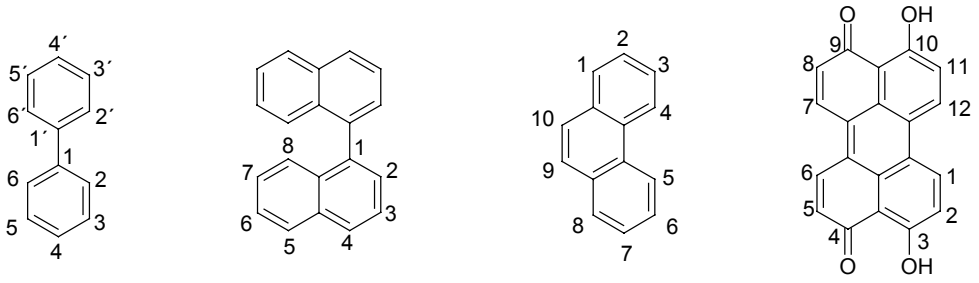

Figure 8. Numbering of the substitution positions in biphenyl, binaphthyl, phenanthrene and perylene quinone.

Quantum chemical studies by Grain confirmed the relationship of the size of the substituents with both the distortion of the molecule expressed in the twist angle θ and the rotational energy barriers.[21a] Additionally, the results obtained by Grain provided a reasonable conclusion on the racemisation mechanism of 2,2´-substituted biphenyl which is in most of the cases an anti-mechanism as shown in Figure 7. Introduction of more than two substituents in the proximity to the chiral axis leads to a significant

increase of the activation energy and thus at room temperature stable conformers could be made available.[31]

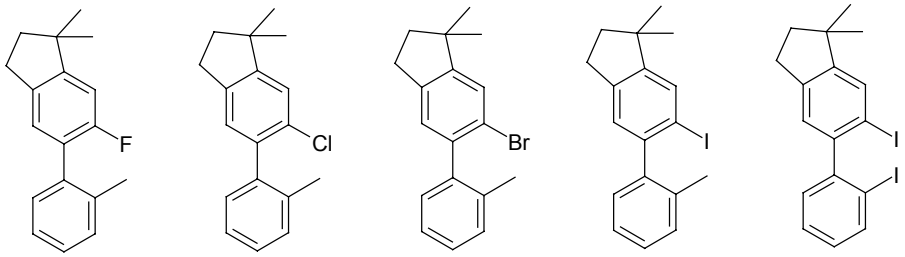

14	**15**	**16**	**17**	**18**
$\Delta G^{\ddagger}$ = 59.6 kJ/mol	78.5 kJ/mol	82.9 kJ/mol	86.3 kJ/mol	97.0 kJ/mol

Figure 9. Structures and activation parameters of the biphenyl derivatives **14**-**18** used for the comparative investigation by Sternhell and co-workers.[30]

Wolf et al. demonstrated on the example of the trifluormethane-substituted biphenyls **19** and **20** (Figure 10), that the interconversion properties further depend on the electronic properties of the compound under consideration. Thus, for the electron-rich amino-substituted compound **19** an interconversion barrier of 113 kJ/mol was determined by polarimetry, whereas for compound **20** with two electron-withdrawing nitro substituents in the 4- and 4´-positions, a free enthalpy of activation $\Delta G^{\ddagger}$ of 103 kJ/mol was obtained.[32] These data clearly show that the interconversion process can be influenced by electronic properties of molecules.

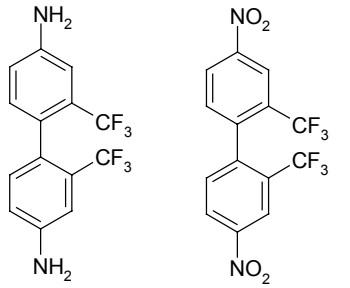

19	**20**
$\Delta G^{\ddagger}$ = 113 kJ/mol	$\Delta G^{\ddagger}$ = 103 kJ/mol

Figure 10. Structures and activation parameters of biphenyl derivatives **19** and **20** used by Wolf et al.[32]

A comparative investigation by Müllen et al. revealed that macrocyclization of biphenyls by connecting the 2- and 2´-positions (Figure 11) influences strongly the activation parameters of biphenyls.[33] An increase of the methylene spacer in these macrocycles leads to an increase of the activation energy resulting from an additional contribution of the conformational changes necessary for the bridging part (Figure 14, **22** vs. **23**). The introduction of macrocycles can also cause a change of the racemisation mechanism of biphenyls from an anti- (**21**) to a syn-mechanism (**22**) which

leads to an increase of the energy barrier owing to the increased steric interactions of the 2,2´-substituents in the transition state for a syn-mechanism (see Figure 7 for mechanism).

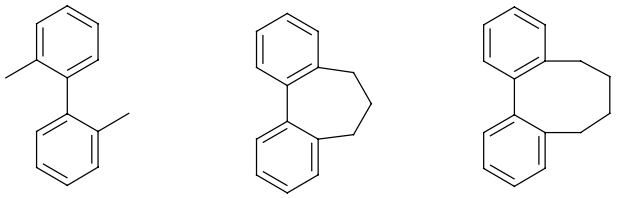

21 $\Delta G^{\ddagger}_{119\,K}$ < 25 kJ/mol **22** $\Delta G^{\ddagger}_{314\,K}$ = 51.5 kJ/mol **23** $\Delta G^{\ddagger}_{314\,K}$ = 96.3 kJ/mol

Figure 11. Structures and thermodynamic parameters for the interconversion process of different biphenyl derivatives **21**-**23**.[33]

Similar effects on the activation parameter were also found for binaphthyl derivatives, whose structural features are related to those of biphenyls. The major difference to biphenyl derivatives is that a steric repulsion imposed by the substituents in the 8,8´-positions (see Figure 8) is already substantial for the parent binaphthyl (i.e. with hydrogens at 8,8´-position). The parent binaphthyl exhibits an interconversion barrier of 101 kJ/mol at 313 K and, thus possesses considerably higher conformational stability than the corresponding unsubstituted biphenyl ($\Delta G^{\ddagger}$ ~ 8 kJ/mol).[4b] The activation parameter of the interconversion process of binaphthyls can further be influenced by attaching substituents in the 2,2´-positions (Figure 8) as the racemisation occurs, similar to biphenyls, via a rotation around the single bond connecting the two aromatic units. A prominent example is 1,1´-binaphth-2-ol (BINOL) which exhibits an interconversion barrier of 158 kJ/mol at 493 K in diphenylether.[4b,34] The importance of the hydrogen atoms in the 8,8´-positions for the stability of the conformational enantiomers was experimentally demonstrated by replacing these hydrogen atoms by nitrogen lone-pairs in 7,7´-dihydroxy-8,8´-biquinolyl.[35] For the latter, a free enthalpy of activation in water was estimated to 103 kJ/mol at 493 K, thus being significantly lower than that of the related BINOL.

Phenanthrenes provide a classical example for molecules in which steric encumbrance leads to a distorted π-conjugated system. Thus, they are distinct from the examples given above, because the interconversion of the enantiomers of phenanthrenes occurs by a movement of both out of plane aromatics through the planarized transition state, as illustrated in Figure 12 (below). For the unsubstituted phenanthrene **24** (Figure12) a twist angle of ~ 5° was reported and the activation barrier is supposed to be very low, if not negligible.[16] As it is apparent from the structure and

the racemisation mechanism, the interconversion process should be influenced by the sterical demand of the substituents in the 4- and 5-positions (Figure 8). Indeed, the free enthalpy of activation for the 4,5-dimethyl-substituted derivative **25** was determined by CD spectroscopy to 67 kJ/mol at 278 K which confirms the effect of the substituents in these positions on the interconversion parameter.[36] Armstrong et al. determined the free enthalpy of activation for phenanthrene derivative **26**, bearing two additional methyl groups in the vicinity, to 96 kJ/mol at 278 K which is 29 kJ/mol larger than that for **25**. This is a convincing example demonstrating the buttressing effect (schematically shown in Figure 15), which is present due to the sterical overcrowding imposed by the additional two methyl groups. Buttressing means that the outer substituents (3,6-positions) enforce a closer proximity of the inner substituents leading to an increased sterical encumbrance and, in turn, to an increased activation energy. Such effects were observed for biphenyl derivatives as well.[4d,37]

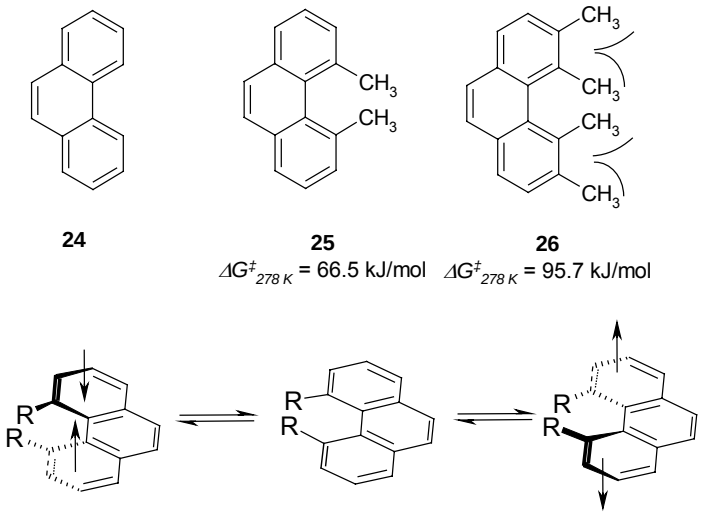

Figure 12. Structures of phenanthrene and 4,5-dimethyl- and 3,4,5,6-tetramethyl-substituted phenanthrenes and the activation parameters of the latters at 278 K (above). The racemisation mechanism of phenanthrenes is shown below.[16,36]

Phenanthrene **24** can be considered as a [3]-helicene, although the ways to influence the dynamic properties in phenanthrenes are significantly different from those of higher homologues helicenes (Figure 13). Experimental values for the activation parameters of helicenes were summarized in a early review article by Laarhoven and Prinsen.[4a] The relation between the activation parameter and the number of annulated rings in helicenes is evident from the experimental free enthalpies of activation (Figure 13) and the quantum chemical studies by Janke et al. confirmed this relation.[38]

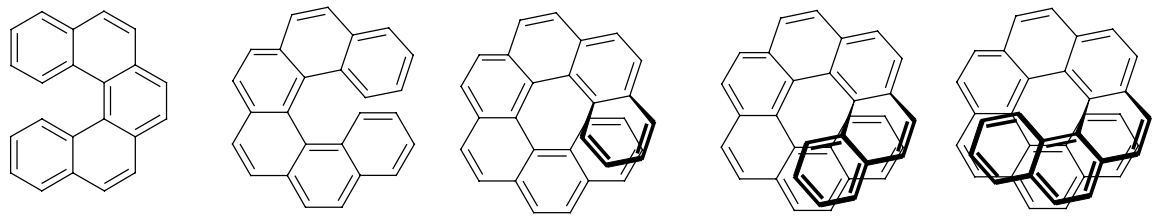

	27	**6**	**12**	**28**	**29**
$\Delta G^{\ddagger}_{300\,K}$ =	100.9 kJ/mol	151.6 kJ/mol	174.6 kJ/mol	177.5 kJ/mol	182.1 kJ/mol

Figure 13. Structures of [5]- (**27**), [6]- (**6**), [7]- (**12**), [8]- (**28**) and [9]-helicene (**29**) and their free activation energies $\Delta G^{\ddagger}$ at 300 K.[4a]

The large span of available activation barriers allows the proper choice of helicenes on the demand of the application (conformational lability or stability) and expands the scope of these compounds. In particular, for larger helicenes (n ≥ 5) the unsubstituted compounds exhibit free enthalpies of activation which are larger than 100.9 kJ/mol. Therefore, similar to binaphthyl derivatives at room temperature stable enantiomers of such helicenes are easily accessible. Like for biphenyl and binaphthyl derivatives, the activation parameter of helicenes can be influenced by introduction of substituents in appropriate positions and by modification of the electronic properties of the aromatic scaffold, e.g., for hexahelicene by attaching electron-donating or electron-withdrawing substituents in the positions A (Figure 14). The free enthalpy of activation for the respective dimethyl derivatives **30** and **31** of hexahelicene were reported to 165 and 186 kJ/mol, respectively, being significantly higher than that of hexahelicene **6** (152 kJ/mol) confirming the influence of substituents in the positions B and D (Figure 14) on the activation parameter of hexahelicenes.[4a,39]

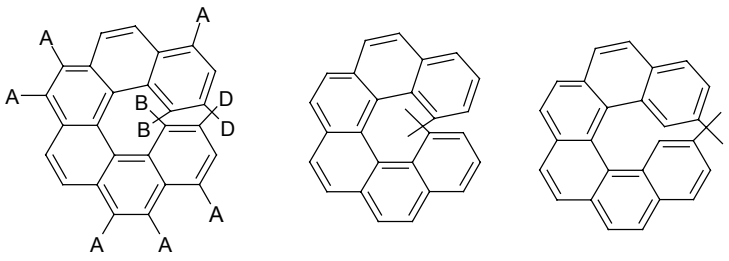

30 **31**

Figure 14. Typical substitution pattern for hexahelicene (left), structures of dimethyl-substituted hexahelicenes **30** and **31**.[4a,39]

The group of Nasini investigated the dynamic properties of cercosporin **32** and pleichrome **33**, that are representative examples for perylene quinones (Figure 15).[40] For perylene quinones, the transition state is assumed to be planar and, thus, the substituents in the bay area (1,6,7,12-positions, Figure 8) can be used to modify the dynamic properties of these compounds. The main structural difference between

cercosporins and pleichromes is that cercosporin **32** bear a dioxomethylene bridge instead of the two methoxy groups in pleichrome **33**. The activation barrier of the perylene quinone derivatives were determined to 115.8 kJ/mol vs. 123.1 kJ/mol for **32** and **33**, respectively, at 298 K by dynamic NMR experiments. The comparison of the activation parameter of cerosporin **32** and pleichrome **33** revealed that the introduction of macrocycles leads, in contrast to biphenyl derivatives,[33] to a decrease of the activation barrier. This effect was attributed to a decreased conformational and sterical restriction imposed by the short methylene bridge in cerosporin **32**.

More important than the effect of macrocyclization observed for these perylene quinones is that another principle of influencing the equilibrium of conformational chiral compounds can be demonstrated by this example. The placement of stereogenic centers in the close vicinity to the chiral plane defined by the bay substituents leads to a shift of the equilibrium towards one of the two atropo-diastereomers, e.g., for **33** a ratio of 79:21 [(*M*,*S*,*S*):(*P*,*S*,*S*)] was found at low temperatures in the ^{1}H NMR spectrum. Such examples were also found for biphenyl and for diasteromeric prezlans as well.[4d,14,41] It has to be noted that the introduction of stereogenic centers does not always lead to a considerable stabilization of one of the atropo-diastereomers and, therefore, to a shift of the racemisation equilibrium. Thus, for dihydrophenanthrenes and hypericins, it was demonstrated that the activation parameter are not significantly influenced by the presence of stereogenic centers.[42]

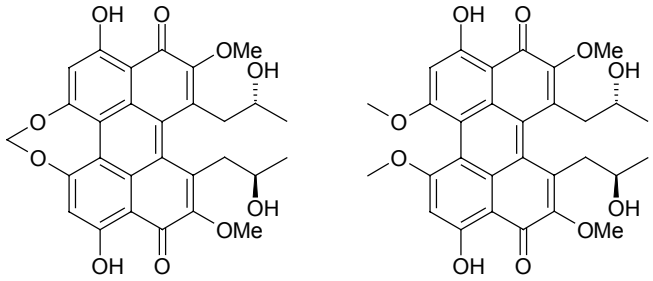

Figure 15. Structures of cercosporin **32** and pleichrome **33**.[40]

Apart from structural modification by covalent attachment of substituents, supramolecular effects can also be utilized for the control of the activation parameter. Faller et al. demonstrated for a biphenyl derivative that the free enthalpy of activation is increased upon coordination of the biphenyl derivative to a metal ion.[43] Likewise, other non-covalent interactions such as hydrogen bonding can be utilized for the stabilization of conformations of chiral chromophores as exemplarily demonstrated for billirubin.[10]

In summary, these examples show that the dynamic properties of conformational chiral compounds can be modified by appropriate structural modifications such as

introduction of substituents in proper positions and incorporation into a macrocyclic structure, as well as by electron-donating or withdrawing substituents. Therefore, it is possible to design chiral molecules with different barriers of inversion between the enantiomers that can be tuned for the respective application if the mechanism of the interconversion process and thus the transition state is known or is apparent from the structure.

1.5 Application of Conformational Chiral Molecules

The classical application of conformational chiral π-systems is in asymmetric catalysis and chiral recognition. The special feature of conformational chiral π-systems is a well-defined extended chiral environment, in particular, after ligation to a catalytic metal center.[44] On the other hand, the dynamic properties of such chiral molecules can be exploited, e.g., in molecular switches and motors.[45]

1.5.1 Asymmetric Catalysis

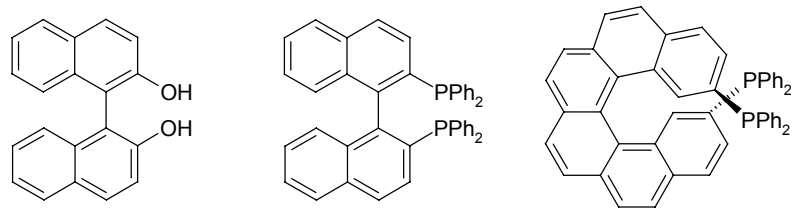

BINOL BINAP Phelix

Figure 16. Structures of 1,1´-binaphth-2-ol (BINOL) and 2,2´-(diphenylphosphanyl)-1,1´-binaphthyl (BINAP) and Phelix. [46-48]

Asymmetric catalysis is one of the most important applications of chiral molecules in chemistry. Binaphthyl derivatives, e.g., BINOL and BINAP (Figure 16), are probably the most extensively used chiral molecules for this purpose,[44,46,47] and also the hexahelicene derivatives, e.g., Phelix (Figure 16), were made available as chiral ligand.[48]

1.5.2 Functional Conformational Chiral Molecules

Most of the compounds mentioned in the previous sections lack of further functionality apart from their chirality. The central chromophore, e.g., biphenyl, binaphthyl, etc, absorb in the UV region of the solar spectrum and are only slightly fluorescent. Thus, to extent the application of such chiral molecules to other fields of chemistry, especially to materials science, the attachment of additional functional units is required. In this

context, the structures of the chromophores were modified or the chiral chromophores were used to control the solid state properties of other functional molecules.

Incorporation of triarylamine functionalities which are known p-type semiconducting molecules, in the chiral scaffold of helicenes was reported by Venkataraman et al.[49] The electrochemical properties and the solid state packing of **34** and **35** (Figure 17) revealed the ability of these chromophores to be applied as p-semiconducting materials in OLEDs. Helicenes **34** and **35** further exhibit pronounced circular polarized emission in solution with a luminescence asymmetry factor *g* ($\Delta I/I$) of 0.001, a large value for molecularly dissolved dyes. For aggregates of hexahelicene quinone, the g factor for luminescence can reach values of up to 0.01.[50] BINOL derivative **36** bearing two hole-transporting triphenylamine units was synthesized by He et al. and LED devices based on **36** revealed an improved performance in comparison to devices made of triphenylamine.[51]

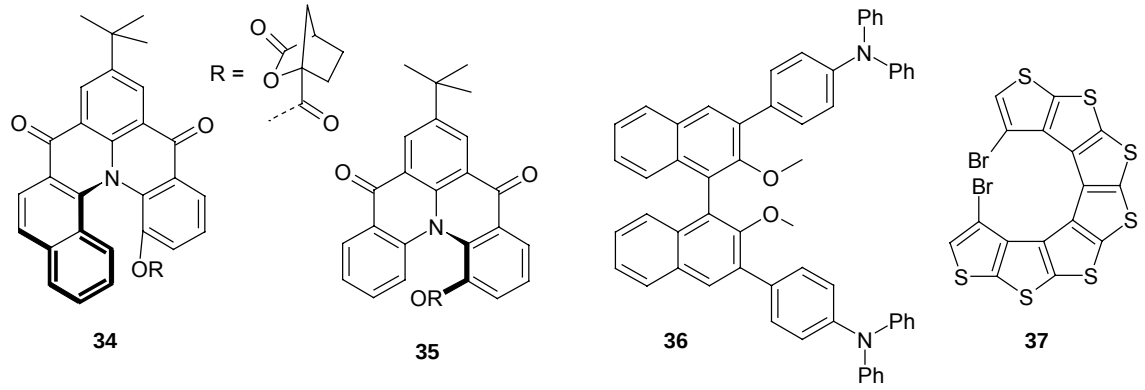

Figure 17. Structures of triarylamine-based helicenes **34**, **35** and binaphthyl **36** and thiophene-based helicene **37**.[50-52]

Helicenes based on β-oligothiophenes were constructed by Rajca and co-workers and advertised for application in optoelectronic devices.[52] Indeed, the solid state properties revealed the formation of a chiral molecular glass with a high glass transition temperature for **37** (Figure 17). Thiophene-based helicene **37** is, therefore, a proper candidate for chiral waveguides and other optical and optoelectronic applications. On the other hand, for outstanding fluorophores and n-type semiconductors such as perylene bisimides, which possess favorable optical and electrochemical properties the synthesis of conformationally stable enantiomers has not been realized yet.[53]

1.5.3 Chiral Recognition and Determination of the Absolute Configuration by Conformational Chiral Molecules

Chiral recognition and the determination of the absolute configuration of a compound is another important field of application for chiral molecules. The essential requirements of chiral molecules for application as sensors or in enantioselective recognition as well as for design principles for supramolecular receptors are surveyed in several reviews, books and articles.[1,54] Therefore, these aspects are not repeated here. The main targets for chiral receptors are given by naturally occurring chiral molecules such as amino acids, and saccharides and DNA.

In Figure 18, some selected examples are presented which all contain a conformational chiral unit responsible for the discrimination of chiral substrates. The classical examples are given by Cram`s receptors based on binaphthyl chromophores such as **38** and **39** (Figure 18).[55] A large variety of these molecules were synthesized in the late 1970s and their use in recognition of amino acids was demonstrated by extraction techniques and monitored by NMR spectroscopy and optical rotation measurements. For **38** ((*P*)-enantiomer), an enantioselective discrimination factor [K(D)/K(L)] of 23.4 was determined for phenylalanine hydroperchlorate by extraction experiments.[55a] The best results were obtained for compound **39** (*P*,*P*-diastereomer) by extraction techniques which exhibited a discrimination factor [K(D)/K(L)] of 52 by recognition of phenylalanine hydroperchlorate. [55b] In both cases the high selectivities were attributed to the increased conformational stability of **38** and **39** owing to the buttressing effects of the ortho substituents present in both compounds.

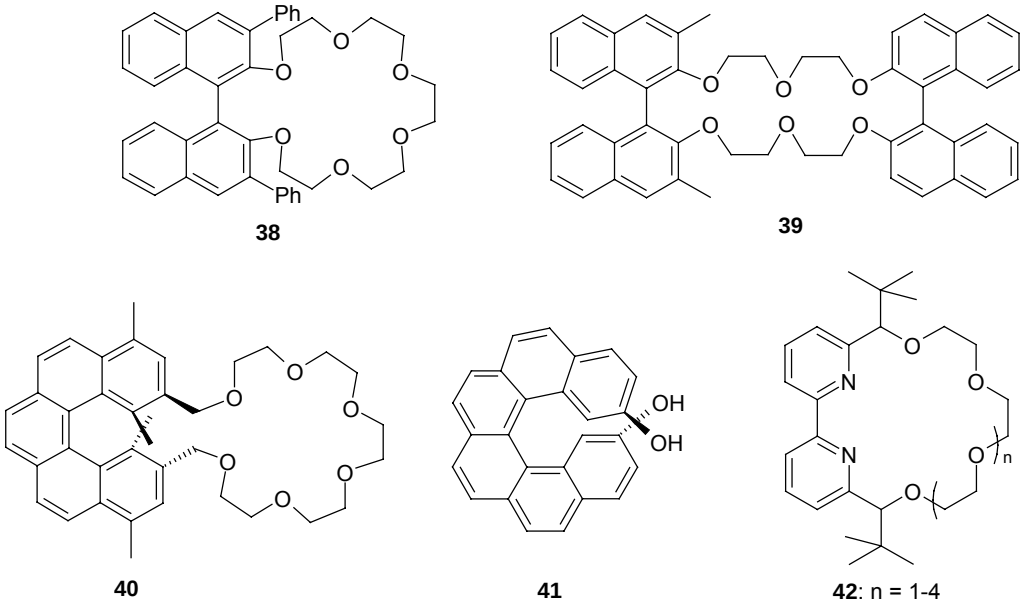

38 **39**

40 **41** **42**: n = 1-4

Figure 18. Binaphthyl, bipyridyl and helicene based molecular receptors.[55-58]

Helicence based chiral macrocycle **40** (Figure 18) was introduced by Yamamoto and co-workers as receptor for the recognition of amino acids.[56] The binding properties of pentahelicene (*M*)-**40** to α-amino acids was investigated by extraction of a racemic mixture of methyl-phenylglycinate from aqueous solution into chloroform. A ratio of 8:1 (*S*:*R*) of the enantiomers in chloroform was determined by NMR spectroscopy thus an applicable enantioselective extraction was achieved.

The ability of chiral HELIXOL **41** (Figure 18) to discriminate between the enantiomers of chiral amines was demonstrated by fluorescence quenching experiments by Reetz and Sostmann.[57] The Stern-Vollmer plot revealed an enantio-discrimination factor ($K_{sv}(R)/ K_{sv}(S)$) of 2.1 for 2-amino-1-propanol which enables **41** to be applied for the determination of the enantiomeric excess of chiral amines.

Bipyridine-based macrocycles **42** (Figure 18) were reported by Lee et al. as chiral receptors.[58] A comparative investigation by UV/Vis and ^{1}H NMR spectroscopy revealed that the smallest macrocycle (**42**: n = 1) exhibited the highest enantioselectivity (K(*S*)/K(*R*)= 2.1) for phenylalanine methylester hydrochloride.

All examples presented so far require an expensive instrumental setup for the determination of the enantiomeric excess (ee). Easy detection of ee for proline was demonstrated by microarrays with a chiral cyanine dye, which enables the detection of samples with large enantiomeric excess by naked eye.[59] Thus, efforts were made to incorporate chromophores into the chiral part of BINOL. Kral and co-workers incorporated a benzthiazolium-pentamethine dye in BINOL and demonstrated the enantioselective recognition of D/L-phenylalanine by UV/Vis spectroscopy.[60]

Introduction of amino functionalities to the chiral scaffold of helicenes allowed the investigation of the binding properties of helically twisted chromophores to DNA. The preferential binding of helicene (*P*)-**43** (Figure 19) to Z-DNA (left-handed) represents the first example, for which a switching from B-DNA to Z-DNA induced by a DNA-binder was experimentally proven.[61] The binding ability of the thia-helicene (*P*)-**43** was attributed to the ammonium groups present under physiological conditions. In contrast, the corresponding (*M*)-**43** did not show any selective binding to B-DNA or Z-DNA.

By changing the position of the amino groups at the helical scaffold, Honzawa et al. showed by fluorescence and CD spectroscopy as well as by isothermal calorimetry that (*P*)-helicene **44** (Figure 19) binds more strongly to calf-thymus DNA (right-handed helicity) than the respective (*M*)-enantiomer.[62] The same selectivity was also observed for small oligonucleotides implying that in addition to the ionic interactions also the nucleosides are involved in the binding process of **44** to DNA.

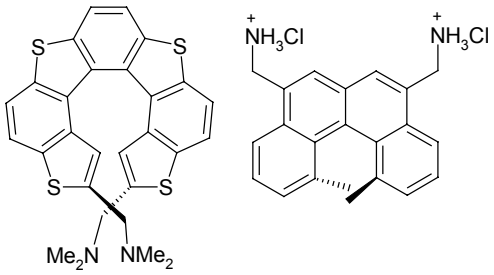

43 **44**

Figure 19. Structures of DNA-binders based on helicenes.[61,62]

Another concept for the application of conformational chirality in chiral recognition is exemplified by the tetraamide macrocycle **45** (Figure 20) of Katoono et al.[63] In contrast to the receptors mentioned above, the macrocycle **45** possesses an achiral rectangular structure in its free form as evidenced by X-ray crystallography. Binding of the chiral analyte **46** caused conformational changes in the host **45** which adopts a screwed and, therefore, chiral conformation in the bound form (Figure 20). This was proven by the observation of an induced bisignated CD signal for the host **45** upon addition of chiral diammonium salt (*S*,*S*)-**46**. Thus, the formation of (*M*)-**45** (Figure 20) was evidenced by exciton chirality method.[63] The flexible macrocycle **45** can therefore be used for the assignment of the absolute stereochemistry of diamines like **46**.

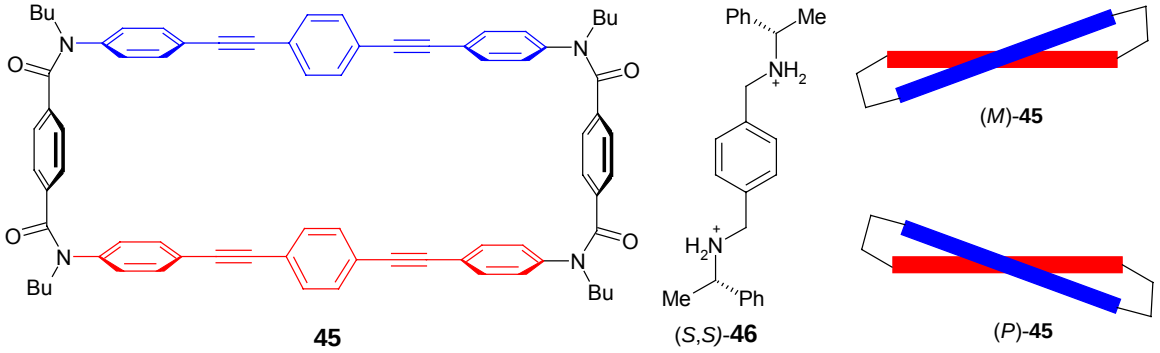

45 (*S*,*S*)-**46**

Figure 20. Structure of diaryl-based macrocycles **45** bearing two tetramide units for chiral recognition and guest **46** (left). Schematic representation of the screwed chiral conformations of host **45** upon binding of chiral guests are shown on the right.[63]

A similar concept was applied for the design of pyridine-based receptors for sugar derivatives. Receptor **47** (Figure 21), reported by Shinkai and co-workers, possesses two chiral axes which can rotate almost freely as no significant steric constraints are present.[64] This is advantageous as upon binding to a sugar substrate, the two pyridine units can adopt different conformations which ensures a high binding constant for a large variety of sugar derivatives.[64] Since different twisted conformations of the pyridine units in **47** give rise to different CD responses, such hosts are proper candidates for

chirality read-out of sugar derivatives. Indeed, it could be demonstrated by CD spectroscopy that the induced chirality observed for **47** is strongly dependent on the sugar molecule and an enhanced selectivity for mannose (K_{Ass} = 940 M^{-1}) in comparison to glucose (85 M^{-1}) and galactose (no binding) was shown by NMR experiments and fluorescence titrations in chloroform.[64] Thus, the major interactions between receptor **47** and the sugar substrates were attributed to hydrogen bonding of the 3-, 4- and 6-hydroxy groups of the sugar molecule to the nitrogen atoms of **47**. This example points out that the flexibility in the receptor and rigidity in the corresponding substrate-receptor complex is a useful combination for chirality read-out, not only for sugar derivatives but in general.

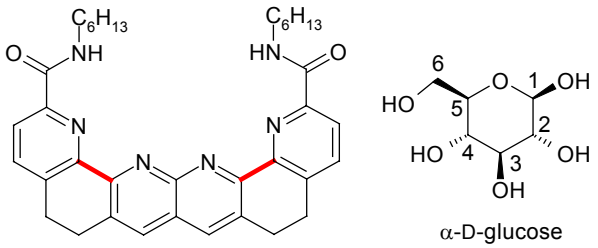

47

Figure 21. Naphthyridine-based receptor **47** for recognition of sugars.[64] The chiral axes of **47** are highlighted in red.

The dynamic properties of biphenyl derivatives can further be used for the determination of the absolute configuration of chiral 2-alkyl or 2-aryl carboxylic acids, diols and alcohols. Thus, biphenyl derivatives **48**, **49** and **50** (Figure 22) were successfully applied for this purpose.[65]

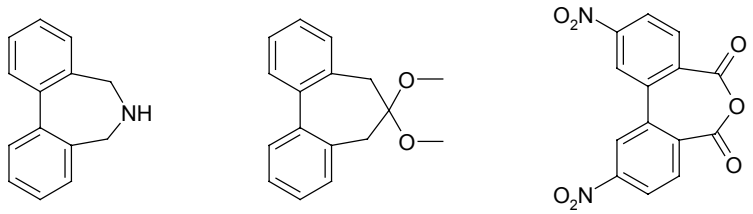

48 **49** **50**

Figure 22. Structures of biphenyl derivatives used for the determination of absolute configurations of acids (**48**), diols (**49**) and alcohols (**50**).[65]

For all these derivatives, the covalent attachment of compounds possessing chiral centers renders a shift of the conformational equilibrium to one of the diastereomers. The concomitant CD signal of the biphenyl core can then be applied to determine the absolute conformation of the substrate molecule. For **48**, X-ray crystallography and consideration of the sterical situation in the covalently bound chiral acid showed that the

conformation of the central biphenyl unit is dependent on the steric demand of the substituents attached to the chiral center of the acid. For biphenyl **49**, the enantiomeric composition of the diol was analyzed by low-temperature NMR spectroscopy and for **50** the configuration of the alcohols was assigned similarly as for **48** by the sign of the CD signal of the covalently bound biphenyl moiety.

1.5.4 Molecular Switches

Molecular switches require a reversible change between two defined states by an external stimuli, e.g., temperature, light or chemical reaction. Therefore, conformational labile chromophores are ideally suited, but also a change of the conformational properties (e.g., the dihedral angle θ) of conformationally stable compounds can be utilized for this purpose.

A temperature dependent shift of the equilibrium between the diastereomers of chiral prezlan **8** (Figure 4) was demonstrated by Stoddart´s group.[14] At room temperature chiral prezlan (*S*,*M*)-**8** was present in a 90% excess in DMSO with respect to (*S*,*P*)-**8** as monitored by ^{1}H NMR spectroscopy. Variable temperature experiments revealed that at elevated temperatures (373 K) the two diastereomers cannot be distinguished by NMR spectroscopy which is apparently due to a fast interconversion between the respective diastereomers on the NMR timescale. This thermal equilibration was further evidenced by the decrease of the CD intensity upon heating of **8** in acetonitrile. Potential applications for such systems might be given in information technology.[14]

For the control of the molecular properties, in particular the dihedral angle θ of conformationally stable chiral compounds by external stimuli, additional functional units, e.g., photo-responsive or electro-responsive groups are required. Molecular switches **51** and **52** (Figure 23) consist of a biphenyl skeleton and two azobenzene functionalties attached to the 2,2´- or 5,5´-positions of the binaphthyl for **51** and **52**, respectively.[66,67] The well-known reversible *E*–*Z*-isomerization of the azophenyl moieties was exploited in these systems to achieve switching between two defined states. In **51**, the (*Z*) form reflects less sterical repulsion of the azo functionalities as in the respective (*E*)-**51** form which enforced a change of the twist angle θ of the biphenyl unit. Consequently, large changes in the CD spectrum were observed upon irradiation of (*E*,*E*)-(*P*)-**51** at 365 nm for the transitions related to the binaphthyl, but also to those of the azo functionalities.[66] In the photostationary state at 365 nm the (*Z*,*Z*) form was present in 30% whereas the (*E*,*E*) form (60%) dominated in the photostationary phase after irradiation at 546 nm.

In contrast, photochemical *E*–*Z*-isomerization (402 nm) of the azo functionalities in the (*E*,*E*) form of (*M*)-**52** retains the CD amplitude related to the binaphthyl unit, as the structural properties are not influenced by substituents in these positions (see above).[67] However, as the absorption properties of the azo functionality differ for the (*E*) (347 nm) and (*Z*) form (454 nm), changes in the CD spectrum were observed in this spectral region revealing the function as molecular switch. Upon irradiation at 402 nm, 44% of all (*E*)-azobenzene moieties were switched to the (*Z*) form whereas upon subsequent irradiation at 466 nm, 76% of all diazo units could be switched back to the (*E*) form reflecting the reversible nature of the photochemical isomerization. For both compounds, **51** and **52**, the use as dopant in liquid crystals and the change of the helical twisting power of a cholesteric liquid crystalline phase upon irradiation at 365 nm or 402 nm, respectively, was demonstrated. In particular the isomerization of the diazo functionalities in **52** revealed an inversion of the helicity of the liquid crystalline phase.[67]

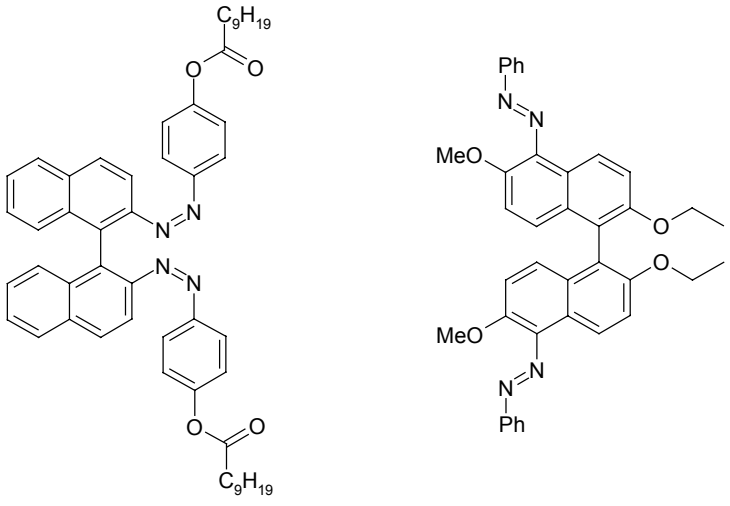

51 **52**

Figure 23. Molecular switches based on binaphthyl chromophores and diazo functionalities.[66,67]

The utilization of electro-responsive tetrathiafulvalene for the design of binaphthyl-based molecular switch **53** (Figure 24) was reported by the group of Zhu.[68] The reversible formation of tetrathiafulvalene cations by chemical oxidation with iron perchlorate increased the CD amplitude of the binaphthyl unit (215-250 nm) in $\mathbf{53}^{2+}$ slightly. Further oxidation under formation of tetrathiafulvalene dications reveals a significant decrease of the respective CD intensity of $\mathbf{53}^{4+}$. As the dihedral angle θ of the neutral form was estimated from quantum chemical calculations to 72.6°, an increase of the CD amplitude should be related to a smaller twist angle and vice versa (see 1.3). These conformational changes of the binaphthyl unit were attributed to the formation of

π-dimers of tetrathiafulvalene radical cations and to repulsive interactions of tetrathiafulvalene dications in **53**$^{4+}$, as schematically shown in Figure 24.

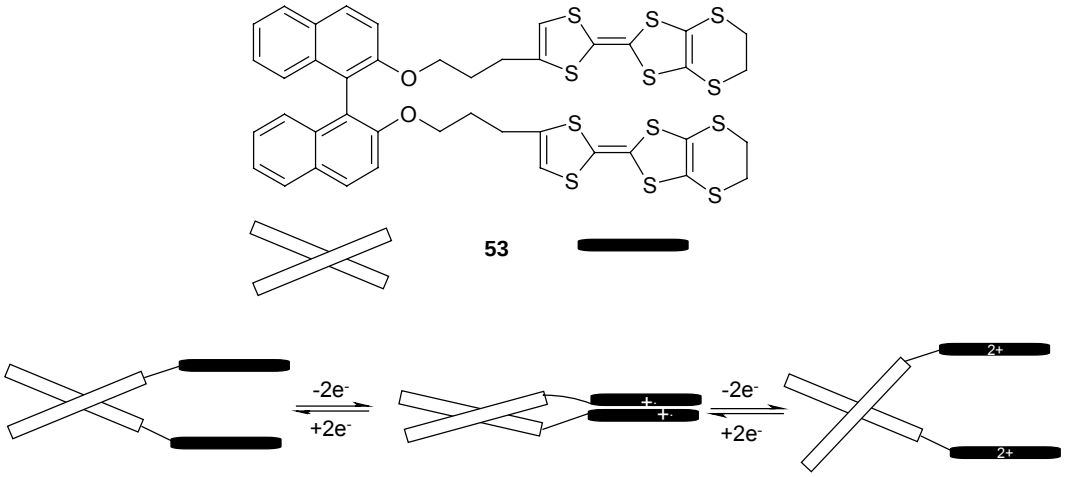

Figure 24. Molecular switch based on binaphthyl with appended electro-responsive tetrathiafulvalene units: Structure of **53** (above) and schematic illustration of the oxidative π-dimerization of tetrathiafulvalene units (below).[68]

Apart from photo- and electrochemical modulation of the structural properties of binaphthyl chromophores, Zhou et al. reported the use of reversible photochemical and chemical reactions for the same purpose.[69] As shown in Figure 25 for binaphthyl derivative **54**, the photochemical ring-opening of spiropyran functionalties *and* subsequent protonation under formation of merocyanine dyes was applied for the design of a molecular switch of "AND" logic gate character.

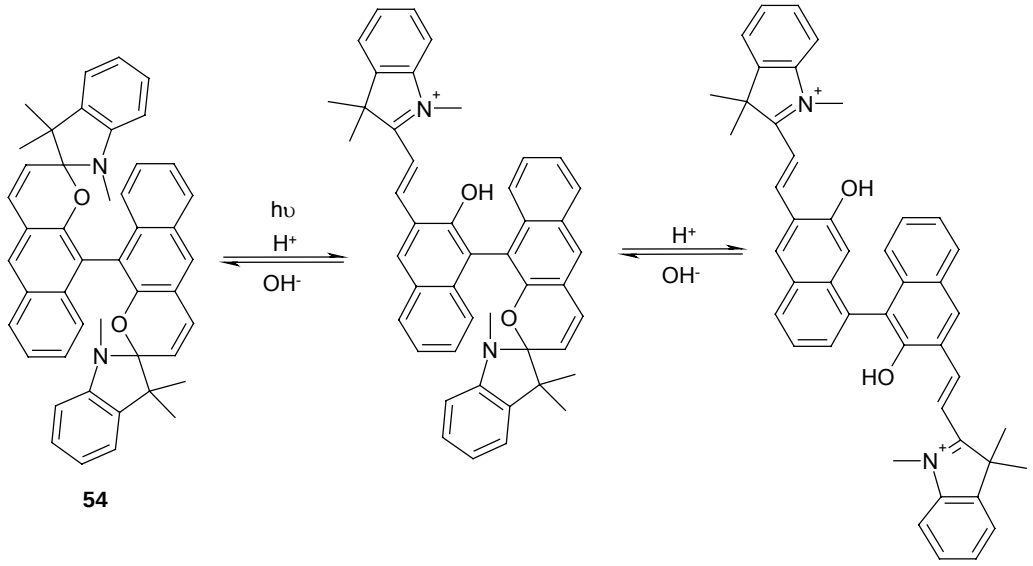

Figure 25. Equilibrium of reversible binaphthyl based AND logic gate **54**.[69]

UV/Vis- and CD-spectroscopic investigations of **54** revealed signification spectral changes of the binaphthyl moiety upon addition of trifluoroacetic acid and illumination

with UV light (250 nm). These spectral changes were attributed to a change of the dihedral angle θ of the binaphthyl unit imposed by repulsive interactions of the positively charged merocyanine moieties. The formation of the merocyanine functionalized binaphthyl was confirmed by ^{1}H NMR titrations. Similarly, the optical rotation was reversibly modulated in dependence on the pH value and UV light exposure, revealing the use of **54** as two input AND logic gate.

One of the most extensively studied conformational chiral π-systems are molecular switches based on overcrowded diarylethenes, e.g. **55a** (Figure 26) which were pioneered by Feringa´s group.[45,70a,b] Here the chirality is switchable in cyclic fashion by alternate thermal or photochemical isomerisation or by irradiation with circular polarized light. Other frequently applied derivatives are 1,2-dithienylethenes such as **55b**.[70c,d] For photochromic helicence **55b** the switching behavior was achieved by photochemical cyclization and ring-opening as shown in Figure 26.[70c] The principle and the remarkable potential of these switches for applications are summarized in several reviews,[45,70] thus these are not repeated here.

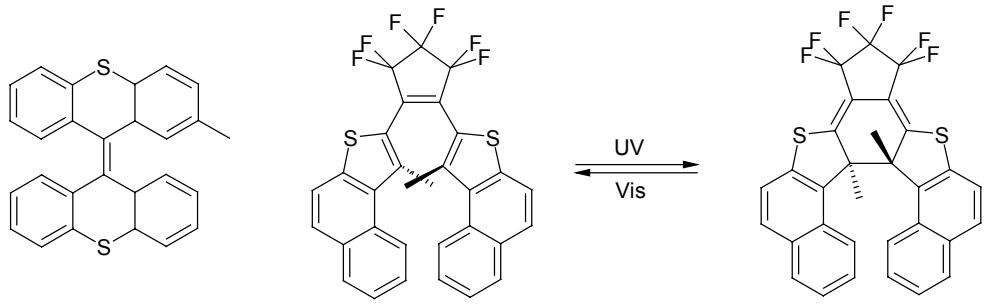

55a **55b**

Figure 26. Structures of diarylethenes **55a** and **55b** and photochemical ring closure and opening of thia-helicene based molecular switch **55b**.[70b,c]

An even more sophisticated example was published recently by Aida´s group.[71] The host molecule in **56** (Figure 27, top) is composed of a azo-functionality, a ferrocene unit and two zinc porphyrin units to which a 1,1´-bis(isoquinoline) guest is bound by non-covalent interactions. Photochemical *E*–*Z*-isomerization of the azo-functionality in **56** leads to a change of the conformation of the two porphyrin moieties and consequently of the bound isoquinoline derivative. Thus, this molecular machine represents the motion of a scissor, as schematically shown in Figure 27 (bottom). Indeed, irradiation dependent UV/Vis and CD spectroscopic investigations revealed a decrease of the CD signal related to the (*M* or *P*)-isoquinoline guest in **56** demonstrating the coupled motion of the azo-functionality and the guest molecule bound to the zinc porphyrin. As pointed out in this article such systems may be used as molecular motors but also the

incorporation into larger self-assembled systems in order to control certain processes seems reasonable.

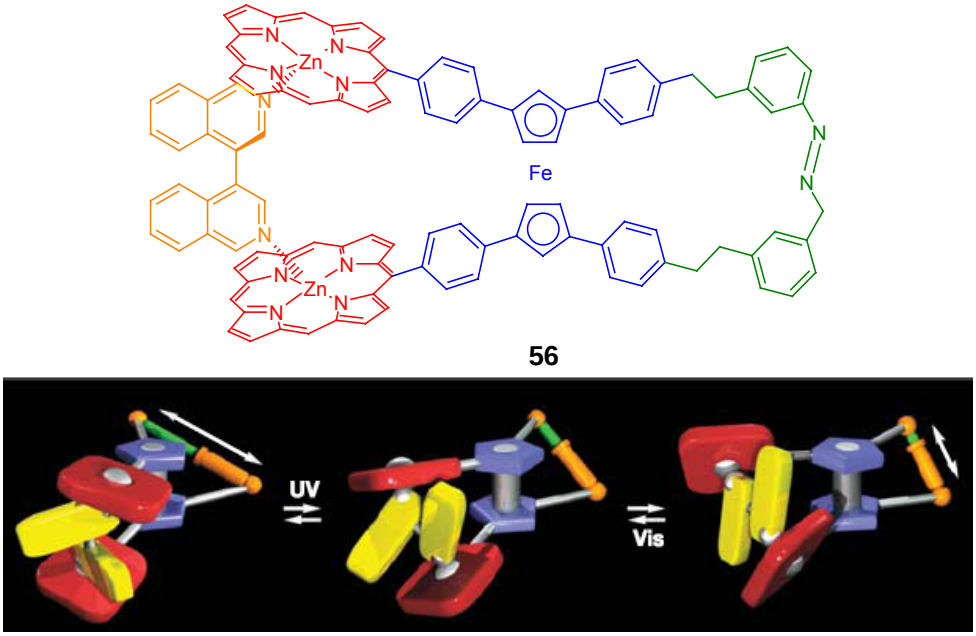

56

Figure 27. Structure (top) and schematic representation of the function (bottom) of molecular machine published by Aida and co-workers.[71] The picture (bottom) was taken from reference 71.

The examples presented here clearly show, that the conformational flexibility of chiral chromophores can be used to control molecular motion by external stimuli.

1.5.5 Conformational Chirality in Self-Assembled Systems

It has already been mentioned in the previous section that chiral π-conjugated molecules such as binaphthyls and helicenes can afford desirable solid state properties of functional molecules and thus improve the performance of solid state devices based on these chromophores.[47-50]

Katz and co-workers investigated by UV/Vis absorption studies the π-π aggregation of enantiopure [6]-helicenequinones **57** in dodecane solution and revealed a preferred formation of helical aggregates for the enantiopure compounds (Figure 28).[50,72] The transfer of the helical structure of these fluorescent aggregates from solution to solid state by spin-coating was evidenced by circular dichroism studies of the obtained thin films. The main application of chiral emitters especially in solid state devices was denoted to stereo-imaging and back-lightening in organic light-emitting diodes as pointed out for aggregates based on chiral oligo(phenylenevinylene).[73]

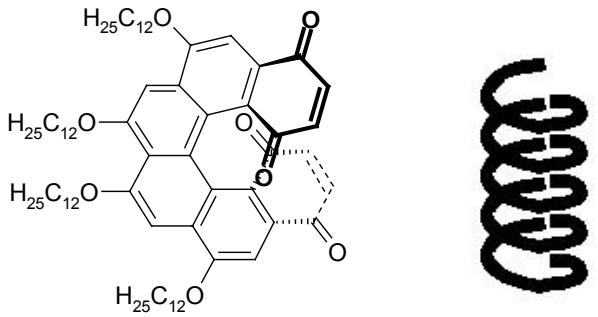

57

Figure 28. Structure of [6]-helicenequinone **57** (left) and schematic representation of the helical π-stacking of **57** (right).[50,72]

In another example from the Katz group, conformationally stable (*M*)-[5]-helicenes were applied to control the enantioselective aggregation of copper and nickel phthalocyanines dyes.[74] The aggregation properties of **58** (Figure 29) were investigated by UV/Vis and CD spectroscopy and atomic force microscopy. From the latter, an average aggregation number of 6-8 molecules was estimated by applying a model obtained from quantum chemical calculations and CD spectroscopy revealed a chiral superstructure imposed by the chiral [5]-helicene substituents in solution and in thin films. Furthermore, notable non-linear optical effects were observed for a thin film of this material on a glass substrate.

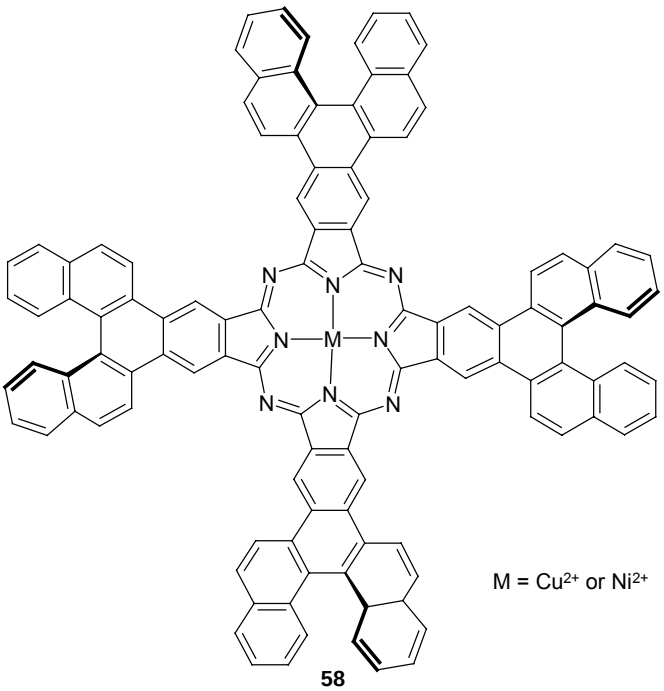

58

Figure 29. Structure of [5]-helicene functionalized phthalocyanine **58**.[74]

Crystallization displays another type of self-assembly. In particular, the spontaneous resolution of enantiomers by crystallization as an convenient method for the separation

of chiral stereoisomers have attracted a great deal of attention.[75] But, crystallization of racemic mixtures most frequently affords racemic crystals (90-95%) whereas the spontaneous resolution of the enantiomers is only rarely observed (5-10%).[76] Examples for chiral crystallization or spontaneous resolution of enantiomers are tartaric acid, divinylbenzene, [4]-helicene and [6]-helicene.[1,75] Resolution of enantiomers by crystallization can be enforced by seeding with enantiomorphic crystals[75f] or by formation of inclusion complexes, e.g. chiral auxiliaries **59-62** (Figure 30) were applied for the resolution of BINOL by Tado and co-workers.[77]

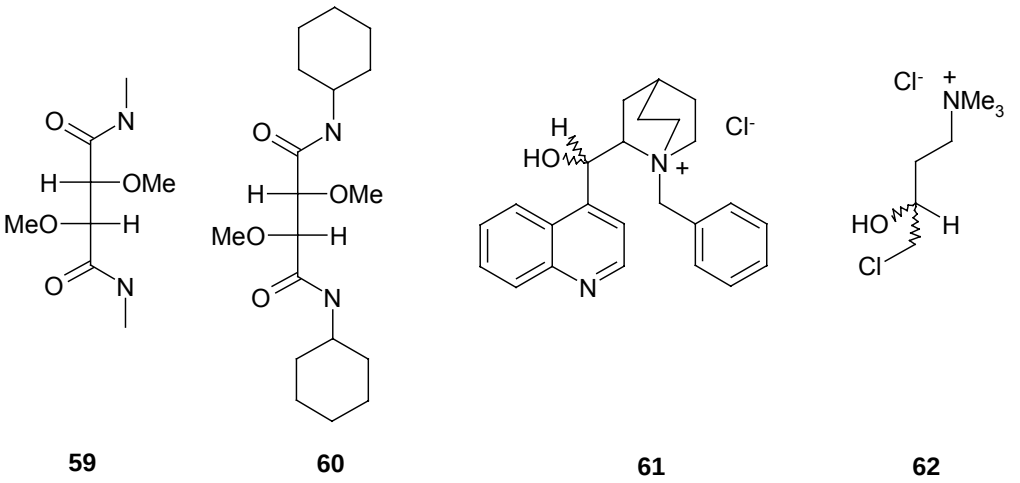

Figure 30. Structures of chiral auxiliaries applied for the resolution of BINOL by inclusion complexation.[77]

The crystallization of racemic 1,1´-binaphthyl from its melt is an exhausting example for the formation of enantiopure crystals from racemic mixtures and has been subject of a variety of studies.[78] In the melt, 1,1´-binaphthyl exhibits a fast interconversion between the enantiomers, whereas at room temperature and in the crystal, the racemisation is slow.[78] Pincock et al. initially demonstrated, that the conglomerate formation (equal amounts of enantiopure crystals of (*P*)- and (*M*)-1,1´-binaphthyl) from the melt is preferred at crystallization temperatures above 145 °C (mp. 158 °C), whereas below this temperature the formation of racemic crystals occured.[78a] Further investigations of the crystallization behavior of 1,1´-binaphthyl revealed that an enrichment of one enantiomer in the crystalline phase from the racemic melt can be achieved either by stirring of the melt (*ee* up to 80%) or by doping the melt with enantiopure (*M*)- or (*P*)-BINOL (~*ee* 100).[78b]

For conformational labile but chiral 2,2´-dipyrrolyl ketone, Branda and co-workers observed the formation of conglomerates upon layering a chloroform solution of a racemic mixture of 2,2´-dipyrrolyl ketone with *n*-hexane.[79] X-ray analysis revealed that

hydrogen-bonds afforded a helical arrangement of one enantiomer which resulted in the formation of enantiopure crystals.

For 7,8-dioxa-[6]-helicene, which similarly exhibits a fast racemisation in solution, Krebs et al. demonstrated the formation of domains of the respective enantiomers in the crystal.[80] Here, the formation of domains and thus the partial resolution of enantiomers seems to be related to the preferred π-stacking of the respective enantiomers.

The spontaneous resolution of the enantiomers of [7]-helicene has been demonstrated by Fasel et al., who visualized by STM investigations the formation of domains of (*M*)-[7]-helicene in the presence of a slight excess of this enantiomer on a Cu (111) surface.[81] Therefore, it seems reasonable that the 2D- and 3D-packing of helicenes is more effective for molecules with the same inherent chirality (*M*-*M* or *P*-*P*) than that of opposite chirality (*M*-*P*). The formation of chiral 2-D adlayers as well as conglomerate formation on surfaces were also demonstrated for a variety of other compounds.[82]

The use of thiol-functionalized BINOL **63** (Figure 30) as molecular wire was investigated by Pu´s group.[83] Although for single molecular devices, as expected, no differences were found for the enantiomers of **63**, the electronic transport properties in nanowell devices revealed that the pure enantiomers showed significantly larger electronic transport ability than in a device of the racemic material. This effect was attributed to the more effective packing of the pure enantiomers within the device.

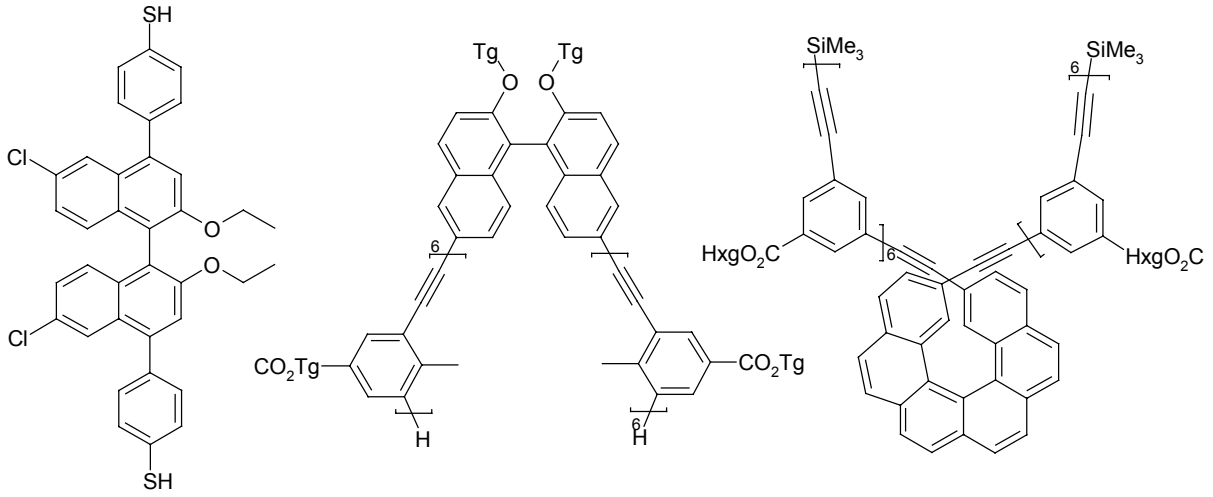

63 **64** **65**

Figure 30. Structures of thiol-functionalized binaphthyl **63** for molecular wires, and oligo(*m*-phenylene ethynylene)-functionalized binaphthyl **64** and helicene **65** applied in foldamers.[83,85,86]

Another possibility arises by incorporation of twisted, conformational stable subunits into a π-conjugated backbone for the control of the chirality in foldamer-type systems. As a model system oligo(*m*-phenylene ethynylene)s (OPE)s, that are know to fold into helical π-stacks in polar solvent,[84] were studied. By incorporation of conformational stable binaphthol or helicence derivatives as central units of OPEs (Figure 30), the helicity thus formed by the OPE unit upon π-π stacking is controlled by the chiral unit. Gin et al. demonstrated in acetonitrile the preferred folding into the (*P*)-helical conformation of the OPE units for **64** by incorporating the (*P*)-enantiomer of BINOL.[85] For a helicene with appended OPE units **65** (see Figure 30) the related foldamer adopts the helicity of the helicene only by applying high water contents in acetonitrile as CD measurements revealed.[86] In acetonitrile, the observed helicity was opposite in sign to that present in the helicene unit. This was related to the conformation of the ethynyl unit directly attached to helicence which has to be changed significantly when adopting the helicity of the helicene. In aqueous solution, hydrophobic effects make the (*M*)-helix (as present in the helicene) more favorable and bring about the necessary conformational changes.

1.6 Concluding Remarks

The origin of conformational chirality has been analyzed and the structural as well as the dynamic properties have been discussed for selected examples. Herein it has been shown, that the barrier of racemisation can be tuned by proper substituents so that molecules can be tailored for a certain application. For the molecules shown, the barrier is most strongly influenced by sterically demanding substituents that are positioned close to a chiral axis. Applications of conformational chiral molecules have been shown in molecular recognition, as chiral catalysts and as molecular switches where conformationally stable as well as conformationally labile molecules can be applied. The presented example revealed the importance and versatility of conformational chiral molecules.

1.7 References and Notes

1 E.L. Eliel, S. H. Wilen, *Stereochemistry of Organic Compounds*, Wiley, London, **1994**.

2 A. B. Harris, R. D. Kamien, T. C. Lubensky, *Rev. Mod. Phys.* **1999**, *71*, 1745-1757 and literature cited in there.

3 P. Atkins, J. de Paula, *ATKINS´ Physical Chemistry*, *Vol. 7*, Oxford Press Inc., New York, **2002**, pp. 453-480.

4 (a) W. H. Laarhoven, W. J. C. Prinsen, *Top. Curr. Chem.* **1984**, *125*, 63-130; (b) L. Pu, *Chem. Rev.* **1998**, *98*, 2405-2494; (c) C. Schmuck, *Angew. Chem.* **2003**, *115*, 2552-2556; *Angew. Chem. Int. Ed.* **2003**, *42*, 2448-2452; (d) G. Bringmann, A. J. Mortimer, P. A. Keller, M. J. Gresser, J. Garner, M. Breuning, *Angew. Chem.* **2005**, *117*, 5518-5563; *Angew. Chem. Int. Ed.* **2005**, *44*, 5384-5427.

5 (a) R. A. Pascal, Jr., W. D. Mc Millan, D. Van Engen, R. G. Eason, *J. Am. Chem. Soc.* **1987**, *109*, 4660-4665; (b) H. M. Duong, M. Bendikov, D. Steiger, Q. Zhang, G. Sonmez, J. Yamada, F. Wudl, *Org. Lett.* **2003**, *5*, 4433-4436; (c) J. Lu, D. M. Ho, N. J. Vogelaar, C. M. Kraml, R. A. Pascal, Jr., *J. Am. Chem. Soc.* **2004**, *126*, 11168-11169; (d) J. E. Norton, K. N. Houk, *J. Am. Chem. Soc.* **2005**, *127*, 4162-4163.

6 L. Eggers, K. Kolster, V. Buss, *Chirality* **1997**, *9*, 243-249.

7 (a) A. P. H. J. Schenning, J. v. Herrikhuyzen, P. Jonkheijm, Z. Chen, F. Würthner, E. W. Meijer, *J. Am. Chem. Soc.* **2002**, *124*, 10252-10253; (b) C. Thalacker, F. Würthner, *Adv. Funct. Mater.* **2002**, *12*, 209-218; (c) E. H. A. Beckers, Z. Chen, S. C. J. Meskers, P. Jonkheijm, A. P. H. J. Schenning, X.-Q. Li, P. Osswald, F. Würthner, R. A. J. Janssen, *J. Phys. Chem. B* **2006**, *110*, 16967-16978.

8 K. C. Nicolaou, C. N. C. Boddy, S. Bräse, N. Winssinger, *Angew. Chem.* **1999**, *111*, 2230-2287; *Angew. Chem. Int. Ed.* **1999**, *38*, 2096-2152.

9 P. Lloyd-Williams, E. Giralt, *Chem. Soc. Rev.* **2001**, *30*, 145-157.

10 S. E. Boidjiev, R. V. Person, G. Puzicha, C. Knobler, E. Maverick, K. N. Trueblood, D. A. Ligthner, *J. Am. Chem. Soc.* **1992**, *114*, 10123-10133.

11 (a) U. Weiss, L. Merlini, G. Nasini, *Prog. Chem. Org. Nat. Prod.* **1987**, *52*, 1-71; (b) H. Falk, *Angew. Chem.* **1999**, *111*, 3306-3326; *Angew. Chem. Int. Ed.* **1999**, *38*, 3116-3136.

12 G. Snatzke, *Chem. unserer Zeit* **1982**, *16*, 160-168.

13 S. E. Boiadjiev, D. A. Lightner, *Chirality* **2005**, *17*, 316-322.

14 (a) Y. Liu, S. A. Vignon, X. Zhang, K. N. Houk, J. F. Stoddart, *Chem. Commun.* **2005**, 3927-3929; (b) Y. Liu, S. A. Vignon, X. Zhang, P. A. Bonvallet, S. I. Khan, K. N. Houk, J. F. Stoddart, *J. Org. Chem* **2005**, *70*, 9334-9344.

15 (a) R. Cosmo, T. W. Hambley, S. Sternhall, *J. Org. Chem.* **1987**, *52*, 3119-3123; (b) H. Bock, M. Sievert, Z. Havlas, *Chem. Eur. J.* **1998**, *4*, 677-685.

16 S. Grimme, J. Harren, A. Sobanski, F. Vögtle, *Eur. J. Org. Chem.* **1998**, 1491-1509

17 A. B. Buba, T. Auf der Heyde, K. Mislow, *Angew. Chem.* **1992**, *104*, 1012-1031; *Angew. Chem. Int. Ed.* **1992**, *31*, 989-1007.

18 O. Katzenelson, J. Edelstein, D. Avnir, *Tetrahedron: Asymmetry* **2000**, *11*, 2695-2704.

19 H. Zabrodsky, D. Avnir, *J. Am. Chem. Soc.* **1995**, *117*, 462-473.

20 D. D. Fitts, M. Siegel, K. Mislow, *J. Am. Chem. Soc.* **1958**, *80*, 480-486.

21 (a) F. Grain, *J. Phys. Chem. B* **2002**, *106*, 3823-3827; (b) S. E. Biali, B. Kahr, Y. Okamoto, R. Aburatani, K. Mislow, *J. Am. Chem. Soc.* **1988**, *110*, 1917-1922.

22 F. Furche, R. Ahlrichs, C. Wachsmann, E. Weber, A. Sobanski, F. Vögtle, S. Grimme, *J. Am. Chem. Soc.* **2000**, *122*, 1717-1724.

23 (a) R. H. Martin, M. J. Marchant, *Tetrahedron* **1974**, *30*, 343-345; (b) E. P. Kyba, G. W. Gokel, F. de Jong, K. Koga, L. R. Sousa, M. G. Siegel, L. Kaplan, G. Dotsevi, Y. Sogah, D. J. Cram, *J. Org. Chem.* **1977**, *42*, 4173-4183; (c) N. Kawano, M. Okigawa, N. Hasaka, I. Kouno, Y. Kawahara, Y. Fujita, *J. Org. Chem.* **1981**, *46*, 389-392.

24 R. B. Bates, F. A. Camou, V. V. Kane, P. M. Mishra, K. Suvannachut, J. J. White, *J. Org. Chem.* **1989**, *54*, 311-317.

25 (a) E. Bunnenberg, C. Djerassi, K. Mislow, A. Moscowitz, *J. Am. Chem. Soc.* **1962**, *84*, 2823-2826 and 5003; (b) K. Mislow, E. Bunnenberg, R. Records, K. Wellman, C. Djerassi, *J. Am. Chem. Soc.* **1963**, *85*, 1342-1349; (c) J. Gawronski, P. Grycz, M. Kwit, U. Rychlewska, *Chem. Eur. J.* **2002**, *8*, 4210-4215.

26 W. Hug, G. Wagnière, *Tetrahedron* **1972**, *28*, 1241-1248.

27 K. Oki in *Topics in Stereochemistry*, *Vol. 14* (Eds. N. L. Allinger, E. E. Eliel, S. H. Wilen), Wiley Interscience, New York, **1983**, pp. 1-76.

28 O. Trapp, G. Schoetz, V. Schuring, *Chirality* **2001**, *12*, 403-414.

29 (a) J. E. Katon, E. R. Lippincott, *Spectrochim. Acta* **1959**, *15*, 627-659; (b) L. A. Carreira, T. G. Towns, *J. Mol. Struct.* **1977**, *41*, 1-9.

30 (a) G. Bott, L. D. Field, S. Sternhell, *J. Am. Chem. Soc.* **1980**, *102*, 5618-5626; (b) R. Cosmo, S. Sternhell, *Aust. J. Chem.* **1987**, *40*, 35-47.

31 N. Kawano, M. Okigawa, N. Hasaka, I. Kouno, Y. Kawahara, Y. Fujita, *J. Org. Chem.* **1981**, *46*, 389-392.

32 C. Wolf, W. A. König, C. Roussel, *Liebigs Ann. Chem.* **1995**, 781-786.

33 K. Müllen, W. Heinz, F.-G. Klärner, W. R. Roth, I. Kindermann, O. Adamczak, M. Wette, J. Lex, *Chem. Ber.* **1990**, *123*, 2349-2371.

34 L. Meca, D. Reha, Z. Havlas, *J. Org. Chem.* **2003**, *68*, 5677-5680.

35 P. R. Blakemore, C. Kilner, S. D. Milicevic, *J. Org. Chem.* **2006**, *71*, 8212-8218.

36 R. N. Armstrong, H. L. Ammon, J. N. Darnow, *J. Am. Chem. Soc.* **1987**, *109*, 2077-2082.

37 M. Rieger, F. H. Westheim, *J. Am. Chem. Soc.* **1950**, *72*, 19-28.

38 R. H. Janke, G. Haufe, E.-U. Würthwein, J. H. Borkent, *J. Am. Chem. Soc.* **1996**, *118*, 6031-6035.

39 H. Meier, M. Schwertel, D. Schollmeyer, *Angew. Chem.* **1998**, *110*, 2224-2226; *Angew. Chem. Int. Ed.* **1998**, *37*, 2110-2113.

40 L. Scaglioni, S. Mazzini, R. Mondelli, L. Merlini, E. Ragg, G. Nasini, *J. Chem. Soc., Perkin Trans. 2*, **2001**, 2276-2286.

41 J.-P. Mazaleyrat, K. Wright, A. Gaucher, N. Toulemonde, L. Dutot, M. Wakselman, Q. B. Broxterman, B. Kaptein, S. Oancea, C. Peggion, M. Crisma, F. Formaggio, C. Toniolo, *Chem. Eur. J.* **2005**, *11*, 6921-6929.

42 (a) R. Altmann, C. Etzlstorfer, H. Falk, *Monatsh. Chem.* **1997**, *128*, 361-370; (b) R. N. Armstrong, D. A. Lewis, *J. Org. Chem.* **1985**, *50*, 907-908.

43 (a) J. W. Faller, N. Sarantopoulos, *Organometallics* **2004**, *23*, 2008-2014; (b) J. W. Faller, P. P. Fontaine, *J. Organomet. Chem.* **2007**, *692*, 1110-1117.

44 R. Noyori, *Angew. Chem.* **2002**, *114*, 2108-2123; *Angew. Chem. Int. Ed.* **2002**, *41*, 2008-2022.

45 B. L. Ferringa, *Molecular Switches*, Wiley VCH, Weinheim, **2001**.

46 J. M. Brunel, *Chem. Rev.* **2005**, *105*, 857-898.

47 (a) M. Berthod, G. Mignani, G. Woodward, M. Lemaire, *Chem. Rev.* **2005**,*105*, 1801-1836; (b) G. M. Aspinall, G. F. Docherty, *Speciality Chem. Mag.* **2005**, 34-35.

48 M. T. Reetz, E. W. Beuttenmüller, R. Goddard, *Tetrahedron Lett.* **1997**, *38*, 3211-3214.

49 (a) J. E. Field, T. J. Hill, D. Venkataraman, *J. Org. Chem.* **2003**, *68*, 6071-6078; (b) J. E. Field, G. Muller, J. P. Riehl, D. Venkataraman, *J. Am. Chem. Soc.* **2003**, *125*, 11808-11809.

50 K. E. S. Phillips, T. J. Katz, S. Jockusch, A. J. Lovinger, N. J. Turro, *J. Am. Chem. Soc.* **2001**, *123*, 11899-11907.

51 Q. He, H. Lin, Y. Weng, B. Zhang, Z. Wang, G. Lei, L. Wang, Y. Qiu, F. Bai, *Adv. Funct. Mater.* **2006**, *16*, 1343-1348.

52 (a) A. Rajca, M. Miyasaka, M. Pink, H. Wang, S. Rajca, *J. Am. Chem. Soc.* **2004**, *126*, 15211-15222; (b) M. Miyasaka, A. Rajca, M. Pink, S. Rajca, *Chem. Eur. J.* **2004**, *10*, 6531-6539.

53 (a) F. Würthner, *Chem. Commun.* **2004**, 1564-1579; (b) F. Würthner, *Pure Appl. Chem.* **2006**, *78*, 2341-2350.

54 (a) T. D. Booth, D. Wahnon, I. W. Wainer, *Chirality* **1997**, *9*, 96-98; (b) A. P. de Silva, H. Q. N. Gunaratne, T. Gunnlaugsson, A. J. M. Huxley, C. P. McCoy, J. T. Rademacher, T. E. Rice, *Chem. Rev.* **1997**, *97*, 1515-1566; (c) V. A. Davankov, *Chirality* **1997**, *9*, 99-102; (d) L. Pu, *Chem. Rev.* **2004**, *104*, 1687-1716; (e) V. Sundaresan, R. Abrol, *Chirality* **2005**, *17*, S30-S39.

55 (a) S. C. Paecock, D. M. Walba, F. C. A. Gaeta, R. C. Helgeson, D. J. Cram, *J. Am. Chem. Soc.* **1980**, *102*, 2043-2052; (b) D. S. Lingenfelter, R. C. Helgeson, D. J. Cram, *J. Org. Chem.* **1981**, *46*, 393-406.

56 K. Yamamoto, T. Ikeda, T. Kitsuki, Y. Okamoto, H. Chikamatsu, N. Nakazaki, *J. Chem. Soc., Perkin Trans. 1*, **1990**, 271-276.

57 M. T. Reetz, S. Sostmann, *Tetrahedron* **2001**, *57*, 2515-2520.

58 C.-S. Lee, P.-F. Teng, W.-L. Wong, H.-L. Kwong, A. S. C. Chan, *Tetrahedron* **2005**, *61*, 7924-7930.

59 G. A. Korbel, G. Lalic, M. D. Shair, *J. Am. Chem. Soc.* **2001**, *123*, 361-362.

60 T. Briza, Z. Kejik, P. Vasek, J. Kralova, P. Martasek, I. Cisarova, V. Kral, *Org. Lett.* **2005**, *7*, 3661-3664.

61 Y. Xu, Y. X. Zhang, H. Sugiyama, T. Umano, H. Osuga, K. Tanaka, *J. Am. Chem. Soc.* **2004**, *126*, 6566-6567.

62 S. Honzawa, H. Okubo, S. Anzai, M. Yamaguchi, K. Tsumoto, I. Kumagai, *Bioorg. Med. Chem.* **2002**, *10*, 3213-3218.

63 R. Katoono, H. Kawai, K. Fujiwara, T. Suzuki, *Chem. Commun.* **2005**, 5154-5156.

64 S.-I. Tamaru, S. Shinkai, A. B. Khasanov, T. W. Bell, *Proc. Natl. Acad. Sci. USA* **2002**, *99*, 4972-4976.

65 (a) S. Hosoi, M. Kamiya, F. Kiuchi, T. Ohta, *Tetrahedron Lett.* **2001**, *42*, 6315-6317; (b) S. Superchi, D. Casarini, A. Laurita, A. Bavoso, C. Rosini, *Angew. Chem.* **2001**, *113*, 465-468; *Angew. Chem. Int. Ed.* **2001**, *40*, 451-454; (c) S. Superchi, R. Bisaccia, D. Casarini, A. Laurita, C. Rosini, *J. Am. Chem. Soc.* **2006**, *128*, 6893-6902.

66 S. Pieraccini, S. Masiero, G. P. Spada, G. Gottarelli, *Chem. Commun.* **2003**, 598-599.

67 R. A. van Delden, T. Mecca, C. Rosini, B. L. Feringa, *Chem. Eur. J.* **2004**, *10*, 61-70.

68 Y. Zhou, D. Zhang, Z. Shuai, D. Zhu, *J. Org. Chem.* **2006**, *71*, 2123-2130.

69 Y. Zhou, D. Zhang, Y. Zhang, Y. Tang, D. Zhu, *J. Org. Chem.* **2005**, *70*, 6164-6170.

70 (a) E. W. Meijer, B. L. Feringa, *Mol. Cryst. Liq. Cryst.* **1993**, *235*, 169-180; (b) B. L. Feringa, R. A. van Delden, N. Koumura, E. M. Geertsema, *Chem. Rev.* **2000**, *100*, 1789-1816; (c) T. J. Wigglesworth, D. Sud, T. B. Norsten, V. S. Lekhi, N. R. Branda, *J. Am. Chem. Soc.* **2005**, *127*, 7272-7273; (d) M. Morimoto, M. Irie, *Chem. Commun*. **2005**, 3895-3905.

71 T. Muraoka, K. Kinbara, T. Aida, *Nature* **2006**, *440*, 512-515.

72 (a) C. Nuckolls, T. J. Katz, L. Castellanos, *J. Am. Chem. Soc.* **1996**, *118*, 3767-3768; (b) C. Nuckolls, T. J. Katz, G. Katz, P. J. Collings, L. Castellanos, *J. Am. Chem. Soc.* **1999**,*121*, 79-88.

73 E. Peeters, M. P. T. Christiaans, R. A. J. Janssen, H. F. M. Schoo, H. P. J. M. Dekkers, E. W. Meijer, *J. Am. Chem. Soc.* **1997**, *119*, 9909-9910.

74 J. M. Fox, T. J. Katz, S. Van Elshocht, T. Verbiest, M. Kauranen, A. Persoons, T. Thongpanchang, T. Krauss, L. Brus, *J. Am. Chem. Soc.* **1999**, *121*, 3453-3459.

75 For some excellent reviews on chiral crystallization, see: (a) A. Collet, M.-J. Brienne, J. Jacques, *Chem. Rev.* **1980**, *80*, 215-230; (b) H. G. Brittain, *Pharm. Res.* **1990**, *7*, 683-690; (c) J. M. McBride, R. L. Carter, *Angew. Chem.* **1991**, *103*, 298-300; *Angew. Chem. Int. Ed.* **1991**, *30*, 293-295; (d) F. Toda, *CrystEngCommun* **2002**, *4*, 215-222; (e) I. Weissbuch, M. Lahav, L. Leiserowitz, *Cryst. Growth Des.* **2003**, *3*, 125-150; (f) T. Matsuura, H. Koshima, *J. Photochem. Photobio. C* **2005**, *6*, 7-24.

76 H. Lorenz, D. Polenske, A. Seidel-Morgenstern, *Chirality* **2006**, *18*, 828-840.

77 (a) F. Toda, K. Tanaka, *J. Org. Chem.* **1988**, *53*, 3607-3609; K. Tanake, T. Odkad, F. Toda, *Angew. Chem.* **1993**, *106,* 1266-1267; *Angew. Chem. Int. Ed.* **1993**, *32*, 1147-1148; (b) F. Toda, K. Yoshizawa, S. Hyoda, S. Toyota, S. Chatziefthimiou, I. M. Mavridis, *Org. Biomol. Chem.* **2004**, *2*, 449-451; K. Yoshizawa, S. Toyota, F. Toda, *Tetrahedron* **2004**, *60*, 7767-7774.

78 (a) R. E. Pincock, R. P. Perkins, A. S. Ma, K. R. Wilson, *Science* **1971**, *174*, 1018-1020; (b) R. B. Kress, E. N. Duesler, M. C. Etter, I. C. Paul, D. Y. Curtin, *J. Am. Chem. Soc.* **1980**, *102*, 7709-7714; (c) D. K. Kondepudi, J. Laudadio, K. Asakura, *J. Am. Chem. Soc.* **1999**, *121*, 1448-1451; (d) K. Asakura, T. Soga, T. Uchida, S. Osanai, D. K. Kondepudi, *Chirality* **2002**, *14*, 85-89; (e) K. Asakura, M. Hayashi, S. Osanai, *Chirality* **2003**, *15*, 238-241.

79 T. B. Norsten, R. McDonald, N. R. Branda, *Chem. Commun.* **1999**, 719-720.

80 F. C. Krebs, A. Faldt, N. Thorup, K. Bechgaard, *CrystEngComm* **1999**, *1*, 21-23.

81 R. Fasel, M. Parschau, K.-H. Ernst, *Nature* **2006**, *439*, 449-452.

82 (a) M. Ortega Lorenzo, C. J. Baddeley, C. Muryn, R. Raval, *Nature* **2000**, *404*, 376-379; (b) J. Crusats, J. Claret, I. Díez-Pérez, Z. El-Hachemi, H. Garcia-Ortega, R. Rubires, F. Sagués, J. M. Ribó, *Chem. Commun.* **2003**, 1588-1589; (c) W. Mamdouh, H. Uji-i, A. Gesquière, S. De Feyter, D. M. Amabilino, M. M. S. Abdel-Mottaleb, J. Veciana, F. C. De Schryver, *Langmuir* **2004**, *20*, 9628-9635; (d) A. Miura, P. Jonkheijm, S. De Feyter, A. P. H. J. Schenning, E. W. Meijer, F. C. De Schryver, *Small* **2005**, *1*, 131-137; for a recent review, see: (e) S. De Feyter, F. C. De Schryver, *Chem. Soc. Rev.* **2003**, *32*, 139-150.

83 Y. Zhu, N. Gergel, N. Majumbar, L. R. Harriot, J. C. Bean, L. Pu, *Org. Lett.* **2006**, *8*, 355-358.

84 (a) J. C. Nelson, J. G. Saven, J. S. Moore, P. G. Wolynes, *Science* **1997**, *277*, 1793-1796; (b) R. B. Prince, J. G. Saven, P. G. Wolynes, J. S. Moore, *J. Am. Chem. Soc.* **1999**, *121*, 3114-3121.

85 (a) M. S. Gin, T. Yokozawa, R. B. Prince, J. S. Moore, *J. Am. Chem. Soc.* **1999**, *121*, 2643-2644; (b) D. J. Hill, J. S. Moore, *Proc. Natl. Acad. Sci. USA* **2002**, *99*, 5053-5057.

86 M. T. Stone, J. M. Fox, J. S. Moore, *Org. Lett.* **2004**, *6*, 3317-3320.

Chapter 2

Structure and Symmetry and Stereochemistry of Bay-Substituted Perylene Bisimides

Abstract: The structural properties of the different bay-substituted perylene bisimides have been discussed based on X-ray crystallographic analysis and molecular modeling studies. The symmetry of perylene bisimides have been deduced from their structural features and the stereochemistry of the conformational enantiomers of bay-substituted perylene bisimides has been defined.

2.1 Introduction

A large number of perylene bisimides (PBIs) bearing different substituents in the imide and the bay positions were reported in literature.[1] The imide positions were mainly used for the introduction of further functionalities such as metal coordination units and dendrons or to promote the solubility of perylene bisimides.[2] It was shown by quantum chemical calculations of the frontier orbitals of unsubstituted PBIs that the electronic properties of the imide substituents possess a negligible effect on the absorption and emission properties of PBIs since their HOMO and LUMO exhibit a knot at the imide nitrogen.[3] This study further revealed, that only the band gap and therefore the spectral position of the absorption and emission maximum remained untouched, whereas the energy of both frontier orbitals increased with increasing electron-donating ability of the imide substituents.[3] This may have an influence on the fluorescence properties of these derivatives, if the orbitals of an electron-donor are located in the same energetical region as the frontier orbitals of PBI.[3] Solid state structures of PBIs bearing different imide substituents demonstrated, that the imide substituents, as attached to both ends of the perylene units, do not affect the structural parameters (bond length, angles) of the perylene core.[1]

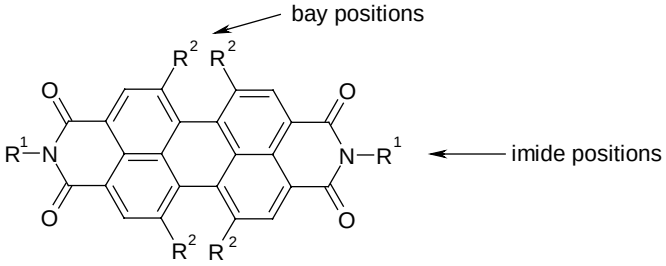

In contrast to the imide positions, the introduction of substituents in the bay positions of the perylene core has significant consequences on the structural and functional properties of perylene bisimides. Substituents such as amines, cyanides, halogens, aryl or aryloxy groups could be attached at the bay positions of perylene bisimides.[1] The influence of the electron-donating or electron-withdrawing substituents on the functional properties of PBIs is apparent from their color in solution which alters from yellow (unsubstituted) to green (diamino-substituted) as well as from the redox potentials as the perylene bisimide core can be tuned from almost an oxidant (diamino-substituted PBIs) to a reductant (for all other derivatives).[1b] Furthermore, the structural properties of PBIs are strongly dependent on the bay-substituents, in particular on their size. The structural properties of PBIs containing different types of bay-substituents are discussed below. The different substitution patterns of perylene bisimides that are frequently reported in literature, and thus considered here for discussion, are shown in Figure 1.

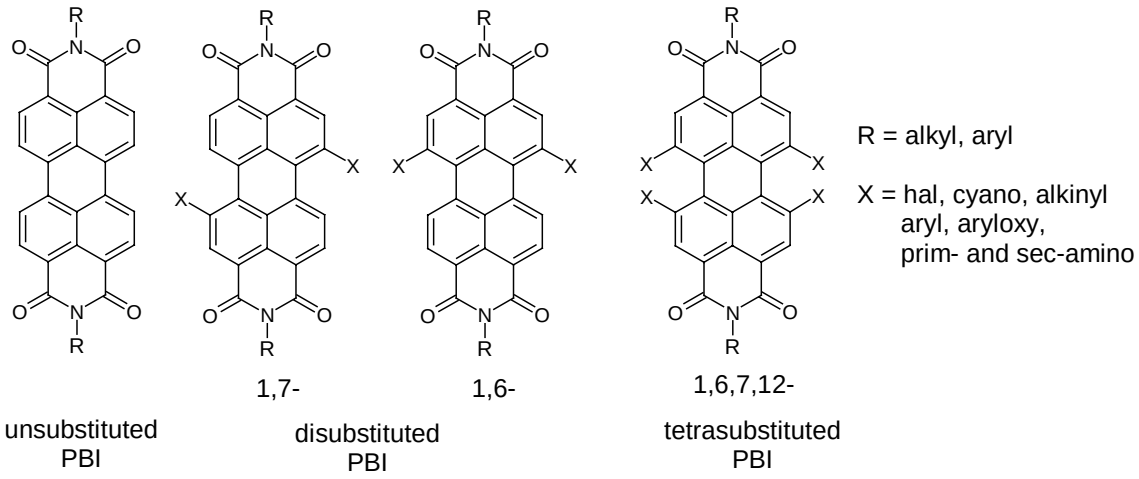

Figure 1. Structures of perylene bisimides with different substitution patterns at the perylene core.

2.2 Structural Properties of Perylene Bisimides

The structural properties of perylene bisimides have been characterized by X-ray crystallographic analysis and molecular modeling investigations. The first X-ray structures of in bay position unsubstituted PBIs were reported by Graser and Hädicke in 1980 and it was shown that unsubstituted PBIs possess, as expected, planar aromatic π-systems.[4] The analysis of the bond lengths (Figure 2) obtained by X-ray diffraction of the unsubstituted PBI revealed that the central perylene unit is composed of two individual naphthalene units, each bearing an imide functionality, which are connected to each other by two C(sp^2)-C(sp^2) single bonds (1.46 Å) in the respective peri-positions (the name perylene is derived from the connectivities).[5]

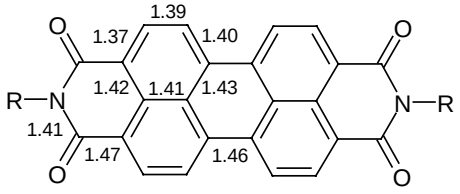

Figure 2. Bond lengths of unsubstituted perylene bisimides in crystals. The bond lengths shown here are the average values obtained from molecular structures of three derivatives with varying imide substituents.[4,5]

X-ray diffraction analysis of different bay-substituted perylene bisimide dyes[6] revealed that the introduction of substituents in the bay area leads to a twist of the two naphthalene units of the former planar perylene core along the connectivities of these two units as shown in Figure 3 for a tetraphenoxy-substituted PBI. This distortion is related to the sterical constrainments of the substituents and can, therefore, be explained by repulsive interactions of the substituents in the bay area. The extent of the

distortion present in bay-substituted PBIs is quantitatively described by the twist angle θ (see Figure 3) between the two naphthalene units. This angle is accessible from X-ray crystallographic data by defining the planes for both naphthalene units and estimating the angle between these planes. An easier and more convenient access to the twist angle θ is given by the twist of the central six-membered ring of the perylene core which can be obtained from the dihedral angles θ (C6-C6´-C7´-C7) and θ (C1-C1´-C12´-C12) (for numbering, see Figure 3, left). The dihedral angles are experimentally available from X-ray analysis and can be calculated by quantum chemistry or molecular modeling. The twist angles θ for different bay-substituted PBIs are summarized in Table 1.

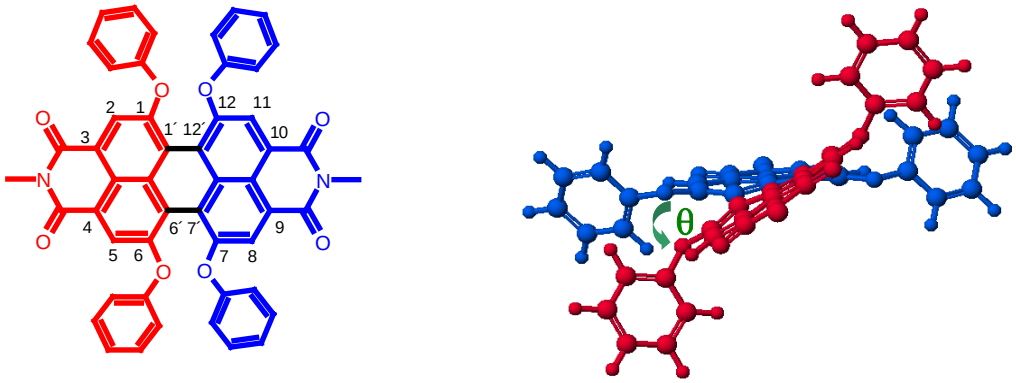

Figure 3. Structure of *N,N'*-dimethyl-1,6,7,12-tetraphenoxyperylene-3,4:9,10-tetracarboxylic acid bisimides (left) and view along the *N,N*-axis of a AM1-optimized geometry of this PBI. The two naphthalene units of the perylene core are highlighted in red and blue.

The twist angles θ determined by X-ray analysis vary from 4° for a 1,7-difluorosubstituted PBI up to 37° for a 1,6,7,12-tetrachloro derivative (Table 1). The twist of tetraphenoxy-substituted PBI (X,Y = OPh) was determined for the first time by X-ray analysis of a structurally related tetraphenoxy-substituted diazadibenzoperylene to 25°.[6a] For other derivatives, whose X-ray crystallographic data are not available, the twist angle were estimated by molecular modeling investigations.[7] The reliability of the twist angles obtained by molecular modeling studies is confirmed by the excellent agreement of the twist angles θ with those obtained from X-ray data (Table 1). The comparison of the values for different bay-substituted PBI derivatives (Table 1) revealed that the degree of the distortion is dependent on the number and size of the substituents in the bay positions. For example, the torsion of 1,7-diphenoxy-substituted perylene bisimides (X = H, Y = OPh) amounts to 15°, whereas a twist angle of 27° is estimated for the 1,6,7,12-tetraphenoxysubstituted PBI (X,Y = OPh). The effect of bay-substituents

on the torsion of perylene bisimides is discussed in more detail in Chapter 6 of this thesis. It is noteworthy that in the crystal structures of core-twisted PBIs, the dihedral angles of the two bay areas are often not identical due to a symmetry breaking effect imparted by the packing of these dyes in the solid state.[1d,6e]

Table 1. Twist Angle θ of the Perylene Core for Different Bay-Substituted Perylene Bisimides obtained from X-Ray Crystallographic Data[4-6] and Semiempirical AM1 calculations.[7]

Substituents	θ (X-ray)	θ (AM1)
X,Y =H	0[4,5]	0
X = H, Y = F	4[6g]	5
X=H, Y = CN	5[6b]	7
X = H, Y = NOctyl	-	15[7b]
X = H, Y = OPh	-	15
X, Y = F	18/28[6g]	22
X = H, Y = Ph	-	22
X = H, Y = Pyr	-	24[7c]
X = H, Y = Br	24[6d,f]	25
X, Y = OPh[a)]	25[6a]	27
X, Y = Cl	35/37[6c,e]	36
X, Y =Br	-	36
X, Y = Ph	-	37

a) determined for 1,6,7,12-tetraphenoxy-substituted diazadibenzoperylene derivative[6a]

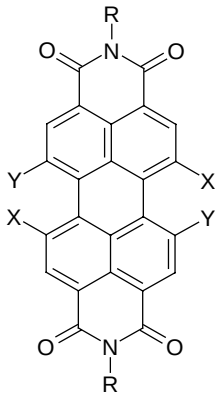

2.3 Symmetry of Perylene Bisimides

In bay area unsubstituted perylene bisimides possess a planar aromatic core as confirmed by single crystal X-ray diffraction.[4,5] The planar unsubstituted perylene bisimides comprise three orthogonal mirror planes as exemplified shown in Figure 4 for unsubstituted perylene bisimide, thus, these molecules are highly symmetrical. It has to be noted, that this symmetry consideration is only valid for the parent unsubstituted perylene bisimide, as the imide substituents can impose symmetry breaking.[8] In addition to the three mirror planes, three orthogonal C_2 axes as the intersection lines of each two mirror planes as well as an inversion center at the intersection of all three mirror planes are given for unsubstituted perylene bisimides. Therefore, unsubstituted

perylene bisimides belong to the symmetry group $\mathbf{D_{2h}}$ and due to the presence of mirror planes in unsubstituted perylene bisimides these molecules are not chiral.

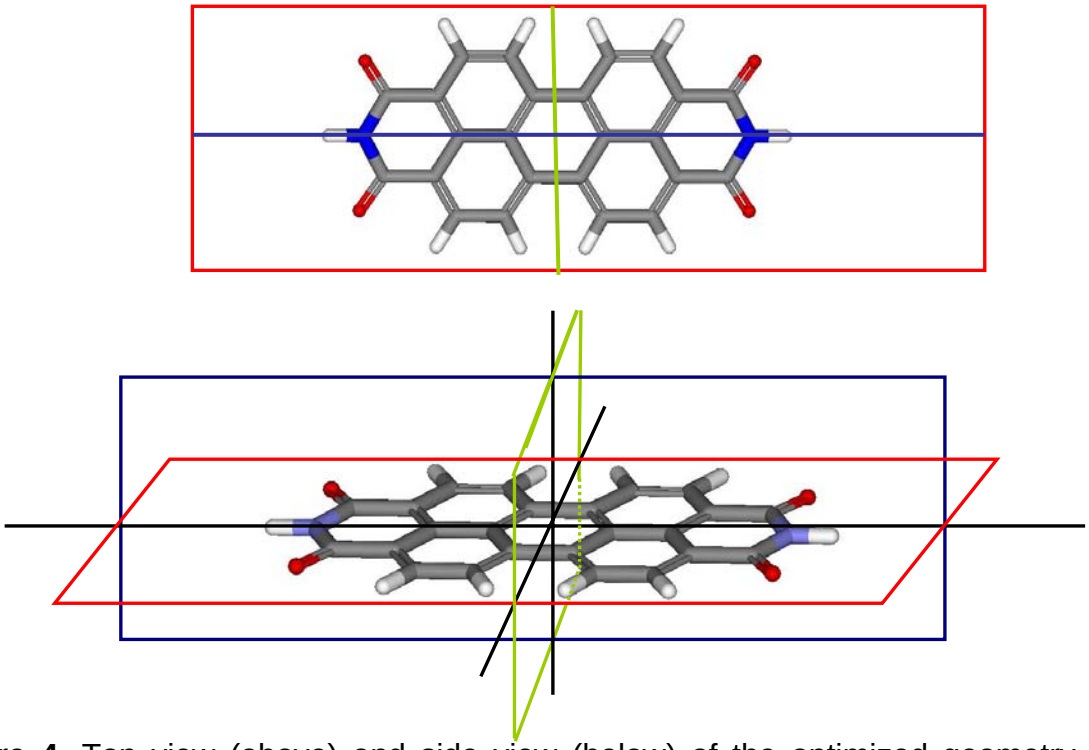

Figure 4. Top view (above) and side view (below) of the optimized geometry of the perylene-3,4:9,10-tetracarboxylic acid bisimide. The red, green and blue rectangles represent the three mirror planes. Note that the inversion center is present at the intersection of the three mirror planes and three C_2 axes are given by the intersection line of each two mirror planes (black lines, below). The structure was optimized by semi-empirical AM1 method using CaChe Quantum CaChe Workspace 5.0.

By considering the two-dimensional projection of 1,6,7,12-tetra bay-substituted perylene bisimide (Figure 1), the same symmetry might be expected for this bay-substituted PBI as for the unsubstituted one. But the twisted nature of the perylene core, as outlined before, leads to symmetry breaking in tetra-substituted PBIs and, therefore to a reduction of the symmetry. The optimized geometry of tetrachloro-substituted PBI depicted in Figure 5 revealed that the mirror planes are lost due to the twisted nature of the perylene core and only the intersection lines of the mirror planes remain as three orthogonal C_2 axes. These axes are the only symmetry elements of tetra bay-substituted PBIs, therefore, they belong to the symmetry group $\mathbf{D_2}$. Due to the absence of mirror plane, inversion center and rotatory reflection axis, bay area tetra-substituted PBIs are inherently chiral.

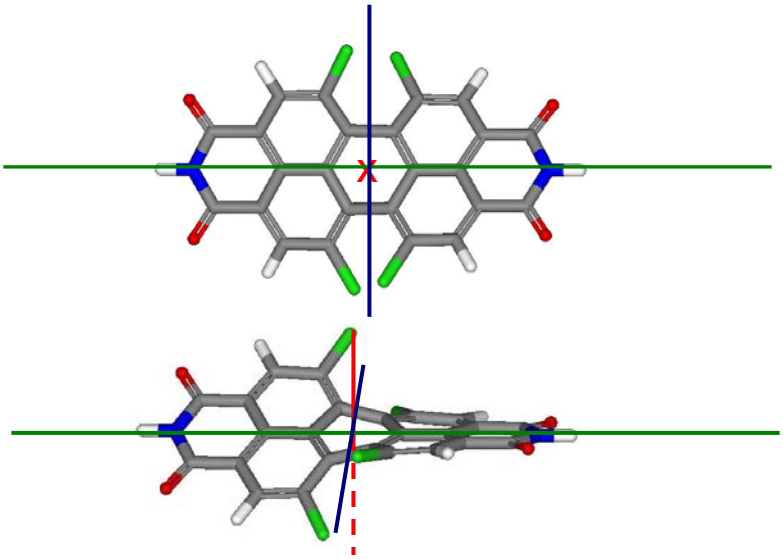

Figure 5. Top view (above) and side view (below) of the optimized geometry of 1,6,7,12-tetrachloroperylene-3,4:9,10-tetracarboxylic acid bisimide ((*M)*-isomer) and its symmetry elements. The three orthogonal C_2 axes are shown as colored lines (in top view, the red axis is represented by a cross). The geometry was optimized by semi-empirical AM1 method using CaChe quantum CaChe Workspace 5.0.

For 1,6- and 1,7-disubstituted perylene bisimides, a further reduction of the symmetry is given owing to the substitution pattern in the bay area. As can be seen from Figure 6, for 1,7-difluorosubstituted perylene bisimide, one C_2 axis remains as the only symmetry element, thus the 1,7-disubstituted PBIs belong to the point group $\mathbf{C_2}$. The C_2 axis of these PBI derivatives is oriented perpendicular to the perylene core (Figure 6). The corresponding 1,6-substituted derivatives possess the same symmetry, except the C_2 axis is oriented along the *N,N*-axis of the perylene bisimide (not shown).

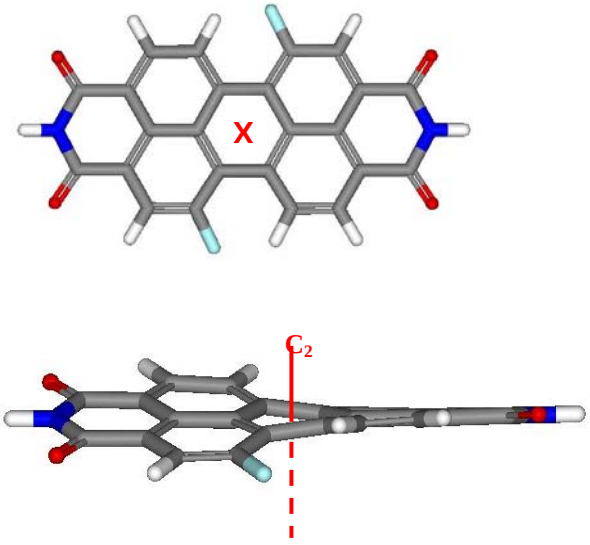

Figure 6. Top view (above) and side view (below) of the optimized geometry of 1,7-difluoroperylene-3,4:9,10-tetracarboxylic acid bisimide ((*M*)-isomer) and its symmetry. The C_2 axis, which is oriented perpendicular to the perylene core, is represented by a

cross (above) and a line (below) in red. The structure was optimized by semi-empirical AM1 method using CaChe quantum CaChe Workspace 5.0.

The remaining bay-substituted perylene bisimides, namely the mono- and 1,6,7-trisubstituted PBIs, do not possess any symmetry element owing to the unsymmetric substitution pattern in the bay area, and thus, they belong to point group $\mathbf{C_1}$ and are chiral as well.

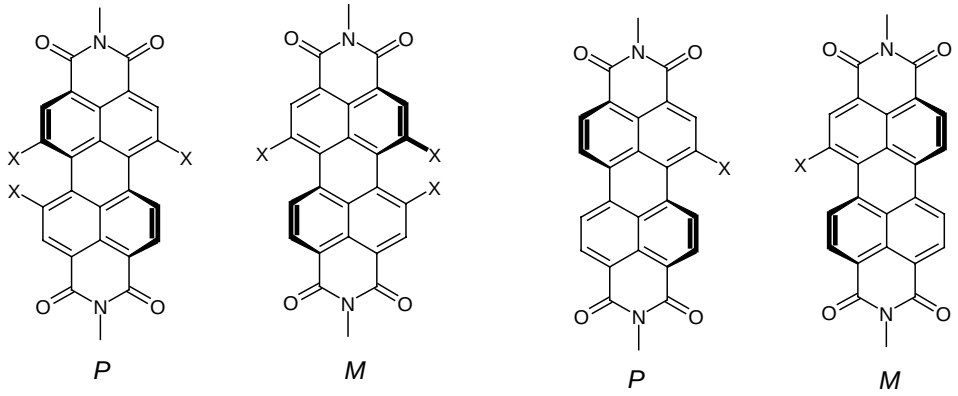

Figure 7. Structures and possible enantiomers for tri-substituted (left) and mono-substituted (right) perylene bisimides.

2.4 Definition of the Stereochemistry of Perylene Bisimides

In the previous section, it was demonstrated by symmetry consideration that all bay-substituted perylene bisimides are in principle chiral. In order to classify the enantiomers arising from the twisted nature of the perylene core, the chirality elements need to be defined. By considering the structure of bay-substituted PBIs, the two peri-bonds connecting the naphthalene units can be thought as chiral axes. Thus, perylene bisimides are axial chiral and the presence of two chiral axes would lead to atropo-diastereomers. But as the configuration of one axis is dependent on that of the other, it is justified to denote the conformers of a core-twisted perylene bisimide as atropo-enantiomers. The view along the *N*,*N*-axis of the perylene bisimide (Figure 8) reveals a helical twist of the two naphthalene units, therefore the core-twisted PBIs can also be considered as helically chiral, the latter is a special case of axial chirality. The definition and nomenclature of the respective enantiomers is similar for both axial and helical chirality and therefore, the enantiomers of the perylene bisimides are designated as (*P*)- and (*M*)-enantiomer.[9]

The two possible enantiomers, *P* and *M,* of bay-substituted perylene bisimides are shown in Figure 8. In the view along the *N,N*-axis of the perylene bisimide, the enantiomers are defined as follows:

If the naphthalene unit in the front (highlighted in red, Figure 8) has to be twisted in a clockwise sense to coincide with the naphthalene unit in the back (labeled in blue), this molecule is called (*P*)-enantiomer (left structure).

The (*M*)-enantiomer is defined as the conformer, in which the naphthalene unit in the front (red) has to be rotated in a counter clockwise sense to coincide with the naphthalene unit in the back (blue) (right structure).

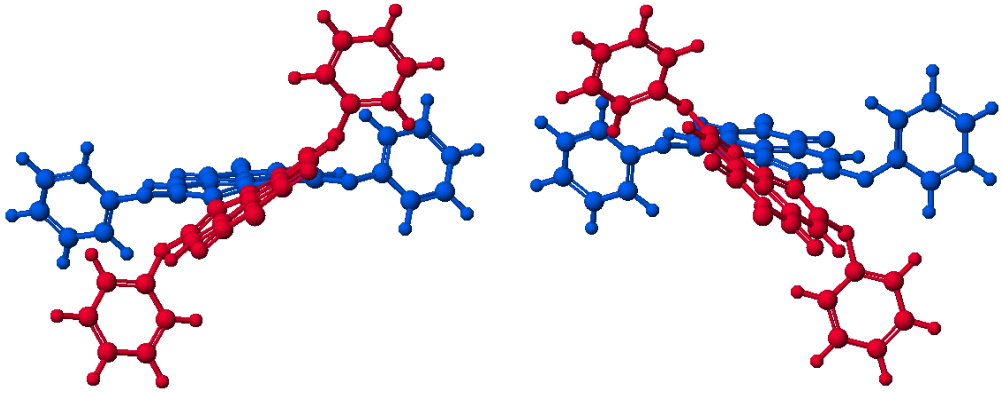

Figure 8. View along the *N,N*-axis of the (*P*)- (left) and (*M*)-enantiomer (right) of a tetraphenoxy-substituted PBI. The naphthalene unit in front is highlighted in red and the back one in blue. Structures were optimized by semi-empirical AM1 method using CaChe quantum CaChe Workspace 5.0.

Although bay-substituted perylene bisimides are inherently chiral, there were no reports on atropo-enantiopure PBIs. Nevertheless, the enantiomers of perylene bisimides were observed in the solid state, but only as racemic mixture.[6] The reason for this may be that the two enantiomers are in a dynamic equilibrium as demonstrated by temperature-dependent NMR spectroscopy of a tetraaryloxy-substituted derivative (Scheme 1).[10] The free enthalpy of activation for this PBI derivative was determined to 60 kJ/mol at 270 K revealing a rather fast interconversion of (*P*)- and (*M*)-enantiomers. For 1,6,7,12-tetrachlorosubstituted PBIs, the free enthalpy of activation was estimated to be larger than 87 kJ/mol demonstrating that not only the twist angle θ, but also the activation parameter of the racemisation process seem to be dependent on the size of the substituents.[9] The influence of the size of the bay-substituents on the activation parameter further suggests a planar structure for the transition state of this equilibrium. The effect of substituents on the activation parameter is discussed in detail in Chapter 6 of this thesis. Due to the equilibrium between the two core-twisted enantiomers, bay-substituted PBIs are conformational chiral (Chapter 1). Thus, it is apparent that conformationally stable chiral perylene bisimides can only be obtained if the

interconversion between the enantiomers can be effectively hindered by the concepts outlined in Chapter 1.

Scheme 1. Equilibrium between (*P*)- and (*M*)-Enantiomer of Tetraaryloxy-Substituted PBI.[9]

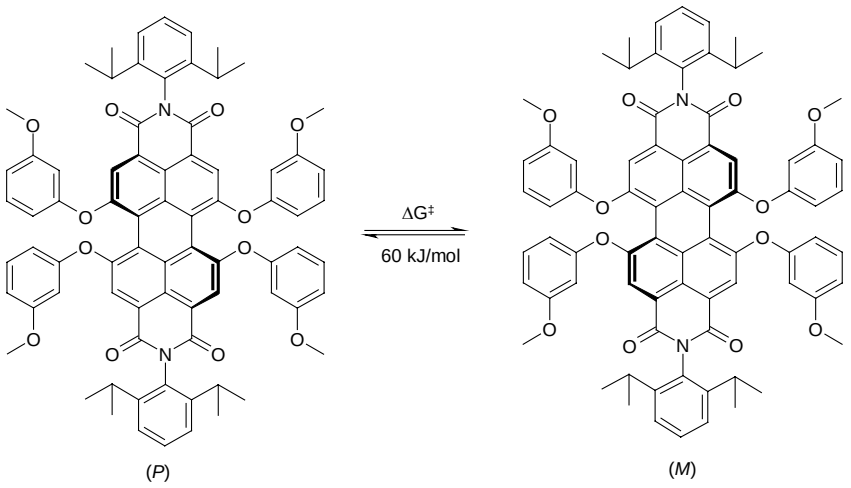

2.5 Conclusion

The characteristic structural feature, i.e. a twisted perylene core, of bay-substituted perylene bisimides was demonstrated by X-ray analysis (literature data) and by molecular modeling. The experimental values for the twist angles θ of bay-substituted PBIs determined by X-ray analysis are in excellent agreement with those estimated by AM1 calculations. A strong dependence of the twist angle of the perylene core on the size of the bay-substituents could be shown. Symmetry consideration revealed that the twisted nature of the perylene core imparts chirality to bay-substituted perylene bisimides. These PBIs are conformational chiral and the atropo-enantiomers undergo rapid interconversion at room or elevated temperatures which prohibited the isolation of enantiopure compounds so far.

2.6 References and Notes

1 For reviews on perylene bisimides see: (a) H. Langhals, *Heterocycles* **1995**, *40*, 477-500; (b) F. Würthner, *Chem. Commun.* **2004**, 1564-1579; (c) A. C. Grimsdale, K. M. Müllen, *Angew. Chem.* **2005**, *117*, 5732-5772; *Angew. Chem. Int. Ed.* **2005**, *44*, 5592-5629; (d) F. Würthner, *Pure Appl. Chem.* **2006**, *78*, 2341-2350; (e) M. R. Wasielewski, *J. Org. Chem.* **2006**, *71*, 5051-5066.

2 (a) F. Würthner, A. Sautter, D. Schmidt, P. J. A. Weber, *Chem. Eur. J.* **2001**, *7*, 894-902; (b) A. Herrmann, T. Weil, V. Sinigersky, U.-W. Wiesler, T. Vosch, J.

Hofkens, F. C. De Schryver, K. Müllen, *Chem. Eur. J.* **2001**, *7*, 4844-4853; (c) R. Dobrawa, F. Würthner, *Macromolecules* **2005**, *38*, 1315-1325; (d) Z. Chen, U. Baumeister, C. Tschierske, F. Würthner, *Chem. Eur. J.*, **2007**, *13*, 450-465.

3 F. Pichierri, *J. Mol. Struct.* **2004**, *686*, 57-63.

4 F. Graser, E. Hädicke, *Liebigs Ann. Chem.* **1980**, 1994-2011.

5 (a) K. Hino, J. Mizuguchi, *Acta Cryst., Section E* **2005**, *61*, o672-o674; (b) J. Mizuguchi, K. Hino, K. Sato, H. Takahashi, S. Suzuki, *Acta Cryst., Section E* **2005**, *61*, o437-o439.

6 (a) F. Würthner, A. Sautter, C. Thalacker, *Angew. Chem.* **2001**, *113*, 4557-4560; *Angew. Chem. Int. Ed.* **2001**, *40*, 4425-4428; (b) B. A. Jones, M. J. Ahrens, M-H. Yoon, A. Fachetti, T. J. Marks, M. R. Wasielewski, *Angew. Chem.* **2004**, *116*, 6523-6526; *Angew. Chem. Int. Ed.* **2004**, *43*, 6363-6366; (c) Z. Chen, M. G. Debije, T. Debaerdemaeker, P. Osswald, F. Würthner, *ChemPhysChem* **2004**, *5*, 137-140; (d) F. Würthner, V. Stepanenko, Z. Chen, C. R. Saha-Möller, N. Kocher, D. Stalke, *J. Org. Chem.* **2004**, *69*, 7933-7939; (e) S. Leroy-Lhez, J. Baffreau, L. Perrin, E. Levillain, P. Hudhomme, *J. Org. Chem.* **2005**, *70*, 6313-6320; (f) C.-C. Chao, M.-k. Leung, Y. O. Su, K.-Y. Chiu, T.-H. Lin, S.-J. Shieh, S.-C. Lin, *J. Org. Chem.* **2005**, *70*, 4323-4331; (g) F. Würthner, P. Osswald, R. Schmidt, T. E. Kaiser, H. Mansikkamaeki, M. Könemann, *Org. Lett.* **2006**, *8*, 3765-3768.

7 For the purpose of comparability, the structures of the PBIs were optimized by the same method (AM 1) and for all PBI derivatives the same imide substituents (cyclohexyl) was used. These values correspond very well to those obtained by applying other quantum chemical methods: (a) J. Hofkens, T. Vosch, M. Maus, F. Köhn, M. Cotlet, T. Weil, A. Herrmann, K. Müllen, F. C. De Schryver, *Chem. Phys. Lett.* **2001**, *333*, 255–263.

For two PBI derivatives (X = H, Y = NH-Octyl and X = H, Y = Pyr), the twist angle was taken from literature: (b) A. S. Lukas, Y. Zhao, S. E. Scott, M. R. Wasielewksi, *J. Phys. Chem. B.* **2002**, *106*, 1299-1306; (c) M. J. Ahrens, M. J. Tauber, M. R. Wasielewski, *J. Org. Chem.* **2006**, *71*, 2107-2114;

8 C. F. Degenhardt III, D. B. Shortell, R. D. Adams, K. D. Shimizu, *Chem. Commun.* **2000**, 929-930.

9 G. Helmchen, *Methods Org. Chem.* (Houben-Weyl), Vol. 21a (Eds. G. Helmchen, R. W. Hoffmann, J. Mulzer, E. Schaumann), Thieme, New York, **1995**, pp.17-21.

10 S. Hien, PhD thesis, University of Regensburg (Germany), **1995**.

Chapter 3

Macrocyclic Perylene Bisimides: Effective Probes for the Assessment of Conformational Effects on the Optical Properties

Abstract: Two regioisomeric macrocycles based on 1,6,7,12-tetraaryloxy-substituted perylene bisimides (APBI) – the diagonally and laterally bridged isomers – have been synthesized for four different chain lengths by a simple one-pot macrocyclization reaction. The different orientations of the aryloxy residues, i.e. horizontal or perpendicular to the perylene core, in the regioisomeric macrocycles have been elucidated by NMR spectroscopy and X-ray analysis and the dynamic properties of the laterally bridged regioisomers have been investigated by temperature-dependent NMR spectroscopy. The influence of the different orientations of the aryloxy residues on the electrochemical properties is demonstrated by cyclic voltammetry which reveals that a perpendicular orientation of the aryloxy residues relative to the perylene core effects an increase of the first reduction potential of the perylene bisimide electrophore. The optical properties of the regioisomeric macrocycles have been determined by UV/Vis and fluorescence spectroscopy. It has been shown that the diagonally bridged macrocycles exhibit optical properties that differ significantly from those of an open-chain reference compound, whereas those of the laterally bridged isomers are identical. This demonstrates that the perpendicular conformation, in contrast to the horizontal one, of the aryloxy residues do not contribute to the optical properties of conformationally unrestricted APBIs in solution. Solvent-dependent fluorescent properties have been exemplified for one diagonally bridged derivative, suggesting an photoinduced electron transfer process as fluorescence quenching mechanism for APBIs. This has been further confirmed by the solvent-dependent fluorescent properties of three different APBI derivatives. Based on these results, a concept for the synthesis of APBIs with high fluorescence quantum yields in polar solvents is suggested.

3.1 Introduction

The synthesis of perylene bisimides bearing four aryloxy substituents in the bay positions (1,6,7,12 positions) was described for the first time in 1987 by BASF scientists and these dyes were initially applied as an industrial colorant in devices such as foils for solar light concentration and for plant growth application in polymeric hosts.[1] Owing to their outstanding optical and electrochemical properties as well as their stability against environmental influences,[2] tetraaryloxy-substituted perylene bisimides (APBIs) have been further used as laser dyes and as chromophores for single molecule spectroscopy.[3] The semiconducting properties of APBIs have enabled applications of these dyes as red chromophores for organic and polymeric light-emitting devices (OLEDs and PLEDs), in solar cell devices and in organic field effect transistors (OFETs).[4] The ability of introducing functional groups at two orthogonal positions (imide and bay positions) has enabled the synthesis of highly functional derivatives and the construction of complex architectures such as rotaxanes,[5] metallosupramolecular squares,[6] rectangles[7] and polymers[8] by self-assembly of APBIs, whilst the introduction of hydrogen-bonding motifs has been utilized for the design of fluorescent organogels[9] based on APBIs. Multichromophore arrays have been designed by combining APBIs either with other perylene bisimide derivatives[10] or other chromophores,[11] in particular, oligo(phenylenevinylene)s,[12] porphyrins,[13] pyrene[14] and fullerenes.[15] In such multichromphore systems efficient energy and electron transfer processes were demonstrated, thus they may serve as artificial light-harvesting systems and show good prospects for application in solar cell devices. Water-soluble APBIs are accessible which exhibit high fluorescent quantum yields in aqueous solution and can be used for cell staining experiments and the investigation of their interaction with DNA.[16] Furthermore, APBIs were used as fluorescence sensors for fluoride anions.[17]

Despite this remarkable versatility of aryloxy-substituted perylene bisimides, the effect of different conformations on the optical properties of this important class of fluorophores has been barely explored. Single-molecule spectroscopic studies revealed that different conformations that originate from the twist of the perylene bisimide chromophore and the orientation of the aryloxy groups have an effect on the photophysical properties of *immobilized* APBIs.[18] It was shown in the solid state structure of a phenoxy-substituted diazadibenzoperylene that the aryloxy units are oriented in the plane of the perylene bisimide unit,[19] whereas quantum chemical calculations suggested another conformation where the aryloxy units are orientated perpendicular to the perylene core.[18] But also other conformations of the aryloxy

residues seem to be easily available within a small energy range.[2c,18] Different conformations of the aryloxy residues might have a significant influence on the optical and electrical properties of these dyes by both inductive and mesomeric effects as it has recently been reported that especially the optical properties of perylene bisimides are sensitive to the type of bay substituent.[2a,10a,20]

To elucidate the conformational effect on the optical properties of APBI chromophores, conformationally restricted macrocyclic systems which are diagonally bridged through 1,7- and 6,12-linkage (Chart 1, A) or laterally bridged through 1,12-

Chart 1. Schematic Representation of Diagonally (A) and Laterally Bridged (B) Macrocyclic Perylene Bisimides.

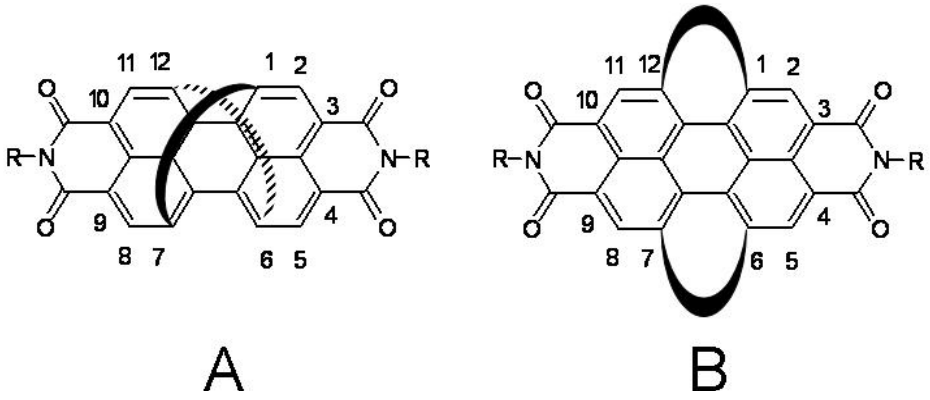

and 6,7-linkage seem to be properly suited since the conformational freedom of the perylene core should be restricted in these systems and a particular conformation of the aryloxy substituents can be achieved through variation of the length of the bridging unit. Furthermore, in diagonally bridged macrocycles an interconversion of the twisted conformers ((*P*)- and (*M*)-enantiomer) is not possible without a bond cleavage. Oligoethylene glycol units were chosen as the bridging unit because, on the one hand, this functionality can be introduced in perylene bisimide by etherification of the resorcin groups in the bay position and, on the other hand, the chain length can be varied through appropriate choice of ditosylates. Here, the synthesis of diagonally bridged macrocyclic perylene bisimides **5a-d** as well as the corresponding laterally bridged isomers **6a-d** are presented and their optical and electrochemical properties are reported in comparison to those of the open-chain reference compound **4**.[21] These studies reveal the conformational effect of aryloxy bay substituents on the optical properties of perylene bisimides. Additionally, the dynamic properties of laterally bridged macrocycles **6a-d** have been investigated to gain a deeper inside into the conformational properties of APBIs.

3.2 Synthesis of Macrocyclic Perylene Bisimides

The synthesis of the macrocyclic perylene bisimides **5a-d** and **6a-d** is outlined in Scheme 1. The perylene bisimides **1-4** were reported in literature.[22]

Scheme 1. Synthesis of Macrocyclic Perylene Bisimides.

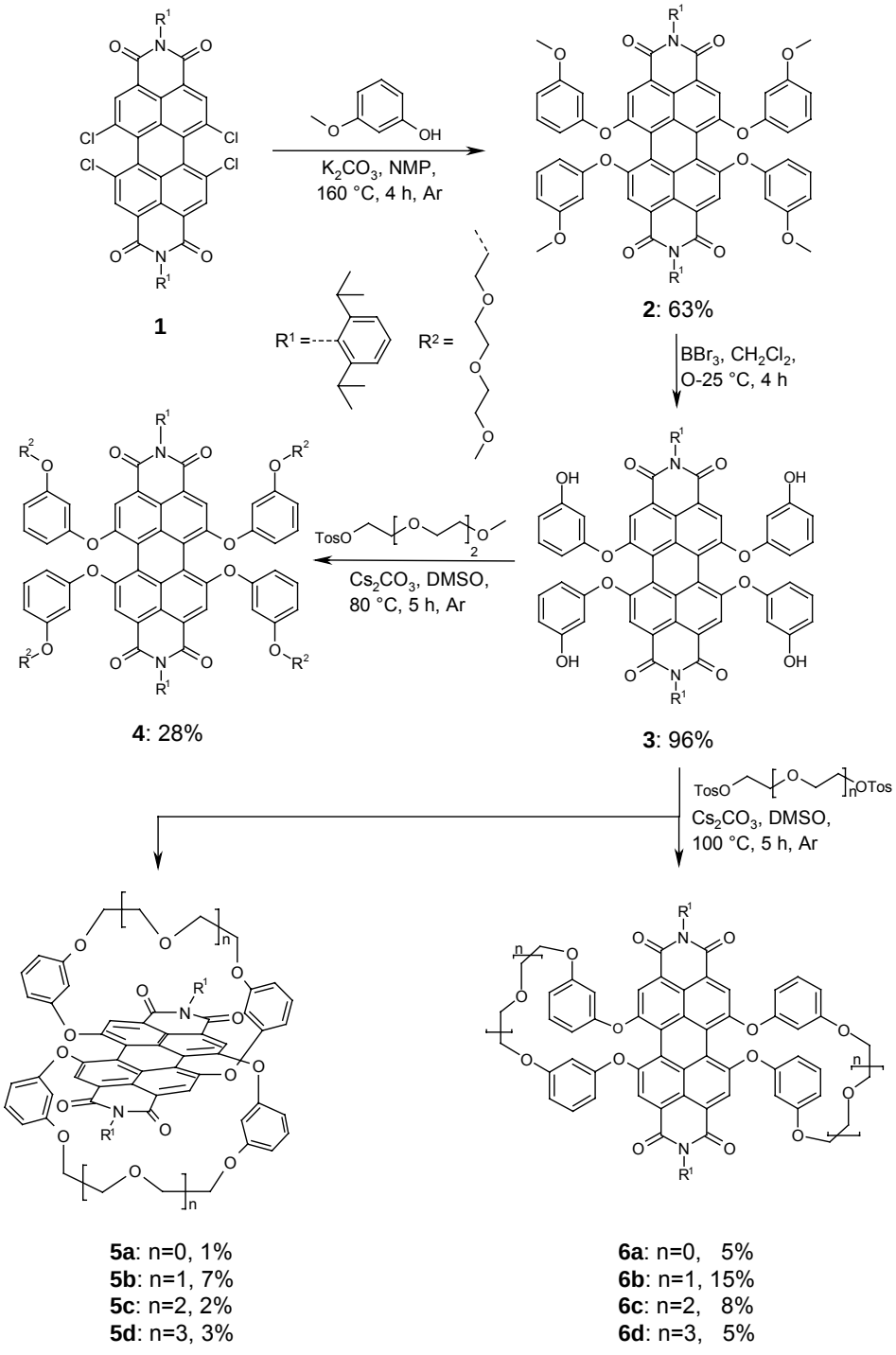

The macrocyclic perylene bisimides **5a-d** and **6a-d** were obtained from perylene bisimide **3** by Williamson´s ether synthesis, a reaction which is frequently applied for the synthesis of macrocyclic compounds.[23] For this purpose, a 10^{-3} M solution of **3** in DMSO was treated at 100 °C with the respective oligoethylene glycol ditosylates and cesium carbonate, the latter being known to facilitate the formation of macrocycles.[24]

After purification by column chromatography the diagonally bridged macrocyclic perylene bisimides **5a-d** were isolated in 1-7% yield and additionally the laterally bridged isomers **6a-d** (Chart 1) were obtained for each chain length in 5-15% yield. The overall yield of macrocyclic compounds obtained upon cyclization with diethylene glycol ditosylate (sum of isomers **5b** and **6b**) is 22% which is about 79% of the yield obtained for the open-chained compound **4** (28%) synthesized under similar conditions. This reveals an effective formation of the macrocycles, although the isolated yield of each individual macrocycle was only moderate. A significantly higher yield was obtained for the laterally bridged isomers compared with those of the diagonally bridged isomers with identical chain length. As the formation of diagonally bridged (**5a-d**) and laterally bridged macrocycles (**6a-d**) occurs from different conformations of the aryloxy residues (perpendicular conformation for **5a-d** and horizontal conformation for **6a-d**, see below) in the precursor **3**, the observed difference in yields of isomers **5a-d** and **6a-d** can be attributed to the different free energies of the respective conformations in solution. Thus, the differing yields for regioisomeric macrocycles with identical chain length suggest that the conformations of the aryloxy residues necessary for the formation of the lateral isomer **6a-d** are of lower energy in solution than those required for the diagonally bridged isomer **5a-d**. Furthermore, the isolated yields are dependent on the chain length of the bridging unit and, in turn, on the size of the macrocycle. The diethylene glycol derivatives **5b** and **6b** display the highest yields in each series of isomeric macrocycles. The lower yields of the monoethylene glycol derivatives **5a** and **6a** can be explained by an increased strain present in these macrocycles, whereas the yields of all other derivatives are determined by the entropy of the transition state of the cyclization reaction which is unfavorable with increasing chain length.[25]

All attempts to resolve the atropo-enantiomers (*P* and *M*) of **5a-d** by chiral HPLC failed. The macrocyclic perylene bisimides **5a-d**, **6a-d** were characterized by ^{1}H NMR spectroscopy and mass spectrometry and two derivatives (**5b** and **6a**) were characterized by X-ray crystallography.[21]

3.3 Structural Properties of Macrocyclic Perylene Bisimide.

The presence of four resorcin units in the precursor bisimide **3** may cause formation of numerous isomeric bis(macrocycles) by etherification whose structures are shown in Figure 1. Only based on spectroscopic data, in particular ^{1}H NMR, reliable assignment of the isolated macrocycles to a particular isomer is not possible. Therefore, crystallization of the macrocycles was carried out and single crystals suitable for X-ray

diffraction[&] were obtained in the case of **5b** and **6a** by dissolving the compounds in dichloromethane, subsequent addition of equal amounts of methanol and slow evaporation of dichloromethane at room temperature.

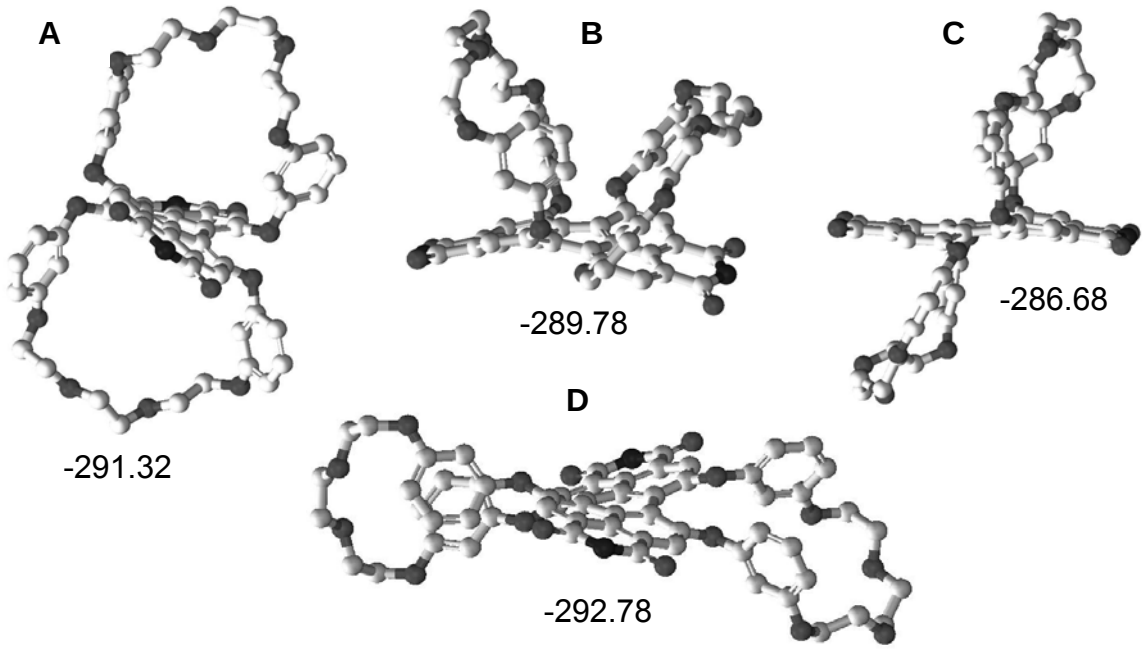

Figure 1. Structures of possible isomeric bis(macrocycles). The structures of the diagonally bridged isomer (A), the two possible straight bridged isomers (B, C; 1,6- and 7,12-linkage) and the laterally bridged isomer (D) were calculated for triethylene glycol as bridging unit and were optimized by the semi-empirical AM1 method (CaChe Quantum CaChe Workspace 5.0). The heats of formation in kcal/mol obtained by AM1 calculations are given below the corresponding structure. Hydrogen atoms and the 2,6-diisopropylphenyl imide substituents were omitted for clarity.

Figure 2 shows the molecular structure of **5b** in the solid state.[26] Compound **5b** possesses a macrocyclic structure with the bridging units lying above and below the perylene core conforming the diagonally bridged structure suggested in Figure 1A. A further characteristic feature for this diagonally bridged isomer is an almost perpendicular orientation of the aryloxy substituents relative to the perylene core which resembles a conformation suggested based on molecular modeling studies of related noncyclic compounds.[18] For the macrocyclic systems **5** an interconversion between the conformational enantiomers ($M \rightleftarrows P$) as observed for non restricted perylene bisimides, is not possible because in the case of **5a-d** a bond cleavage is required for

[&] X-ray measurements and structure determination was performed by Dr. D. Leusser, University of Würzburg, Institute of Inorganic Chemistry.

such interconversion. Therefore, diagonally bridged macrocycles **5a-d** possess favorable structural features to explore the conformational effect of bay aryloxy substituents on the optical and electrochemical properties of this class of chromophores. The twist angle between the two naphthalene units of the perylene core of **5b** was determined to 33° and is thus higher than that known for phenoxy substituted diazadibenzoperylene,[19] which underlines the rigid character of isomers **5a-d**. The size of the cavity formed by the perylene core and the ethylene glycol bridge was determined to 5.9 Å x 6.1 Å for **5b**.

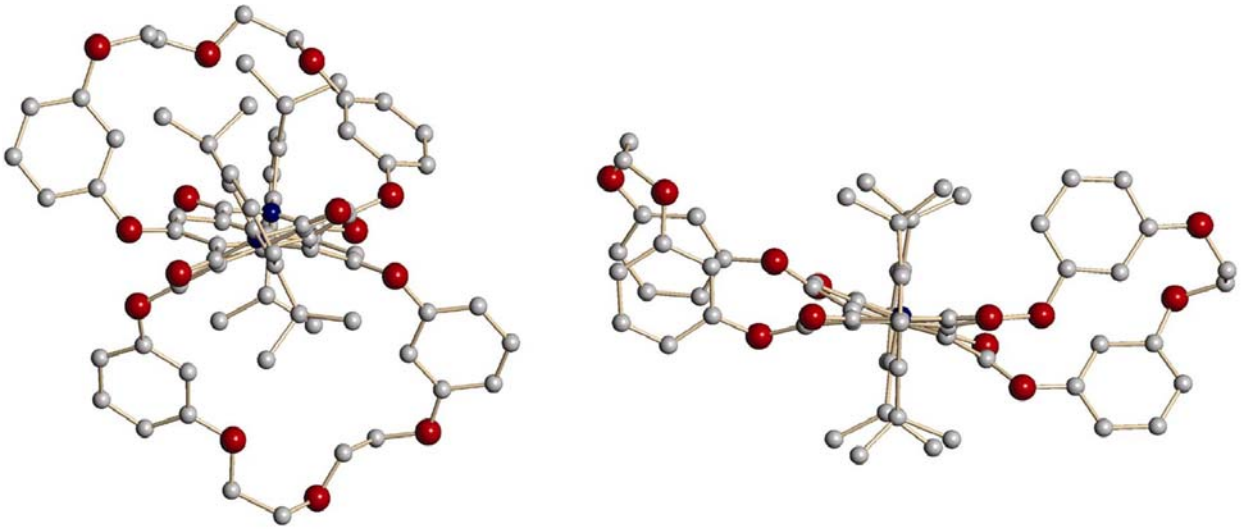

Figure 2. Molecular structure of **5b** (left, (*P*)-enantiomer) and **6a** (right, (*P*)-enantiomer). View along the *N,N*-axis of the perylene bisimide showing the twisted nature and the cyclic structure of both macrocycles. Note that in both crystals (*P*)- and (*M*)-enantiomers are present in equal amounts. Hydrogen atoms as well as co-crystallized solvent molecules were omitted for clarity.

The packing in the solid state of **5b** is shown in Figure 3. The crystals obtained for **5b** belong to the triclinic space group $P\bar{1}$ containing two molecules in the unit cell in a centrosymmetric way, thus a (*M*)- and a (*P*)-enantiomer are present. The two enantiomers are arranged in the crystal in layers of each enantiomer along the b axis of the unit cell (Figure 3). Due to the isolation of the π-systems through the macrocyclic linkages, the closest distance between the perylene π-system of two molecules found in the solid state was 7.3 Å.

The molecular structure of **6a** in the crystal reveals that the two neighboring aryloxy groups are connected and confirms the laterally bridged structure (Figure 2) that has been suggested in Figure 1D. The position of the aryloxy residues changes in comparison to **5b** to a more horizontal orientation relative to the perylene core. For the

laterally bridged isomers, an interconversion of the enantiomers is in principle possible and the barrier of activation for this process should be dependent on the chain length of bridge. Similarly as observed for other perylene bisimides,[27] the two bay areas of the perylene bisimide are no more symmetrical as the aryloxy residues possess slightly different conformational features. The twist angle between the two naphthalene units was determined to 25° being in good agreement with known values.[19] Thus, the laterally bridged isomers **6a-d** comprise an alternate position of the aryloxy residues in comparison to **5b** and therefore the two isomers can be used to determine the influence of the aryloxy substituents on the optical and electrochemical properties of APBIs in solution.

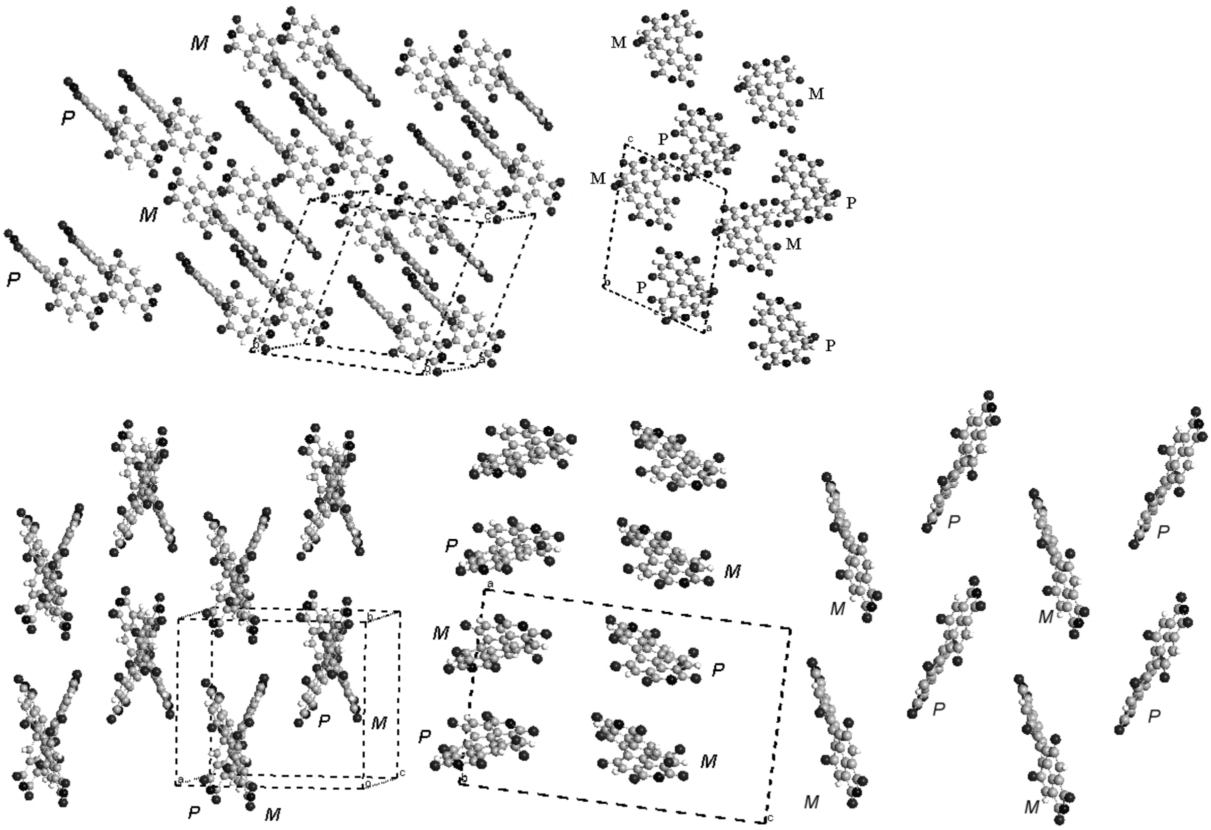

Figure 3. Molecular packing of **5b** along the a axis (right) and the b axis (left) of the unit cell in the crystal showing the alternate layered arrangement of (*P*)- and (*M*)-enantiomers (top). Molecular packing of **6a** (bottom) in the crystal along the b axis (middle) and c axis (left) of the unit cell and 2-dimensional view of the a-b plane (right) showing the herringbone-like arrangement of the chromophores. The substituents in the imide positions as well as in the bay-positions and co-crystallized solvent molecules were omitted for clarity. The assignment of the enantiomers could only be done tentatively since the absolute conformation could not be determined from these X-ray data.

The crystals of **6a** belong to the orthorhombic space group $Pca2_1$. Four molecules belong to the unit cell, namely two (*P*)- and two (*M*)-enantiomers, which are arranged in centrosymmetric way (Figure 3, bottom). Molecules with the same chirality are located in the diagonal opposite corners of the unit cell (Figure 3, bottom). The view along the c axis of the unit cell clearly reveals a herringbone-type arrangement. The closest distance between the perylene π-systems was determined to 9.1 Å and is significantly larger compared to the π–π distance observed for other perylene bisimide derivatives in the solid state.[2a]

Although single crystals could not be obtained for all compounds, the structures of **5a,c,d** and **6b-d** could be assigned by comparison of their ^{1}H NMR data with those of **5b** and **6a**. For this purpose, the resonance of the proton situated between the two oxygen atoms of the resorcin residue is particularly informative, because this proton is differently shielded by the aromatic ring current in lateral and diagonal isomers. In comparison to open-chained reference compound **4**, a typical high field shift of this proton (Figure 4, highlighted resonances) from 6.53 (**4**) to 5.27 ppm for **5a** was observed for the diagonally bridged isomer **5a-d**. Upon increasing length of the oligoethylene glycol bridge, these resonances were shifted continuously downfield up to 6.20 ppm for **5d** in the series of diagonally bridged macrocycles.

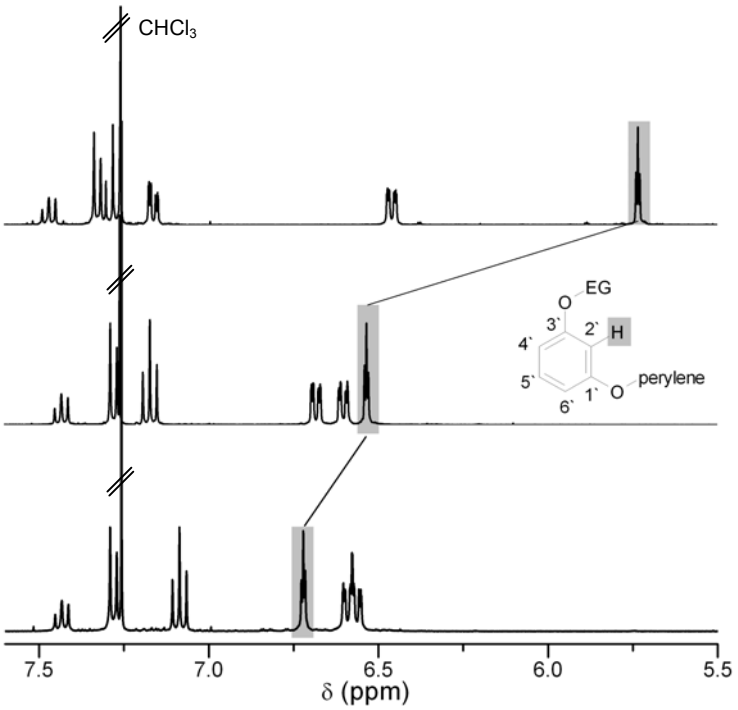

Figure 4. Sections of the ^{1}H NMR spectra (400 MHz) in $CDCl_3$ of the reference compound **4** (middle), **5b** (top) and **6b** (bottom) showing the shift of the proton situated between the two oxygen atoms of the aryloxy substituents (gray). The resonances of the aryloxy residue are displayed.

The shift of this resonance (marked proton H2´) to higher fields is caused by a change of the orientation of the aryloxy residues relative to the perylene core. As the ring current of the perylene bisimide has to be responsible for this observation, the shift of these resonances within the series of diagonally bridged isomers can be attributed to a increasing perpendicular orientation of the aryloxy residues relative to the perylene core upon shortening of the oligoethylene glycol chain (see Figure 5 for illustration). Such a perpendicular orientation was already demonstrated in the solid state structure of **5b** (Figure 2). In contrast, for the lateral isomers **6a-d**, a slight shift of the same proton to lower field from 6.53 ppm (**4**) to 6.70 ppm (**6b-d**) was observed which is caused by more horizontal orientation of the aryloxy residue relative to the perylene core in comparison to open-chained APBI **4**. This implies that the structural features of the laterally bridged isomers **6a-d** are strongly related to those of open-chained perylene bisimides like **4** in solution. Additionally, the laterally and diagonally bridged isomers could be distinguished by the chemical shift of the bridging ethylene glycol unit. The most pronounced effect was observed for **5a** and **6a**. The ethylene glycol proton resonances of **5a** appeared at 3.48 and 3.69 ppm, whereas those of **6a** are situated at 4.49 ppm. The shift to higher fields observed for the corresponding resonances of **5a** indicates that the bridging unit is situated in the deshielding area of the perylene core, further confirming the diagonally bridged structure.

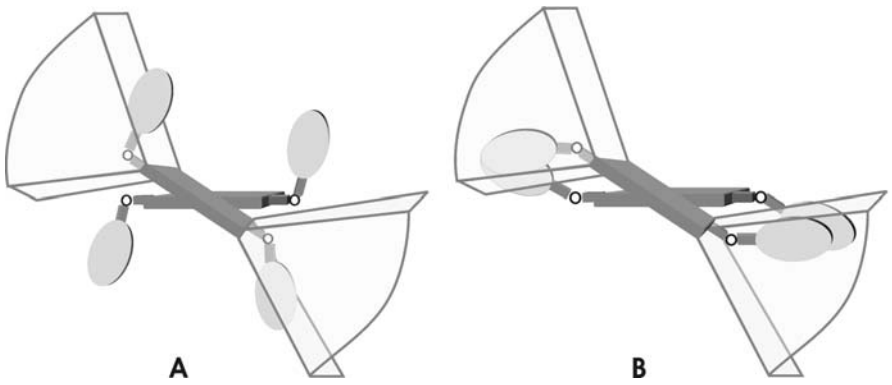

Figure 5. Schematic representation of perpendicular (A) and horizontal (B) conformations. The anisotropy cone of the perylene bisimide core is shown for one naphthalene subunit and the shielding area is highlighted.

3.4 Conformational Properties of Laterally Bridged Macrocycles 6

As outlined in the previous section, the position of the aryloxy substituents is an important structural feature of APBIs and characteristic for each type of regioisomeric macrocycle. The second characteristic structural feature for APBIs is a twisted conformation of the perylene core accompanied by an interconversion process between

the resulting enantiomers (see Chapter 2). As already mentioned before, the diagonally bridged **5a-d** and laterally bridged **6a-d** isomers are expected to have different behavior regarding the interconversion process between (*P*)- and (*M*)-enantiomers. In ^{1}H NMR spectra, this can be detected by the methyl resonances of the diastereotopic isopropyl groups situated at the imide nitrogen position. These resonances are sensitive to chirality present in the molecule and show diagnostic shapes for different stages of the interconversion process. The resonances of these methyl groups for **4**, **5b** and **6b** in ^{1}H NMR spectra in $CDCl_3$ are shown in Figure 6.

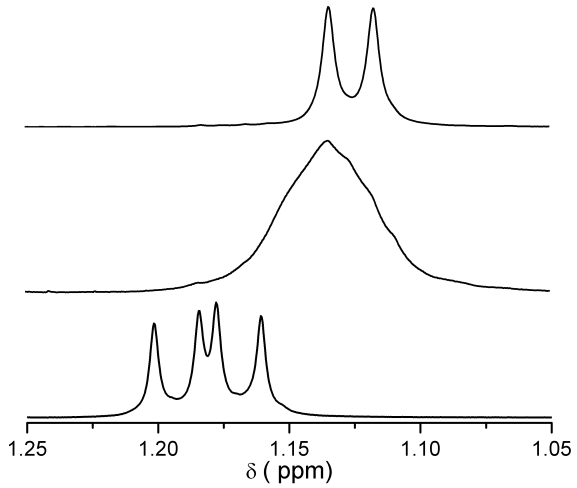

Figure 6. Sections of the ^{1}H NMR spectra (400.13 MHz) of **4** (top), **5b** (bottom) and **6b** (middle) in $CDCl_3$ at 300 K showing the methyl resonances of the diasterotopic isopropyl groups of the imide substituents.

For open-chained reference compound **4**, one doublet was observed for these protons (Figure 6, top). The occurrence of one doublet for the methyl groups of isopropyl substituents is explained by a fast interconversion between the atropo-enantiomers ($M \rightleftharpoons P$), thus, this interconversion is faster than the proton spin relaxation ("NMR time scale") and the two enantiomers cannot be distinguished by NMR spectroscopy. In contrast, for diagonally bridged macrocycles like **5b** two doublets were observed at room temperature (Figure 6 bottom). This represents the region, where the interconversion process is significantly slower than the spin relaxation, and thus the two enantiomers can be monitored by the occurrence of two doublets (see Figure 6, bottom). This is in accordance with the fact that an interconversion for this type of isomers is not possible without a bond cleavage. For the laterally bridged isomers **6b-d**, a broad singlet was observed at room temperature (Figure 6, middle), revealing that the proton spin relaxation occurs at the same time scale as the racemisation process

(coalescence region). This demonstrates that an interconversion between the enantiomers (*P* and *M*) of laterally bridged isomers **6a-d** is indeed possible.

The dynamic properties of the laterally bridged macrocyclic perylene bisimides **6a-d** were investigated in detail by temperature-dependent ^{1}H NMR spectroscopy.[$] The methyl protons of the diastereotopic isopropyl groups in the imide positions of the perylene bisimide are properly suited to monitor the interconversion process. The measurements for the laterally bridged macrocycles **6a-d** were performed in $CDCl_3$ or tetrachorethane-d_2 and additionally the interconversion process of open-chained APBI **2** was investigated in $CDCl_3$ for the purpose of comparison and validation of the experimental set-up. The data were evaluated according to the coalescence method (eqs. 3-1 and 3-2).[28]

$$k_C = \frac{\pi}{\sqrt{2}}|\Delta\nu| \qquad \text{(eq. 3-1)}$$

$$\Delta G^{\#} = R \cdot T_C \cdot \ln\left(\frac{R \cdot T_C}{k_C \cdot N_A \cdot h}\right) \qquad \text{(eq. 3-2)}$$

In Figure 7, the temperature-dependent changes of the signal for the methyl resonances of lateral isomer **6d** are exemplified shown and for the remaining compounds **6a-c**, the spectra are shown in the Appendix. At high temperatures (above 304 K) one doublet was observed, revealing a fast equilibrium between the conformational enantiomers on the NMR time scale as observed for the open-chained APBI **4** at 298 K. Upon cooling of the sample, broadening of the signal occurred and below 280 K two doublets arose which can be attributed to a slow interconversion between the two core-twisted enantiomers (*P* and *M*). From line broadening the coalescence temperature for **6d** was determined to 292 K and the difference in chemical shift of the two enantiomers (*P* and *M*) $\Delta\upsilon$ at low temperatures (253 K) resulted to 19.9 Hz. According to equations 3-1 and 3-2, the free activation enthalpy $\Delta G^{\ddagger}$ for the interconversion process of **6c** was estimated to 63 kJ/mol at 292 K. For **2** and **6a-c** the free activation enthalpies for the interconversion $\Delta G^{\ddagger}$ were estimated analogously and the obtained results are given in Table 1.

[$] DNMR measurements were performed by E. Ruckdeschel and Dr. M. Grüne at a 600 MHz spectrometer at the Institute of Organic Chemistry, University of Würzburg (Germany).

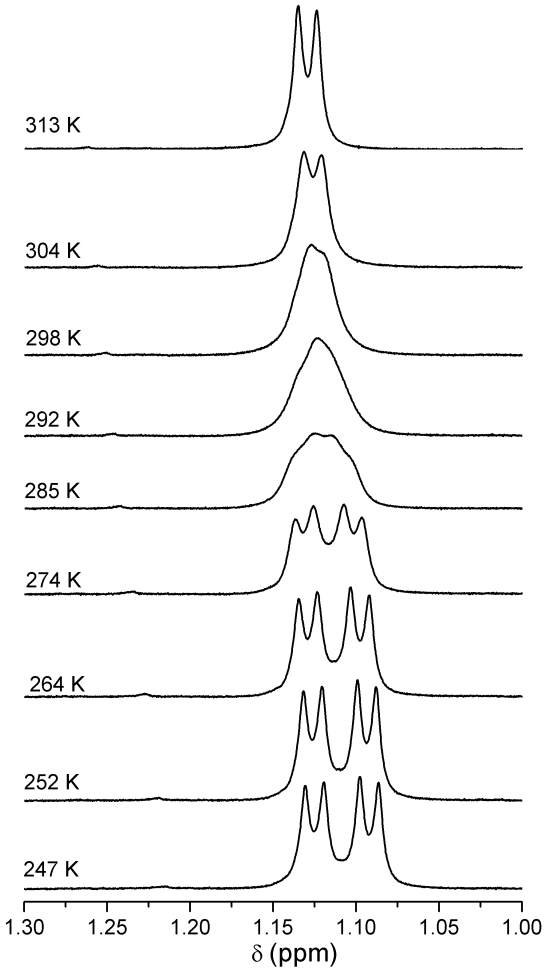

Figure 7. Sections of the temperature-dependent ^{1}H NMR spectra (600 MHz) of **6d** in $CDCl_3$. Displayed are the methyl resonances of the diasteretopic isopropyl groups situated in the imide position.

Within the series of laterally bridged macrocycles **6a-d**, the activation parameter clearly correlate to the ring size of the macrocycle. For the large macrocycles **6b-d**, coalescence temperatures and free enthalpy of activation increased slightly by decreasing the chain length (see Table 1). Furthermore, the inversion barriers are only slightly increased compared to the open-chained APBI **2** demonstrating similar conformational behavior of these compounds (For experimental details for **2**, see Chapter 6). In contrast, macrocycle **6a** showed an increased coalescence temperature (347 K) compared to the other laterally bridged macrocycles **6b-d** and correspondingly the inversion barrier is risen to 74 kJ/mol at 347 K. This trend is rather surprising because for 2,2´-substituted biphenyls the interconversion barriers were shown to increase with increasing chain length of the alkyl bridge (see Chapter 1).[29] But it has to be noted that the conformational restriction imposed by ethylene glycol chains is smaller than that of the corresponding alkyl chains owing to the higher flexibility resulting from the presence of oxygen atoms. Nevertheless, the trend observed for macrocyclic

perylene bisimides **6a-d** highlights the importance of conformational changes of the aryloxy residues for the $M \rightleftarrows P$ interconversion process of APBIs. Especially for **6a** the movement of the aryloxy residues is strongly restricted by the presence of a short bridging unit.

Table 1. Activation Parameters of Laterally Bridged Macrocycles **6** and Open-Chained APBI **2** Determined by Temperature-Dependent NMR Spectroscopy

	solvent	$\Delta\nu$ (Hz)	T_c (K)	$\Delta G^{\ddagger}_{Tc}$ (kJ/mol)
6a	Cl_2DC-$CDCl_2$	26.6	347	74±3
6b	$CDCl_3$	23.6	301	64±3
6c	$CDCl_3$	19.9	295	63±3
6d	$CDCl_3$	19.9	292	63±3
2	$CDCl_3$	6.3	271	60±3

The large energy difference between the ground and the transition state of the racemisation process revealed by the free activation enthalpy of **2** implies that the population of the transition state is negligible at room temperature. To gain a deeper insight into the interconversion process of APBIs, calculations were performed using MM2 force field which seems to be sufficient as it has been widely applied for such purpose.[30] Thus, the heats of formation were calculated for the open-chained APBI **2** with perpendicular orientation of the aryloxy groups in dependence on the twist angle of the perylene core. The calculations were performed for different dihedral angles θ of the central six-membered ring of the perylene core (see Chapter 2 for definition) in the range of –75° to 0° ((*M*)-enantiomer) and the obtained results were mirrored to obtain the heats of formation for the other enantiomer ((*P*)-enantiomer, θ = 0° - 75°). This is justified as enantiomers are considered and no other structural differences, except the opposite twist, have to be taken into consideration. The twist angle dependent distribution of the obtained energies (heat of formation) relative to the local minimum is shown in Figure 8 (left). The local minimum resulted at a twist angle of 28° which is in good agreement to that observed for a structurally related diazadibenzoperylene derivative[19] and **6a** in the solid state.

From these calculations, the energy barrier for the interconversion of **2** was obtained according to equation 3-3 and resulted to 66 kJ/mol which is in excellent agreement to that obtained experimentally by NMR spectroscopy (60 kJ/mol).

$$\Delta H_{rot} = \Delta H_f\,(\theta = 0°) - \Delta H_f\,(\theta = 28°) \qquad \text{(eq. 3-3)}$$

The slight difference between the theoretical and experimental values can be explained by the unknown structure of the transition state and by the fact that the activation enthalpy ΔH is estimated by molecular modeling in the gas phase, while the free enthalpy of activation $\Delta G^{\ddagger}$ was obtained by NMR experiments in solution. From the dependence of the heat of formation on the dihedral angle θ, the population of conformations exhibiting different twist angles was calculated according to Boltzmann statistic (see Experimental Section). The normalized population of conformations with different twist angles at 293 K is shown in Figure 8 (right). The accordance of the calculated values with that determined by NMR spectroscopy confirms that APBIs possess a rather defined twist angle (28°) and reveals a negligible population of the transition state of APBIs in solution.

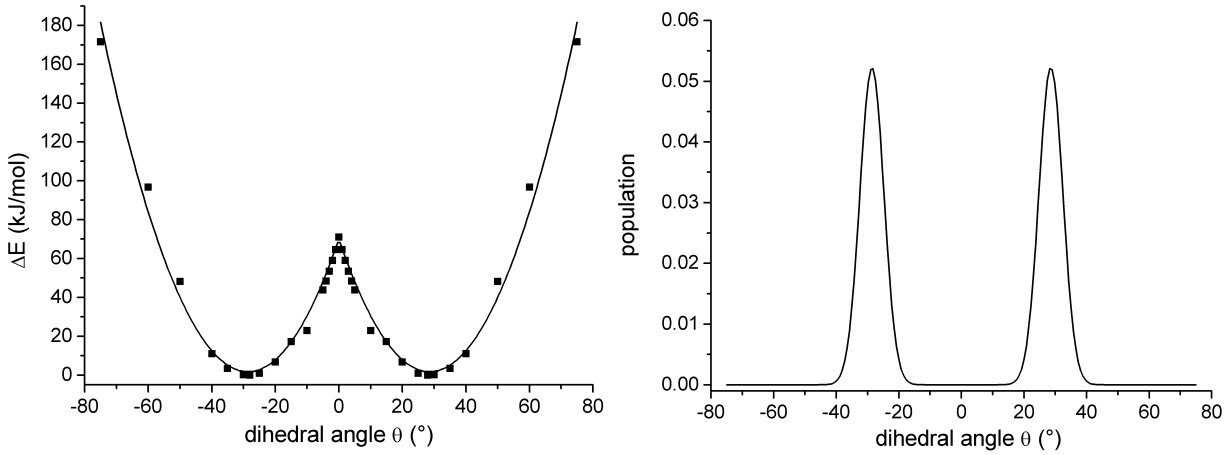

Figure 8. Calculated energy distribution (left) and resulting normalized population of conformations with different dihedral angles θ (right) of **2** at 293 K obtained by MM2 force field calculation.

3.5 Electrochemical Properties of Macrocyclic Perylene Bisimides

Open-chained APBIs like **4** display two reversible reduction waves and one reversible oxidation wave within the potential range from –1.50 V to +1.15 V vs. the ferrocene/ferrocenium couple. In order to investigate the influence of different conformations of the aryloxy substituents on the electrochemical properties, the redox potentials of macrocycles **5a-d** and **6a-d** were determined by cyclic voltammetry in dichloromethane using tetrabutylammonium hexafluorophosphate (TBAHFP) as supporting electrolyte. All half-wave potentials were referred to the redox couple of ferrocence/ferrocenium as internal standard. The first and the second reduction half wave potential as well as the oxidation potential of macrocyclic perylene bisimides **5a-d** and **6a-d** are collected in Table 2, and the cyclic voltammograms of **5c** and **6c** are exemplified in Figure 9. All macrocycles **5a-d** and **6a-d**, showed two reversible

reduction waves, typical for APBIs. Whilst for the macrocycles **5d** and **6a-d** nicely resolved reversible oxidation waves are observed between 0.9 and 1.05 V, the oxidation of diagonal isomers **5a-c** occur at higher potentials and are obscured by a irreversible process.

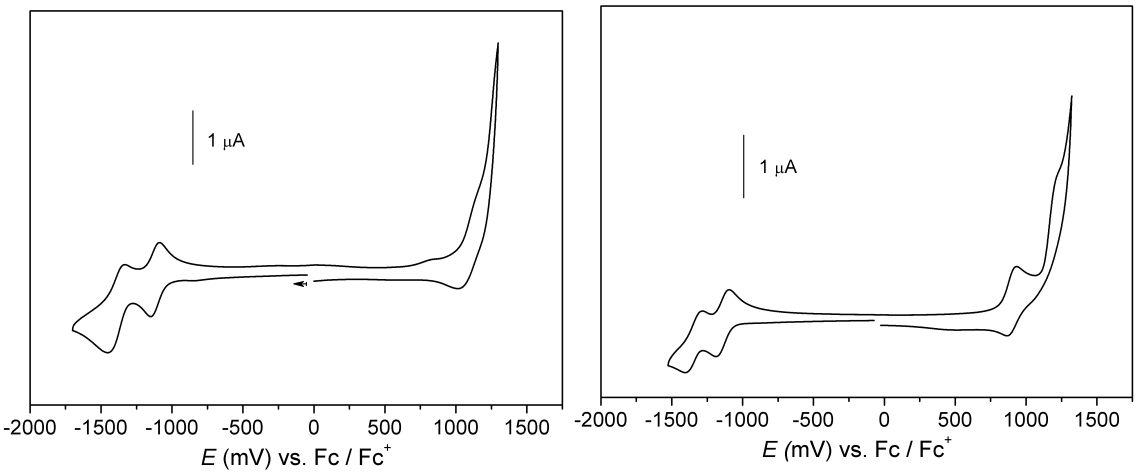

Figure 9. Cyclic voltammogram of **5c** (left) and **6c** (right) in dichloromethane (0.1M TBAHFP, sweep rate 100 mV/min).

For the laterally bridged macrocycles **6b-d**, the determined half-wave potentials for the reduction and oxidation process are similar to those of open-chained APBI **4**. Only the smallest macrocycle **6a** bearing monoethylene glycol bridges exhibits a higher oxidation potential (1.05 V) compared to **4** and **6b-d** (0.90 V), whereas the reduction potentials at –1.07 V and –1.32 V are similar to those determined for **6b-d**. The comparatively high oxidation potential for **6a** can be attributed to the conformational restriction imposed by the shorter spacer unit.

For the diagonally bridged macrocycles with longer bridges **5c,d** the reduction potentials are also in close agreement to that observed for the open-chained reference compound **4**, whilst for the shorter-bridged derivatives **5a,b** an increase of the reduction potential with decreasing chain length was observed. For macrocycle **5a**, a reduction potential of –0.97 V was determined that is almost 0.2 V higher compared to that observed for macrocycle **5d** (–1.17 V). Furthermore, the conformational properties of the aryloxy substituents have a pronounced influence on the respective oxidation potentials of diagonally bridged macrocycles, as the oxidation potentials were found to increase from 0.98 V (**5d**) to 1.16 V (**5b**) with decreasing chain length of the macrocycle (Table 2). For **5a**, no oxidation wave of the perylene bisimide could be observed in the available scanning range due to irreversible oxidation at >1.17 V. The significant changes of the redox potentials observed in the series of macrocyclic perylene bisimides **5a-d** reveal that different conformations of the aryloxy substituents, i.e. the

orientation of the aryloxy residue relative to the perylene core, have an appreciable effect on the redox properties of APBIs.

Table 2. Redox Potentials (in V) of Macrocycles **5a-d** and **6a-d**, and Reference Compound **4** in Dichloromethane (0.1 M TBAHFP) versus Ferrocen/Ferrocenium as Internal Reference[a]

	$E_{1/2}$ (PBI^{-}/PBI^{2-})	$E_{1/2}$ (PBI/PBI^{-})	$E_{1/2}$ (PBI/PBI^{+})
5a	–1.30	–0.97	>1.17
5b	–1.38[b]	–1.07	1.16[b]
5c	–1.39	–1.12	1.09[b]
5d	-1.39	–1.17	0.98
6a	–1.32	–1.07	1.05
6b	–1.30	–1.11	0.91
6c	–1.35	–1.14	0.90
6d	–1.36	–1.14	0.90
4	–1.35	–1.14	0.91

a) determined from reversible redox process with ΔE ~ 60-100 mV between the oxidative and reductive peak maxima, error ± 0.05 V; b) quasi-reversible.

3.6 Optical Properties of Macrocyclic Perylene Bisimides

The optical properties of the macrocyclic perylene bisimides were investigated by UV/Vis and fluorescence (steady-state and time resolved) spectroscopy. In Figure 10, the absorption spectra of macrocycles **6a**,**c-d** are shown in comparison to that of open-chained reference **4**. The absorption spectra of laterally bridged macrocycles **6a-d** (Figure 10) are typical for APBIs with a maximum around 580 nm assigned to the S_0-S_1 transition, a shoulder of the second vibronic progression and a broad maximum at 450 nm related to the S_0-S_2 transition. For the derivatives **6b-d** the absorption maxima as well as the molar absorption coefficients are almost identical to that of open-chained reference compound **4**; therefore, **4** may possess a similar conformation to that of laterally bridged isomers **6a-d** (Figure 10).

Only the smallest macrocycle **6a** adopts an exceptional position because the maximum of the S_0-S_1 transition is hypsochromically shifted by 20 nm compared to that of **6b** and a decrease of the molar absorption coefficient is observed. The exceptional position of **6a** was already demonstrated before by cyclic voltammetry and NMR spectroscopy as the interconversion barrier for this compound (T_c = 347 K) is significantly increased in comparison to the other derivatives (T_c = 295 K). Therefore,

the observed differences in the absorption properties between **6a** and **6b-d** are presumably due to the conformational restriction in **6a** imposed by the short spacer unit.

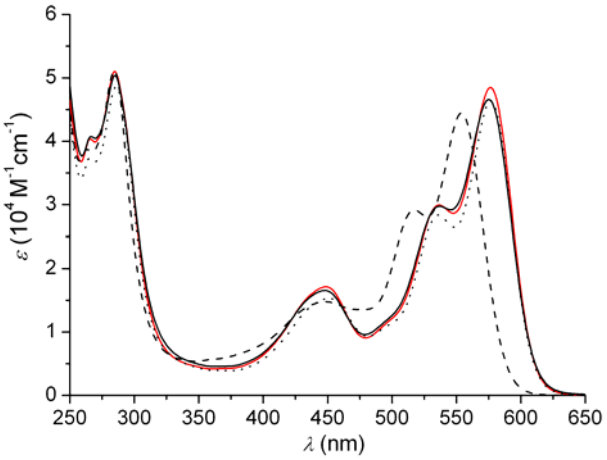

Figure 10. Absorption spectra of **6a** (dashed), **6c** (dotted), **6d** (solid) and **4** (red) in dichloromethane.

For the diagonally bridged isomers **5a-d**, much more pronounced spectral differences are observed in comparison to open-chained reference compound **4** (Figure 11). The absorption maxima related to the S_0-S_1 transition for diagonally bridged macrocycles **5a-d** are shifted up to 41 nm (**5b**) towards shorter wavelength from 575 nm (**4**) to 558 nm (**5d**) and 545 nm (**5a,c**) and 534 nm (**5b**). This hypsochromic shift is further related to the chain length of the bridging unit as the comparison of the absorption maxima of **5b** and **5d** revealed (Figure 11, top). Furthermore, a pronounced hypochromicity is observed for macrocycles **5a-c** in comparison to reference compound **4**. As the transition dipole moments for the S_0-S_1 transition of these diagonally bridged macrocycles **5a-d** (7.6-8.0 Debye) equal that of reference compound **4** (7.8 Debye), the pronounced hypochromicity can be attributed to spectral broadening and shift of intensity into higher vibronic progressions of the S_0-S_1 transitions (see Appendix for details). The observed hypsochromic shift on the other hand may be attributed to the formation of a conformer with less conjugation between the electron-donating aryloxy residue and the electron-deficient perylene bisimide core.

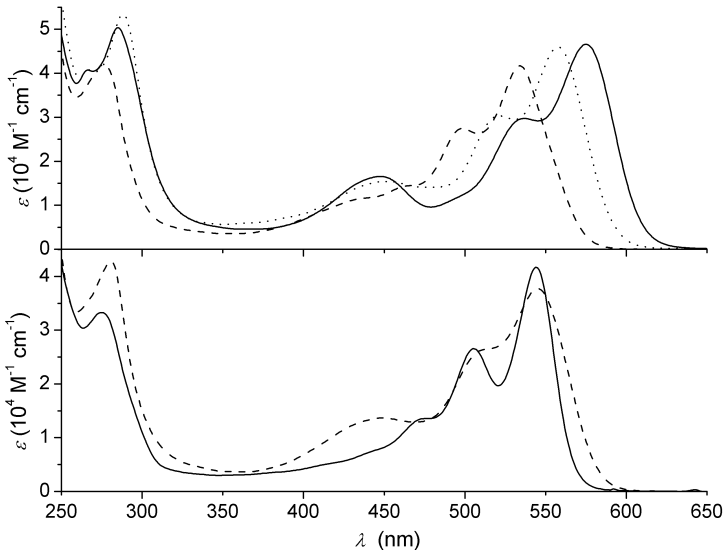

Figure 11. Absorption spectra of **5b** (dashed line, top) and **5d** (dotted line, bottom) in comparison to reference compound **4** (solid black line) and absorption spectra of **5a** (solid line, bottom) and **5c** (dashed line, bottom) in dichloromethane.

The fluorescence properties of reference compound **4** and macrocycles **5a-d** and **6a-d** in dichloromethane are given in Table 3 and the normalized fluorescence spectra are shown in Figure 12. As can be seen from Table 3, the fluorescence quantum yields and lifetimes of the lateral isomers **6b-d** are almost indistinguishable with that of the open-chained reference compound **4**, which again indicates that the behavior of these isomers is similar to that of the open-chain APBI derivatives.

Table 3. Emission Properties of Macrocyclic Perylene Bisimides in Dichloromethane

	λ_{max} (nm)	$\Delta\lambda$ (nm)[a]	Φ_{fl}[b]	τ_{fl} (ns)[c]	k_r (s^{-1})[d]	k_{nr} (s^{-1})[e]
4	609	34	0.89	5.6	$1.7\cdot10^8$	$2.0\cdot10^7$
5a	562	18	< 0.02	< 0.5	> $4.0\cdot10^7$	> $2.0\cdot10^9$
5b	573	39	0.09	0.8	$1.1\cdot10^8$	$1.1\cdot10^9$
5c	582	37	0.43	2.7	$1.6\cdot10^8$	$2.1\cdot10^8$
5d	588	30	0.90	5.5	$1.6\cdot10^8$	$1.8\cdot10^7$
6a	588	34	0.78	5.4	$1.4\cdot10^8$	$4.1\cdot10^7$
6b	605	28	0.82	5.3	$1.6\cdot10^8$	$3.4\cdot10^7$
6c	606	24	0.84	5.6	$1.5\cdot10^8$	$2.9\cdot10^7$
6d	606	29	0.82	5.5	$1.5\cdot10^8$	$3.6\cdot10^7$

a) The stokes shift $\Delta\lambda$ was calculated as the difference in absorption and emission maximum; b) $\Phi_{fl} \pm 0.03$; c) $\tau_{fl} \pm 0.2$; d) $k_r = \Phi_{fl}\cdot\tau_{fl}^{-1}$; e) $k_{nr} = (1-\Phi_{fl})\cdot\tau_{fl}^{-1}$.

In contrast to the situation of lateral isomers **6a-d**, the fluorescence quantum yields of diagonally bridged macrocycles **5a-d** (Table 3) are tremendously decreased from 0.90 for **5d** to 0.02 for **5a** (see Table 3, 4th column). This effect can be attributed to an increase of the non-radiative rate constants k_{nr} (**4~5d<5c<5b<5a**), whereas the radiative rate constants k_r (1.5 x 10^8 s^{-1}) are similar for all compounds presented here.

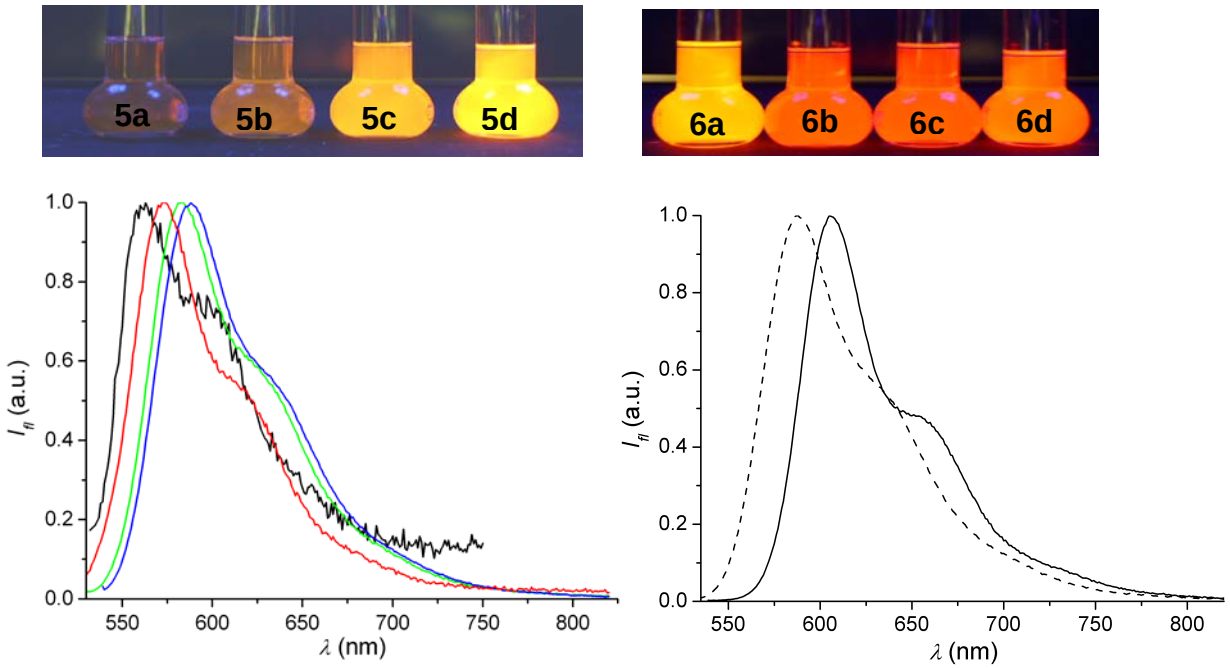

Figure 12. Fluorescence properties of diagonally bridged isomers **5a-d** (left) and laterally bridged isomers **6a-d** (right). Images of 10^{-5} M solutions upon excitation at 258 nm (top) and normalized fluorescence spectra (bottom) of diagonal isomers **5a** (black), **5b** (red), **5c** (green) and **5d** (blue) and lateral isomers **6a** (dashed line) and **6d** (solid line).

3.7 Discussion of the Optical and Electrochemical Properties

In order to explain the observed largely differing optical properties of these APBIs, the optical band gaps and the frontier orbitals of macrocycles **5a-d** and **6a-d** as well as of open-chained APBI **4** were determined. The optical band gap E_{gap}^{OS} was assessed from the cross section of the normalized absorption and emission spectra (Table 4). For the series **5a-d**, Table 4 reveals a continuous increase of E_{gap}^{OS} from 2.17 eV (**5d**) to 2.25 eV (**5a**) with decreasing chain length of the bridging unit. Furthermore the band gaps E_{gap}^{CV} determined from cyclic voltammetry showed excellent agreement to those obtained from optical spectroscopy.

The lateral isomers **6a-d** exhibit ~0.1 eV smaller band gap that show somewhat larger deviations (0.05-0.08 eV) between E_{gap}^{OS} and E_{gap}^{CV}. Again the value of APBI **4** is in perfect agreement with those of **6a-d**. The remarkable agreement of the band gaps

E_{gap}^{OS} and E_{gap}^{CV} is explained by the fact that the S_0-S_1 transition in these APBIs is related to an almost pure electronic excitation of an electron from the HOMO to the LUMO.

Table 4. Optical Band Gaps Determined from Optical Spectroscopy (OS) and Cyclic Voltammetry (CV) and Calculated HOMO and LUMO Levels in eV for Diagonally Bridged **5a-d** and Laterally Bridged Macrocycles **6a-d** and Reference Compound **4**.

	E_{gap}^{OS}[a]	E_{gap}^{CV}[b]	LUMO[c]	HOMO[d]
5a	2.25	>2.14[e]	–3.83	–6.08
5b	2.24	2.23	–3.73	–5.97
5c	2.20	2.21	–3.68	–5.88
5d	2.17	2.15	–3.63	–5.80
6a	2.18	2.12	–3.73	–5.91
6b	2.10	2.02	–3.69	–5.79
6c	2.09	2.04	–3.66	–5.75
6d	2.10	2.04	–3.66	–5.76
4	2.10	2.05	–3.66	–5.71

a) Determined from the intersection of the normalized absorption and emission spectra; b) calculated from the difference of oxidation and reduction potentials; c) calculated from the first reduction potential and the potential of ferrocene relative to the zero vacuum level; d) calculated from E_{gap}^{OS} and the LUMO level; e) not accessible due to irreversible oxidation at 1.17 V.

The energy of the LUMO was assessed from the first reduction potential by taking into consideration the potential of ferrocene (–4.8 eV) with respect to the zero vacuum level.[4b] Then the energy of the HOMO was calculated by subtracting the determined optical band gap E_{gap}^{OS} from the LUMO energy. As can be seen from Table 4 and Figure 13, a continuous decrease of the energy of the HOMO from –5.8 eV (**5d**) to –6.1 eV (**5a**) with respect to the zero vacuum level was observed by shortening of the chain length of the macrocycles. In a similar manner, the energy of the LUMO is decreased from –3.6 eV (**5d**) to –3.8 eV (**5a**), although this effect is less pronounced than that observed for the HOMO energies (Figure 13, left). The different behavior of the frontier orbitals corresponds to the increase of the band gap and thus to the hypsochromic shift of the absorption maximum observed for macrocyclic perylene bisimides **5a-d** (Figure

11). In contrast, the energy of the HOMOs (–3.66 eV) as well as those of the LUMOs (–5.75 eV) remain constant in the series of lateral bridged isomers **6b-d** and resemble those calculated for open-chained reference compound **4** (Table 4).

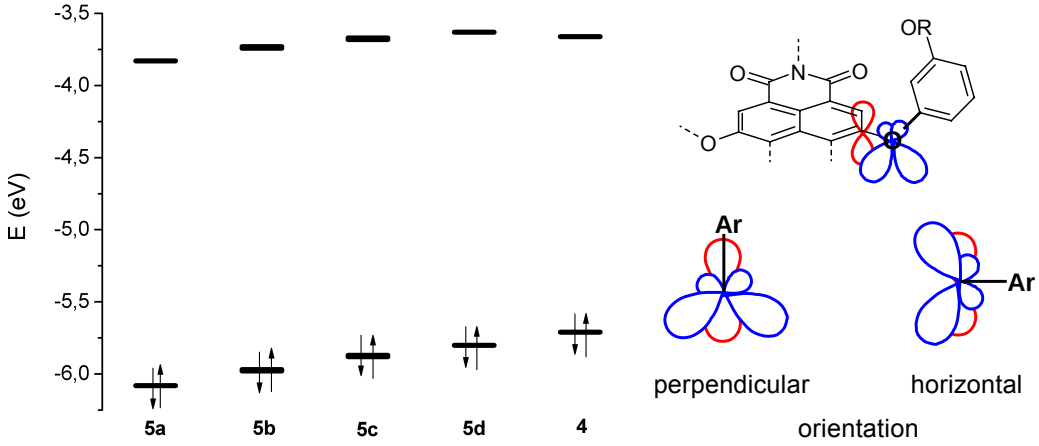

Figure 13. Energies of HOMO and LUMO for diagonally bridged macrocycles **5a-d** and reference compound **4** (left) and schematic representation of the orbital interactions between the perylene core and the aryloxy substituents (right); Ar denotes the 3-alkoxyphenyl residue.

To explain the conformational impact on the HOMO and the LUMO energies of laterally and diagonally bridged isomers **5a-d** and **6a-d**, the electronic coupling between the PBI core and the aryloxy substituents was elucidated. APBIs can be thought to be composed of the electron poor perylene bisimide core and the electron rich aryloxy substituent and thus the MO of APBIs must be a result of the interaction of these molecular fragments accordingly. The comparison of the oxidation potentials determined for open-chained APBI **4** (E_{ox} = +0.91 V; E_{red} = –1.14 V vs. Fc) and macrocyclic perylene bisimides **6b-d** (E_{ox} = +0.90 V; E_{red} = –1.14 V vs. Fc) with that of the unsubstituted *N,N´*-bis(2,6-diisopropylphenyl)perylene-3,4:9,10-tetracarboxylic acid bisimide (E_{ox} = +1.29 V; E_{red} = –1.01 V vs. Fc)[31] reveals that the HOMO is almost 0.4 eV higher for APBIs whilst the LUMO level is only raised by about 0.1 eV. On the other hand, the frontier orbitals of the present APBIs **4** and **6a-d** are not altered in comparison to other APBIs bearing less electron-rich aryloxy substituents in the bay position (e.g. tetraphenoxy-substituted perylene bisimides: E_{ox} = +0.89 V, E_{red} =–1.10 V) revealing that the electrochemical properties of APBIs are little influenced by the type of aryloxy-substituent.[4c] This fact suggests that there is no significant conjugation between the perylene bisimide core and the respective aryloxy residue. The absence of conjugative effects between the perylene bisimide core and the aryloxy residues was also pointed out in literature.[4b] This finding strongly suggest that the electron-rich HOMO of APBIs

originates from the primordial HOMO of the perylene bisimide core upon conjugation to four oxygen atoms (+M-effect) directly attached to the PBI core. In contrast, the LUMO of macrocycles **6b-d** and open-chained reference **4** differ only slightly from that of the unsubstituted perylene bisimide, indicating that the LUMO in APBIs can be ascribed to the primordial perylene bisimide core LUMO.

In order to assess the presence of mesomeric effects between the aryloxy substituent and the perylene core in APBIs, the CO bond length obtained from single crystal X-ray analysis of **5b** and **6a** were analyzed. The length of the bond connecting the perylene bisimide core and the oxygen atom of the aryloxy residue was determined to 1.375±0.003 Å (**5b**) and 1.372±0.007 Å (**6a**) which is significantly lower than the length expected for a C_{sp3}-O single bond (1.440 Å).[32] Furthermore, these values are in good agreement to bond lengths observed for 1,4-dimethoxybenzene (1.360 Å)[33] and 4-nitroanisol (1.351 Å)[34] in the solid state. The observed partial double bond character for these CO bonds thus confirms the presence of mesomeric effects between the perylene bisimide core and the oxygen atoms directly attached to the PBI core.[32]

Therefore, we can relate the observed decrease of the HOMO energy from **5d** to **5a** to a decreased conjugation of the electron-donating oxygen atoms and the electron-poor perylene bisimide core. Since both frontier orbitals determine the optical band gap, also the observed hypsochromic shift can be ascribed to a reduced electron donation of the appended aryloxy substituents in the series of diagonally bridged macrocycles **5a-d**.

The pronounced impact of the orientation of the aryloxy residues on the APBI frontier orbitals, however, remains to be explained. Clearly, the mesomeric effect must be associated with the interaction of the lone pairs of the oxygen atoms directly attached to the perylene bisimide core and the perylene bisimide π-system (Figure 13, right). As the degree of conjugation is related to the overlap of the participating orbitals, it seems reasonable that the angle of the oxygen lone pair orbitals relative to the π-orbitals of the perylene core determines the magnitude of conjugation. As schematically shown in Figure 13 (right), the overlap of the respective orbitals is most effective for a horizontal orientation of the aryloxy residue (as given in **6a-d**) and less effective for a perpendicular orientation of the aryloxy residue (as given in **5a,b**).

Therefore, the electron donation from the aryloxy bay substituents to the PBI core can be directly related to the dihedral angle γ between the aryloxy groups and the perylene bisimide core (see Figure 14). This angle describes the orientation of the aryloxy residues relative to the perylene core and a value of 90° correspond to a perpendicular orientation, whereas a γ value of 0° relates to a horizontal orientation. The dihedral

angle γ was estimated from AM1 calculation as the mean value of the four aryloxy substituents (Figure 14). For the diagonally bridged isomers **5** an increase of the dihedral angle γ was observed with decreasing ring size of the macrocycle from 48° (**5c**) to 79° (**5a**). Therefore, the conjugation between the aryloxy residue and the perylene core is determined by the orientation of the aryloxy residues. Accordingly, the structural origin of the hypsochromicity is given by the different orientations of the aryloxy residue as schematically shown in Figure 14B.

A

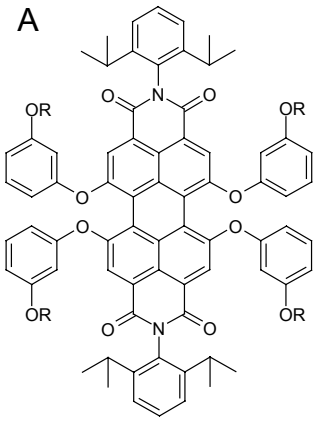

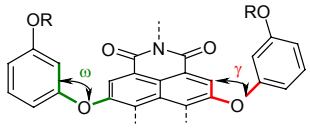

	γ (°)	ω (°)
5a	79.8	11.6
5b	73.6	31.0
5c	48.1	54.4
5d	58.0	39.6
2	47.9	39.1

B

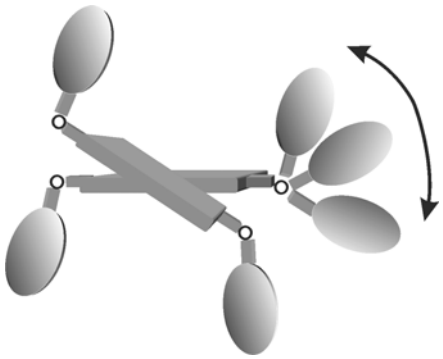

Figure 14. (A) Definition and values of the dihedral angle γ and ω for macrocyclic perylene bisimide **5** and open-chained APBI **2** determined from semiempirical AM1 calculations using Cache Quantum Cache Workspace 5.0. (B) Schematic representation of the possible conformations of the aryloxy residues. The arrow indicates the possible movement of the aryloxy residues.

Likewise, the relative position of the aryloxy residue to the oxygen lone pairs can be assessed from AM1 calculations by the dihedral angle ω (Figure 14A). In accordance to the dihedral angle γ, an angle ω of 0° corresponds to the conformation with the largest interaction between the aryl residue and the oxygen atom, whereas a 90°-conformation do not possess any conjugation, no matter whether a horizontal (γ = 0°) or perpendicular conformation (γ = 90°) is present. The ω-values for diagonally bridged macrocycles **5** increase with increasing ring-size from 11° (**5a**) to 54° (**5c**) which reveal in comparison to the dihedral angle γ, an opposite trend (Figure 14A). These results indicate that for the smallest macrocycle **5a-b**, the lone pairs of the oxygen is conjugated more strongly to the aryl residue, whereas for the larger PBIs **5c-d**, the oxygen lone pairs are more strongly conjugated to the perylene bisimide core.

The pronounced variation of the fluorescence quantum yield of diagonally bridged macrocycles **5a-d** can now be attributed to the different electronic properties that arise

for different dihedral angles γ and ω. On the one hand, Figure 13 reveals the decrease of the HOMO level upon fixation of the aryloxy residue in a perpendicular position by means of short oligoethylene glycol bridge in **5a** (large γ of 80°). On the other hand, the angle ω goes to a minimum (12°) for this compound leading to the most electron-rich resorcin subunit. Indeed, the oxidation potential for 1,3-dimethoxybenzene is 1.08 V vs Fc/Fc^{+}[35] which is lower than the APBI oxidation potential of **5a,b**. Thus, it is reasonable to relate the observed fluorescence quenching for **5a** to a photoinduced electron transfer process from the electron-rich aryloxy subunit to the electron-poor perylene bisimide core. For **5b,c** the quenching is less effective but still substantial. Finally, for the better conjugated conformations, i.e. laterally bridged isomer **6a-d** and the diagonally bridged derivative **5d** with the longest oligoethylene glycol chain in which the electron-deficient perylene bisimide core and the electron-rich resorcin units experience the strongest electronic coupling (see Figure 13), the radiative decay becomes favored.

3.8 Solvent-Dependent Fluorescence Properties of Macrocyclic Perylene Bisimide 5b.

To shed more light into the excited state properties of diagonally bridged macrocyclic perylene bisimides, UV/Vis and fluorescence spectroscopy (steady state and time-resolved) were carried out for diagonal isomer **5b** in solvents of different polarity. The absorption and fluorescence spectra of **5b** in various solvents are shown in Figure 15 and the fluorescence properties are summarized in Table 6.

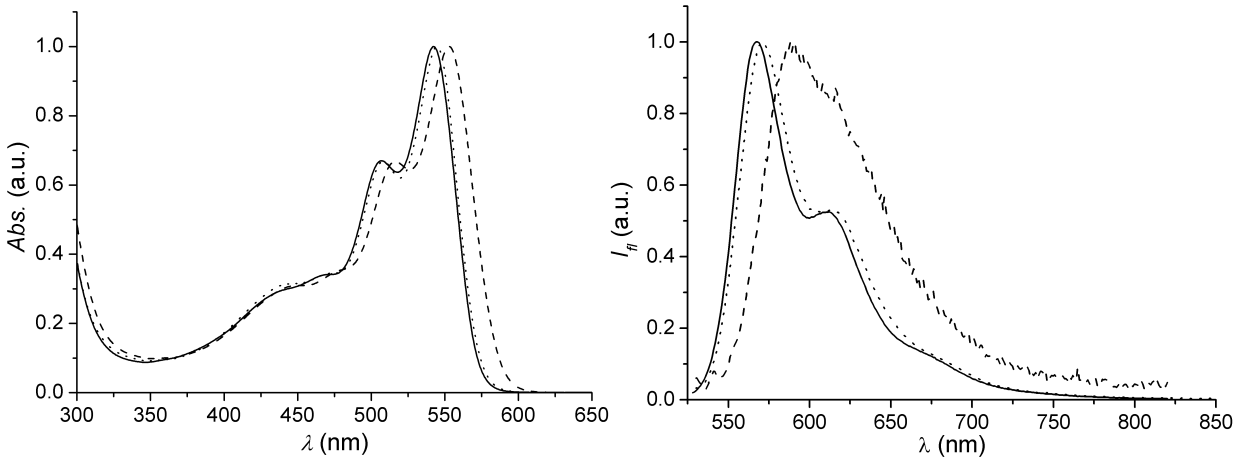

Figure 15. Normalized absorption (left) and emission spectra (right) of **5b** in DMSO (dashed line), THF (dotted line) and diethylether (solid line).

As can be seen from the data in Table 6, the spectral position of the absorption as well as the emission maxima of **5b** are only slightly dependent on the solvent polarity. The observed negligible solvatochromism indicates the apolar character of the ground

and excited state of **5b**.§ Furthermore, the shape of the absorption spectrum is similar for all solvents investigated, indicating no significant conformational changes for **5b**.

Table 6. Solvent-Dependent Absorption and Fluorescence Properties of **5b**

	λ^{abs} (nm)	λ^{em} (nm)	Φ_{fl}[a]	τ_{fl} (ns)[b]	k_r (s^{-1})[c]	k_{nr} (s^{-1})[d]
dimethylsulfoxide	553	590	<0.02	<0.7	>2.9×10^8	>1.4×10^9
dichloromethane	534	573	0.09	<0.8	>1.1×10^8	>1.2×10^9
THF	545	571, (613)[e]	0.14	1.2	1.2×10^8	7.1×10^8
diethylether	543	568, (611)[e]	0.98	5.6	1.8×10^8	3.6×10^6
toluene	548	569, (614)[e]	0.95	5.4	1.8×10^8	9.3×10^6

a) Φ_{fl} ± 0.03; b) τ_{fl} ± 0.5; c) $k_r = \Phi_{fl}\cdot\tau_{fl}^{-1}$; d) $k_{nr} = (1-\Phi_{fl})\cdot\tau_{fl}^{-1}$, e) vibronic progression

The fluorescence intensity of **5b**, on the other hand, is strongly dependent on the polarity of the solvent (see Table 6). In polar solvents such as DMSO, diagonally bridged macrocycle **5b** did not show any fluorescence (Φ_{fl} = 0). In the medium polar solvents dichloromethane and THF (ε_r = 8.9 and 7.4, respectively) the fluorescence quantum yields remain low (0.09 and 0.14, respectively) whereas, in solvents of low polarity like diethylether or toluene (ε_r = 4.3 and ε_r = 2.3, respectively), **5b** exhibits a fluorescence quantum yield of nearly unity (Φ_{fl} = 0.98 and 0.95). Also the fluorescence lifetime increased to 5.6 ns and 5.4 ns in diethylether and toluene, respectively, compared to DMSO (τ_{fl} < 0.7 ns) and are comparable to that determined for the open-chained reference compound **4** (5.6 ns) in dichloromethane and other APBIs (5.9-7.4) [3d,5,8a,18,36].

The observed relationship between the fluorescence quantum yield of **5b** and the relative permittivity of the solvent is characteristic for charge transfer processes.[37] This observation supports the hypothesis of a photoinduced electron transfer process from the electron-rich aryloxy residues to the photoexcited electron-poor perylene bisimide core as explanation for the observed fluorescence properties of diagonally bridged macrocycles **5a-d**. According to Rehm-Weller equation (eq. 3-7), the free enthalpy of a photoinduced electron transfer processes (upon excitation of the acceptor) is related to the solvent polarity ε, but also to the distance between donor and acceptor R_{DA}, to the

§ Correlation of the absorption and emission maxima as well as of the Stokes shift with different solvent parameters such as the dielectric constant ε_r, the refractive index n or the Lippert-Mataga function were not successful. The lack of significant solvatochromism might be due to specific interactions of the applied solvents with the π-systems of perylene bisimides.

electron-donating ability of the donor (E_{ox}) and to the electron-accepting ability (E_{red}) as well as to the band gap of the acceptor (E_{gap}).

$$\Delta G^0 = e(E_{ox}(D) - E_{red}(A)) - E_{gap} - \frac{e^2}{4\pi\varepsilon_0\varepsilon R_{DA}} - \frac{e^2}{8\pi\varepsilon_0}\left(\frac{1}{r^+} + \frac{1}{r^-}\right)\left(\frac{1}{\varepsilon} - \frac{1}{\varepsilon_{ref}}\right) \quad \text{(eq. 3-7)}$$

To further elucidate whether a photoinduced electron transfer process is the general mechanism for fluorescence quenching of APBIs, solvent-dependent fluorescence measurements were additionally performed for the known APBI **7** and compared to the solvent dependent behavior of **4** and **8** reported in literature.[22b,36]

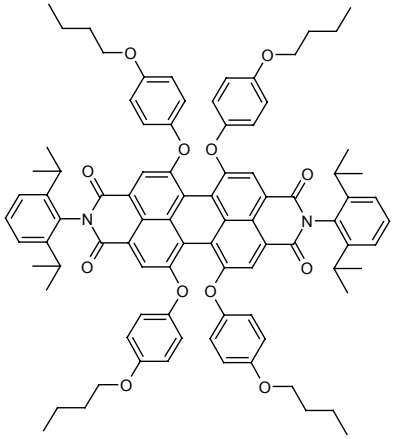

7

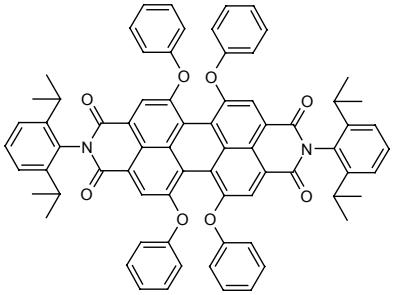

8

APBI **4** was chosen because it comprises different orientation of the aryloxy residues as outlined before (Sections 3.2 and 3.7) and thus a different electronic coupling (Figure 13). APBI **7** was chosen because the aryloxy substituents of this derivative possess a higher electron-donating ability than that of **4** or **5b**. The increased electron-donating ability of the aryloxy residue can be related to the oxidation potential of the corresponding methoxy-substituted benzenes, which were reported to be 1.08 V for 1,3-dimethoxybenzene in contrast to 0.88 V for the 1,4-dimethoxybenzene.[35] Furthermore, APBIs like **7** were reported to be non-fluorescent in dichloromethane.[10a,15a] APBI **8**, on the other hand, exhibits lower electron-donating ability of the aryloxy substituents compared to that of **4**, **5b** and **7** (1.28 V for methoxybenzene vs. ferrocene).[38]

The fluorescence properties of **4** are summarized in Table 7.[22b,#] The fluorescence quantum yields of **4** in polar solvents are low with 0.06 and 0.14 in methanol and acetonitrile, respectively, and increased continuously in dependence on the solvent polarity to 0.21 (ethanol) and 0.40 (1-butanol). In comparison to **5b**, high fluorescence quantum yields (0.75-0.84) were observed in medium polar solvents like ethyl acetate or dichloromethane and remained constant (~0.85) in solvents of lower polarity. These

[#] As quantum yields of **4** in medium polar solvents have not been reported in literature 22b, the values in 1-butanol and ethanol were additionally measured to complete the solvent series.

results reveal a lower driving force for a photoinduced electron transfer according to the Rehm-Weller equation.

Table 7. Fluorescence Quantum Yields of APBI **4** in Different Solvents[22b,#]

solvent	n-hexane	Et_2O	CH_2Cl_2	EtOAc	1-BuOH	ethanol	acetonitrile	methanol
Φ_{fl}	0.79	0.88	0.84	0.75	0.40	0.21	0.14	0.06

The optical properties of APBI **7** were investigated by UV/Vis absorption and fluorescence spectroscopy. The absorption and fluorescence spectra of **7** are shown in Figure 16 and the solvent-dependent fluorescence properties of **7** are given in Table 8.

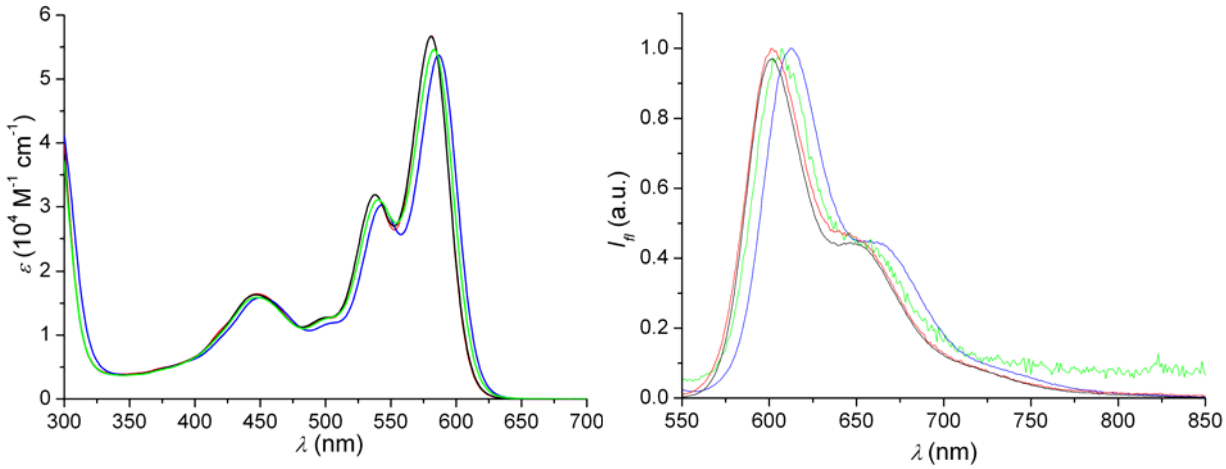

Figure 16. Absorption (left) and normalized fluorescence spectra (right) of **7** in dibutylether (black), diethylether (red), ethyl acetate (green) and toluene (blue).

Table 8. Fluorescence Properties of APBI **7** in Different Solvents

solvent	Φ_{fl}[a]	τ_{fl} (ns)[b]	k_r (s^{-1})[c]	k_{nr} (s^{-1})[d]
dichloromethane	< 0.01	< 0.39	> $2.4x10^7$	> $2.5x10^9$
ethylacetate	< 0.01	< 0.39	> $3.1x10^7$	> $2.5x10^9$
diethylether	0.11	0.71	$1.6x10^8$	$1.3x10^9$
chloroform	0.09	0.71	$1.2x10^8$	$1.3x10^9$
dibutylether	0.73	5.19	$1.4x10^8$	$5.2x10^7$
tetrachloromethane	0.97	7.36	$1.3x10^8$	$4.1x10^6$

a) Φ_{fl} ± 0.03; b) τ_{fl} ± 0.5; c) $k_r = \Phi_{fl} \cdot \tau_{fl}^{-1}$; d) $k_{nr} = (1 - \Phi_{fl}) \cdot \tau_{fl}^{-1}$.

As for the diagonal macrocycle **5b**, APBI **7** does not show a distinct solvatochromism, but the fluorescence quantum yields as well as the corresponding lifetimes show again a strong solvent dependent behavior. APBI **7** is, as reported for similar APBIs, non-fluorescent in dichloromethane.[10a,15a] The fluorescence quantum yields of **7** as well as the fluorescence lifetimes remain low even in diethylether, in which **4** and **5b** exhibit

quantum yields of ca. 90%. Only in lower polar solvents such as dibutylether (ε_r = 3.10) and tetrachloromethane (ε_r = 2.24), an increase of the fluorescence quantum yields was observed and Φ_{fl} becomes almost unity in tetrachloromethane.

This behavior is in contrast to that of tetraphenoxy-substituted perylene bisimide **8** which exhibits quantum yields of almost unity over a wide range of solvent polarity (Table 9).[36a] This behavior is rationalized by the decreased electron-donating ability of the aryloxy residue which cannot provide an exothermic charge separated state according to equation 3-7.

Table 9. Fluorescence Quantum Yields of APBI **8** in Different Solvents[36a]

solvent	cyclohexane	benzene	xylene	$CHCl_3$	THF	1-BuOH	ethanol	methanol
Φ_{fl}	1.01	1.04	0.97	0.96	1.01	0.97	0.91	0.90

By comparing the dependence of the fluorescence quantum yields on the solvent polarity of the four APBIs investigated here (see Figure 17) some general conclusions can be drawn. The fluorescence quantum yields of these APBIs are strongly dependent on the oxidation potential of the aryloxy donor (E_{ox}) and weakly dependent on the conformation. These features can all be rationalized with equation 3-7. Thus, a photoinduced electron transfer process is a very plausible quenching mechanism for APBI. From these results, it is apparent that APBIs with high fluorescence quantum yields in polar solvents should bear electron-poor aryloxy-residues. Indeed, such fluorophores have recently been introduced by Müllen and co-workers which exhibit high fluorescence quantum yields even in the most polar solvent water.[3b,16a,b]

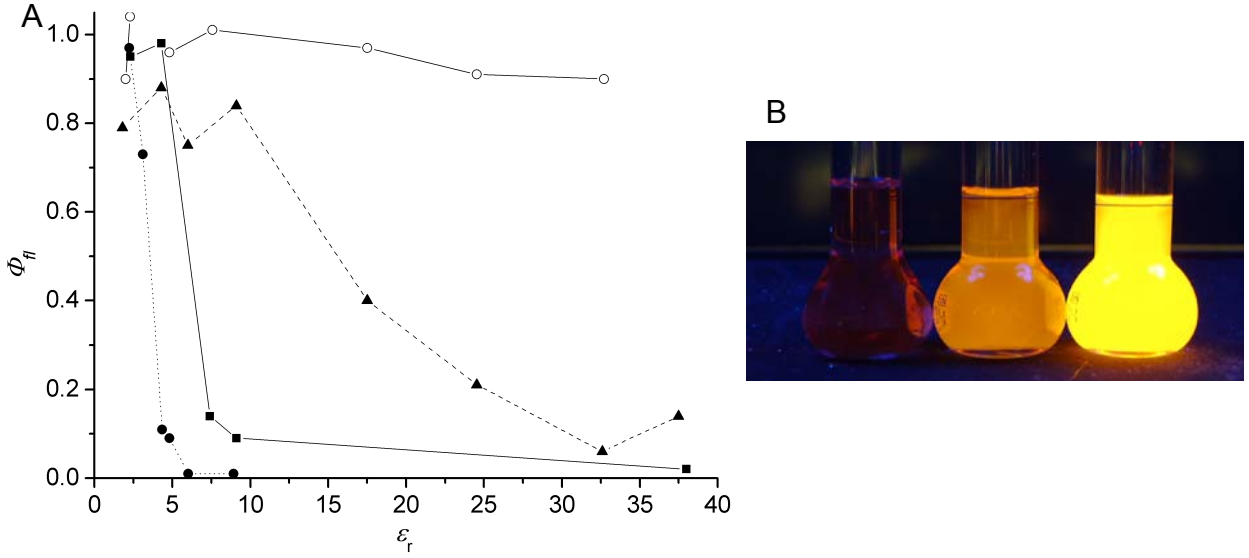

Figure 17. (A) Fluorescence quantum yields of **4** (triangles), **5b** (squares), **7** (circles) and **8** (open circles) in dependence on the solvent polarity (left) and (B) photograph of solutions of **5b** in dimethylsulfoxide (left), THF (middle) and diethylether (right) upon

irradiation at 258 nm. The solvent-dependent fluorescence quantum yields of **8** were taken from literature.[36a]

3.9 Conclusion

In summary, the synthesis of macrocyclic perylene bisimides **5a-d** and **6a-d** with different chain lengths was achieved by Williamson´s ether synthesis and their structures were elucidated by X-ray analysis and NMR spectroscopy. Whilst diagonally bridged derivatives **5a-d** exhibit a rigid twisted core, atropo-enantiomeric laterally bridged macrocycles **6a-d** interconvert on a similar time scale as open-chained APBIs like **2**, according to dynamic NMR spectroscopy. Based on the fact that the spectroscopic data of the diagonally bridged isomers **5a-d** differ significantly from those of reference compound **4**, it can be concluded that conformationally non-restricted APBIs do not exhibit a perpendicular orientation of the aryloxy residues in solution. Instead, based on the observed optical properties of the macrocyclic perylene bisimides **6a-d**, which are similar to reference compound **4**, a conformation with horizontal orientation of the aryloxy groups is most likely for tetraaryloxy-substituted perylene bisimides such as **4** in solution. The detailed analysis of the absorption and fluorescence properties of isomers **5a-d** showed that the degree of conjugation between the electron rich aryloxy residue (+M effect) and the electron poor perylene bisimide core depends on the conformation of the aryloxy residue. Under consideration of the solvent dependent fluorescence properties of APBIs **4**, **7** and **8** as well as macrocycle **5b**, it can be concluded that a photoinduced electron transfer from the electron-rich aryloxy substituent to the electron-deficient perylene core is the most reasonable explanation for the fluorescence quenching of APBIs. Based on these results, aryloxy substituents with an oxidation potential larger than 1.28 V (in CH_2Cl_2 vs. ferrocene) are recommended to achieve highly fluorescent dyes from this class of chromophores in highly polar solvents like alcohols and water.

3.10 Experimental Section

Materials and Methods. Cesium carbonate (99%) purchased from Aldrich (Steinheim, Germany) and dry DMSO (SeccoSolv) obtained from Merck (Darmstadt, Germany) were used as received. *N,N´*-Di(2,6-di*iso*propylphenyl)-1,6,7,12-tetrachloroperylene-3,4:9,10-tetracarboxylic acid bisimide **1** was donated from BASF AG. Perylene bisimides **2-4**[22] and oligoethylene glycol ditosylates[39] were synthesized according to literature procedures.

Flash column chromatography was performed using silica gel Si60 (40-63 µm) from Merck (Hohenbrunn, Germany). Melting points were determined on a Olympus Bx41 polarization microscope and are uncorrected. ^{1}H NMR spectra were recorded on Bruker Advance 400 and calibrated to the internal standard TMS or the residual solvent peak. MALDI-TOF mass spectra were recorded on a Bruker-Franzen Reflex EA240 instrument (at the Institute of Organic Chemistry at the University of Ulm/Germany) and high resolution mass spectra on a ESI MicrOTOF Focus from Bruker Daltonics. Analytical HPLC was performed on a system (PU 2080 PLUS) with a diode array detector (MD 2015) from JASCO equipped with a ternary gradient unit (LG 2080-02) and line-degasser (DG-2080-533). Preparative HPLC was done on a system (PU 2080 PLUS) with a diode array detector (UV 2077 PLUS) from JASCO. HPLC grade solvents (Rectapur) from VWR (Darmstadt, Germany) were used. As column Nucleodur 100-7 C18 ec (Macherey-Nagel; Düren, Germany) was used in the analytical (Ø = 4.6 mm) as well as in the semi-preparative size (Ø = 21 x 250 mm).

Temperature dependent ^{1}H NMR spectroscopy. Temperature-dependent NMR spectroscopy was performed on a Bruker Advance DMX 600 and the spectra referred to the residual solvent peak. Solutions used for high temperature ^{1}H NMR spectroscopy were degassed by three freeze-pump-thaw-cycles and the tubes were molten under vacuum (10^{-3} mbar). The temperature was calibrated to the temperature dependent chemical shift of methanol. Coalescence temperature were determined from spectral broadening and the data evaluated using the coalescence method according to equation 3-1 and 3-2.

Spectroscopy. For all spectroscopic measurements spectroscopic grade solvents (Uvasol®) from Merck (Hohenbrunn, Germany) were used. UV/Vis spectra were recorded on a Perkin Elmer UV/Vis spectrometer Lamda 40 P and fluorescence spectra with a PTI QM-4/2003. All fluorescence measurements were performed under aerobic conditions and fluorescence spectra are corrected. The fluorescence quantum yields were determined as the average value for three different excitation wavelengths using *N,N´*-bis(2,6-diisopropylphenyl)-1,6,7,12-tetraphenoxyperylene-3,4:9,10-tetracarboxylic acid bisimide as reference (Φ_{fl} = 0.96 in chloroform) by applying high dilution conditions (A < 0.05).[36a,40] Fluorescence lifetimes were determined with a PTI GL3330 nitrogen laser and a GL302 dye laser. Decay curves were evaluated with the Felix Software from PTI by fitting 1-4 lifetimes. The quality of the fit was judged by Derbin-Watson factor DW

and χ^2 (for monoexponential decay DW > 1.7 and 0.9 < χ^2 < 1.2) as well as by the correlation function and the residuals.

Cyclic voltammetry. Cyclic voltammetry was performed on a standard commercial electrochemical analyzer (εpsilon; BAS Inc.) in a three electrode single-component cell under argon. Dichloromethane (HPLC grade) was obtained from J. T. Baker (Mumbai, India) and dried over calcium hydride and degassed prior to use. The supporting electrolyte tetrabutylammonium hexafluorophosphate (TBAHFP) was synthesized according to literature[41], recrystallized from ethanol/water and dried in high vacuum. The measurements were carried out under exclusion of air and moisture at a concentration of 10^{-4} M with ferrocene as internal standard for the calibration of the potential. Working electrode: Pt disc; reference electrode: Ag/AgCl; auxiliary electrode: Pt wire.

Computational Details. The geometries of **2** (bearing methyl as imide substituent) were optimized using an MM2 force field with the parameter given in CaChe quantum CaChe workspace 5.0. The dihedral angle was adjusted and fixed before the geometrical optimization and read out after optimization. The calculation was done for twist angles in the range of 0-75° and only for one enantiomer (twist angles from 0-(–75°)). The obtained heat of formation was referred to the energetical minimum, plotted against the dihedral angles and fitted with equation 3-7 in order to obtain a function which can be used to calculate the population of different conformations.

$$E(\theta) = a\left|\theta^2\right| + b\left|\theta\right| + c \quad \text{(eq. 3-7)}$$

The best fit obtained delivered the parameter a = 0.08076, b = -4.53163 and c = 66. The population in dependence of the dihedral angle θ was calculated for the different conformations according to Boltzmann statistics (eq. 3-8) at a temperature of 293 K and normalized by dividing through the integral of this function Z.[42]

$$P(\theta) = \frac{e^{-\frac{E(\theta)}{RT}}}{Z} \quad \text{and} \quad Z = \int e^{-\frac{E(\theta)}{RT}} d\theta \quad \text{(eq. 3-8)}$$

Additionally the geometries of APBI **2** and diagonally bridged macrocycles **5a-d** were optimized by the semi-empirical AM 1 method as implemented in CaChe Quantum CaChe Workspace 5.0.

Synthesis of Macrocyclic Perylene Bisimides 5 and 6

General procedure for macrocyclisation:

Perylene bisimide **3** (1eq), cesium carbonate (16 eq) and the corresponding oligoethylene glycol ditosylates (5-6eq) were suspended under argon in DMSO and heated for 5 h at 100 °C. The reaction mixture was cooled to room temperature and dropped under stirring to 0.33 M hydrochloric acid (150 mL). The resulting precipitate was collected by filtration and dried in vacuum. The crude product was applied on silica gel column chromatography and the resulting macrocycles were isolated by precipitation from dichloromethane with a polar or non-polar solvent. The precipitate was collected by filtration and dried in vacuo (10^{-3} mbar) at 60 °C.

Macrocycles 5a and 6a:

Macrocycles **5a** and **6a** were synthesized according to the general procedure by reaction of **3** (410 mg, 0.36 mmol), ethylene glycol ditosylate (820 mg, 2.21 mmol) and cesium carbonate (1.92 g, 5.90 mmol) in DMSO (65 mL). Column chromatography on silica gel eluting with dichloromethane and reprecipitation from dichloromethane and methanol yielded 4.1 mg (3.43 µmol, 1%) of **5a** as orange crystals and 22.9 mg (19.2 µmol, 5%) of **6a** as orange-red crystals.

5a: Mp: 423–425 °C. ^{1}H NMR (400 MHz, $CDCl_3$, TMS): δ 8.37 (s, 4H), 7.50 (t, *J* = 7.7, 2H), 7.35 (d, *J* = 7.7, 4H), 7.19–7.13 (m, 8H), 6.37 (dd, *J* = 7.6, *J* = 1.9, 4H), 5.27 (t, *J* = 2.2 Hz, 4H), 3.69 (m, 4H), 3.48 (m, 4H), 2.72 (q, *J* = 6.9, 4H), 1.21 and 1.19 ppm (d, *J* = 6.9, 24H); (400 MHz, CD_2Cl_2): δ 8.35 (s, 4H), 7.44 (t, *J* = 7.8, 2H), 7.27 (d, *J* = 7.6, 4H), 7.05 (m, 8H), 6.28 (m, 4H), 3.56 (m, 4H), 3.40 (m, 4H), 2.62 (q, *J* = 6.8, 4H), 1.09 and 1.06 ppm (d, *J* = 6.8, 24H). MS (MALDI-TOF, pos. mode, dithranol): *m/z*: 1195.6 $[M+H]^+$ (calcd. 1194.4). HRMS (ESI-TOF, pos. mode, CH_2Cl_2:acetonitrile = 1:1): *m/z* calcd for $C_{76}H_{63}N_2O_{12}$ 1195.4376 $[M+H]^+$, found 1195.4360. UV/Vis (CH_2Cl_2): λ_{max}/nm (ε_{max}/$M^{-1}cm^{-1}$) 544 (43500), 505 (27600), 474 (14100, sh), 436 (11600), 278 (42000). Fluorescence (CH_2Cl_2): λ_{max} = 562 nm; fluorescence quantum yield Φ_{fl} = 0.02, fluorescence lifetime τ_{fl} < 0.5 ns (λ_{ex} = 520 nm, λ_{em} = 580 nm). CV (CH_2Cl_2, 0.1 M TBAHFP, 100 mV/s): E(PBI/PBI^-) = –0.97 V, E(PBI^-/PBI^{2-}) = –1.30 V.

6a: Mp: > 500 °C. ^{1}H NMR (400 MHz, $CDCl_3$, TMS): δ 8.47 (s, 4H), 7.45 (t, *J* = 7.7, 2H), 7.30 (d, *J* = 7.7, 4H), 7.17 (t, *J* = 8.1, 4H), 6.71 (d, *J* = 8.3, 4H), 6.48 (t, = 2.3, 4H), 6.43 (dd, *J* = 7.6, *J* = 1.9, 4H), 4.43 (s, 8H), 2.72 (q, *J* = 6.9, 4H), 1.16 and 1.13 ppm (d, *J* = 6.9 Hz, 24H); (400 MHz, CD_2Cl_2): δ 8.36 (s, 4H), 7.39 (t, *J* = 7.8, 2H), 7.23 (d, *J* = 7.8,

4H), 7.10 (t, *J* = 8.2, 4H), 6.65 (ddd, *J* = 8.3, *J* = 2.4, *J* = 0.9, 4H), 6.36 (m, 8H), 4.36 (s, 8H), 2.63 (q, *J* = 6.8, 4H), 1.03 and 1.00 ppm (d, *J* = 6.8 Hz, 24H). MS (MALDI-TOF, pos. mode, dithranol): *m/z*: 1195.6 $[M+H]^+$ (calcd 1194.4). HRMS (ESI-TOF, pos. mode, CH_2Cl_2:acetonitrile = 1:1): *m/z* calcd for $C_{76}H_{63}N_2O_{12}$ 1195.4376 $[M+H]^+$, found 1195.4375. UV/Vis (CH_2Cl_2): λ_{max}/nm (ε_{max}/$M^{-1}cm^{-1}$) 554 (43600), 517 (28600), 448 (14500), 284 (50100), 263 (38000). Fluorescence (CH_2Cl_2): λ_{max} = 588 nm, fluorescence quantum yield Φ_{fl} = 0.78, fluorescence lifetime τ_{fl} = 5.4 ns (λ_{ex} = 520 nm, λ_{em} = 600 nm). CV (CH_2Cl_2, 0.1 M TBAHFP, 100 mV/s): E(PBI/PBI^-) = –1.07 V, E(PBI^-/PBI^{2-}) = –1.32 V, E(PBI/PBI^+) = +1.05 V.

Macrocycles 5b and 6b

Perylene bisimide **3** (220 mg, 0.19 mmol), diethylene glycol ditosylate (435 mg, 1.05 mmol) and cesium carbonate (713 mg, 2.19 mmol) were reacted according the general procedure in DMSO (30 mL). The two regioisomers were separated by silica gel column chromatography with dichloromethane and precipitation with methanol afforded 17.1 mg (13.3 µmol, 7%) of **5b** as orange crystals and 37.0 mg (28.8 µmol, 15%) of **6b** as red powder.

5b: Mp 374–376 °C. ^{1}H NMR (400 MHz, $CDCl_3$, TMS) : δ 8.32 (s, 4H), 7.47 (t, *J* = 7.5, 2H), 7.33 (d, *J* = 7.5, 4H), 7.22 (t, *J* = 8.3, 4H), 7.16 (ddd, *J* = 8.3, *J* = 2.3, *J* = 0.8, 4H), 6.46 (ddd, *J* = 8.3, *J* = 2.3, *J* = 0.8, 4H), 5.73 (t, *J* = 2.3, 4H), 3.94–3.89 (m, 4H), 3.72–3.64 (m, 8H), 3.58–3.55 (m, 4H), 2.82 (q, *J* = 6.9, 4H), 1.19 and 1.17 ppm (d, *J* = 6.9 Hz, 24H); (400 MHz, CD_2Cl_2) : δ 8.32 (s, 4H), 7.48 (t, *J* = 7.6, 2H), 7.31 (m, 8H), 7.20 (ddd, *J* = 8.2, *J* = 2.3, *J* = 0.9, 4H), 6.49 (ddd, *J* = 8.2, *J* = 2.3, *J* = 0.9, 4H), 5.72 (t, *J* = 2.3, 4H), 3.85–3.80 (m, 4H), 3.70–3.50 (m, 12H), 2.72 (q, *J* = 6.8, 4H), 1.11 and 1.09 ppm (d, *J* = 6.8 Hz, 24H). MS (MALDI-TOF, pos. mode, dithranol): *m/z*: 1283.8 $[M+H]^+$ (calcd 1282.5). HRMS (ESI-TOF, pos. mode, CH_2Cl_2:acetonitrile = 1:1): *m/z* calcd for $C_{80}H_{71}N_2O_{14}$ 1283.4900 $[M+H]^+$, found 1283.4898, 1305.4713 $[M+Na]^+$. UV/Vis (CH_2Cl_2): λ_{max}/nm (ε_{max}/$M^{-1}cm^{-1}$) 534 (41700), 499 (27500), 467 (14500), 436 (11600), 265 (42000). Fluorescence (CH_2Cl_2): λ_{max} = 573 nm, fluorescence quantum yield Φ_{fl} = 0.09, fluorescence lifetime τ_{fl} = 0.8 ns (λ_{ex} = 520, λ_{em} = 580 nm). CV (CH_2Cl_2, 0.1 M TBAHFP, 100 mV/s): E(PBI/PBI^-) = –1.06 V, E(PBI^-/PBI^{2-}) = –1.38 V, E(PBI/PBI^+) = +1.16 V.

6b: Mp: 365–367 °C, ^{1}H NMR (400 MHz, $CDCl_3$, TMS): δ 8.38 (s, 4H), 7.43 (t, *J* = 7.8, 2H), 7.28 (d, *J* = 7.8, 4H), 7.08 (t, *J* = 8.3, 4H), 6.72 (t, *J* = 7.6, *J* = 1.9, 4H), 6.60–6.55

(m, 8H), 4.18 (bs, 8H), 3.94 (bs, 4H), 3.79 (bs, 4H), 2.71 (q, *J* = 6.8, 4H), 1.14 ppm (bs, 24H). MS (MALDI-TOF, pos. mode, dithranol): *m/z*: 1283.7 $[M+H]^+$ (calcd 1282.5). HRMS (ESI-TOF, pos. mode, CH_2Cl_2:acetonitril = 1:1): *m/z* calcd for $C_{80}H_{71}N_2O_{14}$ 1283.4900 $[M+H]^+$, found 1283.4850, 1305.4723 $[M+Na]^+$. UV/Vis (CH_2Cl_2): λ_{max}/nm (ε_{max}/$M^{-1}cm^{-1}$) 576 (46700), 536 (28600), 451 (15400), 285 (48800), 265 (37500). Fluorescence (CH_2Cl_2): λ_{max} = 605 nm, fluorescence quantum yield Φ_{fl} = 0.82, fluorescence lifetime τ_{fl} = 5.3 ns (λ_{ex} = 520, λ_{em} = 600 nm). CV (CH_2Cl_2, 0.1 M TBAHFP, 100 mV/s): E(PBI/PBI^-) = –1.11 V, E(PBI^-/PBI^{2-}) = –1.30 V, E(PBI/PBI^+) = +0.91 V.

Macrocycles 5c and 6c

The macrocycles **5c** and **6c** were synthesized according to the general procedure by reaction of **3** (197 mg, 0.17 mmol), triethylene glycol ditosylate (518 mg, 1.03 mmol) and cesium carbonate (900 mg, 2.72 mmol) in DMSO (30 mL). After column chromatographic purification on silica gel with dichloromethane (0.3 % methanol) and reprecipitation from dichloromethane with methanol, 4.7 mg (1.60 µmol, 2%) of **5c** were obtained as an orange solid and 21.1 mg (15.3 µmol, 8%) of **6c** as wine-red solid.

5c: Mp: 370–372 °C. ^{1}H NMR (400 MHz, $CDCl_3$, TMS): δ8.29 (s, 4H), 7.45 (t, *J* = 7.7, 2H), 7.32–7.30 (m, 8H), 7.14 (dd, *J* = 8.0, *J* = 2.3, 4H), 6.56 (dd, *J* = 8.0, *J* = 2.2, 4H), 6.03 (t, *J* = 2.3, 4H), 3.93–3.88 (m, 4H), 3.79–3.74 (m, 4H), 3.69–3.50 (m, 16H), 2.77 (q, *J* = 6.9, 4H), 1.16 and 1.14 (d, *J* = 6.4, 24H); (400 MHz, CD_2Cl_2): δ8.28 (s, 4H), 7.47 (t, *J* = 7.6, 2H), 7.38 (t, *J* = 8.2, 4H), 7.30 (d, *J* = 7.8, 4H), 7.21 (ddd, *J* = 8.4, *J* = 2.3, *J* = 0.8, 4H), 6.61 (ddd, *J* = 8.4, *J* = 2.4, *J* = 0.9, 4H), 6.09 (t, *J* = 2.4, 4H), 3.93–3.87 (m, 4H), 3.83–3.78 (m, 4H), 3.67–3.56 (m, 16H), 2.77 (q, *J* = 6.8, 4H), 1.16 and 1.14 (d, *J* = 6.8, 24H). MS (MALDI-TOF, pos. mode, dithranol): *m/z*: 1371.8 $[M+H]^+$ (calcd. 1370.5). HRMS (APCI, pos. mode, chloroform): *m/z* calcd for $C_{84}H_{79}N_2O_{16}$ $[M+H]^+$ 1371.5424, found 1371.5440. UV/Vis (CH_2Cl_2): λ_{max}/nm (ε_{max}/$M^{-1}cm^{-1}$) 545 (37700), 513 (26500, sh), 449 (13700), 281 (42800). Fluorescence (CH_2Cl_2): λ_{max} = 582 nm, fluorescence quantum yield Φ_{fl} = 0.43, fluorescence lifetime τ_{fl} = 2.7 ns (λ_{ex} = 520, λ_{em} = 580 nm); CV (CH_2Cl_2, 0.1 M TBAHFP, 100 mV/s): E(PBI/PBI^-) = –1.13 V, E(PBI^-/PBI^{2-}) = –1.39 V, E(PBI/PBI^+) = +1.09 V.

6c: Mp: 314–315 °C, ^{1}H NMR (400 MHz, $CDCl_3$, TMS): δ 8.30 (s, 4H), 7.43 (t, *J* = 7.8, 2H), 7.27 (d, *J* = 7.8, 4H), 7.13 (t, *J* = 8.2 Hz, 4H), 6.70 (t, *J* = 2.4, 4H), 6.65 (ddd, *J* = 8.4, *J* = 2.4, *J* = 0.8, 4H), 6.56 (ddd, *J* = 8.2, *J* = 2.2, *J* = 0.8, 4H), 4.07–4.02 (m, 8H),

3.85 (bs, 8H), 3.79–3.73 (m, 8H), 2.71 (q, *J* = 6.8, 4H), 1.13 (bd, *J* = 6.8, 24H); (400 MHz, CD_2Cl_2): δ 8.21 (s, 4H), 7.47 (t, *J* = 7.8, 2H), 7.27 (d, ^3J = 7.8, 4H), 7.20 (t, *J* = 8.1 Hz, 4H), 6.73 (m, 8H), 6.58 (ddd, *J* = 8.1, *J* = 2.3, *J* = 0.8, 4H), 4.03 (m, 8H), 3.81 (m, 8H), 3.68 (m, 8H), 2.70 (q, *J* = 6.8, 4H), 1.09 (d, *J* = 6.8, 24H). MS (MALDI-TOF, pos. mode, dithranol): *m/z*: 1371.9 $[M+H]^+$ (calcd 1370.5). HRMS (ESI-TOF, pos. mode, CH_2Cl_2:acetonitrile = 1:1): *m/z* calcd for $C_{84}H_{78}N_2O_{16}Na$ $[M+Na]^+$: 1393.5203; found: 1393.5245. UV/Vis (CH_2Cl_2): λ_{max}/nm (ε_{max}/$M^{-1}cm^{-1}$) 580 (49400), 539 (29900), 450 (16600), 287 (53500), 268 (43300). Fluorescence (CH_2Cl_2): λ_{max} = 606 nm, fluorescence quantum yield Φ_{fl} = 0.84, fluorescence lifetime τ_{fl} = 5.6 ns (λ_{ex} = 520, λ_{em} = 600 nm). CV (CH_2Cl_2, 0.1 M TBAHFP, 100 mV/s): E(PBI/PBI^-) = –1.14 V, E(PBI^-/PBI^{2-}) = –1.35 V, E(PBI/PBI^+) = +0.90 V.

Synthesis of macrocycles 5d and 6d:

Perylene bisimide **3** (197 mg, 0.17 mmol), tetraethylene glycol ditosylate (518 mg, 1.03 mmol) and cesium carbonate (900 mg, 2.72 mmol) were reacted in DMSO (30 mL) according to the general procedure. The two isomeric macrocycles were separated by silica gel column chromatography with dichloromethane and a gradient of 0.3%-1% of methanol. Additional purification by HPLC (Nucleodur 100-7 C18 ec, eluent: methanol) of the first eluted fraction and precipitation with *n*-hexane afforded 7.2 mg (4.93 µmol, 3%) of **5d** as orange crystals. Column chromatography of the second eluted fraction with dichloromethane (0.5% methanol) and reprecipitation from dichloromethane and methanol yielded 12.8 mg (8.76 µmol, 5%) of **6d** as a red-solid.

5d: Mp: 372–374 °C. Retention time t_R (Nucleodur 100-7 C18 ec, methanol, 1ml/min) = 10.8 min. ^{1}H NMR (400 MHz, $CDCl_3$, TMS): δ 8.26 (s, 4H), 7.45 (t, *J* = 7.8, 2H), 7.30 (m, 8H), 7.01 (ddd, *J* = 8.2, *J* = 2.3, *J* = 0.8, 4H), 6.61 (ddd, *J* = 8.3, *J* = 2.4, *J* = 0.8, 4H), 6.20 (t, *J* = 2.3, 4H), 3.99–3.93 (m, 4H), 3.87-3.82 (m, 4H), 3.68–3.66 (m, 8H), 3.58–3.56 (m, 16H), 2.75 (sept., *J* = 6.8, 4H), 1.14 and 1.14 ppm (d, *J* = 6.8, 24H); (400 MHz, CD_2Cl_2): δ 8.21 (s, 4H), 7.42 (t, *J* = 7.8, 2H), 7.36–7.30 (m, 8H), 7.05 (ddd, *J* = 8.1, *J* = 2.3, *J* = 0.8, 4H), 6.65 (ddd, *J* = 8.3, *J* = 2.3, *J* = 0.8, 4H), 6.24 (t, *J* = 2.3, 4H), 3.96–3.91 (m, 4H), 3.86–3.81 (m, 4H), 3.64–3.61 (m, 8H), 3.52–3.45 (m, 16H), 2.70 (sept., *J* = 6.8, 4H), 1.09 (d, *J* = 6.8, 24H). MS (MALDI-TOF, pos. mode, dithranol): *m/z*: 1459.6 $[M+H]^+$ (calcd 1458.6). HRMS (ESI-TOF, pos. mode, CH_2Cl_2:acetonitrile = 1:1): *m/z* calcd for $C_{88}H_{87}N_2O_{18}$ $[M+H]^+$ 1459.5948; found: 1459.5962. UV/Vis (CH_2Cl_2): λ_{max}/nm (ε_{max}/$M^{-1}cm^{-1}$) 558 (46700), 521 (30800), 450 (15700), 288 (54300), 278 (41500). Fluorescence (CH_2Cl_2): λ_{max} = 588 nm, fluorescence quantum yield Φ_{fl} = 0.90, fluorescence lifetime τ_{fl}

= 5.5 ns (λ_{ex} = 520, λ_{em} = 580 nm). CV (CH_2Cl_2, 0.1 M TBAHFP, 100 mV/s): E(PBI/PBI$^-$) = –1.17 V, E(PBI$^-$/PBI^{2-}) = –1.39 V, E(PBI/PBI$^+$) = +0.98 V.

6d: Mp: 314–315 °C. ^{1}H NMR (400 MHz, $CDCl_3$, TMS): δ 8.27 (s, 4H), 7.43 (t, *J* = 7.7, 2H), 7.28–7.27 (d, 4H), 7.15 (t, *J* = 8.3, 4H), 6.69 (d, *J* = 8.5, 4H), 6.60–6.57 (m, 8H), 3.93–3.87 (bm, 16H), 3.71 (bs, 16H), 2.71 (quin, *J* = 6.8, 4H), 1.12 (d, *J* = 6.3, 24H); (400 MHz, CD_2Cl_2): δ 8.21 (s, 4H), 7.46 (t, *J* = 7.7, 2H), 7.31 (d, *J* = 7.7, 4H), 7.20 (t, *J* = 8.4, 4H), 6.74 (ddd, *J* = 8.4, *J* = 2.3, *J* = 1.0, 4H), 6.64–6.60 (m, 8H), 3.94 (bs, 8H), 3.82 (bm, 8H) 3.70–3.63 (bm, 16H), 2.70 (quin, *J* = 6.8, 4H), 1.10 (d, *J* = 6.8, 24H). MS (MALDI-TOF, pos. mode, dithranol): *m/z*: 1459.8 $[M+H]^+$ (calcd 1458.6). HRMS (ESI-TOF, pos. mode, CH_2Cl_2:acetonitrile = 1:1): *m/z* calcd for $C_{88}H_{87}N_2O_{18}$ $[M+H]^+$: 1459.5948, found 1459.5975. UV/Vis (CH_2Cl_2): λ_{max}/nm (ε_{max}/$M^{-1}cm^{-1}$) 577 (49200), 537 (30100), 449 (17200), 285 (51200), 267 (40400). Fluorescence (CH_2Cl_2): λ_{max} = 606 nm, fluorescence quantum yield Φ_{fl} = 0.82, fluorescence lifetime τ_{fl} = 5.5 ns (λ_{ex} = 520, λ_{em} = 600 nm). CV (CH_2Cl_2, 0.1 M TBAHFP, 100 mV/s): E(PBI/PBI$^-$) = –1.14 V, E(PBI$^-$/PBI^{2-}) = –1.36 V, E(PBI/PBI$^+$) = +0.90 V.

***N,N´*-Di(2,6-diisopropylphenyl)-1,6,7,12-tetra(4-butoxyphenoxy)perylene-3,4:9,10-tetracarboxylic acid bisimide 7**

Perylene bisimide **7** was synthesized according to literature.[36b]

^{1}H NMR (400 MHz, $CDCl_3$): δ 8.17 (s, 4H), 7.41 (t, *J* = 7.6, 2H), 7.28 (d, *J* = 7.7, 4H), 6.92 (m, 8H), 6.81 (m, 8H), 3.91 (t, *J* = 6.5, 8H), 2.69 (q, *J* = 6.8, 4H), 1.75 (m, 8H), 1.49 (m, 8H), 1.12 (d, *J* = 6.8, 24H), 0.97 (t, *J* = 7.4, 12H). MS (MALDI-TOF, pos. mode, DCTB): *m/z* 1367.4 $[M]^+$ (calcd 1367.7). Anal. calcd for $C_{80}H_{90}N_2O_{12}$: C; 77.28, H; 6.63, N; 2.05; found: C; 77.10, H; 6.76, N; 2.10. UV/Vis (CH_2Cl_2): λ_{max}/nm (ε_{max}/$M^{-1}cm^{-1}$) 593 (52600), 549 (30400), 458 (16100). Fluorescence (CH_2Cl_2): λ_{max} = 619 nm, fluorescence quantum yield Φ_{fl} < 0.01, fluorescence lifetime τ_{fl} < 0.4 ns (λ_{ex} = 520, λ_{em} = 600 nm).

Supporting Information Available in the Appendix: Estimation of twist angles by shape analysis of fluorescence spectra for APBI **4** and macrocycles **5a-d** and **6a-d**, solvent dependent NMR spectra of **6a**, details for the determination of transition dipole moments for **4** and macrocycles **5a-d**, optimized geometries of diagonally bridged isomers **5a-d**, temperature dependent NMR spectra of **6a-c**, ^{1}H NMR spectra of **5a-d** and **6a-d** and crystallographic details for **5b** and **6a**.

3.11 References and Notes

1 (a) G. Seybold, G. Wagenblast, *Dyes Pigm.* **1987**, *11*, 303-317; (b) G. Seybold, A. Stange (BASF AG), *Ger. Pat.*, DE 35 45 004, **1987** (*Chem. Abstr.* **1988**, *108*, 77134c).

2 (a) F. Würthner, *Chem. Commun.* **2004**, 1564-1579; (b) A. C. Grimsdale, K. Müllen, *Angew. Chem.* **2005**, *117*, 5732-5772; *Angew. Chem. Int. Ed.* **2005**, *44*, 5592-5629; (c) F. Würthner, *Pure Appl. Chem.* **2006**, *78*, 2341-2350; (d) M. R. Wasielewski, *J. Org. Chem.* **2006**, *71*, 5051-5066.

3 (a) T. D. M. Bell, S. Habuchi, S. Masuo, I. Österling, K. Müllen, P. Tinnefeld, M. Sauer, M. van der Auweraer, J. Hofkens, F. C. De Schryver, *Aust. J. Chem.* **2004**, *57*, 1169-1173; (b) A. Margineanu, J. Hofkens, M. Cotlet, S. Habuchi, A. Stefan, J. Qu, C. Kohl, K. Müllen, J. Vercammen, Y. Engelborghs, T. Gensch, F. C. De Schryver, *J. Phys. Chem. B* **2004**, *108*, 12242-12251; (c) F. C. De Schryver, T. Vosch, M. Cotlet, M. van der Auweraer, K. Müllen, J. Hofkens*, Acc. Chem. Res.* **2005**, *38*, 514-522; (d) E. Lang, F. Würthner, J. Köhler, *ChemPhysChem* **2005**, *6*, 935-941; *ChemPhysChem* **2006**, *7*, 292.

4 For OLEDs, see: (a) P. Ranke, I. Bleyl, J. Simmer, D. Haarer, A. Bacher, H. W. Schmidt, *Appl. Phys. Lett.* **1997**, *71*, 1332-1334; (b) P. Pösch, M. Thelakkat, H. W. Schmidt, *Syn. Met.* **1999**, *102*, 1110-1112; (c) F. Würthner, C. Thalacker, S. Diele, C. Tschierske, *Chem. Eur. J.* **2001**, *7*, 2245-2253; (d) L. Fan, W. Zhu, J. Li, H. Tian, *Syn. Met.* **2004**, *145*, 203-210; for PLEDs, see: (e) C. Ego, D. Marsitzky, S. Becker, J. Zhang, A. C. Grimsdale, K. Müllen, J. D. MacKenzie, C. Silva, R. H. Friend, *J. Am. Chem. Soc.* **2003**, *125*, 437-443; for solar cells and OFETS, see: (f) M. Thelakkat, , P. Pösch, H. W. Schmidt, *Macromolecules* **2001**, *34*, 7441-7447; (g) H. Tian, P.-H. Liu, F.-S. Meng, E. Gao, S. Cai, *Syn. Met.* **2001**, *121*, 1557-1558.

5 J. Baggerman, D. C. Jagesar, R. E. Vallée, J. Hofkens, F. C. De Schryver, F. Schelhase, F. Vögtle, A. M. Brouwer, *Chem. Eur. J.* **2007**, *13*, 1291-1299.

6 (a) F. Würthner, A. Sautter, D. Schmidt, P. J. A. Weber, *Chem. Eur. J.* **2001**, *7*, 894-902; (b) C.-C. You, F. Würthner, *J. Am. Chem. Soc.* **2003**, *125*, 9716-9725; (c) C.-C. You, C. Hippius, M. Grüne, F. Würthner, *Chem. Eur. J.* **2006**, *12*, 7510-7519.

7 C. Addicott, I. Österling, T. Yamamoto, K. Müllen, P. J. Stang, *J. Org. Chem.* **2005**, *70*, 797-801.

8 (a) R. Dobrawa, M. Lysteska, P. Ballester, M. Grüne, F. Würthner, *Macromolecules* **2005**, *38*, 1315-1325; (b) Y. Li, N. Wang, H. Gan, H. Liu, H. Li, Y. Li, X. He, C. Huang, S. Cui, S. Wang, D. Zhu, *J. Org. Chem.* **2005**, *70*, 9686-9692.

9 (a) F. Würthner, B. Hanke, M. Lysetska, G. Lambright, G. S. Harms, *Org. Lett.* **2005**, *7*, 967-970; for organogels based on diaryloxy-substituted perylene bisimides, see: (b) K. Sugiyasu, N. Fujita, S. Shinkai, *Angew. Chem.* **2004**, *116*, 1249-1253; *Angew. Chem. Int. Ed.* **2004**, *43*, 1229-1233; (c) Y. Liu, Y. Li, H. Gan, H. Liu, Y. Li, J. Zhuang, F. Lu, D. Zhu, *J. Org. Chem.* **2004**, *69*, 9049-9054.

10 (a) Y. Liu, J. Zhuang, H. Liu, Y. Li, F. Lu, H. Gan, T. Jiu, N. Wang, X. He, D. Zhu, *ChemPhysChem* **2004**, *5*, 1210-1215; (b) C. Hippius, F. Schlosser, M. O. Vysotsky, V. Böhmer, F. Würthner, *J. Am. Chem. Soc.* **2006**, *128*, 3870-3871; for examples of diaryloxy-substituted perylene bisimides, see: (c) A. S. Lukas, Y. Zhao, S. E. Miller, M. R. Wasielwski, *J. Phys. Chem. B* **2002**, *106*, 1299-1306; (d) M. J. Ahrens, L. E. Sinks, B. Rybtchinski, W. Liu, B. A. Jones, J. M. Giaimo, A. V. Gusev, A. J. Goshe, D. M. Tiede, M. R. Wasielwski, *J. Am. Chem. Soc.* **2004**, *126*, 8284-8294;

11 (a) D. Liu, S. De Feyter, M. Cotlet, A. Stefan, U.-M. Wiesler, A. Herrmann, D. Grebel-Koehler, J. Qu, K. Müllen, F. C. De Schryver, *Macromolecules* **2003**, *36*, 5918–5925; (b) J. Qu, N. G. Pschirer, D. Liu, A. Stefan, F. C. De Schryver, K. Müllen, *Chem. Eur. J*. **2004**, *10*, 528–537; (c) C.-C. You, C. R. Saha-Möller, F. Würthner, *Chem. Commun.* **2004**, 2030-2031; (d) J. Pan, W. Zhu, S. Li, W. Zeng, Y. Cao, H. Tian, *Polymer* **2006**, *46*, 7658-7669; (e) J. Pan, W. Zhu, S. Li, J. Xu, H. Tian, *Eur. J. Org. Chem.* **2006**, 986-1001; (f) M. D. Yilmaz, O. A. Bozdemir, E. U. Akkaya, *Org. Lett*. **2006**, *8*, 2871-2873; for a 1,7-disubstituted perylene bisimde, see: (g) T. Ishi-i, K.-i. Murakami, Y. Imai, S. Mataka, *J. Org. Chem.* **2006**, *71*, 5752-5760.

12 (a) A. P. H. J. Schenning, J. v. Herrikhuyzen, P. Jonkheijm, Z. Chen, F. Würthner, E. W. Meijer, *J. Am. Chem. Soc.* **2002**, *124*, 10252-10253; (b) E. H. A. Beckers, S. C. J. Meskers, A. P. H. J. Schenning, Z. Chen, F. Würthner, P. Marsal, D. Beljonne, J. Cornil, R. A. J. Janssen, *J. Am. Chem. Soc.* **2006**, *128*, 649-657; (c) E. H. A. Beckers, Z. Chen, S. C. J. Meskers, P. Jonkheijm, A. P. H. J. Schenning, X.-Q. Li, P. Osswald, F. Würthner, R. A. J. Janssen, *J. Phys. Chem. B* **2006**, *110*, 16967-16978.

13 (a) C.-C. You, F. Würthner, *Org. Lett.* **2004**, *6*, 2401-2404; (b) A. Prodi, C. Chiroboli, F. Scandola, E. Iengo, E. Alessio, R. Dobrawa, F. Würthner, *J. Am. Chem. Soc.* **2005**, *127*, 1454-1462; (c) N. Wang, F. Lu, C. Huang, Y. Li, M. Yuan, X. Liu, H. Liu, L. Gan, L. Jiang, D. Zhu, *J. Poly. Sci. A* **2006**, *44*, 5863-5874; for examples of diaryloxy-substituted perylene bisimides, see: (d) T. van der Boom, R. T. Hayes, Y. Zhao, P. J. Bushard, E. A. Weiss, M. R. Wasielewski, *J. Am. Chem. Soc.* **2002**, *124*, 9582-9590; (e) X. He, H. Liu, Y. Li, Y. Liu, F. Lu, Y. Li, D. Zhu, Macromol. *Chem. Phys.* **2005**, *206*, 2199-2205; (f) S. Xiao, M. E. El-Khouly, Y. Li, Z. Gan, H. Liu, L. Jiang, Y. Araki, O. Ito, D. Zhu, *J. Phys. Chem. B* **2005**, *109*, 3658-3667.

14 B. K. Kaletas, R. Dobrawa, A. Sautter, F. Würthner, M. Zimine, L. De Cola, R. M. Williams, *J. Phys. Chem. A* **2004**, *108*, 1900–1909.

15 (a) Y. Liu, S. Xiao, H. Li, Y. Li, H. Liu, F. Lu, J. Zhuang, D. Zhu, *J. Phys. Chem. B* **2004**, *108*, 6256-6260; (b) J. Hua, F. Ding F. S. Meng, H. Tian, *Chin. Chem. Lett.* **2004**, *15*, 1373-1376; (c) J. Hua, F. Meng, F. Ding, F. Li, H. Tian, *J. Mater. Chem.* **2004**, *14*, 1849-1853; for examples of diaryloxy-substituted perylene bisimides, see: (d) Y. Liu, N. Wang, Y. Li, H. Liu, Y. Li, J. Xiao, X. Xu, C. Huang, S. Cui, D. Zhu, *Macromolecules* **2005**, *38*, 4880-4887; (e) J. Zhuang, W. Zhou, X. Li, Y. Li, N. Wang, X. He, H. Liu, Y. Li, L. Jiang, C. Huang, S. Cui, S. Wang, D. Zhu, *Tetrahedron* **2005**, *61*, 8686-8693.

16 (a) M. A. Abdalla, J. Bayer, J. O. Rädler, K. Müllen, *Angew. Chem.* **2004**; *116*, 4057–4060; *Angew. Chem. Int. Ed.* **2004**, *43*, 3967–3970; (b) C. Kohl, T. Weil, J. Qu, K. Müllen, *Chem. Eur. J.* **2004**, *10*, 5297-5310; (c) S. Krauß, M. Lysetska, F. Würthner, *Lett. Org. Chem.* **2005**, *2*, 349-353.

17 J. Ren, X.-L. Zhao, Q.-C. Wang, C.-F. Ku, D.-H. Qu, C.-P. Chang, H. Tian, *Dyes Pigm.* **2005**, *64*, 193-200.

18 J. Hofkens, T. Vosch, M. Maus, F. Köhn, M. Cotlet, T. Weil, A. Herrmann, K. Müllen, F. C. De Schryver, *Chem. Phys. Lett.* **2001**, *333*, 255–263.

19 A. Sautter, C. Thalacker, F. Würthner, *Angew. Chem.* **2001**, *113*, 4557-4560; *Angew. Chem. Int. Ed.* **2001**, *40*, 4425-4428.

20 (a) M. Cotlet, S. Masuo, M. Lor, E. Fron, M. Van der Auweraer, K. Müllen, J. Hofkens, F. C. De Schryver, *Angew. Chem.* **2004**, *45*, 6242-6246; *Angew. Chem. Int. Ed.* **2004**, *116*, 6116-6120; (b) C. Flors, I. Oesterling, E. Fron, G. Schweitzer, M. Sliwa, A. Herrmann, M. van der Auweraer, F. C. De Schryver, K. Müllen, J.

Hofkens, *J. Phys. Chem. C* **2007**, *111*, 4861-4870; for a recent comparison of different diarylsubstituted perylene bisimides, see: (b) C.-C. Chao, M.-k. Leung, Y. O. Su, K.-Y. Chiu, T.-H. Lin, S.-J. Shieh, S.-C. Lin, *J. Org. Chem.* **2005**, *70*, 4323-4331.

21 A part of this work has been communicated in P. Osswald, D. Leusser, D. Stalke, F. Würthner, *Angew. Chem.* **2005**, *117*, 254-257, *Angew. Chem. Int. Ed.* **2005**, *44*, 250-253.

22 (a) S. Hien, PhD Thesis, University of Regensburg (Germany), **1995**; (b) P. Osswald, Diploma Thesis, University of Ulm (Germany), **2002**.

23 (a) U. Lüning, M. Müller, *Chem. Ber.* **1990**, *123*, 643-645; (b) G. Ferguson, A. J. Lough, A. Notti, S. Pappalardo, M. F. Parasi, A. Petringa, *J. Org. Chem.* **1998**, *63*, 9703-9710; (c) J. A. Wisner, P. D. Beer, M. G. B. Drew, *Angew. Chem.* **2001**, *113*, 3718-3721; *Angew. Chem. Int. Ed.* **2001**, *40*, 3610-3612; for a review on macrocyclisation, see: (d) P. Knops, N. Sendhoff, H. B. Mekelburger, F. Vögtle, *Top. Curr. Chem.* **1992**, *161*, 1-36

24 (a) B. Dietrich, P. Viout, J.-M. Lehn, *Macrocyclic Chemistry*, Wiley VCH, Weinheim, **1993**; (b) A. Ostrowicki, E. Koepp, F. Vögtle, *Top. Curr. Chem.* **1992**, *161*, 37-67.

25 (a) W. L. Mattice, *Macromolecules* **1979**, *12*, 944-948; (b) M. A. Winnik, *Chem. Rev.* **1981**, *81*, 491-524.

26 Selected crystallographic data: **5b**: $C_{79}H_{68}N_2O_{14}$ $(CH_2Cl_2)_{0.66}$, triclinic, space group $P\bar{1}$, $Z = 2$, $a = 1332.3(4)$ pm, $b = 1675.2(6)$ pm, $c = 1722.6(6)$ pm, $\alpha = 104.746(5)°$, $\beta = 100.069(6)°$, $\gamma = 106.408(5)°$, $V = 3.438(2)$ nm^{-3}, $\rho_c = 1.322$ Mgm^{-3}, 71904 reflections measured, 13543 unique, $R1[I>2\sigma(I)] = 0.0469$, $wR2$(all data) = 0.1147, $g_1 = 0.0454$, $g_2 = 2.500$ for 966 parameters and 1002 restraints.

6a: $C_{76}H_{62}N_2O_{12}(CH_2Cl_2)_2(CH_2Cl_2)_{0.58}$, orthorhombic, space group $Pca2_1$, $Z = 4$, $a = 1737.0(3)$ pm, $b = 1555.4(2)$ pm, $c = 2707.6(4)$ pm, $V = 7.3155(18)$ nm^{-3}, $\rho_c = 1.284$ Mgm^{-3}, 50043 reflections measured, 11953 unique, $R1[I>2\sigma(I)] = 0.0605$, $wR2$(all data) = 0.1520, $g_1 = 0.0759$, $g_2 = 7.1271$ for 923 parameters and 36 restraints.

The experimental procedure and detailed crystallographic data are given in the appendix.

27 (a) S. Leroy-Lhez, J. Baffreau, L. Perrin, E. Levillain, M. Allain, M.-J. Blesa, P. Hudhomme, *J. Org. Chem.* **2005**, *70*, 6313-6320; (b) F. Würthner, P. Osswald, R. Schmidt, T. E. Kaiser, H. Mansikkamaeki, M. Könemann, *Org. Lett.* **2006**, *8*, 3765-3768.

28 M. Hesse, H. Meier, B. Zeeh, *Spectroscopic Methods in Organic Chemistry*, Thieme, Stuttgart, **1997**, pp. 88-100.

29 K. Müllen, W. Heinz, F.-G. Klärner, W. R. Roth, I. Kindermann, O. Adamczak, M. Wette, J. Lex, *Chem. Ber.* **1990**, *123*, 2349-2371.

30 (a) I. Petterson, K. Gundertofte, *J. Comp. Chem.* **1991**, *12*, 839-843; (b) C. Etzlstorfer, H. Falk, N. Müller, *Monatsh. Chem.* **1993**, *124*, 431-439; (c) C. Etzlstorfer, H. Falk, N. Müller, W. Schmitzberger, U. G. Wagner, *Monatsh. Chem.* **1993**, *124*, 751-761; (d) C. Etzlstorfer, H. Falk, *Monatsh. Chem.* **1993**, *124*, 1031-1039; (e) S. S. Yilmaz, R. Abbasoglu, B. Hazer, *J. Mol. Model.* **2003**, *9*, 230-234.

31 C.-C. You, R. Dobrawa, C. R. Saha-Möller, F. Würthner, *Top. Curr. Chem.* **2005**, *258*, 39-82.

32 C. Vande Velde, E. Bultinck, K. Tersago, C. Van Alsenoy, F. Blockhuys, *Int. J. Quant. Chem.* **2007**, *107*, 670-679.

33 T. H. Goodwin, M. Przybylska, J. M. Robertson, *Acta Cryst.* **1950**, *3*, 279-284.

34 H. J. Talberg, *Acta Chem. Scand. A* **1978**, *32*, 373-374.

35 The electrochemical potentials in dichloromethane have been taken from the following literature and referred to ferrocene by applying the potential of ferrocene (+ 0.52 V) vs. SCE: T. Higuchi, C. Satake, M. Hirobe, *J. Am. Chem. Soc.* **1995**, *117*, 8879-8880.

36 (a) R. Gvishi, R. Reisfeld, Z. Burshstein, *Chem. Phys. Lett.* **1993**, *213*, 338-344; (b) C.-C.-You, F. Würthner, *J. Am. Chem. Soc.* **2003**, *125*, 9716-9725.

37 (a) D. Rehm, A. Weller, *Ber. Bunsenges. Phys. Chem.* **1969**, *73*, 834-845; (b) A. Weller, *Z. Phys. Chem.* **1982**, *133*, 93-98; (c) N. P. Redmore, I. V. Rubtsov, M. J. Therien, *J. Am. Chem. Soc.* **2003**, *125*, 8769-8778; (d) M. W. Holman, R. Liu, L. Zang, P. Yan, S. A. DiBenedetto, R. D. Bowers, D. A. Adams, *J. Am. Chem. Soc.* **2004**, *126*, 16126-16133.

38 A. Zweig, W. G. Hodgson, W. H. Jura, *J. Am. Chem. Soc*. **1964**, *86*, 4124-4129.

39 (a) D. Marquis, J.-P. Desvergne, H. Bouas-Laurent, *J. Org. Chem.* **1995**, *60*, 7984-7996; (b) S. Chatti, M. Bortolussi, A. Loupy, *Tetrahedron* **2000**, *56*, 5877-5883.

40 J. R. Lakowitz, *Principles of Flourescence Spectroscopy*, *2nd ed*., Kluwer Academic/Plenum, New York, **1999**, pp. 52-55.

41 A. J. Fry in *Laboratory Techniques in Electroanalytical Chemistry*, 2nd edition, (Eds.: P. T. Kessing, W. R. Heineman), Marcel Dekker Inc., New York, **1996**, p. 481.

42 C. J. Adam, S. J. Clark, G. J. Ackland, J. Crain, *Phys. Rev. E* **1997**, *55*, 5641-5650.

Chapter 4

Perylene Bisimide Atropisomers – Synthesis, Resolution and Stereochemical Assignment

Abstract: The macrocyclization of the tetra(hydroxyphenoxy)-substituted perylene bisimide **4** bearing two (*R*)-configured 2-octyl substituents in the imide positions by etherification with diethylene glycol ditosylate afforded both the diagonally bridged (1,7- and 6,12-linkage) and laterally bridged (1,12- and 6,7-linkage) regioisomers **6** and **7**. The atropo-diastereomers of the diagonally bridged macrocycle **6** have been separated by semi-preparative HPLC on a chiral column and their absolute configuration has been determined by circular dichroism (CD) spectroscopy in combination with quantum chemical CD calculations. The isolated epimers (*P*,*R*,*R*)-**6** and (*M*,*R*,*R*)-**6** represent the first examples of diastereomerically pure perylene bisimide atropisomers. The optical and chiroptical properties of these epimers have been investigated by UV/Vis, fluorescence and CD spectroscopy, while their conformational properties have been explored by temperature-dependent ^{1}H NMR spectroscopy.

4.1. Introduction

A strategy to restrict the dynamic racemization process of tetraaryloxy-substituted perylene bisimides by bridging the substituents at the bay positions with oligoethylene glycol chains through macrocyclization was reported in chapter 3 of this thesis.[1] Attempts to separate the enantiomers of diagonally bridged macrocycles by standard techniques[2] such as HPLC on chiral columns or crystallization, which afforded racemic mixtures of the macrocycles, were not successful. Other techniques for the separation include the derivatisation of the enantiomers with chiral substituents and such diastereomeric derivatives were used e.g. for the separation of helicene and is one of the standard technique for the synthesis of enantiopure binaphthyl derivatives.[3]

Therefore, the synthesis of chiral macrocyclic PBIs containing two (*R*)-configured 2-octyl substituents in the imide positions by applying the "macrocyclisation" approach is presented and the resolution of pure PBI epimers is reported. This has allowed the elucidation of the chiroptical properties of twisted PBI fluorophores. The absolute configuration of the atropo-diastereomers is determined by applying CD spectroscopy in combination with quantum chemical CD calculations.

4.2 Synthesis and Separation of Epimerically Pure Macrocyclic Perylene Bisimides

The macrocyclic perylene bisimides **6** and **7** were synthesized in five steps starting with the tetrachloro-substituted perylene bisimide **1**[4] as outlined in Scheme 1. The nucleophilic substitution of the chlorine atoms in **1** by 3-methoxyphenol afforded the tetraaryloxy-substituted perylene bisimide **2** in 36% yield. Subsequent saponification of **2** with potassium hydroxide in isopropanol under reflux provided perylene bisanhydride **3** in 90% yield. The chiral substituents were then introduced by imidization of **3** with 2-(*R*)-octylamine in quinoline employing zinc acetate as a catalyst. After column chromatography of the crude product on silica gel with dichloromethane as eluent, the chiral perylene bisimide **4** was isolated in 58% yield. Cleavage of the methyl ether groups in **4** with boron tribromide in anhydrous dichloromethane provided the (3-hydroxyphenoxy)-functionalized PBI **5** as a synthetic key intermediate. For the macrocyclization of the chiral perylene bisimide **5** a similar procedure was applied as previously described for achiral derivatives.[1] A diethylene glycol linker was chosen as the bridging unit since it provides conformationally rigid macrocycles with reasonable yields.[1] Thus, the tetra(hydroxyphenoxy)-substituted PBI **5** was treated with diethylene glycol ditosylate and cesium carbonate in dimethylsulfoxid at 120 °C under argon, and after column chromatographic purification of the crude product, both the diagonally

bridged (1,7- and 6,12-linkage) macrocycle **6** and its laterally bridged (1,12- and 6,7-linkage) isomer **7** were obtained in 4% and 30% yields, respectively. In comparison to the macrocyclization of perylene bisimides bearing achiral imide groups (Chapter 3 of this thesis), a significantly higher yield for the laterally bridged isomer was observed in the present case.

Scheme 1. Synthesis of Regioisomeric Macrocyclic Perylene Bisimides **6** and **7**, and Resolution of the Atropo-Diastereomers of **6**[a]

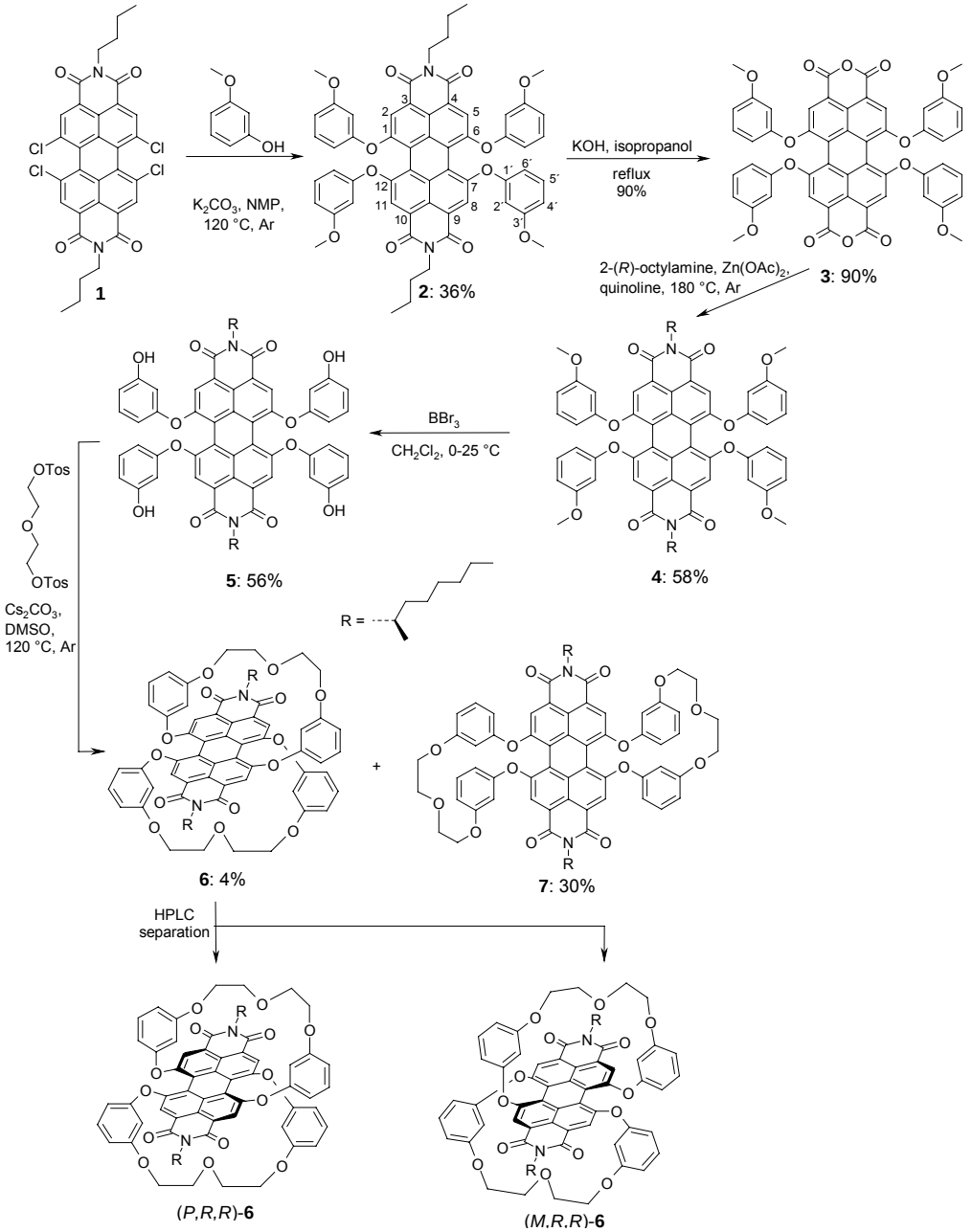

Since the macrocyclic perylene bisimides **6** and **7** contain two (*R*)-configured chiral imide substituents and the perylene core possesses a chirality plane, the occurrence of diastereomers (more precisely, epimers) was to be expected for these compounds. Indeed, the epimers of the diagonally bridged macrocycle **6**, for which an interconversion of the twisted conformers (*P* and *M*) is not possible, proved to be

separable by semi-preparative HPLC on a chiral column (Reprosil 100 chiral-NR) using isopropanol/*n*-hexane (1:1) as the eluent (Figure 1). The absolute configurations of the first (**6´**) and the second eluted (**6´´**) epimers (retention times 25 and 30 min) were determined as (*P*,*R*,*R*) and (*M*,*R*,*R*), respectively, by CD spectroscopy in combination with quantum chemical CD calculations (details are given in next sections). The epimers of the laterally bridged compound **7**, by contrast, could not be resolved, apparently, due to its low isomerization ($M \rightleftharpoons P$) barrier (vide infra).

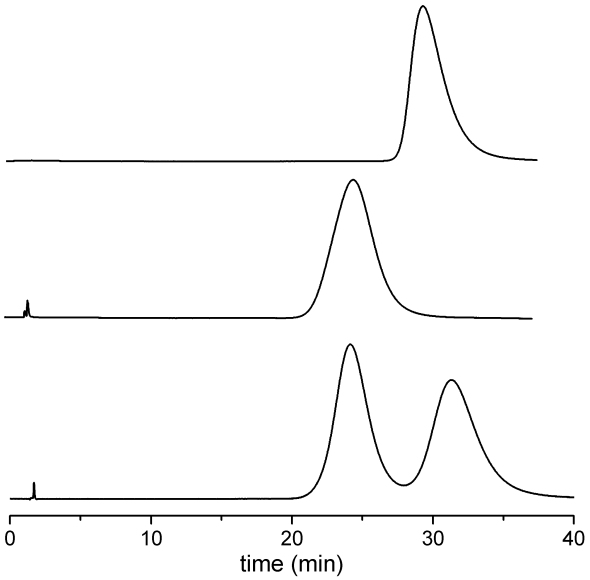

Figure1. HPLC chromatograms before (bottom) and after separation of the epimers of **6** on a Trentec Reprosil 100 chiral-NR column at ambient conditions using isopropanol/*n*-hexane (1:1) as eluent (flow rate: 2 mL/min).

The constitutions of the regioisomeric macrocyclic perylene bisimides **6** and **7** were unambiguously assigned by comparison of their ^{1}H NMR data with those of the previously reported similar macrocycles, whose structures were unequivocally determined by X-ray analysis.[1] Thus, for the diagonally bridged macrocycle **6** a characteristic upfield shift of the signal for the aromatic protons (δ = 5.6 ppm) between the two oxygen atoms of the resorcin residues was observed (Figure 2), indicating that these protons are located above and below the aromatic perylene core. The respective protons of the laterally bridged isomer **7** were found to be shifted to lower field (δ = 6.7 ppm), implying that in this regioisomer the aryloxy residues are oriented more in the plane of the perylene core.

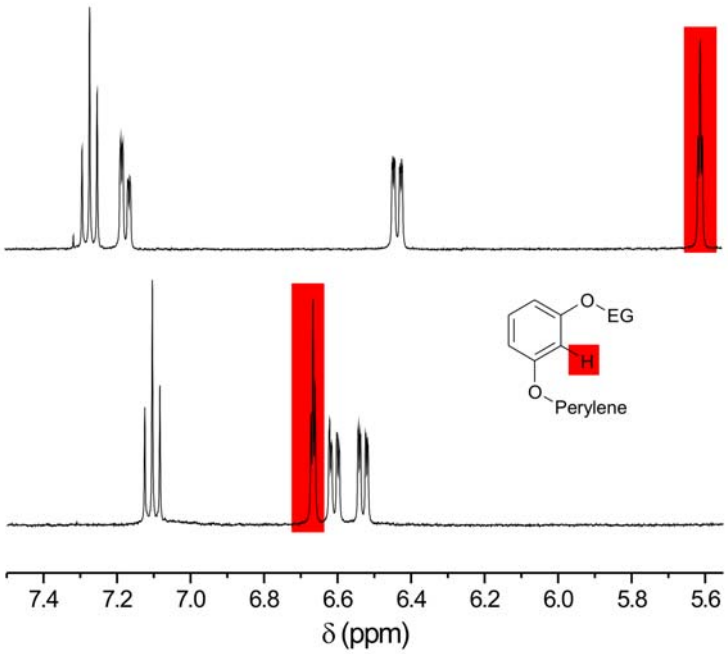

Figure 2. Aromatic region of the ^{1}H NMR spectra (400 MHz) of **6** (top) and **7** (bottom) in CD_2Cl_2 at 300 K. The signals of the protons situated between the two oxygen atoms of the resorcinol residues are highlighted in red. EG denotes ethylene glycol.

Characteristic aromatic shielding effects were also observed for protons of the bridging ethylene glycol units. For the laterally bridged regioisomer **7**, the resonances of these protons appear at 3.8–4.8 ppm, whereas the corresponding protons of the diagonally bridged analog **6** show resonances at considerably higher field (3.5–3.9 ppm). Thus, the bridging units in **6** experience a deshielding due to the aromatic perylene core that is only given for this diagonally bridged macrocycle.

4.3. Optical Properties

The optical properties of the epimeric perylene bisimides **6** and **7** were investigated by UV/Vis and fluorescence (steady state and time-resolved) spectroscopy. The absorption and emission spectra of **6** and **7** in dichloromethane (Figure 3) reveal the characteristic transitions for PBIs, i.e. a S_0-S_1 transition at ~550 nm and a S_0-S_2 transition at 450 nm.

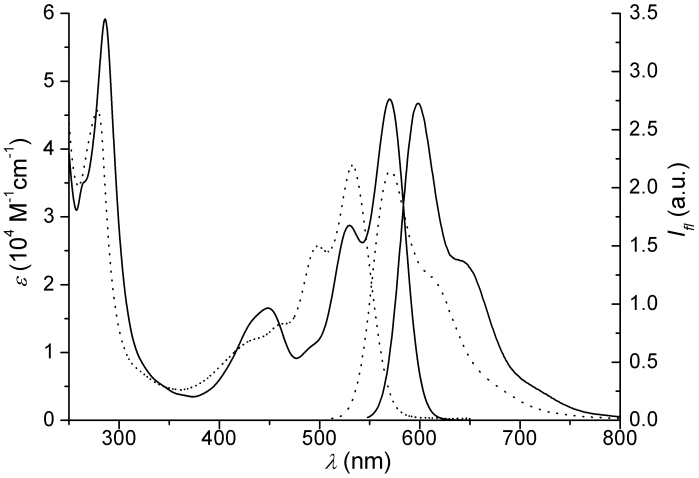

Figure 3. UV/Vis absorption and emission spectra of **6** (dotted line) and **7** (solid line) in dichloromethane at 25 °C.

The UV/Vis absorption spectrum of the diagonally bridged isomer **6** shows a hypsochromic shift of the absorption maximum of the S_0-S_1 transition by 38 nm in comparison to that of **7**, accompanied by a pronounced hypochromicity. Moreover, **6** exhibits a significantly less intense S_0-S_2 transition compared to that of **7**. These spectral features are typical of diagonally bridged PBI macrocycles[1] and, thus, further confirm the structural assignment based on characteristic ^{1}H NMR data.

The fluorescence properties of **6** and **7** in dichloromethane, as summarized in Table 1, reveal that the diagonally bridged isomer **6** is only weakly fluorescent in dichloromethane with a fluorescent quantum yield of 22%. The corresponding fluorescence lifetime was determined as 2.2 ns. The results indicate that the rate constant for the non-radiative processes is increased in comparison to laterally bridged macrocycle **7** (see Table 1).[1] Moreover, for the diagonally bridged isomer **6** a Stokes shift of 38 nm was observed which is 10 nm larger than that of the laterally bridged macrocycle **7**, implying a more pronounced change of the geometry between the ground and the excited states of **6**. By decreasing the solvent polarity an increase of the quantum yield was observed. Thus, **6** exhibits a fluorescence quantum yield of 73% in diethylether, accompanied by an increase of the fluorescence lifetime to 6.2 ns. In contrast to **6**, the fluorescence properties of the laterally bridged perylene bisimide **7** corroborate well to those observed for conformationally flexible, open-chained aryloxy-substituted perylene bisimides such as **4** (Φ_{fl} = 94 %), as for regioisomer **7** a fluorescence quantum yield of 95% was observed in dichloromethane. It is noteworthy that the fluorescence quantum yields of the macrocycles **6** and **7** are slightly higher (by 10-15%) than those of the macrocycles with similar chain-length bearing aryl substituents in the imide position (Chapter 3).[1]

Table 1. Fluorescence Properties of Perylene Bisimides **6** and **7**

	solvent	λ_{max}^{fl} (nm)	Φ_{fl}^{a}	τ_{fl} (ns)^{b}	k_r (s^{-1})^{c}	k_{nr} (s^{-1})^{d}
6	dichloromethane	570	0.22	2.2	1.0×10^8	3.6×10^8
	diethylether	560	0.73	6.2	1.2×10^8	4.4×10^7
7	dichloromethane	598	0.95	6.9	1.4×10^8	7.3×10^6

a) $\Phi_{fl} \pm 0.03$; b) $\tau_{fl} \pm 0.5$ ns; c) $k_r = \Phi_{fl}/\tau_{fl}$, d) $k_{nr} = (1-\Phi_{fl})/\tau_{fl}$

4.4. Stereochemical Assignment and Chiroptical Properties of Atropiosmerically Pure Perylene Bisimides.

The absolute configurations of the isolated epimers (**6´** and **6´´**) of the macrocyclic perylene bisimide **6** were determined by CD spectroscopy in combination with quantum chemical calculations. For this purpose, the chiroptical properties of the epimers were explored beforehand.

The CD spectra of the isolated epimers **6´** and **6´´** show a clear mirror image relation as depicted in Figure 4 (bottom). In the visible region (400–650 nm) of the CD spectra a broad monosignated peak with a maximum at 536 nm can be seen, which properly correlates with the absorption maximum at 532 nm (Figure 4, top). The absolute $\Delta\varepsilon$ values for the longest wavelength transition (536 nm) of the two epimers of **6** are +67 (**6´**) and –63 M^{-1} cm^{-1} (**6``**) giving an absorption dissymmertry factor g = $\Delta\varepsilon/\varepsilon$ of 0.0018. This is in accordance with the values observed for related chiral twisted π-systems, e.g. hypericin derivatives, which, in their 1,6-dioxo form, show a g factor of 0.0014 for the longest wavelength transition.[5] Moreover in the visible part of the CD spectra (400-650 nm) of the epimers two optical transitions are located, i.e. the S_0-S_1 (536 and 495 nm) and the S_0-S_2 transitions (450 nm), whose transition dipole moments are polarized along the long and the short axis of the perylene bisimide, respectively. Since these transitions can be attributed to the whole chromophore, the monosignated CD signal represents the chirality of the whole molecule. These observations are characteristic for molecular chirality and differ from those arising from excitonic coupling.[6]

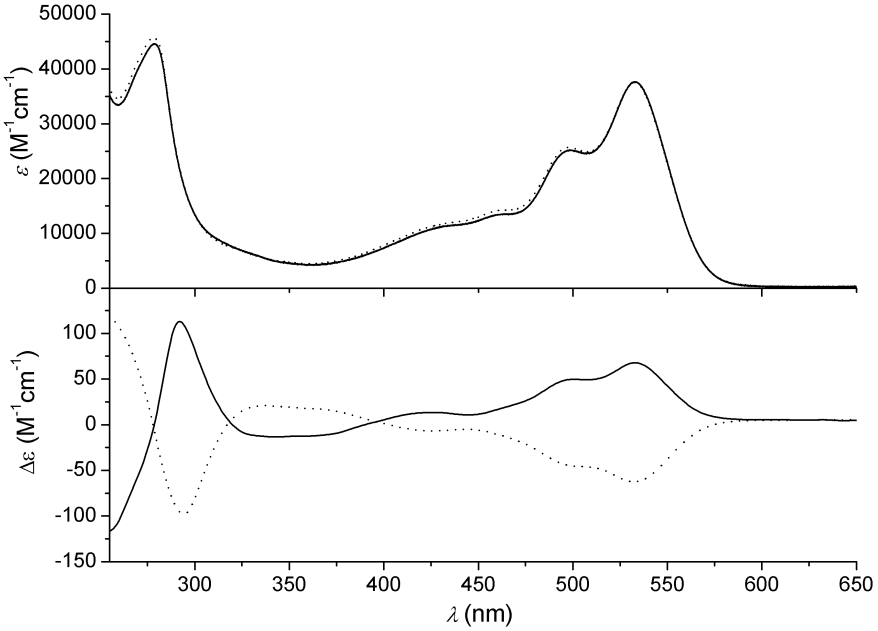

Figure 4. UV/Vis absorption (top) and CD spectra (bottom) of the first (**6´**, solid line) and the second eluted (**6´´**, dotted line) epimers of **6** in dichloromethane at 20 °C.

On the other hand, for the naphthalene-related optical transitions in the UV region (250-400 nm) of the CD spectra, an asymmetric bisignated signal was observed each, with a positive first Cotton effect and a negative second one for the first eluted epimer **6´** and vice versa for second eluted epimer **6´´**. In both cases the peak maxima of the first Cotton effects are located at 292 nm ($\Delta\varepsilon$ values are +113 and –100) and those of the second ones are found at about 250 nm with a cross-over point at 276 nm. This zero transition corresponds very well to the maximum at 278 nm observed in the UV/Vis absorption spectra (Figure 4, top). The observation of an exciton couplet at about 280 nm can be attributed to the excitonic interaction of the two twisted naphthalene imide units of the perylene bisimide core (aryloxy residues absorb at lower wavelengths). Therefore, the exciton chirality method[6] was applied for a first tentative assignment of the absolute configurations of the epimers of **6**. As the first eluted stereoisomer **6´** shows a first positive Cotton effect (at 278 nm), it should be (*P*)-configured and, accordingly, the second eluted epimer **6´´** should have a (*M*)-configuration. Since both imide substituents of **6** are (*R*)-configured, the absolute configuration of the first eluted epimer, **6´**, can be assigned as (*P*,*R*,*R*) and that of the second eluted one, **6´´**, as (*M*,*R*,*R*). The mirror-image relation of the two CD spectra indicates the pseudo-enantiomeric character of these diastereomers, i.e. the chiral alkyl substituents do not contribute to the optical activity in the visible wavelength range. Additionally, the optical rotation values $[\alpha]_D^{20}$ for (*P*,*R*,*R*)-**6** and (*M*,*R*,*R*)-**6** were determined at 20 °C in dichloromethane to be +6600 (c = 0.007) and –6600 (c = 0.006), respectively. Optical

rotations of such large sizes had been previously observed only for twisted π-systems like, e.g., for helicenes.[7] However, in the present case a pronounced dispersion enhancement is present, since the detection wavelength (λ = 589 nm) is close to the absorption maximum of **6**. The identical absolute values of the optical rotations, yet with opposite signs, confirm the pseudo-enantiomeric behavior of these perylene bisimide dyes. Such a pseudo-enantiomeric behavior had been previously demonstrated for related hypericin derivatives, for which the observed chirality emanates from the inherently chiral chromophore.[5]

As mentioned above, the absolute configurations of the epimers of **6** can be tentatively attributed by applying the exciton chirality method. For a more reliable configurational assignment of the epimers, quantum chemical calculations of the CD spectra were performed, with subsequent comparison of the simulated spectra with the measured ones.[§,8]

In a first step, the conformational space of (*P*,*R*,*R*)-**6** was investigated by means of PM3,[9] resulting in 24 minimum geometries within an energy range of 3 kcal/mol.[10] For each single geometry thus obtained, a CD spectrum was calculated using the semiempirical OM2[11] Hamiltonian. These individual spectra were then added up weighted following the Boltzmann statistics, i.e., according to the corresponding heats of formation, to give the overall simulated CD curve, which was then UV-corrected.[12] Comparison with the experimental CD spectrum of the fast eluted epimer **6´** revealed an acceptable agreement for (*P*,*R*,*R*)-**6** and a reversed behavior for (*M*,*S*,*S*)-**6** (Figure 5a),[13] suggesting that the first eluted epimer is (*P*)-configured, and, consequently, the second eluted epimer, **6´´**, is (*M*).

In order to confirm these stereochemical assignments and in view of the molecular flexibility of **6**, further CD calculations for (*P*,*R*,*R*)-**6** were performed, now based on a molecular dynamics (MD) simulation using the TRIPOS[14] force field at a virtual temperature of 800 K. For the geometries extracted from the trajectory of motion, single CD spectra were computed again by means of OM2.[11] Subsequent summation of these curves and UV correction[12] delivered the overall simulated CD spectrum, which now corresponded very well with the experimental spectrum of the first eluted epimer **6´**, while the spectrum predicted for (*M*,*S*,*S*)-**6** was found to be perfectly opposite (Figure

[§] Quantum chemical calculations were performed by Dr. M. Reichert and Prof. G. Bringmann, Institute of Organic Chemistry, University of Würzburg, Germany.

5b). Consequently, the first eluted epimer is unambiguously confirmed to have the (*P*)-configuration, whereas the second eluted one is (*M*)-configured.

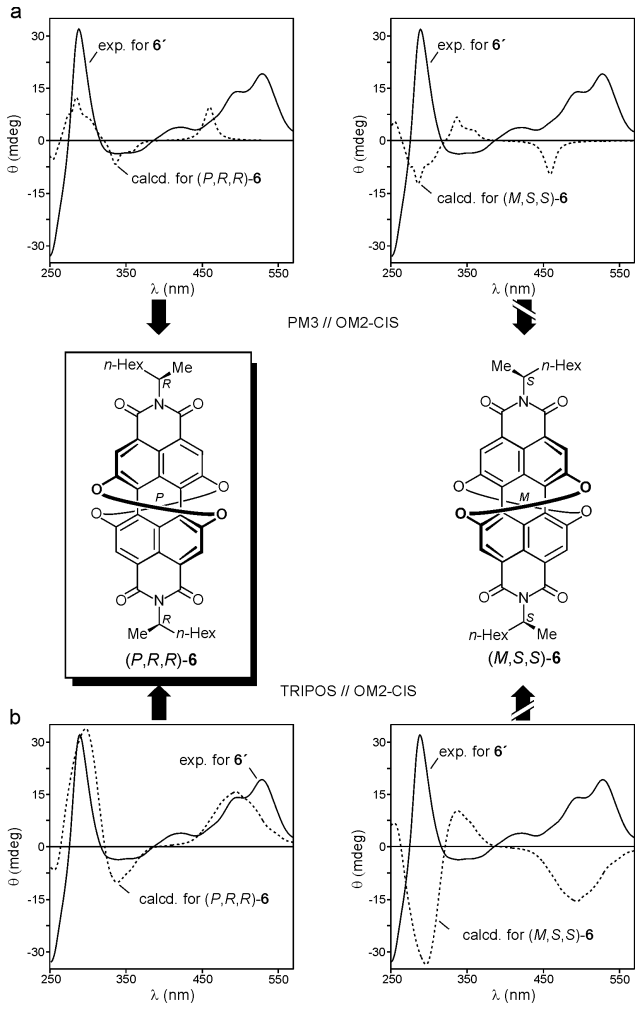

Figure 5. Assignment of the absolute configuration of the first eluted epimer of **6** by comparison of its experimental CD curve (solid lines) with the spectra calculated for (*P*,*R*,*R*)-**6** and (*M*,*S*,*S*)-**6**[24] (a) using the PM3-Boltzmann approach and (b) the TRIPOS-MD method, followed in both cases by OM2-CIS-CD calculations (dotted lines). Shown with the permission of M. Reichert and G. Bringmann.[8]

4.5. Conformational Properties of Perylene Bisimides 4, 6, and 7

In contrast to the diagonally bridged regioisomer **6**, an interconversion of the epimers (*P*,*R*,*R* and *M*,*R*,*R*) of the laterally bridged regioisomer **7** and of the chiral, non-macrocyclic PBI **4** is possible. To gain insight into the equilibrium process ($M \rightleftharpoons P$) for the given pseudo-enantiomeric PBIs **4** and **7**, and to assess whether any additional dynamic processes are involved, temperature-dependent ^{1}H NMR spectroscopic studies were performed for the open-chained tetraaryloxy-substituted PBI **4** and for the

macrocycles **6** and **7**.[#] Figure 6 shows the resonances for the perylene core protons in temperature-dependent ^{1}H NMR spectra of **4** and **6**.

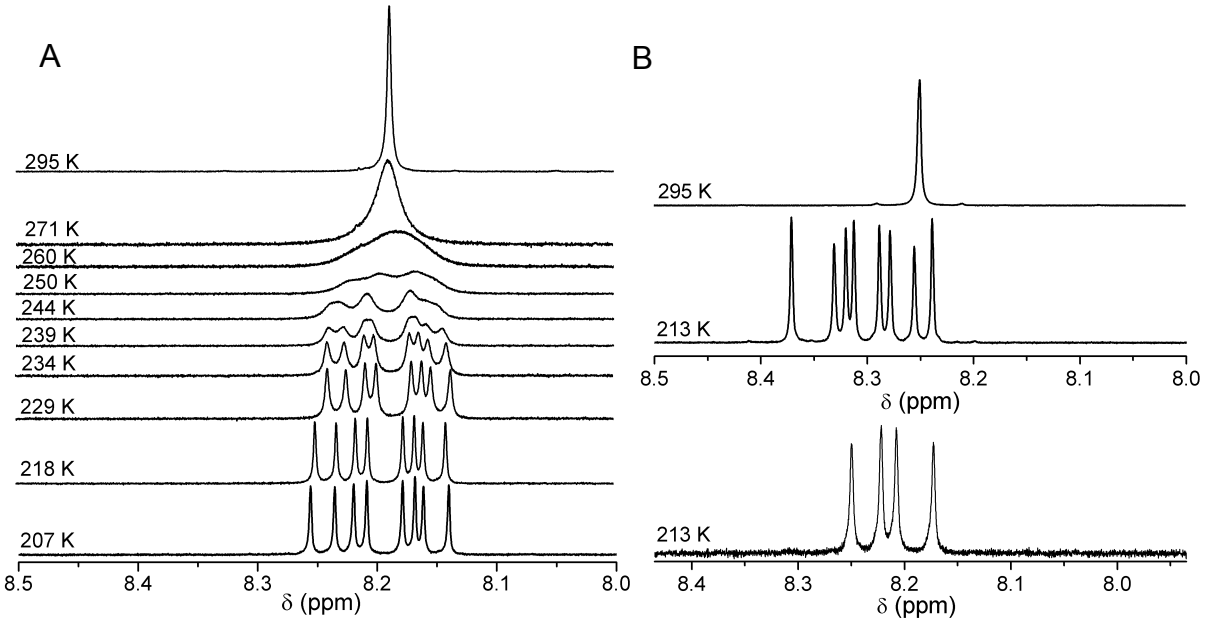

Figure 6. (A) Sections of the temperature-dependent (295–207 K) ^{1}H NMR (600.13 MHz) spectra of aryloxy-substituted PBI **4** in $CDCl_3$ and (B) sections of the ^{1}H NMR spectra (500.13 MHz) of diagonally bridged PBI **6** at 295 K (top) and 213 K (middle) in $CDCl_3$, and of epimerically pure (*M*,*R*,*R)*-**6** in CD_2Cl_2 at 213 K (bottom). Only the resonances of the perylene core protons (H2, H5, H8 and H11) are shown.

The perylene core protons were chosen to monitor the atropisomeric interconversion, which is not a racemisation, but an epimerization, as the atropisomeric PBIs **4**, **6** and **7** contain two (*R*)-configured substituents. The process was investigated upon cooling to a temperature at which the epimerization occurs in the same time scale as the proton spin relaxation (NMR time scale). At even lower temperatures, where the spin relaxation is faster than the epimerization process, two set of signals are expected due to the presence of two epimers (*P*,*R*,*R* and *M*,*R*,*R*). However, as can be seen from Figure 6b (middle), eight signals are observed for the epimeric mixture of **6** at low temperature (213 K). At 295 K, these signals merge into a singlet, again indicating the pseudo-enantiomeric character of the diastereomers. Since for the pure epimer (*M*,*R*,*R*)-**6** (Figure 6b, bottom) only four signals are observed at low temperature (213 K), the eight signals that appear in the respective low-temperature ^{1}H NMR spectrum of **6** can be

[#] Temperature-dependent ^{1}H NMR spectra were recorded by Mrs. M.-L. Schäfer at the Institute of Inorganic Chemistry (500 MHz) and Mrs. E. Ruckdeschel (600 MHz) at the Institute of Organic Chemistry at the University of Würzburg, Germany.

unambiguously assigned to the two respective epimers. The occurrence of four signals, instead of the expected one singlet, for each epimer can be explained either by a self-dimerization[15] or by an intramolecular dynamic process that is frozen on the NMR time scale at lower temperature. As both π-faces of the perylene core in macrocycle **6** are surrounded – and thus shielded – by the bridging units, a dimerization through π-π interactions is not feasible. Thus, the appearance of eight signals for **6** at 213 K can be ascribed to an intramolecular dynamic process. The observed four signals most probably result from a hindered rotation about the imide C-N bond, because rotational barriers around C-N bonds of structurally similar compounds were reported to be around 51 kJ/mol at 228 K.[16]

For a hindered rotation about the C-N bonds of the perylene bisimides **4** and **6**, the preferred conformations at low temperatures are syn and anti as shown in Figure 7b.[17] Such conformational features have been reported by Shimizu et al. for unsubstituted perylene bisimide derivatives bearing aryl substituents in the imide positions.[18d] In both conformations only a C_2 axis remains as a symmetry element, resulting in two singlets for the perylene core protons for each of the two rotamers, syn and anti; as illustrated in Figure 7b. Therefore, the observed four signals for each epimer of **6** can be ascribed to the presence of both rotamers at low temperature. The signal pattern for the rotamers and epimers of **6** are marked in Figure 7a (bottom). The two singlets of one rotamer (marked with red or blue circles) are separated by 24 Hz, whereas for the other rotamer (red or blue squares) a lower distance of 21 Hz was found. Therefore, the signal pattern observed in the ^{1}H NMR spectrum of **6** at low temperature (213 K) is due to the presence of two epimers, whose signals are further split into four signals owing to the presence of syn and anti rotamers.

The temperature-dependent spectral changes for the aryloxy-substituted non-macrocyclic PBI **4** are shown in Figure 6. Upon cooling, the singlet observed for the perylene core protons at room temperature (295 K) gets broadened and at temperatures below 230 K it splits into eight signals, as in the case of **6**. Therefore, the signal pattern of **4** at low temperatures can again be ascribed to the presence of two epimers combined with the occurrence of two rotamers each as in the case of **6** (Figure 7a). In the signal pattern, two corresponding singlets for each rotamer are found that are separated by 24 Hz and 12 Hz, and the chemical shifts of each rotamer results from the mean value of these two singlets. The chemical shifts of the epimers can be assessed as the center of the calculated chemical shift of the two respective rotamers (Figure 7) and are located at 8.22 ppm and 8.17 ppm. Thus, the difference in chemical shift of the epimers $\Delta\upsilon$, which is necessary for the calculation of $\Delta G^{\ddagger}$, was determined

as 31.7 Hz (0.0528 ppm at 600 MHz). The coalescence temperature for the epimerization process was estimated to be 255 K from line broadening. By using the coalescence method,[18] the barrier for the epimerization of **4** was estimated to be 53±3 kJ/mol. Additionally, based on the resonances of the methoxy groups of **4** at 3.5 ppm (not shown in spectra), the coalescence temperature was determined as 244 K and with a $\Delta\upsilon$ value of 7.7 Hz an epimerization barrier of 53±3 kJ/mol was found.

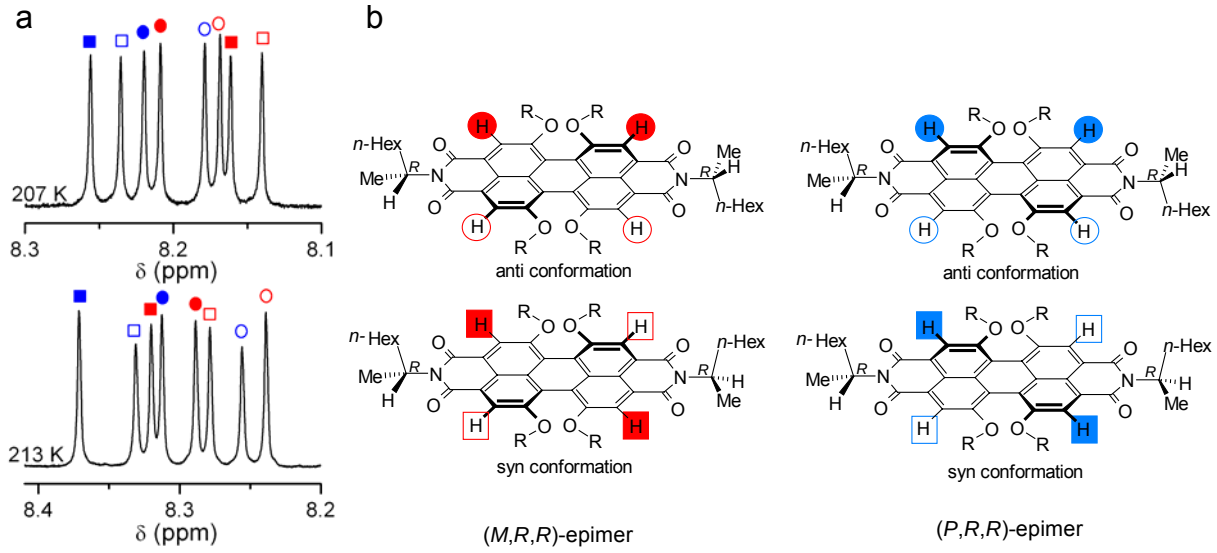

Figure 7. (a) Assignment of the NMR signal pattern of **4** (top) and of **6** (bottom) at low temperature and (b) anti (top) and syn (bottom) conformations of the (*M*,*R*,*R*)- and (*P*,*R*,*R*)-epimers. The blue symbols represent the resonances of the perylene core protons of the (*P*,*R*,*R*)-epimer and the red ones those of (*M*,*R*,*R*) (for **4**, the assignment is analogous to **6**). The circles and squares symbolize the resonances of two rotamers and the filled and empty symbols denote the chemically equivalent core protons of each rotamer (the assignment is tentative).

Figure 8 displays the temperature-dependent ^{1}H NMR spectral changes for the core protons of the laterally bridged macrocycle **7** in $CDCl_3$. Similar changes for the resonances of the perylene core protons as in the case of **4** are observed upon cooling to 233 K, although eight individual signals could not be clearly seen for **7**, because upon cooling below 233 K further broadening of the signals occurred which might be ascribed to an additional dynamic process. In this case, the coalescence temperature was estimated to be 256 K. Thus, compound **7** may have a similar activation barrier as **4**; although absolute values cannot be given because the low temperature spectra could not be resolved. The results of the temperature-dependent NMR studies reveal, that the barrier for the *M* ⇄ *P* racemization is not significantly influenced by the presence of a diethylene glycol linker, while the chiral centers in the imide positions of perylene

bisimide do not affect the dynamics of these dyes. Furthermore, the epimers are present in equal amounts as the integrated intensities of their NMR signals are identical, implying that the chiral substituents do not have any effect on the stability of (*P*)- and (*M*)-atropo-diastereomers.

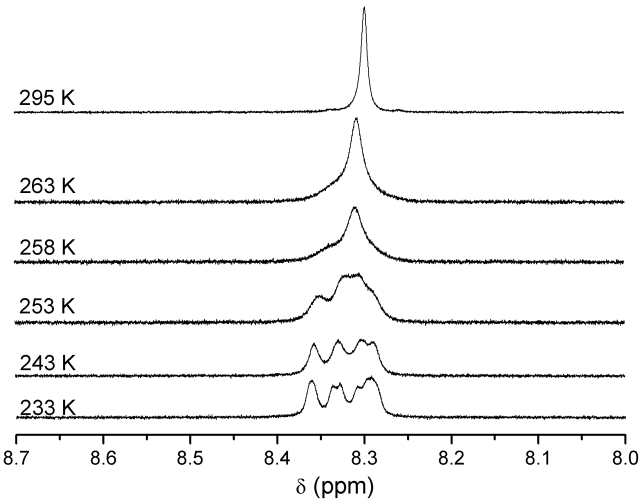

Figure 8. Sections of the temperature-dependent ^{1}H NMR spectra of **7** (500.13 MHz) in $CDCl_3$. The resonances of the perylene core protons are shown.

4.6 Conclusion

These results have shown that pure stereoisomers of perylene bisimides with a (*P*) or (*M*) helically twisted perylene core can be isolated if the interconversion process (*M* ⇄ *P*) is prevented by appropriate bridging of the substituents in the 1,7- and 6,12-positions as demonstrated here for PBI **6**. Since the racemization process for non-macrocyclic 1,6,7,12-tetraaryloxy-substituted PBIs is fairly fast at ambient temperature, owing to an activation energy of only about 54 kJ/mol (as estimated for open-chained PBI **4** and laterally bridged macrocyclic PBI **7**), diagonal bridging through macrocyclization was the method of choice for the synthesis of atropisomerically pure perylene bisimides. The availability of chiral, conformationally stable perylene bisimide dyes could expand the possible application of this very important class of fluorophores to enantioselective recognition and other processes requiring chiral information.

4.7 Experimental Section

Methods and Materials. Cesium carbonate (99%) was purchased from Aldrich (Steinheim, Germany), boron tribromide (≥ 99%), 3-methoxyphenol (97%) and dry DMSO (Secco Solv) were obtained from Merck (Hohenbrunn, Germany), KOH (≥ 99%) and potassium carbonate (99%) were purchased from Grüssing (Filsum, Germany), dichloromethane and isopropanol were obtained from Staub (Nürnberg, Germany) and

N-Methylpyrrolidon (NMP; 99,5%) from Riedel-deHäen (Seelze, Germany). The used 2-(*R*)-octylamine (Lancaster; Karlsruhe, Germany) had an ee value of > 99%. All chemical and reagents were used as received if not otherwise mentioned. NMP and quinoline were fractionally distilled prior to use, dichloromethane was distilled under nitrogen from calcium hydride, pyridine was stored over KOH and potassium carbonate was dried in vacuo at 100 °C for one day. Diethylene glycol ditosylate[19] and *N,N´*-di(*n*-butyl)-1,6,7,12-tetrachloroperylene-3,4:9,10-tetracarboxylic acid bisimide[4] were prepared according to literature procedures. Flash column chromatography was performed using silica gel (Si60, mesh size 40-63 µm) from Merck. Melting points were determined on a Olympus Bx41 polarization microscope and are uncorrected. ^{1}H NMR spectra were recorded on a Bruker Advance 400 spectrometer. Chemical shifts are given in parts per million (ppm) and are referred to TMS as internal standard or to the residual solvent peak. Fast Atom Bombardment (FAB) mass spectra were recorded on Finnigan MAT90, MALDI-TOF mass spectra on a Autoflex II from Bruker Daltonics and high resolution mass spectra were recorded on a MicrOTOF Focus from Bruker Daltonics. Elemental analysis were performed on a CHNS 932 analyzer from Leco Instruments. Analytical HPLC was performed on a system (PU 2080 PLUS) with a diode array detector (MD 2015) from JASCO equipped with a ternary gradient unit (LG 2080-02) and line-degasser (DG-2080-533). Preparative HPLC was done on a system (PU 2080 PLUS) with a diode array detector (UV 2077 PLUS) from JASCO. HPLC grade solvents (Rectapur) from VWR (Darmstadt, Germany) were used, except for isopropanol, which was distilled prior to use. As chiral column Reprosil 100 chiral-NR from Trentec (Gerlingen, Germany) has been used in the analytical (Ø = 4.6 mm) as well as in the semi-preparative size (Ø = 20 mm).

Temperature-Dependent NMR Spectroscopy. Temperature-dependent ^{1}H NMR spectra were recorded on a 500 or 600 MHz spectrometer and for calibration the temperature dependent chemical shift of methanol was used. Coalescence temperatures were determined from the spectral broadening and the data were evaluated using the coalescence method according to equation 4-1.[6]

$$\Delta G^{\ddagger} = RT_C \ln\left(\frac{RT_C\sqrt{2}}{\pi\ N_A h\ |\nu_A - \nu_B|}\right) \qquad \text{(eq. 4-1)}$$

Absorption and Fluorescence Spectroscopy, Circular Dichroism and Optical Rotation. For all spectroscopic measurements spectroscopic grade solvents (Uvasol®) from Merck were used. UV/Vis spectra were recorded with a Perkin Elmer PE 950

under ambient conditions. CD spectra were measured with a JASCO J-810 spectrometer equipped with a CDF-242 peltier element and optical rotation values were determined with a JASCO PE 1020 at 20 °C in the concentrations given in the text. Fluorescence spectra were recorded with a PTI QM-4/2003 instrument and fluorescence lifetimes were determined with PTI GL3330 nitrogen laser and a GL302 dye laser using the stroboscope technique. All fluorescence measurements were performed under aerobic conditions and fluorescence spectra are corrected. The fluorescence quantum yields were determined as the average value for three different excitation wavelengths using *N,N´*-di(2,6-diisopropylphenyl)-1,6,7,12-tetraphenoxyperylene-3,4:9,10-tetracarboxylic acid bisimide as reference (Φ_{fl} = 0.96 in chloroform) by applying high dilution conditions (A < 0.05).[20] Decay curves were evaluated with the Felix software from PTI by fitting 1-4 lifetimes. The quality of the fit was judged by the Derbin-Watson factor DW and χ^2 (for a monoexponential decay DW > 1.7 and 0.9 < χ^2 < 1.2) as well as by the correlation function and the residuals.

Computational Details. The conformational analysis of (*P*,*R*,*R*)-**6** was performed on a Linux AMD MP 2800+ workstation by using the semiempirical PM3 method as implemented in the program package GAUSSIAN 03,[21] starting from a preoptimized structure generated by the TRIPOS force field, as part of the molecular modeling package SYBYL 7.0.

The molecular dynamics (MD) simulation for (*P*,*R*,*R*)-**6** was performed at a virtual temperature of 800 K using the TRIPOS force field as well. The overall simulation time was 500 ps, the single structures were extracted every 0.5 ps yielding 1000 conformers.

The wave functions required for the computation of the rotational strengths for the electronic transitions from the ground state to excited states were obtained by OM2 calculations followed by CIS computations including 900 singly occupied configurations as well as the ground state determinant, by means of the MNDO99[22] software package. In the case of the MD approach, the single CD spectra were added up arithmetically, whilst in the case of the conformational analysis, they were summed energetically weighted following the Boltzmann statistics, i.e., according to the respective heats of formation. The rotational strengths were then transformed into $\Delta\varepsilon$ values and for a better visualization superimposed with Gaussian band shape functions.

Synthesis and Characterization of Macrocyclic Perylene Bisimides

***N,N´*-Di(*n*-butyl)-1,6,7,12-tetra(3-methoxyphenoxy)perylene-3,4:9,10-tetracarboxylic Acid Bisimide (2).**

N,N´-Di(*n*-butyl)-1,6,7,12-tetrachloroperylene-3,4:9,10-tetracarboxylic acid bisimide (**1**)[4] (2.50 g, 3.90 mmol), 3-methoxyphenol (2.42 g, 19.5 mmol) and dry potassium carbonate (1.35 g, 9.76 mmol) were suspended under argon in 35 mL NMP and heated for 42 h at 120 °C. After being cooled to room temperature, the reaction mixture was added dropwise to 150 mL of 0.66 M hydrochloric acid and stirred for additional 2 h. The resulting precipitate was collected by filtration and dried in vacuo. The crude product was chromatographed on silica gel with dichloromethane/*n*-pentane (3/2) as the eluent, dissolved in dichloromethane, precipitated by addition of methanol, and dried in vacuo (10^{-3} mbar) at 60 °C to afford 1.40 g (1.41 mmol, 36 %) of **2** as a red solid:

Mp: 309–311 °C. ^{1}H NMR (400 MHz, $CDCl_3$, TMS): δ 8.20 (s, 4H), 7.17 (t, J = 8.2 Hz, 4H), 6.68 (ddd, J = 8.3 , J = 2.4, and J = 0.9 Hz, 4H), 6.56 (ddd, J = 8.1, J = 2.3, and J = 0.8 Hz, 4H), 6.50 (t, J = 2.3 Hz, 4H), 4.12 (t, J = 7.5 Hz, 4H), 3.67 (s, 12H), 1.65 (m, 4H), 1.38 (m, 4H), 0.94 (t, J = 7.4 Hz, 6H). MS (FAB, pos. mode, 3-nitrophenyloctylether) *m/z*: 990.3 $[M]^+$ (calcd 990.3). Anal. calcd for $C_{60}H_{50}N_2O_{12}$: C, 72.72; H, 5.09; N, 2.83. Found: C, 72.32; H, 5.17; N, 2.75. UV/Vis (CH_2Cl_2): λ_{max}/nm (ε_{max}/$M^{-1}cm^{-1}$) = 573 (43500), 536 (27600), 450 (16200), 289 (55900). Fluorescence (CH_2Cl_2): λ_{max} = 599 nm, fluorescence quantum yield Φ_{fl} = 0.89.

1,6,7,12-Tetra(3-methoxyphenoxy)perylene-3,4:9,10-tetracarboxylic Acid Bisanhydride (3).

Perylene bisimide **2** (500 mg, 0.50 mmol) and potassium hydroxide (3.00 g, 53.5 mmol) were suspended under argon in 25 mL isopropanol and heated to reflux for 2 h. After being cooled to room temperature, the reaction mixture was dropped into 90 mL glacial acetic acid and heated to 50 °C for 30 min. The resulting red precipitate was collected by filtration, washed with water (100 mL), and dried in vacuo (10^{-3} mbar) at 60 °C to give 396 mg (0.45 mmol) **3** in 90% yield. The product was used without further purification.

^{1}H NMR (400 MHz, $CDCl_3$, TMS): δ 8.20 (s, 4H), 7.20 (t, J = 8.2 Hz, 4H), 6.73 (ddd, J = 8.4, J = 2.4, and J = 0.8 Hz, 4H), 6.57 (ddd, J = 8.1, J = 2.3, and J = 0.9 Hz, 4H), 6.49 (t, J = 2.3 Hz, 4H), 3.68 (s, 12H). MS (FAB, pos. mode, 3-nitrobenzylalcohol) *m/z*: 880.1 $[M+H]^+$ (calcd 879.2). Anal. calcd for $C_{52}H_{32}0_{14}$: C, 70.91; H, 3.66. Found: C, 70.44; H, 4.09.

***N,N´*-Di(2-(*R*)-octyl)-1,6,7,12-tetra(3-methoxyphenoxy)perylene-3,4:9,10-tetracarboxylic Acid Bisimide (4).**

Perylene bisanhydride **3** (0.90 g, 1.02 mmol), 2-(*R*)-octylamine (0.69 mL, 0.53 g, 4.09 mmol) and catalytic amounts of zinc acetate were dissolved under argon in 25 mL quinoline and heated for 8 h at 180 °C. The reaction mixture was cooled to ambient conditions and slowly dropped into 50 mL of 0.4 M hydrochloric acid. After addition of 30 mL methanol the resulting precipitate was collected by vacuum filtration and dried in vacuo. Purification by silica gel column chromatography with dichloromethane/*n*-hexane (4/1), precipitation with methanol from dichloromethane solution and drying in vacuo (10^{-3} mbar) at 60 °C afforded 660 mg (0.60 mmol, 58%) of **4** as a red solid.

Mp: 279–281 °C. ^{1}H NMR (400 MHz, $CDCl_3$, TMS): δ 8.18 (s, 4H), 7.17 (t, J = 8.2 Hz, 4H), 6.67 (ddd, J = 8.3, J = 2.5, and J = 0.8 Hz, 4H), 6.57 (ddd, J = 8.1, J = 2.3, and J = 0.9 Hz, 4H), 6.50 (t, J = 2.4 Hz, 4H), 5.18 (m, 2H), 3.67 (s, 12H), 2.11 (m, 2H), 1.82 (m, 2H), 1.49 (d, J = 6.8 Hz, 6H), 1.23 (m, 16H), 0.82 (t, J = 7.0 Hz, 6H). MS (MALDI-TOF, pos. mode, DCTB) *m/z*: 1102.5 $[M]^+$ (calcd 1102.5). Anal. calcd for $C_{68}H_{66}N_2O_{12}$: C, 74.03; H, 6.03; N, 2.54. Found: C, 73.99; H, 6.06; N, 2.50. UV/Vis (CH_2Cl_2): λ_{max}/nm (ε_{max}/$M^{-1}cm^{-1}$) = 568 (45100), 530 (28500), 445 (16500), 285 (57100). Fluorescence (CH_2Cl_2): λ_{max} = 603 nm, fluorescence quantum yield Φ_{fl} = 0.94.

***N,N´*-Di(2-(*R*)-octyl)-1,6,7,12-tetra(3-hydroxyphenoxy)perylene-3,4:9,10-tetracarboxylic Acid Bisimide (5).**

Perylene bisimide **4** (0.60 g, 0.54 mmol) was dissolved in 20 mL dry dichloromethane and cooled to 0 °C. Over a period of 30 min a solution of 0.83 mL (2.18 g, 8.70 mmol) boron tribromide in 40 mL dry dichloromethane was added dropwise and stirred at 0 °C for 1 h and additional 3 h at room temperature. The solvent was removed by distillation and a mixture of water (48 mL) and methanol (12 mL) was added to the residue under ice cooling and treated for 30 min in a ultrasonic bath. The resulting precipitate was collected by filtration, washed with water and dried in vacuo. Column chromatographic purification on silica gel with dichloromethane/methanol (97/3) yielded 314 mg (0.30 mmol, 56%) of **5** as a wine-red solid.

Mp: 311–315 °C. ^{1}H NMR (400 MHz, DMSO-d_6): δ 9.68 (s, 4H), 7.88 (s, 4H), 7.16 (t, J = 8.0 Hz, 4H), 6.62 (ddd, J = 8.2, J = 2.1, and J = 0.8 Hz, 4H), 6.60–6.42 (m, 8H), 5.03 (m, 2H), 2.03 (m, 2H), 1.73 (m, 2H), 1.40 (d, J = 7.0 Hz, 6H), 1.16 (m, 16H), 0.77 (t, J = 6.9 Hz, 6H). MS (MALDI-TOF, pos. Mode, DCTB) m/z: 1046.3 $[M]^+$ (calcd 1046.4).

Anal. calcd for $C_{64}H_{58}N_2O_{12}$: C, 73.41; H, 5.36; N, 2.68. Found: C, 72.76; H, 5.58; N, 2.52.

Macrocyclic Perylene Bisimides 6 and 7.

Perylene bisimide **5** (300 mg, 0.29 mmol), diethylene glycol ditosylate (712 mg, 1.72 mmol) and cesium carbonate (1.23 g, 3.44 mmol) were suspended under argon in 45 mL dry DMSO and heated for 6 h at 120 °C. The reaction mixture was cooled to room temperature and dropped slowly into 75 mL of 0.33 M hydrochloric acid under stirring. The resulting precipitate was collected by vacuo filtration and dried in vacuum. The two regioisomeric macrocycles formed in the reaction were separated by column chromatography with dichloromethane as the eluent and each of the fractions was subjected to an additional column chromatographic purification with dichloromethane as eluent to yield 15.1 mg (12.7 µmol, 4%) of **6** as orange crystals and 106 mg (0.09 mmol, 30%) of **7** as red solid.

6: Mp: 249–251 °C. ^{1}H NMR (500 MHz, $CDCl_3$): δ 8.24 (s, 4H), 7.25 (m, 4H), 7.15 (m 4H), 6.42 (m, 4H), 5.58 (m, 4H), 5.21 (m, 2H), 3.84–3.76 (m, 4H), 3.67–3.58 (m, 8H), 3.56–3.49 (m, 4H), 2.23–2.11 (m, 2H), 1.91–1.79 (m, 2H), 1.54 (m, 6H), 1.37-1.18 (m, 16H), 0.83 (m, 6H). HRMS (ESI, dichloromethane:acetonitrile = 1:1): *m/z* calcd for $C_{72}H_{70}N_2O_{14}Na$ $[M+Na]^+$ 1209.4719, found 1209.4713. UV/Vis (CH_2Cl_2): λ_{max}/nm (ε_{max}/$M^{-1}cm^{-1}$) 532 (37600), 498 (25600), 460 (sh), 438 (sh), 279 (45600). Fluorescence (CH_2Cl_2): λ_{max} = 570 nm, fluorescence quantum yield Φ_{fl} = 0.22, fluorescence lifetime τ_f = 2.2 ns; (Et_2O): λ_{max} = 560 nm, fluorescence quantum yield Φ_{fl} = 0.73, fluorescence lifetime τ_{fl} = 6.2 ns.

7: Mp: 317–320 °C. ^{1}H NMR (400 MHz, $CDCl_3$, TMS): δ 8.29 (s, 4H), 7.07 (t, *J* = 8.2 Hz, 4H), 6.68 (t, *J* = 2.3 Hz, 4H), 6.59 (dd, *J* = 8.2, and *J* = 1.9 Hz, 4H), 6.54 (dd, *J* = 8.2, *J* = 1.7 Hz, 4H), 5.19 (m, 2H), 4.20 (bs, 8H), 4.00–3.70 (m, 8H), 2.20–2.05 (m, 2H), 1.90–1.70 (m, 2H), 1.50 (d, *J* = 6.8 Hz, 6H), 1.35–1.15 (m, 16H), 0.82 (t, *J* = 6.8 Hz, 6H). HRMS (ESI, dichloromethane:acetonitrile = 1:1) *m/z*: calcd for $C_{72}H_{71}N_2O_{14}$ $[M+H]^+$ 1187.4900, found: 1187.4876. Anal. calcd for $C_{72}H_{70}N_2O_{14}$: C, 72.83; H, 5.94; N, 2.36. Found: C, 72.77; H, 5.94; N, 2.36. UV/Vis (CH_2Cl_2): λ_{max}/nm (ε_{max}/$M^{-1}cm^{-1}$) 570 (47800), 530 (29100), 450 (16700), 286 (59600). Fluorescence (CH_2Cl_2): λ_{max} = 598 nm, fluorescence quantum yield Φ_{fl} = 0.95, fluorescence lifetime τ_{fl} = 6.9 ns.

Separation of the Epimers (*P*,*R*,*R*)-(+)-6 and (*M*,*R*,*R*)-(–)-6). Separation of the epimers of **6** was accomplished by HPLC on a semipreparative chiral column (Trentec, Reprosil 100 chiral-NR, Ø = 2 cm) with isopropanol/*n*-hexane (1/1) as eluent (flow rate 10 mL/min). Owing to the low solubility of **6** in the eluent, a dichloromethane solution of **6** was used for injection. The separation was performed on a scale of 8 mg.

(*P*,*R*,*R*)-(+)-6: Retention time (Trentec Reprosil 100 chiral-NR, Ø = 0.8 cm, isopropanol/*n*-hexane (1/1), flow: 2 mL/min): 24.7 min. Optical rotation (CH_2Cl_2, c = 0.007): $[\alpha]^{20}_D$= +6600. CD (CH_2Cl_2): λ_{max}/nm ($\Delta\tilde{\varepsilon}$/$M^{-1}cm^{-1}$) = 536 (67) , 499 (49), 425 (13), 337 (—13), 292 (113).

(*M*,*R*,*R*)-(—)-6: Retention time (Trentec Reprosil 100 chiral-NR, Ø = 0.8 cm, isopropanol/*n*-hexane (1/1), flow: 2 mL/min): 29.6 min. Optical rotation (CH_2Cl_2, c = 0.006): $[\alpha]^{20}_D$ = –6600. CD (CH_2Cl_2): λ_{max}/nm ($\Delta\varepsilon$/$M^{-1}cm^{-1}$) = 536 (–63), 499 (–45), 425 (–6), 337 (21), 292 (–97).

Supporting Information Available in the Appendix: Synthesis and characterization of NH-functionalized perylene bisimides and ^{1}H NMR spectra of compounds **2-7**.

4.8 References and Notes

1 See Chapter 3 of thesis and P. Osswald, D. Leusser, D. Stalke, F. Würthner, *Angew. Chem.* **2005**, *117*, 254-257; *Angew. Chem. Int. Ed.* **2005**, *43*, 250-253.

2 (a) I.-H. Suh, K. H. Park, W. P. Jensen, D. E. Lewis, *J. Chem. Ed.* **1997**, *74*, 800-805; (b) D. Burke, D. J. Henderson, *British J. Aneast.* **2002**, *88*, 563-576:

3 (a) L. Pu, *Chem. Rev.* **1998**, *98*, 2405-2494; (b) J. E. Field, T. J. Hill, D. Venkataraman, *J. Org. Chem.* **2003**, *68*, 6071-6078; (c) J. F. Schneider, M. Nieger, K. Nättinen, B. Lewall, E. Niecke, K. H. Dötz, *Eur. J. Org. Chem.* **2005**, 1541-1560.

4 F. Würthner, A. Sautter, J. Schilling, *J. Org. Chem.* **2002**, *67*, 3037-3044.

5 R. Altmann, C. Etzlstorfer, H. Falk, *Monatsh. Chem.* **1997**, *128*, 785-793.

6 *Exciton Chirality Method: Principles and Applications* in *Circular Dichroism*, 2nd ed., (Eds.: N. Berova, K. Nakanishi, R. W. Woody), Wiley-VCH, Berlin, **2000**, pp. 337-383.

7 W. H. Laarhoven, W. J. C. Prinsen, *Top. Curr. Chem.* **1984**, *125*, 63-130.

8 (a) G. Bringmann, J. Mühlbacher, M. Reichert, M. Dreyer, J. Kolz, A. Speicher, *J. Am. Chem. Soc.* **2004**, *126*, 9283-9290; (b) G. Bringmann, T. Gulder, M.

Reichert, F. Meyer, *Org. Lett.* **2006**, *8*, 1037-1040; (c) A. Muranaka, Y. Asano, A. Tsuda, A. Osuka, N. Kobayashi, *ChemPhysChem* **2006**, *7*, 1235-1240.

9 J. J. P. Stewart, *J. Comput. Chem.* **1989**, *10*, 209-220.

10 The contribution of the CD spectra of those structures that lie energetically higher than 3 kcal/mol above the found global minimum to the overall CD curve is negligible.

11 W. Weber, W. Thiel, *Theor. Chem. Acc.* **2000**, *103*, 495-506.

12 G. Bringmann, S. Busemann in *Natural Product Analysis*; (Eds.: P. Schreier, M. Herderich, H. U. Humpf, W. Schwab); Vieweg, Wiesbaden, **1998**, pp. 195-212.

13 Given the extreme dominance of the chiroptical contributions of the chiral axis vs. the two stereogenic centers, as proven by the inverse experimental CD spectra of the two epimers of **6** (Figure 4), additional calculations for (*M*,*R*,*R*)-**6** appeared unnecessary.

14 SYBYL, Tripos, Inc., 1699 South Hanley Road, St. Louis, MO 63144, USA.

15 Z. Chen, U. Baumeister, C. Tschierske, F. Würthner, *Chem. Eur. J.*, **2007**, *13*, 450-465.

16 S. Kohmoto, K. Sakayori, K. Kishikawa, M. Yamamoto, *J. Chem. Soc., Perk. Trans. 2* **1999**, 833-836.

17 (a) K. D. Shimizu, T. M. Dewey, J. Rebek, Jr., *J. Am. Chem. Soc.* **1994**, *116*, 5145-5149; (b) C. F. Degenhardt III, D. B. Shortell, R. D. Adams, K. D. Shimizu, *Chem. Commun.* **2000**, 929-930; (c) C. F. Degenhardt III, M. D. Smith, K. D. Shimizu, *Org. Lett.* **2002**, *4*, 723-726; (d) C. F. Degenhardt III, J. M. Lavin, M. D. Smith, K. D. Shimizu, *Org. Lett.* **2005**, *7*, 4079-4081.

18 M. Hesse, H. Meier, B. Zeeh, *Spectroscopic Methods in Organic Chemistry*; Thieme, Stuttgart, **1997**, pp. 88-100.

19 D. Marquis, J.-P. Desvergne, H. Bouas-Laurent, *J. Org. Chem.* **1995**, *60*, 7984-7996.

20 (a) J. R. Lakowicz, *Principles of Fluorescence Spectroscopy*; 2nd ed., Kluwer Academic/Plenum, New York, **1999**; pp. 52-55, (b) R. Givshi, R. Reisfeld, Z. Burshstein, *Chem. Phys. Lett.* **1993**, *213*, 338-344.

21 M. J. Frisch, G. W. Trucks, H. B. Schlegel, G. E. Scuseria, M. A. Robb, J. R. Cheeseman, J. A. Montgomery, Jr., T. Vreven, K. N. Kudin, J. C. Burant, J. M. Millam, S. S. Iyengar, J. Tomasi, V. Barone, B. Mennucci, M. Cossi, G. Scalmani, N. Rega, G. A. Petersson, H. Nakatsuji, M. Hada, M. Ehara, K. Toyota, R. Fukuda, J. Hasegawa, M. Ishida, T. Nakajima, Y. Honda, O. Kitao, H. Nakai, M.

Klene, X. Li, J. E. Knox, H. P. Hratchian, J. B. Cross, C. Adamo, J. Jaramillo, R. Gomperts, R. E. Stratmann, O. Yazyev, A. J. Austin, R. Cammi, C. Pomelli, J. W. Ochterski, P. Y. Ayala, K. Morokuma, G. A. Voth, P. Salvador, J. J. Dannenberg, V. G. Zakrzewski, S. Dapprich, A. D. Daniels, M. C. Strain, O. Farkas, D. K. Malick, A. D. Rabuck, K. Raghavachari, J. B. Foresman, J. V. Ortiz, Q. Cui, A. G. Baboul, S. Clifford, J. Cioslowski, B. B. Stefanov, G. Liu, A. Liashenko, P. Piskorz, I. Komaromi, R. L. Martin, D. J. Fox, T. Keith, M. A. Al-Laham, C. Y. Peng, A. Nanayakkara, M. Challacombe, P. M. W. Gill, B. Johnson, W. Chen, M. W. Wong, C. Gonzalez, J. A. Pople, GAUSSIAN 03, Revision B.04, Gaussian, Inc., Carnegie Office Park, Pittsburgh, PA 15106, USA, **2003**.

23 W. Thiel, MNDO99, Version 6.0, Max-Planck-Institut für Kohlenforschung, Kaiser-Wilhelm-Platz 1, D-45470 Mülheim, Germany, **2001**.

Chapter 5

Synthesis, Resolution and Solid State Packing of Macrocyclic 1,7-Diaryloxy-Perylene Bisimide Atropo-Enantiomers

Abstract: The macrocyclization of 1,7-di(hydroxyphenoxy)-substituted perylene bisimide by etherification with diethylene glycol ditosylate has afforded the diagonally bridged macrocycle **4**. The structure of the macrocycle has been confirmed by NMR spectroscopy and X-ray analysis. This is the first single crystal X-ray structure of a 1,7-diaryloxy-substituted perylene bisimide. Furthermore, the optical and electrochemical properties of the present macrocycle have been investigated by UV/Vis and fluorescence spectroscopy and cyclic voltammetry. The resolution of the atropo-enantiomers of this macrocycle has been achieved by semi-preparative HPLC on a chiral column and the chiroptical properties of the enantiomers have been investigated by CD spectroscopy. By comparison of the chiroptical properties of the enantiomers of **4** with those of the epimeric bis(macrocycles) reported in Chapter 4, the dependence of the chiroptical properties on the torsion of the perylene core has been demonstrated. The crystal structure of the (*P*)-enantiomer of macrocycle **4** has revealed an exclusive formation of dimers in the solid state.

5.1 Introduction

In 1997, Böhm et al. have reported a method for the preparation of 1,7-dibromoperylene bisimides.[1] This method has opened an easy access to functional perylene bisimides and numerous disubstituted perylene bisimides bearing pyrrolidino, cyano or aryloxy functionalities in the bay area (1,7-positions) have been reported.[1b,2] Core-extended coronene bisimides could be made available starting by this method from 1,7-diethynyl-substituted perylene bisimides.[1b,2] Especially the introduction of aryloxy-substituents has been widely applied to afford soluble dyes that can be further functionalized by proper derivatization of these substituents. As in the case of most of the perylene bisimide fluorophores, excellent optical properties with quantum yields of up to unity and high stability against environmental influences has been confirmed for these diaryloxy-substituted perylene bisimides (DAPBIs).[2] Thus, it is not surprising that DAPBIs have been evolved to one of the most investigated compounds in the field of perylene bisimide research. Liquid crystalline derivatives became accessible which show promising prospects for application in organic light-emitting diodes.[3] Multichromophoric entities have been realized by combining DAPBIs with other chromophores[4] by covalent or self-assembly approaches. In such multichromophoric systems efficient energy and electron transfer processes have been demonstrated, thus they may serve as artificial light-harvesting systems.[4] Additionally, logic gates based on DAPBIs have been realized,[5] and water soluble dyes have been made available, which can be used as biomarker.[6] Apart from the versatility of these fluorophores, DAPBIs possess like other bay-substituted perylene bisimides a twisted perylene core as revealed by molecular modeling.[3b] Such core-twisting endows these perylene bisimides with conformational chirality (see Chapter 2). Macrocyclization of hydroxyphenoxy-functionalized perylene bisimides has been demonstrated to be a rational method to prevent the racemization process between (*P*)- and (*M*)-enantiomer imposed by the twisted nature of the perylene dyes as demonstrated in Chapter 3.[7a] In Chapter 4 the resolution of atropo-diastereomeric (epimeric) bis(macrocycles) based on tetraaryloxy-substituted perylene bisimides as well as their chiroptical properties are reported.[7b] Atropo-enantiomerically pure perylene bisimides were not known prior to this work. In this chapter, the resolution of the atropo-enantiomers of 1,7-disubstituted perylene bisimides and their chiroptical properties are presented.

To gain an easier and more convenient access to the atropisomers of perylene bisimides a macrocycle based on 1,7-diaryloxy-substituted perylene bisimides was

synthesized. The separation of the enantiomers was accomplished by semi-preparative HPLC on a chiral column and the chiroptical properties were investigated by CD spectroscopy. Comparison of the chiroptical properties of these 1,7-macrocyclic DAPBIs with those determined for the epimeric tetraaryloxy-substituted bis(macrocyclic) perylene bisimides (Chapter 4) allowed the assignment of the absolute configuration of the isolated enantiomers. Also single crystals for the racemic mixture as well as for the (*P*)-enantiomer of macrocycle **4** became available which enable the first single crystal X-ray analysis of DAPBIs. Comparison of the crystal structures of rac-**4** and (*P*)-**4** revealed the formation of π-dimers in the case of homochiral macrocycles (*P*)-**4**, which was not observed for the racemic mixture. Additionally, the optical and electrochemical properties of this macrocycle were investigated.

5.2 Synthesis and Resolution of Enantiomers of Macrocyclic Perylene Bisimides

The macrocyclic perylene bisimide **4** was synthesized according to Scheme 1 in three steps starting from the literature known dibromo-substituted perylene bisimide **1** which contained ca. 5-10% of the 1,6-isomer.[1] Nucleophilic displacement of the bromine atoms of **1** with 3-methoxyphenol in *N*-methylpyrrolidon (NMP) in the presence of anhydrous potassium carbonate as base afforded 1,7-diaryloxy-substituted perylene bisimide along with some 1,6-regioisomer (5-10%). Compound **2** could be isolated after column chromatography with dichloromethane/*n*-hexane (4:1) in 66% yield. The methylether in PBI **2** was cleaved with boron tribromide in dichloromethane to obtain **3** after column chromatographic purification in 96% yield as 9:1 mixture of the respective 1,7- and 1,6-isomers. For the macrocyclization, the previously described method for tetraaryloxy-substituted perylene bisimides was applied.[7] A diethylene glycol linker was chosen as the bridging unit since it provides a rather rigid scaffold and enables reasonable yields for the cyclization reaction.[7] Thus, **3** was treated with diethylene glycol ditosylate and cesium carbonate in DMSO at 120 °C (PBI concentration 10^{-2} M), and after column chromatographic purification of the crude product the desired macrocycle **4** was obtained in 7% isolated yield. The presence of only two resorcin units in **3** afforded the formation of only one racemic macrocyclic product and moreover the number of possible by-products is significantly decreased compared to bis(macrocycles) based on tetraaryloxy-substituted perylene bisimides.[7] Thus, the purification of monobridged macrocycle **4** by column chromatography was much easier compared to that of the tetra(hydroxyphenoxy)-substituted PBIs (see Chapters 3 and 4). The isolated

yield of the monobridged macrocycle **4** (7%) is, however, similar to those observed for analogues diagonally bridged bis(macrocycles) based on tetraaryloxy-substituted perylene bisimides **5** and **6** (4-5%).[7,8] The low yield observed for **4** might be ascribed to the poor solubility of the starting material **3** in DMSO. Additionally, the less twisted perylene core of the precursor **3** (16° instead of 25° for the tetraaryloxy-substituted PBIs) entails a larger distance between the aryloxy functionalities and a less favorable preorganization for the macrocyclization reaction that requires a horizontal orientation.

Scheme 1. Synthesis of Macrocycles based on 1,7-Disubstituted Perylene Bisimides **4**.

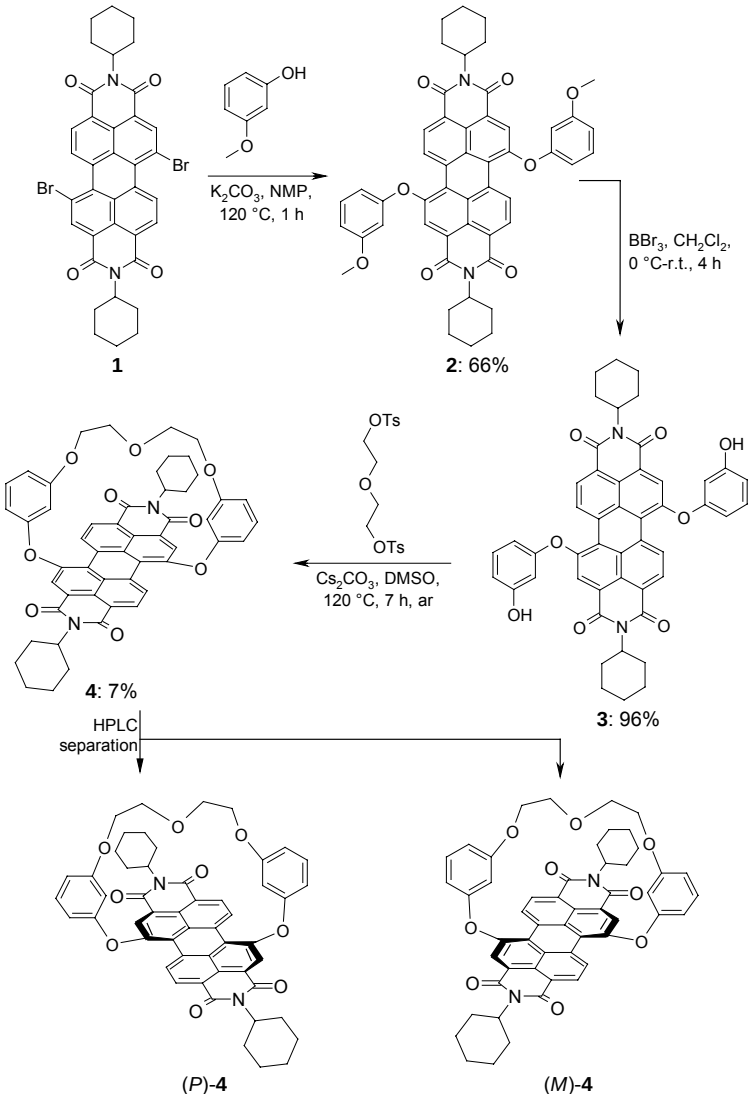

In the case of **4** an interconversion between the twisted conformers (*P* and *M*) is no more possible due to the diagonal bridge (1,7-linkage).[7] Thus, the resolution of the enantiomers of macrocyclic PBI **4** could be achieved by semi-preparative HPLC on a biphenyl-functionalized chiral column (Trentec, Reprosil 100 chiral-NR) with

dichloromethane/*n*-hexane (3:2) as eluent (Figure 1) and a retention time of 6.0 min for the first eluted fraction **4´** and 6.8 min for the second eluted **4´´**.

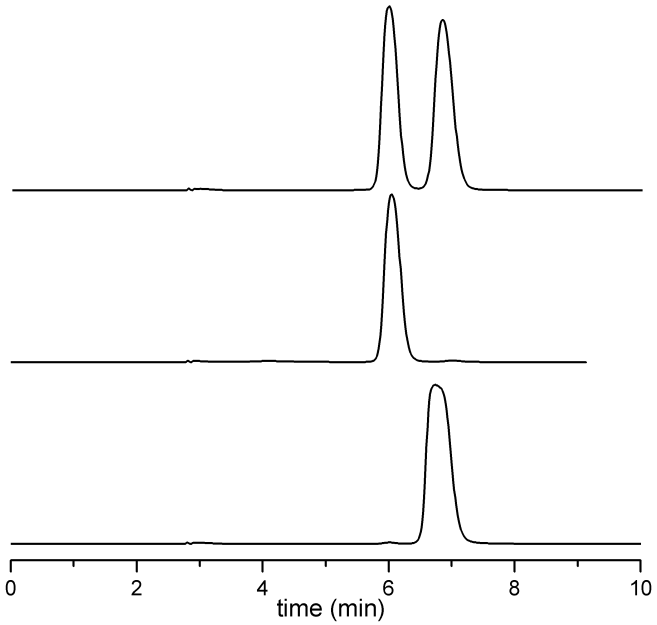

Figure 1. HPLC chromatograms before (top) and after separation of the enantiomers of **4** on a Trentec Reprosil 100 chiral-NR column at ambient conditions using dichloromethane/*n*-hexane (2:1) as eluent (flow rate: 1 mL/min).

As described in Chapter 3, the resolution of the atropo-enantiomers for double-bridged macrocycle **5** was not possible. Therefore, the successful separation of the enantiomers of **4** with Trentec Reprosil 100 chiral-NR column can be ascribed to the presence of only one macrocyclic linkage and/or the sterically less demanding imide substituent. Thus, an increased interaction between the chiral aromatic stationary phase (biphenyl derivative) with the twisted aromatic perylene π-system of **4** might be responsible for its better resolution.[7]

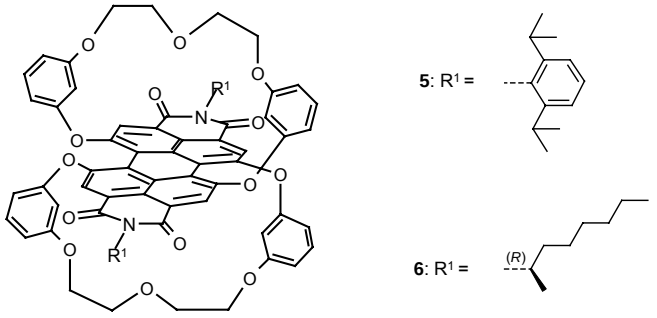

The structural assignment of the racemic macrocycle **4** as a diagonally bridged PBI was made by comparison of the ^{1}H NMR data of this compound with those of the open-chain reference **2** and previously reported macrocycles, whose structures were

unambiguously confirmed by X-ray crystallographic analysis.[7] As can be seen from Figure 2, the resonance of the proton situated between the two oxygens of the resorcin units of **4** (δ = 5.57 ppm) is shifted by about 1.2 ppm to higher field compared to that of the open-chain compound **2** (red marked, Figure 2) which is characteristic for diagonally bridged PBI macrocycles.[7] This pronounced shift can be attributed to a perpendicular orientation of the aryloxy residues relative to the perylene core. Since a macrocyclic product based on the respective 1,6-isomer which was present in an amount of about 10% in starting material **3**, would give rise to similar spectral features, additional prove is required for the assigned structure, which is provided by X-ray analysis of macrocycle **4** (see below).

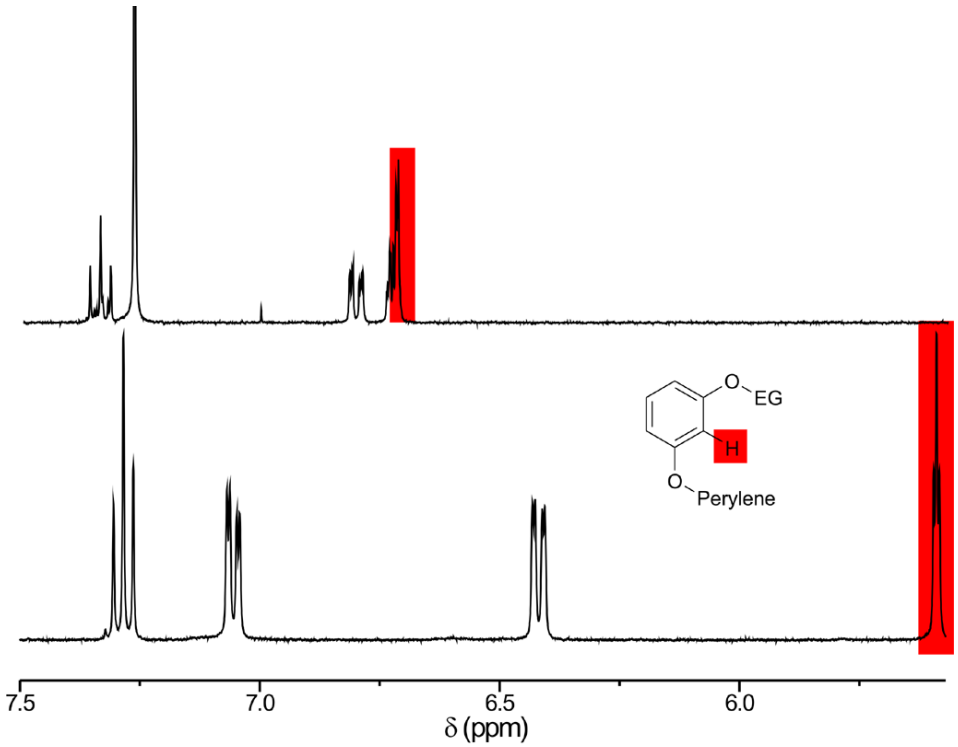

Figure 2. Aromatic region of the ^{1}H NMR spectrum (400.13 MHz) of **2** (top) in $CDCl_3$ and **4** (bottom) in CD_2Cl_2 at 300 K. The resonances highlighted in red belong to the proton situated between the oxygens of the rescorin subunits as schematically shown in the inset (EG denotes ethylene glycol).

5.3 Chiroptical Properties and Stereochemical Assignment of the Enantiomers

The chiroptical properties of the two enantiomers **4´** and **4´´** were determined by circular dichroism and polarimetry in dichloromethane at 20 °C. The stereochemical assignment was achieved by comparison of the measured CD spectra with those of the epimerically pure macrocyclic perylene bisimides **6**, whose stereochemistry was unequivocally

elucidated by CD spectroscopy in combination with quantum chemical calculations as described in Chapter 4.[7]

The UV/Vis absorption and CD spectra of **4´** and **4´´** are shown in Figure 4. In the visible region (400-650 nm), a monosignated CD signal with a maximum at 527 nm was observed for both enantiomers which properly correlates to the absorption maximum at 525 nm. Additionally, good agreement of the shape of the CD spectra for the bands related to the S_0-S_1 transitions (490 – 530 nm) with the absorption spectra was observed. The $\Delta\varepsilon$ values determined for the longest wavelength transition at 527 nm resulted to –51 and +49 $M^{-1}cm^{-1}$ for **4´** and **4´´**, respectively, and revealed the expected mirror image relation between the atropo-enantiomers. By comparison with the CD spectra of the epimeric macrocyclic perylene bisimide **6** presented in Chapter 4,[7] the first eluted fraction **4´** was assigned to the (*M*)-enantiomer by the negative sign of the Cotton effect observed for longest wavelength transition, and accordingly the second eluted fraction **4´´**, to the (*P*)-enantiomer. The same stereochemical assignment results from the analysis of the CD bands in the UV region (250 - 350 nm) of the enantiomers of **4**. An asymmetric bisignated signal was observed with a negative first Cotton effect at 289 nm ($\Delta\varepsilon$ values are –137 and 138 $M^{-1}cm^{-1}$) and a positive second Cotton effect at 265 nm (86 and -83 $M^{-1}cm^{-1}$) for the first eluted enantiomer **4´** and vice versa for the second eluted enantiomer **4´´**. According to exciton chirality method, the observed negative Cotton effect can be related to a (*M*)-configuration of the perylene core for the first eluted enantiomer **4´** and vice versa to a (*P*)-configuration for the second eluted enantiomer **4´´**.[9]

The absorption asymmetry factor $g = \Delta\varepsilon/\varepsilon$ for both enantiomers of **4** was calculated to 9.1 x 10^{-4} for the longest wavelength transition (527 nm). The lower value of the *g* factor obtained for **4** in comparison to the epimers of diagonally bridged macrocycle **6** (g value = 1.8 x 10^{-3}; see Chapter 4)[7b] can be attributed to the less twisted π-system in the present case. Accordingly, a twofold increase of the twist angle from 17° for **4** to 33° for macrocycles with two bridging units like **5** and **6** leads to a doubling of the g factor (see X-ray analysis below). Apart from many similarities with the circular dichroic properties of epimeric tetraaryloxy-substituted macrocycles **6**, it is noteworthy that the bands related to the S_0-S_2 transition are opposite in sign. This might be explained in terms of different polarization of this transition due to the change of the symmetry from D_2 to C_2, or by the presence of another transition (e.g., the S_0-S_3 transition).[10]

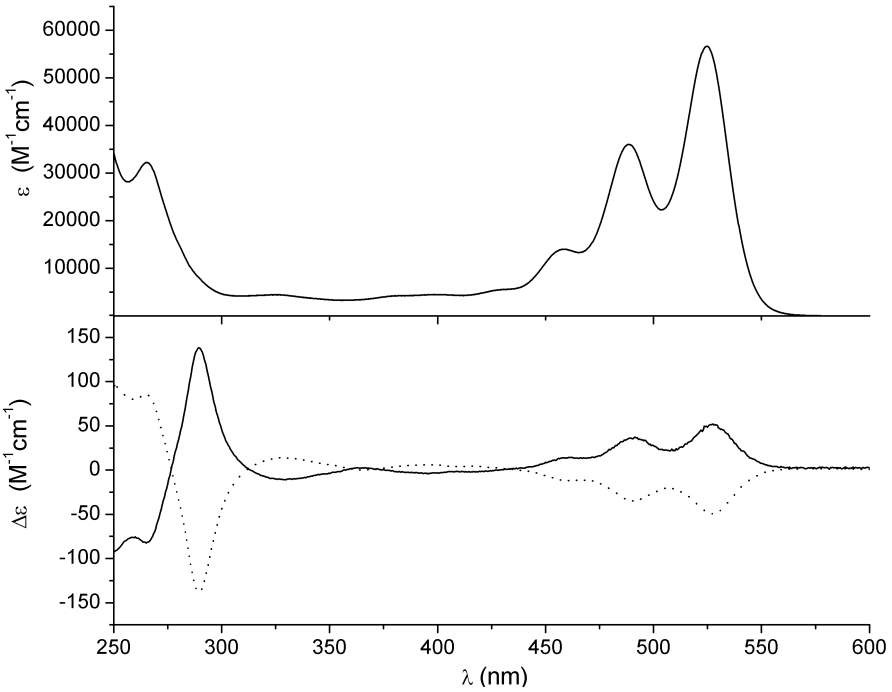

Figure 3. Absorption (top) and circular dichroism (CD) spectra (bottom) of **4´** (dotted line) and **4´´** (solid line) in dichloromethane at 20 °C.

Furthermore, the optical rotation $[\alpha]^{D}_{20}$ of the two enantiomers in dichloromethane was determined to –3761 (c 0.0018) and +3730 (c 0.0015) for (*M*)-**4** and (*P*)-**4**, respectively. The sense of optical rotation of these enantiomers corresponds to that of the isolated epimers of **6** conforming the stereochemical assignment of the enantiomers of **4**.[7b] In comparison to **6** ($[\alpha]^{D}_{20}$ = +6660), the observed values for **4** are reduced by a factor of two in accordance to the g value and the difference in the twist of the perylene core (see section 5.4), albeit, the relatively large values observed for the optical rotation of **4** profit from dispersion enhancement effects as the applied wavelength (589 nm) used in the experiment is pretty close to the absorption maximum (527 nm).

5.4 X-ray Analysis of Racemic 4 and Enantiomerically Pure (*P*)-4

Single crystals of racemic **4** and (*P*)-**4** suitable for X-ray diffraction were obtained by dissolving the compounds in dichloromethane, addition of equal amounts of methanol and subsequent slow evaporation of the solvent. The molecular structure of rac-**4** is shown in Figure 4. Selected crystallographic data for rac-**4** and (*P*)-**4** are given in reference 11 and in the appendix of this thesis and the characteristic features of both

crystals are described below.§ These are the first crystal structures of 1,7-diaryloxy-substituted perylene bisimides. Moreover, the crystal structure of (*P*)-**4** reveal for the first time the packing features of homochiral bay-substituted perylene bisimides.

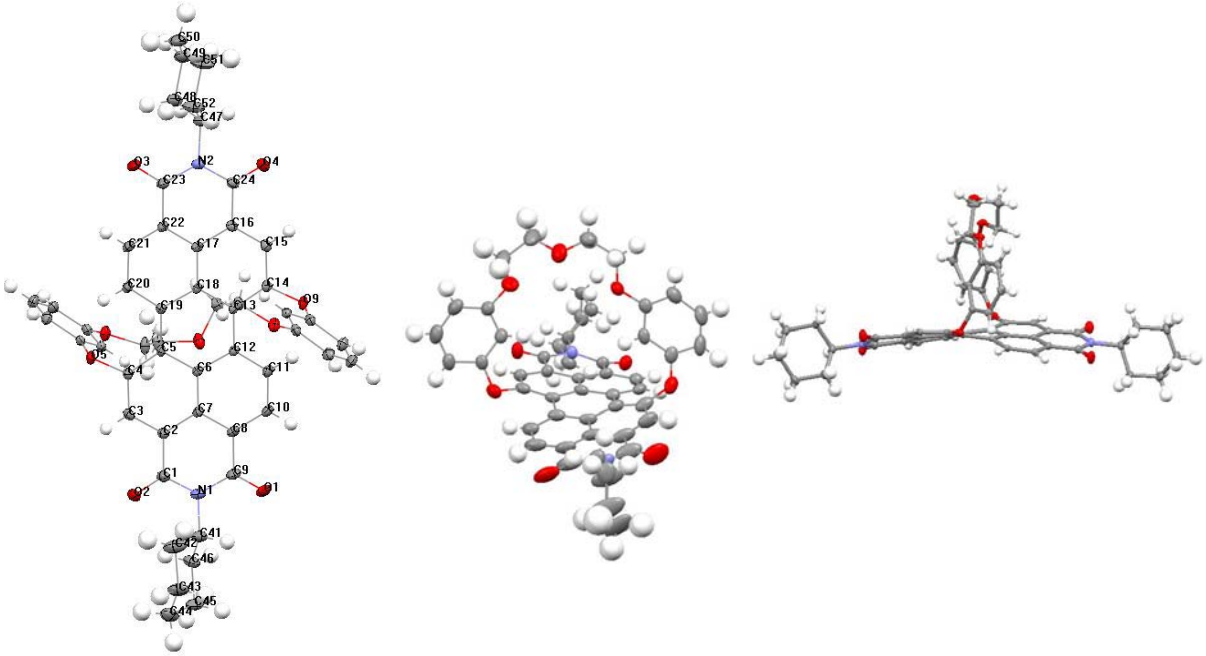

Figure 4. Molecular structure of macrocycle **4** in the racemic crystal (only (*P*)-enantiomer is shown). Fully labeled structure (left), view along the *N*,*N*-axis (middle) and view along the short axis of the perylene bisimide showing the bowl-like distortion of the perylene core (right). The anisotropic displacement parameters are depicted at a 50% probability level. Note that both enantiomers (*P* and *M*) of **4** are present in the crystal in equal amounts.[12]

Racemate **4** crystallized in orthorhombic space group Pna2(1) comprising both enantiomers in the crystal lattice. The molecular structure of **4** clearly reveals the diagonally bridged nature of the macrocycle with the bridge connecting the aryloxy-units in the 1,7-positions of the perylene core, which confirms the structural assignment made by NMR spectroscopic data. Characteristic for bay-substituted perylene bisimides is a twisted π-system which can be expressed either by the torsion of the central six-membered ring (dihedral angle) or by the twist between the two naphthalene units of the perylene bisimide core. It has to be noted at this point that these two quantities must be equal if there is no other distortion present in the twisted π-system. In the case of **4**, the dihedral angels were determined to 16.8° (C4-C5-C19-C20) and 17.3° (C11-C12-C13-

§ X-ray measurements and structure determination was performed by Dr. K. Radaki, University of Würzburg (Germany), Institute of Inorganic Chemistry.

C14) (see fully labeled structure for numbering), thus an average twist of 17.1° of the central six-membered ring is present which is in good agreement with the torsion expected for open-chain 1,7-DAPBIs from molecular modeling investigations (15°).[3b,13] In comparison to tetraaryloxy-substituted macrocycles with similar chain length like **5**, which possess a twist angle of 33° as demonstrated in Chapter 3, the twist of the perylene core of **4** is about half as high.[7a] It is noteworthy that the difference in the torsion of the two bay areas (16.8° vs. 17.3°) leads to symmetry breaking in the solid state, a fact which was also observed for tetraaryloxy-substituted macrocycles (see Chapter 3). Whilst similar dihedral angles were observed for the central six-membered rings, larger twist angles were calculated for the twist of the two naphthalene planes. For different molecular angles, e.g., θ (C1-N1-N2-C23) or θ (C3-C7-C17-C21) (see fully labeled structure for numbering), describing the twist of the two naphthalene units, values in the range of 22-28° were determined that are significantly larger than the torsion of the central six-membered ring. As can be seen from Figure 4 (right), this deviation originates from an unprecedented bowl-type curvature of the perylene core along the *N,N*-axis.

The crystal packing of rac-**4** is characterized by a centrosymetric unit cell composed of two molecules of each enantiomer (*P* and *M*). Enantiomers of the same chirality are located in the diagonal opposite corners of the unit cell as shown in Figure 5 (left).

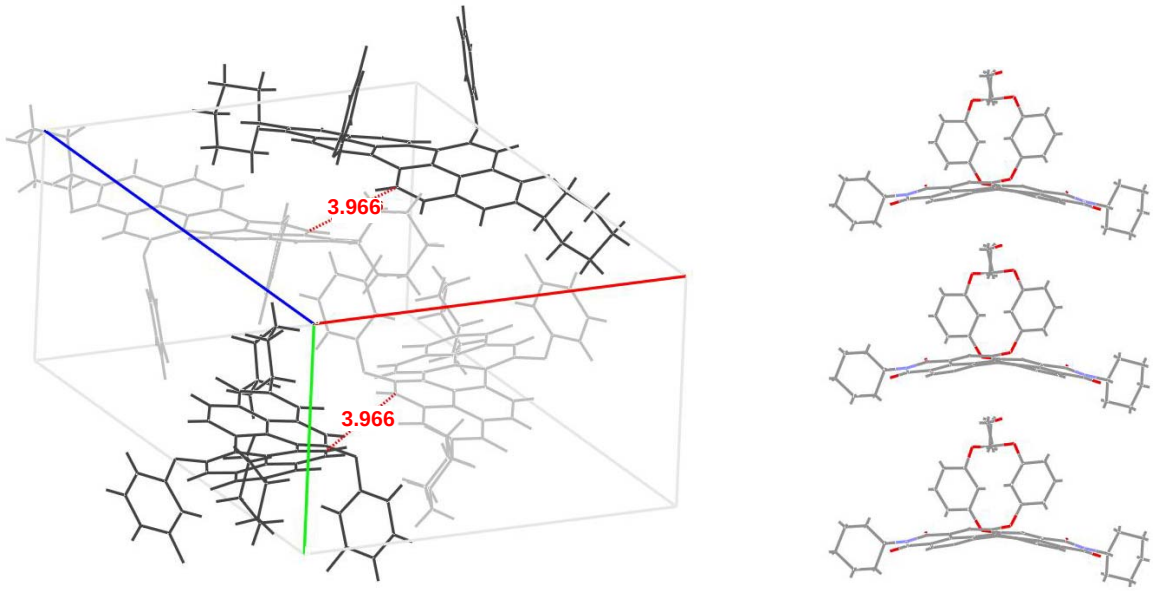

Figure 5. Unit cell of the crystal structure of rac-**4** (left) and packing along the b-axis of the unit cell (right). For representation of the unit cell, the (*P*)-enantiomer is highlighted in dark gray and the (*M*)-enantiomer in light gray and the ethylene glycol bridges are omitted for clarity. The a-axis is labeled red, the b-axis in green and c-axis in blue.

Along the b-axis of the unit cell the molecules are arranged in stacks of one enantiomer with a face-to-edge arrangement as shown in Figure 5 (right). The distance between two perylene bisimide cores in these stacks was determined to 9.9 Å and is mainly determined by the macrocyclic structure of **4**. A closest distances between two molecules of 3.4 Å was found as the distance between two aryloxy residues and of 4.0 Å as the closest distance between two perylene bisimide cores as shown in Figure 5 (left). It is interesting to note that the formation of π-stacked dimers was not observed in the crystal of rac-**4**, although it would have been expected from the structural features of this molecule.

The enantiomerically pure (*P*)-**4** is crystallized in the monoclinic space group C_2 and two crystallographically independent molecules were found in the unit cell (Figure 6). The torsion of the central six-membered ring was determined for one type of molecules (denoted as P2) to 16.9° and 18.5°, and for the other (denoted as P1) to 16.8° and 9.8° being in good agreement with the values obtained for rac-**4**. Molecule P1 possesses a bowl-like structure as described above for rac-**4**, whereas the second type of molecule (P2) does not show any distortion along the *N,N*-axis of the perylene bisimide. The low torsion of 9.8° as well as the bowl-like bending of P1 might be due to packing effects.

Even more interesting than the molecular structures is the solid state packing of the enantiopure macrocycle (*P*)-**4**. In contrast to rac-**4**, the solid state structure of (*P*)-**4** reveals the exclusive formation of π-dimers for these homochiral macrocycles. The dimers are arranged in two perpendicular layers with the perylene plane of **4** being either perpendicular to the a-axis (dimer B of P2 molecules) or the c-axis (dimer A of P1 molecules) of the unit cell (see Figure 6). The closest distance between the molecules was determined to 3.27 Å for dimer B whereas for both π-dimers the mean distance between two perylene bisimide π-surfaces was elucidated to 3.47 Å (see Figure C2 in the Appendix). This is only slightly larger than the distance observed in the solid state for the π–π interactions of the parent fully planar unsubstituted perylene bisimides[14] and of tetrachloro derivatives.[15] The dimers observed in each of the two layer exhibit slightly different geometries and the respective π–π interactions are shown in Figure 7. Both dimers A and B are characterized by a rotational offset of 43° and 58°, respectively. The rotational offset is accompanied by a longitudinal offset along the *N,N*-axis of the perylene bisimide which is negligible for dimer A, but pronounced for dimer B. The chirality of the dimers induced by the rotational offset can be assigned as left-handed for

both dimers A and B. This indicates that the (*P*)-chirality of the twisted perylene core enforces the formation of dimers with left-handed supramolecular chirality.

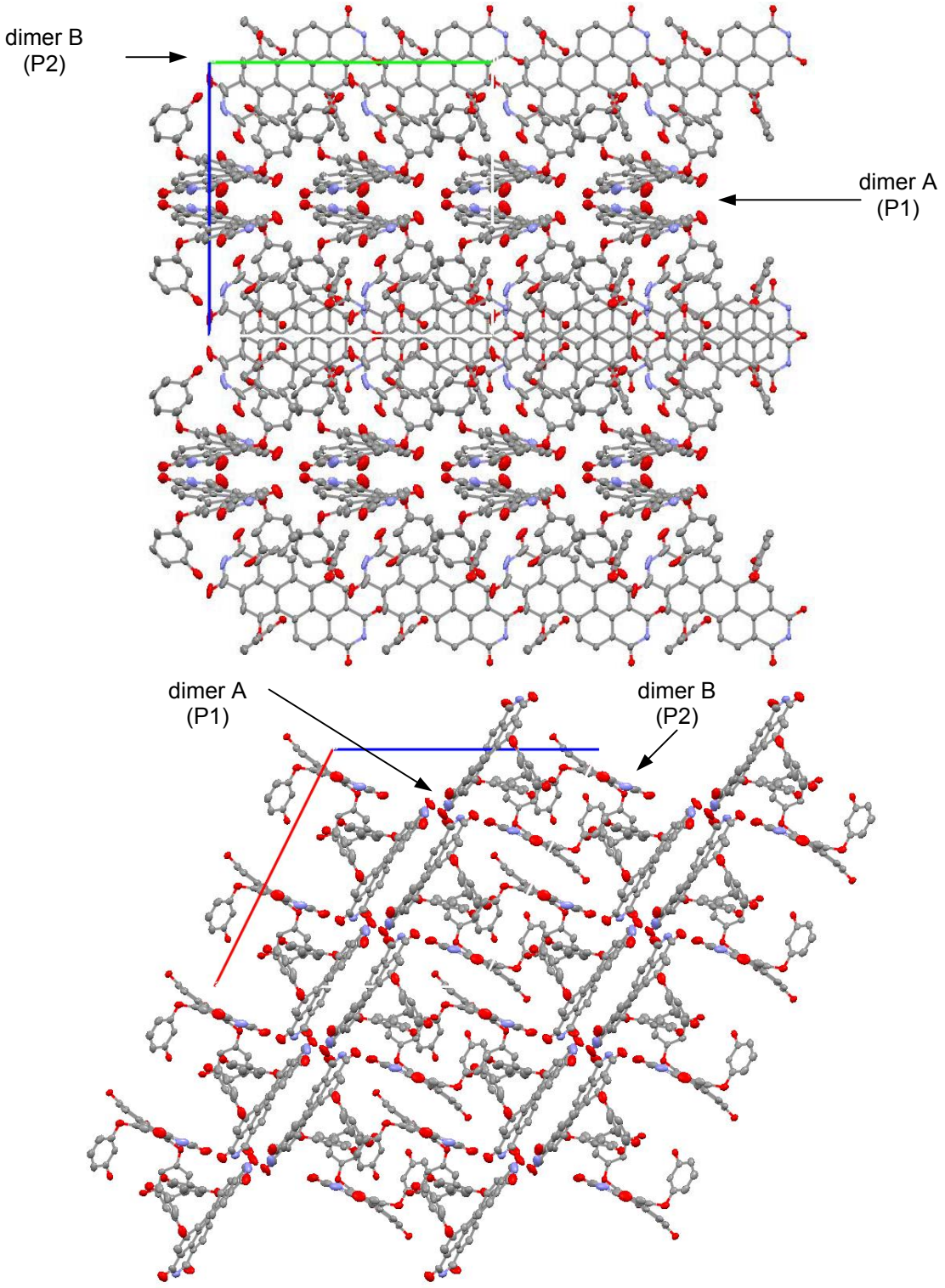

Figure 6. View along along the a-axis (top) and b-axis (bottom) of the crystal structure of (*P*)-**4**. The red line represents the a-axis, the green line the b-axis and the blue line the c-axis of the unit cell. Diethylene glycol bridges and included solvent molecules were omitted for clarity.

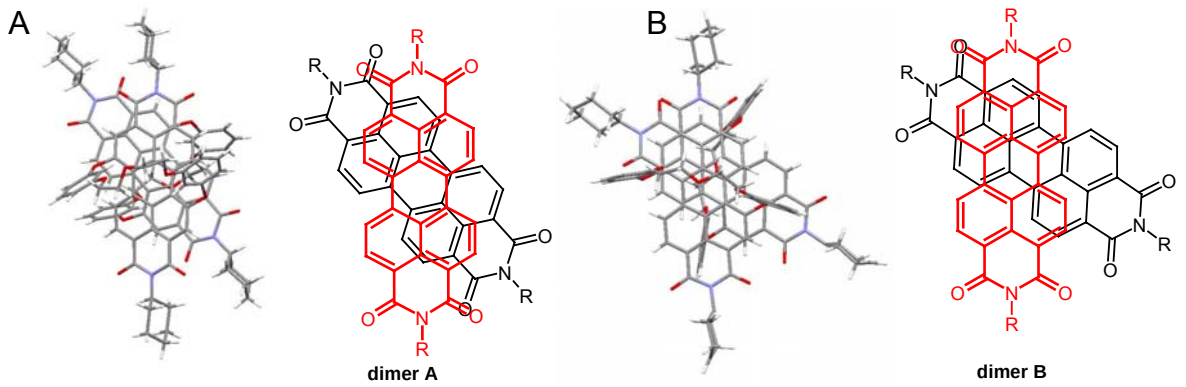

Figure 7. π–π interaction between two molecules in a dimer observed in the solid state structure of (*P*)-**4**: Crystal packing (left) and corresponding structural representation (right) of dimer A (A) and dimer B (B). In the structural representation, the top molecule is highlighted in red and the substituents in the bay area are omitted for clarity.

The comparison of the crystal structure of (*P*)-**4** with that of rac-**4** suggests that the formation of π-stacked dimers is favored for perylene bisimides possessing the same inherent chirality, i.e. homochiral (*P*)-(*P*) or (*M*)-(*M*) dimers than the association of two atropo-enantiomers with opposite chirality, i.e., heterochiral (*P*)-(*M*) dimers, as dimerization was not observed in the crystal of rac-**4**. Homochiral aggregation was previously observed in the crystal structure of racemic *N,N´*-dicyclohexyl-1,7-dibromoperylene-3,4:9,10-tetracarboxylic acid bisimide,[3c,16] and also proposed for self-assembled chiral perylene bisimide aggregates.[17] However, crystal packing of enantiopure (*P*)-**4** provides insight into the pair-wise stacking arrangement of the chromophores in dimers of core-twisted perylene bisimides.

5.5 Optical Properties

The optical properties of racemic DAPBIs **2** and **4** were investigated by UV/Vis absorption and fluorescence (steady state and time-resolved) spectroscopy in dichloromethane. It should be noted at this point that **2** contains about 5% of the corresponding 1,6-isomer. The UV/Vis absorption and emission spectra of **2** and **4** in dichloromethane are shown in Figure 8.

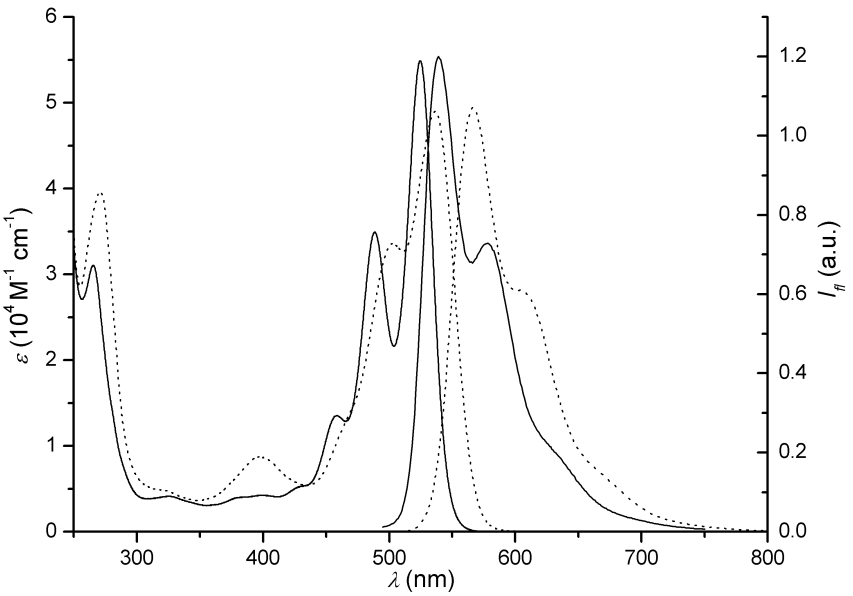

Figure 8. Absorption and emission spectra of open-chain perylene bisimide **2** (dotted line) and macrocycle **4** (solid line) in dichloromethane.

The absorption spectrum of **4** exhibits a maximum at 525 nm which is hypsochromically shifted by 11 nm in comparison to open-chain perylene bisimide **2** (536 nm). This spectral change is typical for diagonally bridged macrocyclic perylene bisimides and can be rationalized by a decreased electronic interaction of the electron-rich aryloxy substituent and the electron-poor perylene bisimide core in comparison to open-chained perylene bisimides like **2**. This results from a perpendicular orientation of the aryloxy substituents relative to the perylene core and was extensively discussed in Chapter 3.[7] The observed hypsochromic shift of **4** is less pronounced as for the diagonally bridged isomers of tetraaryloxy-substituted perylene bisimides with similar length of the bridging unit **5** and **6** (Chapter 3 and 4 of this thesis) which can be attributed to the presence of only two aryloxy residues. In comparison to open-chained perylene bisimides like **2** ($\varepsilon = 49000$ $M^{-1}cm^{-1}$), **4** exhibits hyperchromicity with a molar absorption coefficient of 55800 $M^{-1}cm^{-1}$ for the S_0-S_1 transition. Additionally, the absorption spectra reveal a pronounced vibrational fine structure for the S_0-S_1 transition, not observed for the conformationally unrestricted DAPBI **2**, and this effect is accompanied by a pronounced hypochromicity of the transitions related to the S_0-S_2 transition (Figure 8). As the transition dipole moment μ_{eg} for the S_0-S_1 transition remains almost unchanged for both dyes (7.3 D for **4** and 7.7 D for **2**, see experimental section), the observed increase of the ε_{max} value for **4** is apparently owing to the spectral

narrowing. Furthermore, the clearly visible vibrational progressions for the S_0-S_1 transition indicate the conformational rigidity of macrocycle **4**.

The fluorescence properties of open-chain perylene bisimide **2** and macrocycle **4** are summarized in Table 1. The emission spectrum of **4** shows mirror image relation with an emission maximum at 539 nm (Figure 8). The observed Stokes shift for **4** is reduced to only 14 nm (compared to 30 nm for **2**), again indicative for the rigidity of this system imposed by the macrocyclic linkage. The fluorescence of **4** in dichloromethane (ε_r = 8.7) is moderate with a quantum yield of 27%. The fluorescence quantum yield corresponds to that of tetraaryloxy-based macrocycles **6** as reported in Chapter 4.[7b] In less polar solvents, i.e., diethylether (ε_r = 4.3), the fluorescence quantum yield of **4** increases to 38% (Table 1). Accordingly, the fluorescence lifetime is slightly increased from 1.5 ns in dichloromethane to 2.4 ns in diethylether. The increase of the lifetime of the excited state is due to a decrease of the rate constant for the non-radiative processes, whereas that of the radiative process remains constant (Table 1). Thus, in contrast to earlier reported analogue macrocycles as described in Chapter 3 and 4 of this thesis,[7] macrocycle **4** reveals only a slight increase of the fluorescence by decreasing the solvent polarity.

Table 1. Fluorescence Properties of Macrocyclic Perylene Bisimides **2** and Open-Chain Reference Compound **4**

	solvent	λ_{max}^{fl} (nm)	Φ_{fl} [a]	τ_{fl} (ns)[b]	k_r (s^{-1})[c]	k_{nr} (s^{-1})[d]
2	dichloromethane	566	0.90	4.9	1.8×10^8	2.0×10^7
4	dichloromethane	539	0.27	1.5	1.8×10^8	4.9×10^8
	diethylether	530	0.36	2.4	1.5×10^8	2.7×10^8

a) Φ_{fl} ± 0.03; b) τ_{fl} ± 0.2; c) $k_r = \Phi_{fl} \cdot \tau_{fl}^{-1}$; d) $k_{nr} = (1-\Phi_{fl}) \cdot \tau_{fl}^{-1}$.

5.6 Electrochemical Properties

The electrochemical properties of macrocyclic perylene bisimide **4** were investigated by cyclic voltammetry in dichloromethane with tetrabutylammonium hexafluorophosphate (TBAHFP) as supporting electrolyte. DAPBI **4** showed two reversible reduction waves with a half-wave potential of –1.10 V and –1.33 V, which can be attributed to the formation of perylene bisimide monoanion and dianion, respectively, and no oxidation peak could be found within the available potential range (Figure 9).

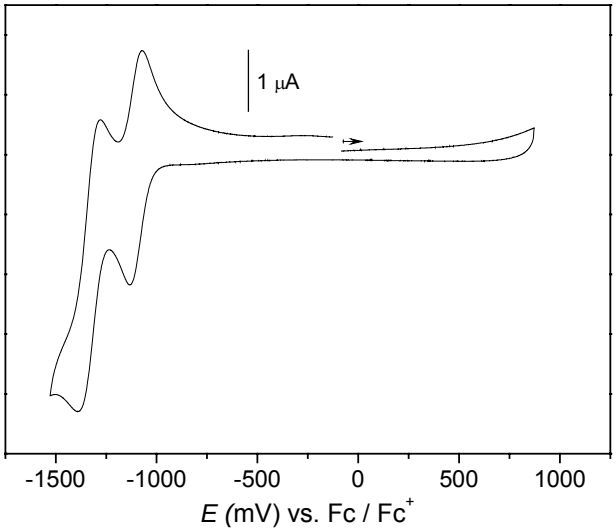

Figure 9. Cyclic voltammogram of **4** in dichloromethane (0.1 M TBAHFP), sweep rate: 100 mV/min.

The reduction potentials of **4** are similar to those observed for the corresponding open-chain 1,7-DAPBI derivatives (–1.10 V and –1.29 V, respectively).[3a] As revealed by the negligible difference between open-chain and macrocyclic compounds, the reduction properties are not significantly influenced by the orientations of the aryloxy substituents. Thus, the larger band gap (equal to a hypsochromic shift of the absorption maximum) observed for **4** by UV/Vis spectroscopy is mainly related to a shift of the oxidation potential toward higher voltages (estimated to 1.30 V from the first reduction potential and the band gap determined by UV/Vis).

5.7 Conclusion

In summary, the synthesis of a macrocycle based on diaryloxy-substituted perylene bisimides was accomplished in three steps and the optical and electrochemical properties of this macrocycle were studied. The resolution of the core-twisted perylene bisimide was achieved by semi-preparative HPLC on a chiral column and, for the first time pure atropo-enantiomers of a perylene bisimide were obtained on a mg scale. The chiroptical properties were determined by CD spectroscopy and the assignment of the stereochemistry was made by comparing the CD spectra with those obtained for epimeric bis(macrocyclic) perylene bisimides described in Chapter 4. X-ray analysis of racemic **4** and homochiral (*P*)-**4** provided insight into the molecular structure of this macrocycle and revealed a strikingly different packing for the racemic mixture and the enantiopure compound. Especially the crystal structure of (*P*)-**4** revealed π-stacked dimeric units for these core-twisted perylene bisimides and provided important

information on the preferred geometrical arrangement of homochiral dimers in solid state. The observed preferred formation of homochiral dimers, i.e., (*P*)-(*P*) or (*M*)-(*M*) and the accessibility of enantiopure macrocycles like **4** provides an ideal starting point for the development of chiral sensors based on perylene bisimide π-dimers.

5.8 Experimental Section

Materials and methods. Cesium carbonate (99%) was purchased from Aldrich (Steinheim, Germany), boron tribromid (≥ 99%), 3-methoxyphenol (97%) and dry DMSO (Secco Solv) were obtained from Merck (Hohenbrunn, Germany) and potassium carbonate (≥99%) from Grüssing (Filsum, Germany). Dichloromethane was purchased from Staub (Nürnberg, Germany) and NMP (99,5%) was obtained from Riedel-deHäen (Seelze, Germany). All chemicals and reagents were used as received if not otherwise mentioned. NMP was fractionally distilled prior to use, dichloromethane was distilled under nitrogen from calcium hydride, potassium carbonate was dried in vacuo at 100 °C for 24 h. Diethylene glycol ditosylate[18] and *N,N´*-dicyclohexyl-1,7-dibromoperylene-3,4:9,10-tetracarboxylic acid bisimide[1] were prepared according to literature procedures.

The two regioisomers of dibromoperylene bisimide **1** (1,6- and 1,7-disubstituted **1**) were not separated by crystallization[16] and, thus **1** was applied as a mixture of the two regiosiomers (1,6-disubstituted **1** and 1,7-disubstituted **1**). As monitored by high field ^{1}H NMR spectroscopy (600 MHz),[16] **1** contained about 5-10 % of the respective 1,6-isomers.

Flash column chromatography was performed using silica gel (Si60, mesh size 40-63 µm) from Merck. ^{1}H NMR spectra were recorded with a Bruker Avance 400 instrument. Chemical shifts are given in parts per million (ppm) and are referred to TMS as internal standard ($CDCl_3$, CD_2Cl_2) or to the residual solvent peak (DMSO). Coupling constants *J* are given in Hertz (Hz). MALDI-TOF mass spectra were recorded on a Autoflex II from Bruker Daltonics and high resolution mass spectra were recorded on a MicrOTOF Focus from Bruker Daltonics. Elemental analysis were performed at the Institute of Organic Chemistry at the University of Stuttgart.

Analytical HPLC was carried out on a JASCO system (PU 2080 PLUS) with a diode array detector (MD 2015) equipped with a ternary gradient unit (DG-2080-533) and inline-degasser (LG 2080-02). Semi-preparative HPLC was performed on a JASCO system (PU 2080 PLUS) with a diode array detector (UV 2077 PLUS). HPLC grade

solvents (Rectapur) from VWR (Darmstadt, Germany) were used. Reprosil 100 chiral-NR chiral columns from Trentec (Gerlingen, Germany) were used for the analytical (Ø = 0.8 cm) as well as the semi-preparative (Ø = 2.0 cm) separation.

Spectroscopy. For all measurements spectroscopic grade solvents (Uvasol®) from Merck were used. UV/Vis spectra were recorded with a Perkin Elmer PE 950 under ambient conditions. CD spectra were measured with a JASCO J-810 spectrometer equipped with a CDF-242 peltier element and optical rotation values were determined with a JASCO PE 1020 at 20 °C in the concentrations given in the text. Fluorescence spectra were recorded with a PTI QM-4/2003 instrument and fluorescence lifetimes were determined with PTI GL3330 nitrogen laser and a GL302 dye laser using the stroboscope technique. All fluorescence measurements were performed under aerobic conditions and fluorescence spectra are corrected. Fluorescence quantum yields were determined as the average value for three different excitation wavelengths with *N,N´*-di(2,6-diisopropylphenyl)-1,6,7,12-tetraphenoxyperylene-3,4:9,10-tetracarboxylic acid bisimide (Φ_{fl} = 0.96 in chloroform) as reference and by applying the high dilution method (A < 0.05).[19] Decay curves were evaluated with the Felix Software from PTI by fitting 1-4 lifetimes. The quality of the fit was judged by Derbin-Watson factor DW and χ^2 (for monoexponential decay DW > 1.7 and 0.9 < χ^2 < 1.2) as well as by the correlation function and the residuals.

Transition dipole moments were calculated according to the equation 5-1:

$$\mu_{eg}^2 = \frac{3hc\varepsilon_0 \ln 10}{2000\pi^2 N_A} \int \frac{\varepsilon}{\tilde{\nu}} \, d\tilde{\nu} \qquad \text{(eq. 5–1)}$$

The integral of the reduced absorption spectra $\int \frac{\varepsilon}{\tilde{\nu}} \, d\tilde{\nu}$ was obtained by peak deconvolution of the reduced absorption spectrum applying gaussian peak functions.

Electrochemical analysis. Cyclic voltammetry was performed on a standard commercial electrochemical analyzer (Epsilon, BAS Inc.) in a three electrode single-component cell under argon. Dichloromethane (HPLC grade) was obtained from J.T. Baker (Mumbai, India), dried over calcium hydride and degassed prior to use. The supporting electrolyte tetrabutylammonium hexafluorophosphate was synthesized according to literature procedures[20], recrystallized from ethanol/water and dried in high vacuum. The measurements were carried out under exclusion of air and moisture at a concentration of 10^{-4} M with ferrocene as internal standard for the calibration of

potential. Working electrode: Pt disc; reference electrode: Ag/AgCl; auxillary electrode: Pt wire.

X-ray analysis. The crystal data of rac-**4** and (*P*)-**4** were collected at a Bruker X8APEX diffractometer with CCD area detector and multi-layer mirror monochromated $Mo_{K\alpha}$ radiation. The structure was solved using direct methods and expanded factor analysis using Fourier techniques. All non-hydrogen atoms were refined anisotropically. Hydrogen atoms were assigned as idealized positions and were included in structure factor calculations.

Synthesis of Macrocyclic Perylene Bisimide 4

***N,N´*-Dicyclohexyl-1,7-(3-methoxyphenoxy)perylene-3,4:9,10-tetracarboxylic Acid Bisimide (2).**

N,N´-Dicyclohexyl-1,7-dibromoperylene-3,4:9,10-tetracarboxylic acid bisimide (500 mg, 0.70 mmol), 3-methoxyphenol (757 mg, 6.10 mmol) and potassium carbonate (303 mg, 3.50 mmol) were dissolved in *N*-methylpyrrolidon (30 mL) and stirred for 1h at 120 °C. The reaction mixture was cooled to room temperature and added dropwise under stirring to 1N hydrochloric acid (50 mL). The precipitate was collected by filtration and dried in vacuo. Silica gel column chromatography with dichloromethane:*n*-hexane (4:1) as eluent, precipitation with methanol from dichloromethane and drying in vacuo afforded 370 mg (0.46 mmol, 66%) of a red solid.

Mp: 317–320 °C. ^{1}H NMR ($CDCl_3$): δ 9.56 (d, J = 8.5, 2H), 8.58 (d, J = 8.3), 8.32 (s, 2H), 7.33 (t, J = 8.5, 2H), 6.80 (ddd, J = 8.2, J = 1.6 Hz, 2H), 6.72 (m, 4H), 4.99 (m, 2H), 2.51 (m, 4H), 1.88 (m, 4H), 1.73 (m, 6H), 1.45-1.26 (m, 6H). MS (MALDI TOF, pos. mode, DCTB): *m/z*: 798.3 $[M]^+$ (calcd 797.3). Analysis calcd for $C_{50}H_{42}N_2O_8$: C 75.17, H 5.30, N 3.51; found: C 75.28, H 5.39, N 3.46. UV/Vis (CH_2Cl_2): λ_{max}/nm (ε_{max}/$M^{-1}cm^{-1}$) 537 (49300), 502 (33800), 397 (8800), 271 (39200). Fluorescence (CH_2Cl_2): λ_{max} = 566 nm, Φ_{fl} = 0.90, τ_{fl} = 4.9 ns.

The obtained product contain 5%-10% of the corresponding 1,6-isomer as the ^{1}H NMR spectra (400 MHz) revealed.

***N,N´*-Dicyclohexyl-1,7-(3-hydroxyphenoxy)perylene-3,4:9,10-tetracarboxylic Acid Bisimide (3).**

N,N´-Dicyclohexyl-1,7-di(3-methoxyphenoxy)perylene-3,4:9,10-tetracarboxylic acid bisimide **2** (740 mg, 0.93 mmol) was dissolved in dichloromethane (42 mL) and cooled to 0 °C. A solution of boron tribromide (4.60 g, 18.52 mmol) in dichloromethane (18 mL) was added dropwise over a period of 30 min and stirred for 1 h at 0 °C and additional 3 h at room temperature. The solvent and excess boron tribromide was removed by distillation and a 4:1 mixture of water and methanol (50 mL) was added to the remaining solid at 0 °C. After treatment for 30 min in an ultrasonic bath, the precipitate was collected by filtration and dried in vacuo. Silica gel column chromatography with dichloromethane:methanol (99:1) as eluent, precipitation with *n*-hexane from dichloromethane solution and drying in vacuo afforded 684 mg (0.89 mmol, 96%) of **3** as a red solid.

Mp: 408–410 °C. ^{1}H NMR ($CDCl_3$): δ 9.85 (s, 2H), 9.29 (bs, 2H, OH), 8.42 (bd, J = 6.3, 2H), 7.86 (bd, 2H), 7.28 (t, J = 8.2, 2H), 6.72 (dd, J = 8.2, J = 1.6, 2H), 6.60 (m, 4H), 4.81 (m, 2H), 2.37 (m, 4H), 1.83 (m, 4H), 1.70 (m, 6H), 1.37-1.21 (m, 6H). MS (MALDI-TOF, pos. mode, DCTB): *m/z*: 770.27 $[M]^+$ (calcd 770.27).

The ratio of two regioisomers could not be determined by ^{1}H NMR spectroscopy (400 MHz). But as the ratio did not change by reaction of **1** with 3-methoxyphenol, the ratio of **3** is expected to be similar to that of starting material **2** and, thus, the obtained product should contain 5-10% of the respective 1,6-isomer.

Macrocyclization of 3.

N,N´-Dicyclohexyl-1,7-(3-hydroxyphenoxy)perylene-3,4:9,10-tetracarboxylic acid bisimide **3** (684 mg, 0.89 mmol), diethylene glycol distosylate (736 mg, 1.78 mmol) and cesium carbonate (2.26 g, 7.10 mmol) were dissolved in DMSO (60 mL) and heated to 120 °C for 7 h. The reaction mixture was cooled to ambient temperature and dropped into 0.33 M hydrochloric acid (150 mL) under stirring. The resulting precipitate was collected by vacuum filtration and dried in vacuo (10 mbar). Silica gel column chromatography with dichloromethane and precipitation with methanol from dichloromethane solution afforded 53.0 mg (0.06 mmol, 7%) of **4** as an orange solid.

Mp. 318–319 °C. ^{1}H NMR (CD_2Cl_2): δ 9.24 (d, 2H, J = 8.2), 8.53 (d, 2H, J = 8.2), 8.40 (s, 2H), 7.26 (t, 2H, J = 8.3), 7.02 (ddd, 2H, J = 8.3, J = 2.5, J = 0.7), 6.40 (ddd, 2H, J = 8.2, J = 2.2, J = 0.7), 5.57 (t, J = 2.4 Hz, 2H), 5.00 (m, 2H), 3.80-3.49 (m, 8H), 2.53 (m, 4H), 1.89 (bd, 4H), 1.74 (bd, 6H), 1.53-1.25 (m, 6H). HRMS (ESI-TOF, pos. mode, dichloromethane:acetonitrile = 1:1): *m/z* calcd for $C_{52}H_{44}N_2O_9Na$ $[M+Na]^+$: 863.2939,

found: 863.2935. Analysis calcd for $C_{52}H_{44}N_2O_9$: C 74.27, H 5.27, N 3.33; found: C 74.46, H 5.80, N 3.06. UV/Vis (CH_2Cl_2): λ_{max}/nm (ε_{max}/$M^{-1}cm^{-1}$) 525 (55800), 488 (35500), 458 (13800), 265 (31600). Fluorescence (CH_2Cl_2): λ_{max} = 539 nm, Φ_{fl} = 0.27, τ_{fl} = 1.5 ns, (Et_2O): λ_{max} = 530 nm, Φ_{fl} = 0.36, τ_{fl} = 2.4 ns.

Separation of enantiomers *P*-(+)-4 and *M*-(-)-4 by HPLC

Separation of the enantiomers was achieved on a semi-preparative column (Trentec Reprosil 100 chiral-NR) with dichloromethane/*n*-hexane (3/2) as eluent. The flow used for separation of the enantiomers was 8 ml/min. **4** was dissolved in a 4:1 mixture of dichloromethane and *n*-hexane for injection owing to tremendously higher solubility than in the eluent. The separation was done on a scale of 15 mg.

M-(–)-**4**: Retention time (Trentec Reprosil 100 chiral-NR, dichloromethane/*n*-hexane (2/1), flow: 1.0 ml/min; Ø = 0.8 cm): 6.0 min. Optical rotation (CH_2Cl_2, 20 °C, c 0.0015): $[\alpha]_D^{20}$ = –3761. CD (CH_2Cl_2): λ_{max}/nm ($\Delta\varepsilon$/$M^{-1}cm^{-1}$) 527 (– 49), 490 (– 35), 459 (– 12), 395 (+ 6), 329 (+ 14), 289 (–138), 266 (+ 86).

P-(+)-**4**: Retention time (Trentec Reprosil 100 chiral-NR, dichloromethane/*n*-hexane (2/1), flow: 1.0 ml/min; Ø = 0.8 cm): 6.8 min. Optical rotation (CH_2Cl_2, 20 °C, c 0.0018): $[\alpha]_D^{20}$ = + 3730. CD (CH_2Cl_2): λ_{max}/nm ($\Delta\varepsilon$/$M^{-1}cm^{-1}$) 527 (+ 51), 490 (+ 37), 459 (+ 13), 395 (– 3), 329 (– 11), 289 (+ 138), 266 (– 83).

Supporting Information Available in the Appendix: Additional graphical materials, crystallographic details for rac-**4** and (*P*)-**4** and ^{1}H NMR spectra of compounds **2-4**.

5.9 References and Notes

1 (a) A. Böhm, H. Arms, G. Henning, P. Blaschka (BASF AG), German Pat. DE19547209 A1, **1997**; *Chem. Abstr.* **1997**, *127*, 96569g; (b) A. Böhm, H. Arms, G. Henning, P. Blaschka (BASF AG), German Pat. DE19547210 A1, **1997**; *Chem. Abstr.* **1997**, *127*, 96570a.

2 (a) U. Rohr, P. Schlichting, A. Böhm, M. Groß, K. Meerholz, C. Bräuchle, K. Müllen, *Angew. Chem.* **1998**, *110*, 1463-1467; *Angew. Chem. Int. Ed.* **1998**, *37*, 1434-1437; (b) Y. Zhao, M. R. Wasielewski, *Tetrahedron Lett.* **1999**, 40, 7047-7050; (c) U. Rohr, C. Kohl, K. Müllen, A. van de Craats, J. Warman, *J. Mater. Chem.* **2001**, *11*, 1789-1799; (d) M. J. Ahrens, M. J. Fuller, M. R. Wasielewski,

Chem. Mater. **2003**, *15*, 2684-2686; (e) C.-C. Chao, M.-k. Leung, Y. O. Su, K.-Y. Chiu, T.-H. Lin, S.-J. Shieh, S.-C. Lin, *J. Org. Chem.* **2005**, *70*, 4323-4331; (f) Y. Li, Y. Li, J. Li, C. Li, X. Liu, M. Yuan, H. Liu, S. Wang, *Chem. Eur. J.* **2006**, *12*, 8378-8385; (g) M. J. Ahrens, M. J. Tauber, M. R. Wasielewski, *J. Org. Chem.* **2006**, *71*, 2107-2114.

3 (a) F. Würthner, C. Thalacker, S. Diele, C. Tschierske, *Chem. Eur. J.* **2001**, *7*, 2245-2253; (b) Z. Chen, U. Baumeister, C. Tschierske, F. Würthner, *Chem. Eur. J.*, **2007**, *13*, 450-465.

4 *Other perylene bismides*: (a) A. S. Lukas, Y. Zhao, S. E. Miller, M. R. Wasielwski, *J. Phys. Chem. B* **2002**, *106*, 1299-1306; (b) M. J. Ahrens, L. E. Sinks, B. Rybtchinski, W. Liu, B. A. Jones, J. M. Giaimo, A. V. Gusev, A. J. Goshe, D. M. Tiede, M. R. Wasielwski, *J. Am. Chem. Soc.* **2004**, *126*, 8284-8294; (c) K. Sugiyasu, N. Fujita, S. Shinkai, *Angew. Chem.* **2004**, *116*, 1249-1253; *Angew. Chem. Int. Ed.* **2004**, *43*, 1229-1233; *Porphyrin*: (d) T. van der Boom, R. T. Hayes, Y. Zhao, P. J. Bushard, E. A. Weiss, M. R. Wasielewski, *J. Am. Chem. Soc.* **2002**, *124*, 9582-9590; (e) X. He, H. Liu, Y. Li, Y. Liu, F. Lu, Y. Li, D. Zhu, *Macromol. Chem. Phys.* **2005**, *206*, 2199-2205; (f) S. Xiao, M. E. El-Khouly, Y. Li, Z. Gan, H. Liu, L. Jiang, Y. Araki, O. Ito, D. Zhu, *J. Phys. Chem. B* **2005**, *109*, 3658-3667; *Phthalocyanine:* (g) X. Li, L. E. Sinks, B. Rybtchinski, M. R. Wasielewski, *J. Am. Chem. Soc.* **2004**, *126*, 10810-10811; (h) M. S. Rodriguez-Morgarde, T. Torres, C. Antienza-Castellanos, D. M. Guldi, *J. Am. Chem. Soc.* **2006**, *128*, 15145-15154; *Fullerene*: (i) Y. Liu, N. Wang, Y. Li, H. Liu, Y. Li, J. Xiao, X. Xu, C. Huang, S. Cui, D. Zhu, *Macromolecules* **2005**, *38*, 4880-4887; (j) J. Zhuang, W. Zhou, X. Li, Y. Li, N. Wang, X. He, H. Liu, Y. Li, L. Jiang, C. Huang, S. Cui, S. Wang, D. Zhu, *Tetrahedron* **2005**, *61*, 8686-8693; *Fluorene:* (k) C. Ego, D. Marsitzky, S. Becker, J. Zhang, A. C. Grimsdale, K. Müllen, J. D. MacKenzie, C. Silva, R. H. Friend, *J. Am. Chem. Soc.* **2003**, *125*, 437-443; (l) S. P. Dudek, M. Pouderoijen, R. Abbel, A. P. H. J. Schenning, E. W. Meijer, *J. Am. Chem. Soc.* **2005**, *127*, 11763- 11768; *other dyes*: (m) T. Ishi-i, K.-i. Murakami; Y. Imai, S. Mataka, *Org. Lett.* **2005**, *7*, 3175-3178; (n) T. Ishi-i, K.-i. Murakami, Y. Imai, S. Mataka, *J. Org. Chem.* **2006**, *71*, 5752-5760.

5 X. Guo, D. Zhang, D. Zhu, *Adv. Mater.* **2004**, *16*, 125-130.

6 C. Kohl, T. Weil, J. Qu, K. Müllen, *Chem. Eur. J.* **2004**, *10*, 5297-5310.

7 See chapters 3 and 4 of this thesis and: (a) P. Osswald, D. Leusser, D. Stalke, F. Würthner, *Angew. Chem.* **2005**, *117*, 254-257; *Angew. Chem. Int. Ed.* **2005**, *43*, 250-253; (b) P. Osswald, M. Reichert, G. Bringmann, F. Würthner, *J. Org. Chem.*, accepted for publication.

8 The overall macrocyclisation yield should correspond to the product of two individual macrocyclisation steps. Thus, the yield of monobridged macrocycles should be the square of that obtained for dibridged macrocycle **5** involving two macrocyclisation steps.

9 *Exciton Chirality Method: Principles and Applications* in *Circular Dichroism* (Eds.: N. Berova, K. Nakanishi, R. W. Woody), 2nd Ed., Wiley-VCH, Berlin, **2000**, pp. 337-383.

10 M. Sadrai, L. Hadel, R. R. Sauers, S. Husain, K. Krogh-Jespersen, J. D. Westbrook, G. R. Bird, *J. Phys. Chem.* **1992**, *96*, 7988-7996.

11 Selected crystallographic data for macrocycles rac-**4** and (*P*)-**4**. Rac-**4**: Crystal system: orthorhombic, space group: Pna2(1), unit cell dimensions: a = 16.7412(7) Å, b = 9.8474 (3) Å, c = 24.5510(9) Å, V = 4047.4(3) $Å^3$, Z = 4, ρ_{calcd} = 1.380 $g \cdot cm^{-3}$, μ = 0.095 cm^{-2} F(000) = 1768, T = 100(2) K, R_1 = 0.0561, ωR^2 = 0.1300, 12590 independent reflections [$2\theta \leq 61.54°$] and 568 parameters.

(*P*)-**4**: Crystal system: monoclinic, space group: C2, unit cell dimensions: a = 21.7834(8) Å, b = 20.2725(7) Å, c = 21.9159(8) Å, α = 90.0°, β = 116.475(2)°, γ = 90.00°, V = 8663.2(5) $Å^3$, Z = 8, ρ_{calcd} = 1.378 $g \cdot cm^{-3}$, μ = 0.154 mm^{-2}, F(000) = 3768, T = 293(2) K, R_1 = 0.1066, ωR^2 = 0.2476, 17437 independent reflections [$2\theta \leq 52.5°$] and 1223 parameters.

Detailed crystallographic data can be found in Appendix C.3 and C.4.

12 Mercury 1.4.1 was applied for preparation of the graphical material.

13 See Chapter 2 of this thesis and F. Würthner, *Pure Appl. Chem.* **2006**, *78*, 2341-2350.

14 (a) K. Hino, J. Mizuguchi, *Acta Cryst., Section E* **2005**, *61*, o672-o674; (b) J. Mizuguchi, K. Hino, K. Sato, H. Takahashi, S. Suzuki, *Acta Cryst., Section E* **2005**, *61*, o437-o439.

15 (a) Z. Chen, M. G. Debije, T. Debardemaeker, P. Osswald, F. Würthner *ChemPhysChem* **2004**, *5*, 137-140; (b) S. Leroy-Lhez, J. Baffreau, L. Perrin, E.

Levillain, M. Allain, M.-J. Blesa, P. Hudhomme, *J. Org. Chem.* **2005**, *70*, 6313-6320.

16 F. Würthner, V. Stepanenko, Z. Chen, C. R. Saha-Möller, N. Kocher, D. Stalke, *J. Org. Chem.* **2004**, *69*, 7933-7939.

17 (a) A. P. H. J. Schenning, J. v. Herrikhuyzen, P. Jonkheijm, Z. Chen, F. Würthner, E. W. Meijer, *J. Am. Chem. Soc.* **2002**, *124*, 10252-10253; (b) C. Thalacker, F. Würthner, *Adv. Funct. Mater.* **2002**, *12*, 209-218; (c) E. H. A. Beckers, Z. Chen, S. C. J. Meskers, P. Jonkheijm, A. P. H. J. Schenning, X.-Q. Li, P. Osswald, F. Würthner, R. A. J. Janssen, *J. Phys. Chem. B* **2006**, *110*, 16967-16978.

18 D. Marquis, J.-P. Desvergne, H. Bouas-Laurent, *J. Org. Chem.* **1995**, *60*, 7984-7996.

19 (a) R. Gvishi, R. Reisfeld, Z. Burshstein, *Chem. Phys. Lett.* **1993**, *213*, 338-344; (b) J. R. Lakowitz, *Principles of Fluorescence Spectroscopy*, 2nd ed., Kluwer Academic/Plenum, New York, **1999**, pp. 52-55.

20 A. J. Fry in *Laboratory Techniques in Electroanalytical Chemistry*, 2nd ed., (Eds.: P. T. Kessing, W. R. Heineman), Marcel Dekker Inc., New York, **1996**, p. 481.

Chapter 6

Effects of Bay-Substituents on the Interconversion Barriers of Perylene Bisimides

Abstract: The activation parameters for the interconversion of axially chiral twisted halogen- and aryloxy-substituted perylene bisimides have been determined by dynamic NMR spectroscopy (DNMR) and time- and temperature-dependent CD-spectroscopy. Furthermore the atropo-enantiomers of tetrachloro- and tetrabromo-substituted perylene bisimides have been separated by HPLC and their chiroptical properties have been investigated. By comparing the activation parameter of four perylene bisimide derivatives with substituents in the 1,7 or 1,6,7,12 “bay” positions, a clear structure-property relationship has been found which demonstrates the size dependence of the inversion parameters and reveals the stability ($\Delta G^{\ddagger}_{368K}$ = 118 kJ/mol) of the atropo-enantiomeric tetrabromo-derivatives in solution. Accordingly, attachment of sterically demanding substituents at the perylene bisimide bay position is a validated concept toward room temperature stable chiral perylene bisimides.

6.1 Introduction

In recent years, bay-functionalized perylene bisimides (PBIs) have received considerable attention for a wide range of application, e.g. as fluorescent dyes for single molecule spectroscopy,[1] bio-imaging[2] or as organic semiconductors for organic light-emitting devices and field effect transistors and solar cells[3]. The molecular properties that enable all these applications are the high fluorescent quantum yield, easily accessible and fairly stable radical anion state and pronounced stability of these dyes against environmental influences.[4] For most of these applications aryloxy-, cyano-, or pyrollidino-substituted PBIs have been chosen, whereas the available halogen-substituted derivatives, i.e. the 1,7-dibromo and the 1,6,7,12-tetrachloro derivatives, have been used as intermediates for their synthesis.[4] In the last five years also the utility of tetrahalogen-substituted PBIs, especially the tetrachloro derivatives has been demonstrated for a variety of applications, e.g. as organic semi-conductor,[5] in multichromophoric systems including tetrathiafulvalene,[6] fullerenes[7] and oligo(phenylenevinylene)s[8], as liquid crystals[9], as laser dyes[10], as g-quartet binder[11] and as functional units in polymers[12]. Recently, the synthesis of tetrabromo-substituted derivatives[13] as well as of di- and tetrafluoro-substituted perylene bisimides[14] have enlarged the number of available halogen-substituted PBIs and raised our expectations with regard to their application as starting material for the next generation of functional PBIs. Apart from the functional diversity of bay-substituted PBIs, they also exhibit interesting structural features, in particular a twisted π-system, which results in a conformational chirality of these dyes.[4a] The distortion of the π-system results from repulsive interactions between the sterically encumbered bay-substituents and can significantly vary dependent on the size of the substituent from 4° (for the difluoro-substituted derivatives) up to 35° (for the tetrachloro derivatives), as known from X-ray analysis.[5a,6,15] However, despite of significant distortion a fast interconversion process between the atropo-enantiomers was found for tetraaryloxy-substituted PBIs which prohibited the isolation of enantiopure derivatives so far.[16] Thus, chiroptical applications of such chiral fluorescent dyes could not be realized yet. The dynamic properties of halogen-functionalized PBIs have not been investigated so far only the interconversion barrier for a tetrachloro derivative has been estimated to be larger than 87 kJ/mol.[16] As it is well known that the activation parameters for conformational chiral systems, e.g. in similar biphenyl-system,[17] are strongly influenced by the size of the substituents, the available series of bromo-, chloro-, aryloxy- and fluoro-substituted PBIs provided a promising starting point for our work.

In order to gain a deeper understanding of the dynamic properties of the racemization process of bay-substituted PBIs, four PBIs **1**, **2**, **4** and **5** bearing three different halogen-substituents in the bay area (1,6,7,12-position) as well as the tetra(3-methoxyphenoxy)-substituted perylene bisimide **3** were chosen and their racemization kinetic was investigated by either dynamic NMR spectroscopy (DNMR)[§] or kinetic measurements applying CD spectroscopy. The series of halogen-substituted perylene bisimides seems to be properly suited, as by variation of the substituents in the bay area the size and, therefore, the structural properties can be tuned in a defined way.[18] In the present investigation the size of the substituents is tunable from fluorine (r_{vdW} 1.35 Å) to bromine (r_{vdW} 1.86 Å). The imide substituents were chosen in order to enable access to the dynamic properties by the respective techniques. Thus, to follow the racemization equilibrium by dynamic NMR diastereotopic methyl groups of 2,6-diisopropylphenyl groups proved to be particularly suited (see Chapter 3), whilst 1-(*R*)-phenylethyl and cyclohexyl groups allowed the separation of the atropo-enantiomers of **1** and the atropo-diastereomers of **2a** by HPLC on a chiral stationary phase.

6.2 Separation and Chiroptical Properties of the Atropisomers of 1 and 2a

The bay-substituted perylene bisimides used for the present investigation and the racemisation process between (*P*)- and (*M*)-enantiomers are shown in Scheme 1. The racemization process for *N,N´*-dicyclohexyl-1,6,7,12-tetrabromoperylene-3,4:9,10-tetracarboxylic acid bisimide **1** and *N,N´*-bis[1-(*R*)-phenylethyl]-1,6,7,12-tetrachloroperylene-3,4:9,10-tetracarboxylic acid bisimide **2a** was investigated by kinetic measurements using CD spectroscopy. Thus, the respective enantiomers of **1** and diastereomers (more precisely epimers) of **2a** were separated with semi-preparative HPLC using a chiral column (Figure 1). In the case of PBI **2a**, the two epimers could not be completely resolved (no baseline separation) with chloroform as eluent, but the separation was good enough to isolate epimerically enriched (de > 90%) (*P*,*R*,*R*)-**2a** and (*M*,*R*,*R*)-**2a** to investigate their chiroptical properties. A better resolution was achieved for the enantiomers of **1** providing almost enantiopure **1** (97% ee). Notably, the enantiomers of PBIs **3**-**5** could not be separated by HPLC as the inversion barrier in these cases is too low for resolving the enantiomers at ambient temperature.[19]

§ DNMR measurements of **4** and **5** were performed by M.-L. Schäfer and Dr. R. Bertermann at a 500 MHz spectrometer at the Institute of Inorganic Chemistry, University of Würzburg (Germany) and that of **2b** and **3** by E. Ruckdeschel and Dr. M. Grüne at a 600 MHz spectrometer at the Institute of Organic Chemistry, University of Würzburg (Germany).

Scheme 1. Racemization Equilibrium and Structures of Bay-Substituted Perylene Bisimides Used for the Present Investigation.

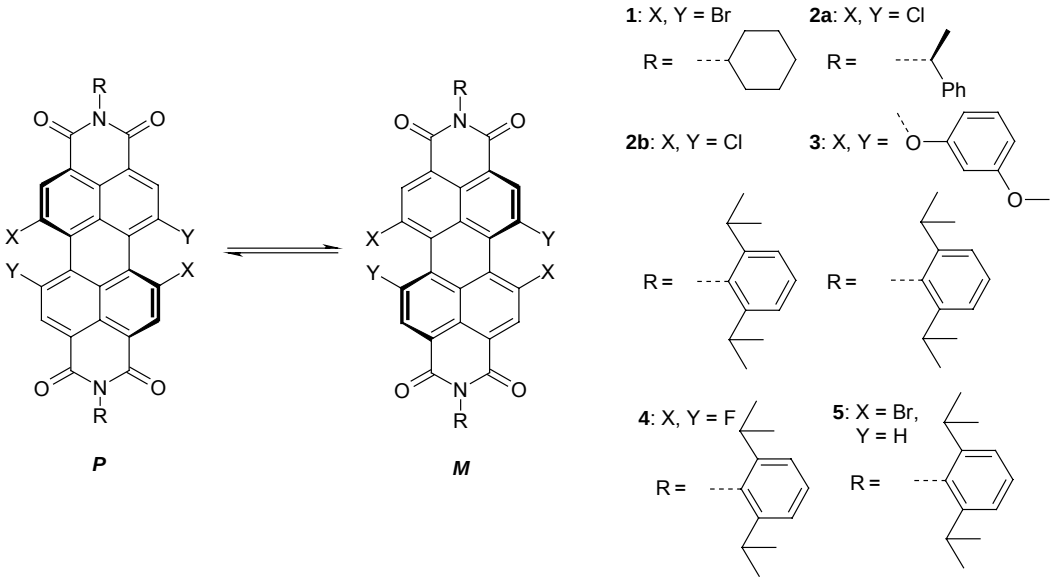

The ability to separate the stereoisomers of **1** and **2a** by HPLC enabled the investigation of their chiroptical properties. Figure 2 shows the absorption and circular dichroism (CD) spectra of the two eluted fractions of **1** and **2a** in chloroform. Based on previously accomplished stereochemical assignment of epimerically pure macrocyclic PBI systems,[20] the positive signal for the longest wavelength transition (λ_{max} = 535 nm) in the CD spectrum of the first eluted fraction of **1** can be attributed to a (*P*)-configuration of the perylene core and, thus, this atropo-enantiomer can be assigned to (*P*)-**1**. The CD spectrum of the second eluted fraction shows a mirror image relation and, therefore, can be assigned to the (*M*)-configuration of **1**.

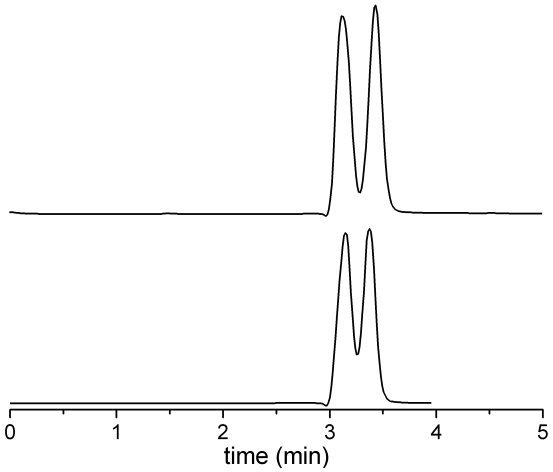

Figure 1. HPLC traces of racemic **1** (top) and **2a** (bottom) on a Trentec Reprosil 100 chiral-NR column at ambient conditions using dichloromethane as eluent (flow: 1 ml/min).

Similarly, the first eluted fraction of **2a** shows a positive signal for the lowest energy transition (λ_{max} = 527 nm). This reveals a (*P*)-configuration of the perylene core and the first eluted fraction of **2a** can thus be assigned to (*P*,*R*,*R*)-**2a**. Likewise, the negative sign for the longest wavelength transition therefore reveals the (*M*)-configuration of the perylene core and the second eluted fraction can be assigned as (*M*,*R*,*R*)-**2a**. Both fractions of **2a** reveal again a mirror image relation, thus pinpointing the pseudo-enantiomeric behavior for these compounds as already discussed for similar aryloxy-substituted derivatives in chapter 4.[20] Likewise in the ^{1}H NMR spectrum the epimers give rise to two singlets for the perylene core protons which are present in equal amounts (see Figure 3).

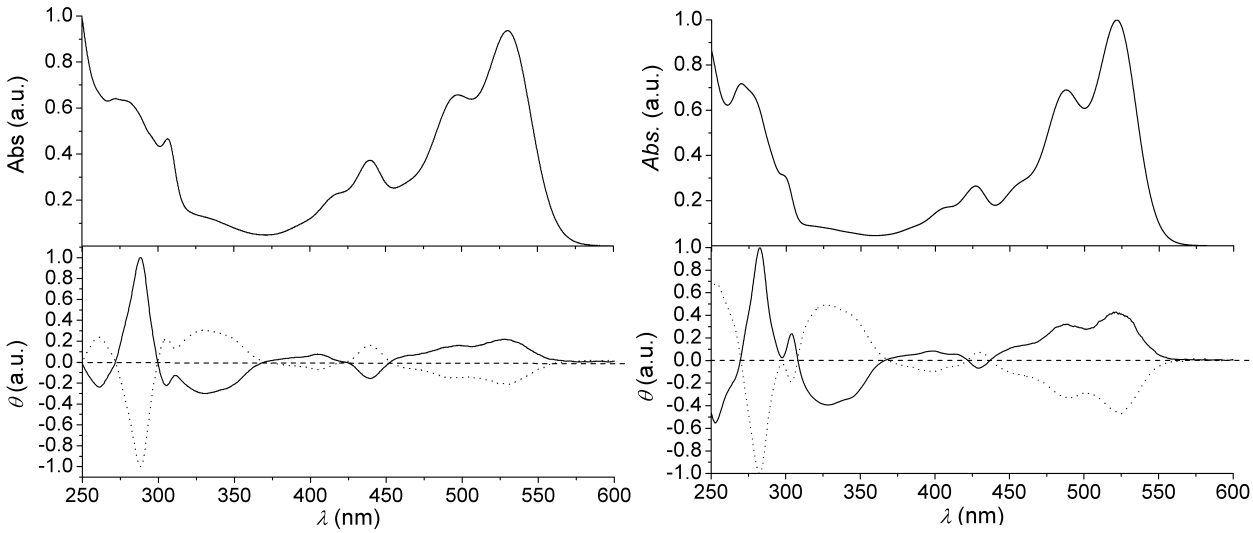

Figure 2. Normalized absorption and circular dichroism spectra of both enantiomers of **1** (left) and epimers of **2a** (right) in chloroform at 20 °C; first eluted fraction (solid line), second eluted fraction (dotted line).

Despite of many similarities, there are also differences in the CD spectra for both halogen-substituted perylene bisimides in comparison to the previously reported aryloxy-substituted ones (Chapter 4.3 and 5.3). Thus, in the spectral region between 350-450 nm, an unconventional CD effect is observed. For such largely twisted π-systems, it was reported that in this range two transition, namely the S_0-S_2 and the S_0-S_3 transitions, are located, the former being polarized out of plane whereas the latter is polarized along the short axis of the molecule.[10] Therefore, the observed CD effect can be explained for both **1** and **2a** by a superposition of the CD effects related to these two transitions which are opposite in sign. Second, in the UV range the occurrence of an intense signal at 360 nm is conspicuous. This might be attributed to the enlarged twist of the perylene core, which due to the resulting symmetry breaking (in comparison to

the parent unsubstituted PBIs; see chapter 2) leads to partial allowance of certain transitions.

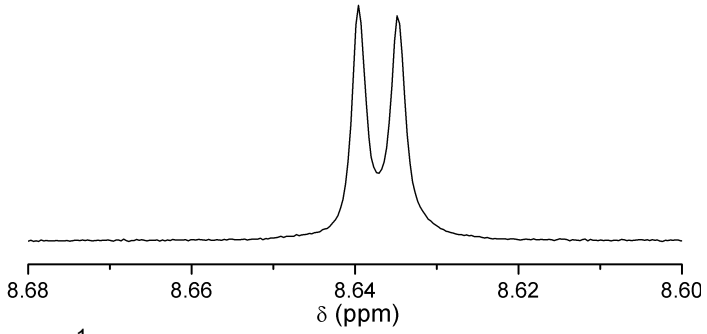

Figure 3. Section of the ^{1}H NMR spectra (400 MHz, 300 K) of **2a** in $CDCl_3$ showing the two diastereotopic resonances of the perylene core protons.

6.3 Determination of Activation Parameter of Bay-Substituted Perylene Bisimides

In order to determine the activation parameters for the racemization of **1** and **2a**, time-dependent CD measurements were performed at different temperatures in the range of 363–383 K for **1** in 1,1,2,2-tetrachloroethane and 293–323 K for **2a** in chloroform. For the racemization process a first order kinetic can be assumed (-d[**1**]/dt = kt).[21] Accordingly, the rate constants were determined from the time dependence of the CD amplitude at 510 nm (**1**) and 500 nm (**2a**), respectively. The kinetic parameters for the racemization at each temperature are collected in Table 1. **1** showed a half-lifetime at 383 K of 36 min and almost complete racemization was observed after 3 hours. Upon decreasing the temperature to 363 K the half-lifetime increased to 326 min and a complete racemization was observed not until after 1.5 days. Experiments at 323 K revealed no significant change of the CD signal of **1** over a period of 3 hours, demonstrating the high stability of these atropo-enantiomers at ambient conditions. The free activation enthalpy for the racemization process $\Delta G^{\ddagger}_{368\ K}$ of **1** was determined according to the Eyring equation (eq. 6-1) to 118±1 kJ/mol which is very similar than the activation barrier observed for a hexahelicene or a trisubstituted biphenyl, both being conformationally stable at ambient conditions.[22] The temperature dependence of the rate constant could also be used to determine the thermodynamic activation parameters $\Delta H^{\ddagger}$ and $\Delta S^{\ddagger}$ by linear regression analysis according to the Eyring equation (eq. 6-2).

$$\Delta G^{\ddagger} = -RT \ln\left(\frac{hk}{\kappa\ k_b T}\right) \qquad \text{(eq. 6-1)}$$

$$k = \kappa \frac{k_B T}{h} \exp\left[\frac{\Delta S_0^{\ddagger}}{R} - \frac{\Delta H_0^{\ddagger}}{RT}\right] \qquad \text{(eq. 6-2)}$$

The parameter κ was taken as 0.5 as the probability of the transition state to transform into one or the other stereoisomer is equal.[23] For PBI **1**, the activated complex exhibited an enthalpy $\Delta H^{\ddagger}$ of 126±3 kJ/mol and only a slightly positive entropy $\Delta S^{\ddagger}$ of 13±10 J/molK. Furthermore, the activation energy E_A was determined according to Arrhenius. The obtained value of 123±3 kJ/mol is in good agreement to the activation enthalpy $\Delta H^{\ddagger}$ determined by Eyring equation, which are related by $E_A = \Delta H^{\ddagger} + RT$.

Table 1. Kinetic Data for the Racemization Process of **1** in Chloroform and **2a** in 1,1,2,2-Tetrachloroethane at Different Temperatures

1	T (K)	k ($10^{-5}s^{-1}$)	$t_{1/2}$[a] (min)	$\Delta G^{\ddagger}$ (kJ/mol)	**2a**	T (K)	k ($10^{-5}s^{-1}$)	$t_{1/2}$[a] (min)	$\Delta G^{\ddagger}$ (kJ/mol)
	363	3.54±0.08	326±7	118.2±0.1		293	1.40±0.03	825±14	97.3±0.1
	368	6.33±0.19	183±6	118.1±0.1		303	4.54±0.08	255±5	97.7±0.1
	373	10.50±0.30	110±4	118.1±0.1		313	15.30±0.40	76±2	97.8±0.1
	378	17.87±0.60	67±2	118.2±0.1		323	50.68±1.30	23±1	97.8±0.1
	383	32.55±1.00	36±1	117.8±0.1					

a) calculated according to $t_{1/2} = \ln 2/k$

In contrast to the tetrabromo PBI **1**, a significantly accelerated racemisation process was observed for the tetrachloro derivative **2a** as can be seen from the half-lifetimes given in Table 1. Thus, **2a** exhibited almost the same half-lifetime at 323 K as **1** did at 383 K. At 293 K an almost complete racemization was observed after 1 day, as can be seen from Figure 4. Upon increasing the temperature to 313 K a decrease of the half-lifetime of the racemization process to 23 minutes was observed and a complete racemization was given after 3 hours. The free enthalpy of activation for the racemization of **2a** at 303 K was determined to 98±1 kJ/mol which is in the same range as the activation barriers observed for pentahelicene[22a] or unsubstituted 1,1´-binaphthyl[24].

The activation energy E_A according to Arrhenius resulted to 94±2 kJ/mol and showed again the expected correlation to the activation enthalpy $\Delta H^{\ddagger}$ (92±2 kJ/mol). The activation entropy of **2a** revealed a slightly negative value of –20±15 J/molK. The negligible entropic contribution to the free enthalpy of activation indicates that the latter can be considered as temperature independent, at least in a particular temperature region.

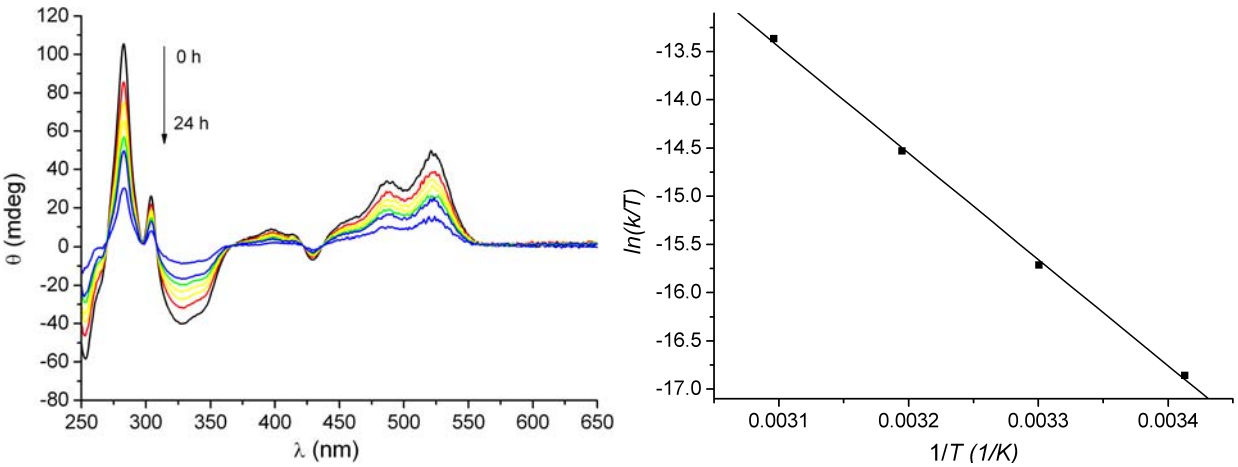

Figure 4. Time-dependent CD spectra of (*P*,*R*,*R*)-**2a** in chloroform at 20 °C and Eyring plot for **2a**.

The atropo-enantiomers of perylene bisimides **3**-**5** could not be separated by HPLC, apparently, the interconversion barriers in these cases are too low for resolving the enantiomers at room temperature. Thus, dynamic NMR experiments were performed in order to obtain the activation parameters for the interconversion of the atropisomers.

For perylene bisimide **3** bearing four aryloxy-substituents in the bay position, dynamic NMR experiments in deuterated chloroform were reported in literature and were remeasured in order to validate the experimental setup.[16] For data evaluation, the resonances of the methyl protons of the diastereotopic isopropyl groups situated in the imide positions were used. The temperature dependent changes of these signals are shown in Figure 5. At room temperature, the methyl protons of the diisopropyl groups show one doublet, which suggests that the interconversion process is faster than the spin-relaxation at this temperature (see also chapter 3 and 4).

Upon decreasing the temperature this signal is broadened and at low temperatures (230 K) two doublets (overlapped to a triplet) arose for the two enantiomers, namely (*P*)-**3** and (*M*)-**3**. The coalescence temperature was determined from the line broadening to 270 K and the difference in chemical shift $\Delta\upsilon$ of the two enantiomers at low temperature (230 K) was estimated to 6.3 Hz. With these data, the free enthalpy of activation was calculated to 60 kJ/mol according to the coalescence method (eqs. 6-3 and 6-4) which is in perfect agreement with the value reported in the literature.[16,25]

$$k_C = \frac{\pi}{\sqrt{2}}\left|\Delta\nu\right| \qquad \text{(eq. 6-3)}$$

$$\Delta G^{\#} = R \cdot T_C \cdot \ln\left(\frac{R \cdot T_C}{k_C \cdot N_A \cdot h}\right) \qquad \text{(eq. 6-4)}$$

The free activation enthalpy of 60 kJ/mol reveals a strong decrease of the activation parameter in comparison to **1** (118 kJ/mol) and **2a** (98 kJ/mol). From equation 6-3, the half-lifetime of **3** at the coalescence temperature (270 K) was approximated to 10 s under assumption of a first order kinetic which demonstrates a fast interconversion process for **3** and the impossibility to resolve the respective atropo-enantiomers at room temperature. The proper agreement between $\Delta G^{\ddagger}$ values from DNMR experiments and kinetic measurements can be visualized by the example of the tetrachloro-derivative **2b**. By temperature-dependent NMR experiments in 1,1,2,2-tetrachlorethane-d_2, a lower limit of the free enthalpy of activation was estimated from the difference of the chemical shifts of the two enantiomers $\Delta\upsilon$ (6.7 Hz) and the highest available temperature for this solvent (383 K) to 87 kJ/mol.[16,26] Thus, the activation parameters of **2** determined by kinetic measurements and DNMR show a rather good agreement.

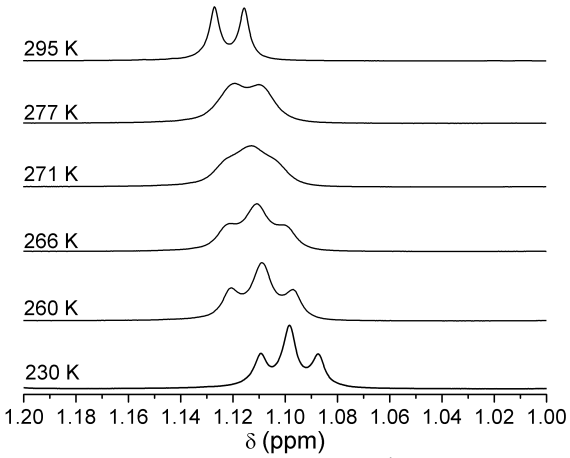

Figure 5. Section of the temperature-dependent ^{1}H NMR spectra of **3** (600 MHz) in $CDCl_3$. The signals of the diastereotopic methyl groups of the diisopropylphenyl imide substituents are shown.

For perylene bisimide **4** bearing four fluorine substituents in the bay position, dynamic NMR experiments were performed in deuterated dichloromethane. As can be seen from Figure 6 (left), the changes of the methyl protons is similar to that observed for the tetraaryloxy substituted PBI **3**. Unfortunately, the static case in the slow exchange region could not be realized owing to the experimental limitations (melting point of dichloromethane) and only the coalescence temperature of 180 K could be determined from the experiment. However, as the splitting of the signal $\Delta\upsilon$ in the static region was not significantly different for similar perylene bisimides, e.g. **2b** (6.7 Hz) or **3** (6.3 Hz) as shown before, we can assume that the differences in the chemical shift $\Delta\upsilon$ of the two enantiomers should be similar for **4** as well. Therefore, the free enthalpy of activation $\Delta G^{\ddagger}$ is estimated according to equations 6-3 and 6-4 to 40 kJ/mol at 180 K.

In the series of 1,7-dihalogenated PBIs only the bromo and fluoro derivatives are available.[4a,4d,14] Owing to the only slightly twisted perylene core the torsional barrier is expected to be rather small for the fluoro compound. For the dibromo-substituted PBI **5** similar temperature dependent changes were observed as for **4** and the coalescence of the methyl resonances was reached at 180 K (Figure 6, right). Thus, the free energy of activation is similarly estimated to 40 kJ/mol. This related behavior strongly suggests that similar steric constraints are given with regard to the planarization of the two π-conjugated systems, despite large structural differences.

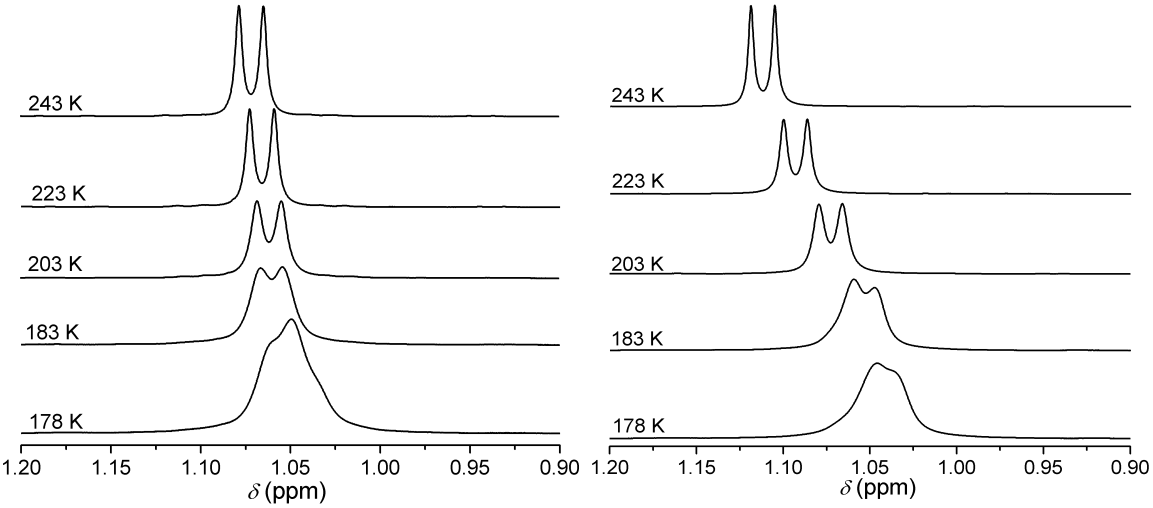

Figure 6. Section of the temperature-dependent ^{1}H NMR spectra (500 MHz) of **4** (left) and **5** (right) in CD_2Cl_2. The signals of the diastereotopic methyl groups of the 2,6-diisopropylphenyl imide substituents are shown.

Table 2 collects the thermodynamic parameters for all investigated PBIs. The comparison of the five bay-substituted perylene bisimides reveals a strong dependence of the free enthalpy of activation for this racemization process on the substituents. Although these $\Delta G^{\ddagger}$ values were determined at different temperatures their comparison is justified due to the negligible entropic influence.

Table 2. Free Enthalpy of Activation for the Racemization of PBIs **1**-**5**

	$\Delta G^{\ddagger}$ (kJ/mol)
1	118 ± 1[a]
2a	98 ± 1[b]
3	60 ± 3[c]
4	40 ± 5[d]
5	40 ± 5[d]

a) at 368 K; b) at 303 K;
c) at 270 K; d) at 183 K.

6.4 Relation between Activation Parameters and the Size of Bay Substituents

The value which has been most frequently applied to account for the steric stress of a distorted system due to the size of the substituents is the apparent overlap parameter ∑r* of the substituents that cause the distortion. The apparent overlap is defined as the overlap of the substituents in a 2-dimensional projection of a presumably planar transition state as shown in Figure 7.

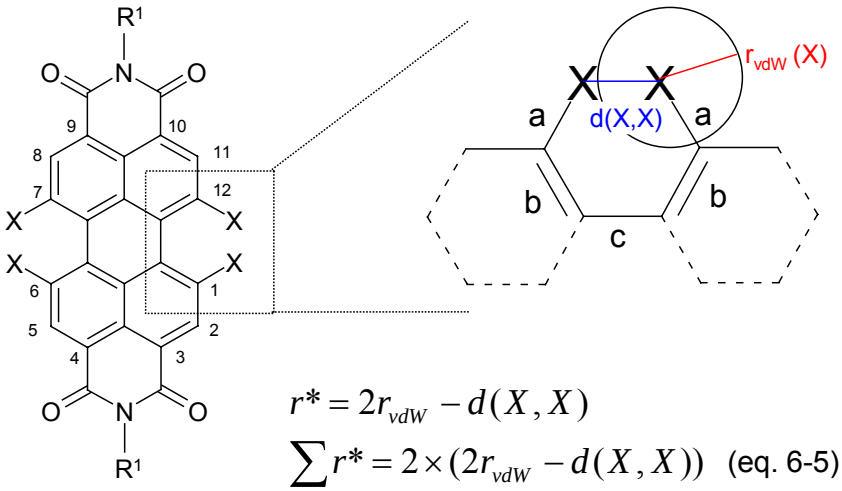

	r_{vdW}(X)	a(x)	∑r* (Å)
1	1.86	1.92	5.56
2	1.73	1.76	4.76
3	1.52	1.43	3.22
4	1.47	1.38	2.92

$$r^* = 2r_{vdW} - d(X,X)$$

$$\sum r^* = 2 \times (2r_{vdW} - d(X,X)) \quad \text{(eq. 6-5)}$$

Figure 7. Definition of geometrical parameters for 1,6,7,12-tetrabay-substituted perylene bisimides and the formulas necessary for the calculation of the apparent overlap ∑r*. The table on the right summarizes the apparent overlap for PBIs **1-4**. The apparent overlap of **3** was calculated for a hypothetical PBI bearing only oxygen atoms in the bay positions. For the calculation of 1,7-substituted PBIs, see Appendix.

Thus, r* depends on the geometry of the system under consideration and can be calculated according to equation 6-5 by applying standard bond length and bond angles, as well as the van der Waals radius r_{vdW} of the substituents.[27] In the present case the bond lengths and angles were taken from single crystal X-ray data of the parent planar unsubstituted PBI (see Chapter 2) which yields a value d(X,X) = 2.862 Å - a(x) (see Appendix).[28] The ∑r* values for the disubstituted dye **5** was calculated by a similar procedure to be 3.06 Å (see Appendix) and the ∑r* values of the investigated tetrasubstituted perylene bisimides **1-4** are summarized in Figure 7.

As can be seen from Figure 8, the free enthalpy of activation of the investigated PBI derivatives depends linearly on the apparent overlap of the substituents indicating a direct relationship of the activation parameters on the size of the substituents and, thus, on the steric repulsion imparted by the substituents. For the purpose of comparison the unsubstituted perylene bisimide is also included in Figure 8, which possesses a free enthalpy of activation of zero due to its planar structure.

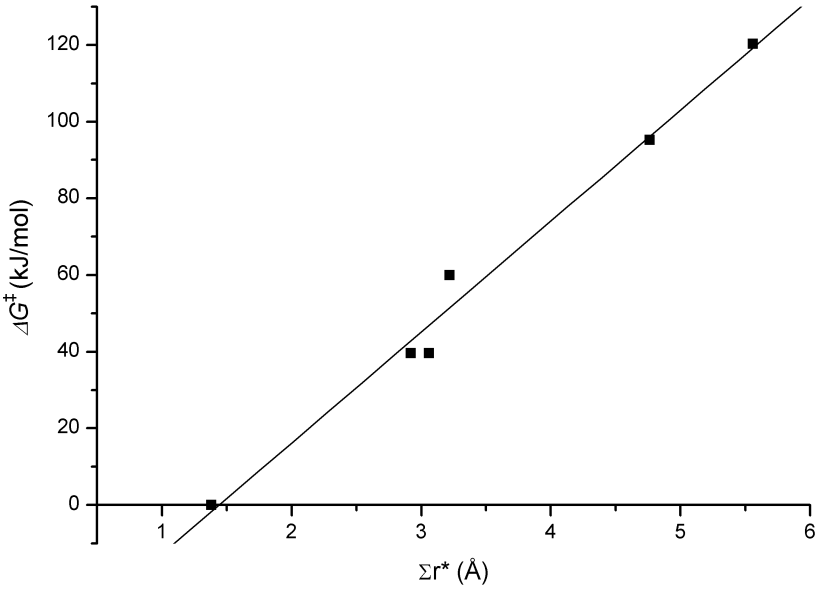

Figure 8. Dependence of the free activation enthalpy of racemization on the apparent overlap ∑r* for PBIs **1**-**5**.

The observed linear dependence of free enthalpy of activation on the apparent overlap can be expressed by the equation 6-6 (correlation factor r² of 0.98).

$$\Delta G^{\ddagger}_{180K}\,(\text{kJ/mol}) = 29.0\ \sum r^{*} - 41.8 \qquad \text{(eq. 6-6)}$$

This demonstrates that the major factor determining the activation energy for the racemization of bay-substituted PBIs is the steric overlap of substituents in the planarized transition state.[&] However, the zero crossing at ∑r* = 1.40 Å indicates that the planarity can be maintained at small steric encumbering. This is convincingly demonstrated for the parent PBI (X = Y = H; ∑r* = 1.38 Å) as well as for the difluoro-substituted derivative (∑r* = 2.06 Å).[14]

This point is further elucidated by relation between the magnitude of the torsional twist upon attachment of bay-substituents and the apparent overlap parameter. If we look at the dependence of the dihedral angles (taken from quantum chemical calculations that are in good accordance with crystallographic data) on the apparent overlap a S-shaped curve is obtained (Figure 9). For apparent overlaps between 2.1 (for 1,7-difluoro-substituted PBI) and 3.1 (for dibromo-substituted PBI **5**) an almost linear increase of the dihedral angle is given. However, by introducing larger substituents, the dihedral angle

[&] Perylene bisimides do not fulfill all requirements for application of the apparent overlap ∑r*, as considerable steric interactions are present in the ground state. Similar as observed for 9,10-dihydrophenanthrenes, the observed linear dependence of the free enthalpy of activation on the apparent overlap (Figure 8) reveals that the energetics of interconversion process for PBIs are dominated by the transition state energy, which justifies the application of the apparent overlap theory.

saturates at a value of about 37° whilst for the smallest hydrogen substituents planarization takes place.

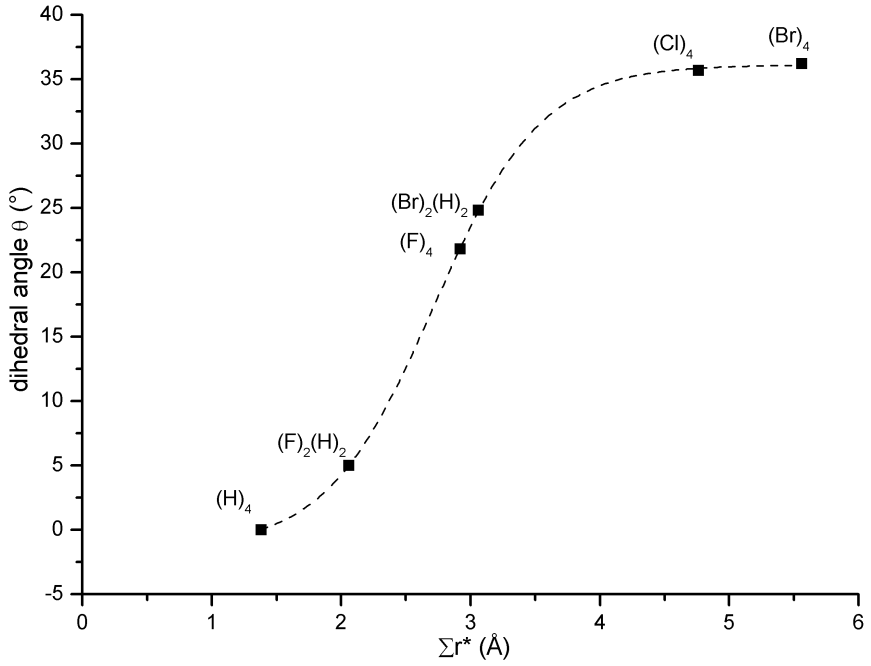

Figure 9. Dependence of the dihedral angle and the apparent overlap for different halogen-substituted perylene bisimides (substituents with numbers are given). The dihedral angles are taken from AM1 calculations and are the average value of two dihedral angles (see Chapter 2).

Obviously, in the most demanding cases of sterical encumbering other distortions of the π-system come into play rather than a further twisting of the π-system around the central axis. On the other hand, in the region of small apparent overlaps, an increased sterical demand of the respective substituents does not immediately lead to a twist of the perylene core, but to slight expansions of the bond angles in such systems. For the unsubstituted perylene bisimide, which was demonstrated to be planar by X-ray crystallography, the bond angles at the two bay areas have to be expanded only slightly in order to obtain an overlap of zero.

Apparently, this analysis provides a profound correlation between the interconversion barrier $\Delta G^{\ddagger}$ for known perylene bisimide dyes and the structural parameter ∑r*. Accordingly, with the simple geometrical tool of apparent overlap values, interconversion barriers of known and unknown bay-substituted perylene bisimide dyes can now be calculated and conformationally stable atropisomers become more predictable. This approach is exemplified in the following section for a variety of bay-substituted perylene bisimides (Chart 1). The first example is di(NHoctyl)-substituted perylene bisimide,[29] for which the apparent overlap was calculated by taking the van-

der-Waals radius of NH-alkyl substituents from literature (for the definitions and the use of group radii, see Appendix).[30] With a value of ∑r* = 3.66 Å and equation 6-6, a free enthalpy of activation in the order of 64 kJ/mol is expected for this PBI, which is slightly higher than that of tetraaryloxy-substituted perylene bisimide **3** revealing a fast interconversion of the enantiomers of these dyes at room temperature.

Chart 1. Structures, Van Der Waals Radii r_{vdW}, Bond Length a (x) and Apparent Overlap Values (∑r*) of Different PBIs.

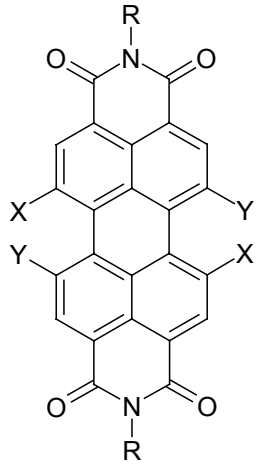

R = alkyl, aryl

PBI	r_{vdw}	a(x)[31]	∑r*
X = H, Y = NHOctyl	1.86[30]	1.47	3.66
X, Y = OH	1.52[30]	1.43	3.22
X, Y = NH_2	1.55[30]	1.47	3.41
X, Y = SH	1.80[30]	1.81	5.10
X, Y = PH_2	1.80[30]	1.80	5.08
X, Y = CH_3	1.80[30,a]	1.54	4.56
X, Y = SiH_3	1.90[30]	1.85	5.48
X, Y = *tert*-Bu	2.40[30]	1.54	6.96
X, Y = $SiMe_3$	2.60[30,a]	1.85	8.37
X, Y = CN	2.71[b]	1.44	8.00
X, Y = ethynyl	3.50[b]	1.53	11.34
X, Y = Ph	3.35	1.53	10.22
X, Y = $P(Ph)_2$	4.05[b]	1.80	14.15

a) minimal van der Waals radius; b) axial van der Waals radius (for definition, see Appendix).

More importantly, the presented correlation allows the prediction and the design of conformationally stable core-twisted PBIs. For this purpose it can be derived from the Eyring equation, that the free enthalpy of activation must be in the order of 113 kJ/mol at 295 K to obtain at room temperature stable atropo-enantiomers of PBIs.[17,19,32] Thus, from equation 6-6, it can be predicted that the apparent overlap ∑r* has to be larger than 5.3 Å. By comparing the apparent overlap calculated for 1,6,7,12-tetrasubstituted PBIs bearing only the respective hydrogen saturated atoms in the bay positions, it can be predicted that the attachment of sulfur, phosphor and silicon substituents allows the synthesis of conformationally stable atropo-enantiomeric PBIs (estimated $\Delta G^{\ddagger}$ = 106 - 118 kJ/mol) whereas the attachment of oxygen substituents and primary amins results in conformationally labile PBIs, as already demonstrated for PBI **3** (Chart 1). Therefore,

tetrathioaryloxy substituted PBIs, for which an free enthalpy of racemisation $\Delta G^{\ddagger}$ of 106 kJ/mol is estimated from equation 6-6, seems to be a suitable candidate for the synthesis of functional atropo-enantiomerically pure PBIs. As another reasonable synthetical strategy for an effective prevention of the racemisation for PBIs, the introduction of bulky substituents in the bay area can be proposed as for *tert*-butyl- and trimethylsilyl-substituents $\Delta G^{\ddagger}$ values of 160 kJ/mol and 201 kJ/mol, respectively, are estimated from equation 6-6 (Chart 1). Furthermore, also the tetracyano and tetraalkynyl substituted PBIs as well as the tetra(diphenylphosphino) substituted PBI, which is particular interesting for catalytic purposes, are suitable targets for the synthesis of conformationally stable perylene bisimides. But also the known tetraphenyl substituted perylene bisimides[13b] for which an effective van der Waals radius of 3.35 was proposed in literature,[30] should afford stable chiral dyes. This can also be seen from an AM1 optimized geometry for this derivative (Figure 10). Here an interconversion of the enantiomers is not easily possible due to the overlap of the two phenyl substituents in the two bay areas.

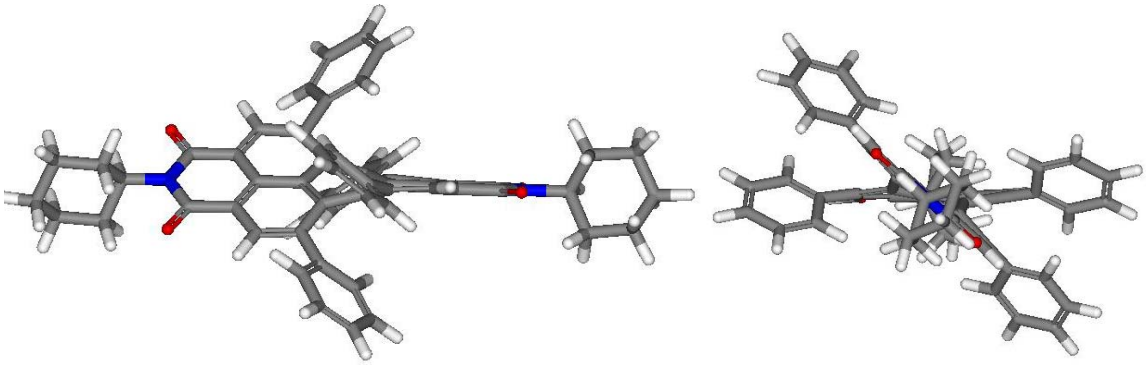

Figure 10. AM1 optimized geometry of tetraphenyl-substituted PBI: Side view (left) and view along the *N*,*N*-axis of the (*M*)-enantiomer (right). Structures were optimized by using the AM1 method as parameterized in CaChe Quantum CaChe workspace 5.0.

6.5 Conclusion

In conclusion, activation parameters for the racemization of five core-twisted perylene bisimides bearing substituents of different size in bay position have been determined. These activation parameters revealed a close correlation with the size of the substituents attached in the bay area and confirm that the transition state in the interconversion process proceeds through an essentially planarized molecule. Additionally, it was found that four sterical demanding substituents attached to the bay area can prevent the dynamic racemization at ambient temperature. Thus, for tetrabromo derivatives for the first time atropo-enantiomeric PBIs could be isolated on a

chiral column. The pronounced stability allowed us to determine their chiroptical properties. The correlation of substituent size with $\Delta G^{\ddagger}$ is useful for the prediction of activation barriers for other bay-substituted PBI dyes that might be promising targets for the future research. Conformationally stable atropo-enantiomeric PBI should be useful for many applications namely as chiral building blocks with catalytic and sensory functionality. Based on the relationship between size and racemization barrier such dyes can now be developed by design.

6.6 Experimental Section

Methods and Materials. Potassium fluoride (99%) was obtained from Grüssing (Filsum, Germany) and sulpholane (>97%) from Merck (Hohenbrunn, Germany). 1-(*R*)-Phenylethylamine was purchased from Fluka (Buchs, Switzerland) and had an *ee* of > 99%. All chemical and reagents were used as received. 1,6,7,12-Tetrachloroperylene-3,4:9,10-tetracarboxylic bisanhydride was donated from BASF AG. Perylene bisimides **1,**[13] **2a,**[16] **2b,**[5a] **3**[16] and **5**[33] as well as the catalyst CNC^{+}[34] were synthesized according to the literature.

Flash column chromatography was performed using silica gel (Si60, mesh size 40-63 µm). The melting point of **4** was determined on a Olympus Bx41 polarization microscope and is uncorrected. ^{1}H NMR spectra and ^{19}F NMR were recorded with a Bruker Avance 400 instrument. The spectra are referred to TMS as internal standard ($CDCl_3$, CD_2Cl_2) and chemical shifts δ are given in parts per million. Coupling constants *J* are given in Hertz. MALDI-TOF mass spectra were recorded on a Bruker Autoflex II and high resolution mass spectra were recorded on a MicrOTOF Focus from Bruker Daltonics.

Analytical HPLC was performed on a system (PU 2080 PLUS) with a diode array detector (MD 2015) from JASCO equipped with a ternary gradient unit (DG-2080-533) and line-degasser (LG 2080-02). Preparative HPLC was done on a system (PU 2080 PLUS) with a diode array detector (UV 2077 PLUS) from JASCO. HPLC grade solvents (Rectapur) from VWR (Darmstadt, Germany) were used except chloroform (Staub; Filsum, Germany) which was distilled prior to use. As chiral column Reprosil 100 chiral-NR from Trentec (Gerlingen, Germany) was used in the analytical (Ø = 4.6 mm) as well as in the semi-preparative size (Ø = 20 mm).

Spectroscopy. For all measurements spectroscopic grade solvents (Uvasol®) from Merck were used expect for the CD-measurements. UV/Vis spectra were recorded with

a Perkin Elmer PE 950 under ambient conditions. Fluorescence spectra were recorded with a PTI QM-4/2003 and fluorescence lifetimes were determined with PTI GL3330 nitrogen laser and a GL302 dye laser using the stroboscope technique. All fluorescence measurements were performed under aerobic conditions and fluorescence spectra are corrected. Fluorescence quantum yields were determined as the average value for three different excitation wavelengths with *N,N´*-di(2,6-diisopropylphenyl)-1,6,7,12-tetraphenoxyperylene-3,4:9,10-tetracarboxylic acid bisimide (Φ_{fl} = 0.96 in chloroform) as reference and by applying the high dilution method (A < 0.05).[35] Decay curves were evaluated with the Felix Software from PTI by fitting 1-4 lifetimes. The quality of the fit was judged by Derbin-Watson factor DW and χ^2 (for monoexponential decay DW > 1.7 and 0.9 < χ^2 <1.2) as well as by the correlation function and the residuals. Circular Dichroism was measured using a JASCO J-810 spectrometer equipped with a CDF 426-S temperature control unit.

Temperature-dependent ^{1}H NMR spectroscopy. Temperature dependent ^{1}H NMR spectra were recorded on a Bruker Avance 500 MHz (**4** and **5**) and on a Bruker Avance 600 MHz spectrometer (**2b** and **3**). Temperature was calibrated with the temperature dependent chemical shift of methanol. Coalescence temperature was determined from the spectral broadening and the data evaluation was performed by using the coalescence method according to equations 6-3 and 6-4.

Kinetic measurements. For the kinetic measurements, the atropo-enantiomers of **1** and the atropo-diastereomers of **2a** were separated by semi-preparative HPLC using chloroform as eluent. The separation was done directly before each kinetic measurement and only the amount necessary for one measurement was separated (< 0.5 mg). As starting time for the kinetic measurements of **2a** the peak maximum of the first eluted peak was used. The first CD spectrum was measured after ~90 seconds. The obtained fraction was diluted with chloroform (spectroscopic grade) to have ideal concentration for the CD measurement. For the kinetic measurements of **1** either the first or the second eluated fraction was used. The solvent was removed in a nitrogen flow and the solid was dissolved in 1,1,2,2-tetrachloroethane (1,1,2,2-tetrachloroethane used for the CD-measurements was fractionally distilled under vacuum prior to use). The Peltier element was heated to the starting temperature and as starting time the beginning of the measurement was chosen as no racemization was observed at RT. The purity of the samples were checked by HPLC. For data evaluation the Eyring (eqs.

6-1 and 6-2) and Arrhenius equation (eq. D-6 in Appendix) were used as outlined in the Appendix. The errors for the velocity constant k (Table 1), the activation energy E_A, the enthalpy $\Delta H^{\ddagger}$ as well as the entropy of activation $\Delta S^{\ddagger}$ are the standard deviation obtained by linear regression analysis. The errors for $\Delta G^{\ddagger}$ and $\tau_{1/2}$ were calculated by main error estimation (see Appendix for details).

Synthesis and Characterization

***N,N´*-Dicyclohexyl-1,6,7,12-tetrabromoperylene-3,4:9,10-tetracarboxylic Acid Bisimide (1).[13]**

The separation of the enantiomers by semi-preparative HPLC (Flow: 7ml/min) was realized only in very small amounts (~ 0.5 mg). The separation of larger amounts is possible but very time-consuming due to the low solubility of **1** in chloroform.

^{1}H NMR ($CDCl_3$): δ 8.79 (s, 4H), 5.01 (m, 2H), 2.53 (m, 4H), 1.92 (bd, 4H), 1.75 (bd, 6H), 1.53–1.25 (m, 6H). MS (MALDI-TOF, pos. mode, DCTB): *m/z*: 865.86 $[M]^+$ (calcd 865.86). UV/Vis (CH_2Cl_2): λ_{max}/nm (ε_{max}/$M^{-1}cm^{-1}$) 528 (32500), 495 (22800), 438 (12700). Fluorescence (CH_2Cl_2): λ_{max} = 563 nm, fluorescence quantum yield Φ_{fl} = 0.52, fluorescence lifetime τ_{fl} = 4.2 ns.

***N,N´*-Di(1-(*R*)-phenylethyl)-1,6,7,12-tetrachloroperylene-3,4:9,10-tetracarboxylic Acid Bisimide (2a).[16]**

The separation of the diastereomers was done by HPLC (Flow: 7 ml/min) using chloroform as eluent. The separation was done on a scale of 0.5 mg and an ee of 90% was realized under the conditions given. A baseline separation might be achieved by using mixtures of dichloromethane and hexane as eluent.

^{1}H NMR ($CDCl_3$): δ 8.65 (s, 4H), 8.64 (s, 4H), 7.51 (bd, *J* = 7.2, 8H) 7.36–7.31 (m, 8H), 7.28–7.23 (m, 8H), 6.54 (q, 2H, *J* = 7.2), 2.01 ppm (d, *J* = 7.2 Hz, 6H). MS (FAB, pos. mode, 3-nitrobenzylalcohol): *m/z*: 735.0 $[M+H]^+$ (calcd 735.0). Analysis calcd for $C_{40}H_{22}Cl_4N_2O_4$ C 65.24 H 3.01 N 3.80 found C 65.02 H 3.27 N 3.72. UV/Vis (CH_2Cl_2): λ_{max}/nm (ε_{max}/$M^{-1}cm^{-1}$) 520 (41300), 487 (28700), 426 (10900), 269 (30000). Fluorescence (CH_2Cl_2): λ_{max} = 545 nm, fluorescence quantum yield Φ_{fl} = 0.60, fluorescence lifetime τ_{fl} = 4.7 ns.

***N,N´*-Di(2,6-diisopropylphenly)-1,6,7,12-tetrachloroperylene-3,4:9,10-tetracarboxylic Acid Bisimide (2b).[5a]**

^{1}H NMR ($CDCl_3$): δ 8.77 (dd, 8H), 7.53 (t, *J* = 8.0, 2H), 7.37 (d, *J* = 8.0, 4H), 2.75 (sept, *J* = 7.0, 4H), 1.20 (d, *J* = 7.0, 24H). Fluorescence (CH_2Cl_2): λ_{max} = 548 nm, fluorescence quantum yield Φ_{fl} = 0.93. CV (CH_2Cl_2, 0.1 M TBAHFP, vs. Fc/Fc^+): $E_{1/2}$ (PBI/PBI^-) = –0.79, $E_{1/2}$ (PBI^-/PBI^{2-}) = –1.04 V.

***N,N´*-Di(2,6-diisopropylphenly)-1,6,7,12-tetra(3-methoxyphenoxy)perylene-3,4:9,10-tetracarboxylic Acid Bisimide (2a).[16]**

^{1}H NMR ($CDCl_3$): δ 8.30 (s, 4H), 7.43 (t, *J* = 8.0, 2H), 7.28 (d, *J* = 8.0, 4H), 7.18 (d, *J* = 8.0, 4H), 6.67 (ddd, *J* = 8.5, *J* = 2.5, *J* = 1.0, 4H), 6.60 (ddd, *J* = 8.0, *J* = 2.5, *J* = 1.0, 4H), 6.52 (d, *J* = 2.5, 4H), 3.67 (s, 12H), 2.71 (sept, *J* = 7.0, 4H), 1.13 (d, *J* = 7.0, 24H).

***N,N´*-Di(2,6-diisopropylphenly)-1,6,7,12-tetrafluoroperylene-3,4:9,10-tetracarboxylic Acid Bisimide (4).**

N,N´-Di(2,6-diisopropylphenly)-1,6,7,12-tetrachloroperylene-3,4:9,10-tetracarboxylic acid bisimide **2b** (238 mg, 0.28 mmol), potassium fluoride (115 mg, 1.98 mmol), CNC^+ (12 mg) and 1,1-oxo-tetrahydrothiophene (sulpholane) (4 g) were reacted for 5 h at 160 °C and 17 h at 170 °C. The crude product was purified by three subsequent columns using dichloromethane/*n*-hexane (7/3), dichloromethane/*n*-hexane (6/4) and chloroform/*n*-hexane (7/3). After precipitation with methanol from dichloromethane solution and drying in vacuum, 54 mg (0.007 mmol, 25%) of **4** was isolated as an orange solid.

Mp: 256–258 °C. ^{1}H NMR ($CDCl_3$): δ 8.58 (dd, *J*(H,F) = 5.2, *J*(H,F) = 5.2, 4H), 7.52 (t, *J*(H,H) = 7.8, 2H), 7.37 (d, *J*(H,H) = 7.7, 4H), 2.71 (sept, *J*(H,H) = 6.9, 4H), 1.18 (d, *J*(H,H) = 6.8, 24H). ^{19}F NMR (376.5 MHz, $CDCl_3$): δ –93.95 (t, *J*(F,H) = 5.31). MS (MALDI-TOF, neg. mode, DCTB): *m/z*: 782.26 $[M]^-$ (calcd 782.28). HRMS (ESI, pos. mode, dichloromethane/acetonitrile = 1:1): *m/z* calcd for $C_{48}H_{38}F_4N_2O_4$ 783.2841, found 783.2842 $[M+H]^+$. UV/Vis (CH_2Cl_2): λ_{max}/nm (ε_{max}/$M^{-1}cm^{-1}$) = 503 (77200), 469 (48300), 439 (17700). Fluorescence (CH_2Cl_2): λ_{max} = 512 nm, fluorescence quantum yield Φ_{fl} = 0.94, fluorescence lifetime τ_{fl} = 3.4 ns. CV (CH_2Cl_2, 0.1 M TBAHFP, vs. Fc/Fc^+): $E_{1/2}$ (PBI/PBI^-) = –0.92, $E_{1/2}$ (PBI^-/PBI^{2-}) = –1.22 V.

***N,N´*-Di(2,6-diisopropylphenly)-1,7-dibromoperylene-3,4:9,10-tetracarboxylic Acid Bisimide (5).[32]**

^{1}H NMR (CD_2Cl_2): δ 9.56 (d, J = 8.1, 2H), 9.02 (s, 2H), 8.81 (d, J = 8.1, 2H), 7.52 (t, J = 7.8, 4H), 7.36 (t, J = 7.8, 4H), 2.74 (sept., J = 6.8, 4H), 1.19 (2d, J = 6.8, 24H). HRMS (ESI-TOF, pos. mode, acetonitrile:chloroform = 1:1): *m/z* calcd for $C_{48}H_{41}Br_2N_2O_4$ $[M+H]^+$: 867.1428, found: 867.1419.

Supporting Information Available in the Appendix: Details for data evaluation of kinetic measurements, calculation of sterical encumbering in bay substituted perylene bisimides, calculation of group radii, main error estimation for $\Delta G^{\ddagger}$ and $t_{1/2}$, as well as ^{1}H NMR and ^{19}F NMR spectrum of **4**.

6.7 References and Notes

1 (a) J. Hofkens, T. Vosch, M. Maus, F. Köhn, M. Cotlet, T. Weil, A. Herrmann, K. Müllen, F. C. De Schryver, *Chem. Phys. Lett.* **2001**, *333*, 255-263; (b) T. D. M. Bell, S. Habuchi, S. Masuo, I. Österling, K. Müllen, P. Tinnefeld, M. Sauer, M. van der Auweraer, J. Hofkens, F. C. De Schryver, *Aust. J. Chem.* **2004**, *57*, 1169-1173; (c) A. Margineanu, J. Hofkens, M. Cotlet, S. Habuchi, A. Stefan, J. Qu, C. Kohl, K. Müllen, J. Vercammen, Y. Engelborghs, T. Gensch, F. C. De Schryver, *J. Phys. Chem. B* **2004**, *108*, 12242-12251; (d) F. C. De Schryver, T. Vosch, M. Cotlet, M. van der Auweraer, K. Müllen, J. Hofkens*, Acc. Chem. Res.* **2005**, *38*, 514-522; (e) E. Lang, F. Würthner, J. Köhler, *ChemPhysChem* **2005**, *6*, 935-941; *ChemPhysChem* **2006**, *7*, 292; (f) C. Jung, B. K. Müller, D. C. Lamb, F. Nolde, K. Müllen, C. Bräuchle, *J. Am. Chem. Soc.* **2006**, *128*, 5283-5291.

2 (a) C. Kohl, T. Weil, J. Qu, K. Müllen, *Chem. Eur. J.* **2004***, 10*, 5297-5310; (b) J. Qu, J. Zhang. A. C. Grimsdale, K. Müllen, F. Jaiser, X. Yang, D. Neher, *Macromolecules* **2004**, *37*, 8297-8306; (c) S. Krauß, M. Lysetska, F. Würthner, *Lett. Org. Chem.* **2005**, *2*, 349–353; (d) F. Yukruk, A. L. Dogan, H. Canpinar, D. Guc, E. U. Akkaya, *Org. Lett.* **2005**, *7*, 2885-2887.

3 (a) P. Ranke, I. Bleyl, J. Simmer, D. Haarer, A. Bacher, H. W. Schmidt, *Appl. Phys. Lett.* **1997**, *71*, 1332-1334; (b) P. Pösch, M. Thelakkat, H.-W. Schmidt, *Syn. Met.* **1999**, *102*, 1110-1112; (c) B. A. Jones, M. J. Ahrens, M.-H. Yoon, A. Fachetti, T. J. Marks, M. R. Wasielewski, *Angew. Chem.* **2004**, *116*, 6523-6526; *Angew. Chem. Int. Ed.* **2004**, *43*, 6363-6366; W. S. Shin, H.-H. Jeong, M.-K. Kim,

S.-H. Jin, M.-R. Kim, J.-K. Lee, J. W. Lee, Y.-S. Gal, *J. Mater. Chem.* **2006**, *16*, 384-390.

4 For recent review, see: (a) F. Würthner, *Chem. Commun.* **2004**, 1564-1579; (b) A. C. Grimsdale, K. M. Müllen, *Angew. Chem.* **2005**, *117*, 5732-5772; *Angew. Chem. Int. Ed.* **2005**, *44*, 5592-5629; (c) M. R. Wasielewski, *J. Org. Chem.* **2006**, *71*, 5051-5066; (d) F. Würthner, *Pure Appl. Chem*. **2006**, *78*, 2341-2350.

5 (a) Z. Chen, M. G. Debije, T. Debaerdemaeker, P. Osswald, F. Würthner, *ChemPhysChem* **2004**, *5*, 137-140; (b) H. Graaf, W. Michaelis, G. Schnurpfeil, N. Jaeger, D. Schlettwein, *Org. Electronics* **2004**, *5*, 237-249; (c) M. G. Debije, Z. Chen, J. Piris, R. B. Neder, M. M. Watson, K. Müllen, F. Würthner, *J. Mater. Chem.* **2005**, *15*, 1270-1276.

6 S. Leroy-Lhez, J. Baffreau, L. Perrin, E. Levillain, M. Allain, M.-J. Blesa, P. Hudhomme, *J. Org. Chem.* **2005**, *70*, 6313-6320.

7 J. Baffreau, L. Perrin, S. Leroy-Lhez, P. Hudhomme, *Tetrahedron Lett.* **2005**, *46*, 4599-4603.

8 (a) E. H. A. Beckers, S. C. J. Meskers, A. P. H. J. Schenning, Z. Chen, F. Würthner, R. A. J. Janssen, *J. Phys. Chem. A* **2004**, *108*, 6933-6937; (b) H. Uji-i, A. Miura, A. Schenning, E. W. Meijer, Z. Chen, F. Würthner, F. C. De Schryver, M. van der Auweraer, S. De Feyter, *ChemPhysChem* **2005**, *6*, 2389-2395; (c) P. Jonkheijm, N. Stutzmann, Z. Chen, D. M. de Leeuw, E. W. Meijer, A. P. H. J. Schenning, F. Würthner, *J. Am. Chem. Soc.* **2006**, *128*, 9535-9540.

9 Z. Chen, U. Baumeister, C. Tschierske, F. Würthner, *Chem. Eur. J.* **2007**, *13*, 450-465.

10 M. Sadrai, L. Hadel, R. R. Sauers, S. Husain, K. Krogh-Jespersen, J. D. Westbrook, G. R. Bird, *J. Phys. Chem.* **1992**, *96*, 7988-7996.

11 C. L. Mazzitelli, J. S. Brodbelt, J. T. Kern, M. Rodriguez, S. M. Kerwin, *J. Am. Soc. Mass Spectrom.* **2006**, *17*, 593-604.

12 J. Baier, P. Pösch, G. Jungmann, H. W. Schmidt, A. Seilmeier, *J. Chem. Phys.* **2001**, *114*, 6739-6743.

13 (a) L. Fan, X. Xu, H. Tian, *Tetrahedron Lett.* **2005**, *46*, 4443-4447; (b) W. Qiu, S. Chen, X. Sun, Y. Liu, D. Zhu, *Org. Lett.* **2006**, *8*, 867-870.

14 F. Würthner, P. Osswald, R. Schmidt, T. E. Kaiser, H. Mansikkamaeki, M. Könemann, *Org. Lett.* **2006**, *8*, 3765-3768.

15 (a) F. Würthner, V. Stepanenko, Z. Chen, C. R. Saha-Möller, N. Kocher, D. Stalke, *J. Org. Chem.* **2004**, *69*, 7933-7939; (b) P. Osswald, D. Leusser, D. Stalke, F. Würthner, *Angew. Chem.* **2005**, *117*, 254-257; *Angew. Chem. Int. Ed.* **2005**, *44*, 250-253.

16 See Chapter 2 and S. Hien, PhD thesis, University of Regensburg (Germany), **1995**.

17 G. Bringmann, A. J. Price Mortimer, P. A. Keller, M. J. Gresser, J. Garner, M. Breuning, *Angew. Chem.* **2005**, *117*, 5518-5563; *Angew. Chem. Int. Ed.* **2005**, *44*, 5384-5427.

18 G. Bott, L. D. Field, S. Sternhell, *J. Am. Chem. Soc.* **1980**, *102*, 5618-5626.

19 K. Oki *in Topics in Stereochemistry, Vol. 14* (Eds.: N.-L. Allinger, E. E. Eliel, S. H. Wilen), Wiley, New York, **1983**, pp. 1-76.

20 See chapter 3 and 4 of this thesis and P. Osswald, M. Reichert, G. Bringmann, F. Würthner, *J. Org. Chem.*, accepted for publication.

21 C. Wolf, W. A. König, C. Roussel, *Liebigs Ann. Chem.* **1995**, 781-786.

22 (a) W. H. Laarhoven, W. J. C. Prinsen, *Top. Curr. Chem.* **1984**, *125*, 63-130; (b) A. I. Meyers, R. J. Himmelsbach, *J. Am. Chem. Soc.* **1985**, *107*, 682-685.

23 G. Schoetz, O. Trapp, V. Schuring, *Electrophoresis* **2001**, *22*, 3185-3190.

24 A. S. Cooke, M. M. Harris, *J. Chem. Soc.* **1963**, 2365-2373.

25 M. Hesse, H. Meier, B. Zeeh, *Spectroscopic Methods in Organic Chemistry*, Thieme, Stuttgart, **1997**, pp. 88-100.

26 The used 1,1,2,2-tetrachloroethane-d_2 contained small amounts of water which limited the available temperature for this solvent.

27 (a) R. Cosmo, T. W. Hambley, S. Sternhell, *J. Org. Chem.* **1987**, *52*, 3119-3123; (b) R. Cosmo, S. Sternhell, *Aust. J. Chem.* **1987**, *40*, 35-47.

28 The planar unsubstituted PBI resembles the geometry of the presumably planar transition state. The values were taken as the average value of three different solid state structures as given in Chapter 2.

29 M. J. Ahrens, M. J. Tauber, M. R. Wasielewski, *J. Org. Chem.* **2006**, *71*, 2107-2114.

30 M. Charton, *Top. Curr. Chem.* **1983**, *114*, 57-91.

31 *CRC Handbook of Chemistry and Physics*, 67th edition (Ed. R. C. Weast), CRC Press Inc., Boca Raton, **1986**.

32 The free enthalpy of activation was calculated by the Eyring equation for a half-lifetime of 1 year.

33 C.-C. Chao, M.-k. Leung, Y. O. Su, K.-Y. Chiu, T.-H. Lin, S.-J. Shieh, S.-C. Lin, *J. Org. Chem.* **2005**, *70*, 4323-4331.

34 A. Pleschke, A. Marhold, M. Schneider, A. Kolomeitsev, G.-V. Röschenthal, *J. Fluorine Chem.* **2004**, *125*, 1031-1038.

35 (a) R. Givshi, R. Reisfeld, Z. Burshstein, *Chem. Phys. Lett.* **1993**, *213*, 338-344; (b) J. R. Lakowicz, *Principles of Fluorescence Spectroscopy*, 2nd ed., Kluwer Academic/Plenum, New York, **1999**, pp. 52–55.

CHAPTER 7

DABCO-mediated Self-Assembly of Zinc Porphyrin Perylene Bisimide Monodisperse Nanoparticles

Abstract: Four zinc porphyrin dyes have been appended to a central perylene bisimide dye unit through esterification. Upon addition of DABCO a well-defined intramolecular macrocyclic 2:1 complex was formed according to UV/Vis and NMR spectroscopy. The fluorescence properties of the self-assembly has been investigated by fluorescence spectroscopy. Deposition of the self-assembled 2:1 complex on HOPG afforded a well-defined 2D adlayer of discrete nanoparticles in contrast to the formation of pourly defined agglomerates in the absence of DABCO.

7.1 Introduction

Metalloporphyrins are versatile building blocks for self-assembly.[1] Especially, assemblies composed of zinc porphyrins and diaza-[2.2.2]-bicyclooctane (DABCO) have gained considerable attention as the defined binding site and the high binding constants enable the formation of stable two- and three-dimensional architectures.[2] Perylene bisimides, on the other hand, represent a class of functional dyes which exhibit outstanding photophysical and electrochemical properties and have been applied in a variety of highly luminescent self-assembled systems such as squares[1c,d,3] and rectangles[4]. The combination of both chromophores by either covalent or non-covalent means has led to systems with remarkable optical properties. Wavelength-dependent charge and energy transfer[5] as well as efficient charge separation[6] have been demonstrated for such multichromophoric systems depending on the incorporated perylene bisimide.

In order to realize well-defined discrete architectures composed of aryloxy-substituted perylene bisimides (APBIs) and porphyrins by self-assembly,[5,7] porphyrin-perylene bisimide bichromophoric system **4** which contains four zinc porphyrins tethered to the aryloxy arms of the APBI was synthesized. The self-assembly of building block **4** upon addition of DABCO was investigated by UV/Vis, ^{1}H NMR and ^{1}H DOSY NMR spectroscopy and atomic force microscopy (AFM). Spectroscopic studies revealed the formation of a 2:1 (DABCO:**4**) complex and highly ordered structure of this complex on HOPG surface could be demonstrated by AFM.

7.2 Synthesis of Zinc Porphyrin Functionalized Perylene Bisimide 4

As shown in Scheme 1, the synthesis of porphyrin-functionalized perylene bisimide **4** was accomplished by esterification of tetra(3-hydroxyphenoxy) perylene bisimide **1** with free base porphyrin carboxylic acid **2** using dicyclohexylcarbodiimide (DCC) and 4-(*N*-dimethylamino)pyridinium toluene sulfonate (DPTS) as coupling reagent in dichloromethane at room temperature. The crude free base porphyrin functionalized perylene bisimide **3** was isolated in 33% yield and was characterized by ^{1}H NMR and MALDI-TOF mass spectrometry. Subsequent metallation of **3** with saturated methanolic zinc acetate solution in dichloromethane affords the target zinc porphyrin-functionalized perylene bisimide **4** that was purified by silica-gel column chromatography with

chloroform as eluent and isolated in 21% overall yield. Compound **4** was fully characterized by ^{1}H NMR, MALDI-TOF mass spectrometry and elemental analysis.

Scheme 1. Synthesis of Tetra(Zinc Porphyrin) Substituted Perylene Bisimide **4**

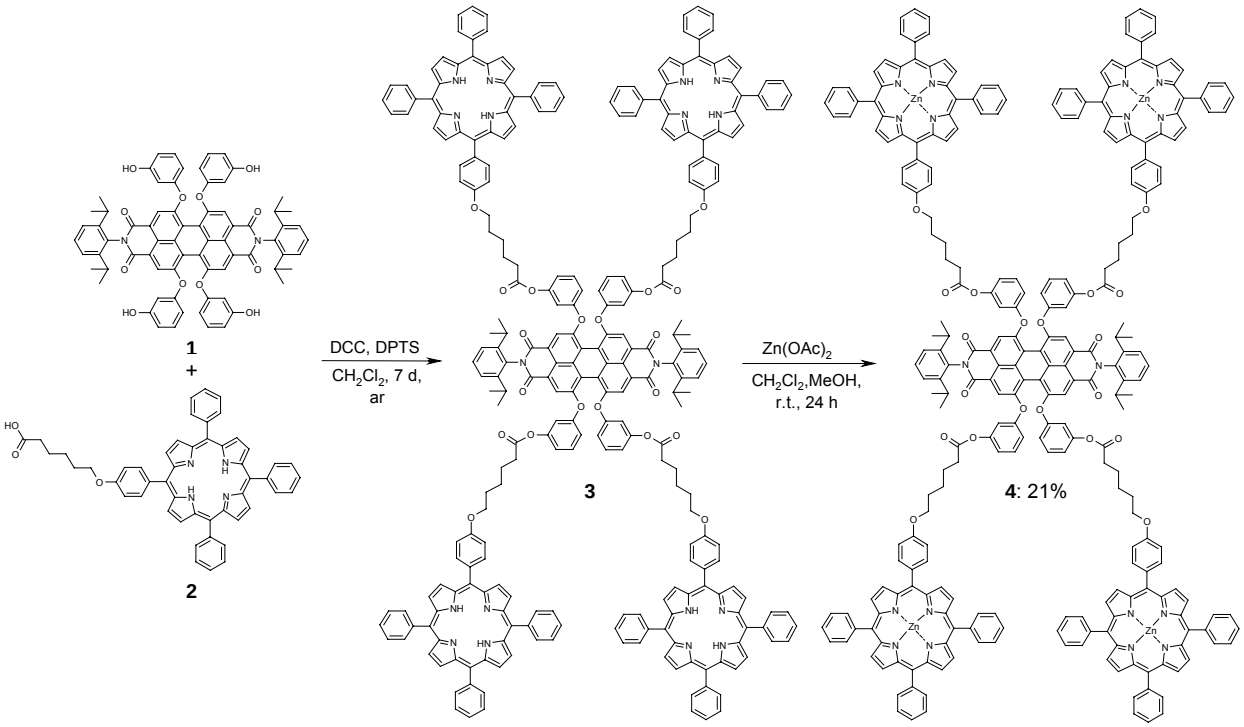

7.3 Optical Properties of Zinc Porphyrin Functionalized Perylene Bisimide 4

The optical properties of **4** were investigated by UV/Vis and fluorescence (steady state and time-resolved) spectroscopy in chloroform and tetrahydrofuran. The absorption and emission spectra of **4** in chloroform and tetrahydrofuran are shown in Figure 1. The absorption properties of **4** in both solvents are dominated by the intense Soret band of the zinc porphyrin (420-430 nm), whereas in the Q band region of the porphyrin (500-650 nm) the spectra of both chromophores overlap. In THF, the Soret band of **4** is shifted bathochromically by 7 nm to 430 nm compared to chloroform (423 nm) and a clearly visible absorption band at 605 nm appears in the Q band region (450-650 nm).

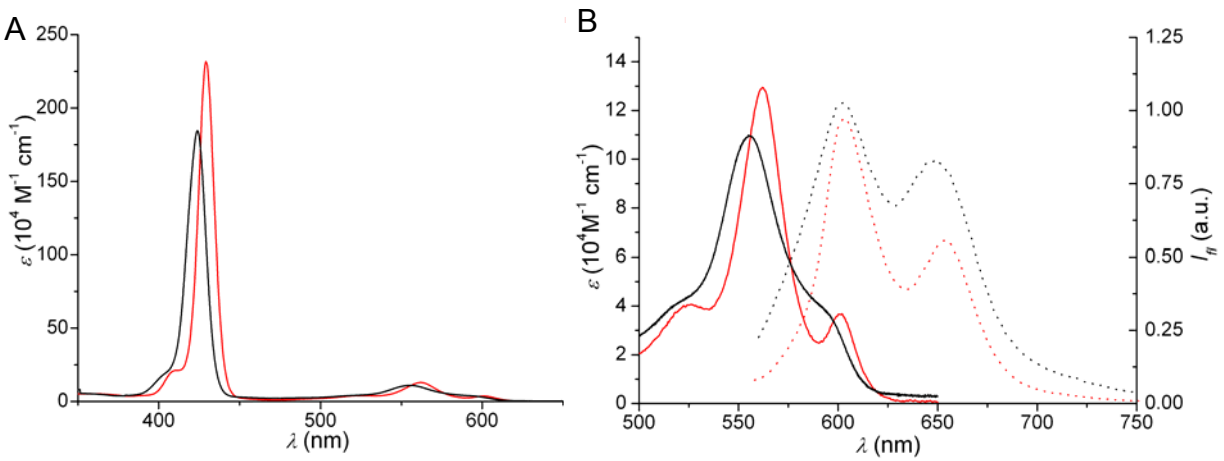

Figure 1. Absorption (A) and expanded view of the Q-band absorption (solid line) and emission spectra (dotted line) of **4** in chloroform and tetrahydrofuran (B). The spectra in chloroform are shown in black and those in THF in red.

In Figure 2, the UV/Vis absorption spectrum of **4** in chloroform is compared with the spectrum of the parent zinc tetraphenylporphyrin (ZnTPP), which was magnified by a factor of four.[8] For the Soret band (423 nm), a good agreement of the absorption spectrum of **4** and ZnTPP was found indicating that no ground state interaction between the zinc porphyrin units and the perylene bisimide of **4** are present. In contrast, in the Q-band region significant spectral differences were observed which can be attributed to the perylene bisimide chromophore. By subtracting the spectrum of four ZnTPP from that of **4**, the obtained spectrum (Figure 2B) revealed the characteristic spectral features of perylene bisimide dyes and a good agreement of the molar absorption coefficient with those of similar perylene bisimides was observed. Thus, the absorption maximum of the perylene bisimide unit can be estimated from the differential spectra to 569 nm. Accordingly, the longest wavelength transition in the absorption spectra can be clearly attributed to the zinc porphyrin units.

The emission spectra of **4** exhibit maxima at 601 and 648 nm in chloroform, and at 603 and 660 nm in tetrahydrofuran. Small Stokes shifts were observed in chloroform (9 nm) as well as in tetrahydrofuran (2 nm). Since perylene bisimides do not possess such small Stokes shifts (in general 30 nm), the observed Stokes shifts for the bichromophoric building block **4** indicate that the emission of the bichromophoric system results from the excited state of the zinc porphyrin. This is further evidenced by the fact that the absorption maximum of the longest wavelength transition (ca. 590 nm) can be

attributed to the zinc porphyrin units as the maximum of the perylene bisimide is situated at 569 nm (Figure 2). The spectral differences observed in chloroform and tetrahydrofuran, that are the bathochromic shift of the absorption and emission maxima, can be attributed to the complexation of the solvent THF to the zinc porphyrin units.

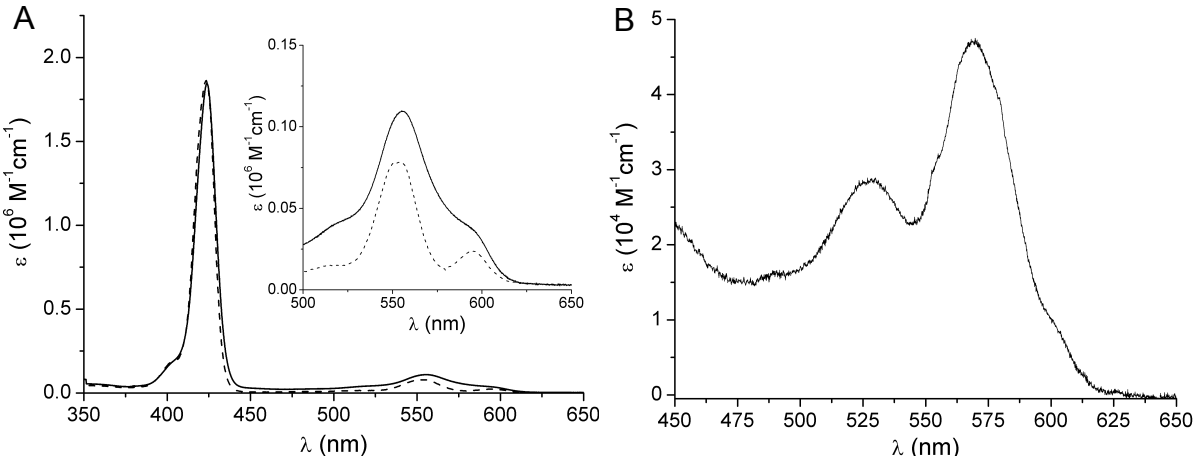

Figure 2. Comparison of the absorption spectra of **4** (solid line) and ZnTPP (magnified by a factor of 4, dotted line) in chloroform (A) and Q-band region of the differential spectra of **4** and ZnTPP (B).

Compound **4** showed only moderate fluorescence upon excitation at 540-560 nm with a quantum yield of 3% in chloroform and tetrahydrofuran. The excitation spectrum of **4** in chloroform (Figure 3) revealed that both chromophores, the perylene bisimide and the zinc porphyrin, contribute to the emission spectrum of **4** although the emission results exclusively from the excited state of the zinc porphyrin unit. This behavior might be explained by an energy transfer from the perylene bisimide core to the zinc porphyrin units. The fluorescence lifetime of **4** was determined in chloroform upon excitation at 550 nm and two emission lifetimes with a major component of τ_1 = 0.5 ns (95%) and a minor component τ_2 = 3.5 ns (5%) were found. The determined fluorescence lifetime reveal that the excited state of **4** exhibits a significantly shorter lifetime (0.5 ns) than that of both of the individual chromophores (5.6-7.4 ns for aryloxy-substituted perylene bisimides and 1.1 ns for ZnTPP).[1c] The fact that the fluorescence of perylene bisimide is completely quenched and the quantum yield corresponds to that of ZnTPP suggests an energy transfer process from perylene bisimide to zinc porphyrin.[1b,7] Therefore, the major pathway of deactivation of the excited state of **4** might be the population of the

zinc porphyrin triplet state as this deactivation pathway was reported to be very fast and efficient[9]

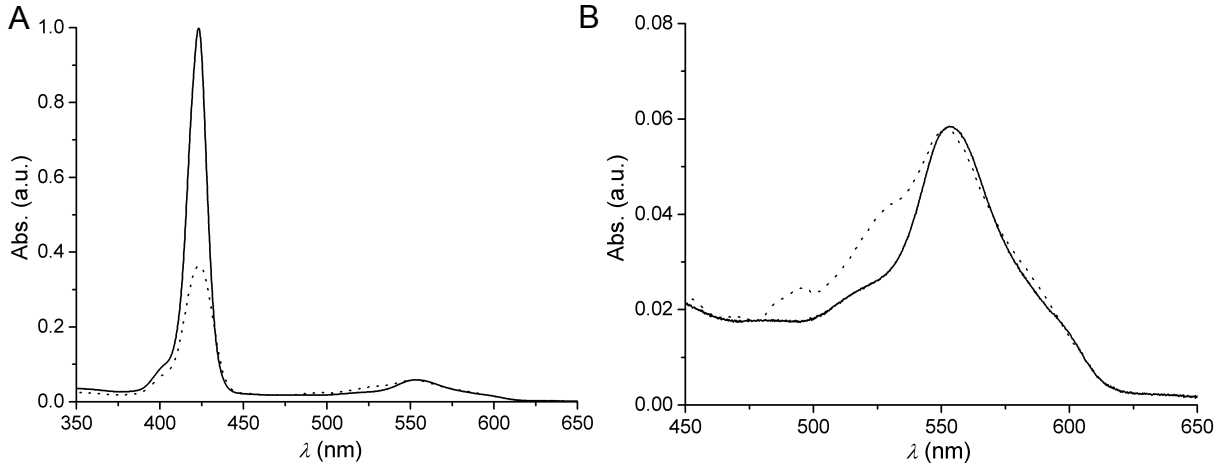

Figure 3. Absorption (solid) and excitation spectra (dotted line) of **4** in chloroform (A) and expanded view of the Q-band region (B). The detection wavelength for excitation spectra was 620 nm.

7.4 DABCO-Directed Self-Assembly of Building Block 4

The self-assembly of **4** with 1,4-diazabicyclo-[2.2.2]-undecan (DABCO) was investigated by constant host titration using UV/Vis spectroscopy. Figure 4 shows the absorption spectra of **4** in chloroform upon addition of DABCO.

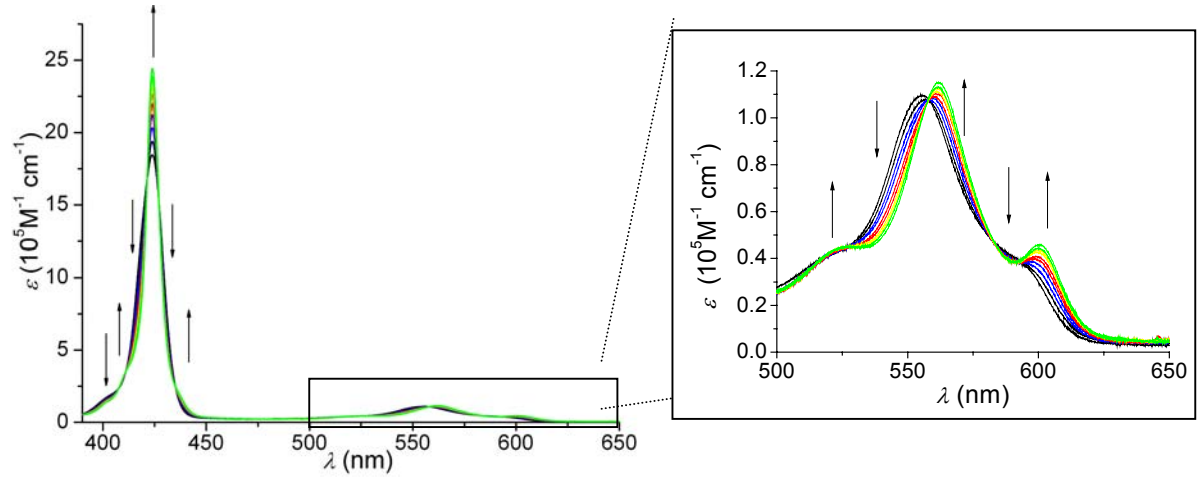

Figure 4. UV/Vis titration of **4** with DABCO in $CHCl_3$ at 23 °C. Inset: Expanded view of the Q-band region. Arrows indicate spectral changes with increasing amounts of DABCO.

During the titration, a new band arises at 601 nm and the broad Soret band gets narrowed with a concomitant increase in intensity as the half-width of the Soret band

changes from initially 770 cm^{-1} to 436 cm^{-1}. The changes in the Q band region of the absorption spectra upon addition of DABCO in chloroform are similar to those observed for **4** in THF. Thus, the appearance of a clearly visible absorption band at 601 nm reveals the ligation of DABCO by the zinc porphyrin units. Moreover, the position of the Soret band at 424 nm, as previously observed for similar systems,[2g] indicates the formation of a sandwich complex.[§]

During the titration isosbestic points (at 421, 427, 435, 557, 579, 592 nm) were observed up to a ratio of 1:1 (**4**:DABCO), implying that two species are present in equilibrium. On subsequent addition of DABCO up to a ratio of 1:2 (**4**:DABCO), a second process arises with slightly displaced isosbestic points (421, 427, 434, 558, 582, 591 nm). These observations reveal, that two individual two-state equilibria are involved in this self-assembly process. A schematic representation of the possible equilibria is given in Figure 5. The titration data were analyzed by non-linear least square analysis[10] using a model consisting of 1:0, 1:1 and 1:2 species (see Figure 5). The binding constant for the formation of the 1:1 species K_{11} was determined to (1.3 ± 0.3) x 10^7 M^{-1}, while for the equilibrium between the 1:1 and the 1:2 species (K_{12}) a value of (5.6 ± 1.5) x 10^6 M^{-1} was obtained (Figure 5).

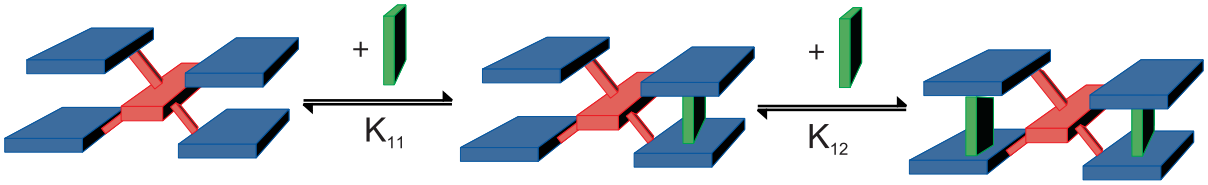

Figure 5. Schematic representation of a two step formation of self-assembled macrocycles and definition of binding constants. The perylene bisimide is shown in red, the porphyrin in blue and DABCO ligand in green.

UV/Vis titration indicates the ligation of DABCO at the zinc coordination site, but self-assembly of multifunctional compounds can result either in the formation of polymeric structures or macrocycles. The comparison of the binding constants observed for the DABCO mediated self-assembly of **4** with those of other systems leading to macrocyclic

[§] It has to be noted that a red-shift of 5 nm (from 420 to 425 nm) is related to presence of a sandwich complex. This red shift was not observed in the present case, but the narrowing of the Soret band indicates that additional processes, e.g. the presence of slight amounts of water or ethanol (stabilizer of chloroform), might be responsible for the absence of this indicative red shift. See also: (a) S. Yagi, M. Ezoe, I. Yonekura, T. Takagishi, H. Nakazumi, *J. Am. Chem. Soc.* **2003**, *125*, 4068-4069; (b) W.-S. Li, D.-L. Liang, Y. Suna, T. Aida, *J. Am. Chem. Soc.* **2005**, *127*, 7700-7702.

structures[2k] suggests the formation of an intramolecular macrocyclic structure in the present case, as schematically shown in Figure 5.

To elucidate the structural features of the self-assemblies, detailed ^{1}H NMR studies were performed. First, ^{1}H NMR titration was carried out in deuterated chloroform at 300 K under constant host conditions with a 0.67 mM solution of **4**. The aromatic region as well as the region of the DABCO resonances are shown in Figure 6.

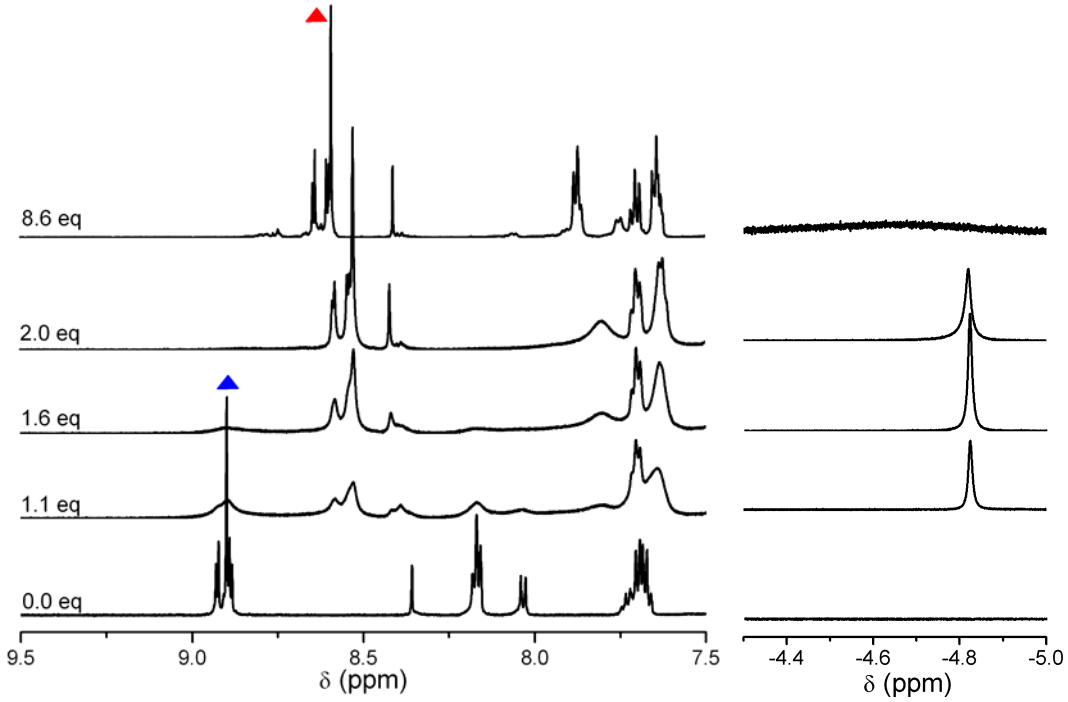

Figure 6. Sections of the ^{1}H NMR spectra (600 MHz) of **4** (6.4 x 10^{-4} M) in $CDCl_3$ upon successive addition of DABCO. Shown are the aromatic resonances (left) the high field region (right), showing the DABCO resonances. The equivalents of DABCO are denoted for each spectrum.

Upon subsequent addition of DABCO to a solution of **4**, the porphyrin resonance at 8.8 ppm (blue triangle, Figure 6) decreased in intensity and a new resonance arose at around 8.5 ppm (red triangle, Figure 6). At a 1:2 ratio of **4** and DABCO, the signal at 8.8 ppm completely disappeared and only the resonance at 8.5 ppm was present for the porphyrin resonances. This confirms the 1:2 stoichiometry of the complex already deduced by UV/Vis spectroscopy. The characteristic high field shift of these resonances (0.3 ppm) indicates the formation of a double decker structure where the aromatic ring current of the two porphyrins influence each other. This is further confirmed by the

DABCO resonances, which are located at –4.8 ppm. The large deshielding effect demonstrates that the DABCO molecule is situated between two porphyrin molecules. By addition of more than 2 equivalents of DABCO, the corresponding DABCO signal gets broadened and shifted to lower field and almost disappeared at a ratio of 8:1 (DABCO:**4**). Such behavior was frequently observed in similar systems and can be attributed to a fast exchange of the bound and free DABCO molecules on the NMR time scale.[2] At a stoichiometry of ≥ 2:1, all perylene bisimide and zinc porphyrin resonances appear sharp indicating the presence of a defined supramolecular species as well as a high binding constant which is in accordance with the results of UV/Vis studies. Thus, the NMR titration clearly reveals, on one hand, the strong binding of **4** and DABCO and second the formation of a double decker like structure for the 2:1 complex. The well resolved and sharp signals obtained by addition of two equivalents of DABCO further substantiate the formation of a structurally defined assembly rather than polymeric species.

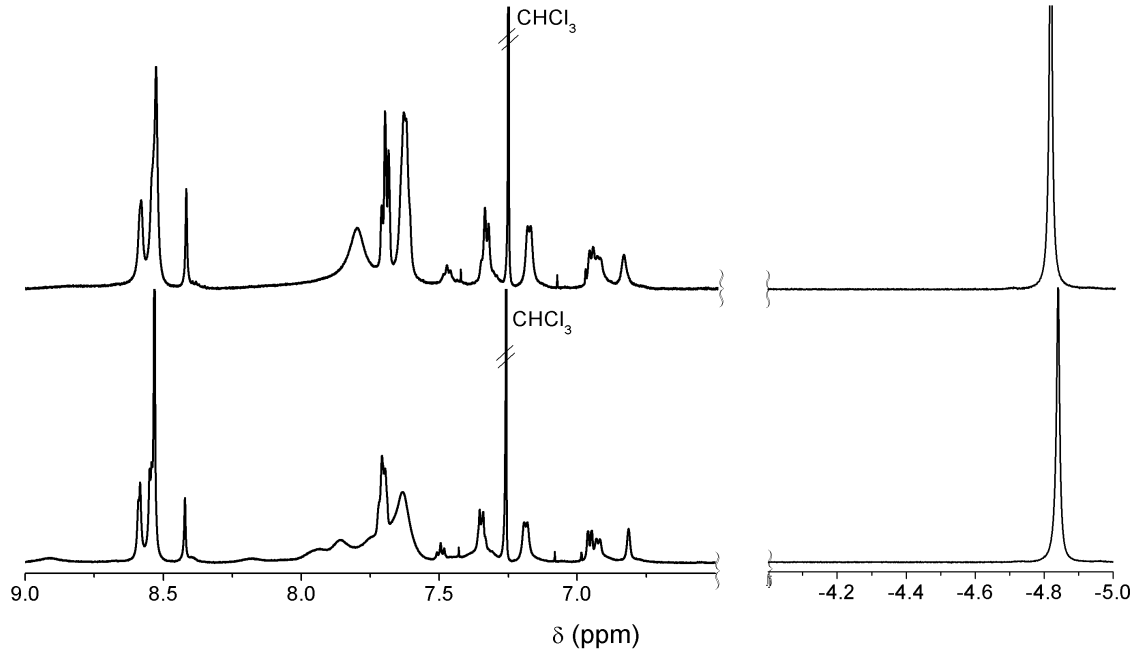

Figure 7. ^{1}H NMR spectra (400 MHz) of **4**•$(DABCO)_2$ in $CDCl_3$ at 273 K (bottom) and 293 K (top).

The slight broadening of the signals is presumably related to an intramolecular dynamic process resulting from the increased barrier for the inversion process between the (*P*)- and (*M*)-enantiomers of the perylene bisimide which can be clearly seen from

the temperature-dependent spectra shown in Figure 7. Upon cooling from 293 K to 273 K a clear sharpening of the signals was observed, especially of the resonances related to the aryloxy residues attached to the perylene core, whereas the DABCO protons remained unchanged, revealing that the complexation is not significantly influenced by temperature change.

To provide further evidence that no polymers or higher cyclic oligomers are created by self-assembly of **4** and DABCO, two-dimensional DOSY (diffusion ordered spectroscopy) NMR experiments were performed in $CDCl_3$. The DOSY spectra were recorded first for the host **4** and after addition of 2 equivalent of DABCO for the complex **4**•$(DABCO)_2$. The diffusion coefficients were determined as the mean value of ten individual signals and the obtained values for the free host **4** (2.29×10^{-10} m^2s^{-1}) and a 1:2 (**4**:DABCO) sample (2.33×10^{-10} m^2s^{-1}) did not differ significantly, revealing that the species formed by self-assembly of **4** with DABCO at a 1:2 ratio should be of similar size as **4**. From the diffusion coefficients, the hydrodynamic radius of the molecules was calculated employing the Stokes-Einstein-equation (eq. 7-1) under the assumption of spherical particles.[8]

$$D = \frac{k_B T}{6\pi\eta r} \qquad \text{(eq. 7-1)}$$

According to equation 7-1, radii of 1.59 nm and 1.56 nm were estimated for **4** and **4**•$(DABCO)_2$ complex, respectively. Indeed, this value (1.56 nm) for the **4**•$(DABCO)_2$ complex is in excellent agreement with the radius (1.54 nm) obtained from molecular modeling (Figure 8). These results corroborate that oligomers or polymers are not formed by self-assembly of **4** and DABCO, rather discrete structures, in particular intramolecular complex **4**•$(DABCO)_2$, are formed at a 1:2 (**4**:DABCO) stoichiomertry.

Owing to the high complexation constant observed in $CDCl_3$, self-assembly of **4** and DABCO seemed to be feasible even in a competitive solvent like THF with the ability to coordinate to zinc ions. Indeed, ^1H NMR experiments in THF-d^8 revealed the formation of expected complex. Thus, a broad singlet for the DABCO protons at –2.2 ppm can be observed, again showing the sandwich structure of **4**•$(DABCO)_2$ (Figure 9). As a further result of the formation of sandwich complex, the porphyrin protons are shifted by 0.3 ppm to lower field compared to pure **4** as already observed for NMR experiments in

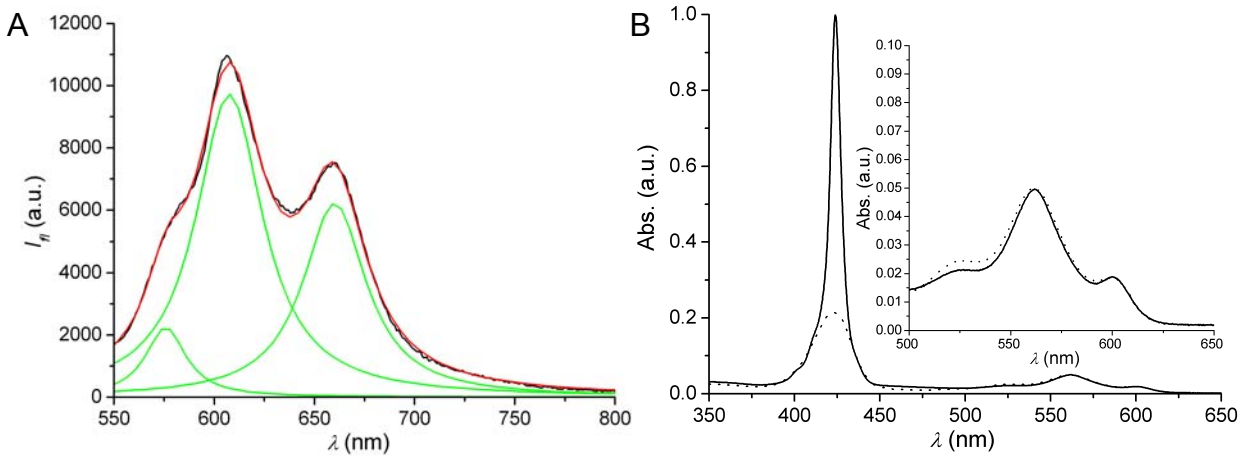

Figure 12. Lorentzian peak deconvolution of the emission spectra (black line) obtained by excitation at 540 nm (A). The peaks obtained by deconvolution are highlighted in green and the corresponding sum spectra in red. Absorption (solid line) and excitation spectra (dotted line, λ_{ems} = 660 nm) of **4**•(DABCO)$_2$ (B). Inset: Expanded view of the Q-band region.

The lifetime of the excited state of **4**•(DABCO)$_2$ was determined in chloroform upon excitation at 550 nm. Similar as for **4**, two emission lifetimes with a major component τ_1 of 0.8 ns (92 %) and a minor component τ_2 of 4.3 ns (8 %) were observed for **4**•(DABCO)$_2$. The determined fluorescence lifetimes show rather good agreement with those observed for **4** (τ_1 = 0.5 ns, τ_2 = 3.4 ns), except that the ratio changed slightly from 95:5 to 92:8 (τ_1:τ_2). Furthermore, the amount of τ_2 is in good agreement with the contribution of the perylene bisimide emission determined from the fluorescence spectra of **4**•(DABCO)$_2$, indicating that the larger fluorescence lifetime can be attributed to the perylene bisimide unit in the bichromophoric system. The low fluorescence quantum yields observed for **4**•(DABCO)$_2$ as well as the minor contribution of the perylene bisimide to the total emission suggest that also for self-assembled **4**•(DABCO)$_2$ an energy transfer from the perylene bisimide to the porphyrin is present. The excitation spectra (λ_{dect} = 660 nm) of **4**•(DABCO)$_2$ again show good agreement with the absorption spectra as can be seen from Figure 12B, indicating, that both chromophores contribute to the total emission at 660 nm. Therefore, the emission properties of **4**•(DABCO)$_2$ suggest that the fluorescence properties (Φ_{fl} and τ_{fl}) of **4** do not change significantly upon complexation, apart from the shift of the emission maxima.

$CDCl_3$. For all signals, no significant line broadening is observed, showing that a defined species is present rather than a polymeric one.

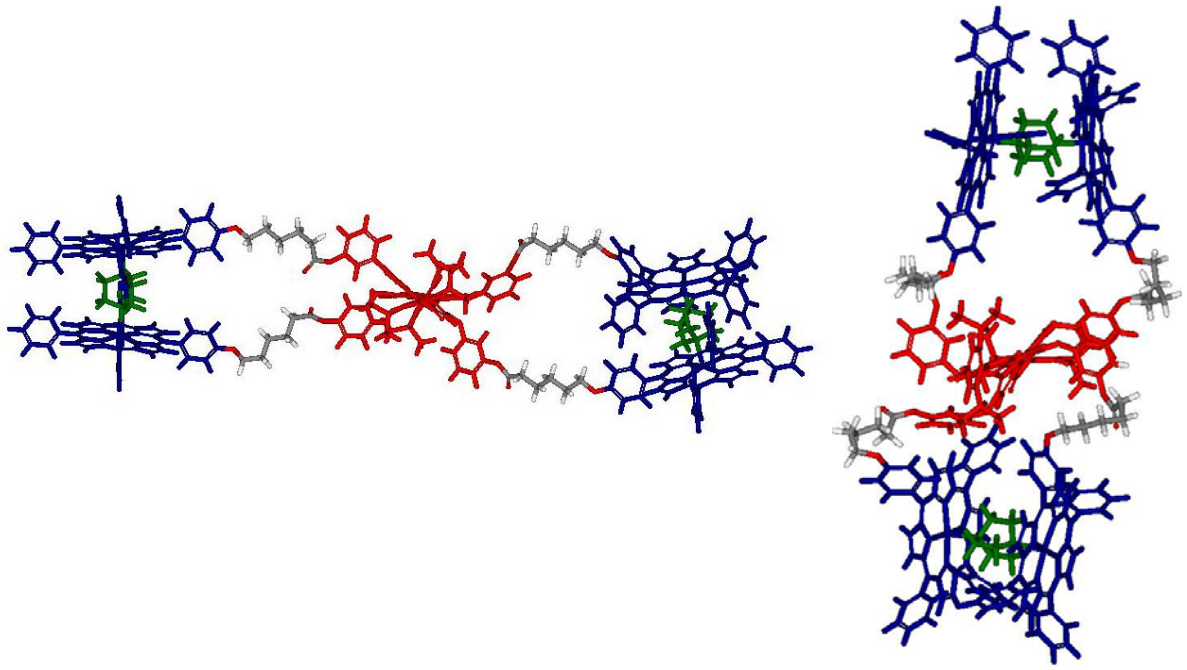

Figure 8. Structure of the two possible cyclic isomers **4**•$(DABCO)_2$ obtained from molecular modeling. Laterally (left, stretched conformation) and diagonally (right, squeezed conformation) bridged structures were calculated with a MM3 force field using CaChe Quantum CaChe Workspace 5.0. All views are along the *N,N*-axis of the perylene bisimide, the perylene bisimide is highlighted in red, the porphyrin in blue and DABCO in green.

Additionally ^1H DOSY spectra in THF-d^8 were recorded first for the host **4** and after addition of DABCO for the **4**•$(DABCO)_2$ complex (Figure 10). The diffusion coefficients were determined as the mean value of ten individual signals and resulted for the host **4** to (2.78 x 10^{-10} m^2s^{-1}) and for the **4**•$(DABCO)_2$ complex to (2.88 x 10^{-10} m^2s^{-1}).[8] The calculated hydrodynamic radius of the molecules in solution is 1.57 nm and 1.52 nm for **4** and **4**•$(DABCO)_2$, respectively. The spectral properties for **4**•$(DABCO)_2$ as well as the calculated hydrodynamic radius is in excellent agreement with the results obtained in chloroform, revealing the formation of intramolecular macrocyclic structure also in the competitive solvent THF. This demonstrates the high thermodynamic driving force for the formation of an intramolecular macrocyclic complex.

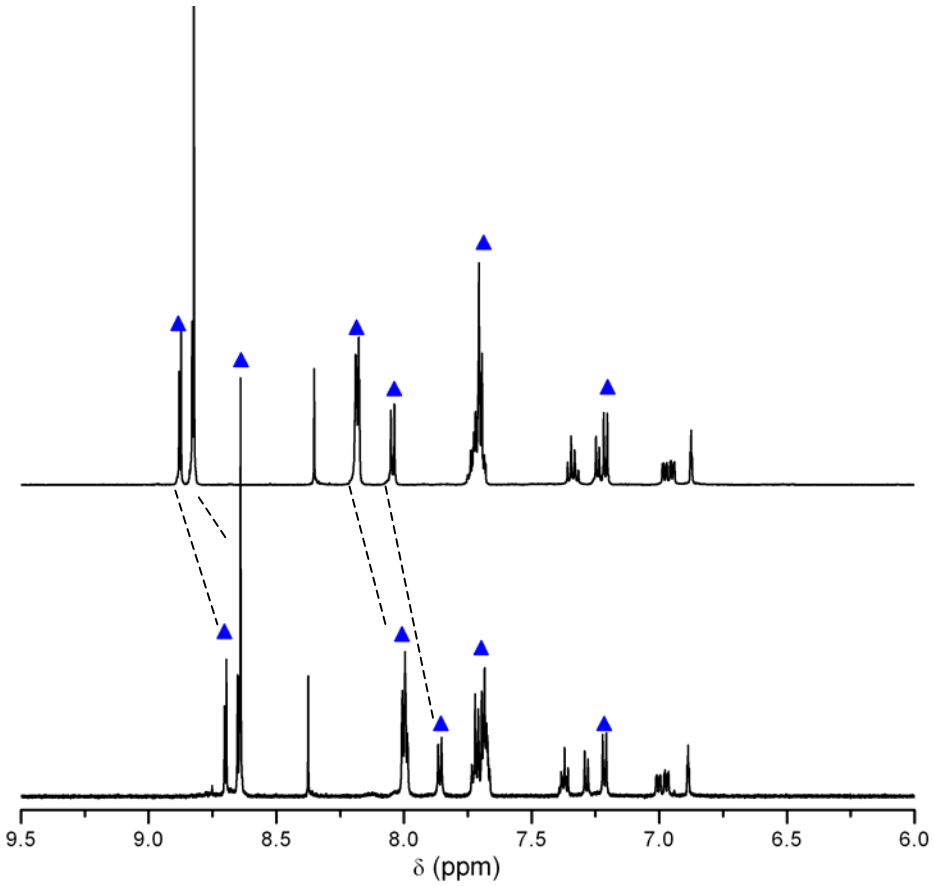

Figure 9. Aromatic region of the ^{1}H NMR spectra (600.13 MHz) of **4** (top) and **4**•(DABCO)$_2$ (bottom) in THF-d^8. The signals of the porphyrin protons are marked blue.

Unfortunately, all attempts to record mass spectra for the complex **4**•(DABCO)$_2$ by ESI-TOF MS and MALDI-TOF MS failed. Only the molecular ion of **4** was observed. This is frequently observed for self-assembled systems and is attributed to the reversible nature of the self-assemblies and the lability of such self-assembled systems under the conditions necessary for ionisation.[1c]

As outlined in Chapter 3, two isomers are possible for an intramolecular macrocyclic structure of **4**•(DABCO)$_2$.[11,$] Upon complexation, the DABCO molecules can either link two porphyrins in a lateral or diagonal fashion (as shown in Figure 8). These two possible structures cannot be distinguished by UV/Vis, ^{1}H NMR or DOSY spectroscopy in the present case as the long alkyl spacer in **4** enforce similar conformational

[$] As already annotated in Chapter 3 of this thesis, two additional isomeric macrocycles are possible by 1,6- and 7,12-linkage. In contrast to the lateral and diagonal isomer (D_2), these two isomers exhibit less symmetry as they belong to the symmetry group C_2. Therefore, these isomers can be excluded due to the observed symmetrical NMR pattern of the self-assemblies. This is further supported by the fact that these two straight bridged isomers are energetically less favored as shown in chapter 3 (Figure 1) of this thesis.

properties for both isomers. Thus, characteristic spectral features (high field shift of the aryloxy-resonances in the ^{1}H NMR spectrum and the hypschromic shift of the absorption maximum) as observed for covalent macrocycles in Chapter 3 cannot be observed. Only due to the fact that aryloxy-substituted perylene bisimides (Chapter 3) prefer a horizontal orientation of the aryloxy residues, the most likely conformation should be the laterally bridged species for the self-assembled intramolecular macrocyclic species **4**•$(DABCO)_2$ as well.[11]

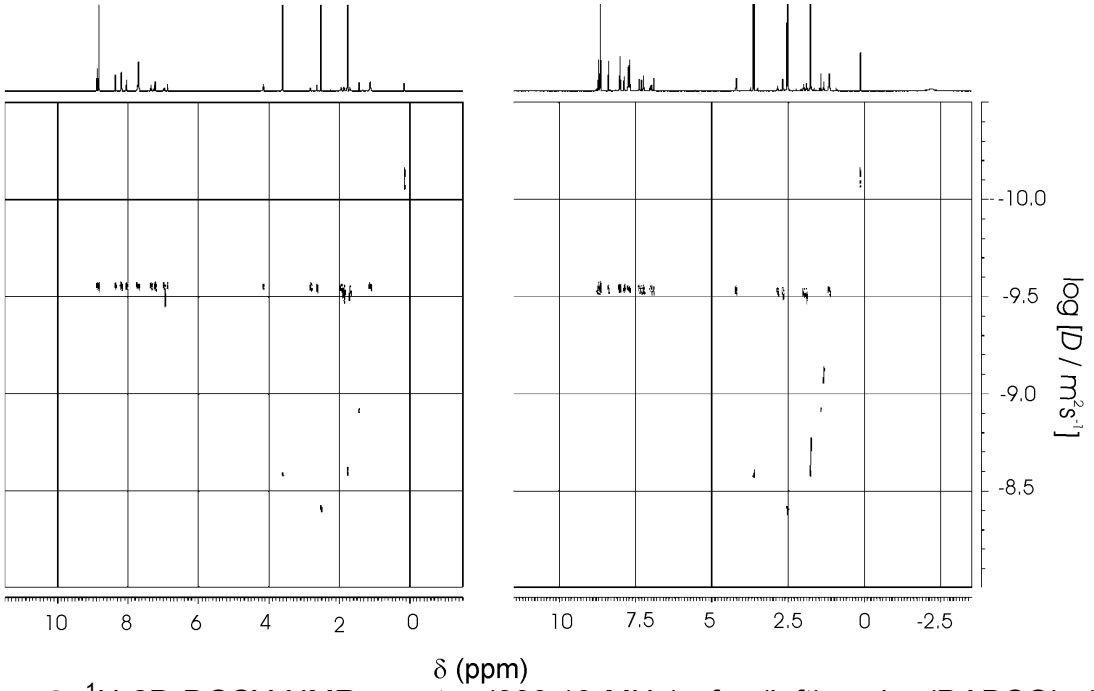

Figure 10. ^{1}H 2D-DOSY NMR spectra (600.13 MHz) of **4** (left) and **4**•$(DABCO)_2$ (right) in THF-d^8. The diffusion coefficient D (in m^2/s) in logarithmic scale is plotted against the chemical shift δ.

7.5 Optical Properties of the Self-Assembled Species 4•$(DABCO)_2$

To explore the fluorescence properties of the self-assembled species **4**•$(DABCO)_2$, fluorescent titration experiments were performed in chloroform at room temperature (21 °C). The emission spectra, which were corrected by the absorption at the excitation wavelength (540 nm), and the change of the fluorescence quantum yields of **4** upon addition of DABCO are shown in Figure 11. The fluorescence quantum yields of **4** and **4**•$(DABCO)_2$ were determined to 0.03 and 0.04, respectively, indicating that the fluorescence properties of **4** are not affected by addition of DABCO (Figure 11B). The low quantum yields observed for **4**•$(DABCO)_2$ reveal that the emission is determined by

the porphyrin units in this bichromophoric array, as it is the case for the free building block **4**. Furthermore, upon addition of DABCO the shape of the fluorescence spectra changes significantly which can be attributed to the formation of the complex **4**•$(DABCO)_2$ as similar spectral properties were observed also for the emission of **4** in tetrahydrofuran. The emission maximum of **4** at 602 nm is shifted to 605 nm and a more pronounced shift was observed for the second emission maximum from 648 to 660 nm upon addition of DABCO.

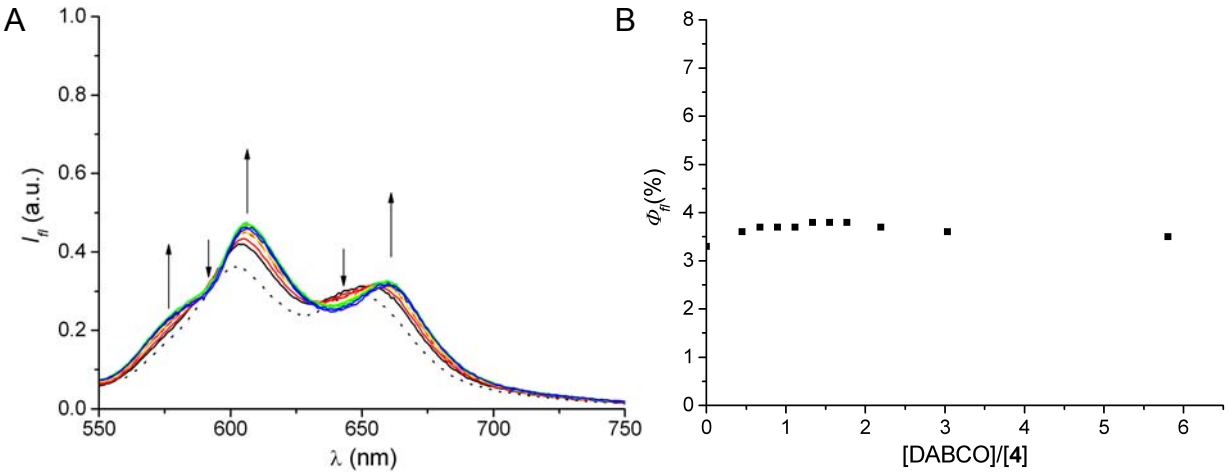

Figure 11. Changes of emission spectra (absorption corrected) upon excitation at 540 nm (A) and change of the fluorescence quantum yields (B) of **4** upon addition of DABCO in chloroform (1.03 x 10^{-6} M) at 20 °C. Arrows indicate spectral changes upon increasing amounts of DABCO.

Another interesting feature is the occurrence of a clearly visible shoulder in the high energy region of the emission spectra. By peak deconvolution the maximum of this shoulder was determined to 582 nm (see Figure 12A) which is located at shorter wavelength than the maximum of the longest wavelength transition (601 nm) observed in the absorption spectra of **4**•$(DABCO)_2$. This suggests that the shoulder originates from the emission of the perylene bisimide core. From the areas obtained by peak deconvolution, it can be estimated that the perylene bisimide emission contributes with 8 % to the total emission of the complex **4**•$(DABCO)_2$. This is further confirmed by the fluorescence spectrum of **4**•$(DABCO)_2$ upon excitation at 423 nm where mainly the zinc porphyrin part of the bichromophoric system is excited. In this case no high energy shoulder was observed which demonstrates that the fluorescence results exclusively from the complexed zinc porphyrin units (Figure 13).

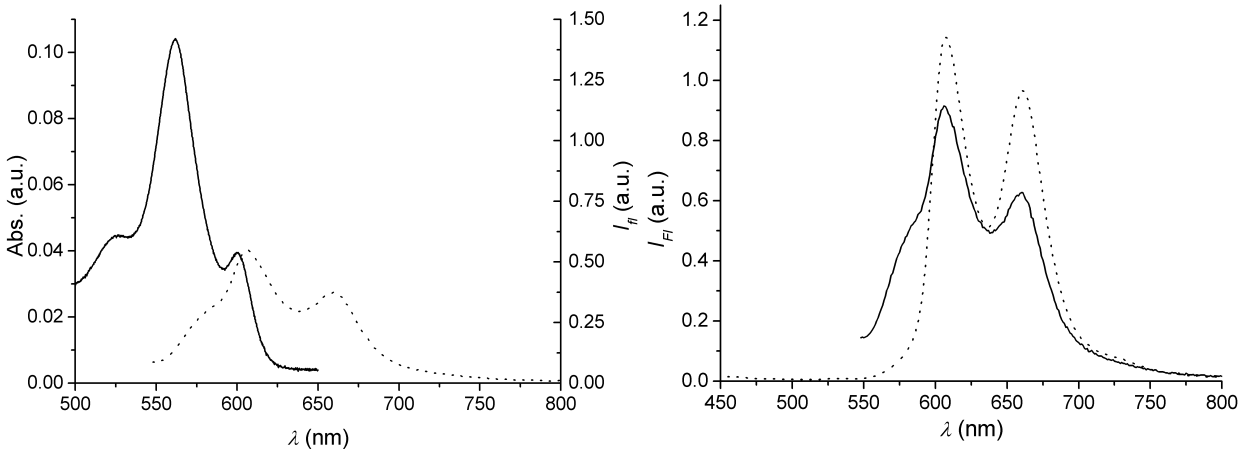

Figure 13. Q-band region of the absorption spectra and emission spectra of **4**•$(DABCO)_2$ in chloroform at 20 °C (λ_{ex} = 540 nm) (left) and comparison of the emission spectra of **4**•$(DABCO)_2$ upon excitation at 540 nm (solid line) and 423 nm (dotted line) (right).

7.6 Organization of Self-Assembled 4•$(DABCO)_2$ complexes on HOPG surfaces

To assess the ability of these well-defined self-assembled macrocycles **4**•$(DABCO)_2$ to organize on surfaces, AFM analysis was performed on highly ordered pyrolytic graphite (HOPG) in the tapping mode.[#] Figures 14 and 15 show the AFM images obtained for **4** and **4**•$(DABCO)_2$.

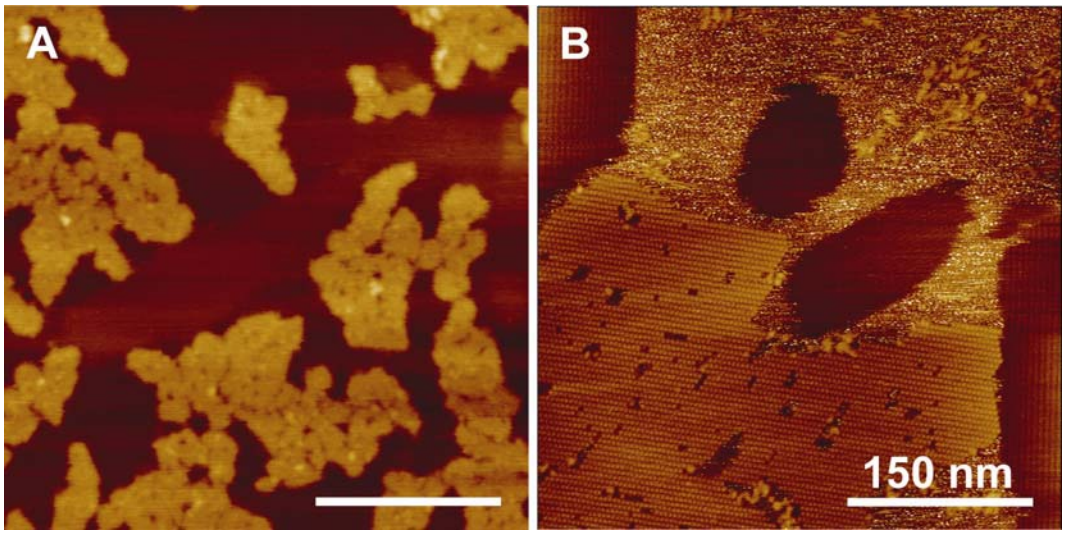

Figure 14 AFM-image of **4** (A) and **4**•$(DABCO)_2$ (B) on HOPG (spin-coated). The bar represents 150 nm for both images and dark areas indicate the graphite surface.

[#] AFM measurements have been performed by V. Stepanenko, Institute of Organic Chemistry, University of Würzburg/Germany.

In AFM images of self-assembled macrocyclic complex (Figure 14B), a highly ordered pattern was observed over a wide range of the surface. For comparison a sample of uncomplexed **4** was analyzed under similar conditions (Figure 14A). In contrast to **4**•$(DABCO)_2$, uncomplexed **4** showed only ill-defined agglomerates on surface indicating that the defined arrangement of the chromophores in macrocycles **4**•$(DABCO)_2$ is responsible for the observed unique ordering on the surface. High resolution AFM image of **4**•$(DABCO)_2$ (Figure 15, C) clearly showed small isolated nanosized particles that are arranged in a distorted hexagonal packing on the surface. For these ellipsoid particles, an average length 4.7 ± 0.5 nm and width of 3.4 ± 0.5 nm were determined by Fourier transformation. The height of the particles was elucidated by cross-section analysis as 0.48 nm, indicating the presence of a monolayer. Based on these data, the area covered by each supramolecular particle was estimated to 12.6 nm^2. Again, the particle size determined by AFM analysis fits well with the dimensions (10.9 nm^2) of the macrocyclic structure calculated by molecular modeling, confirming the monodispers nature of the particles. These results clearly demonstrate, that the well-defined self-assembled macrocycles **4**•$(DABCO)_2$ can be deposited on surfaces by spin-coating as single molecular entities in a highly ordered pattern.

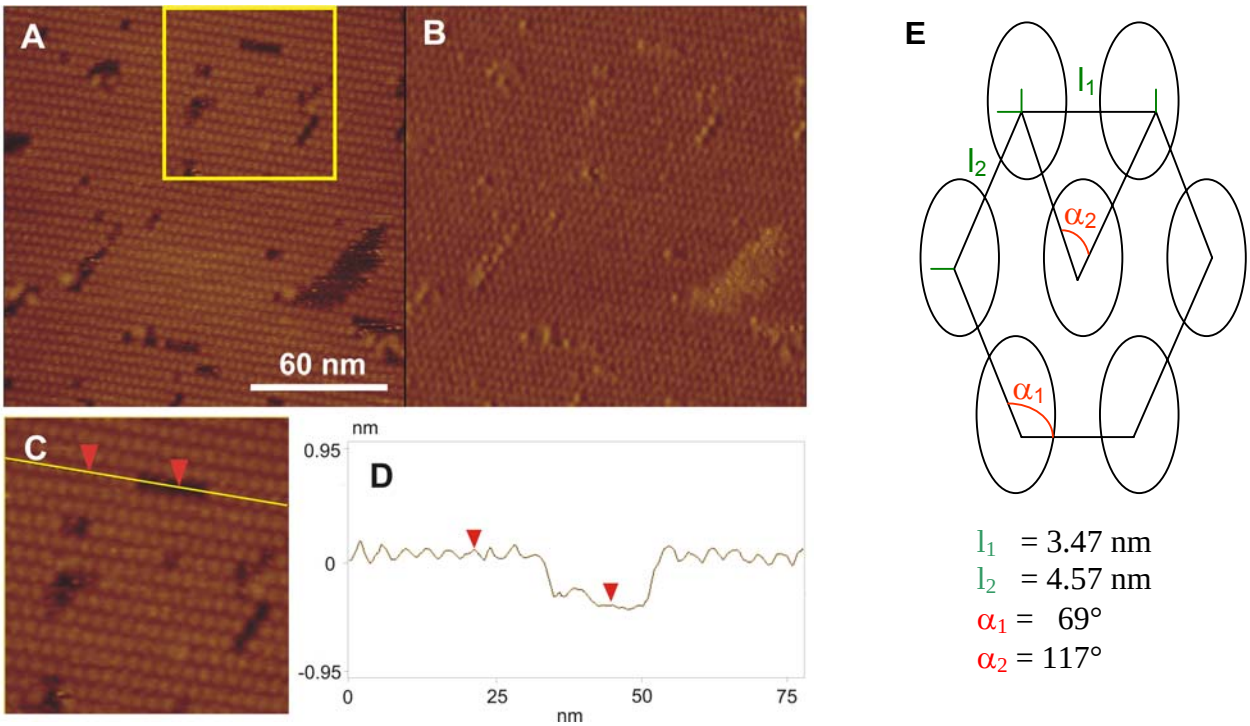

Figure 15. AFM-image of a 1 x 10^{-5} M solution of **4**•$(DABCO)_2$ on HOPG (spin-coated). height (A) and phase image (B), high resolution image of A (c; yellow square in A) and

cross-section-analysis (D, yellow line in C). The z-scale is 2 nm. The hexagonal structure of **4**•$(DABCO)_2$ and its dimensions on the surface are schematically shown in E.

7.7 Conclusion

In summary, a new zinc porphyrin-functionalized perylene bisimide **4** was synthesized. The DABCO-mediated self-assembly of **4** occurred with high binding constants under exclusive formation of one species upon addition of two equivalents of DABCO over a wide range of concentration. The structure of the self-assembled species **4**•$(DABCO)_2$ was assigned to an intramolecular macrocycle by ^{1}H NMR spectroscopy in combination with DOSY NMR spectroscopy and atomic force microscopy. Furthermore, it was demonstrated that the complex **4**•$(DABCO)_2$ was deposited on a graphite surface by spin-coating to give a regular 2D adlayer of photofunctional monodisperse nanoparticles. The defined arrangement of the chromophores as well as the highly ordered structure of the particles observed on HOPG may lead to applications as electro- or photoactive materials where such particles can be addressed individually.[12]

7.8 Experimental Section

Methods and Materials. Dichloromethane and methanol were purchased from Staub (Filsum, Germany), DCC (99%) and DABCO (≥ 97%) were obtained from Acros Organics (Geel, Belgium) and zinc acetate (99%+) from Grüssing (Nürnberg, Germany). All chemical and reagents were used as received if not otherwise mentioned. Perylene bisimide **1**, free base porphyrin **2**, and DPTS were synthesized according to literature procedure.[8,13] Anhydrous dichloromethane was obtained by distillation from calcium hydride under nitrogen. Flash column chromatography was performed using silica gel (Si60 mesh size 40-63 µm) as stationary phase. 1,8-Diazabicyclo-[2.2.2]-octane was sublimed prior to use and chloroform used for titration experiments was filtered over basic aluminum oxide. ^{1}H NMR spectra were recorded with a Bruker Avance 400 spectrometer. The spectra are referred to TMS as internal standard ($CDCl_3$) or to the residual solvent peak (THF-d^8) and the chemical shifts δ are given in parts per million. Coupling constants *J* are given in Hertz. MALDI-TOF mass spectra were recorded on a Bruker-Franzen Reflex EA240 instrument. Elemental analysis were performed on a CHNS 932 analyzer from Leco Instruments.

Spectroscopy. Spectroscopic grade solvents (Uvasol®) from Merck were used for all spectroscopic measurements. UV/Vis spectra were recorded with a Perkin Elmer Lamba 40P under ambient conditions. Fluorescence spectra were recorded with a PTI QM-4/2003 and fluorescence lifetimes were determined with a PTI GL3330 nitrogen laser and a GL302 dye laser using stroboscope technique. All fluorescence measurements were performed under aerobic conditions and fluorescence spectra are corrected. Fluorescence quantum yields were determined as the average value for three different excitation wavelengths with *N,N´*-bis(2,6-diisopropylphenyl)-1,6,7,12-tetraphenoxyperylene-3,4:9,10-tetracarboxylic acid bisimide (Φ_{fl} = 0.96 in chloroform) as reference and by applying the high dilution method (A < 0.05).[14] Decay curves were evaluated with the Felix Software from PTI by fitting 1-4 lifetimes. The quality of the fit was judged by Derbin-Watson factor DW and χ^2 (for a diexponential decay DW > 1.7 and $0.9 < \chi^2 < 1.2$) as well as by the correlation function and the residuals.

DOSY NMR Spectroscopy. ^{1}H DOSY experiments were carried out at 299.2 K on a Bruker Advance DMX 600 spectrometer equipped with a gradient unit and a conventional 5 mm broadband (^{15}N-^{31}P)/^{1}H probe with automatic tune/match accessory and z axis gradient coil that is capable of producing pulsed magnetic field gradients in the z direction of 52 G/cm^{-1}. Data were acquired and processed using the software XWIN-NMR 3.5, patch level 6. Signal averaging was done with 160 scans per increment. The ^{1}H NMR data were recorded in deuterated chloroform and THF-d^8 solutions in 5 mm NMR tubes. The detailed experimental setup and pulse sequences, and the equation for data analysis used for these experiments were recently published by our group, and are therefore not reported here.[15]

For calculating the hydrodynamic radius of the molecules, the Stokes-Einstein-equation (eq. 7-1) was used. This equation is only valid for spherical particles.[16]
The dynamic viscosity μ of THF-d^8 (0.000501 kg m^{-1}s^{-1}) and $CDCl_3$ (0.000542 kg m^{-1}s^{-1}) used for calculating of the hydrodynamic radius were taken from literature 16.

Atomic Force Microscopy (AFM). Atomic force microscopy was performed on a Nanoscope IV controller Veeco Multi Mode AFM using silicon tips with a resonance frequency of 300 kHz. The measurements were done in the tapping mode. The samples

were prepared by spin-coating (5000 rpm) of a 1.1 x 10^{-5} M solution of **4** or **4**•$(DABCO)_2$ on highly pyrolytic graphite (HOPG).

Quantum Chemical Calculations. All calculations were done in the gas phase by applying a MM3 force field (CaChe Quantum CaChe Workspace 5.0) and solvent effects are, therefore, not considered. The size of the two possible cyclic isomers was determined by analyzing atom distances as implemented in the CaChe Quantum CaChe Workspace 5.0. As different conformations are possible for the alkyl chains the dimensions the molecules possess a length of 4.0 nm (squeezed) to 6.3 nm (stretched), a width along the *N*,*N*-axis of the perylene bisimide of 2.2 nm and a height of 1.1-1.2 nm.

For comparison with the DOSY-experiments, the volume of the molecules was calculated by assuming cuboids. By applying the formula for spheres the desired radius was determined from this volume. For comparison with the AFM measurements, it was assumed, that the aromatic units have a high affinity to the HOPG surface and the molecules are oriented flat on the surface (porphyrin lying next to the surface). Therefore, the area was calculated with the length and the width of the molecules by underlying an ellipsoid shape, as observed by AFM.

UV/Vis titration experiments. Titration experiments were carried out on a Perkin Elmer Lamda 950 (1.0 µM) or on a Perkin Elmer Lamda 40P photospectrometer with a peltier temperature control unit (10.0 µM).

To a 9.3 x 10^{-7} M solution of **4** in chloroform in a 1 cm quartz cuvette at 23 °C were added via a microliter syringe 5 µl aliquots of a solution of DABCO (4 x 10^{-6} M) and **4** (9.3 x 10^{-7}M). After each addition, a UV/Vis spectrum was recorded. The titration experiments were analyzed by fitting the whole series of spectra at 0.5 nm intervals using the software SpecFit/32, which uses a global analysis system with expanded factor analysis and a Marquardt least-square minimization to obtain globally optimized parameters. The individual binding constants were calculated from the logβ values obtained by the program.

Additionally, the titration experiments were similarly performed at a concentration of 1 x 10^{-5} M of **4** and 4 x 10^{-4} M of DABCO for analyzing the Q-band region at higher

concentrations of the host **4**. Although the error of the experiments in this case was quite high, the fit of the titration curve and the match of the experimental spectra with calculated ones were good. The binding constants determined in this case were (1.8 ± 1.0) x 10^7 M^{-1} and (1.1 ± 0.6) x 10^7 M^{-1} and the values agree well with those determined at lower concentrations. Both experiments were reproduced once.

Fluorescence titration experiments. Titration experiments were carried out on a Perkin Elmer Lamda 950 UV/Vis spectrometer and PTI QM-4/2003 fluorescence spectrometer.

To a 1.0 x 10^{-6} M solution of **4** in chloroform in a 1 cm quartz cuvette at 23 °C were added via a microliter syringe 5 µl aliquots of a solution of DABCO (7.0 x 10^{-5} M) and **4** (1.0 x 10^{-6} M). After each addition, a UV/Vis spectrum and fluorescence spectra for three different excitation wavelength (527, 540 and 550 nm) were recorded. At the beginning and the end of the titration experiment, the fluorescence lifetime was determined and an excitation spectrum (λ_{ex} = 550 nm) was recorded after the procedures given above. Fluorescence quantum yields were determined for each addition of DABCO according to the procedure given in the section spectroscopy. For analysis of the spectral changes, the emission intensities were divided by the absorption of **4**•$(DABCO)_2$ at the excitation wavelength.

^{1}H NMR titration and DOSY NMR experiments. ^{1}H NMR titration was performed under constant host conditions on a Bruker Advance 600 spectrometer at 300 K. To 600 µL of a 0.67 mM solution of **4** in deuterated chloroform were added 10 µl aliquots of a solution of DABCO (16.9 mM) and **4** (0.67 mM) via a microliter syringe. After each addition, a ^{1}H NMR spectrum was recorded. Before the first addition and after the sixth addition a DOSY spectrum was recorded under the conditions given above.

Synthesis and Characterization of Perylene Bisimide 4

N,N`-Di(2,6-diisopropylphenyl)-1,6,7,12-tetrakis(3-hydroxyphenoxy)perylene-3,4:9,10-tetracarboxylic acid bisimide **1** (50 mg, 43.7 µmol), porphyrin **2** (164 mg, 0.22 mmol), DCC (159 mg, 0.77 mmol) and DPTS (168 mg, 0.57 mmol) were suspended under argon in anhydrous dichloromethane (5 mL) and stirred for seven days at room

temperature. The reaction mixture was filtered and evaporated to dryness. After silica gel column chromatography with chloroform 59 mg (14.6 µmol, 33%) **3** could be obtained as crude product.

^{1}H NMR ($CDCl_3$): δ 8.81 (m, 32H), 8.36 (s, 4H), 8.16 (m, 24H), 8.04 (m, 8H), 7.75–7.65 (m, 36H), 7.37 (t, *J* = 8.2, 2H), 7.28 (t, *J* = 8.1, 4H), 7.16 (d, *J* = 7.8, 4H), 7.29 (m, 2H), 6.90–6.88 (m, 8H), 6.81 (t, *J* = 2.2, 4H), 4.13 (t, *J* = 6.8, 8H), 2.73 (q, *J* = 6.5, 4H), 2.60 (t, *J* = 7.5, 8H),1.97–1.80 (m, 16H), 1.68 (m, 8H), 1.12 (d, *J* = 6.4, 24H), –2.77 (s, 8H). MS (MALDI-TOF, pos. mode, dithranol): *m/z*: 4047.5 $[M]^+$ (calcd 4047.6). Anal. calcd for $C_{272}H_{210}N_{18}O_{20}\cdot CH_2Cl_2$: C 79.29 H 5.17 N 6.18; found: C 79.26 H 5.40 N 5.80.

Without further purification, the crude product was dissolved in dichloromethane (5 mL) and after addition of a saturated methanolic zinc acetate solution (5 mL), the reaction mixture was stirred for 24 h at room temperature. The reaction mixture was washed three times with water (90 mL), dried over anhydrous sodium sulfate and evaporated to dryness. Subsequent silica gel column chromatography with chloroform as eluent afforded 36 mg of **4** (8.38 µmol, 21%) as a violet solid.

Mp: 285–290 °C. ^{1}H NMR (THF-d^8): δ 8.84 (d, *J* = 4.6, 8H), 8.79 (d, *J* = 3.5, 8H), 8.32 (s, 4H), 8.14 (m, 24H), 8.01 (m, 8H), 7.72–7.62 (m, 36H), 7.30 (m, 6H), 7.19 (m, 12H), 6.94–6.88 (m, 8H), 6.84 (t, *J* = 2.2, 4H), 4.13 (t, *J* = 6.3, 8H), 2.78 (q, *J* = 6.9, 4H), 2.59 (t, *J* = 7.4, 8H),1.93–1.80 (m, 16H), 1.68 (m, 8H), 1.09 (d, *J* = 6.6, 24H). MS (MALDI-TOF, dithranol): *m/z* calcd for $C_{272}H_{202}N_{18}O_{20}Zn_4$: 4295.3 $[M]^+$, found 4295.2 and 4296.3. Anal. calcd for $C_{272}H_{202}N_{18}O_{20}Zn_4\cdot H_20$: C 75.45 H 4.93 N 5.82; found: C 75.30 H 4.98 N 5.51. UV/Vis (CH_2Cl_2): λ_{max}/nm (ε_{max}/nm) 555 (117300), 424 (1890500); (tetrahydrofuran): 602 (36600), 562 (129600), 429 (2318500). Fluorescence ($CHCl_3$): λ_{max} = 602, 647 nm, fluorescence quantum yield Φ_{fl} = 0.03, fluorescence lifetime τ_{fl} = 0.8 (95%) and 3.5 ns (5%); (tetrahydrofuran): λ_{max} = 603, 656 nm; fluorescence quantum yield Φ_{fl} = 0.03.

Supporting Information available in the Appendix: Graphical material for data evaluation with SpecFit/32 and ^{1}H NMR spectrum of **4**.

7.9 References and Notes

1 For recent reviews, see: (a) C. M. Drain, J. T. Hupp, K. S. Suslick, M. R. Wasielewski, X. Chen, *J. Porph. Phthalo.* **2002**, *61*, 243-258; (b) A. Satake, Y. Kobuke, *Tetrahedron* **2005**, *1*, 13-41; (c) C. M. Drain, I. Goldberg, I. Sylvain, A. Falber, *Top. Curr. Chem.* **2005**, *245*, 55-88; (d) C.-C. You, R. Dobrawa, C. R. Saha-Möller, F. Würthner, *Top. Curr. Chem.* **2005**, *258*, 39-82.

2 (a) H. L. Anderson, C. A. Hunter, M. N. Meah, J. K. M. Sanders, *J. Am. Chem. Soc.* **1990**, *112*, 5780-5789; (b) C. A. Hunter, M. N. Meah, J. K. M. Sanders, *J. Am. Chem. Soc.* **1990**, *112*, 5773-5780; (c) C. C. Mak, N. Bampos, J. K. M. Sanders, *Angew. Chem.* **1998**, *111*, 3009-3012; *Angew. Chem. Int. Ed.* **1998**, *37*, 3020-3023; (d) C. C. Mak D. Pomeranc, M. Montalti, L. Prodi, J. K. Sanders, *Chem. Commun*. **1999**, 1083-1084; (e) P. N. Taylor, H. L. Anderson, *J. Am. Chem. Soc.* **1999**, *121*, 11538-11545; (f) C. C. Mak, N. Bampos, S. L. Darling, M. Montalti, L. Prodi, J. K. M. Sanders, *J. Org. Chem.* **2001**, *66*, 4476-4486; (g) L. Baldini, P. Ballester, A. Casnati, R. M. Gomila, C. A. Hunter, F. Sansone, R. Ungaro, *J. Am. Chem. Soc.* **2003**, *125*, 14181-14189; (h) T. Hirao, K. Saito, *Macromol. Sympo.* **2003**, *204*, 103-112; (i) M. C. Lensen, S. J. T. van Dingenen, J. A. A. W. Elemans, H. P. Dijkstra, G. P. M. van Klink, G. van Koten, J. W. Gerritsen, S. Speller, R. J. M. Nolte, A. E. Rowan, *Chem. Commun.* **2004**, 762-763; (j) D. I. Schuster, K. Li, D. M. Guldi, J. Ramey, *Org. Lett.* **2004**, *6*, 1919-1922; (k) P. Ballester, A. Costa, A. M. Castilla, P. M. Deyà, A. Frontera, R. M. Gomila, C. A. Hunter, *Chem. Eur. J.* **2005**, *11*, 2196-2206; (l) T. Kishida, N. Fujita, O. Hirata, S. Shinkai, *Org. Biomol. Chem.* **2006**, *4*, 1902-1909; (m) T. Ishida, Y. Morisaki, Y. Chujo, *Tetrahedron Lett.* **2006**, *47*, 5265-5268.

3 (a) F. Würthner, A. Sautter, D. Schmid, P. J. A. Weber, *Chem. Eur. J.* **2001**, *7*, 894-902; for reviews, see: (b) F. Würthner, C.-C. You, C. R. Saha-Möller, *Chem. Soc. Rev.* **2004**, *33*, 133-146; (c) J. A. A. W. Elemans, R. van Hameren, R. J. M. Nolte, A. E. Rowan, *Adv. Mater.* **2006**, *18*, 1-17; (d) F. Würthner, *Pure Appl. Chem*. **2006**, *78*, 2341-2350.

4 C. Addicott, I. Österling, T. Yamamoto, K. Müllen, P. J. Stang, *J. Org. Chem.* **2005**, *70*, 797-801.

5 A. Prodi, C. Chiroboli, F. Scandola, E. Iengo, E. Alessio, R. Dobrawa, F. Würthner, *J. Am. Chem. Soc.* **2005**, *127*, 1454-1462.

6 (a) T. van der Boom, R. T. Hayes, Y. Zhao, P. J. Bushard, E. A. Weiss, M. R. Wasielewski, *J. Am. Chem. Soc.* **2002**, *124*, 9582-9590; (b) S. Xiao, M. E. El-Khouly, Y. Li, Z. Gan, H. Liu, L. Jiang, Y. Araki, O. Ito, D. Zhu, *J. Phys. Chem. B* **2005**, *109*, 3658-3667; (c) Y. Liu, N. Wang, Y. Li, H. Liu, Y. Li, J. Xiao, X. Xu, C. Huang, S. Cui, D. Zhu, *Macromolecules* **2005**, *38*, 4880-4887; (d) M. O. Liu, C.-H. Tai, C.-W. Chen, W.-C. Chang, A. T. Hu, *J. Photochem. Photobiol., A* **2004**, *163*, 259-266.

7 C.-C. You, F. Würthner, *Org. Lett.* **2004**, *6*, 2401-2404.

8 F. D´Souza, S. Gadde, M. E. Zandler, K. Arkady, M. E. El-Khouly, M. Fujitsuka, O. Ito, *J. Phys. Chem. A* **2002**, *106*, 12393-12404.

9 (a) B. M. Hoffman, *J. Am. Chem. Soc.* **1975**, *97*, 1688-1694; (b) D. Quimby, F. Longo, *J. Am. Chem. Soc.* **1975**, *97*, 5111-5117; (c) T. A. Moore, D. Benin, R. Tom, *J. Am. Chem. Soc.* **1982**, *104*, 7356-7357.

10 SpecFit/32 from Spectrum Software Associates (Marlborough, MA, 2000-2001) was used for data analysis.

11 see Chapter 3 and 4 of this thesis and P. Osswald, D. Leusser, D. Stalke, F. Würthner, *Angew. Chem.* **2005**, *117*, 254-257; *Angew. Chem. Int. Ed.* **2005**, *44*, 250-253.

12 H. Uji-i, A. Miura, A. P. H. Schenning, E. W. Meijer, Z. Chen, F. Würthner, F. C. De Schryver, M. van der Auweraer, S. De Feyter, *ChemPhysChem* **2005**, *6*, 2389-2395.

13 (a) C.-C. You, F. Würthner, unpublished results; (b) B. W. Messmore, J. F. Hulvat, E. D. Sone, S. I. Stupp, *J. Am. Chem. Soc.* **2004**, *126*, 14452-14458; (c) S. Hien, PhD Thesis, University of Regensburg (Germany), **1995**.

14 (a) R. Givshi, R. Reisfeld, Z. Burshstein, *Chem. Phys. Lett.* **1993**, *213*, 338-344; (b) J. R. Lakowicz, *Principles of Fluorescence Spectroscopy*; 2nd ed., Kluwer Academic/Plenum, New York, **1999**; pp. 52–55.

15 (a) R. Dobrawa, M. Lysetska, P. Ballester, M. Grüne, F. Würthner, *Macromolecules* **2005**, *38*, 1315–1325; (b) T. Megyes, H. Jude, T. Grosz, I.

Bakó, T. Radnai, G. Tárkányi, G. Pálinkás, P. J. Stang, *J. Am. Chem. Soc.* **2005**, *127*, 10731-10738.

16 M. Holz, X.-A. Mao, D. Seiferling, *J. Chem. Phys.* **1996**, *104*, 669-679.

Chapter 8

Alignment of a Linear π-Conjugated Polymer by Zinc Porphyrin/Perylene Bisimide Supramolecular Cross-Linker

Abstract: The self-assembly of a tetra zinc porphyrin/perylene bisimide cross-linker **1** with linear π-conjugated polymer **3** containing di(*N*-methylaminomethyl)benzene units has been investigated by UV/Vis spectroscopy and atomic force microscopy (AFM). Prior to the investigations with polymer **3**, UV/Vis spectroscopic titrations have been performed with the monomeric model compound 1,4-di(*N*-methylaminomethyl)-2,5-diiodobenzene **2**, which contains the same binding unit as linear polymer **3**, and an effective binding of this model compound to the zinc porphyrin units of cross-linker **1** has been observed. In the case of linear polymer **3**, AFM studies have revealed the formation of extended lamellar structures for the self-assemblies of **1** and **3**, demonstrating two-dimensional alignment of the linear polymer by bichromophore cross-linker. In accordance with the UV/Vis and AFM data, these lamellar structures are attributed to the formation of macrocyclic sandwich complexes of ditopic zinc porphyrin tweezer units of **1** and the diamine binding sites in linear polymer **3**. Our studies have shown that three different types of chromophores, i.e., zinc porphyrin, perylene bisimide and π-conjugated polymer can be aligned by this self-assembly approach.

8.1 Introduction

The organization of functional π-conjugated chromophores by self-assembly into well-defined architectures is an important topic of material science,[1] because by this approach a defined arrangement of the chromophores can be achieved which results in a modulation of their functional properties both in solution and in the solid state. Thus, π-conjugated molecules such as oligothiophenes, oligo(phenylenevinylene)s (OPVs), porphyrins, phthalocyanines, hexabenzocoronenes, and perylene bisimides (PBIs) have been intensively studied in the past years to develop functional materials with desirable properties.[1] In particular, $\pi-\pi$ aggregation has been widely explored and numerous one-dimensional stacks of chromophores were shown to form columnar liquid crystals.[1b,2] On the other hand, hydrogen bonding[1a,b] and metal-ion-directed self-assembly[1b,c] have been exploited for the construction of rosettes,[3] squares,[4] linear arrays,[5] and a large variety of other architectures[6]. However, most of these studies are still focused on the formation of self-assembled architectures based on mono-chromophore building blocks, although the incorporation of different types of chromophores into self-assembled systems may provide many interesting new features. Thus, recently effective energy transfer and electron transfer processes have been demonstrated in such co-self-assembled arrays of PBIs and other chromophores such as OPVs,[7] porphyrins,[8] fullerenes,[9] phthalocyanines,[10] as well as for oligothiophenes in combination with fullerenes[11] and in porphyrin/fullerene assemblies.[12]

From the view point of material science, not only the defined arrangement of chromophores by self-assembly in solution but also the organization of multichromophoric arrays on surfaces is of particular interest. Such “modified” surfaces may provide redoxactive interfaces for electronic devices (e.g. OFETS, OLEDs, solar cells) or exhibit catalytic activity.[13] Different methods have been developed in the past to achieve defined arrangements of π-systems on surfaces, e.g., self-assembly,[14] Langmuir-Blogett techniques,[1,13g] and the layer-by-layer method[15], the latter utilizes ionic interactions to obtain defined arrangements of two oppositely charged chromophores on a surface. It has been demonstrated that additional non-covalent interactions are very useful to control the morphology of the deposited material by layer-by-layer approach. This concept was extended to well-designed multi-functional molecules which form extended two-dimensional architectures by self-assembly.[1b,c,9f,12c,16] Recently, the two-dimensional alignment of diamino-functionalized linear π-conjugated polymers by rigid zinc porphyrin scaffolds into defined supramolecular assemblies has been demonstrated.[17] These two-dimensional networks

could be deposited on graphite surfaces by maintaining their supramolecular structures observed in solution.

We asked the question whether this approach for the alignment of π-conjugated polymers by zinc porphyrin tweezers can be applied for the self-assembly of zinc porphyrin/perylene bisimide bichromophore system with linear π-conjugated polymers to achieve defined 3-dimensional arrangements of these three different types of chromophores. To explore this possibility, we have studied the binding properties of zinc porphyrin/perylene bisimide cross-linker **1** (see Chapter 7) with monomeric reference compound 1,6-di(*N*-methylaminomethyl)-2,5-diiodobenzene **2** by UV/Vis spectroscopy. Atomic force microscopy (AFM) investigations revealed a perfect parallel alignment of the linear polymer **3** by zinc porphyrin/perylene bisimide aligner **1** on HOPG surface.

8.2 General Considerations for the Alignment of Linear π-Conjugated Polymer 3 by Cross-Linker 1

The molecular structures of the tetra(zinc porphyrin)-functionalized perylene bisimide **1**,[18] and linear π-conjugated polymer **3** (M_n = 48000)[17] and monomeric reference 1,4-di(*N*-methylaminomethyl)-2,5-diiodobenzene **2** used here are shown in Figure 1.

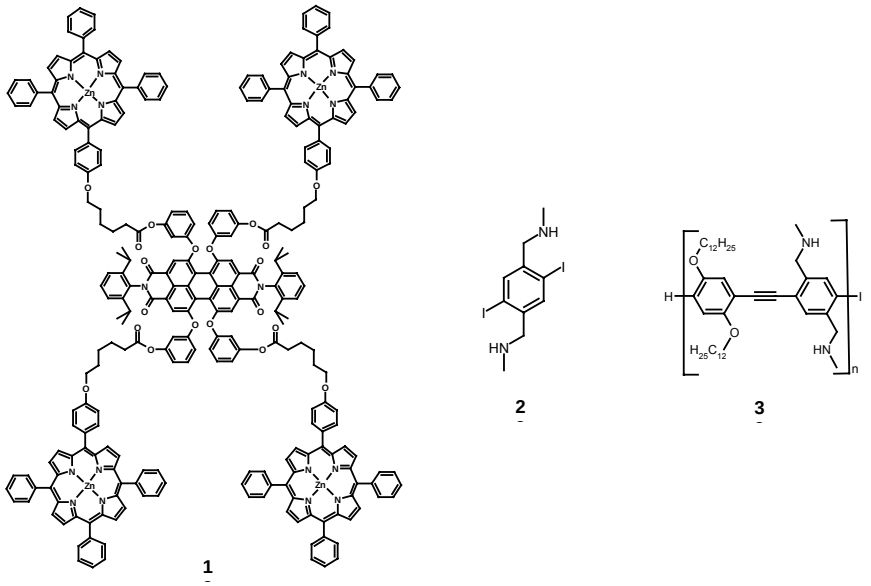

Figure 1. Structures of cross-linker **1**, reference **2** and polymer **3**.

The linear π-conjugated polymer **3** is supposed to exhibit a random orientation in solution and on HOPG surface in the absence of an aligner as schematically shown in Figure 2.[17] Upon addition of bichromophore cross-linker **1**, its zinc porphyrin tweezers should enforce a parallel orientation of polymer **3** strands which, in turn, can provide a defined arrangement of the three different chromophores, namely, zinc porphyrin,

perylene bisimide and π-conjugated polymer **3** (Figure 2). For the present case, the self-assembly is directed by the coordination of amine-functionalities in polymer **3** to zinc porphyrins of bichromophore cross-linker **1**. For the latter system, the formation of sandwich-type complexes between two zinc porphyrins and diazabicyclo-[2.2.2]-undecane (DABCO), resulting in discrete macrocycles, was demonstrated in Chapter 7.[18] As pointed out in literature,[17] the presence of two zinc porphyrin tweezers in the present cross-linker which are capable of forming intramolecular macrocyclic sandwich complexes is an essential requirement for the defined parallel alignment of the diamine-functionalized π-conjugated polymer **3**. Therefore, the formation of such macrocyclic sandwich complexes of **1** with two polymer **3** strands would provide a parallel orientation of the polymer as schematically shown in Figure 2, and two-dimensional ordering will then be facilitated by the multiple diamine binding sites of polymer **3**.

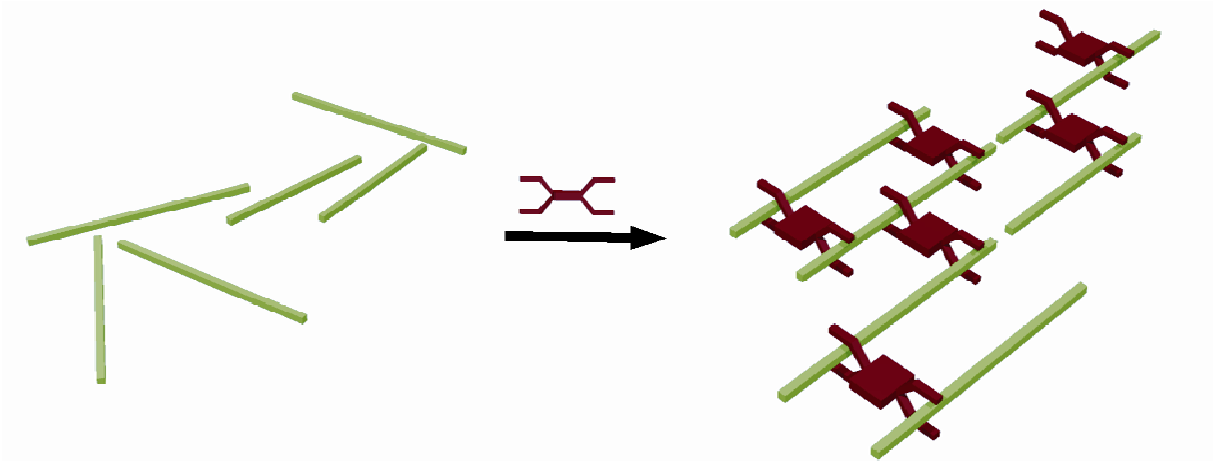

Figure 2. Schematic representation of the alignment of polymer **3** (green) by cross-linker **1** (red).

8.3 Studies of Complexation Between Cross-Linker 1 and Monomeric Model Compound 2

The binding sites for the self-assembly of polymer **3** and cross-linker **1** are given by the diamine functionalities in polymer **3** and ditopic zinc porphyrin tweezers of **1**. Therefore, complexation experiments with zinc porphyrin/perylene bisimide cross-linker **1** and monomeric reference compound 1,4-di(*N*-methylaminomethyl)-2,5-diiodobenzene **2** can provide valuable structural and thermodynamic information for the more demanding self-assembly of **1** with polymer **3**. Diaminomethyl benzene **2**, which is a building block for the synthesis of polymer **3**, exhibits good solubility that is important for the determination of binding properties in the absences of other effects such as π-π interactions. Figure 3 (left) shows the UV/Vis absorption spectra of the Q-band region of **1** upon successive addition of **2** in chloroform at room temperature. Similar to the self-

assembly of **1** with DABCO (see Chapter 7), the absorption maximum for the Q-bands of **1** at 552 nm decreases with increasing amount of bidentate ligand **2** and new maxima arise at 563 and 603 nm, which can be attributed to the formation of a complex between the amine functionalities of **2** and the zinc porphyrin units of **1**. The presence of five well-defined isosbestic points (593, 582, 558, 517 and 473 nm) upon successive addition of **2** demonstrates the formation of a well-defined supramolecular architecture by the self-assembly of **1** and **2**. The change of the absorbance at 603 nm upon addition of **2** shown in Figure 3 (right) reveals a strong binding of the cross-linker **1** to the guest **2**, suggesting the formation of a single species, apparently a 1:2 complex **1**•(**2**)$_2$ as observed for the self-assembly of **1** and DABCO (see chapter 7). For larger excess of **2** (more than 6-fold), a slight shift of the isosbestic points and a small increase of the absorbance at 603 nm (Figure 3, right) were observed which can be taken as indication for the formation of a 1:3 complex **1**•(**2**)$_3$ as schematically shown in Figure 4.

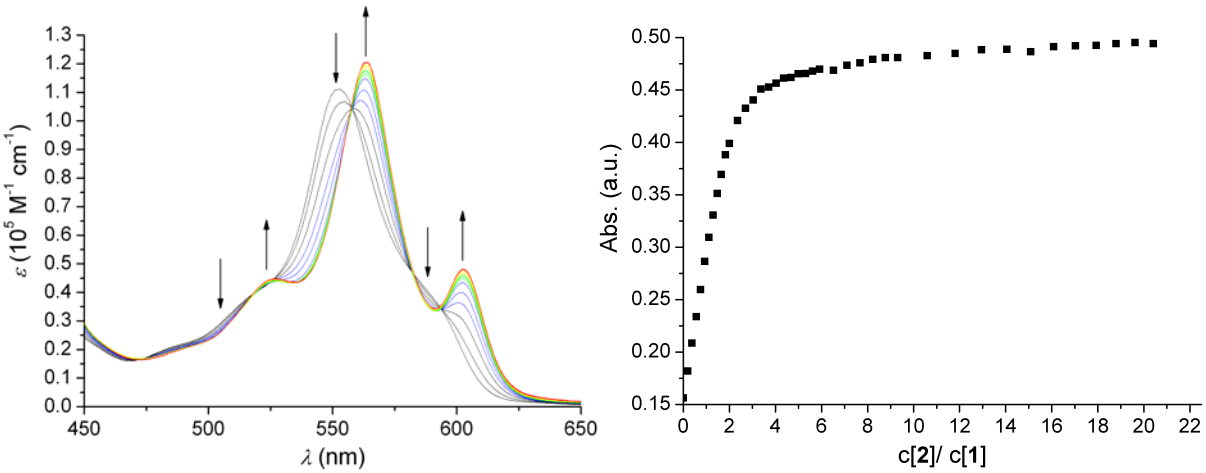

Figure 3. UV/Vis titration of **1** (c = 1.1 x 10^{-5} M) with **2** in chloroform at 25 °C (left) and binding isotherm at 603 nm (right). The arrows indicate spectral changes with increasing amount of **2**.

The titration data were evaluated by applying non-linear regression analysis[19] with a binding model consisting of 1:0, 1:1, 1:2, and 1:3 complexes of **1** and **2** and binding constants K_1, K_2, and K_3 (see Figure 4 for definition). Concentration profiles, residuals, calculated spectra, and titration isotherms obtained by non-linear regression analysis are depicted in Figure 5. A binding constant K_1 of 1.4 ± 0.3 x 10^6 M^{-1} was obtained for the formation of 1:1 species whereas a slightly smaller binding constant K_2 of 3.9 ± 0.9 x 10^5 M^{-1} was estimated for the subsequent formation of the 1:2 species. The binding constants for the formation of the 1:3 species (see Figure 4) in the presence of diamine **2** in high excess was determined as 7.7 ± 3.3 x 10^3 M^{-1}.[20]

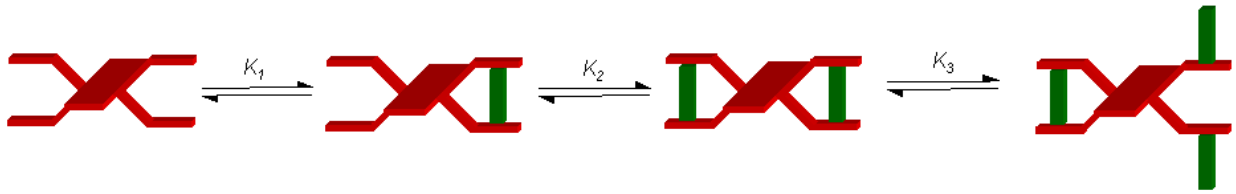

Figure 4. Schematic representation of the chemical equilibria and definition of the binding constants for the self-assembly of **1** and **2**. The green bars represent the diamine **2** and **1** is highlighted in red.

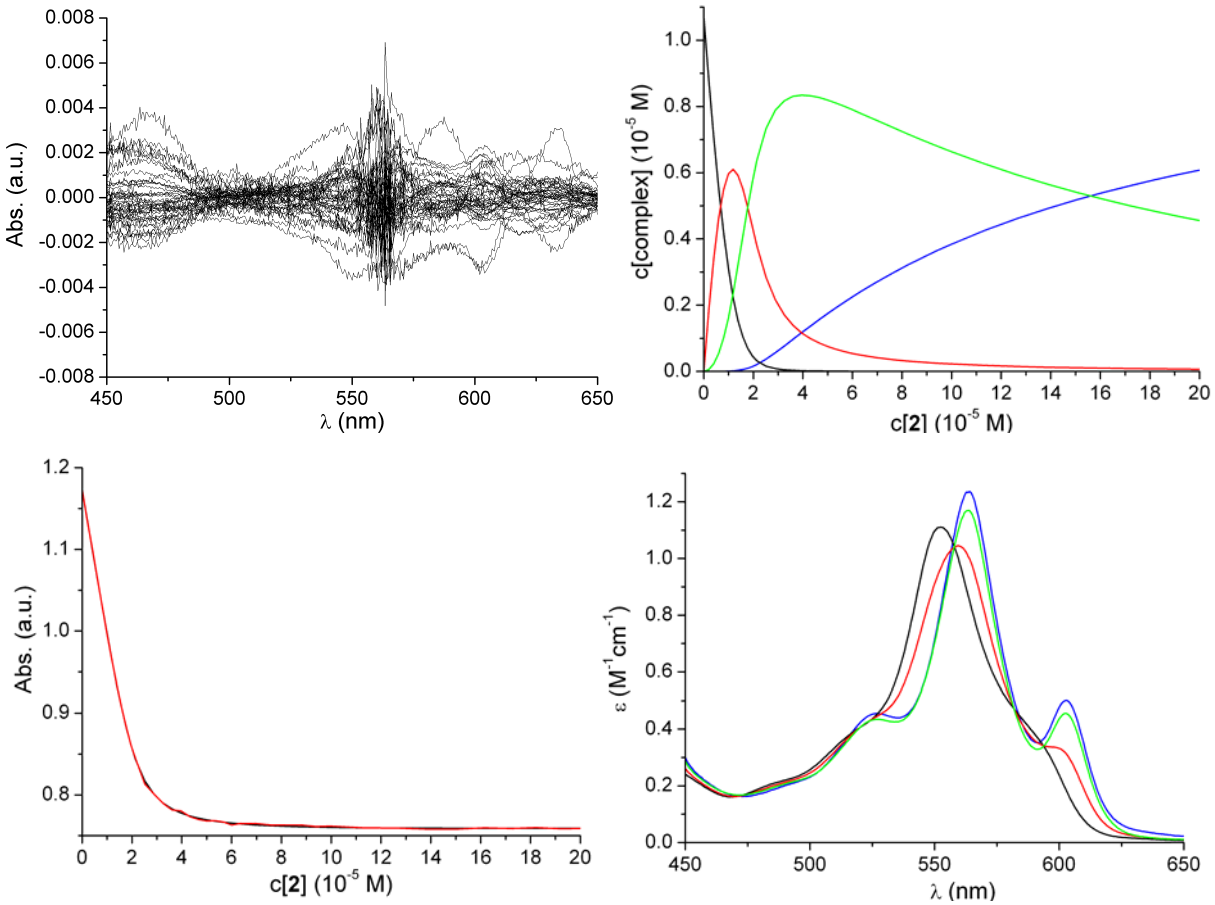

Figure 5. Non-linear regression analysis for the UV/Vis titration of **1** with diamino benzene derivative **2**. Top: Residuals of the calculated and experimental spectra (left) and change of the concentration for different species during the titration (right). Bottom: Experimental (red) and calculated (black) titration curves at 550 nm (left) and calculated spectra of different species (right). For the spectra and the concentration profile, the black lines represent the cross-linker **1** and the red, green and blue lines represent the complexes **1**•(**2**), **1**•(**2**)$_2$ and **1**•(**2**)$_3$, respectively.

The significantly larger binding constants K_1 and K_2 compared to that for the formation of 1:3 complex (K_3) suggest a thermodynamically favored bis-macrocyclic sandwich structure for the 1:2 complex **1**•(**2**)$_2$.[21] The binding constants K_1 and K_2 for the self-

assembly of cross-linker **1** and diamine **2** are decreased by one order of magnitude in comparison to that for the self-assembly of **1** and DABCO (Chapter 7; $K_1 \approx K_2 \approx 1 \times 10^7$ M^{-1}), for which the macrocyclic nature of the self-assembly was confirmed by DOSY NMR spectroscopy.[18] This was expected, because the binding constants for the complexation of secondary amines to zinc porphyrins are smaller than that of quinuclidine.[6h] Moreover, the determined binding constants K_1 and K_2 are in good agreement with those reported for the self-assembly of **2** with similar, but monochromic, tetra zinc porphyrin tweezer.[17] For the latter system, formation of macrocyclic sandwich complexes was reported which is also in support of a macrocyclic structure of **1**•(**2**)$_2$. However, in contrast to literature reported system,[17] a negative cooperativity was observed for the binding of cross-linker **1** and diamine **2** as K_2 is about one third of K_1. The observed negative cooperativity for the present system might be related to the flexibility of **1** due to the long alkyl spacer. The observed effective binding of model compound **2**, which contains the same binding site as polymer **3** suggests that the tetra zinc porphyrin/perylene bisimide **1** is a promising candidate for the alignment of polymer **3** to achieve defined networks of three different chromophores.

8.4 Alignment of Linear π-Conjugated Polymer 3 by Bichromophore Cross-Linker 1 on HOPG Surface

To elucidate the alignment of polymer **3** by the cross-linker **1** to afford two-dimensional networks, solutions with different ratios α of **1** and **3** in chloroform were deposited onto highly ordered pyrolytic graphite (HOPG) and analyzed by AFM. The ratio α was calculated according to α = c[**1**]/c[**3**] (mol/mol) and represents the ratio of **1** to the repeating units of polymer **3**. Thus, the concentrations given for the polymer **3** refer to the concentration of *one repeating unit*. For example, a ratio of α = 0.5 means that 2 equivalents of the repeating units of polymer **3** and one equivalent of the cross-linker **1** are present which corresponds to the stoichiometry of a 1:2 complexation. At a ratio α < 0.5 the amine binding sites of **3** are present in excess, while at α > 0.5 the cross-linker **1** is in excess. In Table 1, the concentrations of polymer **3** and cross-linker **1** and the respective α values used for the AFM investigations are collected.

Table 1. Ratios α and Concentrations of Supramolecular Cross-Linker **1** and Polymer **3** used for AFM Investigations

α	4	2	0.5	0.03
c [**1**] (10^{-6} M)	3.36	7.20	6.61	1.63
c [**3**] (10^{-6} M)	0.91	3.60	13.21	47.5

For different ratios α of **1** and **3**, different binding situations are expected as schematically shown in Figure 6. For a large excess of polymer **3** (low ratio α), the polymer strands are connected by a small amount of supramolecular cross-linker **1**, hence not every binding site of polymer **3** is occupied which leads to a deficient cross-linking (Figure 6A). For a ratio α = 0.5, the binding sites in **1** and **3** are present in equal amounts (Figure 6B), thus, the cross-linking should be most effective in this case. In contrast, for an excess of cross-linker **1** (higher ratio α), no cross-linking is expected rather alternating complexation of **1** with isolated strands of **3** may take place which is in agreement with the fact that $K_1 > K_2$ (Figure 6C).

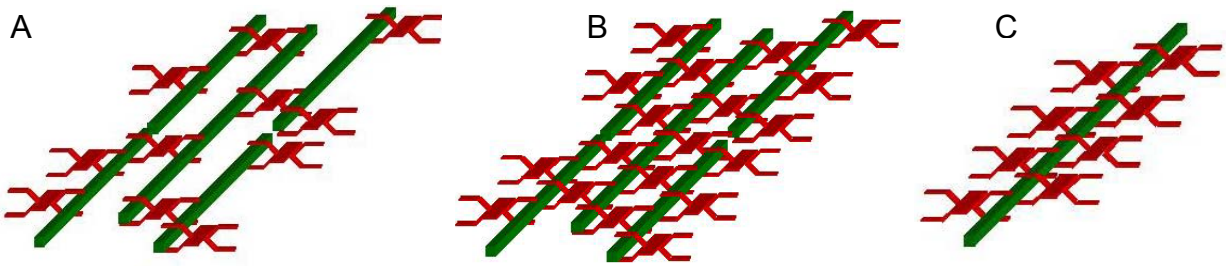

Figure 6. Possible binding motifs of supramolecular networks for large excess (α < 0.5) of polymer **3** (A), at a ratio α of 0.5 (B) and at large excess (α > 0.5) of cross-linker **1** (C). Red clips represent cross-linker **1** and the green bars denote polymer **3**.

Initially, a sample of pure polymer **3** was analyzed by AFM on HOPG. In low resolution image of polymer **3** only agglomerates were observed (see Figure F1 in Appendix F). High resolution image of polymer **3** (Figure 7A) revealed the formation of small, but distinct lamellar structures of the polymer **3** that are grown epitaxially at 60° angles on HOPG. These lamellar structures are embedded in a unstructured monolayer of polymer **3**. A lamellar distance of 3.96 ± 0.50 nm which can be related to the spacing between the individual polymer strands of **3**, was determined to by Fourier transformation and an average height of 0.30 ± 0.10 nm was estimated for the monolayer to by cross-section analysis. The size of the lamellar structures observed in the monolayer was determined as 0.008 μm^2 – 0.010 μm^2. The ordered lamellae domains within the monolayer might be related to short polymer strands that epitaxially

grown on the surface as schematically shown in Figure 7B, while the long polymer strands form the unstructured monolayer. The epitaxial growth of polymer **3** on the graphite surface can be rationalized by the interaction of the C_{12} chains with HOPG as the observed distance in the lamellae (3.96± 0.50 nm) corresponds well to the width of polymer **3** (3.8 nm) as estimated by molecular modelling. In contrast to polymer **3**, **1** forms only ill-defined structures on HOPG substrate upon spin coating of a 1 x 10^{-5} M solution in chloroform as shown in Chapter 7.

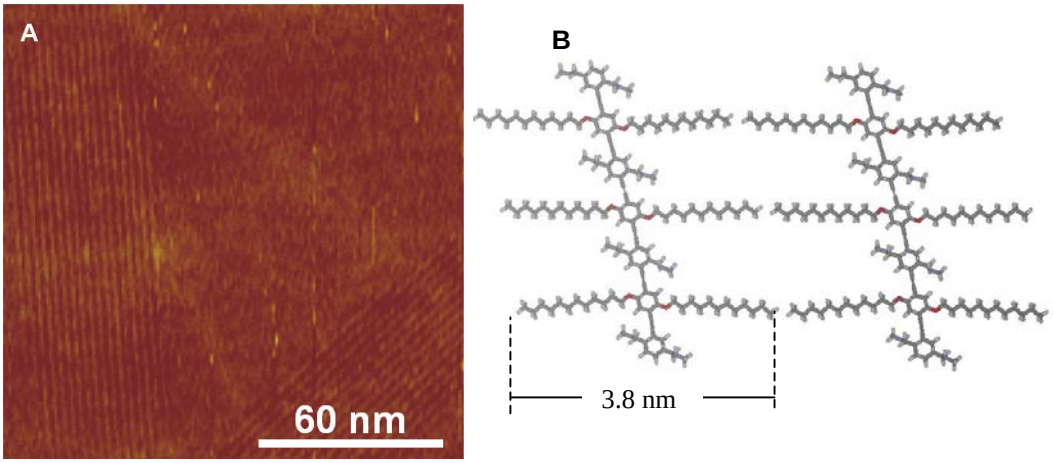

Figure 7. (A) High resolution AFM height image of a solution of polymer **3** (c = 1.2 x 10^{-5} M) in chloroform on HOPG. The z-scale was 3 nm. (B) Proposed arrangement of polymer **3** in ordered lamellae domains. Molecular structure was optimized with MM3 force field using Cache Quantum Cache 5.0.

Next, solutions with different ratios of polymer **3** and cross-linker **1** were investigated by AFM. At a ratio of α = 0.03, the concentration of the repeating unit of polymer **3** is about 30 times higher than that of **1**, thus, every 15 repeating unit of polymer **3** can be occupied by a ditopic zinc porphyrin tweezer unit of **1**. The AFM images obtained for this ratio are shown in Figure 8.

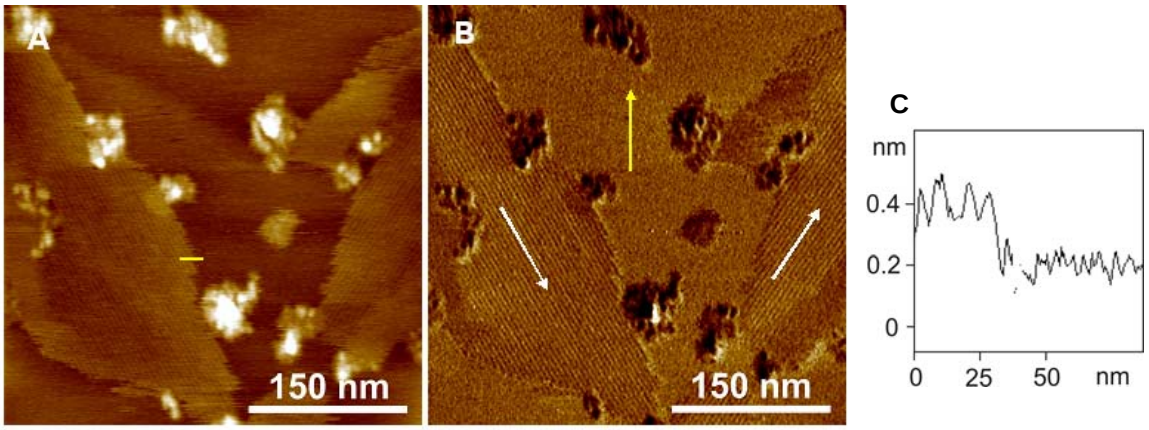

Figure 8. AFM images of a chloroform solution of **1** and **3** at a ratio of α = 0.03 spin-coated onto HOPG: (A) High resolution height image, (B) phase image and (C) cross

section analysis along the yellow line in A. The corresponding AFM images showing a larger surface area are given in Appendix (Figure F2). White arrows in (B) show the main direction of ordered lamellae and the yellow arrow points at an amorphous section. The z-scale for all images was 2 nm.

For α = 0.03, lamellar structures were observed over a large area of the surface, as high resolution images 8A,B show (see also low resolution images in Figure F2 in Appendix). In contrast to the pure polymer **3**, no unstructured monolayer was present at this ratio α. The height *h* of the surface pattern was determined as 0.30 ± 0.05 nm by cross-section analysis, which corresponds well to that observed for polymer **3**, and an average lamellar distance *l* (distance of two linear strands of the lamellae) of 4.5 ± 0.5 nm was obtained, the latter value is larger than that observed for pure polymer **3** (4.0 ± 0.5 nm). The domain size of the lamellar structures increased in comparison to that of pure polymer **3** (0.008-0.010 μm^2) to 0.02-0.04 μm^2, and large areas of the surface are now covered by ordered lamellar structures. AFM images revealed also amorphous parts on the surface (yellow arrow, Figure 8B) which can be attributed either to a ill-defined assembly of pure polymer **3** or to a three-dimensional arrangement of polymer **3** and cross-linker **1**.[17] Furthermore, different orientations for the lamellar structures were found which are almost in a 60° angle to each other as can be seen from the high resolution images (white arrows, Figure 8B). This is indicative for a surface-induced orientation of the self-assemblies of **1** and **3** along the graphite axes. The increased domain size of the lamellar structures and the absence of an unstructured monolayer suggest that these structures are due polymer **3** and cross-linker **1** networks.

High resolution AFM images for ratio of α = 0.5 are shown in Figure 9. At this ratio the binding sites of **1** and **3** are present in equal amounts. Therefore extended cross-linking of polymer **3** by **1** is expected to provide a dense 2D array with the highest possible occupancy of the cross-linker. High resolution images (Figure 9A,B) clearly show domains of ordered lamellar structures with different heights. Moreover no monolayer is present as in the case of ratio α = 0.03. An average lamellar distance *l* of 4.7 ± 0.3 nm was determined by cross-section analysis which is in good agreement with that determined for lower amount of cross-linker **1** (4.5 ± 0.5 nm) and significantly larger than that observed for polymer **3** alone. Furthermore, high resolution images (Figure 9A,B) reveal different orientations of the lamellae, and the angle between two lamellar structures is 60°, which is in proper agreement with the angle of the graphite lattice.

This suggests that also in this case the orientation of the assemblies is induced by the graphite surface. In contrast to the extended lamellar structures (width of ~148 nm) observed at lower amounts of **1** (ratio α = 0.03), ordered structures with smaller width (perpendicular to the linear strands) were observed in the present case (α = 0.5): Lamellae with widths of 14-19 nm and larger than 52 nm were found (Figure 9B).

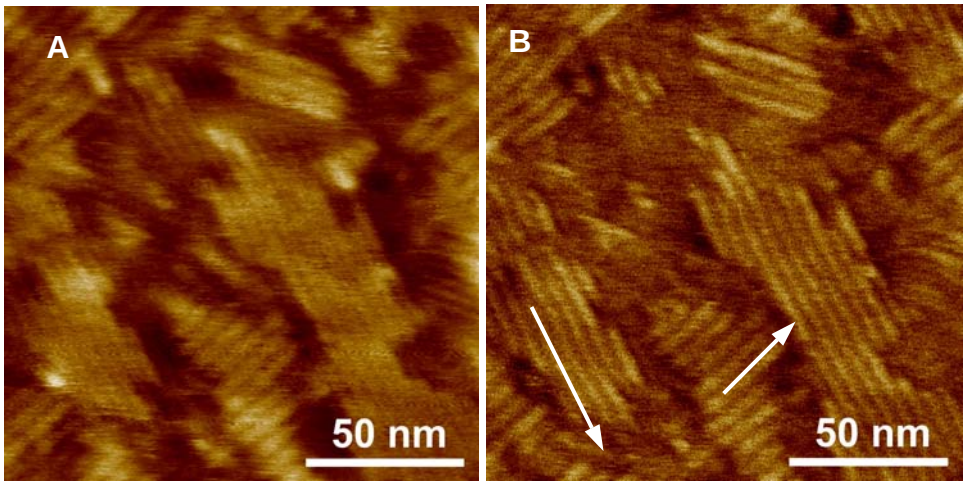

Figure 9. High resolution AFM images, height (A) and phase (B), of a mixture of **1** and **3** at a ratio α = 0.5 spin-coated onto HOPG. The z-scale is 1.5 nm. The white arrows indicate the main directions of ordered lamellae. Images showing a larger surface area are depicted in Figure F3 in Appendix.

Furthermore, AFM investigations for the ratios α = 2 and 4 were performed (Figure 10A,B). As can be seen from the low resolution image for ratio α = 2 (Figure 10 A), well-defined lamellar structures (indicated by yellow arrows) were formed. The areas occupied by each of these lamellar assemblies varies between 0.04 μm^2 (149 nm x 149 nm) and 0.11 μm^2 (567 nm x 187 nm), thus a large area of the HOPG surface is covered. Amorphous parts are also present on the surface which can be related to the excess of free **1**. High resolution image of a sample of **1** and **3** with a ratio α = 2 (Figure 10B) revealed small isolated particles of ellipsoid shape that are arranged densely packed within the lamellar structure. A lamellar distance *l* of 4.8 ± 0.2 nm and a intralamellar distance *a* (along the linear strands) of 2.4 ± 0.1 nm, as marked in Figure 10B, was determined by Fourier transformation. Thus, unit cell parameters for the arrangement of the ellipsoid particles in lamellar structures are *a* = 2.4 ± 0.1 nm and *l* = 4.8 ± 0.2 nm with an angle of 74°. The height *h* of the lamellar structure was determined by cross-section analysis as 0.34 ± 0.05 nm (Figure 10B), which is larger than that observed for pure polymer **3** (h ≈ 0.3 nm) indicating that the observed structures can be attributed to self-assemblies of **1** and **3.**

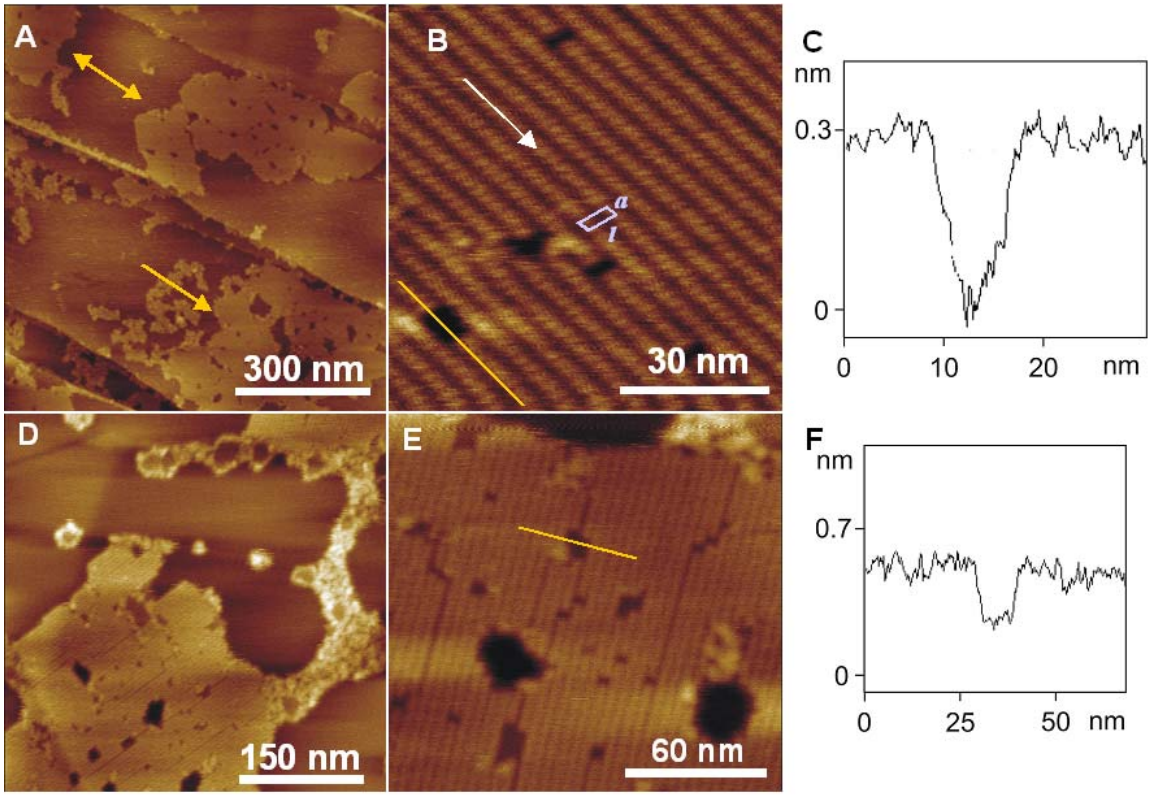

Figure 10. AFM height images of samples of **1** and **3** in ratios α = 2 (A,B) and α = 4 (D,E): Low resolution images (A, D), high resolution images (B, E), and cross-section analysis (C, F) along the yellow lines in (B) and (E), respectively. The yellow arrows in (A) point at the ordered structures on the surface and the white arrow in (B) indicate the lamellar orientation. The gray lines in B highlight the unit cell. The z-scales were 3.0 nm (A), 1.0 nm (B), 2 nm (D), and 1.5 nm (E). The dark areas in the AFM images correspond to the graphite surface.

For a larger excess of cross-linker **1** (α = 4), AFM investigations revealed similar structural pattern for the self-assemblies of **1** and polymer **3** on HOPG surface (Figure 10D,E). As in the case of α = 2, extended lamellar structures were observed (Figure 10D,E) with a height *h* of 0.32 ± 0.05 nm and a lamellar distance *l* of 4.90 ± 0.50 nm which correspond very well to the values observed for lower amounts of **1** (for α = 2: height *h* ≈ 0.35 nm; distance *l* ≈ 4.8 nm). Furthermore, high resolution image (Figure 10E) revealed also for this case (α = 4) the presence of single particles. However, the distance between these particles along the lamellae could not be determined due to deficient lateral resolution. The dimensions of the lamellar structures on the HOPG surface ranged from 0.06 μm^2 (169 x 347 nm) to 0.10 μm^2 (235 x 344) and are comparable with those observed for a ratio of α = 2, revealing that a broad area of the surface is covered by ordered structures.

8.5 Binding Model

The dimensions of the lamellar structures observed for different ratios of cross-linker **1** and polymer **3** are summarized in Table 2 and the data are discussed briefly here, as based on these data a binding model for the networks created by self-assembly of **1** and **3** is proposed.

Table 2. Dimensions of Lamellar Structures Determined by AFM for Different Ratios of **1** and **3**

ratio α	*h* (nm)	*l* (nm)	area (μm^2)
0	~0.30	4.0	0.008-0.010
0.03	0.30	4.5	0.02 - 0.04
0.5	n.d.[a]	4.7	n.d.[a]
2	0.35	4.8	0.04 - 0.11
4	0.30	4.9	0.05 - 0.10

a) dimension could not be determined due to the mulitlayer structure at this ratio α.

For all investigated ratios of **1** and **3**, extended lamellar structures were observed which differ significantly from that obtained for pure polymer **3**. The areas of the lamellar structures observed in the presence of cross-linker **1** varied from 0.02 μm^2 to 0.11 μm^2, which is two to ten times larger than those observed for pure polymer **3** (see last column in Table 2). The larger extension of the ordered structures as well as the absence of an unstructured monolayer (as present for pure polymer **3**) clearly indicate that the observed lamellar structures (for ratios $\alpha > 0$) can be attributed to the formation of networks between the conjugated polymer **3** and cross-linker **1**, and, in turn, to an effective cross-linking and alignment of **3** by **1**. The ordered structures for polymer **3** in the presence of supramolecular cross-linker **1** are characterized by two parameters, namely the lamellar distance *l* and the height *h* of the structure. These parameters are almost independent of the applied ratio α as the data shown in Table 2 reveal. The characteristic dimensions observed for all applied ratios is the lamellar distances *l* which were determined to 4.5-4.9 nm (3rd column, Table 2). In comparison to the pure polymer **3**, the lamellar distances *l* are appreciably increased in the presence of **1**, implying that cross-linker **1** is incorporated in the lamellar structures formed by self-assembly of **1** and **3**. The height *h* of the surface pattern varied from 0.30 nm for low amounts of cross-linker **1** (α = 0.03) to 0.34 nm for large amounts of **1** (α = 2). The observed heights indicate the formation of macrocyclic sandwich complexes of zinc porphyrin/perylene bisimide tweezer **1** and amine-functionalized polymer **3**, since the heights *h* are in reasonable agreement with that obtained for the self-assembly of **1** and DABCO (0.48 nm, see Chapter 7)[18] and nearly identical with the heights (0.30 - 0.35 nm) observed for

the sandwich complexes of polymer **3** with other zinc porphyrin tweezers reported in literature.[17] Furthermore, nanosized particles were observed for large excess of **1** (α = 2) and an intralamellar distance *a* of 2.4 ± 0.5 nm between these particles was determined by AFM analysis.

Based on the above-mentioned structural discussion, the observed ordered structure on HOPG can be explained in terms of supramolecular complexes formed between **1** and **3**. Thus, the geometry of the macrocyclic sandwich complex of ditopic tweezer **1** with a unit of the polymer **3** was optimized by force field method (MM3) and the energy-minimized structure is shown in Figure 12.

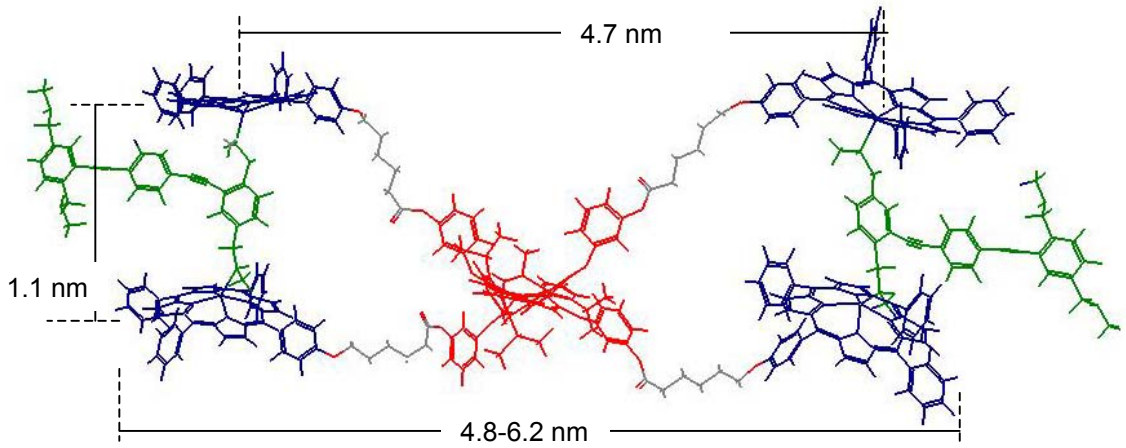

Figure 11. Structure of the complex between a short polymer unit and the ditopic zinc porphyrin/perylene bisimide receptor obtained by molecular modeling with MM3 force field calculations using Cache Quantum Cache Workspace 5.0.

The dimensions for the sandwich complex depicted in Figure 11 were estimated to 4.8-6.2 nm in width (depending on the conformation of the alkyl spacers) and 1.1 nm in height. The lamellar distance *l* of 4.5-4.8 nm determined by AFM for mixtures of **1** and **3** in different ratios is in good agreement with the distance between to zinc atoms of two porphyrins oriented to opposite directions estimated for the calculated structure of the sandwich complex (4.7 nm for an extended conformation, Figure 11). This indicates that one molecule of cross-linker **1** forms sandwich complexes with two neighboring polymer strands. This is in accordance with the literature report, where the spacing between the polymer **3** strands was clearly correlated to the dimensions of the zinc porphyrin aligner applied.[17] Therefore it is reasonable that the perylene bisimide core of cross-linker **1** is located in between the linear polymer strands as schematically shown in Figure 12. Furthermore, the dimensions of the porphyrin units in **1** (MM3 force field: 1.6 x 1.6 nm) and the distance between the binding sites in polymer **3** (MM3 force field: 1.3-1.4 nm) suggest that the porphyrin units which occupy two neighboring binding sites of the

polymer **3** are twisted against each other as shown in Figure 12 (see also Appendix F). Such binding geometries were also suggested in literature for a rigid porphyrin tweezer.[17]

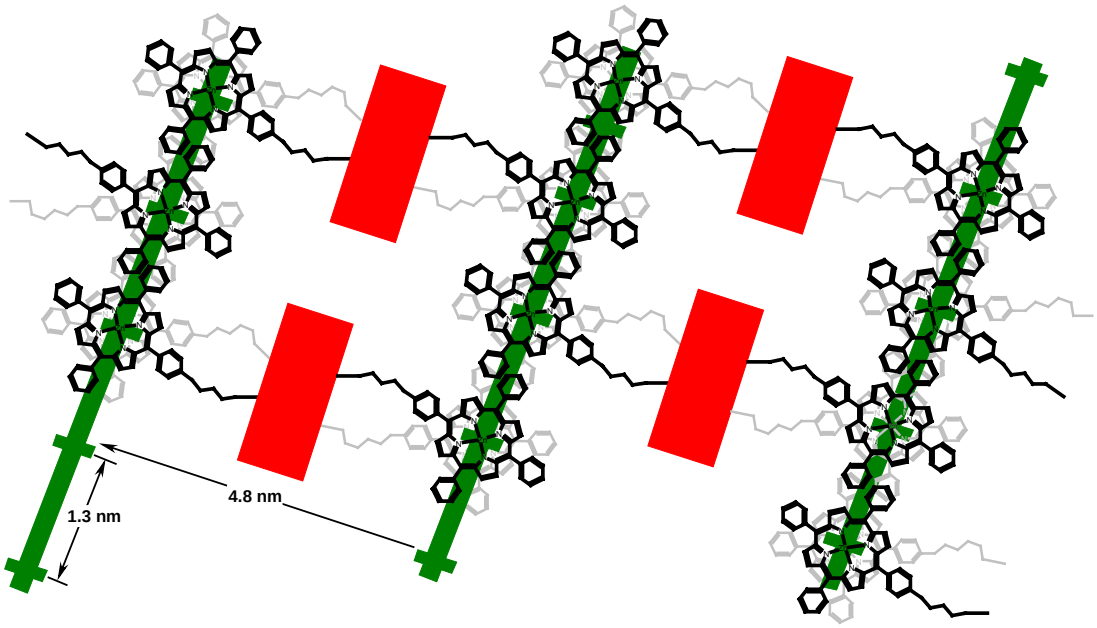

Figure 12. Schematic representation of lamellar structures for the self-assembly of **1** and **3**. The polymer strands are shown in green, perylene bisimide in red and zinc porphyrins on top and below the polymer strand in black and gray, respectively.

Single nanosized particles could only be observed for a ratio α of 2, whereas for all other ratios no such particles were observed which is due to lower lateral resolution in the latter cases. For α = 2, a interlamellar distance *a* (along the linear polymer strands) of 2.4 nm was determined. These nanoparticles can be attributed to the zinc porphyrin units of **1**, as the perylene bisimide must be located in between the linear polymer strands (see before). As shown above, two neighboring zinc porphyrin units possess a twisted geometry along the polymer strand. As the center-to-center distance between two porphyrins in such a twisted geometry was estimated to be 1.05-1.15 nm, the observed single particles have to be resulted from two neighboring sandwich complexes of **1** and polymer **3** which provide a periodicity of 2.1-2.3 nm. This is supported by the fact that the distance *a* (2.4 nm) determined for the particles corresponds more properly to the distance between the first and third binding site (2.6 nm) rather than to that of two neighboring binding sites (1.3 nm). Therefore, the observed surface pattern can be attributed to the formation of networks between **1** and **3**. Since the obtained lamellar structures showed great resemblance for all investigated amounts of supramolecular cross-linker **1** (different ratio α), the formation of networks between polymer **3** and **1** appears to be the most preferred binding motif on the HOPG surface. As the cross-

linker **1** is incorporated into the ordered structure, this supramolecular approach provides a well-defined arrangement of three different chromophores – zinc porphyrin, perylene bisimide, and π-conjugated polymer – on HOPG surface.

8.6 Conclusion

In summary, the self-assembly of linear π-conjugated polymer **3** and a zinc porphyrin/perylene bisimide tweezer **1** was elucidated by UV/Vis spectroscopy and AFM. The binding constants between **1** and monomeric reference compound **2** were determined by UV/Vis spectroscopic titration experiments and revealed effective binding of this model compound with cross-linker **1**. The formation of macrocyclic sandwich complex could be confirmed based on the observed binding constants. The binding between polymer **3** and cross-linker **1** was investigated by AFM. It was demonstrated that the lamellar structures formed on HOPG surface were almost indistinguishable for different ratios of polymer **3** and cross-linker **1** which revealed the parallel alignment of polymer **3** in the presence of different amounts of **1**. By comparison of the dimensions determined by AFM investigations with those obtained from molecular modeling, the structure of the self-assembled species on the HOPG surface was attributed to macrocyclic sandwich complexes of **1** and **3**. The observed well-defined arrangement of three different chromophores on HOPG surface is a promising starting point for the design of functional materials for information technology, sensory or catalysis.[13] The alignment of polymers bearing asymmetric carbon atoms might lead to chiral functional surfaces for asymmetric catalysis.[17]

8.7 Experimental Section

Methods and Materials. 1,4-Di(*N*-methylaminomethyl)-2,5-diiodobenzene **2** and the boc-protected polymer **3** were obtained from the group of Dr. M. Takeuchi and Prof. S. Shinkai (University of Tokio, Japan) and used as received. The synthesis of zinc porphyrin/perylene bisimide cross-linker **1** was described in Chapter 7 of this thesis. Dichloromethane (obtained from Grüssing; Filsum, Germany) was dried by distillation from calcium hydride, and trifluoroacetic acid (99%) obtained from Aldrich (Steinheim, Germany) was used as received. For all experiment spectroscopic grade solvents (Uvasol®) from Merck (Hohenbrunn, Germany) were used and chloroform was filtered over basic aluminium oxide (Merck) to remove traces of HCl prior to use.

The deprotection of boc-**3** was done according to literature procedure:[17]
1 mg of the Boc-protected polymer **3** was dissolved in anhydrous dichloromethane (10 mL) and 1 mL of trifluoroacetic acid was added. The reaction mixture was stirred for 24 h at room temperature and subsequently diluted with 10 mL of dichloromethane. The solution was neutralized with 1*N* sodium hydroxid. The combined organic layers were dried over Na_2SO_4, filtered via a syringe filter and condensed by heating with a hair dryer. Spectroscopic grade chloroform was added (4 mL) and the solution was further condensed. The concentration of the solution was determined by UV/Vis spectroscopy. An absorption at 403 nm of 0.544 corresponds to a concentration of the repeating unit of polymer **3** of 42.3 µm.[17]

UV/Vis Spectroscopic Titration Experiments.

Titration with 1,4-Di(*N*-methylaminomethyl)-2,5-diiodobenzene 2. Titration experiments were carried out on a Perkin Elmer Lamda 40 equipped with a peltier element for temperature control. To 1.1 x 10^{-5} M solution of **1** in chloroform in a 1 cm quartz cuvette at 23 °C were added via a microliter syringe 5 µl aliquots of a solution of 1,4-di(*N*-methylaminomethyl)-2,5-diiodobenzene **2** (6.1 x 10^{-4} M) and **1** (1.1 x 10^{-5} M). After each addition, a UV/Vis spectrum was recorded. The titration experiments were analyzed by fitting the whole series of spectra at 0.5 nm intervals using the software SpecFit/32, which uses a global analysis system with expanded factor analysis and a Marquardt least-square minimization to obtain globally optimized parameters. The individual binding constants were calculated from the log β values obtained by the program.

Atomic Force Microscopy (AFM). The AFM measurements were carried out by Vladimir Stepanenko (AK Würthner) at Institute of Organic Chemistry, University of Würzburg. Atomic force microscopy was performed on a Nanoscope IV controller, Veeco Multi Mode AFM using silicon tips with a resonance frequency of 300 kHz. The measurements were done in tapping mode with a resonance frequency of 300 kHz. The samples were prepared by spin coating (5000 rpm) of the respective solutions onto highly ordered pyrolytic graphite (HOPG). Samples for AFM were prepared by mixing stock solutions of **1** and **3** in chloroform via a microliter syringe. The concentrations of the mixtures used are shown in Table 1.

Supporting Information Available in the Appendix. Additional graphical materials and UV/Vis binding studies for **1** with polymer **3**.

8.8 References and Notes

1 For recent reviews, see: (a) F. Würthner, *Chem. Commun.* **2004**, 1564-1579; (b) F. J. M. Hoeben, P. Jonkheijm, E. W. Meijer, A. P. H. Schenning, *Chem. Rev.* **2005**, *105*, 1491-1546; (c) C. M. Drain, I. Goldberg, I. Sylvain, A. Falber, *Top. Curr. Chem.* **2005**, *245*, 55-88; (d) *Supramolecular Dye Chemisty*, *Topics in Current Chem*istry; *Vol. 258*, (Ed.: F. Würthner), Springer Verlag, Berlin, **2005**; (e) J. A. A. W. Elemans, R. van Hameren, R. J. M. Nolte, A. R. Rowan, *Adv. Mater.* **2006**, *18*, 1-17; (f) L.-J. Wan, *Acc. Chem. Res.* **2006**, *39*, 334-342.

2 (a) C. F. van Nostrum, R. J. M. Nolte, *Chem. Commun*. **1996**, 2385-2392; (b) A. M. van de Craats, J. M. Warman, *Adv. Mater.* **2001**, *13*, 130-133; (c) F. Würthner, C. Thalacker, S. Diele, C. Tschierske, *Chem. Eur. J.* **2001**, *7*, 2245-2253; (d) F. Nolde, W. Pisula, S. Müller, C. Kohl, K. Müllen, *Chem. Mater* **2006**, *18*, 3715-3725; (e) M.-h. Yoon, A. Facchetti, C. L. Stern, T. J. Marks, *J. Am. Chem. Soc.* **2006**, *128*, 5792-5801; (f) Z. Chen, U. Baumeister, C. Tschierske, F. Würthner, *Chem. Eur. J.* **2007**, *13*, 450-465; for reviews, see: (g) H. Ringsdorf, P. Schumacher, W. Baumeister, T. Scheybani in *Comprehensive Supramolecular Chemistry*, *Vol. 9*, (Eds.: J.-P. Sauvage, M. W. Hosseini), Elsevier, Oxford, **1996**, pp. 313-350; (h) K. Otha, K. Hatsusaka, M. Sugibayashi, M. Ariyoshi, K. Ban, F. Maeda, R. Naito, K. Nishizawa, A. N. van de Craats, J. M. Warman, *Mol. Cryst. Liq. Cryst.* **2003**, *397*, 325-345; (i) S. Kumar, *Chem. Soc. Rev.* **2006**, *35*, 83-109.

3 (a) E. E. Simanek, L. Isaacs, X. Li, C. C. C. Wang, G. M. Whiteside, *J. Org. Chem.* **1997**, *62*, 8994-9000; (b) X.-B. Shao, X.-K. Jiang, S.-Z. Zhu, Z.-T. Li, *Tetrahedron* **2004**, *60*, 9155-9162; (c) S. Yagai, T. Nakajima, T. Karatsu, K.-i. Saitow, A. Kitamura, *J. Am. Soc. Chem.* **2004**, *126*, 11500-11508; (d) A. Miura, P. Jonkheijm, S. De Feyter, A. P. H. J. Schenning, E. W. Meijer, F. C. De Schryver, *Small* **2005**, *1*, 131-137.

4 (a) P. J. Stang, J. Fan, B. Olenyuk, *Chem. Commun.* **1997**, 1453-1454; (b) C. Ikeda, N. Nagahara, E. Motegi, N. Yoshioka, H. Inoue, *Chem. Commun.* **1999**, 1759-1760; (c) F. Würthner, A. Sautter, D. Schmidt, P. J. A. Weber, *Chem. Eur. J.* **2001**, *7*, 894-902; (d) C.-C. You, F. Würthner, *J. Am. Chem. Soc.* **2003**, *125*, 9716-9725; (e) K. F. Cheng, N. A. Thai, L. C. Teague, K. Grohmann, C. M. Drain,

Chem. Commun. **2005**, 4678-4680; (f) C.-C. You, C. Hippius, M. Grüne, F. Würthner, *Chem. Eur. J.* **2006**, *12*, 7510-7519; for a review see: F. Würthner, C.-C. You, C. R. Saha-Möller, *Chem. Soc. Rev.* **2004**, *33*, 133-146.

5 (a) U. Michelsen, C. A. Hunter, *Angew. Chem.* **2000**, *112*, 780-783; *Angew. Chem. Int. Ed.* **2000**, *39*, 764-767; (b) D. M. Drain, *Proc. Nat. Acad. Sci. USA* **2002**, *99*, 5178-5182; (c) K. Sugiyasu, N. Fujita, S. Shinkai, *Angew. Chem.* **2004**, *116*, 1249-1253; *Angew. Chem. Int. Ed.* **2004**, *43*, 1229-1233; (d) R. Dobrawa, M. Lysteska, P. Ballester, M. Grüne, F. Würthner, *Macromolecules* **2005**, *38*, 1315-1325; (e) Y. Li, N. Wang, H. Gan, H. Liu, H. Li, Y. Li, X. He, C. Huang, S. Cui, S. Wang, D. Zhu, *J. Org. Chem.* **2005**, *70*, 9686-9692; (f) P. K. Iyer, J. B. Beck, C. Weder, S. J. Rowan, *Chem. Commun.* **2005**, 319-321; (g) F. Würthner, B. Hanke, M. Lysetska, G. Lambright, G. S. Harms, *Org. Lett.* **2005**, *7*, 967-970; (h) H. Sato, O. Tsutsumi, K. Takeda, H. Tanaka, T. Ogawa, *Jap. J. Appl. Phys.* **2006**, *45*, 2324-2327; for a review, see: (i) R. Dobrawa, F. Würthner, *J. Polym. Sci. Part A: Polym. Chem.* **2005**, *43*, 4981-4995.

6 (a) C. Thalacker, F. Würthner, *Adv. Func. Mater.* **2002**, *12*, 209-218; (b) Y. Liu, J. Zhuang, H. Liu, Y. Li F. Lu, H. Gan, T. Jiu, N. Wang, X. He, D. Zhu, *ChemPhysChem* **2004**, *5*, 1210-1215; (c) M. G. J. ten Cate, M. Crego-Calama, D. N. Reinhoudt, *J. Am. Chem. Soc.* **2004**, *126*, 10840-10841; (d) L. E. Sinks, B. Rybtchinski, M. Limura, B. A. Jones, A. J. Goshe, X. Zuo, D. M. Tiede, X. Li, M. R. Wasielewski, *Chem. Mater.* **2005**, *17*, 6295-6303; (e) P. Jonkheijm, J. K. L. van Duren, M. Kemerink, R. A. J. Janssen, A. P. H. J. Schenning, E. W. Meijer, *Macromolecules* **2006**, *39*, 784-788; (f) S. Bhosale, A. L. Sisson, P. Talkudar, A. Fürstenberg, N. Banerji, E. Vauthey, G. Bollot, J. Mareda, C. Röger, F. Würthner, N. Sakai, S. Matile, *Science* **2006**, *313*, 84-86; for reviews on porphyrins, see: (g) K. S. Suslick, P. Bhyrappa, J.-H. Chou, M. E. Kosal, S. Nakagaki, D. W. Smithenry, S. R. Wilson, *Acc. Chem. Res.* **2005**, *38*, 283-291; (h) A. Satake, Y. Kobuke, *Tetrahedron* **2005**, *61*, 13-41.

7 (a) A. P. H. J. Schenning, J. v. Herrikhuyzen, P. Jonkheijm, Z. Chen, F. Würthner, E. W. Meijer, *J. Am. Chem. Soc.* **2002**, *124*, 10252-10253; (b) E. H. A. Beckers, S. C. J. Meskers, A. P. H. J. Schenning, Z. Chen, F. Würthner, P. Marsal, D. Beljonne, J. Cornil, R. A. J. Janssen, *J. Am. Chem. Soc.* **2006**, *128*, 649-657; (c) E. H. A. Beckers, Z. Chen, S. C. J. Meskers, P. Jonkheijm, A. P. H.

J. Schenning, X.-Q. Li, P. Osswald, F. Würthner, R. A. J. Janssen, *J. Phys. Chem. B* **2006**, *110*, 16967-16978.

8 (a) T. van der Boom, R. T. Hayes, Y. Zhao, P. J. Bushard, E. A. Weiss, M. R. Wasielewski, *J. Am. Chem. Soc.* **2002**, *124*, 9582-9590; (b) C.-C. You, F. Würthner, *Org. Lett.* **2004**, *6*, 2401-2404; (c) M. O. Liu, C.-H. Tai, C.-W. Chen, W.-C. Chang, A. T. Hu, *J. Photochem. Photobiol. A* **2004**, *163*, 259-266; (d) S. Xiao, M. E. El-Khouly, Y. Li, Z. Gan, H. Liu, L. Jiang, Y. Araki, O. Ito, D. Zhu, *J. Phys. Chem. B* **2005**, *109*, 3658-3667; (e) A. Prodi, C. Chiroboli, F. Scandola, E. Iengo, E. Alessio, R. Dobrawa, F. Würthner, *J. Am. Chem. Soc.* **2005**, *127*, 1454-1462.

9 (a) Y. Liu, S. Xiao, H. Li, Y. Li, H. Liu, F. Lu, J. Zhuang, D. Zhu, *J. Phys. Chem. B* **2004**, *108*, 6256-6260; (b) J. Hua, F. Ding, F. S. Meng, H. Tian, *Chin. Chem. Lett.* **2004**, *15*, 1373-1376; (c) J. Hua, F. Meng, F. Ding, F. Li, H. Tian, *J. Mater. Chem.* **2004**, *14*, 1849-1853; (d) Y. Liu, N. Wang, Y. Li, H. Liu, Y. Li, J. Xiao, X. Xu, C. Huang, S. Cui, D. Zhu, *Macromolecules* **2005**, *38*, 4880-4887; (e) J. Zhuang, W. Zhou, X. Li, Y. Li, N. Wang, X. He, H. Liu, Y. Li, L. Jiang, C. Huang, S. Cui, S. Wang, D. Zhu, *Tetrahedron* **2005**, *61*, 8686-8693; (f) J. A: Theobald, N. S. Oxtoby, N. R. Champness, P. H. Beton, T. J. S. Dennis, *Langmuir* **2005**, *21*, 2038-2041.

10 (a) X. Li, L. E. Sinks, B. Rybchinski, M. R. Wasielewski, *J. Am. Chem. Soc.* **2004**, *126*, 10810-10811; (b) M. S. Rodriguez-Morgade, T. Torres, C. Castellanos, D. M. Guldi, *J. Am. Chem. Soc.* **2006**, *128*, 15145-15154.

11 (a) T. Otsubo, Y. Aso, K. Takimiya, *J. Mater. Chem.* **2002**, *12*, 2565-2575; (b) C.-H. Huang, N. D. McClenaghan, A. Kuhn, G. Bravic, D. M. Bassani, *Tetrahedron* **2006**, *62*, 2050-2059.

12 (a) H. Sato, K. Tashiro, H. Shinmori, A. Osuka, T. Aida, *Chem. Commun.* **2005**, 2324-2326; (b) R. Marczak, V. Sgobba, W. Kutner, S. Gadde, F. D´Souza, D. M. Guldi, *Langmuir* **2007**, *23*, 1917-1923; (c) V. Sgobba, G. Giancane, S. Conoci, S. Casilli, G. Ricciardi, D. M. Guldi, M. Prato, L. Valli, *J. Am. Chem. Soc.* **2007**, *129*, 3173-3181; for review, see: (d) K. Tashiro, T. Aida, *Chem. Soc. Rev.* **2007**, *36*, 189-197.

13 (a) A. P. H. J. Schenning, P. Jonkheijm, F. J. M. van Herrikhuyzen, S. C. J. Meskers, E. W. Meijer, L. M. Herz, C. Daniel, C. Silva, R. T. Phillips, R. H. Friend, D. Beljonne, A. Miura, S. De Feyter, M. Zdanowska, H. Uji-i, F. C. De Schryver,

Z. Chen, F. Würthner, M. Mas-Torrent, D. den Boer, M. Durkut, P. Hadley, *Syn. Met.* **2004**, *147*, 43-48; (b) V. Humbolt, S. M. Barlow, R. Raval, *Prog. Surf. Sci.* **2004**, *76*, 1-19.

14 Recent reviews: (a) V. Kriegisch, C. Lambert, *Top. Curr. Chem.* **2005**, *258*, 257-313; (b) J. J. Davis, *Chem. Commun.* **2005**, 3509-3513; (c) B. A. Hermann, L. J. Scherer, C. E. Hourscroft, E. C. Constable, *Adv. Funct. Mater.* **2006**, *26*, 221-235.

15 (a) G. Decher, *Science* **1997**, *277*, 1232-1237; (b) M. Schütte, D. G. Kurth, M. R. Linford, H. Cölfen, H. Möhwald, *Angew. Chem.* **1998**, *110*, 3058-3061; *Angew. Chem. Int. Ed.* **1998**, *37*, 2891-2893; (c) R. Dobrawa, D. G. Kurth, F. Würthner, *Polymer Prepr.* **2004**, *45*, 378-379; (d) T. Tang, J. Qu, K. Müllen, S. E. Webber, Langmuir **2006**, *22*, 26-28; for reviews, see: (e) G. Decher in *Comprehensive Supramolecular Chemistry*, *Vol. 9*, (Eds.: J.-P. Sauvage, M. Hosseini), Elsevier, Oxford, **1996**, pp. 507-528; (f) C. F. J. Faul, M. Antonietti, *Adv. Mater.* **2003**, *15*, 673-683; (g) D. M. Guldi, M. Prato, *Chem. Commun.* **2004**, 2517-2525.

16 T. Yamaguchi, N. Ishii, K. Tashiro, T. Aida, *J. Am. Chem. Soc.* **2003**, *125*, 13934-13935.

17 (a) R. Wakabayashi, Y. Kubo, K. Kaneko, M. Takeuchi, S. Shinkai, *J. Am. Chem. Soc.* **2006**, *128*, 8744-8745; (b) Y. Kubo, Y. Kitada, R. Wakabayashi, T. Kishida, M. Ayabe, K. Kaneko, M. Takeuchi, S. Shinkai, *Angew. Chem.* **2006**, *118*, 1578-1583; *Angew. Chem. Int. Ed.* **2006**, *45*, 1548-1553.

18 See Chapter 7 of this thesis.

19 SpecFit/32 from Spectrum Software Associates (Marlborough, MA, 2000-2001) was used for data analysis.

20 Non-linear regression analysis with an open-chained 1:4 species instead of a 1:3 species provided a reasonable fit of the experimental data as well. A binding constant of 2.3 x 10^8 M^{-2} was obtained for direct formation of a 1:4 species from the macrocyclic 1:2 species.

21 V. V. Borovkov, J. M. Lintuluoto, G. A. Hembury, M. Sugiura, R. Arakawa, Y. Inoue, *J. Org. Chem.* **2003**, *68*, 7176-7192.

Chapter 9

Summary

The importance of conformational chiral molecules for chiral recognition processes and enantioselective catalysis have evolved them to an attractive research object for academies and the pharmaceutical and chemical industry. In combination with functional properties such as an absorption in the visible region or luminescence the detection of recognition processes becomes more cost-effective. The excellent optical properties of perylene bisimides and the conformational chirality arising from the “bay” substituents should facilitate the application of this class of dyes as sensors and molecular switches and machines.

This thesis deals with the synthesis of atropo-enantiomeric and atropo-diastereomeric chromophores based on perylene bisimides and the elucidation of their optical and chiroptical properties. For this purpose, three concepts have been followed in order to fix the inherent chirality of “bay” substituted perylene bisimides and thus to obtain isolatable chiral perylene bisimides: On the one hand, the linkage of the aryloxy-substituents through macrocyclisation by covalent or non-covalent interactions and, on the other hand, the introduction of sterically demanding substituents in the bay positions (1,6,7,12-positions) to increase the racemisation barrier.

The special features of conformational chiral molecules have been outlined in an introductory way in Chapter 1. Particular emphasis has been given to the dynamic properties of such molecules and fundamental concepts for the sterically and electronically inhibition of the racemisation equilibrium have been discussed. Additionally, application potentials of conformational chiral molecules have been shown on selected examples such as binaphthyls and helicenes. The special structural features of bay-substituted perylene bisimides have been outlined in Chapter 2 on the basis of molecular modelling and literature known X-ray structures. In addition, the symmetry properties of different bay-substituted perylene bisimides have been analyzed and the stereochemistry of the two expected conformational enantiomers was defined.

In the extensive Chapter 3 the concept of macrocyclization for the synthesis of perylene bisimide atropo-enantiomers was applied. The synthesis of macrocyclic perylene bisimides was achieved by using a tetra(hydroxyphenoxy)-functionalized perylene bisimide with achiral 2,6-diisopropylphenyl as imide substituent through Williamson´s etherfication which could be realized for four different oligoethylene glycol bridging units. Two regioisomeric macrocycles, namely the diagonally bridged (1,7- and 6,12- linkage) and the laterally bridged (1,12- and 6,7-linkage) isomers, were obtained for each bridging unit (Scheme 1). The structural assignment of the isolated regioisomeric macrocycles was unambiguously accomplished by X-ray analysis of two

macrocycles and by characteristic chemical shifts of reference protons in the ^{1}H NMR spectra for all isomers.

Scheme 1. Synthesis of Macrocyclic Perylene Bisimides.

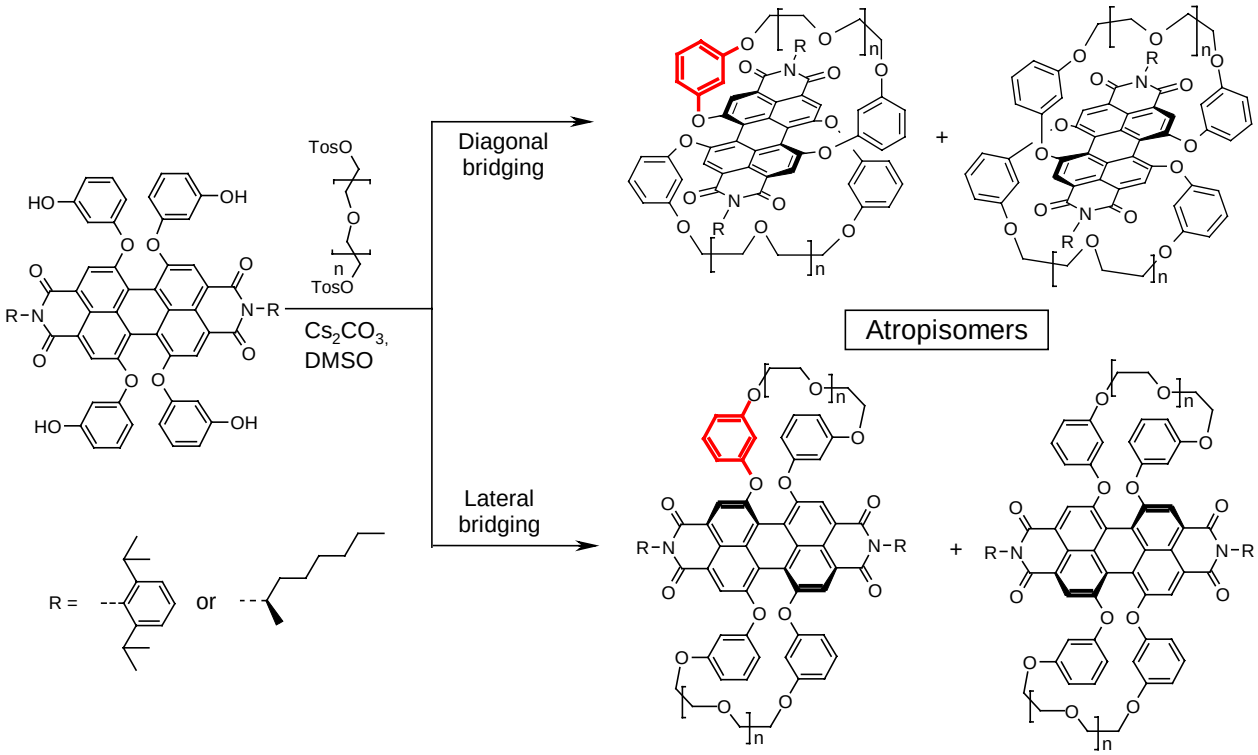

From the crystallographic data and the observed chemical shifts of characteristic protons in the NMR spectra, it was apparent that the two regioisomers comprise different orientations of the aryloxy residues relative to the perylene core, i.e. a perpendicular orientation in the diagonally bridged isomer and a horizontal orientation in the laterally bridged isomer (Scheme 1). By comparison of the optical properties of both regioisomers for each chain-length with those of an open-chained reference compound, it was shown that the excellent fluorescence properties of aryloxy-substituted perylene bisimides are due to the presence of these chromophores in a lateral conformation. Furthermore, the fluorescence properties of the diagonally bridged isomers and three noncyclic perylene bisimides indicated that a photoinduced electron transfer process is of importance for the fluorescence quenching of electron-rich aryloxy-substituted perylene bisimides. The dynamic properties of the lateral isomers were investigated by dynamic NMR spectroscopy and quantum chemical calculations providing an insight into the twisting and the racemisation barrier of these chromophores in solution.

The atropo-enantiomers of the diagonally bridged isomers (containing achiral imide substituents) could not be resolved by HPLC on a chiral column or by crystallization.

Therefore, macrocyclic perylene bisimides with chiral 2-(*R*)-octylamine as imide substituent were synthesized for diethylene glycol bridging units (Chapter 4) and the resolution of the (*P*,*R*,*R*)- and (*M*,*R*,*R*)-atropo-diastereomers for the diagonally bridged regioisomer could be accomplished by semi-preparative HPLC on a chiral column. The chiroptical properties of the isolated epimerically pure macrocycles were determined by CD spectroscopy and the obtained absorption dissymmetry factor g (g = $\Delta\varepsilon/\varepsilon$) revealed typical values for conformational chiral molecules as e.g. helicenes. Based on the experimental CD spectra, the stereochemical assignment of the isolated epimers was accomplished by application of the excition chirality method and confirmed by quantum chemical calculation of the CD spectra

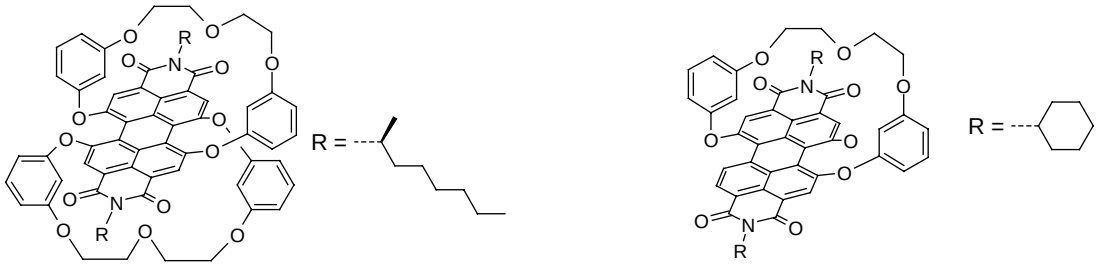

Figure 1. Structures of epimeric macrocycles based on 1,6,7,12-tetraaryloxy-substituted perylene bisimides (left) reported in Chapter 4 of this thesis and atropo-enantiomeric macrocycles based on 1,7-diaryloxy-substituted perylene bisimide (right) presented in Chapter 5.

The synthetical concept was extended successfully to 1,7-diaryloxy-substituted perylene bisimides in the fifth chapter. The synthesis of the macrocycle (Figure 1, right) was achieved by the established method starting from 1,7-di(hydroxyphenoxy)-substituted perylene bisimide. Diethylene glycol was chosen as bridging unit since it provides conformationally rigid macrocycles in reasonable yields. In the present case, the diagonally bridged macrocycle is the only possible isomer, whose structure was unambiguously confirmed by X-ray analysis and NMR spectroscopy. Furthermore, the optical and electrochemical properties of the racemate were investigated by UV/Vis and fluorescence spectroscopy and cyclic voltammetry. The atropo-enantiomers of this macrocycle could be resolved by semi-preparative HPLC on a chiral column which allowed the characterization of the chiroptical properties by CD spectroscopy. The assignment of the absolute configuration was achieved by comparison of the CD spectra of the resolved enantiomers with those of epimerically pure bis(macrocycles) reported in Chapter 4. As single crystals were available for both, the racemic mixture and one atropo-enantiomer, important information could be extracted from these solid

state structures. In particular, the formation of π-dimers, in which the (*P*)-enantiomers are stacked in a (*M*)-helical fashion, could only be observed in the solid state of the homochiral compound. This represents a very promising starting point for the construction of chiral sensors based on π-dimers of enantiopure macrocyclic perylene bisimides.

The dependence of the interconversion barrier on the bulkiness of the bay-substituents was investigated in Chapter 6. For this purpose, four halogen-substituted perylene bisimides were applied, the literature known tetrabromo, tetrachloro and dibromo derivatives, and the newly synthesized tetrafluoro-substituted perylene bisimide. The dynamic properties were investigated by temperature-dependent NMR spectroscopy and kinectic measurements using CD spectroscopy. By applying the concept of the “apparent overlap” a convincing linear relationship between the size of the substituents and the free enthalpy of activation could be derived. Furthermore, the resolution of the atropo-diastereomers or enantiomers of the tetrachloro and tetrabromo-substituted derivates was accomplished, whereupon especially the 1,6,7,12-tetrabromosubstituted perylene bisimide provided at room temperature stable enantiomers. Additionally, the derived structure-property relationship allows the design of conformationally stable perylene bisimide enantiomers by proper choice of the bay substituents.

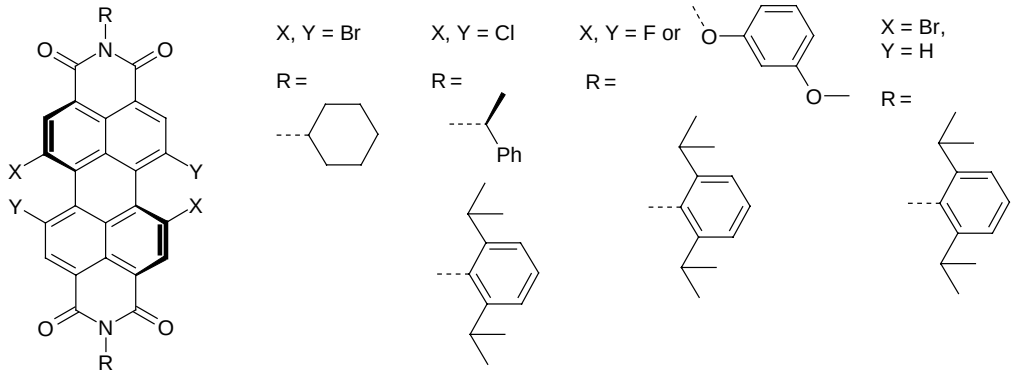

Figure 2. Structure of bay-substituted perylene bisimides used in Chapter 6.

In order to utilize the reversibility of self-assembly for the quantitative formation of macrocyclic perylene bisimides, a tetrazinc porphyrin-functionalized perylene bisimide was synthesized. The self-assembly of the zinc porphyrin perylene bisimide bichromophoric building block and diazabicyclo-[2.2.2]-undecane into the desired 1:2 sandwich complex was investigated by UV/Vis and ^{1}H NMR spectroscopy and the macrocyclic structure was unequivocally proven by diffusion-ordered NMR spectroscopy (DOSY NMR). An assignment of the obtained macrocycle to one of the two possible

regioisomers (diagonal/lateral) was just as little possible as the experimental evidence or even the isolation of conformationally stable atropo-enantiomers. The similarity of the optical properties of the bichromophoric system and the self-assembled macrocycle with those of tetraphenyl zinc porphyrin indicates an energy transfer from the perylene bisimide to the zinc porphyrin. Furthermore, the controlled deposition of these well-defined macrocycles on highly ordered pyrolitic graphite (HOPG) was demonstrated by atomic force microscopy (AFM) investigations.

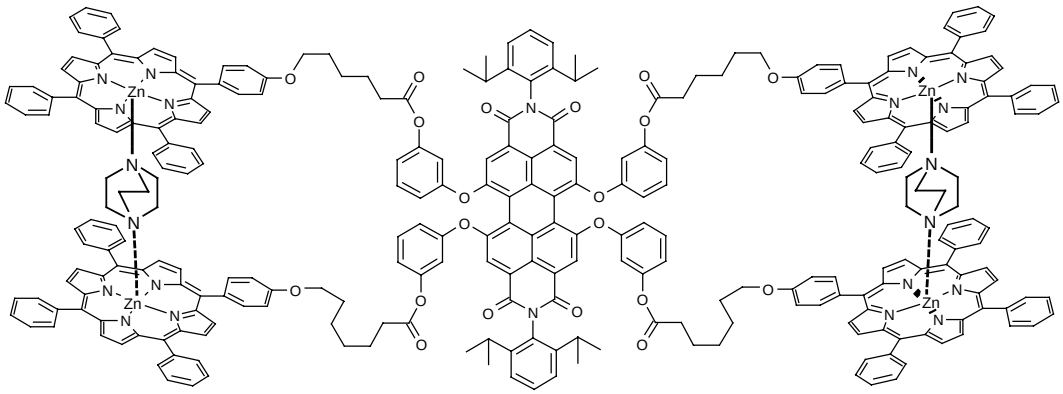

Figure 3. Probable regioisomer of the macrocycle obtained by self-assembly of zinc porphyrin perylene bisimide bichromophoric system and DABCO (Chapter 7).

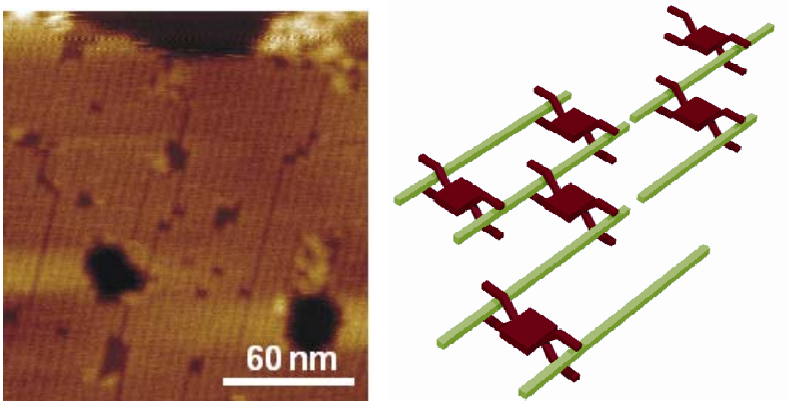

Figure 4. AFM image (left) and schematic representation (right) for the alignment of linear polymer by zinc porphyrin functionalized perylene bisimide. The green bars (right) represent the polymer and the bichromophoric system is shown as clip in red.

In the final Chapter 8, the alignment of a linear π-conjugated polymers containing two amino functionalities per repeating unit upon addition of the bichromphoric tetrazinc porphyrin-perylene bisimide was investigated by UV/Vis spectroscopy and AFM measurement. The binding of bichromophoric system under formation of macrocyclic structure was demonstrated for a simple reference compound. The surface analysis by AFM investigations revealed that the bichromophoric system composed of perylene bisimide and zinc porphyrin is able to cross-link the linear π-conjugated polymer over a

wide range of the graphite surface which provided a defined arrangement of three different functional π-systems. This is of particular interest for the design of functional surfaces for catalysis or sensory.

In conclusion, two concepts for the synthesis of conformational stable chiral perylene bisimides have been realized: (i) Synthesis of macrocyclic perylene bisimides and subsequent resolution of the atropo-diastereomers (epimers) of diagonally bridged macrocycles based on tetraaryloxy-substituted perylene bisimides and the resolution of the enantiomers of diaryloxy-substituted macrocyclic perylene bisimides and (ii) the introduction of large bay substituents to increase the racemisation barrier which enabled the resolution of the atropo-enantiomers of tetrabromo-substituted perylene bisimides. Finally, the principle of self-assembly for the synthesis of macrocycles was demonstrated for a zinc porphyrin functionalized perylene bisimides by coordination with DABCO, although enantiomers could not be resolved by this approach. The alignment of a linear π-conjugated polymer by this bichromophoric system, revealed that a defined alignment of π-conjugated polymers was possible in solution and on surfaces as well.

Chapter 10

Zusammenfassung

Die Bedeutung konformativ chiraler Moleküle für chirale Erkennungsprozesse und die enantioselektive Katalyse macht sie zu attraktiven Forschungsobjekten sowohl in der Hochschule als auch in der chemischen und pharmazeutischen Industrie. In Kombination mit funktionellen Eigenschaften wie etwa Absorption im sichtbaren Bereich oder Fluoreszenz werden Erkennungsprozesse kostengünstig detektierbar. Die herausragenden optischen Eigenschaften von Perylenbisimiden und die durch „Bay“-Substituenten resultierende Chiralität dieser Moleküle sollten Anwendungen dieser Farbstoffklasse als Sensoren, molekulare Schalter und Maschinen ermöglichen.

Die vorliegende Arbeit beschäftigt sich mit der Synthese von atropo-enantiomeren und atropo-diastereomeren Farbstoffen auf Basis von Perylenbisimiden und der Bestimmung ihrer optischen und chiroptischen Eigenschaften. Hierzu wurden drei unterschiedliche Konzepte verfolgt, um die inhärente konformative Chiralität „bay“-substituierter Perylenbisimide zu fixieren und somit zu isolierbaren chiralen Farbstoffen zu gelangen: Einerseits die Verknüpfung von Aryloxysubstituenten durch Makrocyclisierung kovalenter und nicht-kovalenter Wechselwirkungen, andererseits die Einführung von sterisch anspruchsvollen Substituenten in den Bay-Positionen (1,6,7,12-Positionen) zur Erhöhung der Razemisierungsbarrieren.

Im einleitenden Kapitel 1 wurden die Besonderheiten konformativ chiraler Moleküle aufgezeigt. Hierbei wurde besonderes Augenmerk auf die dynamischen Eigenschaften dieser Moleküle gelegt und grundlegende Konzepte zur sterischen und elektronischen Inhibierung der Razemisierung diskutiert. Außerdem wurden Anwendungsmöglichkeiten für konformativ chirale Moleküle an Hand von ausgewählten Beispielen, wie etwa Binaphthylen und Helicenen, aufgezeigt. In Kapitel 2 wurden dann die strukturellen Besonderheiten bay-substituierter Perylenbisimide anhand von Molecular Modeling Untersuchungen und literaturbekannten Kristallstrukturen aufgezeigt. Darüber hinaus wurden die Symmetrieeigenschaften dieser Farbstoffe analysiert und die Stereochemie der zu erwartenden konformativen Enantiomere definiert.

In umfangreichen Kapitel 3 wurde die Makrocyclisierung zur Herstellung von atropo-enantiomeren Perylenbisimiden eingesetzt. Die Darstellung makrocyclischer Perylenbisimide erfolgte ausgehend von einem vierfach (3-Hydroxyphenoxy)-funktionalisierten Perylenbisimid mit achiralen 2,6-Diisopropylphenylsubstituenten an den Imidpositionen durch Williamsonsche Ethersynthese. Die Synthese konnte für vier unterschiedliche Oligoethylenglykol-Kettenlängen realisiert werden, wobei für jede Brückenlänge jeweils zwei regioisomere Makrocyclen, nämlich das diagonal verbrückte (1,7- und 6,12-Verküpfung) und das seitlich verbrückte Isomer (1,12- und 6,7-

Verknüpfung) isoliert werden konnten (Schema 1). Die strukturelle Zuordnung der isolierten Makrocyclen zu einem der beiden Regioisomeren gelang zweifelsfrei anhand von Röntgenstrukturanalysen für zwei Makrocyclen und mittels charakteristischer chemischer Verschiebungen von Referenzprotonen in den ^{1}H NMR-Spektren für alle Isomere.

Schema 1. Synthese von macrocyclischen Perylenbisimiden.

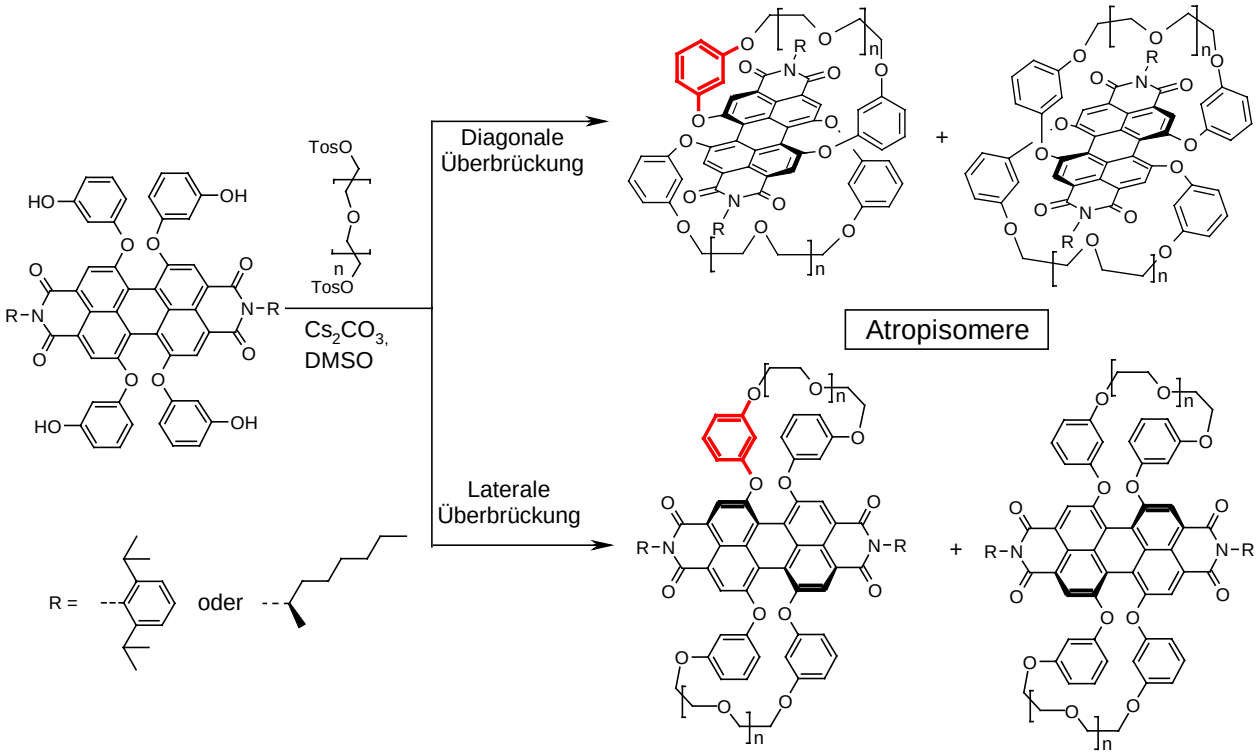

Aus den kristallographischen Daten und den beobachteten chemischen Verschiebungen charakteristischer Protonen in den ^{1}H-NMR-Spektren wurde offensichtlich, dass die beiden Regioisomere unterschiedliche Stellungen der Aryloxy-Reste beinhalten, nämlich eine senkrechte Orientierung relative zum Perylengrundgerüst im diagonal verbrückten Isomer und eine horizontale Orientierung in den seitlich überbrückten Isomeren (Schema 1). Durch Vergleich der optischen Eigenschaften der beiden Regioisomere für alle vier erhaltenen Brückenlängen mit einer offenkettigen Referenzverbindung konnte gezeigt werden, dass die vorzüglichen Fluoreszenzeigenschaften Aryloxy-substituierter Perylenbisimide in Lösung auf deren Vorliegen in der lateralen Konformation beruhen. Darüber hinaus konnte anhand der Fluoreszenzeigenschaften der diagonal verbrückten Makrocyclen und dreier offenkettigen Derivaten gezeigt werden, dass ein photoinduzierter Elektronentransferprozess für die Fluoreszenzlösung für elektronenreiche Aryloxy-Substituenten von Bedeutung ist. Die dynamischen Eigenschaften der seitlichen

Isomere wurden mittels dynamischer NMR-Spektroskopie und quantenchemischen Rechnungen untersucht. Hierbei konnte ein Einblick in den Verdrillungsgrad und die Razemisierungsbarrieren dieser Farbstoffe in Lösung erhalten werden.

Versuche zur Trennung der Atropo-Enantiomere (im Fall der achiralen Imidsubstituenten) blieben für die diagonal verbrückten Isomere sowohl mittels HPLC an einer chiralen stationären Phase als auch durch Kristallisation ohne Erfolg. Deshalb wurden in Kapitel 4 makrocyclische Verbindungen mit chiralen 2-(*R*)-Octylamin Imidsubstituenten und Diethyleneglykol als Brückenkette synthetisiert, deren Trennung in (*P*,*R*,*R*) und (*M*,*R*,*R*)-diagonal verbrückte Atropo-Diastereomere mittels semi-preparativer HPLC an einer chiralen stationären Phase gelang. Die chiroptischen Eigenschaften der isolierten epimerenreinen Makrocyclen wurden mittels CD-Spektroskopie untersucht. Die ermittelten Absorptions-Anisotropie Faktoren g ($g = \Delta\varepsilon/\varepsilon$) liegen im typischen Bereich für konformativ chirale Moleküle wie z.B. Helicene. Die Zuordnung der absoluten Stereochemie konnte anhand der erhaltenen CD-Spektren durch Anwendung der „Theorie der excitonischen Kopplung“ abgeleitet und durch quantenchemische Berechnung der CD-Spektren bestätigt werden.

Das Synthesekonzept wurde im fünften Kapitel auf 1,7-diaryloxy-substituierten Perylenbisimide erweitert. Die Darstellung des Makrocyclus erfolgte nach der bereits etablierten Methode ausgehend von einem 1,7-di(3-hydroxyphenoxy)-substituierten Perylenbisimid. Erneut wurde Diethylenglycol verwendet, da dieses die besten Ausbeuten und eine ausreichende konformative Rigidität des Makrocyclus bedingt. Hierbei kann lediglich das diagonal verbrückte monocyclische Isomer entstehen, dessen Struktur erneut durch NMR-Spektroskopie und Röntgenstrukturanalyse eindeutig bestimmt werden konnte. Des weiteren wurden die optischen und elektrochemischen Eigenschaften dieses Makrocyclus mittels UV/Vis- und Fluoreszenzspektroskopie, sowie mit Cyclovoltammetrie untersucht. Die Trennung der Atropo-Enantiomere gelang mittels semi-preparativer HPLC an einer chiralen stationären Phase, so dass die chiroptischen Eigenschaften mittels CD-Spektroskopie charakterisiert werden konnte. Die Zuordnung der Stereochemie gelang anhand des Vergleichs der CD-Spektren mit den zuvor für epimerenreine Bismakrocyclen (Kapitel 4) erhaltenen CD-Spektren. Da sowohl für die racemische Mischung als auch für das Atropo-Enantiomer Einkristalle erhalten werden konnten, ließen sich bedeutende Informationen aus diesen Festkörperstrukturen ableiten. So bilden sich nur für den homochiralen Fall π-Dimere aus, in denen (*P*)-Atopo-Enantiomere (*M*)-helikal stapeln. Dies stellt einen vielversprechenden Ausgangspunkt zur Darstellung von chiralen

Sensoren auf Basis von π-Dimeren enantiomerenreiner makrocyclischer Perylenbisimide dar.

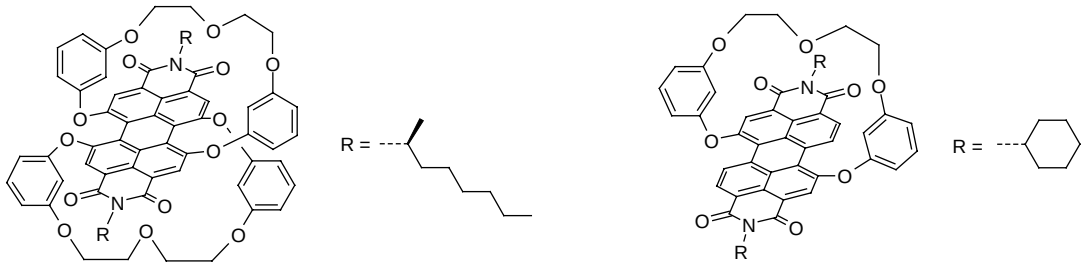

Abbildung 1. Strukturen von in dieser Arbeit isolierten chiralen Makrocyclen basierend auf tetraaryloxy-substitutierten Perylenbisimiden (links, Kapitel 4) und 1,7-diaryloxy-substituierten Perylenbisimiden (rechts, Kapitel 5).

Die Abhängigkeit der Razemisierungsbarriere von der Größe der Bay-Substituenten wurde in Kapitel 6 untersucht. Hierzu wurden vier halogensubstituierte Derivate, die literaturbekannten tetrabrom-, tetrachlor- und 1,7-dibrom-substituierten Perylenbisimide, sowie eine neu synthetisierte 1,6,7,12-tetrafluor-substituierte Verbindung verwendet. Die dynamischen Eigenschaften wurden mittels temperaturabhängiger NMR-Spektroskopie und kinetischer Messungen mittels CD-Spektroskopie bestimmt. Unter Anwendung des „Apparent Overlap“-Konzeptes konnte eine überzeugende lineare Beziehung zwischen der Größe der Substituenten und der Inversionsbarriere hergestellt werden. Darüber hinaus war es möglich die Atropo-Diastereomere bzw. Enantiomere der tetrachlor- und tetrabrom-substituierten Derivate zu trennen, wobei vor allem das 1,6,7,12-tetrabrom-substituierte Perylenbisimid stabile Enantiomere bei Raumtemperatur lieferte. Die abgeleitete Struktur-Eigenschaftsbeziehung sollte zukünftig die Herstellung von stabilen Enantiomeren durch geeignete Wahl der Substituenten in den Bay-Positionen ermöglichen.

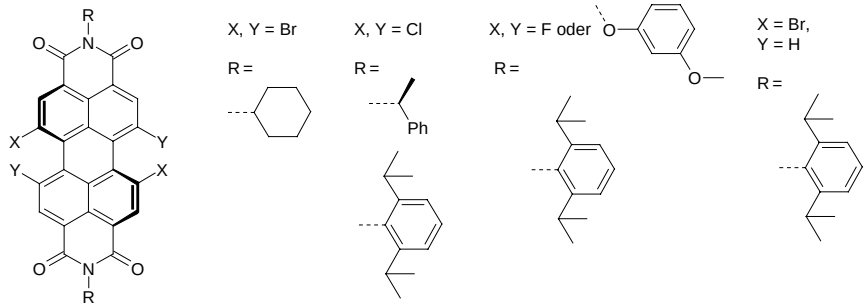

Abbildung 2. Strukturen der in Kapitel 6 verwendeten Perylenbisimide.

Um die Reversibilität der Selbstorganisation zur quantitativen Synthese makrocyclischer Perylenbisimide ausnützen zu können, wurde ein tetra(zinkporphyrin)-funktionalisiertes Perylenbisimid synthetisiert. Die Ausbildung des angestrebten 1:2-

Sandwichkomplexes aus Tetra-Zinkporphyrin-Perylenbisimid und Diazabicyclo-[2.2.2]-undecan (DABCO) wurde mittels UV/Vis und ^{1}H NMR Spektroskopie untersucht und die makrocyclische Struktur des Komplexes konnte mittels diffusionsabhängiger NMR Spektroskopie (DOSY NMR) eindeutig bewiesen werden. Eine Zuordnung des entstanden Makrocycluses zu einem der beiden Regioisomere (diagonal/lateral) war hierbei genauso wenig möglich wie der Nachweis oder gar die Isolierung konformativ stabiler Atropo-Enantiomere. Die optischen Eigenschaften des bichromophoren Moleküls als auch die des 1:2-Sandwichkomplexes wurden mittels UV/Vis und Fluoreszenzspektroskopie untersucht. Die Ähnlichkeit der Fluoreszenzeigenschaften des bichromophoren Systems als auch des durch Selbstoganisation erhaltenen Makrocyclus mit denen von Zinktetraphenylporphyrin weisen hierbei auf einen Energietransfer vom Perylenbisimid auf das Zinkporphyrin hin. Weiterhin konnte mittels rasterkraftmikroskopischer (AFM) Untersuchungen gezeigt werden, dass diese funktionellen makrocyclischen Verbindungen sehr geordnet auf einer Graphitoberfläche (HOPG) abgeschieden werden können.

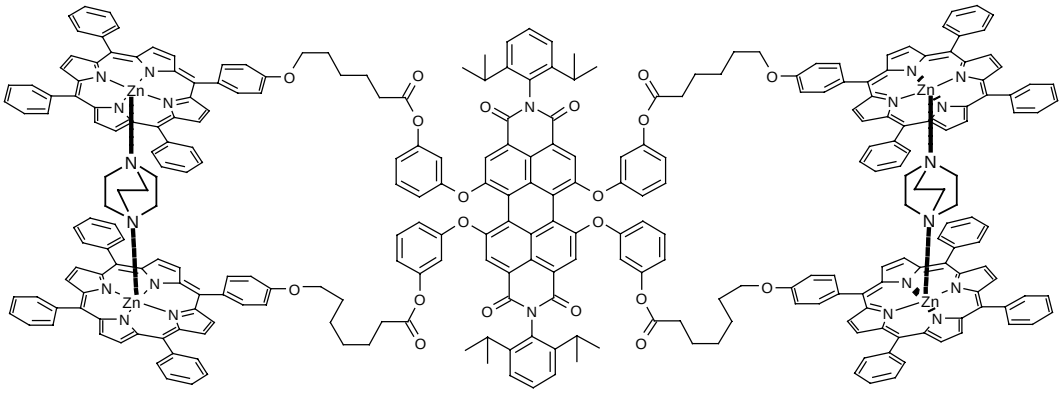

Abbildung 3. Mögliche Struktur der durch DABCO-Zugabe in Kapitel 7 erhaltenen bichromophoren Komplexverbindung.

Im letzten Kapitel wurde die Ausrichtung eines π-konjugierten Polymers, welches zwei Amino-Funktionalitäten pro Wiederholungseinheit aufweist, durch Zugabe des bichromphoren Tetra-Zinkporphyrin-Perlyenbisimids mittels UV/Vis-Spektroskopie und AFM-Messungen untersucht. Hierbei konnte die Bindung des bichromophoren Systems unter Ausbildung makrocyclischer Strukturen sowohl für eine einfache Referenzverbindung als auch für das Polymer festgestellt werden. Die Oberflächenanalyse mittels AFM zeigte, dass die bichromophore Verbindung die linearen π-konjugierten Polymere über weite Teile der Oberfläche auszurichten vermag, so dass eine definierte Anordnung von drei π-Systemen auf der Graphitoberfläche

ermöglicht wurde. Dies ist von besonderem Interesse im Hinblick auf funktionelle Oberflächen für die Katalyse oder Sensorik.

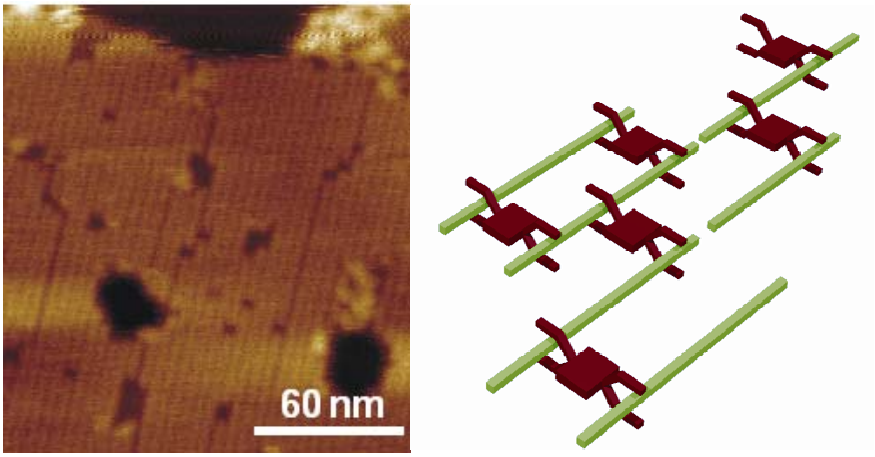

Abbildung 4. AFM Bild (links) und schematische Darstellung (rechts) der Ausrichtung eines linearen π-konjugierten Polymers mittels des zinkporphyrin-funktionalisierten Perylenbisimids. Das grüne Rechteck rechts repräsentiert das lineare Polymer, die rote Klammer das Tetra-Zinkporphyrin-Perylenbisimid.

Zusammenfassend wurden in dieser Arbeit drei Konzepte zur Synthese von konformativ stabilen chiralen Perylenbisimiden realisiert, beginnend mit der Synthese von makrocyclischen Perylenbisimiden, der Trennung atropo-diastereomerer diagonal verbrückter Makrocyclen auf Basis tetraaryloxy-substituierter Perylenbisimide und der Trennung der Atropo-Enantiomere 1,7-diaryloxy-substituierter makrocyclischer Perylenbisimide. Desweiteren wurde gezeigt, das die Razemisierungsbarriere der Perylenbisimid Atropisomere von der Größe der Bay-Substitutenten abhängt und dass deren Separation für die tetrabromierten Perylenbisimide möglich ist. Schließlich konnte das Prinzip der Selbstorganisation zur Synthese von Makrocyclen auf der Basis eines tetra(zinkporphyrin)-substituierten Perylenbisimids durch DABCO-Koordination gezeigt werden, wobei die Enantiomere hierbei aber nicht auftrennbar waren. Die Ausrichtung eines linearen π-konjugierten Polymers durch dieses bichromophore Zinkporphyrin/Perylenbisimid-System zeigte, dass mittels dieser Selbstassoziation eine definierte Ausrichtung π-konjugierter Polymere und somit eine definierte Anordnung von drei unterschiedlichen funktionellen Chromophoren sowohl in Lösung als auch auf Oberflächen möglich ist.

Appendix

A Supplement for Chapter 3

A.1 Single Crystal X-ray Structure of Compound 5d

Additionally, single crystals were available for **5d** by the evaporation method applying a dichloromethane solution and cyclohexane for precipitation. The refinement of the reflection data in the case of **5d** could not be accomplished at a fully satisfactory level.[$] This can be attributed to an extreme disorder of the bridging ethylene glycol units. Furthermore, the crystal seemed to be a twin and also insufficient solid state packing might be responsible for the obtained refinement parameter. However, the connectivites in the molecular structures are reliable.

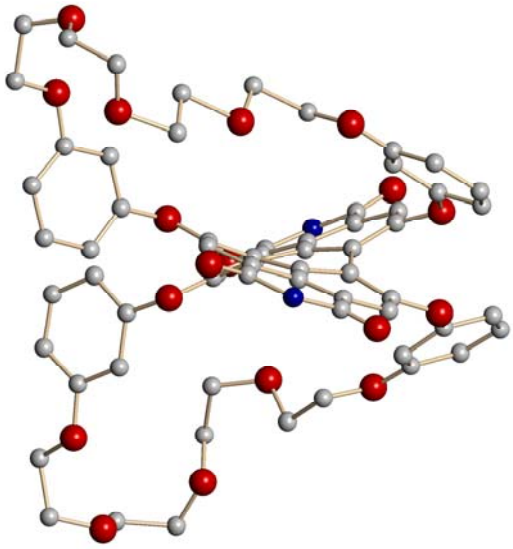

Figure A1. Molecular structure of **5d** ((*M*)-enantiomer). View along the *N,N*-axis of the perylene bisimide showing the twisted nature and the cyclic structure of both macrocycles. Note that in both crystals (*P*)- and (*M*)-enantiomers are present in equal amounts. Hydrogen atoms and the imide substituents as well as co-crystallized solvent molecules were omitted for clarity.

The macrocyclic structure of **5d** is clearly discernible with the bridges lying above and below the perylene core. The twist of the two naphthalene units of the perylene core of **5d** was determined to 34°, and is comparable to that obtained for **5b**. In contrast to **5b**, the increased length of the bridge enables this macrocycle to adopt different conformations of the phenoxy units. As can be seen from the molecular structure in Figure A1, for one bay area of the perylene core of **5d**, the phenoxy residues are arranged in the preferred horizontal orientation with the phenoxy residues being in the

[$] Structure refinement was communicated by Dr. D. Leusser, University of Würzburg, Institute of Inorganic Chemisty.

plane of the perylene core, whereas for the other bay area, the phenoxy-units exhibit a conformation with close contact between the phenoxy substituents and the perylene core. Furthermore, the unequivalence of the two bay areas leads to a symmetry breaking in the solid state which was also observed in the solid state structures of the other macrocyclic perylene bisimides **5b** and **6a**.[A1] The molecular structures of **5b** and **5d** in the solid state reveal that the restriction of the available conformations is strongly dependent on the length of the bridging unit in this type of isomer. Short bridging units as for **5b** enforce a conformational restriction whereas for larger bridging units, e.g. for **5d**, the available conformational space of the phenoxy substituents is significantly increased.

A.2 Solvent Dependet NMR Spectra of 6a

In addition to the different twist angles resulting from the interconversion process, the polarity of the solvent has an influence on the conformational properties of macrocyclic perylene bisimides **5a-d** and **6a-d**. It is well known, that oligoethylene glycol based macrocycles exhibit different conformations dependent on the solvent polarity which enables the high solubility of such macrocycles in a large variety of solvents.[A2] The two major conformations were attributed to the “oxygen-in” conformation for low polarity solvents and “oxygen-out” conformation for highly polar solvents.[A2] Similar behavior was also observed for the present macrocycles. Figure A2 shows sections of the ^{1}H NMR spectra of **6a** in $CDCl_3$, CD_2Cl_2 and DMSO. In $CDCl_3$ and CD_2Cl_2 one singlet was observed for the ethylene glycol protons (at about 4.30 ppm) which presumably results from symmetrical ethylene glycol bridges (Figure A2, top), thus the coupling between the protons was not observable in the NMR spectra. In contrast to chloroform and dichloromethane, two doublets were observed in DMSO which can be attributed to an unsymmetrical conformation which is characteristic for polar solvents. In the case of such small chain lengths as in the case of **6a**, the conformation of the ethylene glycol bridge additionally has a significant influence on the conformation of the aryloxy residues. The position of the aryloxy residues changes slightly from a horizontal orientation to a more perpendicular orientation upon change of the ethylene glycol conformation, as the signal of the proton situated between the two oxygens (dotted red line, Figure A2A) is shifted to lower fields (from 6.41 in chloroform to 6.23 ppm in DMSO). This can be attributed to a change of the conformation of the aryloxy residue, as schematically shown in Figure A2B. However, this conformational effect is only of

significance for macrocyclic perylene bisimides with short bridging units, whereas in the case of larger bridges, i.e for **6b-d**, such conformational effects might be neglected.

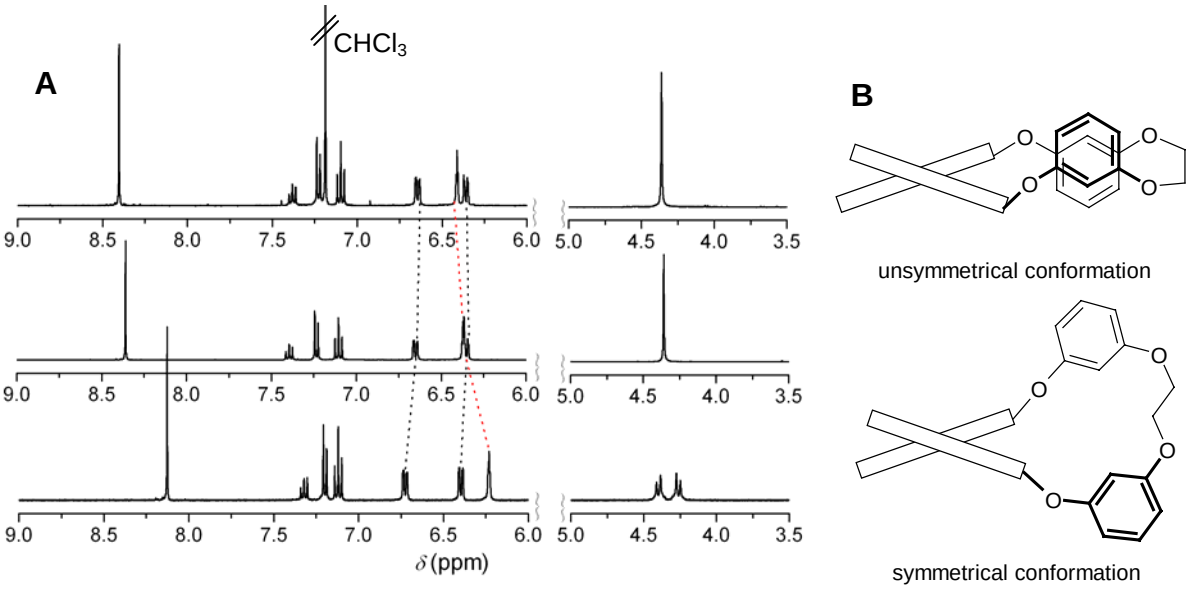

Figure A2. (A) Sections of 400 MHz ^{1}H NMR spectra of **6a** in $CDCl_3$ (top), CD_2Cl_2 (middle) and DMSO-d^6 (bottom). (B) Schematic representation of a symmetrical and unsymmetrical conformation for **6a** (view along the *N*,*N*-axis of the perylene core). The bars represent the naphthalene units of the perylene core and only one bay area is shown for clarity.

A.3 Determination of the Transition Dipole Moments for Diagonally Bridged Macrocycles 5a-d and Reference Compound 4

As can be seen from Figure 13 in Chapter 3, the diagonally bridged macrocycles **5a-d** show reduced molar absorption coefficients for the S_0-S_1 transition in comparison to open-chained perylene bisimide **4**. In order to explain this phenomenon, the first and the second moment of the dipole strength for the S_0-S_1 transitions were determined. The first moment of dipole strength, which corresponds to the transition dipole moment of the S_0-S_1 transition, was calculated for the diagonally bridged macrocycles **5a-d** and reference **4** according to equation A-1. For the determination of this moment, the integral of the reduced absorption spectrum is required. The absorption bands related to the S_0-S_1 transition are superimposed by those related to the S_0-S_2. Peak deconvolution by applying either Lorentzian or Gaussian peak functions did not result in a sufficient separation of the transitions as the S_0-S_2 transition was overestimated.

$$\mu_{eg}^2 = \frac{3hc\varepsilon_0 \ln 10}{2000\pi^2 N_A} \int \frac{\varepsilon}{\tilde{\nu}} d\tilde{\nu} \qquad \text{(eq. A1–1)}$$

Therefore, the fluorescence spectra were mirrored assuming mirror image relation between the absorption and the fluorescence spectra. It is important to note that this approach bears some inaccuracy as the wavelength and intensity of the maximum has to be adjusted to the reduced absorption spectra. The desired integral was than obtained from the integration of the mirrored fluorescence spectra and was corrected by the spectral differences of the absorption and emission spectra (see Figure A3). These corrections are necessary as the mirror image relation is only valid to a certain extent.

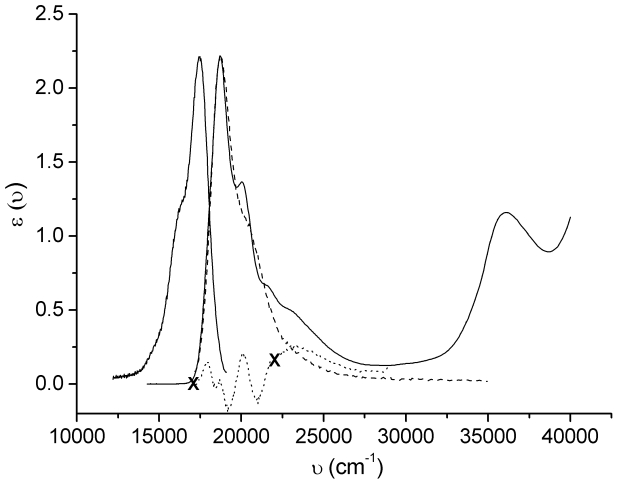

Figure A3. Reduced absorption spectrum and emission spectrum (solid line) of **5b**. The transition dipole moment was calculated from the mirrored fluorescence spectrum (dotted line) and the differential spectrum between absorption and mirrored emission spectrum (dashed line). The crosses mark the integral area used for the correction of the area of the mirrored fluorescence spectrum.

As can be seen from Table A1, the transition dipole moments μ_{eg} for the S_0-S_1 transition are in the order of 7.6-8.0 Debye and are almost similar for all macrocycles **5a-d**. Furthermore, these μ_{eg} values are in good agreement with that determined for the open-chained reference **4** and correspond well to those reported for other PPBI derivatives (6.9-8.0)[A3] revealing a similar strength of this transition for all compounds.

Additionally, the second moment of dipole strength was calculated according to equation A-2.

$$\tilde{\nu}_D = \frac{\int \varepsilon \; d\tilde{\nu}}{\int \frac{\varepsilon}{\tilde{\nu}} \; d\tilde{\nu}} \qquad \text{(eq. A-2)}$$

The required integral of the absorption spectrum was determined from the mirrored fluorescence spectra according to the procedure described before. The second moment of dipole strength is the dipole strength-weighted band center frequency and the

difference to the absorption maximum Δ can be used to describe the asymmetry of an absorption band. Asymmetric absorption bands are obtained when intensity is shifted from the first vibrational progression into the higher vibrational progression of the respective transition. As can be seen from Table A1, the highest "asymmetry" was obtained for **5c**, which exhibits the lowest extinction coefficients within the series of diagonally bridged macrocycles.

Table A1. Absorption Maxima and Transition Dipole Moments μ_{eg}, Second Moment of Dipole Strength υ_D and Difference Δ Between Absorption Maximum $\tilde{\nu}_{\max}$ and $\tilde{\nu}_D$ for Diagonally Bridged Macrocycles **5** and Reference Compound **4** in Dichloromethane

	$\tilde{\nu}_{\max}$ (cm^{-1})	μ_{eg} (Debye)	$\tilde{\nu}_D$ (cm^{-1})	Δ (cm^{-1})
5a	18400	7.7	19800	1430
5b	18700	7.9	20100	1450
5c	18300	7.6	19800	1540
5d	17900	8.0	19300	1360
4	17400	7.8	18700	1260

Thus, the detailed analysis of the absorption spectra for diagonally bridged isomers **5a-d** revealed that the S_0-S_1 transition possesses a similar strength for all diagonally bridged macrocycles. The observed hypochromicity can be attributed to spectral broadening effects and a shift of the intensity into the higher vibrational progressions of the respective transition.

A.4 Estimation of Twist Angle of Macrocycles 5a-d and 6a-d as well as Open-Chained PPBI 4 in Solution by Shape Analysis of the Fluorescence Spectra

To elucidate the twist angle of the perylene bisimide core in solution, the shape of the fluorescence spectra of macrocycles **5a-d** and **6a-d**, and reference compound **4** were analyzed. The shape parameter *S* (eq. A-2) was used which was applied in literature for similar purpose and relates the twist of aromatic systems to the fine structure of the emission band.[A4]

$$S = \frac{2I_v}{I_{P1} + I_{P2}} \qquad \text{(eq. A-2)}$$

where I_{P1} is the intensity of the fluorescence maximum and I_{P2} the intensity of the first vibrational progression and I_V the fluorescence intensity of the valley between the two peaks. Values of S = 1 corresponds to totally unstructured emission bands, whereas a

value of *S* = 0 reflects two baseline separated peaks. For perylene bisimides, large values of *S* were attributed to conformations with large twist angle of the perylene bisimide core and vice versa and the S parameter can thus be used to deduce the twist angle of PPBIs in solution.[A4b] The obtained parameter S for all macrocycles are summarized in Table A2.

Table A2. *S* Parameter for the Fluorescence Spectra of Macrocycles **5a-d** and **6a-d** and Reference Compound **4**

	4	**5a**	**5b**	**5c**	**5d**	**6a**	**6b**	**6c**	**6d**
S	0.69	0.89	0.75	0.76	0.76	0.83	0.69	0.69	0.69

It is worth noting, that the determination of the fluorescence intensities, especially of unstructured emission bands, is somehow arbitrary as the peaks are not well resolved. Nevertheless, the values obtained for the macrocycles **5** show that the macrocycles **5b-d** possess similar twist angles of the perylene core in solution and that these angles are larger in comparison to open-chained PPBI **4**. Furthermore, these results suggest that the macrocycle **5a** possesses a larger twist of the perylene core in solution than the other diagonally bridged macrocycles **5b-d**. For validation of this concept, the observed *S* parameter for laterally bridged macrocycles **6** were determined and a perfect agreement with those observed for **4** was found. Macrocycle **6a** takes an exceptional position and the *S* parameter obtained for **6a** is even larger than those observed for diagonally bridged macrocycles **5b-d**. This suggests that macrocycle **6a** exhibits a larger twist angle in solution than that observed in the solid state. As similar twist angles are present in the series of diagonally bridged macrocycles **5**, different conformations of the phenoxy-residues have to be responsible for the observed differences in absorption and emission.

A.5 Spectroelectrochemical Measurement for Diagonal Isomer 5b

In order to assign the observed reduction properties, spectroelectrochemistry[#] was performed for **5b** as a representative example and the absorption spectra obtained upon stepwise reduction of the negative potential are shown in Figure A4. Upon subsequent decrease of the applied potential, the S_0-S_1 absorption band of **5b** at 535 nm is gradually reduced and completely disappeared at a potential of –0.9 V. Simultaneously, a new intense band at 770 nm and two less intense bands at 930 and

[#] Spectroelectrochemical measurements were performed by D. Novak at the group of Prof. Lambert at the Institute of Organic Chemistry, University of Würzburg (Germany).

1030 nm arose. The observed spectral changes are characteristic for the formation of radical anions of perylene bisimides dyes,[A5] thus, the first reduction wave observed by cyclovoltammetry can be clearly assigned to the reduction of the perylene bisimide core.

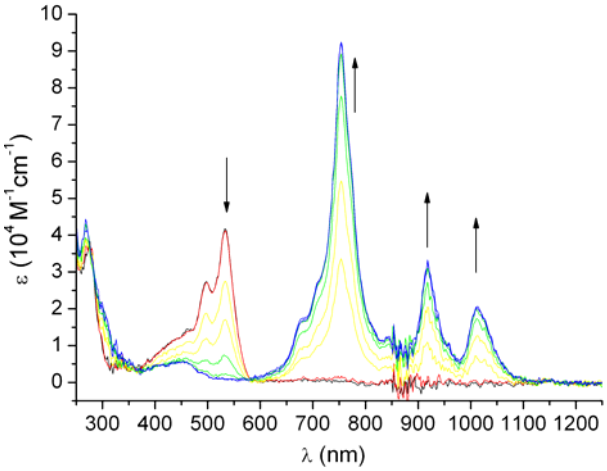

Figure A4. Spectroelectrogram of **5b** in dichloromethane (0.1M TBAHFP) by applying different potentials. The arrows indicates the spectral changes upon decreasing the applied voltage from 0 V (black line) to -0.90 V (blue line).

Experimental Details for Spectroelectochemistry. Spectroelectrochemical measurements were carried out on a Jasco V-570 UV/Vis/NIR spectrometer with a special mirror optical accessory. A cylindrical glass cell was used as cuvette. The absorption spectra were recorded by reflection on the working electrode and referred to the solvent/electrolyte spectra. The stepwise application of negative potentials was realized with a electrochemical work station (BAS CV-50 W). The solvent and the electrolyte were dried as described in the section cyclic voltammetry in Chapter 3 and all measurements were carried out under argon and exclusion of moisture. Working electrode: Pt disc; reference electrode: Ag/AgCl; auxiliary electrode: gold covered nickelated V2A disk.

A.6 AM1 Optimized Structures for Diagonally Bridged Isomers 5a-d

All structures of macrocyclic perylene bisimides **5a-d** were optimized by semiempirical AM1 caclualtions using CaChe Quantum CaChe Workspace 5.0

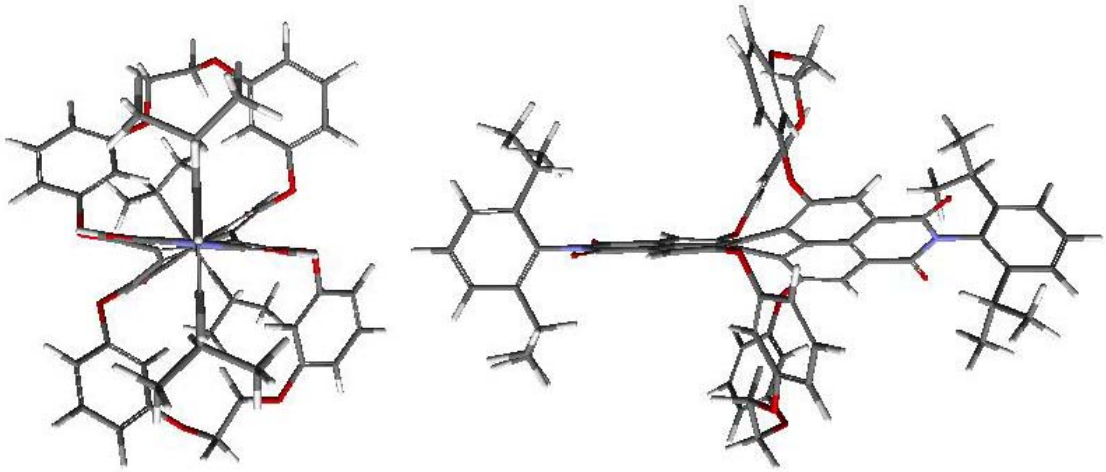

Figure A5. View along the *N*,*N*-axis of the perylene bisimide (left) and side view (right) of the optimized structures for macrocyclic perylene bisimides **5a**.

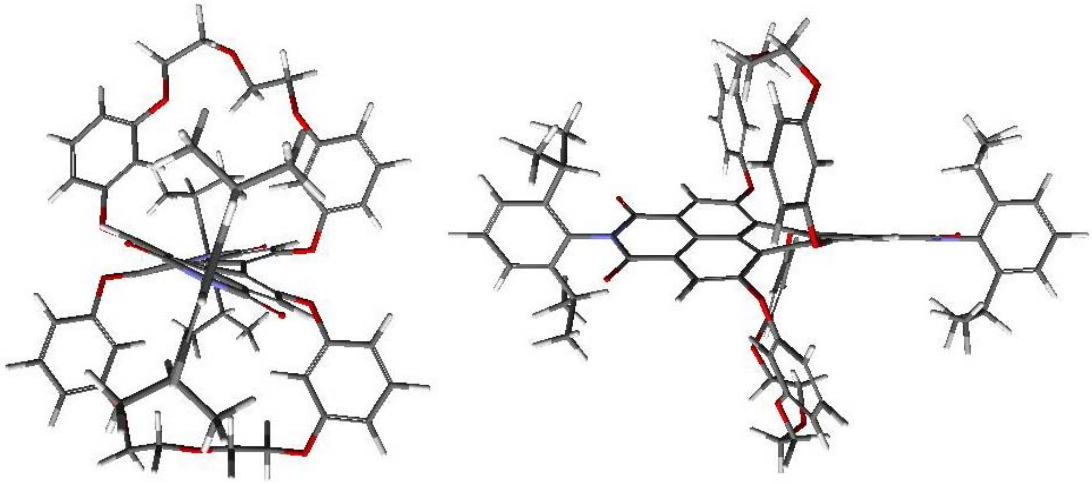

Figure A6. View along the *N*,*N*-axis of the perylene bisimide (left) and side view (right) of the optimized structures for macrocyclic perylene bisimides **5b**.

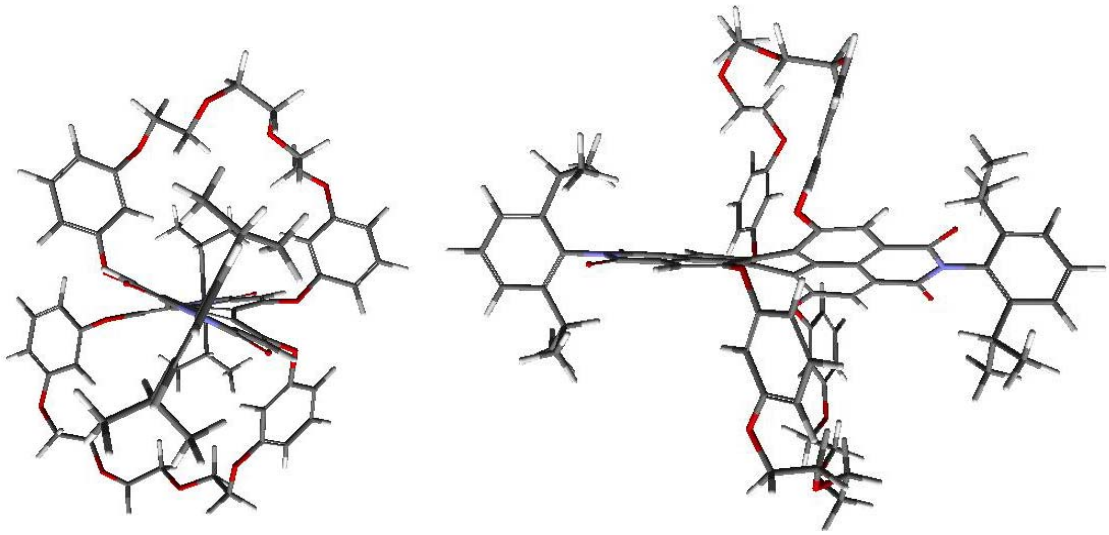

Figure A7. View along the *N*,*N*-axis of the perylene bisimide (left) and side view (right) of the optimized structures for macrocyclic perylene bisimides **5c**.

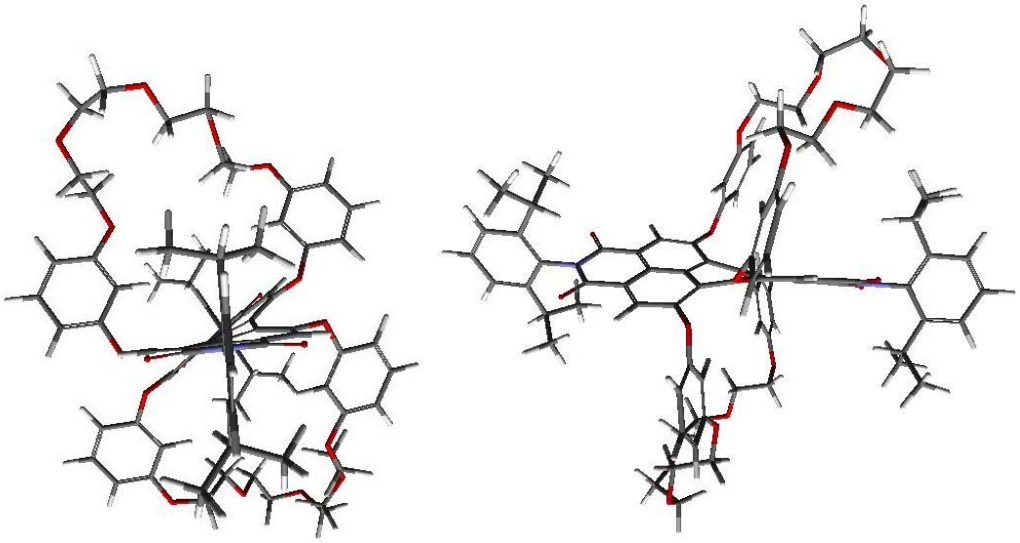

Figure A8. View along the *N*,*N*-axis of the perylene bisimide (left) and side view (right) of the optimized structures for macrocyclic perylene bisimides **5d**.

A.7 Temperature-Dependent ^{1}H NMR Spectra of 6a, 6b and 6d.

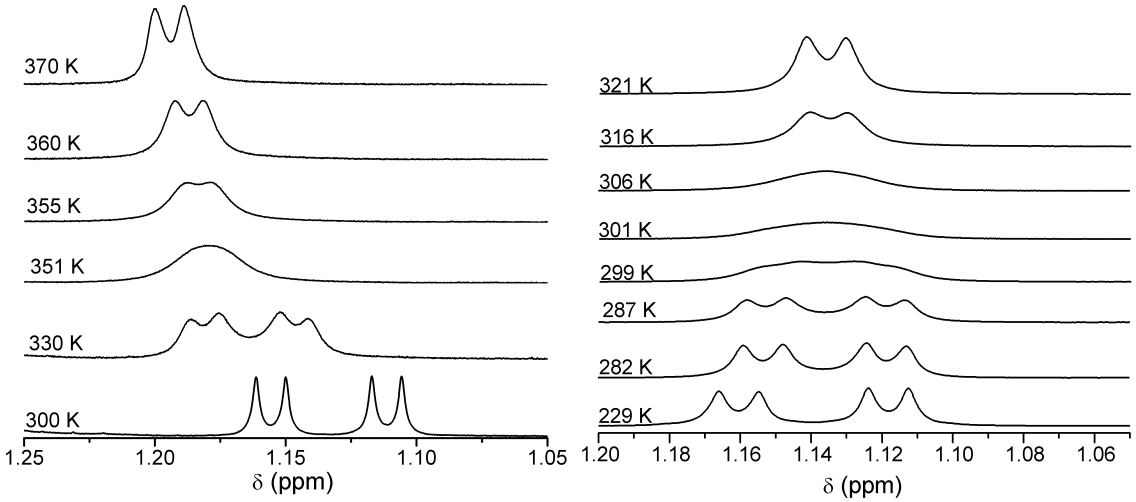

Figure A9. Section of the temperature dependent ^{1}H NMR spectra of **6a** (left) and **6b** (right). Shown are the resonances of the methyl groups of diastereotopic isopropyl groups situated at the imide substituent

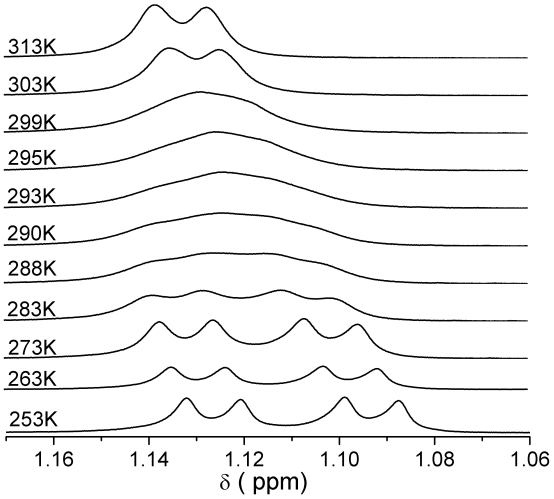

Figure A10. Section of the temperature dependent ^{1}H NMR spectra of **6d**. Shown are the resonances of the methyl groups of diastereotopic isopropyl groups situated at the imide substituents.

A.8 ^{1}H NMR Spectra of Macrocycles 5a-d and 6a-d

^{1}H NMR spectrum (400 MHz) of **5a** in CD_2Cl_2

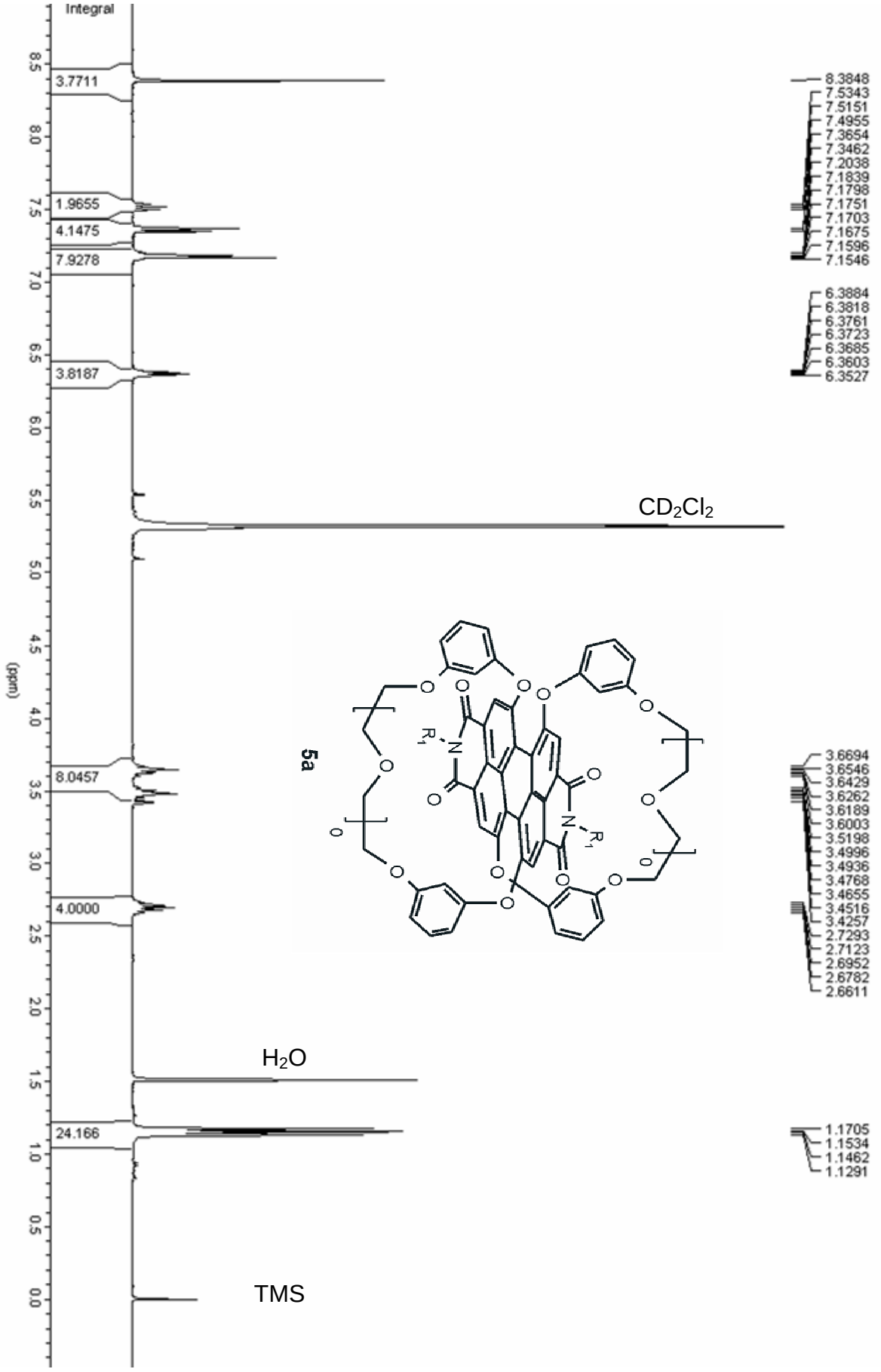

^{1}H NMR spectrum (400 MHz) of **6a** in CD_2Cl_2

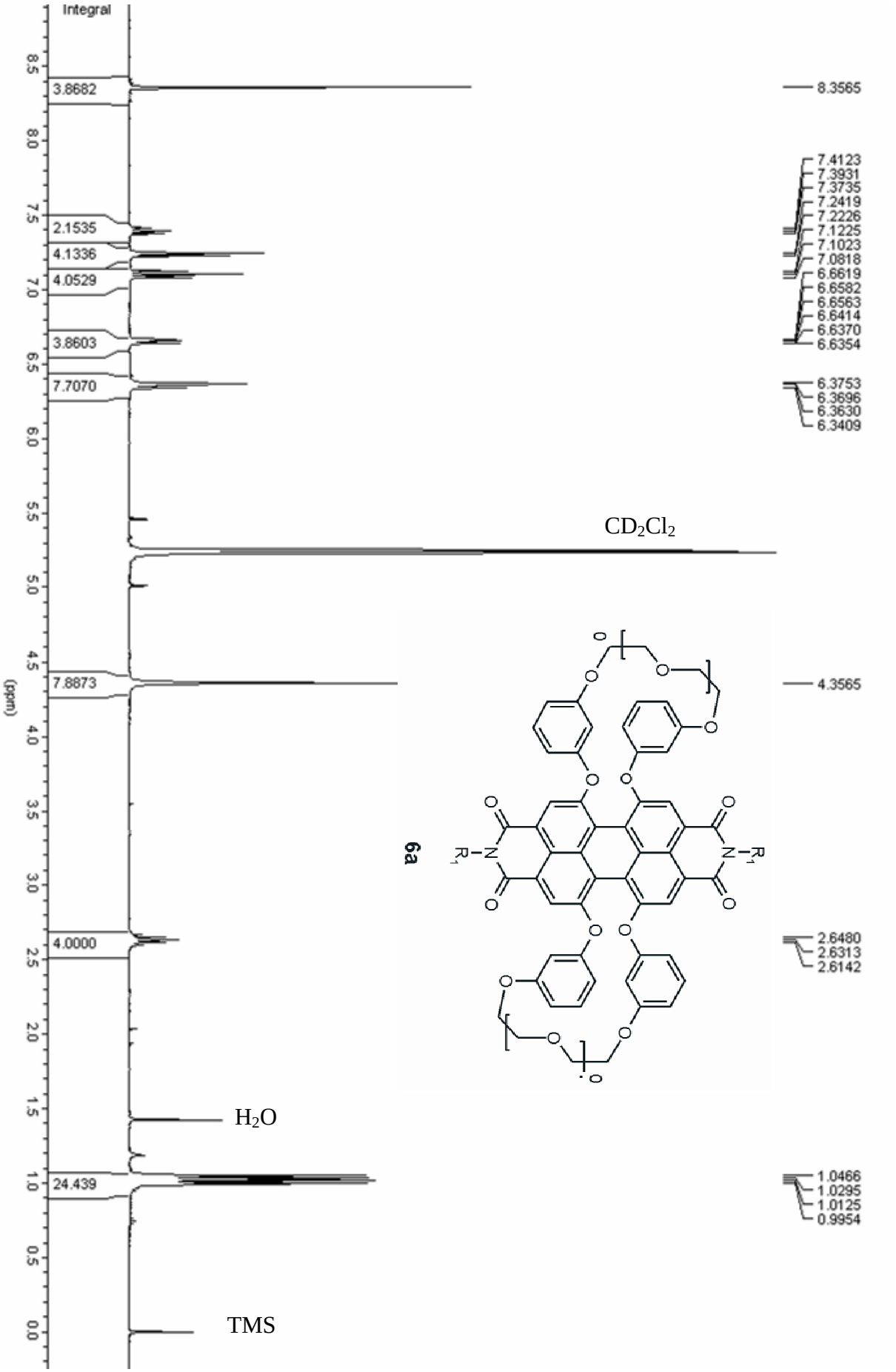

^{1}H NMR (400 MHz) of **5b** in CD_2Cl_2

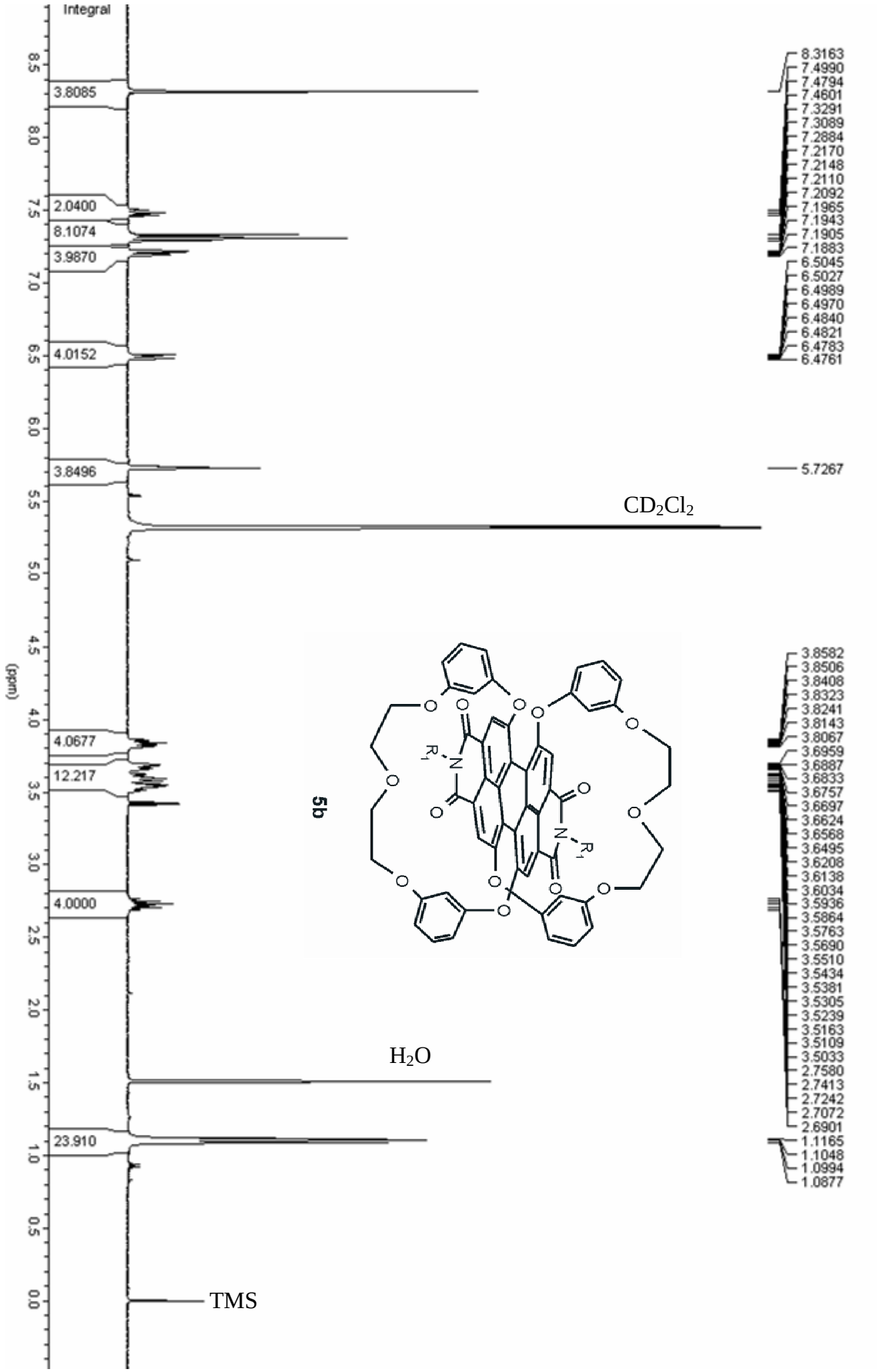

^{1}H NMR spectrum (400 MHz) of **6b** in $CDCl_3$

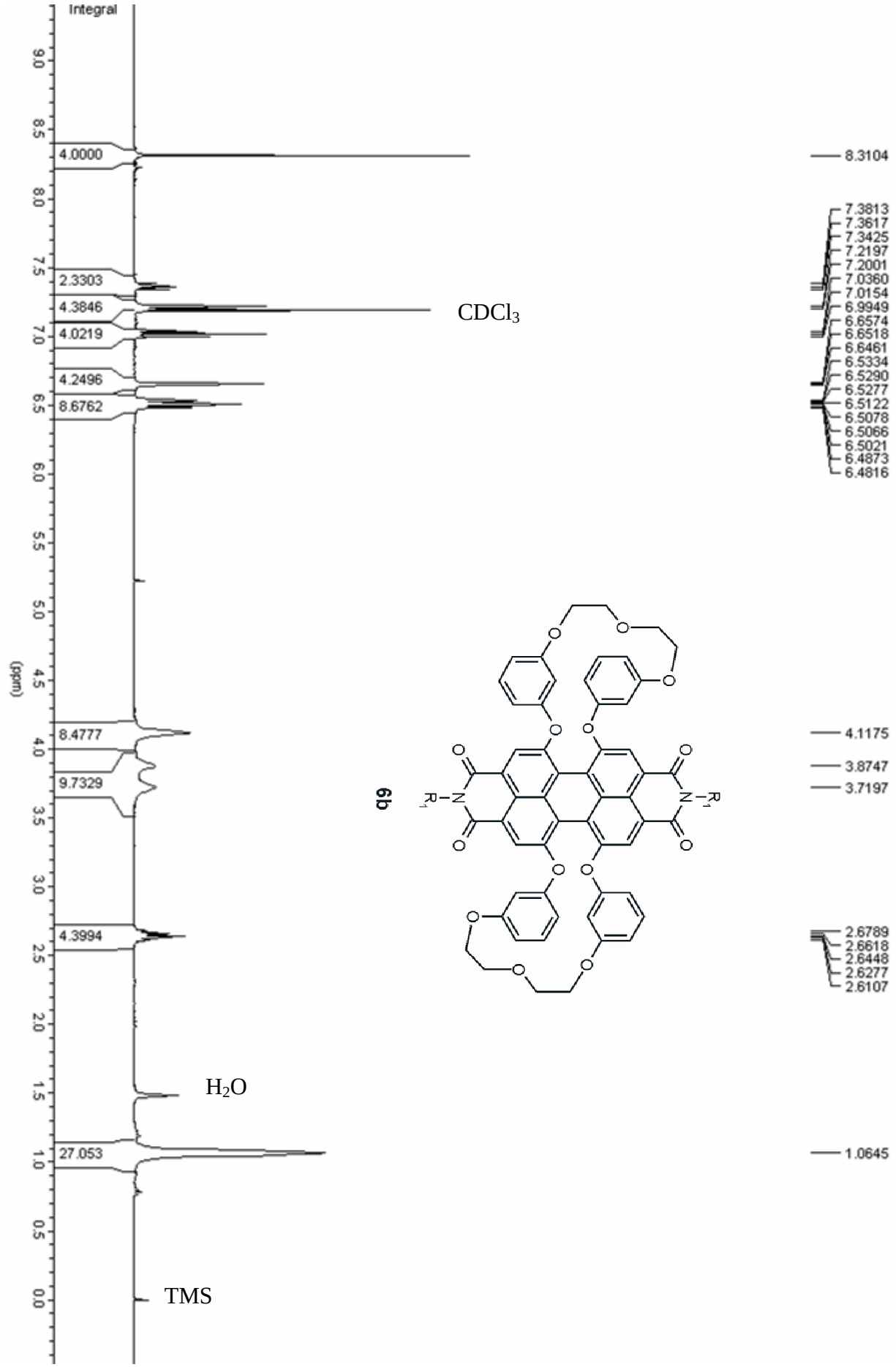

^{1}H NMR spectrum (400 MHz) of **5c** in CD_2Cl_2

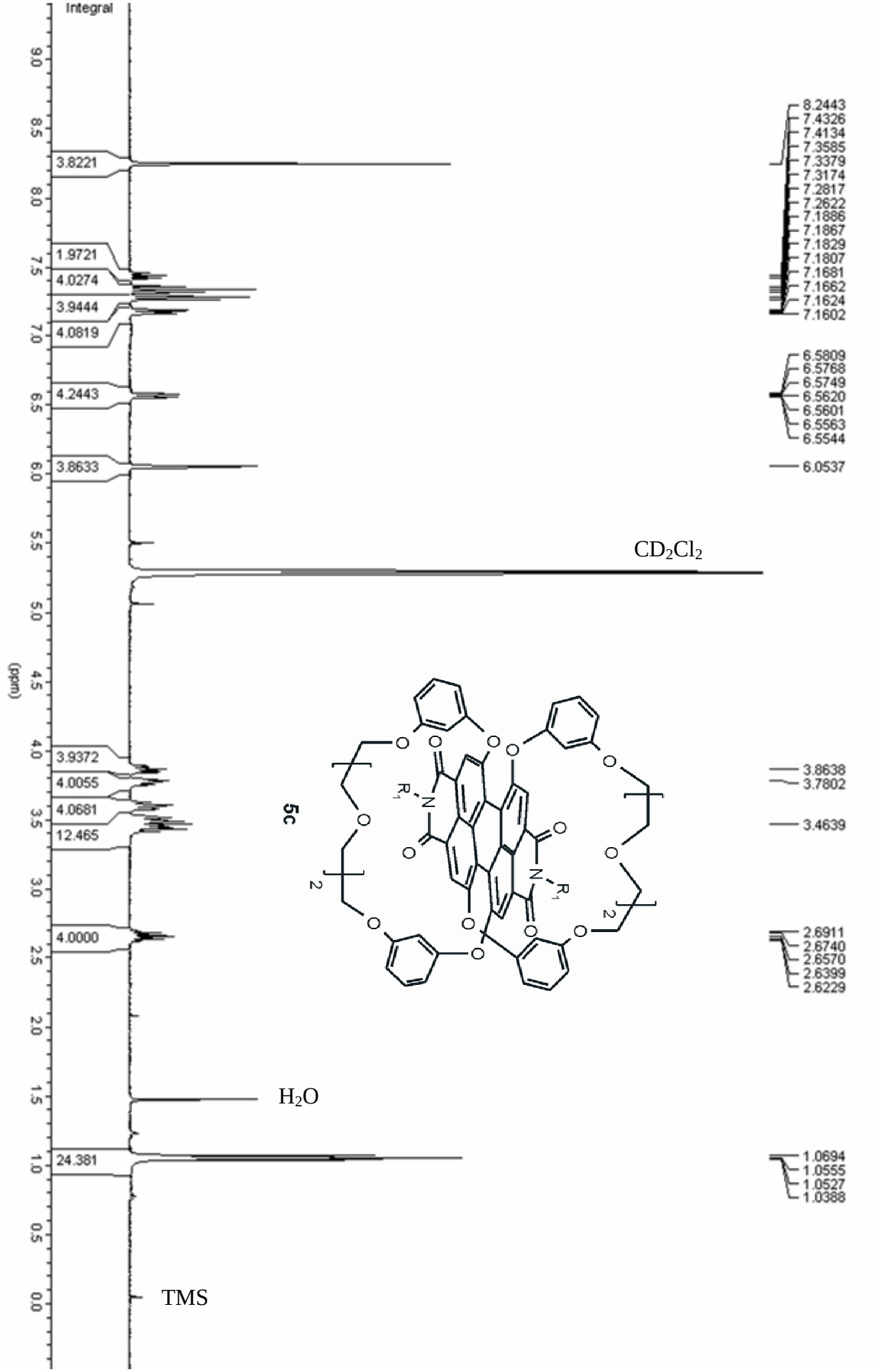

^{1}H NMR spectrum (400 MHz) of **6c** in CD_2Cl_2

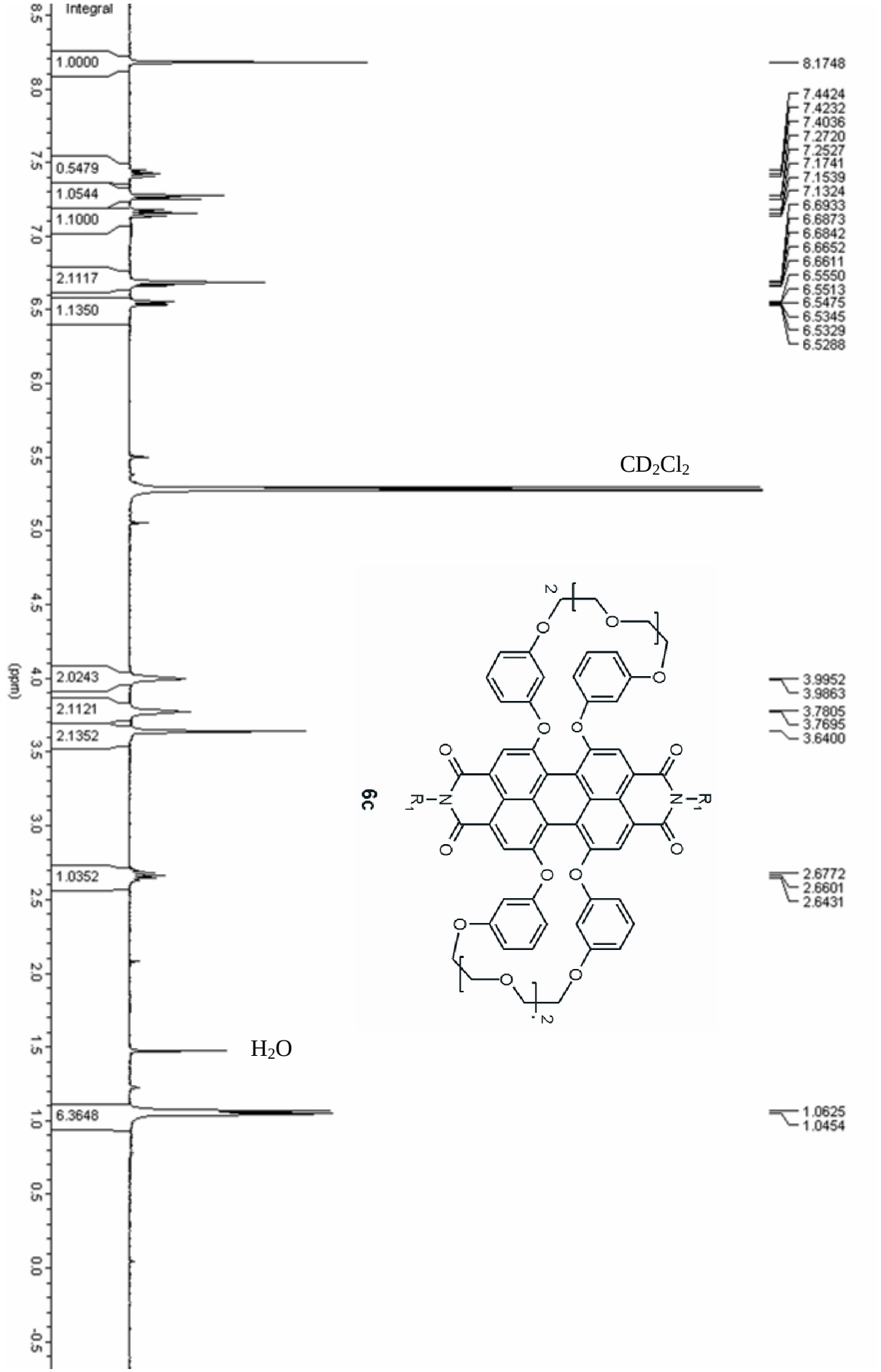

^{1}H NMR spectrum (400 MHz) of **5d** in $CDCl_3$

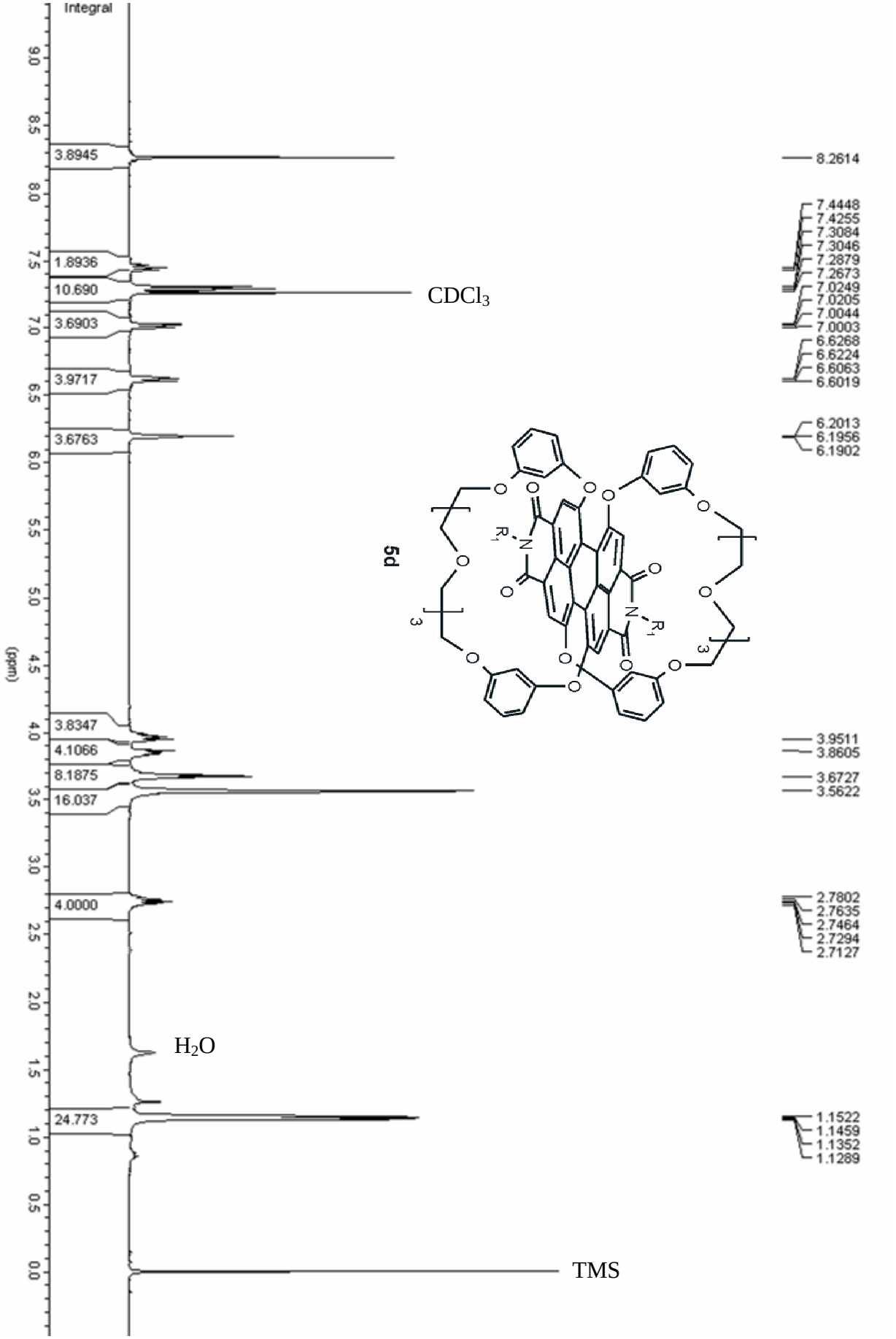

^{1}H NMR spectrum (400 MHz) of **6d** in $CDCl_3$

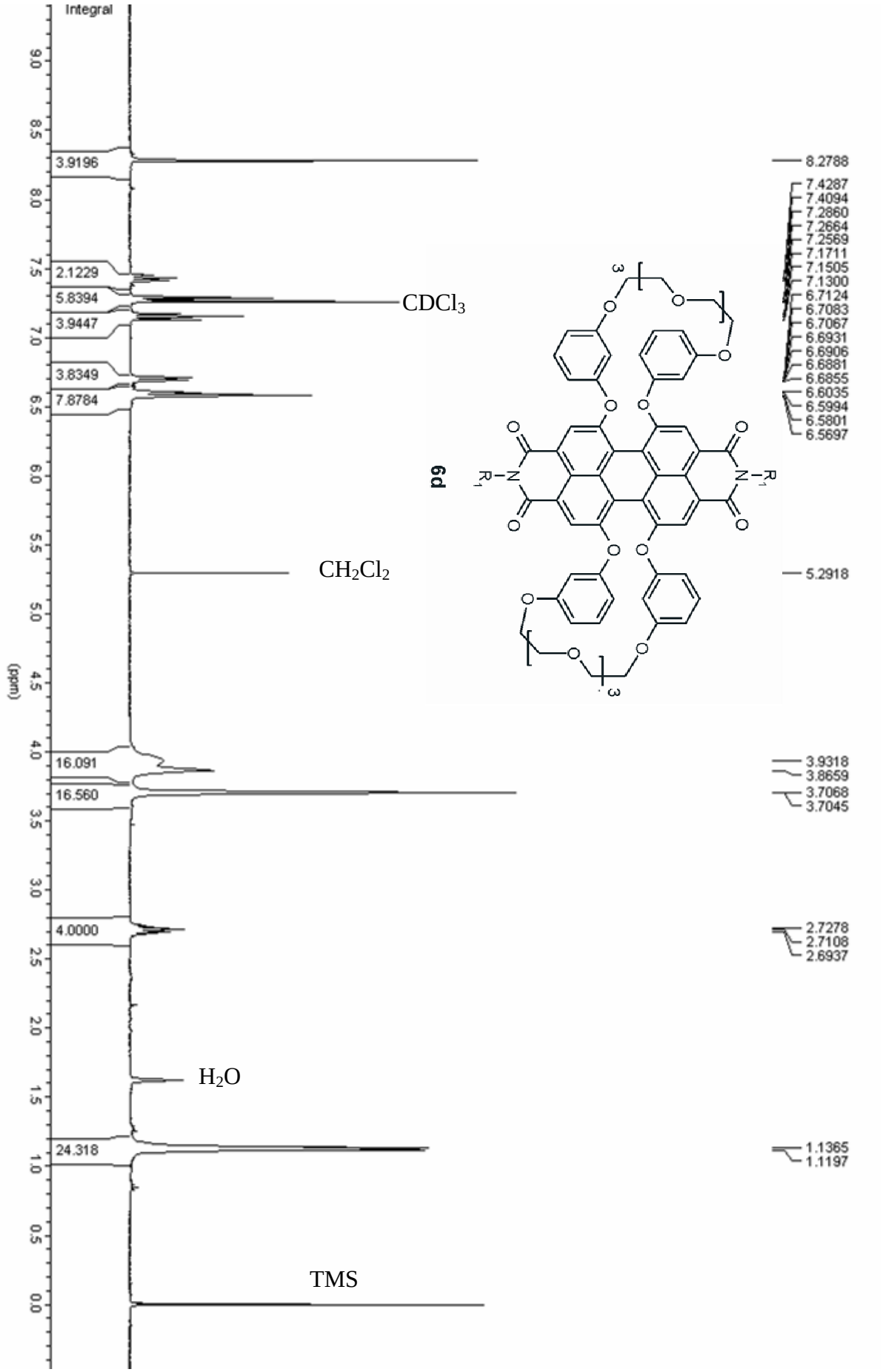

A.9 Detailed Crystallographic Data for the Crystal Structures of Compounds 5b and 6a.

A.9.1 X-Ray structure determination for 5b and 6a

All data were collected from shock-cooled crystals on a BRUKER SMART-APEX diffractometer with D8 goniometer (graphite-monochromated Mo-Kα radiation, λ = 71.073 pm) equipped with a low temperature device at 100(2) K.[A6] An empirical absorption correction was employed.[A7] The structures were solved by direct methods (SHELXS-97[A8]) and refined by full-matrix least squares methods against F^2 (SHELXL-97[A9]). R values: $R1 = \Sigma||F_o|-|F_c||/\Sigma|F_o|$, $wR2 = [\Sigma w(F_o^2-F_c^2)^2/\Sigma w(F_o^2)^2]^{0.5}$, $w = [\sigma^2(F_o^2)+(g_1P)^2+g_2P]^{-1}$, $P = 1/3[\max(F_o^2,0)+2F_c^2]$.

5b: All non-hydrogen atoms were refined with anisotropic displacement parameters. The hydrogen atoms were assigned ideal positions and refined isotropically using a riding model with U_{iso} constrained to 1.2 times the U_{eq} of the parent atom for hydrogen atoms bonded to C(sp^2) and 1.5 times the U_{eq} for hydrogen atoms bonded to C(sp^3), respectively. One of the $O(CH_2)_2O(CH_2)_2O$ chains, connecting the phenoxy residues is disordered. The site occupation factors refined to split occupancies of 0.6/0.4. A cocrystallized solvent molecule CH_2Cl_2 was refined to an site occupancy of 0.66 using distance and similarity restraints.

6a: All non-hydrogen atoms were refined with anisotropic displacement parameters. The hydrogen atoms were assigned ideal positions and refined isotropically using a riding model with U_{iso} constrained to 1.2 times the U_{eq} of the parent atom for hydrogen atoms bonded to C(sp^2) and 1.5 times the U_{eq} for hydrogen atoms bonded to C(sp^3), respectively. The structure was refined as racemic twin using the TWIN-command in SHELXL. The corresponding BASF-parameter refined to 0.38. Besides the $C_{76}H_{62}N_2O_{12}$ unit, the asymmetric unit contains four CH_2Cl_2 solvent molecules, of which three were disordered. One CH_2Cl_2 could not be refined satisfactory. Therefore the program SQUEEZE implemented in PLATON[A10] was used to remove the contributions to the data from this solvent molecule. The structure reported here was refined against the corrected data. The two remaining disordered CH_2Cl_2 molecules were refined using distance and similarity restraints. The site occupation factors were determined to split occupancies of 0.70/0.30 and 0.61/0.39, respectively. The remaining solvent molecule CH_2Cl_2, which showed no signs for a disorder was refined to a site occupancy of 0.58.

Crystallographic data (excluding structure factors) for the structures reported in this chapter have been deposited with the Cambridge Crystallographic Data Centre as

supplementary publication no. CCDC-246746 and no. CCDC-246747. Copies of the data can be obtained free of charge on application to CCDC, 12 Union Road, Cambridge CB2 1EZ, UK [fax: (internat.) + 44(1223)336-033; e-mail: deposit@ccdc.cam.ac.uk].

A.9.2 Crystal Structure of 5b.

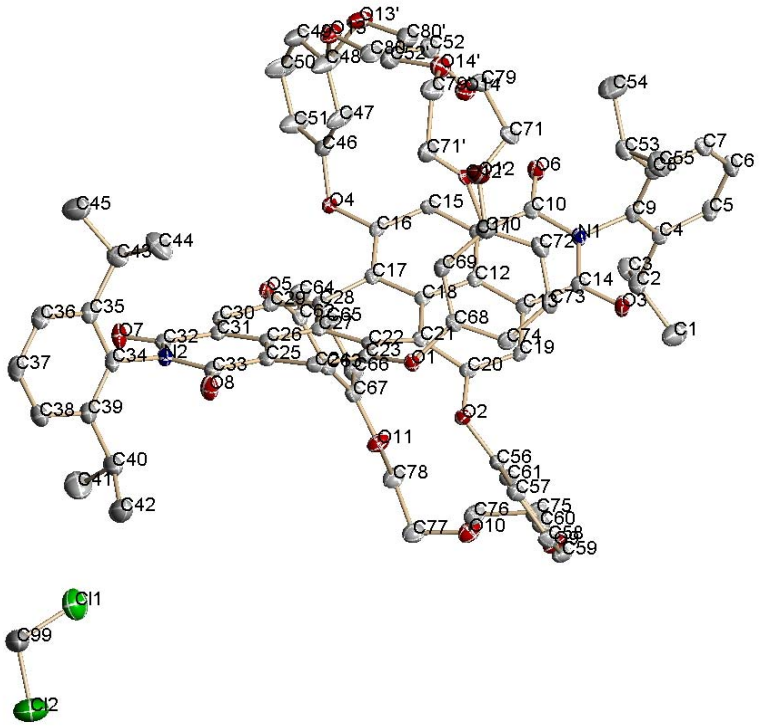

Figure A11. Fully labelled diagram of **5b** ($C_{80}H_{70}N_2O_{14}$ $(CH_2Cl_2)_{0.66}$). Anisotropic displacement parameters are depicted on 50% probability level. Hydrogen atoms are omitted for clarity.

Table A3. Crystal Data and Structure Refinement for **5b**

Empirical formula	$C_{80}H_{70}N_2O_{14}$ $(CH_2Cl_2)_{0.66}$	
Formula weight	1339.43	
Temperature	100(2) K	
Wavelength	0.71073 Å	
Crystal system	Triclinic	
Space group	P-1	
Unit cell dimensions	a = 13.323(4) Å	α= 104.746(5)°.
	b = 16.752(6) Å	β= 100.069(6)°.
	c = 17.226(6) Å	γ = 106.408(5)°.
Volume	3438(2) $Å^3$	
Z	2	
Density (calculated)	1.294 Mg/m^3	
Absorption coefficient	0.137 mm^{-1}	
F(000)	1407	
Crystal size	0.4 x 0.2 x 0.02 mm^3	

Theta range for data collection	2.57 to 26.08°.
Index ranges	-16<=h<=15, -20<=k<=20, 0<=l<=21
Reflections collected	71904
Independent reflections	13543 [R(int) = 0.0322]
Completeness to theta = 26.08°	99.2 %
Absorption correction	Empirical
Max. and min. transmission	0.9187 and 0.99
Refinement method	Full-matrix least-squares on F^2
Data / restraints / parameters	13543 / 1002 / 966
Goodness-of-fit on F^2	1.038
Final R indices [I>2sigma(I)]	R1 = 0.0469, wR2 = 0.1084
R indices (all data)	R1 = 0.0596, wR2 = 0.1147
Largest diff. peak and hole	0.607 and -0.335 e.$Å^{-3}$

Table A4. Atomic Coordinates (x 10^4) and Equivalent Isotropic Displacement Parameters ($Å^2$x 10^3) for **5b**. U(eq) is defined as One Third of the Trace of the Orthogonalized U^{ij} Tensor.

x	y	z	U(eq)	
Cl(1)	1531(1)	8850(1)	3986(1)	50(1)
Cl(2)	77(1)	9771(1)	3591(1)	76(1)
C(99)	1153(4)	9753(3)	4311(3)	81(2)
O(1)	4475(1)	3585(1)	2183(1)	18(1)
O(2)	4745(1)	3409(1)	675(1)	18(1)
O(3)	6341(1)	1002(1)	-304(1)	27(1)
O(4)	10333(1)	5200(1)	3056(1)	21(1)
O(5)	9976(1)	6526(1)	2743(1)	19(1)
O(6)	9863(1)	2142(1)	1253(1)	26(1)
O(7)	8285(1)	8280(1)	4560(1)	28(1)
O(8)	4828(1)	6487(1)	4123(1)	28(1)
N(1)	8087(1)	1562(1)	501(1)	18(1)
N(2)	6589(1)	7352(1)	4396(1)	20(1)
C(1)	7711(2)	944(1)	-1906(1)	37(1)
C(2)	8604(1)	1311(1)	-1088(1)	23(1)
C(3)	9721(2)	1635(1)	-1235(1)	31(1)
C(4)	8539(1)	639(1)	-638(1)	20(1)
C(5)	8750(1)	-127(1)	-972(1)	23(1)
C(6)	8691(1)	-744(1)	-568(1)	25(1)
C(7)	8382(1)	-623(1)	165(1)	24(1)
C(8)	8151(1)	128(1)	525(1)	22(1)
C(9)	8259(1)	749(1)	115(1)	19(1)
C(10)	8983(1)	2233(1)	1092(1)	19(1)
C(11)	8794(1)	3047(1)	1506(1)	17(1)
C(12)	7762(1)	3120(1)	1286(1)	16(1)
C(13)	6896(1)	2439(1)	657(1)	17(1)
C(14)	7050(1)	1610(1)	236(1)	19(1)
C(15)	9625(1)	3723(1)	2120(1)	17(1)
C(16)	9472(1)	4513(1)	2492(1)	16(1)
C(17)	8472(1)	4628(1)	2278(1)	16(1)
C(18)	7584(1)	3884(1)	1719(1)	15(1)
C(19)	5907(1)	2538(1)	431(1)	17(1)

C(20)	5721(1)	3284(1)	885(1)	16(1)
C(21)	6500(1)	3895(1)	1594(1)	16(1)
C(22)	6287(1)	4526(1)	2244(1)	16(1)
C(23)	5320(1)	4375(1)	2487(1)	17(1)
C(24)	5140(1)	5044(1)	3061(1)	18(1)
C(25)	5929(1)	5859(1)	3409(1)	18(1)
C(26)	6957(1)	6013(1)	3248(1)	17(1)
C(27)	7163(1)	5326(1)	2704(1)	16(1)
C(28)	8244(1)	5436(1)	2624(1)	16(1)
C(29)	8973(1)	6294(1)	2902(1)	18(1)
C(30)	8752(1)	6987(1)	3407(1)	18(1)
C(31)	7785(1)	6842(1)	3618(1)	18(1)
C(32)	7601(1)	7557(1)	4221(1)	20(1)
C(33)	5710(1)	6569(1)	3990(1)	21(1)
C(34)	6411(1)	8006(1)	5043(1)	23(1)
C(35)	6770(1)	8045(1)	5866(1)	24(1)
C(36)	6544(2)	8646(1)	6475(1)	29(1)
C(37)	5995(2)	9176(1)	6264(1)	31(1)
C(38)	5659(2)	9125(1)	5448(1)	31(1)
C(39)	5858(2)	8536(1)	4811(1)	27(1)
C(40)	5485(2)	8493(1)	3916(1)	36(1)
C(41)	6183(2)	9295(2)	3768(2)	54(1)
C(42)	4275(2)	8372(2)	3659(1)	52(1)
C(43)	7349(2)	7440(1)	6095(1)	31(1)
C(44)	6525(2)	6584(1)	6076(2)	45(1)
C(45)	8194(2)	7868(2)	6930(1)	52(1)
C(46)	10988(1)	5060(1)	3693(1)	19(1)
C(47)	10547(2)	4490(1)	4089(1)	34(1)
C(49)	12305(2)	4962(1)	5059(1)	34(1)
C(50)	12715(2)	5517(2)	4649(1)	39(1)
C(51)	12066(2)	5568(1)	3953(1)	35(1)
C(53)	7776(2)	232(1)	1316(1)	27(1)
C(54)	8595(2)	169(2)	2020(1)	45(1)
C(55)	6648(2)	-441(1)	1152(1)	36(1)
C(56)	4202(1)	3141(1)	-164(1)	18(1)
C(57)	3081(1)	2790(1)	-376(1)	21(1)
C(58)	2521(1)	2546(1)	-1208(1)	24(1)
C(59)	3060(1)	2648(1)	-1806(1)	25(1)
C(61)	4769(1)	3281(1)	-748(1)	20(1)
C(62)	10055(1)	6330(1)	1928(1)	19(1)
C(63)	9183(1)	6086(1)	1244(1)	19(1)
C(64)	11106(1)	6460(1)	1848(1)	25(1)
C(65)	11267(1)	6359(1)	1064(1)	28(1)
C(66)	10415(1)	6133(1)	366(1)	24(1)
C(68)	4700(1)	2814(1)	2156(1)	17(1)
C(69)	5541(1)	2804(1)	2745(1)	24(1)
C(70)	5717(2)	2017(1)	2687(1)	28(1)
C(72)	5066(1)	1253(1)	2042(1)	25(1)
C(73)	4209(1)	1279(1)	1477(1)	23(1)
C(74)	4011(1)	2059(1)	1531(1)	21(1)
C(60)	4188(1)	3030(1)	-1575(1)	21(1)
O(9)	4653(1)	3136(1)	-2203(1)	26(1)

C(75)	5815(1)	3466(1)	-2009(1)	26(1)
C(76)	6326(1)	4441(1)	-1505(1)	25(1)
O(10)	7000(1)	4831(1)	-1953(1)	28(1)
C(77)	7598(2)	5737(1)	-1543(1)	27(1)
C(78)	8661(1)	5901(1)	-942(1)	25(1)
O(11)	8469(1)	5782(1)	-178(1)	24(1)
C(67)	9372(1)	5998(1)	461(1)	21(1)
C(48)	11218(2)	4449(2)	4781(1)	48(1)
O(13)	10770(2)	4046(2)	5324(1)	27(1)
C(80)	9721(3)	3369(2)	4984(2)	26(1)
C(52)	9779(3)	2587(3)	4320(3)	28(1)
O(14)	8796(2)	2146(1)	3686(1)	27(1)
C(79)	7949(2)	1642(2)	3942(2)	27(1)
C(71)	6911(2)	1358(2)	3272(2)	26(1)
O(12)	6409(5)	1906(3)	3287(4)	48(1)
O(13')	11094(3)	3667(3)	5032(2)	34(1)
C(80')	10139(5)	2901(4)	4606(4)	31(1)
C(52')	9170(5)	2986(4)	4890(3)	33(1)
O(14')	8343(3)	2166(2)	4503(2)	33(1)
C(79')	7346(4)	2149(3)	4676(3)	33(1)
C(71')	6697(4)	2480(3)	4109(3)	32(1)
O(12')	6691(6)	2172(4)	3286(6)	22(1)

Table A5. Anisotropic Displacement Parameters ($Å^2x10^3$) for **5b**. The Anisotropic Displacement Factor Exponent takes the Form: $-2\pi^2[h^2 a^{*2}U^{11} + ... + 2 h k a^* b^* U^{12}]$

	U^{11}	U^{22}	U^{33}	U^{23}	U^{13}	U^{12}
Cl(1)	53(1)	37(1)	58(1)	13(1)	18(1)	10(1)
Cl(2)	87(1)	81(1)	59(1)	27(1)	-10(1)	39(1)
C(99)	124(4)	52(2)	48(2)	-6(2)	-31(2)	53(3)
O(1)	18(1)	16(1)	20(1)	3(1)	5(1)	6(1)
O(2)	18(1)	21(1)	16(1)	3(1)	3(1)	10(1)
O(3)	21(1)	20(1)	30(1)	-5(1)	-1(1)	8(1)
O(4)	20(1)	16(1)	21(1)	3(1)	-2(1)	5(1)
O(5)	18(1)	17(1)	18(1)	4(1)	3(1)	4(1)
O(6)	19(1)	22(1)	31(1)	0(1)	2(1)	11(1)
O(7)	32(1)	16(1)	28(1)	0(1)	10(1)	5(1)
O(8)	26(1)	25(1)	31(1)	0(1)	12(1)	11(1)
N(1)	19(1)	15(1)	20(1)	1(1)	5(1)	8(1)
N(2)	26(1)	17(1)	17(1)	2(1)	5(1)	11(1)
C(1)	35(1)	38(1)	33(1)	13(1)	2(1)	7(1)
C(2)	25(1)	20(1)	24(1)	3(1)	8(1)	9(1)
C(3)	32(1)	27(1)	40(1)	13(1)	15(1)	10(1)
C(4)	15(1)	17(1)	24(1)	2(1)	2(1)	4(1)
C(5)	19(1)	20(1)	25(1)	-1(1)	6(1)	6(1)
C(6)	18(1)	16(1)	35(1)	0(1)	3(1)	7(1)
C(7)	20(1)	16(1)	33(1)	7(1)	2(1)	6(1)
C(8)	17(1)	19(1)	24(1)	4(1)	2(1)	5(1)
C(9)	15(1)	15(1)	22(1)	0(1)	1(1)	6(1)
C(10)	19(1)	18(1)	19(1)	4(1)	5(1)	7(1)
C(11)	20(1)	16(1)	17(1)	5(1)	6(1)	7(1)
C(12)	19(1)	15(1)	14(1)	5(1)	5(1)	6(1)
C(13)	19(1)	16(1)	16(1)	4(1)	6(1)	7(1)
C(14)	19(1)	18(1)	19(1)	3(1)	4(1)	7(1)
C(15)	15(1)	20(1)	17(1)	7(1)	4(1)	8(1)
C(16)	18(1)	15(1)	14(1)	5(1)	4(1)	4(1)
C(17)	20(1)	16(1)	13(1)	5(1)	5(1)	6(1)
C(18)	19(1)	16(1)	13(1)	6(1)	5(1)	7(1)
C(19)	18(1)	17(1)	13(1)	3(1)	2(1)	4(1)
C(20)	16(1)	18(1)	17(1)	7(1)	6(1)	8(1)
C(21)	19(1)	14(1)	16(1)	7(1)	6(1)	6(1)
C(22)	20(1)	15(1)	14(1)	5(1)	3(1)	8(1)
C(23)	19(1)	16(1)	15(1)	5(1)	1(1)	7(1)
C(24)	19(1)	21(1)	16(1)	6(1)	6(1)	9(1)
C(25)	24(1)	19(1)	14(1)	6(1)	4(1)	12(1)
C(26)	23(1)	16(1)	14(1)	5(1)	3(1)	9(1)
C(27)	21(1)	17(1)	13(1)	7(1)	4(1)	9(1)
C(28)	20(1)	17(1)	11(1)	5(1)	2(1)	8(1)
C(29)	18(1)	19(1)	15(1)	6(1)	2(1)	6(1)
C(30)	23(1)	13(1)	15(1)	4(1)	0(1)	5(1)
C(31)	24(1)	17(1)	14(1)	5(1)	3(1)	10(1)
C(32)	27(1)	17(1)	16(1)	4(1)	3(1)	9(1)
C(33)	25(1)	20(1)	17(1)	4(1)	4(1)	10(1)
C(34)	26(1)	18(1)	21(1)	0(1)	7(1)	8(1)
C(35)	26(1)	21(1)	24(1)	4(1)	8(1)	7(1)

C(36)	33(1)	28(1)	21(1)	1(1)	8(1)	10(1)
C(37)	37(1)	25(1)	27(1)	-3(1)	10(1)	14(1)
C(38)	40(1)	25(1)	31(1)	3(1)	8(1)	19(1)
C(39)	33(1)	22(1)	25(1)	2(1)	5(1)	12(1)
C(40)	54(1)	31(1)	26(1)	4(1)	6(1)	26(1)
C(41)	84(2)	49(1)	37(1)	20(1)	18(1)	26(1)
C(42)	64(2)	51(1)	36(1)	-1(1)	-4(1)	36(1)
C(43)	43(1)	35(1)	22(1)	10(1)	13(1)	22(1)
C(44)	69(2)	39(1)	49(1)	25(1)	34(1)	31(1)
C(45)	62(2)	65(2)	35(1)	11(1)	3(1)	41(1)
C(46)	20(1)	20(1)	17(1)	3(1)	3(1)	10(1)
C(47)	23(1)	40(1)	26(1)	15(1)	-5(1)	-7(1)
C(49)	30(1)	38(1)	28(1)	15(1)	-5(1)	6(1)
C(50)	16(1)	54(1)	42(1)	25(1)	-2(1)	0(1)
C(51)	23(1)	41(1)	37(1)	24(1)	2(1)	1(1)
C(53)	32(1)	24(1)	27(1)	8(1)	9(1)	12(1)
C(54)	44(1)	63(2)	31(1)	16(1)	9(1)	24(1)
C(55)	34(1)	35(1)	43(1)	13(1)	16(1)	13(1)
C(56)	20(1)	14(1)	18(1)	3(1)	1(1)	8(1)
C(57)	21(1)	22(1)	23(1)	9(1)	7(1)	10(1)
C(58)	17(1)	26(1)	29(1)	11(1)	2(1)	6(1)
C(59)	24(1)	27(1)	20(1)	8(1)	-2(1)	7(1)
C(61)	17(1)	19(1)	21(1)	5(1)	2(1)	7(1)
C(62)	23(1)	13(1)	20(1)	6(1)	6(1)	6(1)
C(63)	18(1)	16(1)	24(1)	7(1)	7(1)	6(1)
C(64)	20(1)	29(1)	25(1)	8(1)	2(1)	8(1)
C(65)	20(1)	35(1)	33(1)	12(1)	10(1)	12(1)
C(66)	26(1)	26(1)	23(1)	8(1)	10(1)	10(1)
C(68)	20(1)	17(1)	19(1)	7(1)	10(1)	8(1)
C(69)	27(1)	21(1)	19(1)	2(1)	2(1)	9(1)
C(70)	31(1)	28(1)	25(1)	8(1)	2(1)	16(1)
C(72)	31(1)	19(1)	29(1)	8(1)	11(1)	12(1)
C(73)	24(1)	17(1)	25(1)	3(1)	8(1)	3(1)
C(74)	19(1)	22(1)	22(1)	6(1)	4(1)	6(1)
C(60)	24(1)	20(1)	20(1)	7(1)	6(1)	9(1)
O(9)	22(1)	35(1)	18(1)	8(1)	3(1)	6(1)
C(75)	22(1)	34(1)	21(1)	7(1)	6(1)	9(1)
C(76)	25(1)	32(1)	20(1)	8(1)	8(1)	8(1)
O(10)	26(1)	34(1)	21(1)	8(1)	7(1)	5(1)
C(77)	30(1)	31(1)	23(1)	12(1)	7(1)	9(1)
C(78)	26(1)	29(1)	21(1)	10(1)	8(1)	6(1)
O(11)	21(1)	33(1)	18(1)	9(1)	5(1)	7(1)
C(67)	21(1)	17(1)	22(1)	6(1)	4(1)	6(1)
C(48)	41(1)	48(1)	36(1)	27(1)	-12(1)	-12(1)
O(13)	27(1)	29(1)	21(1)	11(1)	4(1)	4(1)
C(80)	25(2)	28(2)	24(2)	11(1)	7(2)	7(2)
C(52)	25(2)	22(2)	34(3)	8(2)	4(2)	7(2)
O(14)	24(1)	26(1)	29(1)	9(1)	5(1)	6(1)
C(79)	25(2)	24(2)	33(2)	14(2)	2(1)	7(1)
C(71)	26(2)	16(1)	33(2)	11(1)	3(1)	7(1)
O(12)	59(4)	47(3)	34(2)	1(3)	-7(2)	38(3)
O(13')	26(2)	39(2)	32(2)	19(2)	-4(2)	5(2)

C(80')	38(4)	26(3)	27(4)	10(3)	3(3)	12(3)
C(52')	31(3)	31(3)	30(3)	6(2)	-2(2)	8(2)
O(14')	29(2)	25(2)	38(2)	7(2)	-1(2)	7(1)
C(79')	32(2)	30(3)	35(3)	14(2)	3(2)	8(2)
C(71')	30(2)	23(2)	32(2)	3(2)	-5(2)	5(2)
O(12')	23(3)	8(2)	28(2)	4(2)	-5(2)	3(2)

Table A6. Bond Lengths [Å] for **5b**.

Cl(1)-C(99)	1.718(4)	C(17)-C(28)	1.471(2)	C(57)-C(58)	1.391(2)
Cl(2)-C(99)	1.737(4)	C(18)-C(21)	1.429(2)	C(58)-C(59)	1.373(3)
O(1)-C(23)	1.3757(19)	C(19)-C(20)	1.407(2)	C(59)-C(60)	1.394(2)
O(1)-C(68)	1.3970(19)	C(20)-C(21)	1.392(2)	C(61)-C(60)	1.389(2)
O(2)-C(20)	1.3761(19)	C(21)-C(22)	1.459(2)	C(62)-C(63)	1.384(2)
O(2)-C(56)	1.3918(19)	C(22)-C(23)	1.399(2)	C(62)-C(64)	1.393(2)
O(3)-C(14)	1.210(2)	C(22)-C(27)	1.427(2)	C(63)-C(67)	1.394(2)
O(4)-C(16)	1.3711(19)	C(23)-C(24)	1.401(2)	C(64)-C(65)	1.379(3)
O(4)-C(46)	1.3894(19)	C(24)-C(25)	1.372(2)	C(65)-C(66)	1.388(3)
O(5)-C(29)	1.378(2)	C(25)-C(26)	1.409(2)	C(66)-C(67)	1.390(2)
O(5)-C(62)	1.388(2)	C(25)-C(33)	1.481(2)	C(68)-C(69)	1.381(2)
O(6)-C(10)	1.217(2)	C(26)-C(31)	1.411(2)	C(68)-C(74)	1.381(2)
O(7)-C(32)	1.212(2)	C(26)-C(27)	1.414(2)	C(69)-C(70)	1.386(2)
O(8)-C(33)	1.214(2)	C(27)-C(28)	1.436(2)	C(70)-O(12)	1.348(7)
N(1)-C(10)	1.400(2)	C(28)-C(29)	1.392(2)	C(70)-C(72)	1.392(3)
N(1)-C(14)	1.408(2)	C(29)-C(30)	1.401(2)	C(70)-O(12')	1.423(9)
N(1)-C(9)	1.455(2)	C(30)-C(31)	1.372(2)	C(72)-C(73)	1.383(3)
N(2)-C(33)	1.400(2)	C(31)-C(32)	1.480(2)	C(73)-C(74)	1.388(2)
N(2)-C(32)	1.401(2)	C(34)-C(39)	1.390(2)	C(60)-O(9)	1.363(2)
N(2)-C(34)	1.455(2)	C(34)-C(35)	1.395(2)	O(9)-C(75)	1.434(2)
C(1)-C(2)	1.529(3)	C(35)-C(36)	1.395(2)	C(75)-C(76)	1.526(3)
C(2)-C(4)	1.513(2)	C(35)-C(43)	1.522(3)	C(76)-O(10)	1.412(2)
C(2)-C(3)	1.523(2)	C(36)-C(37)	1.376(3)	O(10)-C(77)	1.419(2)
C(4)-C(5)	1.392(2)	C(37)-C(38)	1.371(3)	C(77)-C(78)	1.508(2)
C(4)-C(9)	1.393(2)	C(38)-C(39)	1.396(2)	C(78)-O(11)	1.435(2)
C(5)-C(6)	1.379(3)	C(39)-C(40)	1.512(3)	O(11)-C(67)	1.371(2)
C(6)-C(7)	1.379(3)	C(40)-C(41)	1.512(3)	C(48)-O(13)	1.405(3)
C(7)-C(8)	1.396(2)	C(40)-C(42)	1.534(3)	C(48)-O(13')	1.456(4)
C(8)-C(9)	1.388(2)	C(43)-C(45)	1.518(3)	O(13)-C(80)	1.436(4)
C(8)-C(53)	1.518(2)	C(43)-C(44)	1.529(3)	C(80)-C(52)	1.535(5)
C(10)-C(11)	1.481(2)	C(46)-C(47)	1.370(2)	C(52)-O(14)	1.412(4)
C(11)-C(15)	1.378(2)	C(46)-C(51)	1.370(2)	O(14)-C(79)	1.417(4)
C(11)-C(12)	1.410(2)	C(47)-C(48)	1.389(3)	C(79)-C(71)	1.504(4)
C(12)-C(18)	1.413(2)	C(49)-C(50)	1.359(3)	C(71)-O(12)	1.276(7)
C(12)-C(13)	1.413(2)	C(49)-C(48)	1.382(3)	O(13')-C(80')	1.440(7)
C(13)-C(19)	1.376(2)	C(50)-C(51)	1.387(3)	C(80')-C(52')	1.488(9)
C(13)-C(14)	1.481(2)	C(53)-C(55)	1.530(3)	C(52')-O(14')	1.404(7)
C(15)-C(16)	1.404(2)	C(53)-C(54)	1.531(3)	O(14')-C(79')	1.405(6)
C(16)-C(17)	1.399(2)	C(56)-C(57)	1.383(2)	C(79')-C(71')	1.505(6)
C(17)-C(18)	1.428(2)	C(56)-C(61)	1.386(2)	C(71')-O(12')	1.377(11)

A.9.3 Crystal Structure of 6a.

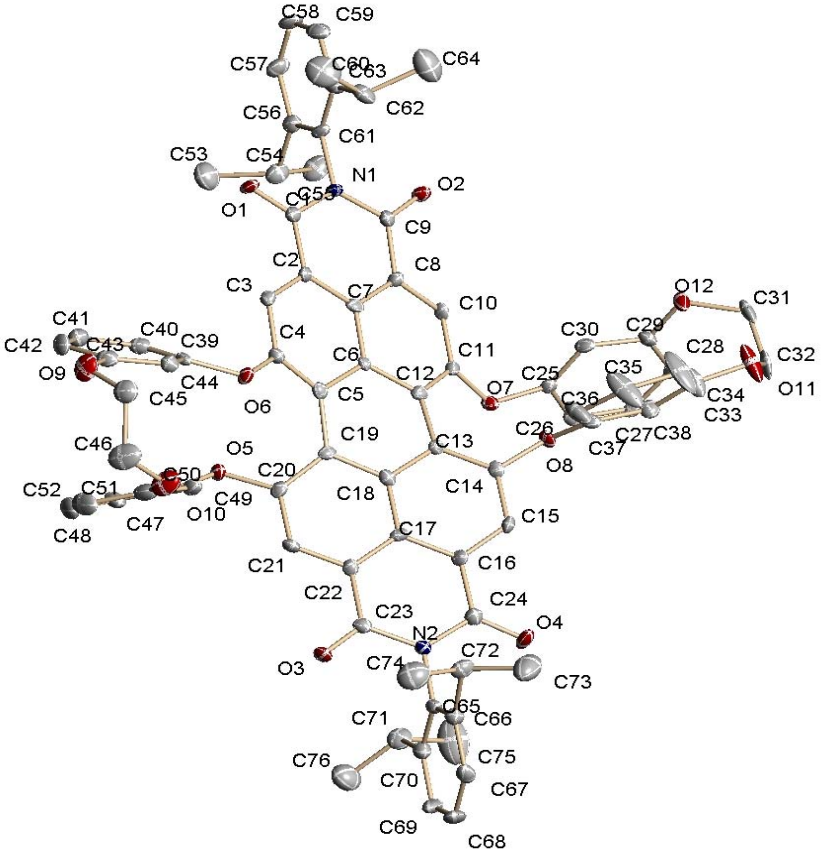

Figure A12. Fully labelled diagram of **6a** ($C_{76}H_{62}N_2O_{12}(CH_2Cl_2)_2(CH_2Cl_2)_{0.58}$). Anisotropic displacement parameters are depicted on 50% probability level. Hydrogen atoms and dichloromethane molecules are omitted for clarity.

Table A7. Crystal Data and Structure Refinement for **6a**.

Empirical formula	$C_{76}H_{62}N_2O_{12}(CH_2Cl_2)_2(CH_2Cl_2)_{0.58}$	
Formula weight	1414.59	
Temperature	100(2) K	
Wavelength	71.073 pm	
Crystal system	Orthorhombic	
Space group	Pca2(1)	
Unit cell dimensions	a = 1737.0(3) pm	α = 90°.
	b = 1555.4(2) pm	β = 90°.
	c = 2707.6(4) pm	γ = 90°.
Volume	7.3155(18) nm^3	
Z	4	
Density (calculated)	1.284 Mg/m^3	
Absorption coefficient	0.267 mm^{-1}	
F(000)	2946	
Crystal size	0.2 x 0.2 x 0.1 mm^3	
Theta range for data collection	3.49 to 25.03°.	
Index ranges	0<=h<=20, 0<=k<=18, -32<=l<=23	
Reflections collected	50043	
Independent reflections	11953 [R(int) = 0.0633]	

Completeness to theta = 25.03°	99.7 %
Absorption correction	Empirical
Max. and min. transmission	0.85 and 0.99
Refinement method	Full-matrix least-squares on F^2
Data / restraints / parameters	11953 / 36 / 923
Goodness-of-fit on F^2	1.060
Final R indices [I>2sigma(I)]	R1 = 0.0605, wR2 = 0.1475
R indices (all data)	R1 = 0.0688, wR2 = 0.1520
Absolute structure parameter	0.0(3)
Largest diff. peak and hole	0.793 and -0.363 e.$Å^{-3}$

Table A8. Atomic Coordinates ($x10^4$) and Equivalent Isotropic Displacement Parameters ($pm^2 x\ 10^{-1}$) for **6a**. U(eq) is defined as One Third of the Trace of the Orthogonalized U^{ij} Tensor.

	x	y	z	U(eq)
C(64)	8044(3)	7686(4)	6475(2)	51(2)
C(34)	10360(3)	4443(4)	4102(2)	62(2)
C(35)	10341(3)	3897(4)	4499(2)	57(2)
O(5)	7443(2)	978(2)	6683(1)	19(1)
O(8)	8358(2)	3113(2)	4378(1)	18(1)
O(6)	8164(2)	2345(2)	6984(1)	18(1)
O(3)	8870(2)	-1213(2)	5661(1)	22(1)
O(7)	6959(2)	3529(2)	4546(1)	16(1)
N(2)	9033(2)	-587(2)	4914(1)	17(1)
O(1)	6864(2)	5216(2)	7182(1)	22(1)
O(4)	9255(2)	60(2)	4177(1)	32(1)
O(10)	9545(2)	178(2)	7694(1)	39(1)
O(9)	9006(2)	1432(2)	8561(1)	34(1)
O(12)	8242(2)	5787(2)	3696(1)	28(1)
N(1)	6626(2)	5680(2)	6404(1)	15(1)
O(2)	6398(2)	6148(2)	5618(1)	21(1)
O(11)	9810(2)	5056(2)	3392(1)	45(1)
C(22)	8437(2)	223(2)	5588(2)	15(1)
C(60)	6816(2)	7090(2)	6805(2)	23(1)
C(12)	7521(2)	3186(2)	5321(1)	15(1)
C(61)	6308(2)	6475(2)	6615(1)	18(1)
C(15)	8675(2)	1654(2)	4513(1)	16(1)
C(38)	9093(2)	3974(2)	3861(2)	21(1)
C(6)	7449(2)	3301(2)	5843(1)	12(1)
C(7)	7172(2)	4098(2)	6027(2)	16(1)
C(40)	7247(2)	2330(2)	7667(2)	22(1)
C(25)	7032(2)	4080(2)	4146(1)	15(1)
C(9)	6625(2)	5576(2)	5885(2)	17(1)
C(17)	8391(2)	955(2)	5284(1)	14(1)
C(16)	8674(2)	924(2)	4798(1)	16(1)
C(13)	7971(2)	2447(2)	5144(1)	13(1)
C(2)	7191(2)	4254(2)	6540(1)	14(1)
C(67)	10385(3)	-2331(2)	4557(2)	25(1)
C(28)	7265(2)	4951(2)	3268(1)	20(1)
C(42)	7725(3)	1834(3)	8454(2)	28(1)

C(1)	6887(2)	5067(2)	6742(2)	17(1)
C(14)	8338(2)	2409(2)	4690(1)	15(1)
C(68)	9882(3)	-2906(3)	4359(2)	32(1)
C(57)	5214(3)	7306(3)	6846(2)	26(1)
C(21)	8135(2)	246(2)	6052(2)	18(1)
C(11)	7132(2)	3778(2)	5017(1)	14(1)
C(20)	7831(2)	1012(2)	6244(1)	16(1)
C(18)	8062(2)	1733(2)	5469(2)	15(1)
C(10)	6843(2)	4551(2)	5203(1)	16(1)
C(66)	10111(2)	-1552(2)	4754(2)	21(1)
C(37)	9072(2)	3480(2)	4289(2)	19(1)
C(19)	7855(2)	1781(2)	5977(1)	14(1)
C(4)	7749(2)	2866(2)	6675(1)	16(1)
C(30)	7543(2)	4758(2)	4132(2)	19(1)
C(8)	6897(2)	4732(2)	5699(1)	16(1)
C(56)	5515(2)	6552(2)	6637(2)	21(1)
C(23)	8792(2)	-578(2)	5408(1)	18(1)
C(39)	7977(2)	2268(2)	7488(1)	17(1)
C(69)	9102(3)	-2746(3)	4342(2)	30(1)
C(49)	8512(3)	445(2)	7160(2)	25(1)
C(54)	4963(2)	5875(3)	6431(2)	26(1)
C(5)	7673(2)	2636(2)	6184(1)	15(1)
C(27)	6730(2)	4293(3)	3295(2)	21(1)
C(3)	7491(2)	3664(2)	6854(2)	15(1)
C(65)	9332(2)	-1397(2)	4724(1)	18(1)
C(29)	7671(2)	5177(2)	3684(2)	21(1)
C(51)	7209(3)	63(3)	7361(2)	28(1)
C(72)	10680(2)	-941(3)	5013(2)	25(1)
C(58)	5706(3)	7931(3)	7035(2)	29(1)
C(62)	7689(2)	6998(3)	6796(2)	26(1)
C(71)	7950(2)	-1798(3)	4487(2)	28(1)
C(50)	7737(3)	457(2)	7067(2)	21(1)
C(41)	7131(3)	2123(3)	8165(2)	26(1)
C(59)	6488(3)	7821(3)	7012(2)	27(1)
C(46)	9803(3)	273(3)	8194(2)	44(1)
C(24)	9011(2)	124(2)	4594(2)	20(1)
C(32)	9163(3)	5227(3)	3079(2)	30(1)
C(53)	4417(3)	5539(3)	6835(2)	39(1)
C(36)	9670(3)	3427(3)	4606(2)	35(1)
C(26)	6614(2)	3832(2)	3728(1)	16(1)
C(31)	8672(3)	5947(3)	3253(2)	29(1)
C(44)	8599(2)	2016(2)	7772(2)	19(1)
C(43)	8463(2)	1770(2)	8257(2)	23(1)
C(70)	8804(2)	-1978(3)	4522(2)	23(1)
C(47)	8771(3)	74(3)	7600(2)	33(1)
C(45)	9761(3)	1194(3)	8385(2)	31(1)
C(55)	4510(3)	6240(3)	5995(2)	34(1)
C(48)	8255(3)	-342(3)	7905(2)	39(1)
C(33)	9741(3)	4480(3)	3776(2)	35(1)
C(73)	11348(3)	-681(4)	4686(2)	49(1)
C(74)	10984(3)	-1362(4)	5481(2)	47(1)
C(52)	7483(4)	-352(3)	7782(2)	44(1)

C(76)	7442(3)	-2547(3)	4645(2)	45(1)
C(75)	7738(4)	-1499(5)	3977(2)	71(2)
C(103)	4869(4)	1084(4)	6670(3)	30(2)
Cl(5)	5267(2)	100(2)	6469(1)	54(1)
Cl(6)	5636(2)	1753(3)	6863(2)	108(2)
C(101)	6044(3)	8176(3)	5700(2)	38(1)
Cl(1)	6736(1)	8997(1)	5679(1)	52(1)
Cl(2)	5250(8)	8473(3)	5374(7)	79(4)
Cl(2')	5076(4)	8502(6)	5607(6)	60(2)
C(102)	9354(3)	6653(4)	5573(2)	58(2)
Cl(3)	8577(1)	5927(1)	5569(1)	67(1)
Cl(4)	9982(2)	6501(2)	6080(1)	72(1)
Cl(4')	10212(3)	6171(4)	5646(3)	76(3)

Table A9. Anisotropic Displacement Parameters ($pm^2 x\ 10^{-1}$) for Angles [°] for **6a**. The Anisotropic Displacement Factor Exponent takes the Form:
$-2\pi^2[\ h^2\ a^{*2}\ U^{11} + ... + 2\ h\ k\ a^*\ b^*\ U^{12}]$

	U^{11}	U^{22}	U^{33}	U^{23}	U^{13}	U^{12}
C(63)	43(3)	55(3)	56(4)	3(3)	-16(3)	-1(3)
C(64)	41(3)	49(3)	64(4)	21(3)	6(3)	2(2)
C(34)	52(3)	67(4)	69(4)	43(3)	-32(3)	-44(3)
C(35)	61(4)	48(3)	62(4)	31(3)	-43(3)	-33(3)
O(5)	31(2)	15(1)	11(1)	3(1)	5(1)	4(1)
O(8)	24(1)	11(1)	19(2)	8(1)	5(1)	5(1)
O(6)	27(1)	18(1)	10(1)	1(1)	2(1)	5(1)
O(3)	38(2)	10(1)	19(2)	3(1)	5(1)	3(1)
O(7)	24(1)	12(1)	12(1)	1(1)	-3(1)	1(1)
N(2)	25(2)	11(2)	14(2)	1(1)	2(1)	2(1)
O(1)	40(2)	14(1)	12(2)	-3(1)	4(1)	8(1)
O(4)	55(2)	22(2)	17(2)	3(1)	16(2)	16(1)
O(10)	53(2)	42(2)	22(2)	-2(2)	-12(2)	14(2)
O(9)	41(2)	45(2)	16(2)	8(1)	-6(1)	9(2)
O(12)	49(2)	24(2)	12(2)	-1(1)	3(1)	-18(1)
N(1)	23(2)	10(1)	12(2)	-1(1)	2(1)	3(1)
O(2)	35(2)	14(1)	15(2)	-1(1)	2(1)	7(1)
O(11)	36(2)	57(2)	42(2)	36(2)	-15(2)	-25(2)
C(22)	17(2)	15(2)	12(2)	2(2)	-1(2)	1(1)
C(60)	36(2)	11(2)	23(2)	1(2)	1(2)	-1(2)
C(12)	16(2)	13(2)	16(2)	-2(2)	1(2)	-3(1)
C(61)	31(2)	11(2)	12(2)	-1(2)	2(2)	9(2)
C(15)	20(2)	18(2)	10(2)	0(2)	5(2)	0(2)
C(38)	26(2)	21(2)	16(2)	-1(2)	-3(2)	-4(2)
C(6)	13(2)	10(2)	12(2)	2(1)	2(1)	-2(1)
C(7)	17(2)	11(2)	20(2)	-2(2)	2(2)	-4(2)
C(40)	29(2)	15(2)	21(2)	-1(2)	-5(2)	3(2)
C(25)	20(2)	11(2)	13(2)	1(2)	2(2)	5(2)
C(9)	21(2)	14(2)	16(2)	2(2)	4(2)	-1(2)
C(17)	16(2)	13(2)	14(2)	-4(2)	-2(2)	3(1)
C(16)	25(2)	15(2)	9(2)	1(2)	-2(2)	2(2)
C(13)	14(2)	13(2)	14(2)	0(2)	1(2)	0(1)
C(2)	17(2)	13(2)	13(2)	1(2)	6(2)	-1(2)

C(67)	31(2)	16(2)	27(2)	5(2)	10(2)	6(2)
C(28)	33(2)	19(2)	8(2)	3(2)	2(2)	3(2)
C(42)	46(3)	25(2)	12(2)	6(2)	3(2)	-1(2)
C(1)	20(2)	14(2)	17(2)	0(2)	5(2)	-2(2)
C(14)	16(2)	16(2)	12(2)	4(2)	-2(2)	1(2)
C(68)	52(3)	13(2)	31(3)	-7(2)	16(2)	2(2)
C(57)	31(2)	26(2)	22(2)	-5(2)	3(2)	10(2)
C(21)	27(2)	9(2)	19(2)	1(2)	3(2)	0(2)
C(11)	17(2)	13(2)	11(2)	0(2)	2(2)	-3(1)
C(20)	22(2)	18(2)	10(2)	-1(2)	-1(2)	2(2)
C(18)	16(2)	14(2)	16(2)	3(2)	-1(2)	0(1)
C(10)	20(2)	14(2)	12(2)	6(2)	-1(2)	2(2)
C(66)	28(2)	17(2)	19(2)	0(2)	3(2)	1(2)
C(37)	30(2)	13(2)	14(2)	-3(2)	-3(2)	-1(2)
C(19)	13(2)	13(2)	15(2)	-4(2)	0(2)	-2(1)
C(4)	21(2)	12(2)	14(2)	2(2)	1(2)	1(1)
C(30)	31(2)	14(2)	11(2)	-3(2)	-5(2)	2(2)
C(8)	21(2)	15(2)	11(2)	-1(2)	2(2)	3(2)
C(56)	30(2)	18(2)	14(2)	2(2)	0(2)	3(2)
C(23)	23(2)	13(2)	16(2)	0(2)	-1(2)	-1(2)
C(39)	32(2)	9(2)	10(2)	2(2)	0(2)	-4(2)
C(69)	43(3)	19(2)	27(3)	-11(2)	15(2)	-10(2)
C(49)	46(3)	15(2)	15(2)	2(2)	5(2)	7(2)
C(54)	24(2)	29(2)	26(2)	-4(2)	2(2)	2(2)
C(5)	13(2)	15(2)	17(2)	3(2)	3(2)	-1(1)
C(27)	26(2)	24(2)	12(2)	-6(2)	-3(2)	2(2)
C(3)	20(2)	15(2)	11(2)	-1(2)	1(2)	-3(2)
C(65)	32(2)	10(2)	13(2)	1(2)	3(2)	0(2)
C(29)	32(2)	10(2)	20(2)	2(2)	3(2)	0(2)
C(51)	48(3)	15(2)	21(2)	0(2)	1(2)	-7(2)
C(72)	24(2)	24(2)	26(2)	-5(2)	2(2)	6(2)
C(58)	49(3)	16(2)	24(2)	-6(2)	6(2)	11(2)
C(62)	30(2)	17(2)	31(3)	5(2)	-1(2)	-5(2)
C(71)	30(2)	29(2)	24(3)	-3(2)	-6(2)	-2(2)
C(50)	49(3)	4(2)	10(2)	-1(2)	3(2)	2(2)
C(41)	35(2)	20(2)	25(3)	-2(2)	8(2)	0(2)
C(59)	45(3)	17(2)	19(2)	-3(2)	-5(2)	-1(2)
C(46)	62(3)	42(3)	27(3)	1(2)	-20(2)	16(3)
C(24)	25(2)	17(2)	18(2)	1(2)	4(2)	3(2)
C(32)	35(2)	41(3)	14(2)	18(2)	0(2)	-12(2)
C(53)	35(3)	40(3)	41(3)	6(2)	2(2)	-7(2)
C(36)	57(3)	21(2)	27(3)	11(2)	-15(2)	-14(2)
C(26)	17(2)	12(2)	19(2)	2(2)	3(2)	0(2)
C(31)	47(3)	24(2)	16(2)	11(2)	-5(2)	-19(2)
C(44)	21(2)	16(2)	19(2)	0(2)	3(2)	0(2)
C(43)	34(2)	18(2)	17(2)	-1(2)	-5(2)	-1(2)
C(70)	34(2)	19(2)	16(2)	1(2)	2(2)	-3(2)
C(47)	61(3)	18(2)	20(2)	-2(2)	0(2)	7(2)
C(45)	40(3)	30(2)	21(2)	3(2)	-6(2)	3(2)
C(55)	30(2)	46(3)	26(3)	-6(2)	-6(2)	3(2)
C(48)	76(4)	25(2)	16(2)	7(2)	-9(2)	3(2)
C(33)	34(2)	38(3)	31(3)	18(2)	-11(2)	-13(2)

C(73)	55(3)	54(3)	40(3)	-15(3)	9(3)	-18(3)
C(74)	48(3)	50(3)	41(3)	-5(3)	-9(3)	3(2)
C(52)	86(4)	25(2)	20(3)	5(2)	12(3)	-11(3)
C(76)	44(3)	38(3)	55(4)	1(2)	6(3)	-8(2)
C(75)	50(4)	109(6)	53(4)	29(4)	-16(3)	-16(4)
C(103)	37(4)	28(4)	24(4)	-1(3)	8(3)	-1(3)
Cl(5)	64(2)	45(1)	54(2)	10(1)	16(1)	17(1)
Cl(6)	73(2)	119(3)	131(4)	-67(3)	-22(2)	-25(2)
C(101)	37(2)	29(2)	47(3)	9(2)	2(2)	2(2)
Cl(1)	42(1)	40(1)	73(1)	17(1)	-2(1)	-3(1)
Cl(2)	81(4)	25(2)	133(8)	9(2)	-82(5)	-8(2)
Cl(2')	41(2)	60(4)	78(6)	29(4)	-17(3)	4(2)
C(102)	58(3)	55(3)	63(4)	20(3)	8(3)	9(2)
Cl(3)	61(1)	53(1)	86(1)	16(1)	8(1)	-1(1)
Cl(4)	68(2)	59(2)	89(2)	30(1)	-5(1)	11(1)
Cl(4')	50(3)	59(3)	120(7)	43(4)	8(3)	15(2)

Table A10. Bond Lengths [Å] for **6a**.

C(63)-C(62)	1.506(7)	C(12)-C(6)	1.429(5)	C(66)-C(65)	1.377(6)
C(64)-C(62)	1.509(7)	C(12)-C(13)	1.471(5)	C(66)-C(72)	1.539(6)
C(34)-C(35)	1.370(7)	C(61)-C(56)	1.385(6)	C(37)-C(36)	1.349(6)
C(34)-C(33)	1.393(7)	C(15)-C(16)	1.374(5)	C(19)-C(5)	1.477(5)
C(35)-C(36)	1.406(7)	C(15)-C(14)	1.398(5)	C(4)-C(5)	1.382(5)
O(5)-C(20)	1.366(5)	C(38)-C(33)	1.391(6)	C(4)-C(3)	1.406(5)
O(5)-C(50)	1.414(5)	C(38)-C(37)	1.392(6)	C(30)-C(29)	1.396(6)
O(8)-C(14)	1.383(4)	C(6)-C(7)	1.421(5)	C(56)-C(54)	1.529(6)
O(8)-C(37)	1.388(5)	C(6)-C(5)	1.441(5)	C(39)-C(44)	1.383(6)
O(6)-C(4)	1.371(5)	C(7)-C(8)	1.410(5)	C(69)-C(70)	1.389(6)
O(6)-C(39)	1.409(5)	C(7)-C(2)	1.412(6)	C(49)-C(50)	1.370(6)
O(3)-C(23)	1.210(5)	C(40)-C(39)	1.360(6)	C(49)-C(47)	1.396(6)
O(7)-C(11)	1.368(5)	C(40)-C(41)	1.401(6)	C(54)-C(55)	1.530(6)
O(7)-C(25)	1.386(4)	C(25)-C(30)	1.378(5)	C(54)-C(53)	1.539(6)
N(2)-C(23)	1.402(5)	C(25)-C(26)	1.400(6)	C(27)-C(26)	1.388(6)
N(2)-C(24)	1.406(5)	C(9)-C(8)	1.483(5)	C(65)-C(70)	1.398(6)
N(2)-C(65)	1.457(5)	C(17)-C(16)	1.406(5)	C(51)-C(50)	1.362(6)
O(1)-C(1)	1.212(5)	C(17)-C(18)	1.428(5)	C(51)-C(52)	1.393(7)
O(4)-C(24)	1.209(5)	C(16)-C(24)	1.482(5)	C(72)-C(73)	1.515(7)
O(10)-C(47)	1.378(6)	C(13)-C(14)	1.384(5)	C(72)-C(74)	1.520(7)
O(10)-C(46)	1.432(6)	C(13)-C(18)	1.426(5)	C(58)-C(59)	1.372(7)
O(9)-C(43)	1.358(5)	C(2)-C(3)	1.355(5)	C(71)-C(75)	1.502(8)
O(9)-C(45)	1.444(6)	C(2)-C(1)	1.476(5)	C(71)-C(70)	1.514(6)
O(12)-C(29)	1.373(5)	C(67)-C(68)	1.360(6)	C(71)-C(76)	1.522(7)
O(12)-C(31)	1.436(5)	C(67)-C(66)	1.407(6)	C(46)-C(45)	1.524(7)
N(1)-C(1)	1.398(5)	C(28)-C(29)	1.376(6)	C(32)-C(31)	1.483(7)
N(1)-C(9)	1.416(5)	C(28)-C(27)	1.384(6)	C(44)-C(43)	1.386(6)
N(1)-C(61)	1.469(5)	C(42)-C(41)	1.372(6)	C(47)-C(48)	1.381(7)
O(2)-C(9)	1.212(5)	C(42)-C(43)	1.392(6)	C(48)-C(52)	1.383(8)
O(11)-C(33)	1.376(5)	C(68)-C(69)	1.378(7)	C(103)-Cl(5)	1.765(6)
O(11)-C(32)	1.434(5)	C(57)-C(58)	1.391(6)	C(103)-Cl(6)	1.769(6)
C(22)-C(21)	1.363(6)	C(57)-C(56)	1.403(6)	C(101)-Cl(2)	1.703(6)
C(22)-C(17)	1.406(5)	C(21)-C(20)	1.403(5)	C(101)-Cl(1)	1.754(5)
C(22)-C(23)	1.473(5)	C(11)-C(10)	1.398(5)	C(101)-Cl(2')	1.774(9)

C(60)-C(59)	1.389(6)	C(20)-C(19)	1.399(5)	C(102)-Cl(4')	1.680(8)
C(60)-C(61)	1.400(6)	C(18)-C(19)	1.425(5)	C(102)-Cl(3)	1.761(6)
C(60)-C(62)	1.523(6)	C(10)-C(8)	1.375(5)	C(102)-Cl(4)	1.770(6)
C(12)-C(11)	1.407(5)				

A.9 Additional References and Notes

A1 (a) S. Leroy-Lhez, L. Perrin, E. Levillain, J. Baffreau, P. Hudhomme, *J. Org. Chem.* **2005**, *70*, 6313-6320; (b) F. Würthner, P. Osswald, R. Schmidt, T. E. Kaiser, H. Mansikkamaeki, M. Könemann, *Org. Lett.* **2006**, *6*, 3765-3768.

A2 V. P. Solov´ev, N. N. Strakhova, O. A. Raevsky, V. Rüdiger, H.-J. Schneider, *J. Org. Chem.* **1996**, *61*, 5221-5226.

A3 (a) R. Gvishi, R. Reisfeld, Z. Burshtein, *Chem. Phys. Lett.* **1993**, *213*, 338-344; (b) E. Lang, F. Würthner, J. Köhler, *ChemPhysChem* **2005**, *6*, 935-941.

A4 (a) G. F Swiatkowski, R. Menzel, W. Rapp, *J. Lumin.* **1987**, *37*, 183-189; (b) J. Hofkens, T. Vosch, M. Maus,. Köhn, M. Cotlet, T. Weil, A. Herrmann, K. Müllen, F. C. De Schryver, *Chem. Phys. Lett.* **2001**, *333*, 255-263.

A5 (a) E. K. Todd, S. Wang, X. Wan, Z. Y. Wang, *Tetrahedron Lett.* **2005**, *46*, 587-590; (b) F. Würthner, A. Sautter, D. Schmidt, P. J. A. Weber, *Chem. Eur. J.* **2001**, *7*, 894-902.

A6 (a) T. Kottke, D. Stalke*, J. Appl. Crystallogr*. **1993**, *26*, 615-619; (b) T. Kottke, R. J. Lagow, D. Stalke, *J. Appl. Crystallogr*. **1996**, *29*, 465-468; (c) D. Stalke, *Chem. Soc. Rev.* **1998**, *27*, 171-178.

A7 G. M. Sheldrick, SADABS 2.05: Program for Area Detector Absorption Correction, University of Göttingen, **2002**.

A8 G. M. Sheldrick, *Acta Crystallogr. Sect. A: Found. Crystallogr.* **1990**, *46*, 467-473.

A9 G. M. Sheldrick, *SHELXL-97 – Program for Structure Refinement*, University of Göttingen, **1997**.

A10 P. van der Sluis, A. L. Spek, *Acta Crystallogr. Sect. A: Found. Crystallogr.* **1990**, *46*, 194-201.

B Supplement for Chapter 4

B.1 Synthesis of NH-Functionalized Perylene Bisimides.

The synthesis of epimeric macrocycles based on 1-(*R*)-phenylethylamine as chiral substituent in the imide position failed already at the stage of the tetra(3-hydroxyphenoxy)-functionalized precursor **10** (Scheme B1). Instead, the additional cleavage of the imide substituent by boron tribromide was observed. This reaction displays a feasible reaction pathway to NH-functionalized perylene bisimides.

The chiral amine 1-(*R*)-phenylethylamine was introduced in perylene bisanhydride **3** by reaction of **3** in pyridine with imidazol as catalyst as shown in Scheme B1. After column chromatography perylene bisimides **8** was obtained in 36% isolated yield. The cleavage of the methyl ether in **8** was realized by applying standard conditions using boron tribromide in dichloromethane. In the present case the cleavage of the chiral imide substituent 1-(*R*)-phenylethylamine was additionally observed under the formation of perylene bisimide **9** in 64% yield. This was confirmed by ^{1}H NMR spectroscopy and MALDI TOF mass spectrometry. Therefore, the cleavage of the imide substituent with boron tribromide offers a new reaction pathway to NH-functionalized perylene bisimides from a defined and well-soluble precursor.

Scheme B1. Synthesis of NH-Functionalized Perylene Bisimides

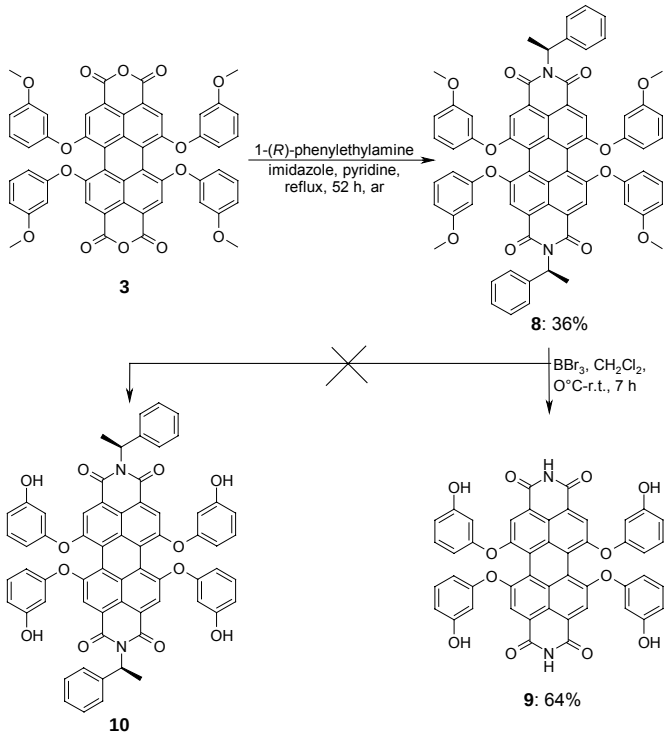

A possible mechanism for the cleavage of the imide substituent is shown in Scheme B2. The suggested mechanism involves the coordination of the lewis acid boron

tribromide to the carbonyl oxygen which leads to strong polarization of the CN-imide bond. This is reasonable due to the high oxophilicity of boron-containing compounds. This enables the formation of the methylbenzyl cation which in a second step abstracts a bromide from the complexed boron tribromide moiety under formation of the respective benzylbromide. Finally, hydrolysis of the boron compound yields the corresponding NH-functionalized perylene bisimide. The generation of the NH functionality by hydrolysis in a separate step prevents the reverse reaction of bisimide **9** with methylbenzylbromide. This finding might also explain the moderate yields for the formation of **5** as the cleavage of the methylether for APBI can in general be achieved quantitatively as demonstrated in Chapter 3.

Scheme B2. Possible Mechanism for the Formation of NH-Functionalized Perylene Bisimides

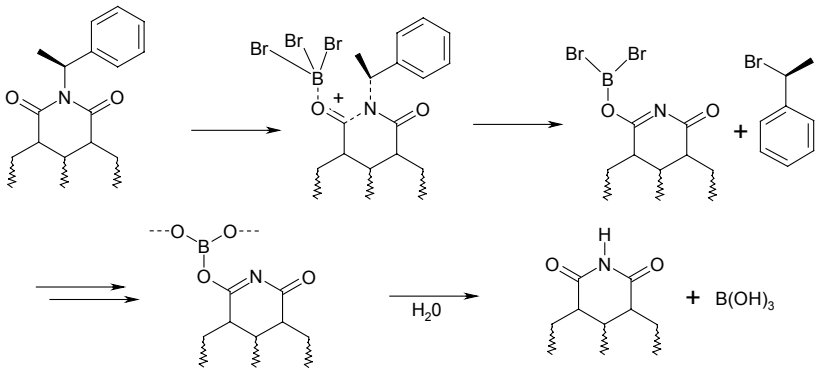

B.2 Experimental Section

Methods and Materials. Boron tribromid (≥ 99%) was purchased from Merck (Hohenbrunn, Germany), imidazole (> 97%) from Riedel-deHaen (Seelze, Germany) and pyridine (>99.5%) were obtained from Grüssing (Filsum, Germany). 1-(*R*)-phenylethylamine was purchased from Fluka (Buchs, Switzerland) and had an ee > 99%. All chemical and reagents were used as received if not otherwise mentioned. Dichloromethane was distilled under argon from calcium hydride and pyridine was stored over KOH. Flash column chromatography was performed using silica gel (Si60, mesh size 40-63 µm) from Merck. ^{1}H NMR spectra were recorded on a Bruker Advance 400 spectrometer. Chemical shifts are given in parts per million (ppm) and are referred toTMS ($CDCl_3$) or the residual solvent peak (Acetone-d^6 and DMSO-d^6). MALDI-TOF mass spectra were recorded on a Autoflex II from Bruker Daltonics.

Synthesis of NH-functionalized Perylene Bisimides

***N,N´*-Di(1-(*R*)-phenylethyl))-1,6,7,12-tetrakis(3-methoxyphenoxy)perylene-3;4:9:10-tetracarboxylic Acid Bisimide 8**

1,6,7,12-Tetrakis(3-methoxyphenoxy)perylene3:4;9:10-tetracarboxylic acid bisanhydride **3** (0.60 g, 0.68 mmol), 1-(*R*)-phenylethylamine (0.37 g, 3.07 mmol) and imidazole (2.57 g (31.3 mmol) were dissolved under argon in pyridine (40 mL) and heated to reflux for 47 h. After addition of additional amounts of imidazole (1.00 g, 12.2 mmol) the reaction was kept under reflux for 5 h. After cooling to rt, the reaction mixture was dropped into 75 mL of 0.33 M hydrochloric acid, the resulting precipitate was collected by filtration washed with 1M hydrochloride solution to remove excess imidazole and dried in vacuo. Silica gel column chromatography with dichloromethane as eluent yielded 266 mg (0.25 mmol, 36%) of **8** as a wine-red solid.

Mp: 345–348 °C; ^{1}H NMR (400 MHz, $CDCl_3$, TMS): δ 8.16 (s, 4H), 7.42 (d, ^{3}J = 7.8, 4H), 7.29 (m, 4H), 7.21 (d, ^{3}J = 7.3, 2H), 7.15 (t, ^{3}J = 8.2, 4H), 6.67 (ddd, ^{3}J = 8.3, ^{4}J = 2.4, ^{4}J = 0.7, 4H), 6.49 (d, ^{3}J = 8.0, 4H), 6.47 (t, ^{3}J = 2.3, 4H), 6.43 (m, 2H), 3.65 (s, 12H), 1.91 (d, ^{3}J = 7.1, 6H). MS (MALDI-TOF, pos. mode, DCTB) m/z: 1086.3 $[M]^+$ (calcd 1086.3). Anal. calcd for $C_{68}H_{50}N_20_{12}$: C, 75.13; H, 4.64; N, 2.58. Found: C, 74.82; H, 4.82; N, 2.49. UV/Vis (CH_2Cl_2): λ_{max}/nm (ε_{max}/$M^{-1}cm^{-1}$) 578 (45800), 539 (28400), 451 (15900), 288 (50100). Fluorescence (CH_2Cl_2): λ_{max} = 599 nm, fluorescence quantum yield Φ_{fl} = 0.94.

1,6,7,12-Tetrakis(3-hydroxyphenoxy) perylene-3;4:9;10-tetracarboxylic Acid Bisimide 9

Perylene bisimide **8** (483 mg, 0.44 mmol) was dissolved in dichloromethane (30 mL) and cooled to 0 °C. A solution of boron tribromide (0.67 mL, 1.78 g, 7.11 mmol) in dichloromethane (20 mL) was added over a period of 30 min and the reaction mixture was stirred for 2 h at 0 °C and additional 5 h at rt. The solvent and excess boron tribromide was removed by destilliation and a 4:1-mixture of water and methanol (50 mL) was added to the residue under ice cooling and was ultrasonicated for 30 min. The precipitate was collected by filtration, washed with water (3 x 20 mL) and dried at 60 °C in vacuo. The reaction afforded **9** in 64% (229 mg, 0.28 mmol) crude yield as violet solid.

^{1}H NMR (400 MHz, Aceton-d^6): δ 10.54 (s, 1H, NH), 8.61 (s, 2H, OH), 8.09 (s, 4H), 7.17 (t, ^{3}J = 8.2, 4H), 6.65 (ddd, ^{3}J = 8.3, ^{4}J = 2.4, ^{4}J = 0.7, 4H), 6.49 (ddd, ^{3}J = 8.0, ^{4}J = 2.4, ^{4}J = 0.7, 4H), 6.62 (t, ^{3}J = 2.3, 4H); (400 MHz, DMSO-d^6): δ 11.90 (s, 2H, NH), 9.70 (s,

4H, OH), 7.85 (s, 4H), 7.18 (t, ^{3}J = 8.2, 4H), 6.65 (ddd, ^{3}J = 8.3, ^{4}J = 2.4, ^{4}J = 0.7, 4H), 6.62 (t, ^{3}J= 2.3, 4H), 6.49 (ddd, ^{3}J = 8.0, ^{4}J = 2.4, ^{4}J = 0.7, 4H). MS (MALDI-TOF, pos. mode, DCTB): m/z: 822.16 $[M]^{+}$ (calcd. 822.15); (a small amount of the mono-cleaved product was observed by MALDI-TOF MS: m/z: 926.21 $[M]^{+}$ (calcd. 926.21).

B3 ^{1}H NMR Spectra of 2-7

^{1}H NMR spectrum (400.13 MHz) of **2** in $CDCl_3$

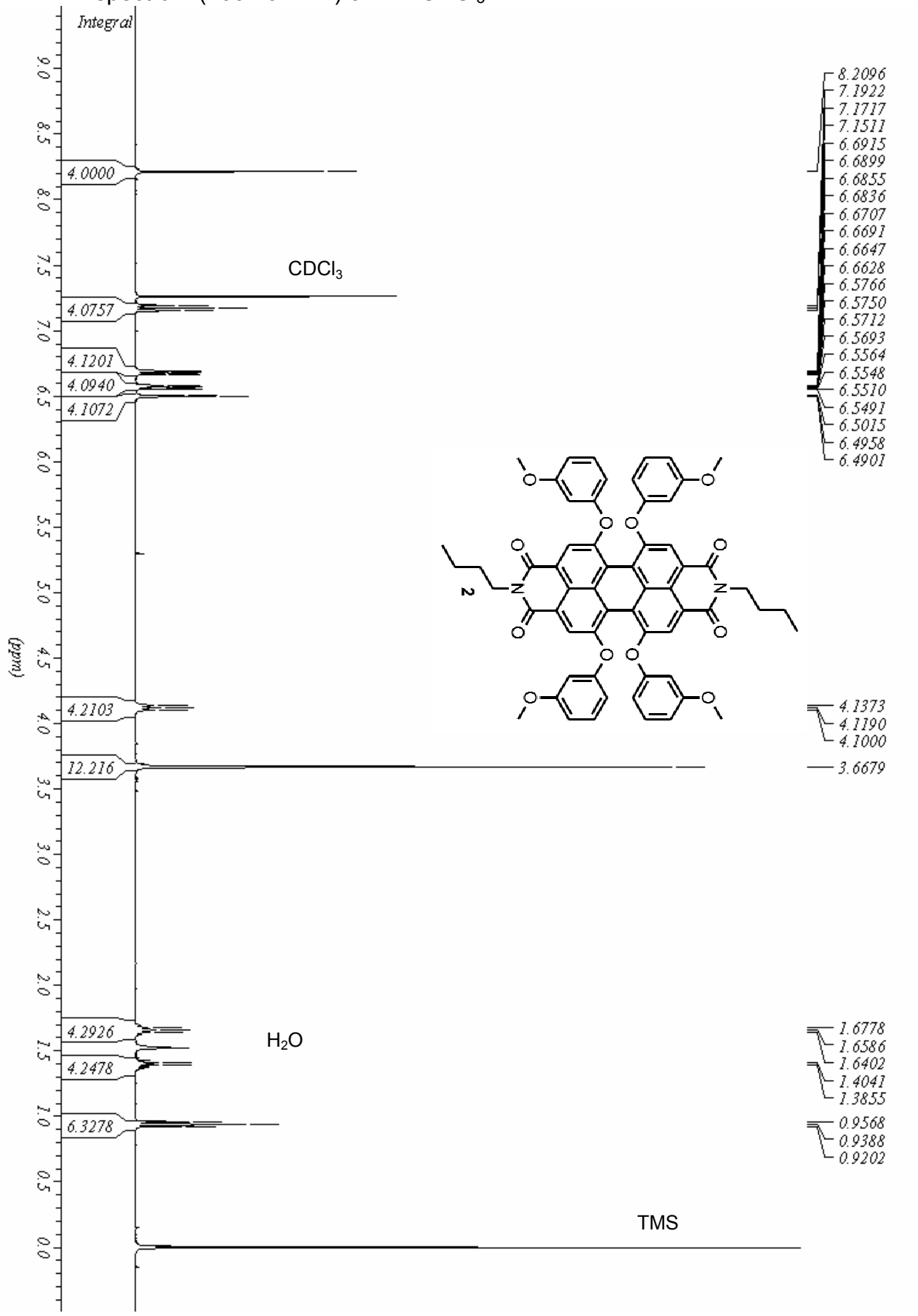

^{1}H NMR spectrum (400.13 MHz) of **3** in $CDCl_3$

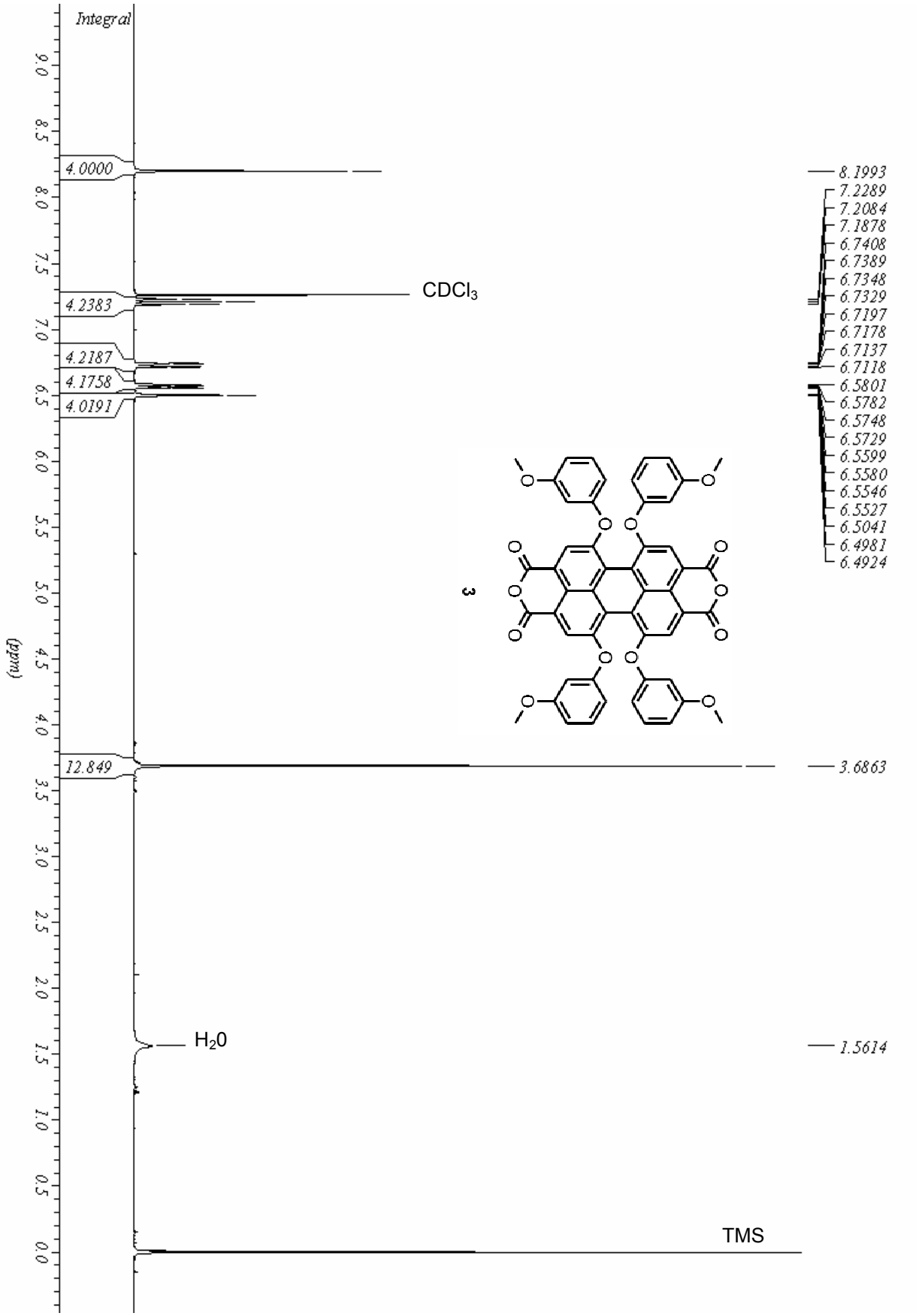

^{1}H NMR spectrum (400.13 MHz) of **4** in $CDCl_3$

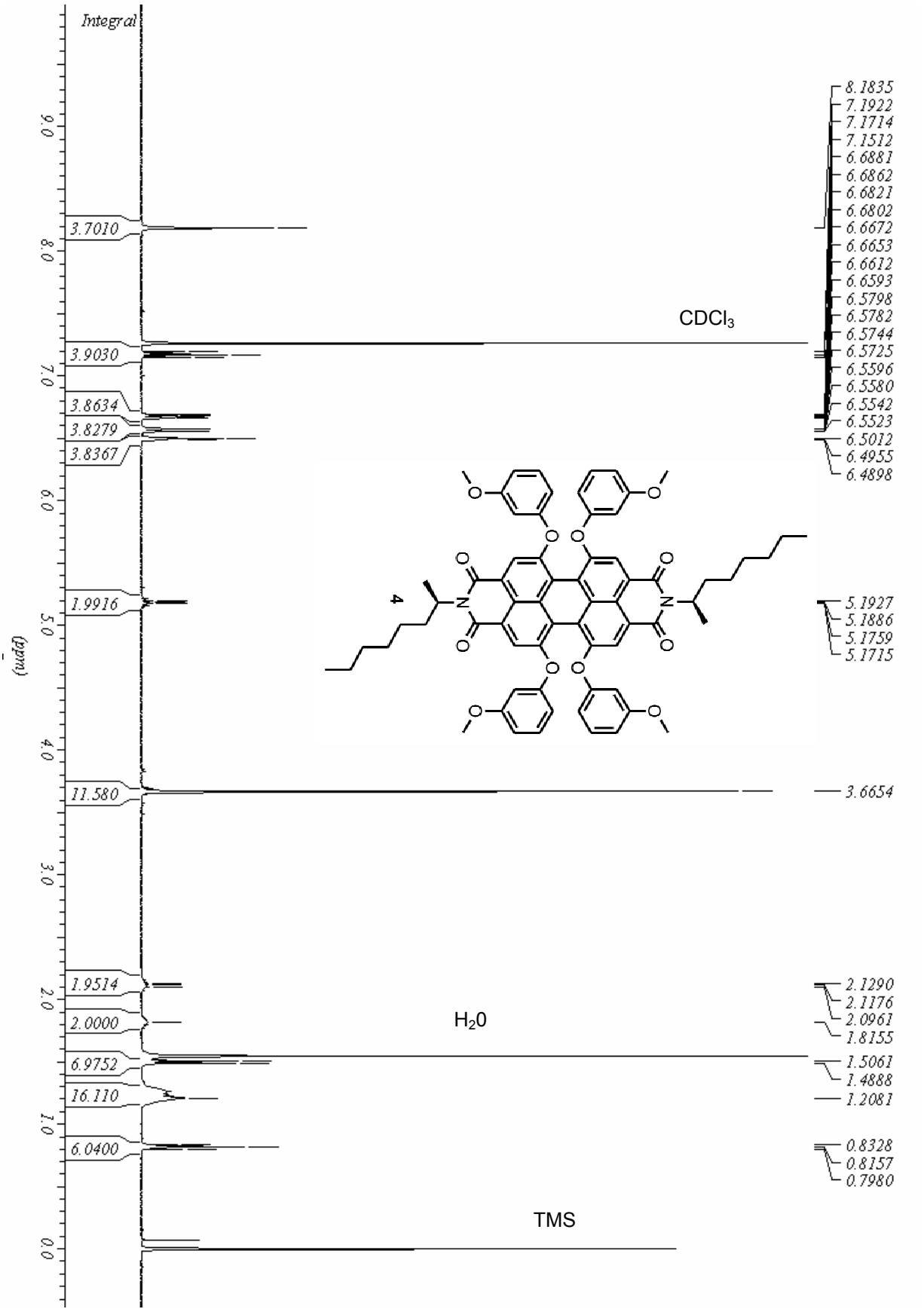

^{1}H NMR spectrum (400.13 MHz) of **5** in DMSO-d_6

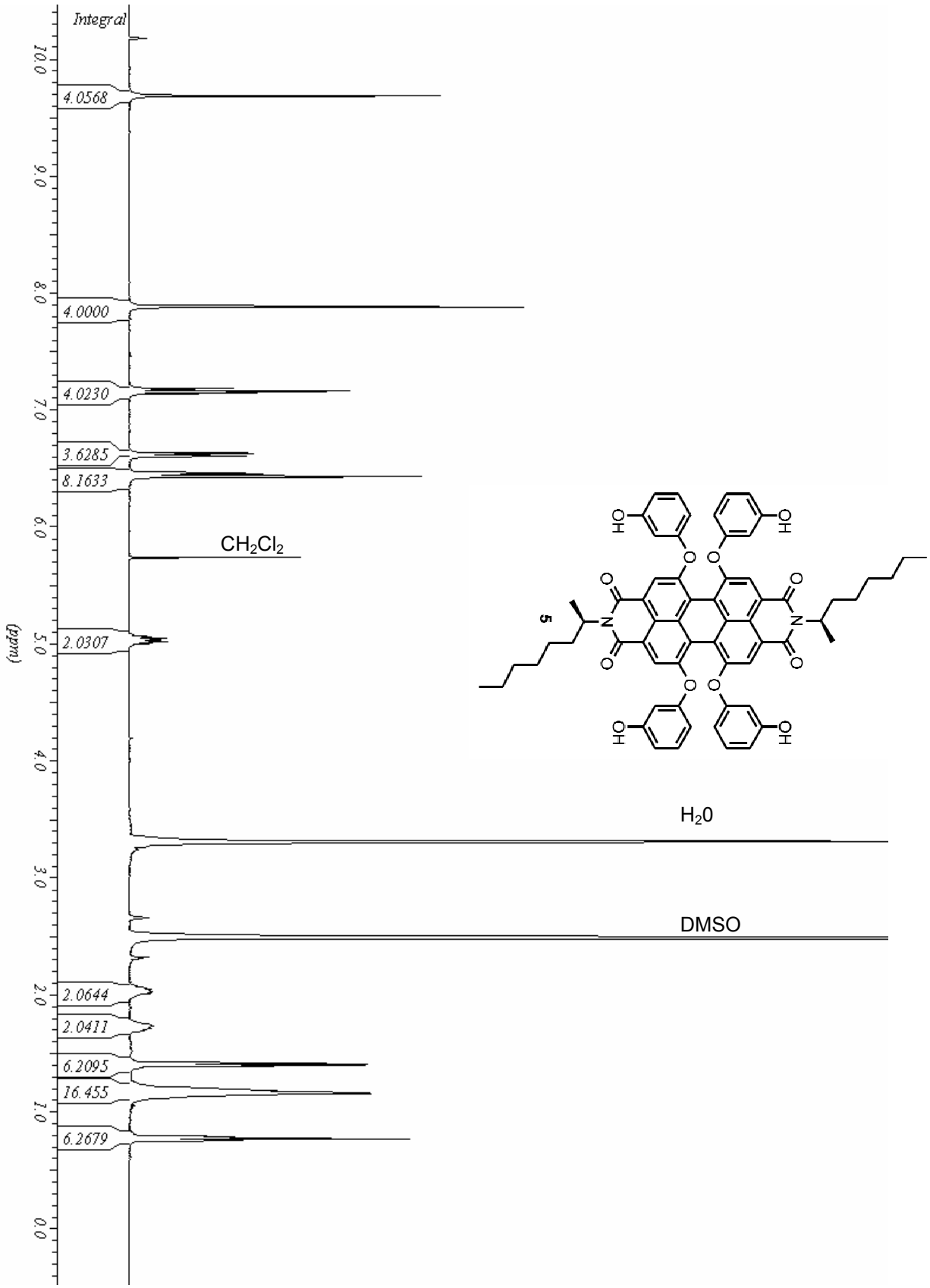

^{1}H NMR spectrum (500.13 MHz) of **6** in $CDCl_3$

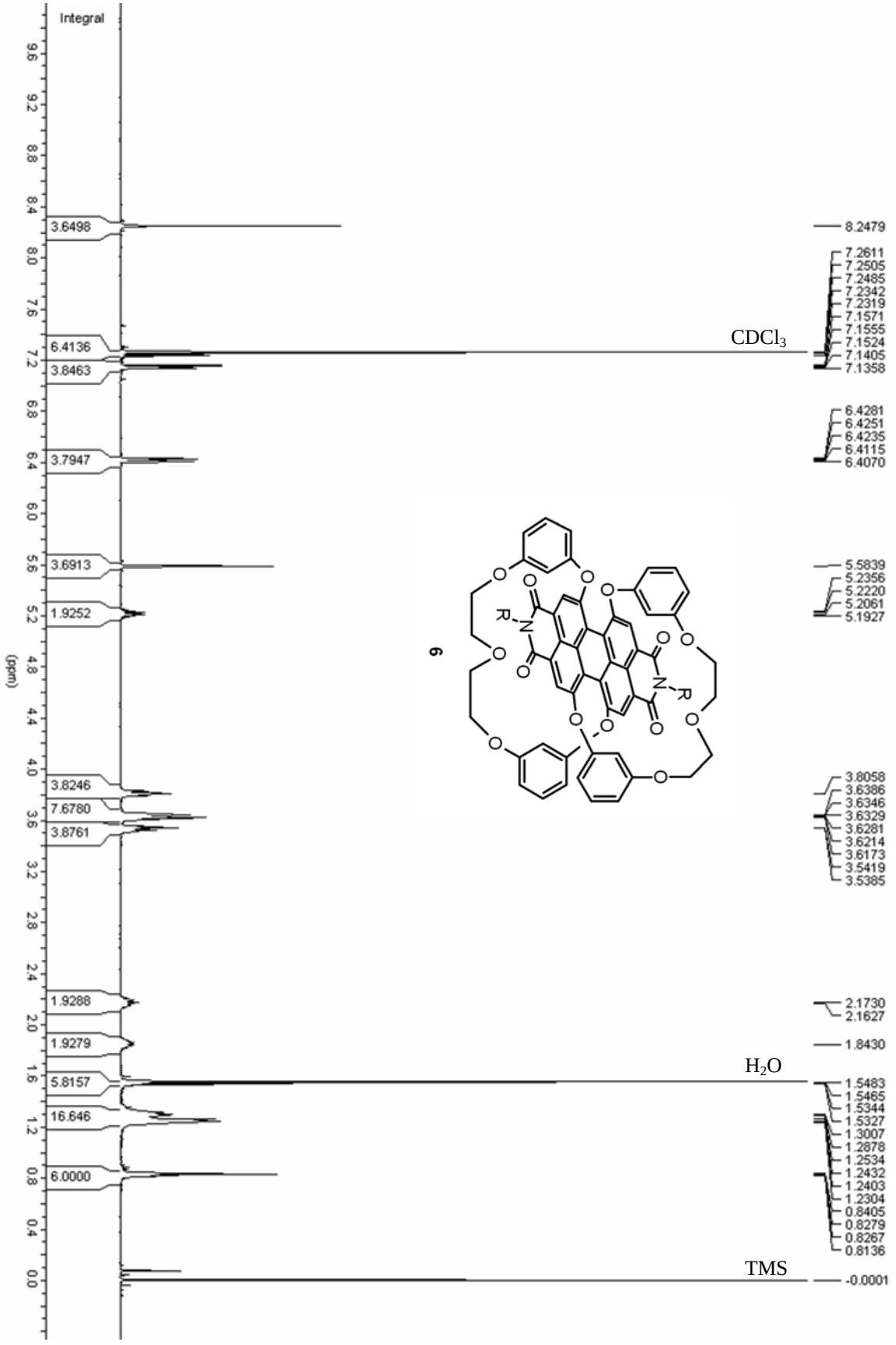

^{1}H NMR spectrum (400.13 MHz) of **7** in $CDCl_3$

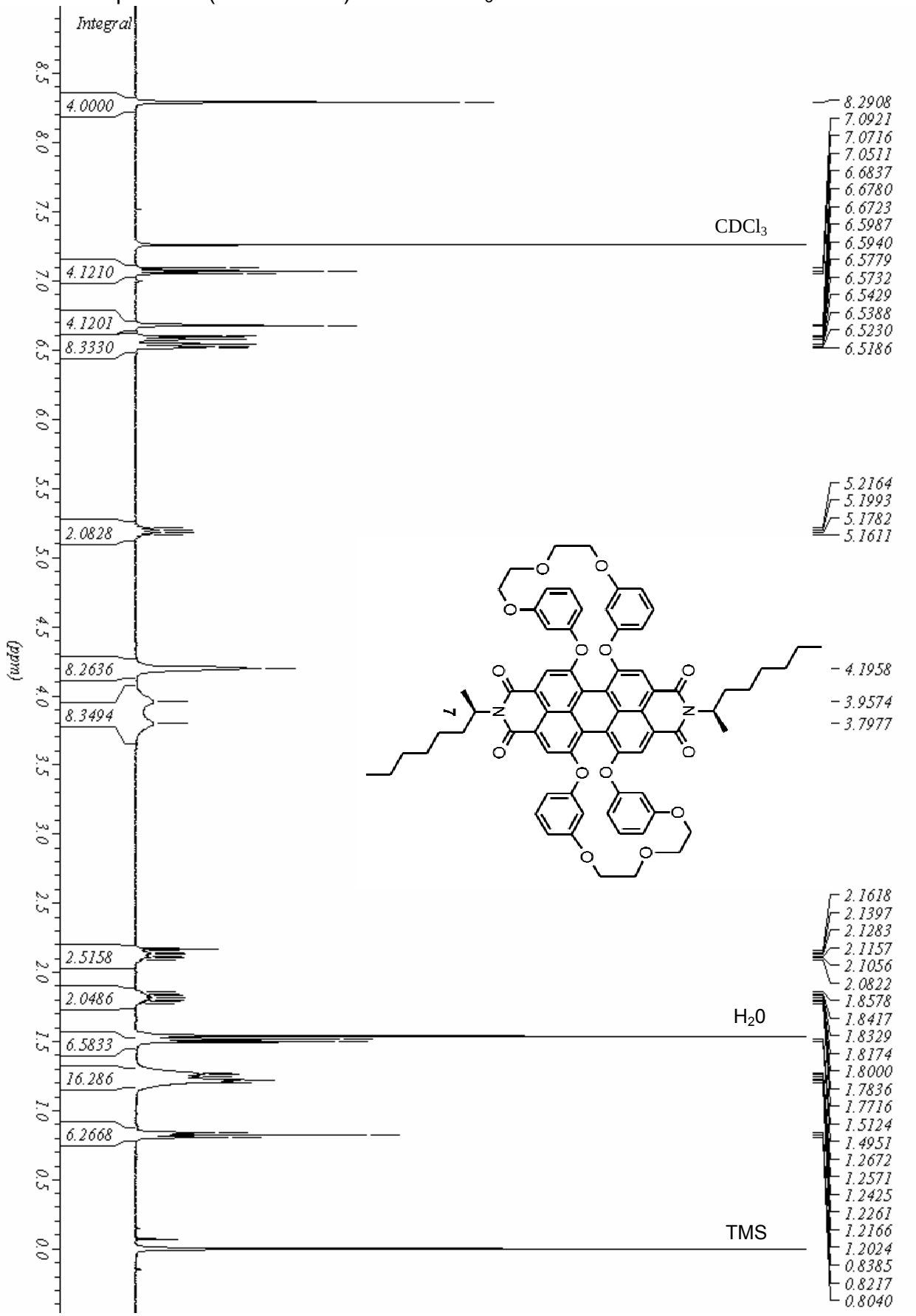

^{1}H NMR spectrum (400.13 MHz) of **8** in $CDCl_3$

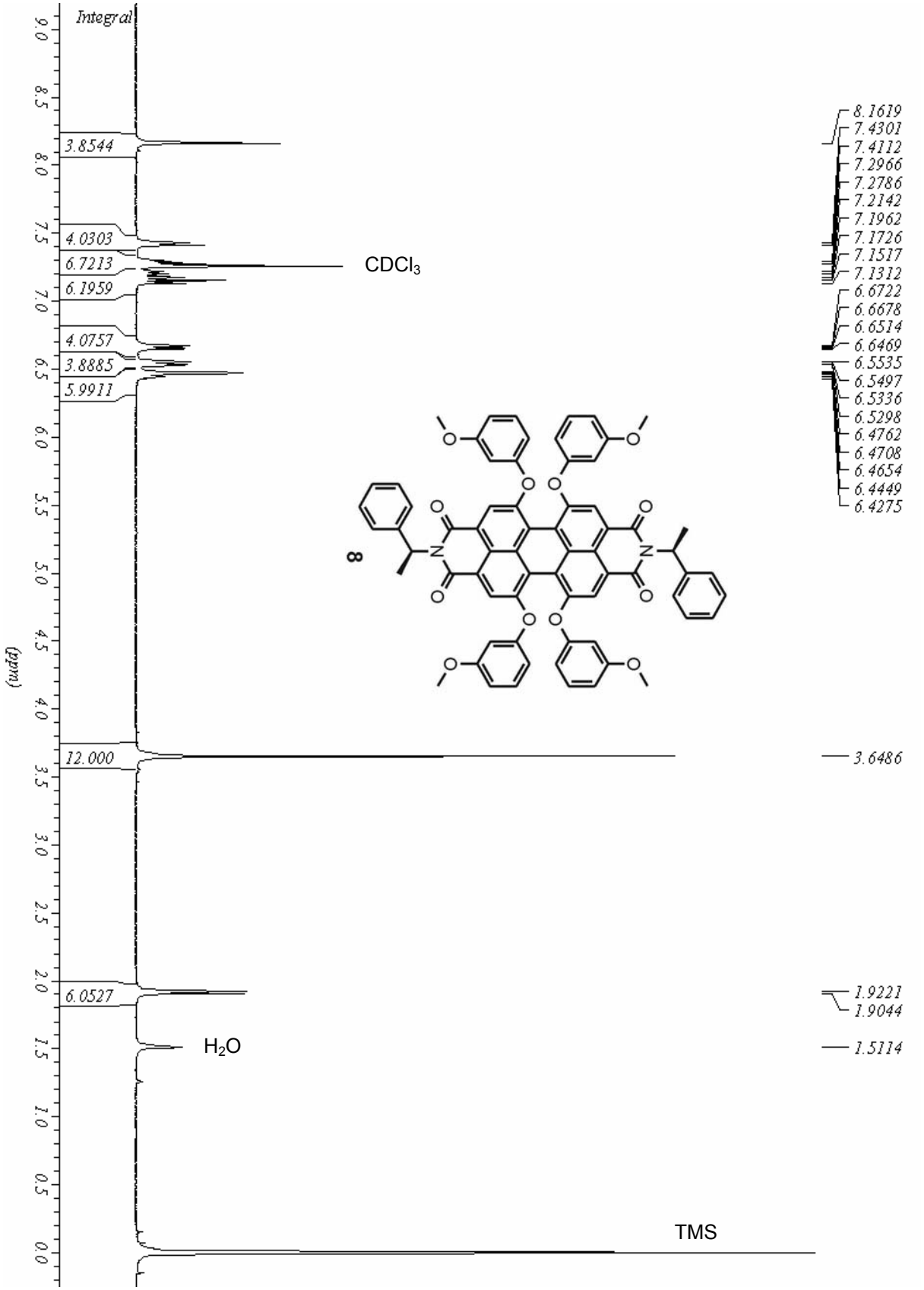

^{1}H NMR spectrum (400.13 MHz) of **9** in acetone-d_6

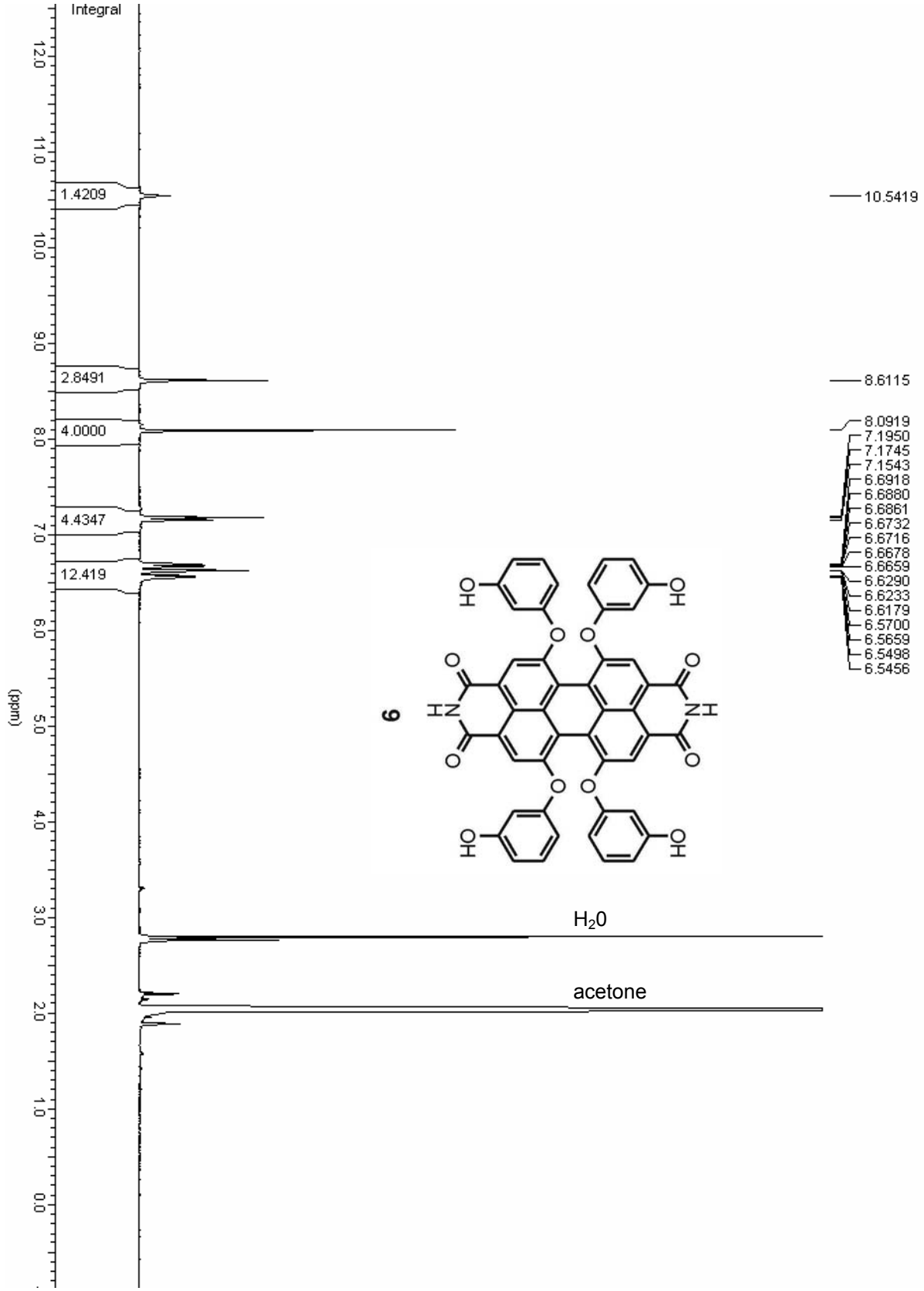

C Supplement for Chapter 5

C.1 Additional Graphical Material

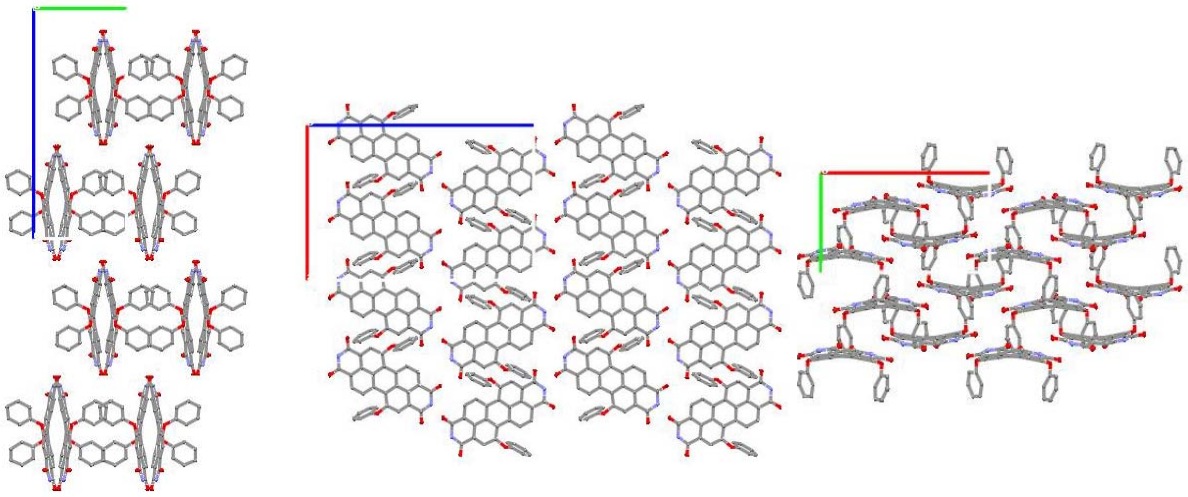

Figure C1. View along the a- (left), b- (middle) and c-axis (right) of the solid state structure rac-**4**. The red line represents the a-axis, the green line the b-axis and the blue line the c-axis of the unit cell.

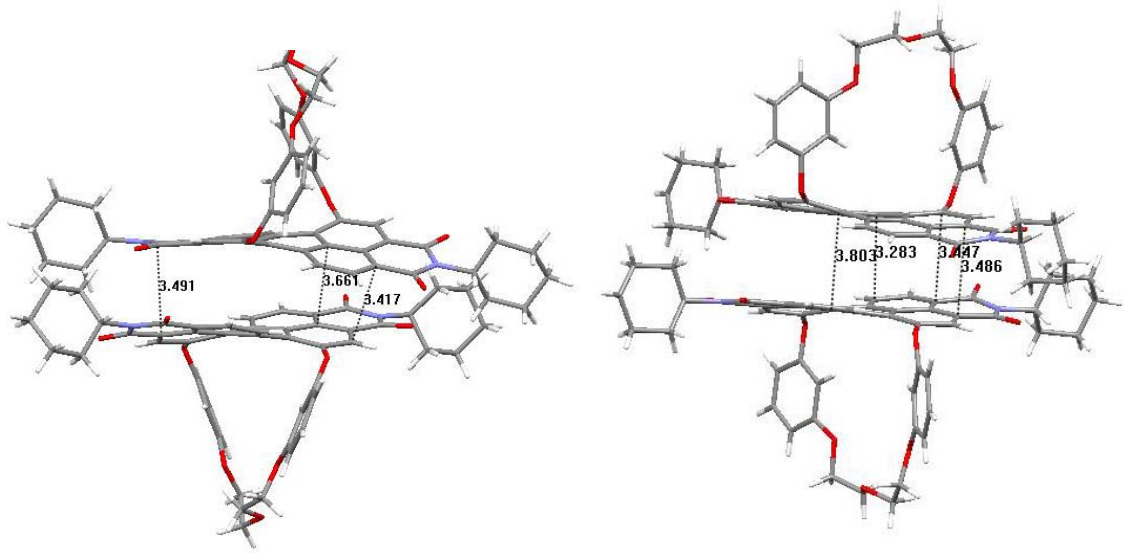

Figure C2. Closest π-π Distances in Dimer A (left) and Dimer B (rigth) observed in the solid state structure of (*P*)-**4**.

C.2 ^{1}H NMR spectra of 2-4

^{1}H NMR spectrum (400 MHz) of **2** in $CDCl_3$

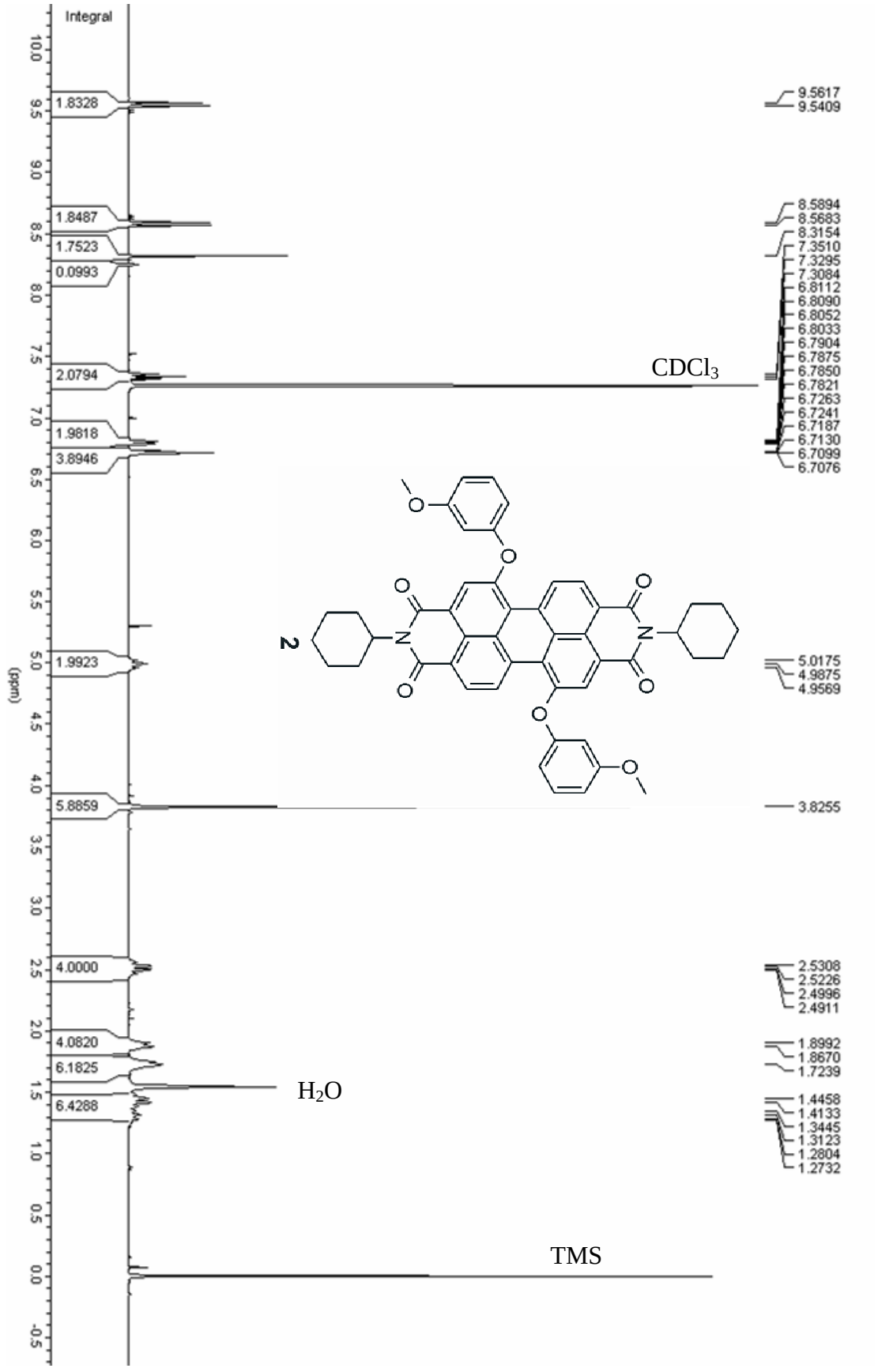

^{1}H NMR spectrum (400 MHz) of **3** in DMSO-d^{6}

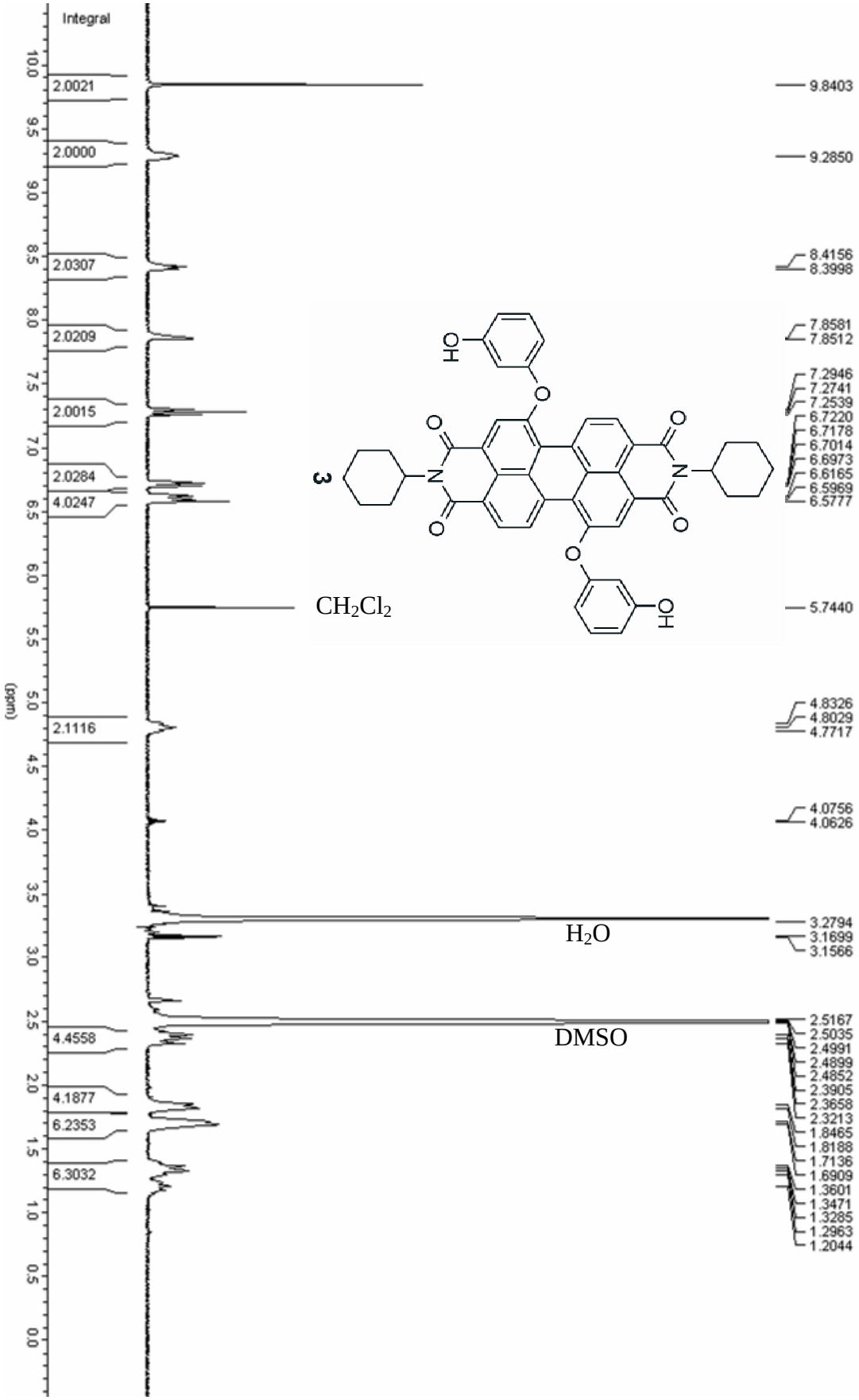

^{1}H NMR spectrum (400 MHz) of **4** in CD_2Cl_2

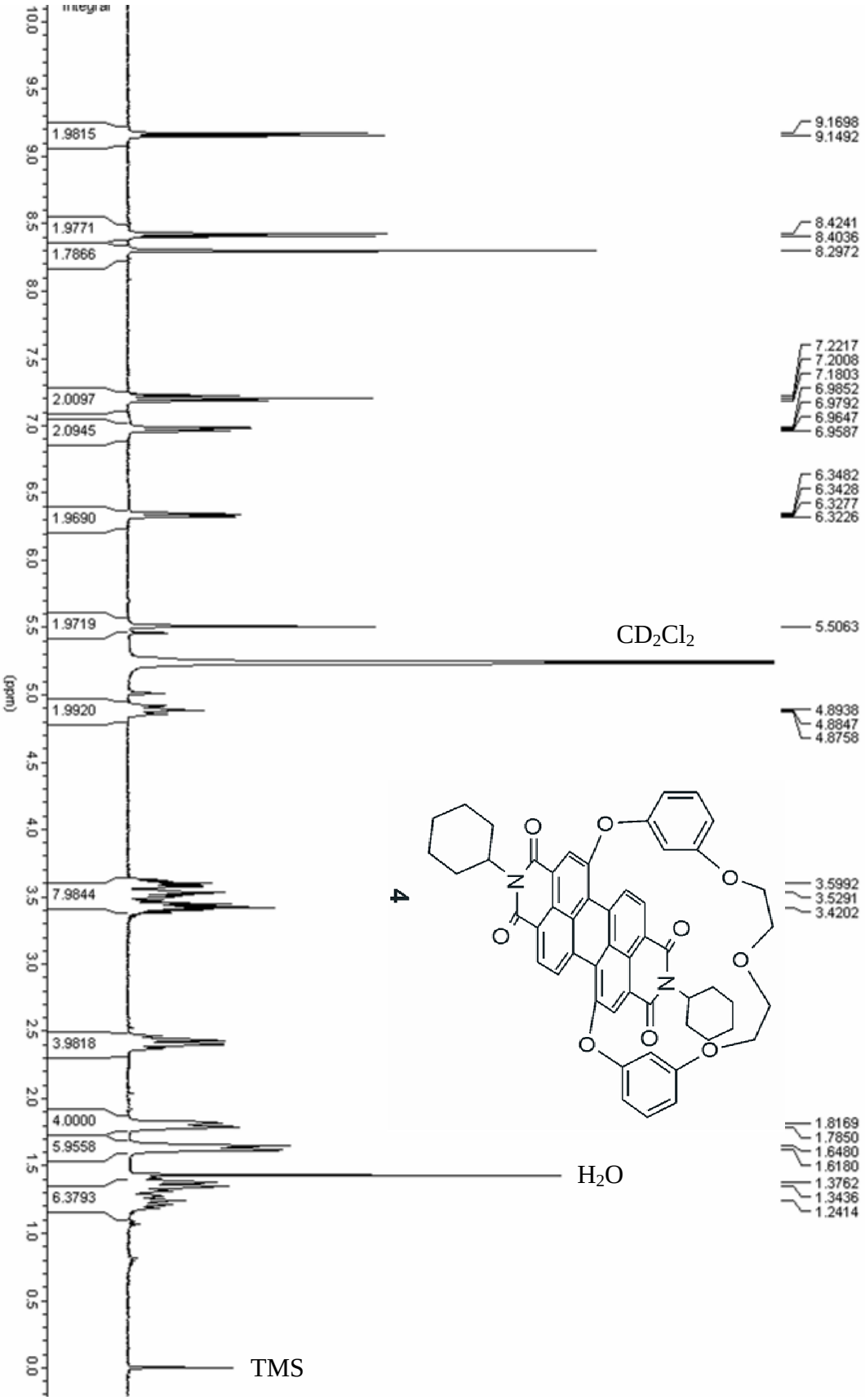

C.3 Crystal structure of (*P*)-4

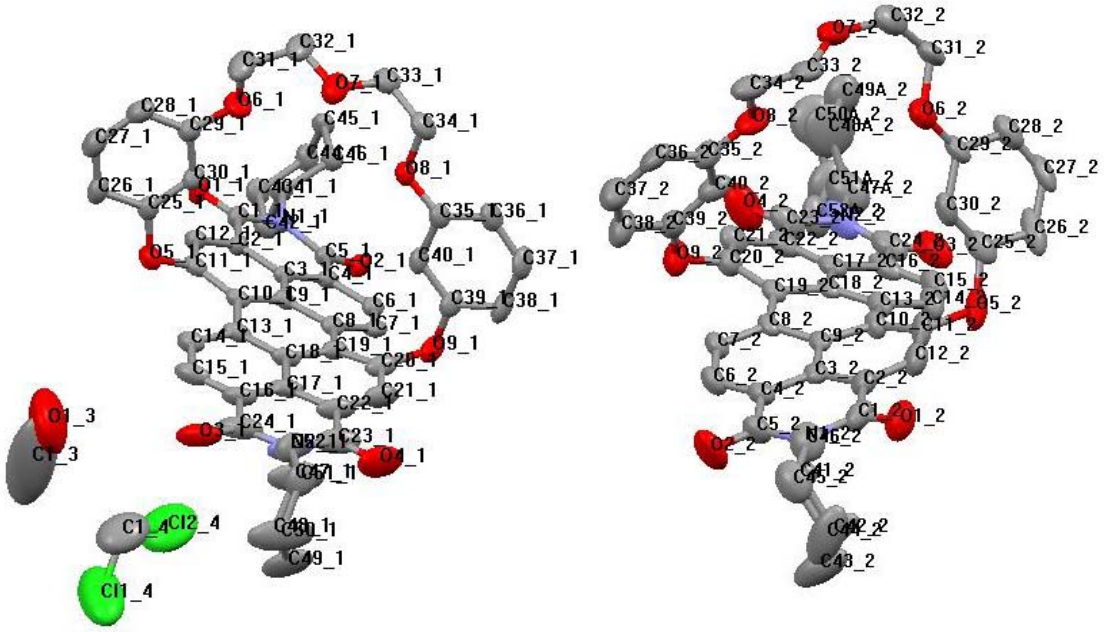

Figure C3. Fully labelled diagram of both crystallographic independent molecules of (*P*)-**4** $C_{52}H_{44}N_2O_9 \cdot (CH_2Cl_2)_{0.5}(H_3COH)_{0.5}$. Anisotropic displacement parameters are depicted on 50% probability level. Hydrogen atoms are omitted for clarity.

Table C1. Crystal Data and Structure Refinement for (*P*)-**4**.

Empirical formula	$C_{53}H_{47}ClN_2O_{9.50}$	
Formula weight	899.86	
Temperature	293(2) K	
Wavelength	0.71073 Å	
Crystal system	monoclinic	
Space group	C_2	
Unit cell dimensions	a = 21.7834(8) Å	α = 90°
	b = 20.2725(7) Å	β = 116.475(2)°
	c = 21.9159(8) Å	γ = 90°
Volume	8663.2(5) $Å^3$	
Z	8	
Density (calculated)	1.377 Mg/m^3	
Absorption coefficient	0.154 mm^{-1}	
F(000)	3764	
Crystal size	0.29 x 0.011 x 0.11 mm	
θ range for data collection	1.49 to 26.25°	
Index ranges	-27<=h<=27, -25<=k<=25, -27<=l<=27	
Reflections collected	157288	
Independent reflections	17437 [R_{int} = 0.0535]	
Completeness to θ = 26.00°	99.9 %	
Refinement method	Full-matrix least-squares on F^2	
Data / restraints / parameters	17437 / 184 / 1220	
Goodness-of-fit on F^2	S = 1.047	

R indices [for 13910 reflections with I>2σ(I)] R_1 = 0.0849, wR_2 = 0.2279

R indices (for all 17437 data)	R_1 = 0.1064, wR_2 = 0.2474
Absolute structure (Flack) parameter	0.1(2)
Largest diff. peak and hole	1.027 and -0.906 eÅ^{-3}

Table C2. Atomic Coordinates (x 10^4) and Equivalent Isotropic Displacement Parameters (Å^2 x 10^3) for (*P*)-**4**. U(eq) is defined as One Third of the Trace of the Orthogonalized U_{ij} Tensor

	x	y	z	U(eq)
N1_1	4789(2)	5465(2)	11016(2)	26(1)
N2_1	3427(3)	506(3)	8293(4)	73(2)
O1_1	4180(2)	5996(2)	10010(2)	37(1)
O2_1	5531(2)	4911(2)	11961(2)	34(1)
O3_1	3061(2)	1034(3)	7253(3)	76(2)
O4_1	3842(3)	13(2)	9337(4)	85(2)
O5_1	3124(2)	4273(2)	8225(2)	38(1)
O6_1	1294(2)	4249(2)	8819(2)	49(1)
O7_1	831(2)	3330(2)	9498(2)	55(1)
O8_1	1998(2)	2592(2)	10388(2)	36(1)
O9_1	4236(2)	1784(2)	11002(2)	42(1)
C1_1	4375(2)	5481(2)	10319(2)	29(1)
C2_1	4181(2)	4834(2)	9956(2)	26(1)
C3_1	4401(2)	4233(2)	10320(2)	25(1)
C4_1	4828(2)	4245(2)	11023(2)	27(1)
C5_1	5086(2)	4884(2)	11379(2)	27(1)
C6_1	5025(2)	3666(2)	11382(2)	30(1)
C7_1	4788(2)	3068(2)	11056(2)	31(1)
C8_1	4371(2)	3032(2)	10358(2)	29(1)
C9_1	4188(2)	3626(2)	9969(2)	28(1)
C10_1	3793(2)	3620(2)	9238(2)	28(1)
C11_1	3564(2)	4226(3)	8918(2)	33(1)
C12_1	3752(2)	4825(2)	9270(2)	30(1)
C13_1	3682(2)	2977(2)	8886(3)	34(1)
C14_1	3419(2)	2922(3)	8179(3)	39(1)
C15_1	3307(3)	2295(3)	7858(3)	52(2)
C16_1	3447(3)	1725(3)	8230(3)	47(1)
C17_1	3715(2)	1758(3)	8935(3)	45(1)
C18_1	3855(2)	2387(2)	9275(3)	34(1)
C19_1	4128(2)	2399(2)	10002(3)	33(1)
C20_1	4134(2)	1805(2)	10318(3)	44(1)
C21_1	4012(3)	1206(3)	9985(4)	53(2)
C22_1	3835(3)	1171(3)	9332(4)	54(2)
C23_1	3704(3)	519(4)	9000(5)	70(2)
C24_1	3299(3)	1077(4)	7876(4)	71(2)
C25_1	2446(2)	4415(2)	8073(2)	31(1)
C26_1	2043(3)	4680(2)	7430(3)	40(1)
C27_1	1359(3)	4795(3)	7247(3)	49(1)
C28_1	1074(3)	4666(3)	7691(3)	45(1)
C29_1	1489(3)	4405(2)	8322(2)	36(1)
C30_1	2186(2)	4295(2)	8527(2)	33(1)
C31_1	585(3)	4145(4)	8615(4)	67(2)

C32_1	534(3)	3956(4)	9261(4)	69(2)
C33_1	1026(3)	3247(3)	10190(3)	48(1)
C34_1	1362(3)	2587(3)	10435(3)	45(1)
C35_1	2476(3)	2123(2)	10746(2)	33(1)
C36_1	2402(3)	1646(2)	11165(3)	43(1)
C37_1	2949(3)	1221(3)	11518(3)	49(1)
C38_1	3555(3)	1262(3)	11460(3)	49(1)
C39_1	3603(3)	1738(2)	11040(2)	36(1)
C40_1	3080(3)	2166(2)	10676(2)	33(1)
C41_1	4963(2)	6114(2)	11378(2)	29(1)
C42_1	5671(3)	6358(2)	11498(3)	34(1)
C43_1	5762(3)	7067(2)	11770(3)	38(1)
C44_1	5644(3)	7122(2)	12399(2)	39(1)
C45_1	4945(2)	6851(2)	12275(2)	32(1)
C46_1	4856(2)	6137(2)	12015(2)	32(1)
C47_1	3261(4)	-166(4)	7981(6)	99(4)
C48_1	3741(3)	-390(3)	7736(5)	82(3)
C49_1	3622(4)	-1115(4)	7518(5)	95(3)
C50_1	2921(5)	-1297(5)	7131(8)	136(6)
C51_1	2427(4)	-1041(3)	7380(3)	59(2)
C52_1	2554(3)	-336(3)	7622(3)	53(2)
N1_2	-2117(2)	1408(3)	6069(2)	49(1)
N2_2	2368(4)	-617(3)	5362(3)	69(2)
O1_2	-2222(3)	425(2)	6529(3)	69(1)
O2_2	-1921(3)	2394(3)	5692(3)	83(2)
O3_2	1870(3)	-1630(3)	5208(2)	75(2)
O4_2	2716(3)	438(3)	5330(4)	93(2)
O5_2	-335(3)	-1059(2)	6624(3)	67(1)
O6_2	1583(2)	-410(2)	8724(2)	59(1)
O7_2	2529(2)	597(2)	9490(2)	61(1)
O8_2	1921(2)	1428(2)	8316(2)	53(1)
O9_2	1311(2)	1893(2)	6020(2)	53(1)
C1_2	-1913(3)	765(3)	6301(3)	49(1)
C2_2	-1291(3)	502(3)	6264(3)	43(1)
C3_2	-908(2)	904(2)	6046(2)	34(1)
C4_2	-1096(3)	1571(3)	5874(2)	39(1)
C5_2	-1739(3)	1825(3)	5864(3)	50(1)
C6_2	-696(3)	1978(3)	5708(3)	45(1)
C7_2	-77(3)	1753(3)	5739(3)	39(1)
C8_2	122(3)	1098(2)	5888(2)	33(1)
C9_2	-313(2)	657(2)	6014(2)	30(1)
C10_2	-153(3)	-33(2)	6129(3)	38(1)
C11_2	-512(3)	-399(3)	6414(3)	49(1)
C12_2	-1076(3)	-139(3)	6468(3)	52(1)
C13_2	362(3)	-304(2)	5935(2)	37(1)
C14_2	411(3)	-977(3)	5835(3)	48(1)
C15_2	889(4)	-1212(3)	5631(3)	53(2)
C16_2	1343(3)	-791(3)	5548(3)	51(2)
C17_2	1314(3)	-106(3)	5654(2)	40(1)
C18_2	793(3)	143(2)	5816(2)	33(1)
C19_2	742(3)	848(2)	5879(2)	34(1)
C20_2	1282(3)	1224(3)	5896(3)	44(1)

C21_2	1794(3)	973(3)	5754(3)	47(1)
C22_2	1796(3)	318(3)	5608(3)	48(1)
C23_2	2323(4)	64(4)	5430(4)	65(2)
C24_2	1866(4)	-1053(4)	5354(3)	61(2)
C25_2	310(4)	-1152(3)	7214(3)	54(2)
C26_2	495(5)	-1833(3)	7270(4)	76(2)
C27_2	1097(4)	-1984(3)	7842(3)	57(2)
C28_2	1499(4)	-1540(3)	8316(4)	60(2)
C29_2	1288(3)	-877(3)	8250(3)	43(1)
C30_2	662(3)	-713(3)	7674(3)	47(1)
C31_2	2249(3)	-563(3)	9272(3)	58(2)
C32_2	2488(4)	-4(4)	9784(4)	72(2)
C33_2	1980(3)	1041(3)	9344(3)	51(1)
C34_2	2014(3)	1626(4)	8984(3)	59(2)
C35_2	1737(3)	1898(3)	7833(3)	48(1)
C36_2	1664(3)	2580(3)	7921(3)	51(2)
C37_2	1467(4)	2973(4)	7369(4)	67(2)
C38_2	1334(4)	2751(3)	6738(4)	65(2)
C39_2	1427(3)	2077(3)	6660(3)	49(1)
C40_2	1623(3)	1664(3)	7193(3)	50(1)
C41_2	-2753(3)	1677(4)	6062(3)	55(2)
C42_2	-3388(3)	1315(5)	5552(5)	95(3)
C43_2	-4014(4)	1666(6)	5528(6)	116(4)
C44_2	-3985(5)	1777(5)	6225(8)	129(5)
C45_2	-3355(5)	2117(4)	6692(4)	78(2)
C46_2	-2701(4)	1767(4)	6757(4)	69(2)
C47_A2	2939(4)	-914(5)	5264(4)	96(3)
C48_A2	3590(5)	-714(14)	5876(9)	126(5)
C49_A2	4210(5)	-1058(11)	5891(10)	80(6)
C50_A2	4284(8)	-934(13)	5249(13)	112(10)
C51_A2	3627(10)	-1073(13)	4619(10)	97(9)
C52_A2	3022(9)	-731(9)	4639(7)	71(6)
C47_B2	2939(4)	-914(5)	5264(4)	96(3)
C48_B2	3666(5)	-698(10)	5705(9)	126(5)
C49_B2	4163(5)	-1075(9)	5527(8)	96(6)
C50_B2	3957(8)	-1052(12)	4774(9)	116(8)
C51_B2	3241(8)	-1302(11)	4351(7)	140(9)
C52_B2	2722(8)	-941(10)	4507(5)	99(6)
O1_3	6786(15)	2528(13)	3933(12)	295(13)
C1_3	6470(20)	2354(9)	4140(13)	340(30)
C1_4	5855(6)	1112(7)	3383(8)	139(5)
Cl1_4	5349(2)	769(4)	3683(2)	224(3)
Cl2_4	5353(2)	1342(2)	2534(2)	167(2)

Table C3. Anisotropic Displacement Parameters ($Å^2$ x 10^3) for (*P*)-**4**. The Anisotropic Displacement Factor Exponent takes the Form: $-2\pi^2$ [$h^2 a^{*2} U_{11}$ + ... + 2 h k a* b* U_{12}]

	U_{11}	U_{22}	U_{33}	U_{23}	U_{13}	U_{12}
N1_1	34(2)	19(2)	26(2)	0(1)	13(2)	-2(1)
N2_1	46(3)	34(3)	122(6)	-39(3)	23(3)	-3(2)
O1_1	50(2)	26(2)	28(2)	1(1)	11(1)	0(1)

O2_1	37(2)	27(2)	31(2)	-3(1)	8(1)	1(1)
O3_1	49(2)	78(3)	86(3)	-52(3)	15(2)	8(2)
O4_1	89(4)	25(2)	141(5)	-21(3)	52(4)	-8(2)
O5_1	40(2)	46(2)	27(2)	-7(2)	14(1)	-6(2)
O6_1	31(2)	66(3)	48(2)	-4(2)	16(2)	-7(2)
O7_1	44(2)	58(2)	50(2)	5(2)	8(2)	-6(2)
O8_1	45(2)	34(2)	37(2)	5(1)	24(2)	-1(1)
O9_1	38(2)	27(2)	51(2)	7(2)	11(2)	-4(1)
C1_1	30(2)	25(2)	29(2)	-1(2)	11(2)	-1(2)
C2_1	28(2)	21(2)	29(2)	-2(2)	12(2)	-1(2)
C3_1	26(2)	19(2)	33(2)	-5(2)	17(2)	-4(2)
C4_1	28(2)	21(2)	34(2)	-7(2)	15(2)	-2(2)
C5_1	31(2)	22(2)	30(2)	-4(2)	14(2)	-3(2)
C6_1	30(2)	27(2)	37(2)	-2(2)	18(2)	-4(2)
C7_1	27(2)	25(2)	44(3)	1(2)	20(2)	3(2)
C8_1	26(2)	26(2)	39(2)	-6(2)	18(2)	-7(2)
C9_1	29(2)	27(2)	32(2)	-10(2)	19(2)	-7(2)
C10_1	26(2)	30(2)	33(2)	-13(2)	17(2)	-7(2)
C11_1	29(2)	42(3)	32(2)	-9(2)	18(2)	-5(2)
C12_1	31(2)	29(2)	31(2)	-5(2)	14(2)	-1(2)
C13_1	28(2)	34(2)	45(3)	-19(2)	21(2)	-10(2)
C14_1	31(2)	45(3)	39(3)	-14(2)	14(2)	-3(2)
C15_1	34(3)	67(4)	56(3)	-37(3)	21(3)	-10(3)
C16_1	37(3)	41(3)	66(4)	-27(3)	26(3)	-4(2)
C17_1	29(2)	41(3)	66(3)	-29(3)	23(2)	-6(2)
C18_1	34(2)	25(2)	51(3)	-18(2)	25(2)	-9(2)
C19_1	29(2)	23(2)	50(3)	-6(2)	20(2)	-2(2)
C20_1	30(2)	26(2)	70(4)	-9(2)	18(2)	-5(2)
C21_1	48(3)	23(2)	88(5)	-11(3)	32(3)	-1(2)
C22_1	40(3)	25(3)	100(5)	-25(3)	34(3)	-8(2)
C23_1	44(3)	46(4)	117(7)	-43(4)	33(4)	-17(3)
C24_1	36(3)	80(5)	87(5)	-61(4)	17(3)	-6(3)
C25_1	39(2)	22(2)	26(2)	-6(2)	10(2)	-5(2)
C26_1	56(3)	27(2)	34(2)	2(2)	16(2)	0(2)
C27_1	56(3)	38(3)	37(3)	0(2)	6(2)	3(2)
C28_1	39(3)	39(3)	45(3)	-5(2)	8(2)	6(2)
C29_1	37(2)	31(2)	35(2)	-2(2)	13(2)	0(2)
C30_1	32(2)	26(2)	35(2)	1(2)	10(2)	-4(2)
C31_1	35(3)	81(5)	77(4)	33(4)	19(3)	5(3)
C32_1	38(3)	85(5)	93(5)	41(4)	37(3)	14(3)
C33_1	44(3)	50(3)	55(3)	-2(3)	27(3)	-4(2)
C34_1	54(3)	41(3)	53(3)	-3(2)	35(3)	-13(2)
C35_1	42(3)	23(2)	31(2)	-5(2)	15(2)	-9(2)
C36_1	61(3)	33(3)	42(3)	-4(2)	29(3)	-12(2)
C37_1	65(4)	33(3)	44(3)	10(2)	20(3)	-12(3)
C38_1	59(3)	29(3)	41(3)	11(2)	6(2)	-5(2)
C39_1	41(2)	20(2)	38(2)	-2(2)	10(2)	-7(2)
C40_1	44(3)	22(2)	25(2)	-2(2)	10(2)	-8(2)
C41_1	35(2)	16(2)	33(2)	-6(2)	13(2)	-2(2)
C42_1	40(2)	30(2)	38(2)	-8(2)	22(2)	-8(2)
C43_1	49(3)	26(2)	42(3)	-5(2)	21(2)	-12(2)
C44_1	51(3)	31(2)	31(2)	-7(2)	16(2)	-10(2)

C45_1	40(2)	29(2)	28(2)	-9(2)	14(2)	0(2)
C46_1	34(2)	27(2)	31(2)	-6(2)	13(2)	-5(2)
C47_1	64(4)	54(4)	173(10)	-76(6)	47(5)	-21(4)
C48_1	50(3)	39(3)	126(7)	-47(4)	11(4)	5(3)
C49_1	78(5)	47(4)	127(7)	-46(5)	16(5)	18(4)
C50_1	78(6)	72(6)	236(14)	-99(8)	51(8)	-21(5)
C51_1	69(4)	35(3)	54(3)	-19(3)	9(3)	-17(3)
C52_1	54(3)	33(3)	57(3)	-14(2)	10(3)	-7(2)
N1_2	37(2)	56(3)	47(3)	-7(2)	12(2)	6(2)
N2_2	93(4)	67(4)	66(3)	18(3)	52(3)	46(3)
O1_2	79(3)	53(3)	96(4)	-15(3)	57(3)	-10(2)
O2_2	71(3)	69(3)	118(5)	42(3)	52(3)	37(3)
O3_2	101(4)	64(3)	62(3)	0(2)	38(3)	43(3)
O4_2	105(4)	91(4)	128(5)	37(4)	93(4)	41(3)
O5_2	110(4)	33(2)	78(3)	-8(2)	60(3)	-17(2)
O6_2	57(2)	55(2)	59(3)	21(2)	22(2)	5(2)
O7_2	47(2)	76(3)	42(2)	11(2)	3(2)	-9(2)
O8_2	49(2)	69(3)	41(2)	-26(2)	20(2)	-10(2)
O9_2	71(3)	40(2)	63(3)	-7(2)	42(2)	-7(2)
C1_2	51(3)	51(3)	53(3)	-17(3)	30(3)	-18(3)
C2_2	42(3)	36(3)	46(3)	-8(2)	15(2)	-4(2)
C3_2	37(2)	34(2)	26(2)	-7(2)	9(2)	-1(2)
C4_2	37(2)	41(3)	32(2)	1(2)	11(2)	11(2)
C5_2	45(3)	47(3)	56(3)	11(3)	21(3)	16(3)
C6_2	54(3)	36(3)	44(3)	11(2)	22(3)	14(2)
C7_2	48(3)	33(2)	38(3)	8(2)	20(2)	8(2)
C8_2	46(3)	28(2)	20(2)	3(2)	10(2)	6(2)
C9_2	37(2)	27(2)	21(2)	-4(2)	7(2)	2(2)
C10_2	52(3)	24(2)	38(3)	-3(2)	22(2)	6(2)
C11_2	72(4)	22(2)	65(4)	-5(2)	42(3)	-5(2)
C12_2	64(4)	34(3)	64(4)	-9(3)	35(3)	-9(3)
C13_2	51(3)	31(2)	28(2)	-2(2)	16(2)	9(2)
C14_2	75(4)	31(3)	44(3)	-1(2)	31(3)	5(3)
C15_2	79(4)	33(3)	46(3)	2(2)	28(3)	17(3)
C16_2	71(4)	50(3)	25(2)	2(2)	16(2)	32(3)
C17_2	44(3)	44(3)	26(2)	4(2)	9(2)	13(2)
C18_2	42(3)	32(2)	16(2)	2(2)	7(2)	8(2)
C19_2	42(3)	34(2)	25(2)	2(2)	13(2)	9(2)
C20_2	48(3)	37(3)	46(3)	3(2)	19(2)	4(2)
C21_2	49(3)	52(3)	47(3)	13(3)	29(3)	8(3)
C22_2	57(3)	55(3)	34(3)	9(2)	21(2)	20(3)
C23_2	67(4)	77(5)	68(4)	31(4)	45(4)	27(4)
C24_2	75(4)	66(4)	42(3)	7(3)	27(3)	33(4)
C25_2	70(4)	59(4)	48(3)	15(3)	41(3)	26(3)
C26_2	154(8)	34(3)	71(5)	9(3)	77(5)	14(4)
C27_2	97(5)	36(3)	51(3)	22(3)	46(4)	22(3)
C28_2	74(4)	52(4)	62(4)	22(3)	37(3)	24(3)
C29_2	56(3)	38(3)	36(3)	14(2)	21(2)	17(2)
C30_2	57(3)	31(2)	67(4)	13(3)	40(3)	10(2)
C31_2	44(3)	56(4)	56(3)	28(3)	7(3)	10(3)
C32_2	60(4)	88(5)	63(4)	37(4)	24(3)	0(4)
C33_2	43(3)	64(4)	30(3)	-10(3)	3(2)	-4(3)

C34_2	44(3)	87(5)	40(3)	-17(3)	13(2)	-9(3)
C35_2	51(3)	50(3)	46(3)	-7(3)	24(3)	-13(3)
C36_2	41(3)	54(3)	59(4)	-31(3)	22(3)	-20(3)
C37_2	74(4)	61(4)	61(4)	-8(3)	26(4)	-16(3)
C38_2	79(5)	47(4)	77(5)	-14(3)	41(4)	-20(3)
C39_2	45(3)	46(3)	55(3)	0(3)	21(3)	-7(2)
C40_2	36(3)	64(4)	51(3)	-25(3)	22(2)	-9(3)
C41_2	39(3)	67(4)	58(3)	-13(3)	22(3)	6(3)
C42_2	37(3)	114(7)	130(7)	-73(6)	34(4)	-12(4)
C43_2	47(4)	137(9)	154(9)	-83(8)	37(5)	-8(5)
C44_2	94(7)	80(6)	271(16)	-53(8)	132(9)	-14(5)
C45_2	102(6)	70(5)	87(5)	1(4)	63(5)	26(4)
C46_2	84(5)	64(4)	78(5)	-12(4)	53(4)	13(4)
C47_A2	110(6)	104(6)	95(5)	9(5)	65(5)	38(5)
C48_A2	92(6)	158(9)	189(11)	3(8)	117(7)	18(6)
C49_A2	68(10)	76(10)	122(14)	-11(10)	65(10)	2(8)
C50_A2	119(14)	140(17)	130(16)	-17(12)	103(13)	16(11)
C51_A2	86(14)	106(14)	134(15)	-21(11)	80(12)	-12(11)
C52_A2	90(11)	59(9)	93(11)	15(8)	67(9)	2(8)
C47_B2	110(6)	104(6)	95(5)	9(5)	65(5)	38(5)
C48_B2	92(6)	158(9)	189(11)	3(8)	117(7)	18(6)
C49_B2	119(11)	101(10)	99(10)	0(9)	76(9)	33(8)
C50_B2	82(11)	154(14)	129(14)	-6(10)	62(10)	27(10)
C51_B2	137(13)	171(15)	149(13)	-6(11)	96(11)	62(11)
C52_B2	102(11)	113(12)	108(11)	33(8)	70(9)	46(9)
O1_3	390(30)	330(30)	240(20)	-140(20)	220(20)	-60(20)
C1_3	730(90)	68(9)	148(17)	40(10)	140(30)	-10(20)
C1_4	69(6)	136(11)	177(13)	4(9)	23(7)	2(7)
Cl1_4	79(2)	432(10)	146(3)	-80(5)	35(2)	-5(3)
Cl2_4	72(2)	185(4)	176(4)	27(3)	-6(2)	13(2)

C.4 Crystal structure of rac-4

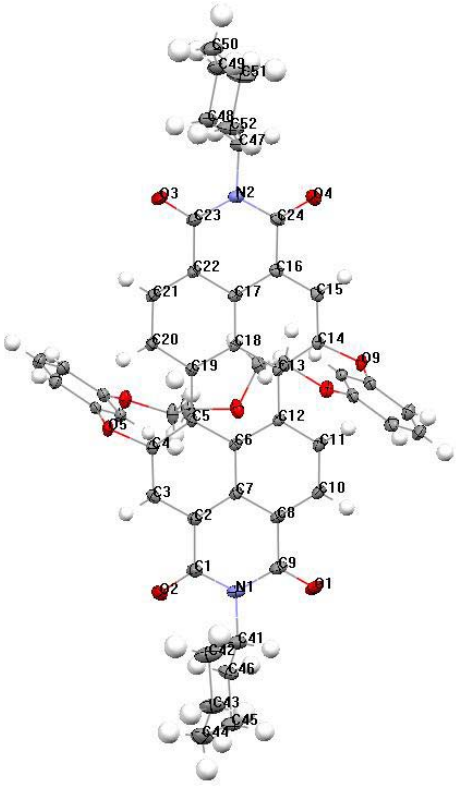

Figure C4. Fully labelled diagram of rac-**4** ($C_{52}H_{44}N_2O_9$). Anisotropic displacement parameters are depicted on 50% probability level. Hydrogen atoms are omitted for clarity.

Table C4. Crystal Data and Structure Refinement for rac-**4**

Empirical formula	$C_{52}H_{44}N_2O_9$	
Formula weight	840.89	
Temperature	100(2) K	
Wavelength	0.71073 Å	
Crystal system	Orthorhombic	
Space group	Pna2(1)	
Unit cell dimensions	a = 16.7412(7) Å	α = 90°
	b = 9.8474(3) Å	β = 90°
	c = 24.5510(9) Å	γ = 90°
Volume	4047.4(3) $Å^3$	
Z	4	
Density (calculated)	1.380 Mg/m^3	
Absorption coefficient	0.095 mm^{-1}	
F(000)	1768	
Crystal size	0.17 x 0.12 x 0.06 mm	
θ range for data collection	2.23 to 30.77°	
Index ranges	-24<=h<=22, -14<=k<=13, -35<=l<=35	
Reflections collected	128887	
Independent reflections	12590 [R_{int} = 0.0740]	

Completeness to θ = 26.00°	100.0 %
Absorption correction	Semi-empirical from equivalents
Max. and min. transmission	0.99 and 0.98
Refinement method	Full-matrix least-squares on F^2
Data / restraints / parameters	12590 / 1 / 568
Goodness-of-fit on F^2	S = 1.056
R indices [for 11469 reflections with I>2σ(I)]	R_1 = 0.0478, wR_2 = 0.1238
R indices (for all 12590 data)	R_1 = 0.0561, wR_2 = 0.1300
Absolute structure (Flack) parameter	-0.1(5)
Largest diff. peak and hole	0.746 and -0.335 e$Å^{-3}$

Table C5. Atomic Coordinates (x 10^4) and Equivalent Isotropic Displacement Parameters ($Å^2$ x 10^3) for rac-**4**. U(eq) is defined as One Third of the Trace of the Orthogonalized U_{ij} Tensor

	x	y	z	U(eq)
O(9)	6394(1)	891(1)	8087(1)	16(1)
O(5)	10769(1)	1147(1)	8759(1)	16(1)
C(5)	9430(1)	1468(1)	8394(1)	13(1)
C(18)	8183(1)	1521(1)	8943(1)	12(1)
C(19)	9035(1)	1632(1)	8923(1)	12(1)
O(8)	7114(1)	-3866(1)	8003(1)	19(1)
O(6)	10263(1)	-3669(1)	8975(1)	19(1)
C(6)	8956(1)	1598(1)	7913(1)	13(1)
C(16)	6969(1)	1361(2)	9497(1)	15(1)
C(7)	9332(1)	1760(2)	7399(1)	14(1)
C(17)	7798(1)	1591(1)	9459(1)	13(1)
C(8)	8879(1)	2076(2)	6930(1)	17(1)
C(13)	7714(1)	1378(1)	8460(1)	13(1)
C(14)	6899(1)	1098(1)	8527(1)	14(1)
C(3)	10612(1)	1300(2)	7807(1)	16(1)
N(2)	6997(1)	1776(1)	10482(1)	19(1)
C(4)	10250(1)	1272(1)	8321(1)	14(1)
N(1)	10102(1)	2177(2)	6377(1)	21(1)
C(24)	6547(1)	1428(2)	10026(1)	18(1)
C(22)	8232(1)	1913(2)	9931(1)	16(1)
C(11)	7679(1)	1929(2)	7462(1)	17(1)
C(2)	10165(1)	1597(2)	7352(1)	15(1)
C(21)	9043(1)	2138(2)	9899(1)	17(1)
C(9)	9269(1)	2323(2)	6398(1)	21(1)
C(12)	8102(1)	1616(1)	7934(1)	13(1)
O(4)	5829(1)	1210(2)	10057(1)	27(1)
C(15)	6533(1)	1074(2)	9037(1)	16(1)
O(7)	8628(1)	-5305(1)	8280(1)	22(1)
O(1)	8884(1)	2645(2)	5998(1)	31(1)
C(23)	7823(1)	2031(2)	10466(1)	19(1)
C(20)	9442(1)	1964(2)	9401(1)	16(1)
O(2)	11281(1)	1592(2)	6770(1)	30(1)
C(30)	6782(1)	-1478(2)	8074(1)	14(1)

C(1)	10567(1)	1770(2)	6819(1)	20(1)
C(39)	10796(1)	-69(2)	9040(1)	14(1)
O(3)	8184(1)	2347(2)	10877(1)	30(1)
C(36)	10971(1)	-2444(2)	9631(1)	19(1)
C(40)	10467(1)	-1259(1)	8834(1)	14(1)
C(25)	6423(1)	-361(2)	7829(1)	15(1)
C(28)	6399(1)	-2837(2)	7291(1)	21(1)
C(47)	6553(1)	1906(2)	11006(1)	21(1)
C(10)	8062(1)	2194(2)	6968(1)	19(1)
C(29)	6768(1)	-2715(2)	7799(1)	16(1)
C(35)	10562(1)	-2446(2)	9137(1)	15(1)
C(38)	11196(1)	-36(2)	9535(1)	19(1)
C(34)	9657(1)	-3666(2)	8567(1)	21(1)
C(32)	7954(1)	-5056(2)	8621(1)	21(1)
C(41)	10479(1)	2481(2)	5840(1)	24(1)
C(31)	7554(1)	-3716(2)	8498(1)	17(1)
C(46)	10855(1)	1239(2)	5579(1)	25(1)
C(26)	6057(1)	-446(2)	7324(1)	20(1)
C(37)	11279(1)	-1229(2)	9826(1)	21(1)
C(48)	6826(1)	870(2)	11430(1)	28(1)
C(45)	11207(1)	1596(2)	5025(1)	28(1)
C(33)	9379(1)	-5136(2)	8539(1)	27(1)
C(27)	6055(1)	-1698(2)	7058(1)	23(1)
C(49)	6261(1)	947(2)	11919(1)	31(1)
C(52)	6551(1)	3344(2)	11223(1)	32(1)
C(50)	6209(2)	2374(3)	12146(1)	39(1)
C(51)	5984(2)	3410(2)	11712(1)	40(1)
C(43)	11370(2)	4040(2)	5308(1)	36(1)
C(42)	11022(2)	3705(2)	5867(1)	40(1)
C(44)	11763(1)	2779(2)	5054(1)	37(1)

Table C6. Anisotropic Displacement Parameters ($Å^2$ x 10^3) for rac-**4**. The Anisotropic Displacement Factor Exponent takes the Form: $-2\pi^2$ [h^2 a^{*2} U_{11} + ... + 2 h k a* b* U_{12}]

	U_{11}	U_{22}	U_{33}	U_{23}	U_{13}	U_{12}
O(9)	15(1)	14(1)	20(1)	-2(1)	-6(1)	3(1)
O(5)	14(1)	15(1)	20(1)	2(1)	-5(1)	-4(1)
C(5)	14(1)	11(1)	13(1)	1(1)	-2(1)	-1(1)
C(18)	14(1)	11(1)	12(1)	0(1)	-3(1)	1(1)
C(19)	14(1)	10(1)	14(1)	0(1)	0(1)	-1(1)
O(8)	20(1)	14(1)	22(1)	-3(1)	-5(1)	3(1)
O(6)	18(1)	14(1)	25(1)	4(1)	-7(1)	-2(1)
C(6)	16(1)	10(1)	13(1)	-1(1)	-1(1)	-1(1)
C(16)	16(1)	14(1)	16(1)	0(1)	1(1)	3(1)
C(7)	17(1)	13(1)	13(1)	-1(1)	-1(1)	-2(1)
C(17)	17(1)	10(1)	13(1)	0(1)	0(1)	2(1)
C(8)	23(1)	17(1)	11(1)	0(1)	-1(1)	-1(1)

C(13)	14(1)	11(1)	13(1)	0(1)	-2(1)	2(1)
C(14)	14(1)	11(1)	16(1)	1(1)	-2(1)	2(1)
C(3)	14(1)	14(1)	20(1)	-2(1)	2(1)	-4(1)
N(2)	21(1)	21(1)	15(1)	1(1)	4(1)	0(1)
C(4)	14(1)	12(1)	17(1)	0(1)	-2(1)	-2(1)
N(1)	27(1)	22(1)	15(1)	-1(1)	5(1)	0(1)
C(24)	18(1)	19(1)	18(1)	2(1)	3(1)	4(1)
C(22)	19(1)	16(1)	13(1)	-2(1)	-1(1)	0(1)
C(11)	18(1)	18(1)	16(1)	1(1)	-4(1)	2(1)
C(2)	16(1)	15(1)	15(1)	-3(1)	2(1)	-3(1)
C(21)	21(1)	18(1)	13(1)	0(1)	-3(1)	-3(1)
C(9)	29(1)	22(1)	14(1)	-3(1)	2(1)	1(1)
C(12)	16(1)	12(1)	13(1)	-1(1)	-1(1)	0(1)
O(4)	17(1)	41(1)	24(1)	1(1)	2(1)	0(1)
C(15)	15(1)	14(1)	19(1)	1(1)	0(1)	4(1)
O(7)	15(1)	18(1)	34(1)	-6(1)	-4(1)	2(1)
O(1)	36(1)	43(1)	13(1)	2(1)	0(1)	6(1)
C(23)	22(1)	22(1)	14(1)	-2(1)	2(1)	-2(1)
C(20)	17(1)	16(1)	15(1)	0(1)	-3(1)	-3(1)
O(2)	18(1)	48(1)	23(1)	-2(1)	4(1)	-9(1)
C(30)	12(1)	15(1)	14(1)	-2(1)	-1(1)	1(1)
C(1)	21(1)	22(1)	17(1)	-3(1)	3(1)	-7(1)
C(39)	10(1)	16(1)	16(1)	1(1)	1(1)	-1(1)
O(3)	28(1)	50(1)	14(1)	-7(1)	1(1)	-10(1)
C(36)	18(1)	21(1)	17(1)	5(1)	-1(1)	1(1)
C(40)	11(1)	14(1)	16(1)	1(1)	-2(1)	0(1)
C(25)	12(1)	14(1)	17(1)	-1(1)	0(1)	0(1)
C(28)	20(1)	23(1)	20(1)	-6(1)	-2(1)	1(1)
C(47)	24(1)	23(1)	16(1)	0(1)	6(1)	0(1)
C(10)	23(1)	21(1)	12(1)	1(1)	-4(1)	2(1)
C(29)	12(1)	16(1)	19(1)	-1(1)	0(1)	1(1)
C(35)	11(1)	15(1)	18(1)	1(1)	0(1)	0(1)
C(38)	19(1)	21(1)	19(1)	-3(1)	-4(1)	0(1)
C(34)	17(1)	14(1)	33(1)	3(1)	-10(1)	-2(1)
C(32)	17(1)	15(1)	30(1)	3(1)	0(1)	1(1)
C(41)	29(1)	26(1)	18(1)	2(1)	7(1)	2(1)
C(31)	14(1)	13(1)	24(1)	0(1)	-3(1)	1(1)
C(46)	27(1)	22(1)	27(1)	-5(1)	12(1)	-3(1)
C(26)	21(1)	21(1)	19(1)	1(1)	-5(1)	2(1)
C(37)	20(1)	27(1)	16(1)	1(1)	-5(1)	2(1)
C(48)	30(1)	31(1)	22(1)	5(1)	7(1)	6(1)
C(45)	34(1)	29(1)	21(1)	-2(1)	10(1)	6(1)
C(33)	17(1)	13(1)	51(1)	-1(1)	-11(1)	1(1)
C(27)	23(1)	29(1)	15(1)	-3(1)	-5(1)	0(1)
C(49)	37(1)	35(1)	22(1)	8(1)	8(1)	1(1)
C(52)	47(1)	20(1)	30(1)	-1(1)	21(1)	1(1)
C(50)	43(1)	52(1)	22(1)	-7(1)	12(1)	-6(1)
C(51)	53(1)	27(1)	39(1)	-6(1)	26(1)	1(1)
C(43)	54(1)	27(1)	27(1)	4(1)	15(1)	-10(1)
C(42)	64(2)	29(1)	26(1)	-4(1)	14(1)	-16(1)
C(44)	37(1)	44(1)	31(1)	5(1)	10(1)	-6(1)

D. Supplement for Chapter 6

D.1 Details for Data Evaluation of the Kinetic Measurements of 1 and 2a

The rate law of the racemisation process between (*P*)- and (*M*)-enantiomers is given by

$$v = -\frac{d(A)}{A_0} = kdt \qquad \text{(eq. D-1)}$$

where A is the concentration of the enantiomer which is present in excess and A_0 the respective initial concentration.

The integrated form of the rate law is given by

$$\ln\frac{A}{A_0} = -kt \qquad \text{(eq. D-2)}$$

$$\Rightarrow \quad \frac{A}{A_0} = e^{-kt} \Leftrightarrow A = A_0\, e^{-kt} \qquad \text{(eq. D-3)}$$

Owing to a linear relationship between CD amplitude and the concentration of initial enantiomer, the latter can be directly replaced by the experimentally determined CD amplitude. According to equation D-3 the rate constant at a certain temperature can than be determined from the exponential decay of the CD signal in dependence on the time as shown in Figure D1 and can be used to calculate the half lifetimes according to $t_{1/2} = \ln 2/k$. The half lifetimes and rate constants of **1** and **2a** at different temperatures are given in Table 1 in the main text.

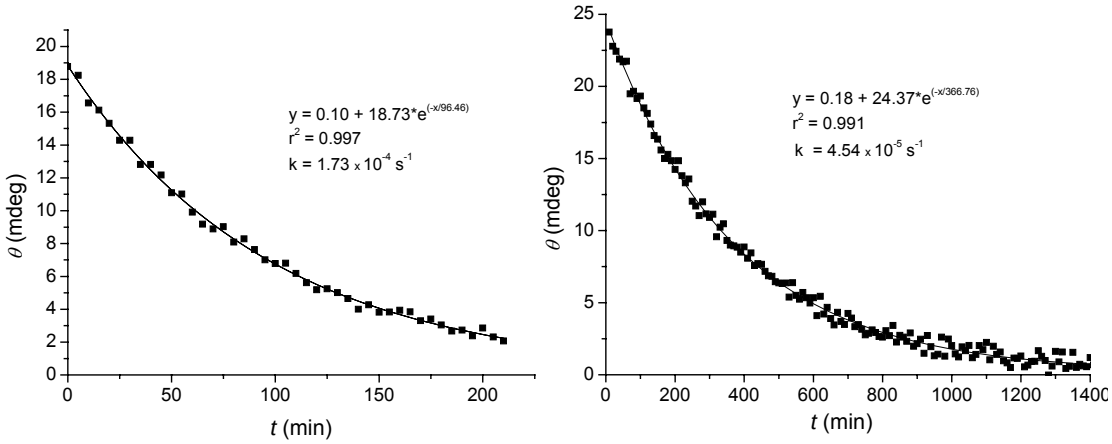

Figure D1. Exponential decay of the CD amplitude of (*P*)-**1** at 378 K in 1,1,2,2-tetrachlorethane and (*P*,*R*,*R*)-**2a** at 303 K in chloroform. The detection wavelength was 510 nm and 500 nm, respectively.

Additionally, the rate constant can be accessed by linear regression analysis according to equation D-4 and can be obtained from the slope of the straight line (eq. D-5) as shown in Figure D2.

$$\ln A = -kt - \ln A_0 \quad \text{(y = mx + c)} \qquad \text{(eq. D-4)}$$

$$m = -k \qquad \text{(eq. D-5)}$$

The determination according to equation D-3 is more accurate as the error for the linear regression analysis is amplified by the signal to noise ratio at low CD amplitudes.

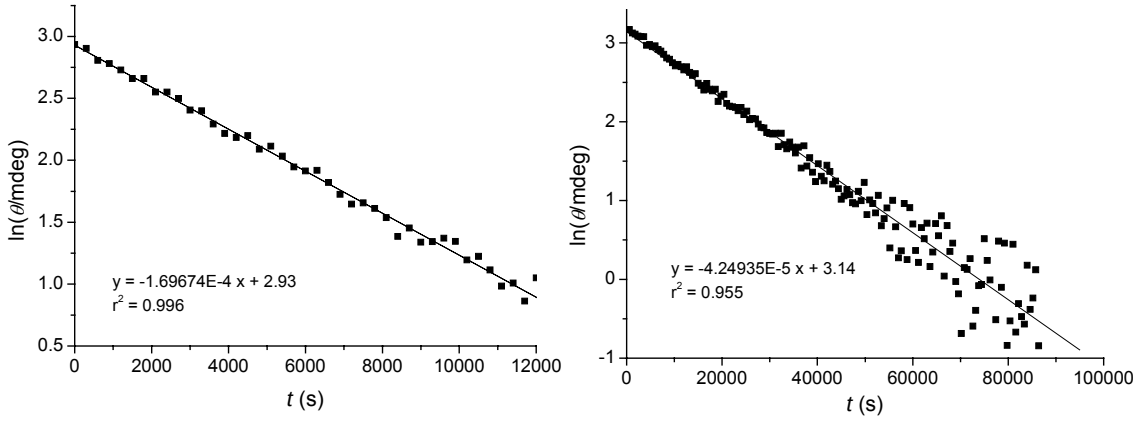

Figure D2. Data evaluation by linear regression analysis for the kinetic measurements of (*P*)-**1** at 378 K in 1,1,2,2-tetrachlorethane and of (*P*,*R*,*R*)-**2a** at 303 K in chloroform. The detection wavelength was 510 nm and 500 nm, respectively.

The temperature dependence of the rate constant can be used to determine the activation energy of a process according to the Arrhenius equation (eq. D-6).

$$k = Ae^{-\frac{E_A}{RT}} \quad \Rightarrow \quad \ln k = -\frac{E_A}{R}\frac{1}{T} + \ln A \qquad \text{(y = mx + c)} \qquad \text{(eq. D-6)}$$

$$m = -\left(\frac{E_A}{R}\right) \quad \text{and} \quad c = \ln A \qquad \text{(eq. D-7)}$$

The activation energy of a reaction E_A can therefore be evaluated by determination of k at different temperatures and linear regression analysis according to equation D-6. The activation energy E_A can be calculated from the slope of the straight line according to equation D-7. Data evaluation according to Arrhenius for **1** and **2a** are shown in Figure D3.

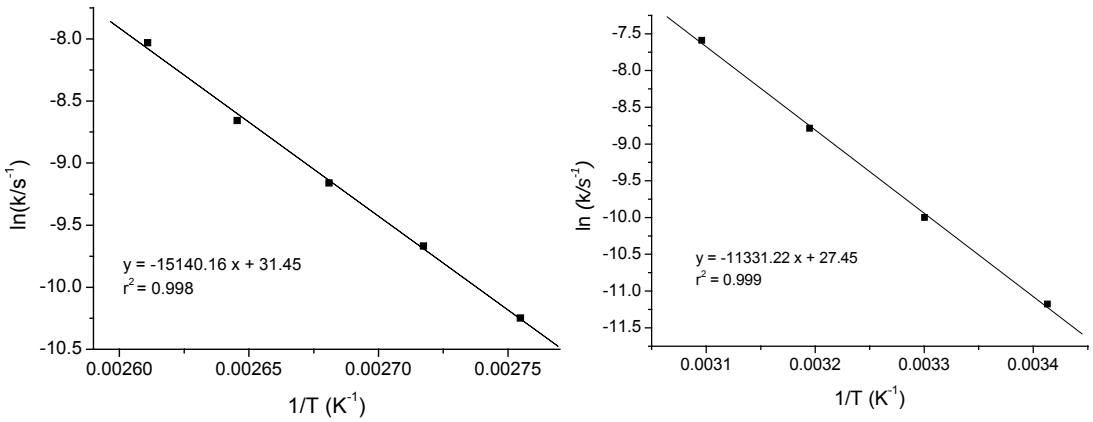

Figure D3. Temperature dependence of k for **1** and **2a** according to Arrhenius.

The thermodynamic parameters of the transition state of a reaction are expressed in the Eyring equation. The enthalpy and entropy as well as the free enthalpy of the transition state can be determined from the temperature dependency of the rate constant as shown by equations 6-1 and 6-2 in the main text

$$\Delta G^{\ddagger} = \Delta H^{\ddagger} - T\Delta S^{\ddagger} = -RT \ln K^{\ddagger} \qquad \text{(eq. D-8)}$$

$$\Delta G^{\ddagger} = -RT \ln \frac{k\ h}{\kappa\ k_B T} \qquad \text{(eq. 6-1)}$$

$$k = \kappa \frac{k_B T}{h} \exp\left[\frac{\Delta S^{\ddagger}}{R}\right] \exp\left[-\left(\frac{\Delta H^{\ddagger}}{RT}\right)\right] \qquad \text{(eq. 6-2)}$$

$$\ln \frac{k}{T} = -\left(\frac{\Delta H^{\ddagger}}{R}\right)\frac{1}{T} + \frac{\Delta S^{\ddagger}}{R} + \ln \frac{\kappa\ k_B}{h} \quad (y = mx + c) \qquad \text{(eq. D-9)}$$

$$m = -\left(\frac{\Delta H^{\ddagger}}{R}\right) \text{ and } c = \frac{\Delta S^{\ddagger}}{R} + \ln \frac{\kappa\ k_B}{h} \qquad \text{(eq. D-10)}$$

From linear regression analysis according to equation 6-2, $\Delta H^{\ddagger}$ can be determined from the slope m and $\Delta S^{\ddagger}$ from the y-axis intercept (eq. D-10). Exemplified, data evaluation of **1** is shown in Figure D4.

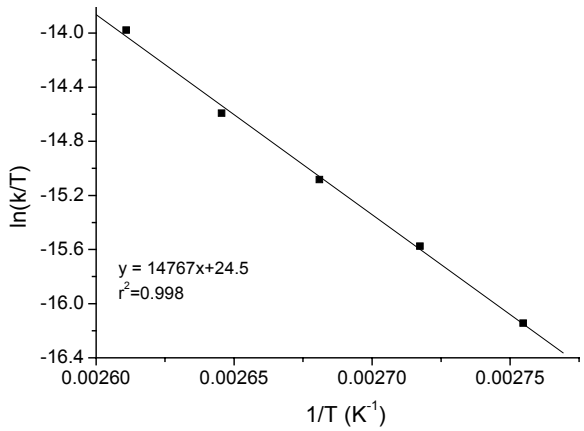

Figure D4. Temperature dependence of k according to Eyring for **1**.

Comparison of the Eyring (eqs. 6-1 and 6-2) and the Arhenius equation (eq. D-6) reveals that $\Delta H^{\ddagger}$ is correlated to the activation energy of the reaction according to equation D-11 as well as the activation entropy $\Delta S^{\ddagger}$ is correlated to preexponential factor of the Arrhenius equation.

$$E_A = \Delta H^{\ddagger} + RT \qquad \text{(eq. D-11)}$$

$$\ln A = \frac{\Delta S^{\ddagger}}{R} + \ln \frac{\kappa \; k_B}{h} \qquad \text{(eq. D-12)}$$

The chiroptical properties of (*P*)-**1** and (*M*)-**1** in 1,1,2,2-tetrachlorethane are show in Figure D5, left and no significant differences are observed to those determined in chloroform as shown in Figure D5, right.

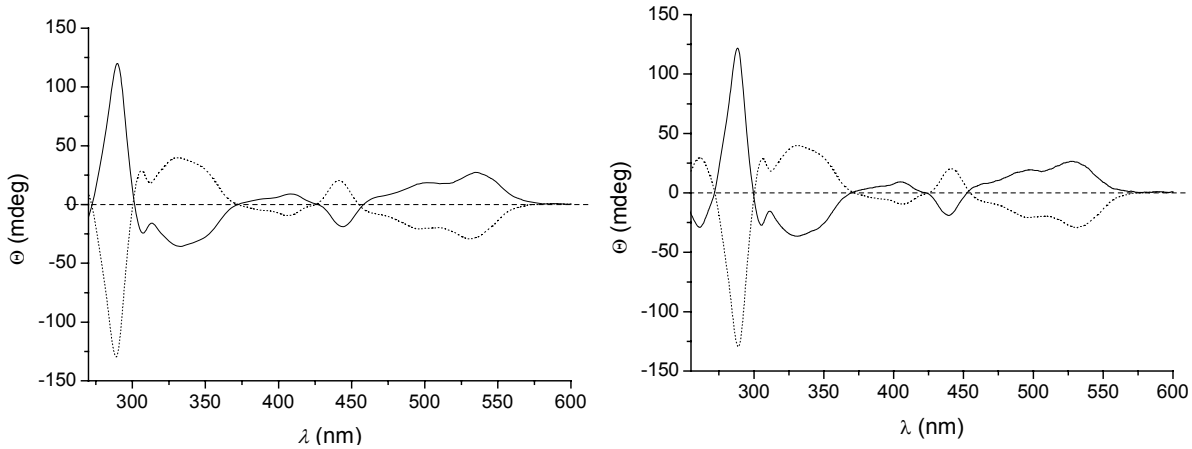

Figure D5. CD-spectra (left) of (*P*)**-1** (dotted line) and (*M*)**-1** (solid line) in 1,1,2,2-tetrachlorethane and comparison (right) of the CD-spectra of (*P*)**-1** in chloroform (dotted line) and of (*M*)**-1** in 1,1,2,2-tetrachlorethane (solidline).

D.2 Calculation of Sterical Encumbering in Bay Substituted Perylene Bisimides

The apparent van der Waals overlap ∑r* of the substituents that cause the distortion of a molecule can be used to describe sterical encumbering of the hypothetical undistorted molecule.[D1] For several series of compounds correlation between this parameter and the interconversion processes have demonstrated the usefulness of this parameter.[D1] In the following section the procedure for the calculation of the ∑r*-value for perylene bisimide dyes is outlined.

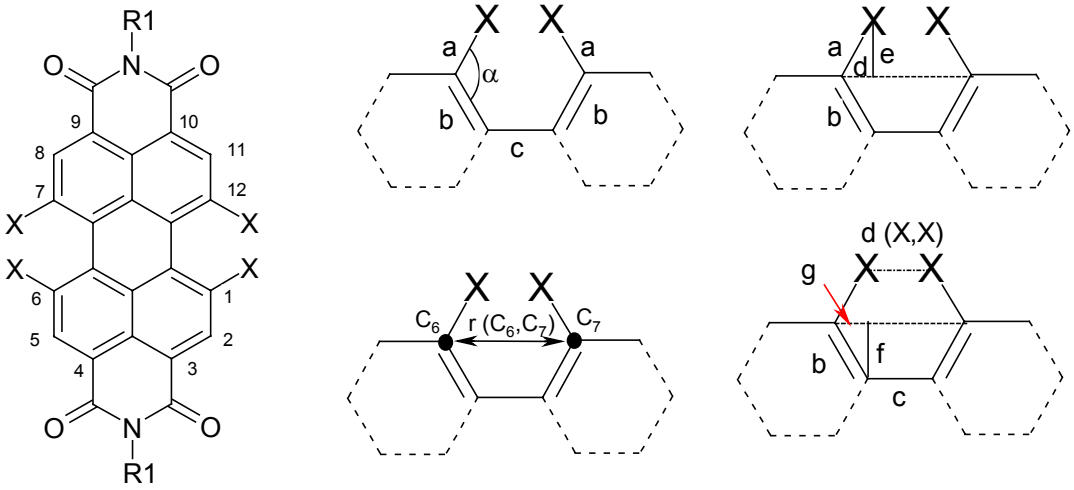

Figure D6. Definition of sizes and angles used for the calculation of the apparent overlap.

The apparent overlap ∑r* is defined as the overlap of the substituents in a hypothetical planar structure. The overlap r* of two substituents is given by the difference of the sum of their van der Waals radii and the center-to-center distance of the substituents (see Figure 7 in the main section). The van der Waals radii can be taken from literature,[D2] but the center-to-center distance d(X,X) has to be calculated from the geometry of the molecule. Per definition, the planar structure necessary for the calculations of r* should possess an idealized geometry and thus standard bond lengths and bond angles should be used. The structural parameters required for the calculation are shown in Figure D6. The CC-bond length (b and c in Figure D6) of the aromatic perylene core were taken from X-ray structure analysis of the parent unsubstituted perylene bisimide derivatives (as described in Chapter 2).[D3] The average value calculated from three individual structures of the bond length results to 1.394±0.016 Å (b) and 1.468±0.025 Å (c). These values are considered as very precise as all parent PBI derivatives possess a planar structure. Furthermore, all bond angles were set at 120°, characteristic for aromatic compounds, and the length of the

C(sp^2)-X bonds were taken from literature.[D4] The specific parameters for the substituents are summarized in Table D1.

Table D1. Van der Waals radii r_{vdW}[D2] and C(sp^2)-X Bond Length a[D4] for Different Substituents X in Å (left) and C(sp^2)-C(sp^2) Bond Lengths b,c.[D3]

X	r_{vdW}	a
H	1.20	1.10
F	1.47	1.39
Cl	1.73	1.76
Br	1.87	1.92
O	1.52	1.43

	X = H
b	1.394
c	1.468

For the symmetrical dyes **1**-**4**, having four similar substituents in the bay positions, the apparent overlap can be calculated according to the following equations.

The distances d(X,X) between the substituents X in a planar conformation can be calculated by simple trigometric consideration for α = 120°.

$$d = a \times \cos(\alpha/2) = a \times \cos(60°) = a \times 0.5$$

$$g = b \times \cos(\alpha/2) = b \times \cos(60°) = b \times 0.5$$

$$r(C_6, C_7) = (2g + c) = b + c \qquad \text{(eq. D-13)}$$

$$r(C_6, C_7) = 2.862\ \text{Å}$$

$$d(X, X) = r(C_6, C_7) - 2d$$

$$= 2.862\ \text{Å} - 2 \times (0.5a)$$

$$d(X, X) = 2.862\ \text{Å} - a \qquad \text{(eq. D-14)}$$

with equation 6-5 (Figure 7, Chapter 6), the r* results to

$$r^* = 2r_{vdW}(X) - d(X, X)$$

$$r^* = 2r_{vdW}(X) - (2.862\text{Å} - a) \qquad \text{(eq. D-15)}$$

The apparent overlap is the sum of the r* values for both sides of the perylene core. Owing to the symmetry of the planar conformation the apparent overlap results to

$$\sum r^* = \sum\left(2\times r_{vdW}(X) - (c+b-a)\right) = 2\times\left(2\times r_{vdW}(X) - (r(C_6,C_7)-a)\right)$$

$$\sum r^* = \left(4r_{vdW}(X) - 2(r(C_6,C_7)-a)\right)$$

$$\sum r^* = 4r_{vdW}(X) + 2a - 5.724\ \text{Å} \qquad \text{(eq. D-16)}$$

For perylene bisimides bearing two different substituents (H,Y) in the bay-position, as in the case of 1,7-disubstituted perylene bisimides (see Figure D7), the calculation of r* is more complicated and can be accomplished according to the following equations.

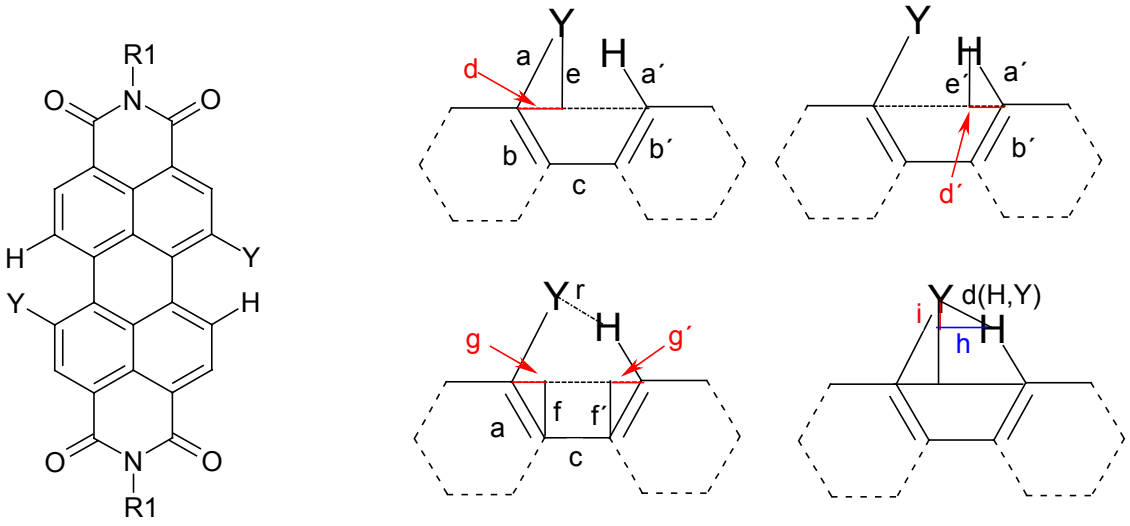

Figure D7. Definition of sizes and angles used for the calculation of the apparent overlap of 1,7-disubstituted perylene bisimides.

The distance r(C_6,C_7) is still obtained by equation D-13 as discussed above:

$$r(C_6,C_7) = 2.862\ \text{Å}$$

The values of d and d´ can be calculated similarly as described above, except that the substituents pattern is now asymmetrical and d and d´ have to be distinguished.

$$d = a\times\cos(\alpha/2) = a\times\cos(60°) = a\times 0.5$$

$$d' = a'\times\cos(\alpha/2) = a'\times\cos(60°) = a'\times 0.5$$

The vertical distance between the substituents h can be calculated with equation D-17 by applying the distance r (C_6,C_7) according to the formula:

$$h = r(C_6,C_7) - d - d'$$

$$= 2.862\ \text{Å} - 0.5a - 0.5a' \qquad \text{(eq. D-17)}$$

The horizontal distance between the substituents i can be obtained as the difference of the horizontal distance e and e´ of the substituents as shown in Figure D7

$$i = |e - e'| = |a - a'| \sin 60° \qquad \text{(eq. D-18)}$$

Finally, the distance between the two substituents d(H,Y) can be obtained by applying the sentence of Pythagoras.

$$(d(H,Y))^2 = h^2 + i^2$$

$$d(H,Y) = \sqrt{h^2 + i^2}$$

to give

$$d(H,Y) = \sqrt{(2.862\ \text{Å} - 0.5a - 0.5a')^2 + (|a - a'| \sin 60°\ )^2} \qquad \text{(eq. D-19)}$$

The apparent overlap can be calculated similar as before from the difference between the distance of the substituents H and Y and the sum of their van der Waals radii:

$$r^* = r_{vdW}(Y) + r_{vdW}(H) - d(H,Y)$$

$$\sum r^* = 2r^* = 2r_{vdW}(Y) + 2r_{vdW}(H) - 2\sqrt{(2.862\ \text{Å} - 0.5a - 0.5a')^2 + (|a - a'| \sin 60°)^2}$$

with the bond length and the van der Waals radius of hydrogen we can simplify this equation to

$$\sum r^* = 2r^* = 2r_{vdW}(Y) + 2.40\text{Å} - 2\sqrt{(2.312\ \text{Å} - 0.5a)^2 + (-0.953\text{Å} + 0.866a)^2} \qquad \text{(eq. D-20)}$$

Now, only the values a and r_{vdW} of the substituents Y have to be applied to calculate the apparent overlap. The apparent overlap for the different perylene bisimides are given in Figure 7 and Chart 1 in Chapter 4.

D.3 Calculation of group radii

As outlined in section D2, the van der Waals radius of the substituents in the bay area is required for the calculation of the apparent overlap of bay-substituted perylene bisimide. In contrast to simple substituents, as e.g. fluorine, chlorine or bromine atoms, the van der Waals radius of complex substituents (group radii), e.g. alkyl groups or aromatics, has to be calculated from the geometry of the respective substituent.[D2] The group radii for large variety of substituents as well as principles and formulas for the calculation of group radii were reported by Charton and coworkers.[D2] Furthermore, it was pointed out by these authors that three different van der Waals radii are necessary to describe the steric encumbering of any substituent.[D2] These radii are a result of the three dimensional arrangement of the substituents and were denoted as the minimal van der Waals radius $r_{vdW,min}$, the maximal van der Waals radius $r_{vdW,max}$ and the axial van der Waals radius

$r_{vdW,ax}$. The minimal and maximal van der Waals radii are defined perpendicular to the group axis and describe the minimal and maximal extension of the substituents, respectively, whereas the axial van der Waals radius is defined along the group axis (see Figure D8) and describes the maximal extension of the substituent in this direction.[D2] The group axis is defined as the extension of the bond connecting the substituent to the central unit which is in the present case the perylene bisimide core.

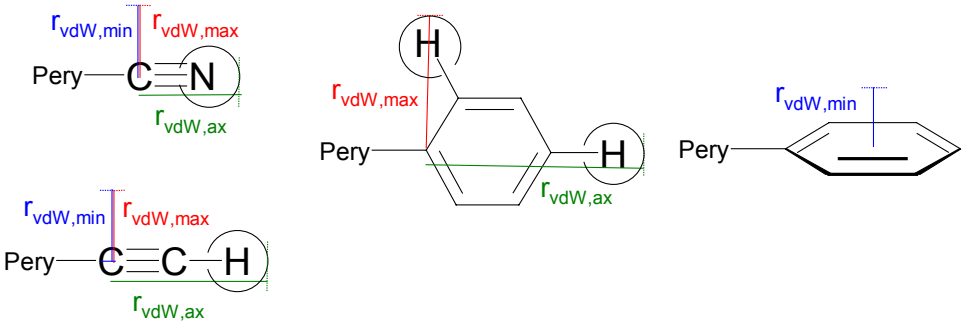

Figure D8. Definition of the minimal $r_{vdW,min}$ and maximal van der Waals radius $r_{vdW,max}$ as well as the axial van der Waals radius $r_{vdW,ax}$ for planar π-conjugated groups. The radii $r_{vdW,max}$, $r_{vdW,min}$ and $r_{vdW,ax}$ are displayed as red, blue and green lines, respectively. Pery denotes perylene bisimide.

The use of the three different van der Waals radii is dependent on the sterical situation in the system under consideration.[D2] In most of the cases, the minimal radius $r_{vdW,min}$ has to be applied, e.g. for the 2-ethynyl-2´-bromo-1,1´-biphenyl in which the sterical encumbering is govern by the repulsion of the bromine atom and the π-system of the alkynyl group (Figure D9). For 1,6,7,12-tetraalkynyl substituted perylene bisimides the sterical encumbering is determined by the length of the substituents as can be seen from Figure D9. Thus, for PBIs bearing four extended planar π-systems in the bay area, e.g. phenyl, alkynyl or cyano, the length of the substituents which is expressed in the axial van der Waals radii $r_{vdW,ax}$ should be used for calculation of the apparent overlap rather than the minimum or maximum van der Waals radii which relate to the thickness of the substituents.

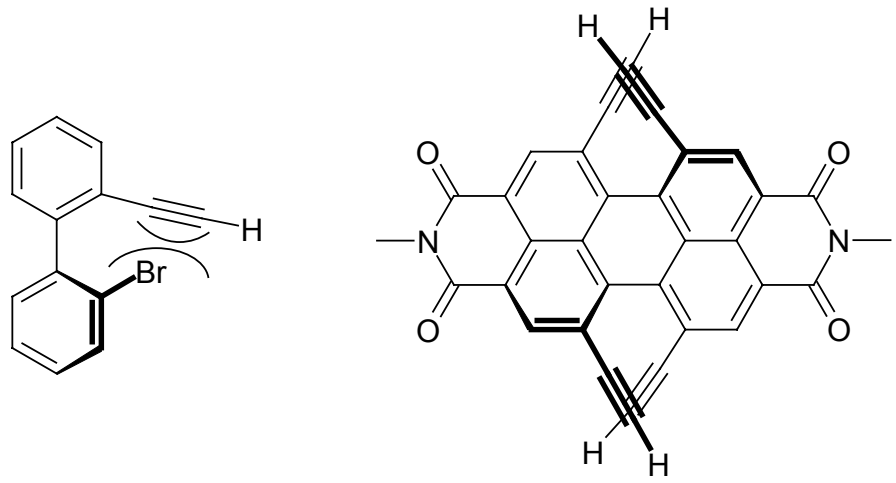

Figure D9. Structure of 2´-methyl-2-ethynyl-1,1´-biphenyl and *N*,*N*´-dimethyl-1,6,7,12-tetraethynylperylene-3,4:9,10-tetracarboxylic acid bisimide.

The minimum van der Waals radius $r_{vdW,min}$ of planar π-conjugated substituents is given by the half thickness of the π-system. The maximal van der Waals radius $r_{vdW,max}$ on the other hand represents the largest possible extension of the substituent perpendicular to the group axis, which is given for cylindrical groups such as cyano or alkynes, by the half-thickness of the π-system, whereas for phenyl substituents this radius is given by the width of the phenyl ring as defined in Figure D8. The half thickness of the π-system can be taken from literature[D2] as 1.60 Å for the cyano group, 1.78 Å for alkynyl groups and 1.77 Å for phenyl groups (Table D3). The maximum van der Waals radius as well as the axial van der Waals radii of substituents can be calculated from the geometry of the substituents (see Figure D10 for definiton) by applying standard bond length and bond angles (Table D2).[D2,D4]

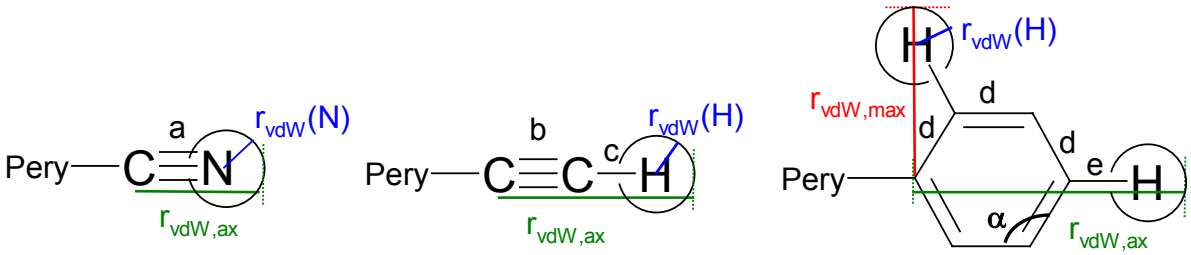

Figure D10. Definiton of bond length and bond angles used for the calculation of the axial van der Waals radius of cyano, ethynyl and phenyl substituents.

For linear cylindrical groups such as cyano or alkynyl groups (Figure D10), the axial radius can be assessed by simple summation of the bond lengths. For cyano substituents $r_{vdW,ax}$ can be calculated according to

$$r_{vdW,ax} = a + r_{vdW}(N)$$

and for ethynyl substituents the axial van der Waals radius results to

$$r_{vdW,ax} = b + c + r_{vdW}(H).$$

Table D2. Bond Length[D4] and Van Der Waals Radii[D2] in Å used for the Calculation of the Group Radii of Cyano, Ethynyl, Phenyl and Diphenylphosphino Substituents as defined in Figure D9 and D10.

	length
a	1.16
b	1.20
c	1.10
d	1.39
e	1.10
f	1.80
r_{vdW} (H)	1.20
r_{vdW} (N)	1.55

For phenyl substituents (Figure D10), the axial radius can be calculated according to the following equations:

$$r_{vdW,ax} = d + 2(d\cos(\alpha/2)) + e + r_{vdW}(H)$$

with α = 120°

$$r_{vdW,ax} = 2d + e + r_{vdW}(H)$$

For diphenylphospino substituents the group radii have not been reported in literature. Similar as for phenyl substituents, the minimal van der Waals radius is given by the half-thickness of the phenyl substituents and therefore results to 1.77 Å. The remaining van der Waals radii, $r_{vdW,max}$ and $r_{vdW,ax}$, were calculated from the molecular geometry of the diphenylphosino group as depicted in Figure D11 by applying standard bond length (Table D2).[4]

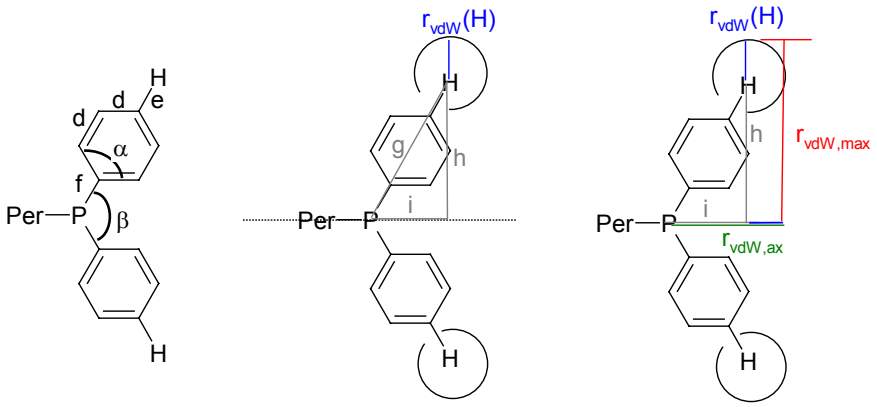

Figure D11. Definition of geometrical parameters for the calculation of the group radii of diphenylphosphine substituents.

The maximum van der Waals radius $r_{vdW,max}$ of diphenylphosphine substituents was calculated according to the following equations:

$$g = f + d + 2(d\cos(\frac{\alpha}{2})) + e$$

with α = 120°

$$g = f + 2d + e \qquad \text{(eq. D-21)}$$

$$h = g\sin(\beta/2) = 0.87(f + 2d + e)$$

$$r_{vdW,\max} = h + r_{vdW}(H) = 0.87(f + 2d + e) + r_{vdW}(H)$$

The axial van der Waals radius $r_{vdW,ax}$ can be assessed from the distance g and equation D-21 according to the following equation:

$$i = g\cos(\beta/2) = 0.5(f + 2d + e)$$

$$r_{vdW,ax} = i + r_{vdW}(H) = 0.5(f + 2d + e) + r_{vdW}(H)$$

The axial van der Waals radii as well as the minimum and maximum van der Waals radii for cyano, ethynyl, phenyl and diphenylphosphino substituents are reported in Table D3.

Table D3. Group Radii in Å for Different π-Conjugated Substituents

	$r_{vdW,min}$	$r_{vdW,max}$	$r_{vdW,ax}$
cyano	1.60[a]	1.60[a]	4.17
alkynyl	1.78[a]	1.78[a]	4.94
phenyl	1.77[a]	3.35[a]	6.32
PPh_2	1.77	6.20	4.05

a) taken from reference D2

D.4 Main Error Estimation for $\Delta G^{\ddagger}$ and the Half Lifetime $t_{1/2}$

The main error of $\Delta G^{\ddagger}$ and $t_{1/2}$ (Table 1 in main text) was estimated according to the following equations:

$$\Delta(\Delta G^{\ddagger}) = \left| R\ T \left(\ln \frac{h}{\kappa\ k_B T\ k} \right) \right| \Delta k + \left(\left| R\ \ln\left(\frac{h\ k}{\kappa\ k_B T} \right) \right| + \left| -R\ \frac{h\ k}{\kappa\ k_B} \right| \right) \Delta T \quad \text{(eq. D-22)}$$

$$\Delta(t_{1/2}) = \left| -\frac{\ln 2}{k^2} \right| \Delta k \quad \text{(eq. D-22)}$$

The temperature error ΔT was taken as 2 K and Δk as given in Table 1 (main text).

D.5 ^{1}H and ^{19}F NMR spectra of 4.

^{19}F NMR spectra of **4** in $CDCl_3$

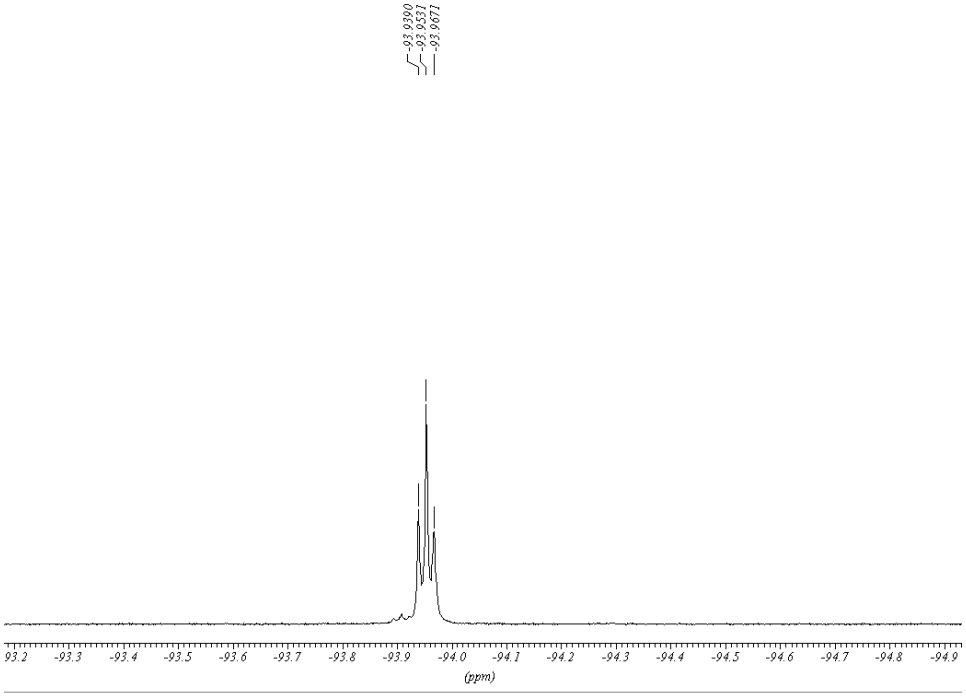

^{1}H NMR spectra of **4** in $CDCl_3$

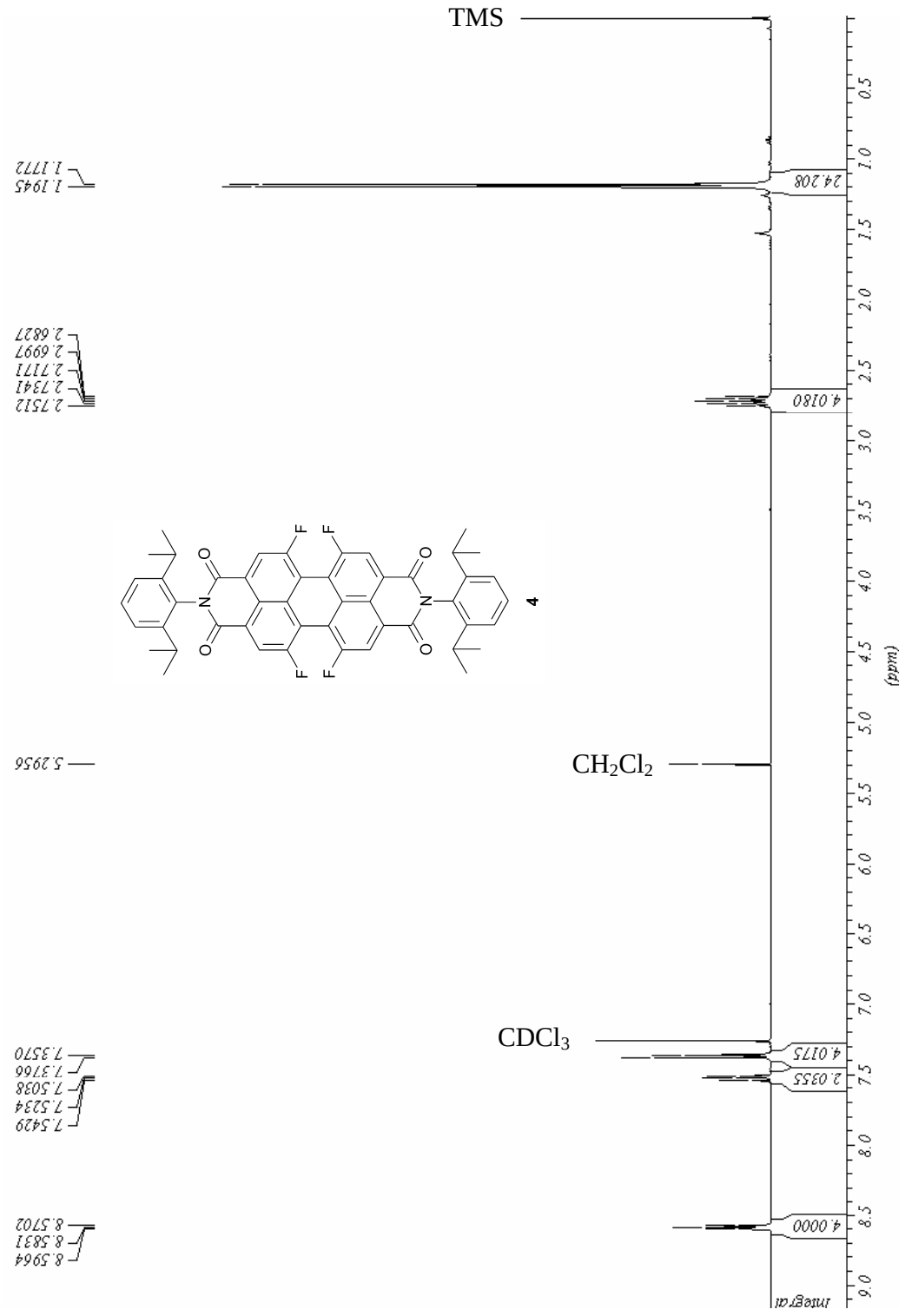

D.6 Additional References and Notes

D1 (a) R. Cosmo, T. W. Hambley, S. Sternhell, *J. Org. Chem.* **1987**, *52*, 3119-3123; (b) R. Cosmo, S. Sternhell, *Aust. J. Chem.* **1987**, *40*, 35-47.

D2 M. Charton, *Top. Curr. Chem.* **1983**, *114*, 57-91 and literature cited in there.

D3 The planar unsubstituted PBI resembles the geometry of the presumably planar transition state. The values were taken as the average value of three different solid state structures as given in Chapter 2.

D4 *CRC Handbook of Chemistry and Physics*, 67th edition (Ed.: R. C. Weast), CRC Press Inc., Boca Raton, **1986**.

E. Supplement for Chapter 7

E.1Graphical Material for Data Evaluation with SpecFit/32

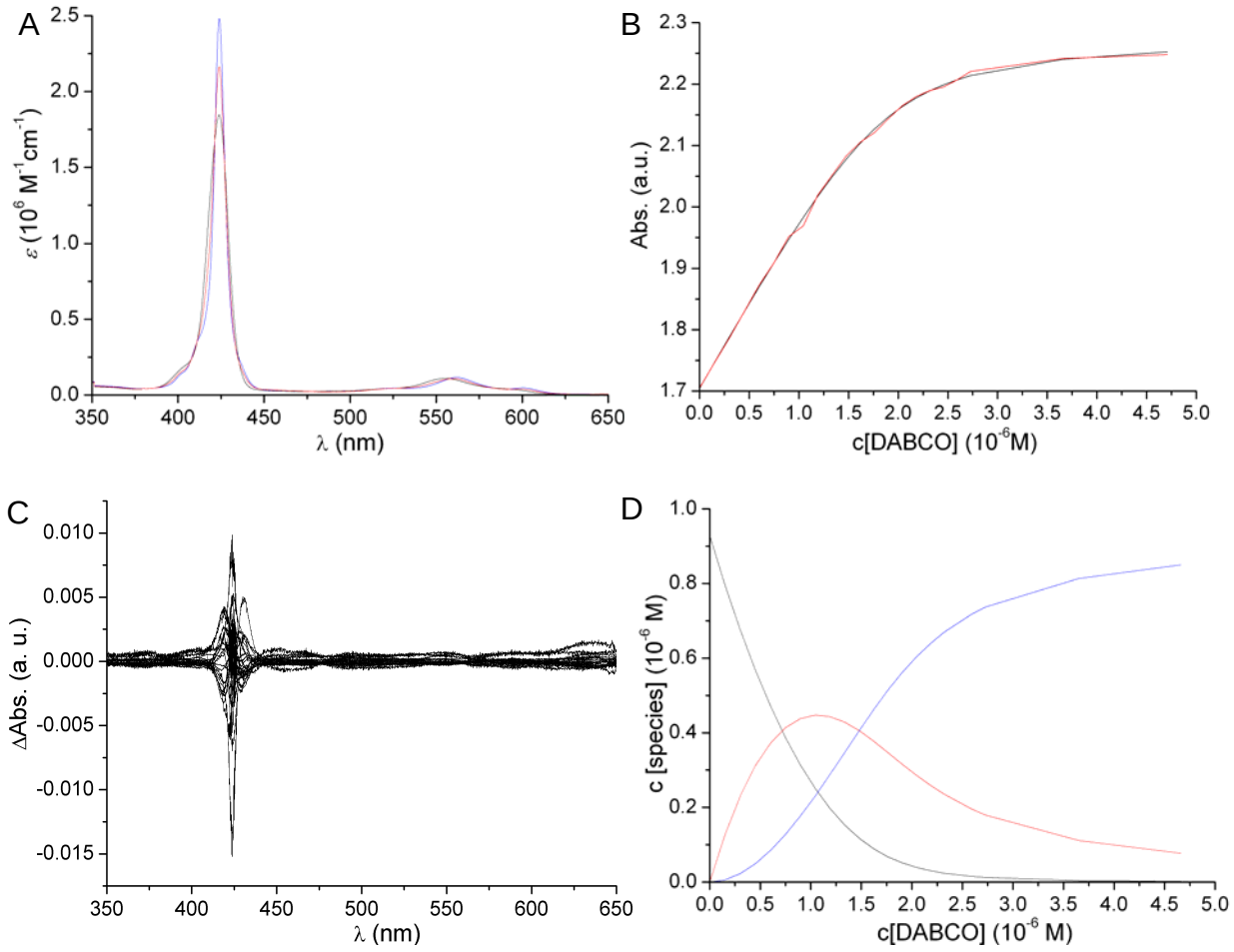

Figure A5-1. Exemplified data evaluation with SpecFit/32 for UV/Vis titration experiments at a concentration of 1 x 10^{-6} M. Calculated spectra for the different species (A; **4** [black line], **4**•(DABCO) [red line] and **4**•$(DABCO)_2$ [blue line]), experimental (red) and calculated (black) binding isotherm at 424 nm (B), residuals of the calculated and the experimental spectra (C) and concentration profiles for the different species (D; colour corresponds to those of A).

E.2 ^{1}H NMR Spectrum of 4

^{1}H NMR spectrum (400 MHz) of **4** in THF-d_8

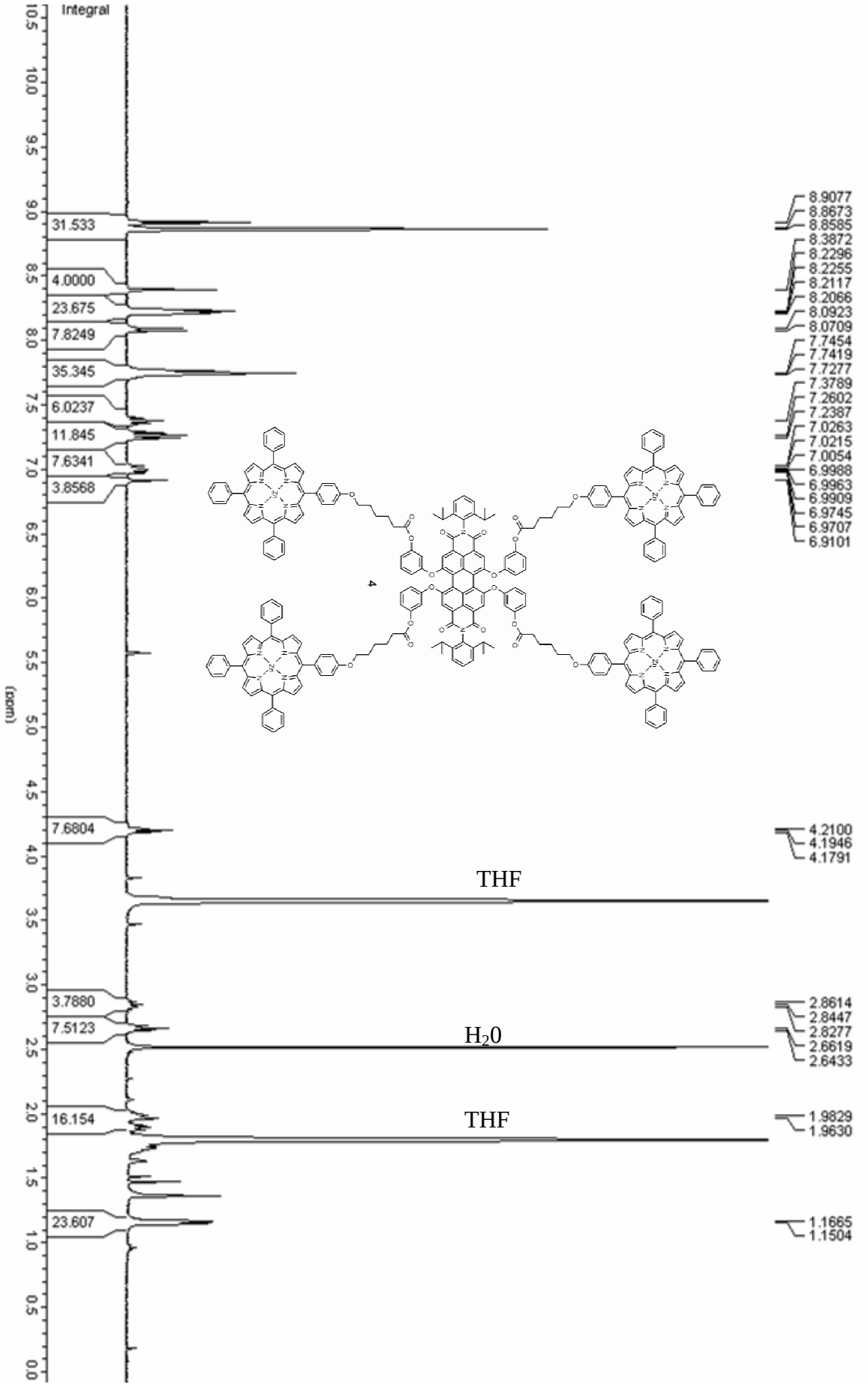

F. Supplement for Chapter 8

F.1 Additional Graphical Materials

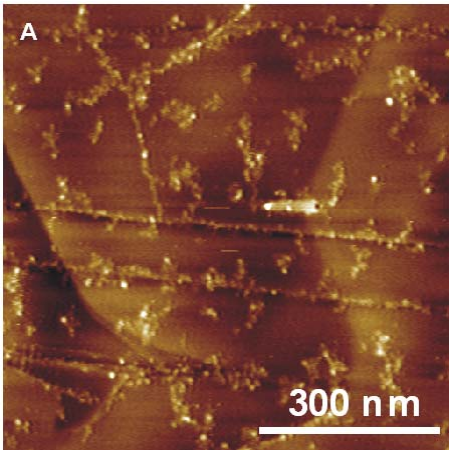

Figure F1. AFM image of a solution of polymer **3** (c = 1.2 x 10^{-5} M) in chloroform on HOPG. The z-scale was 3 nm.

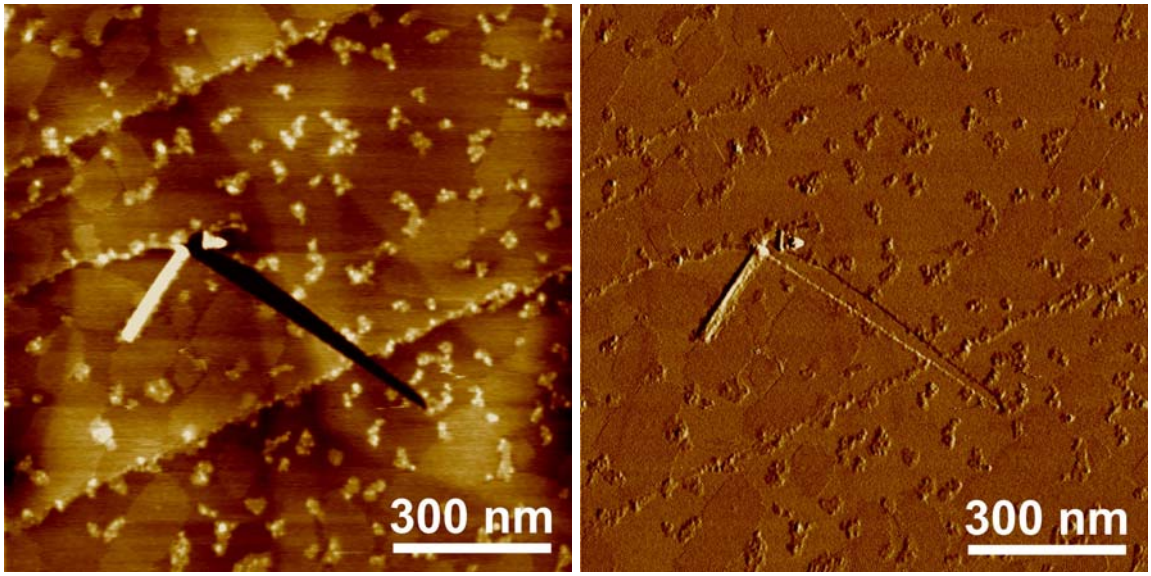

Figure F2. AFM images of a chloroform solution of **1** and **3** at a ratio of α = 0.33 spin-coated onto HOPG: Height image (left) and phase image (right). The z-scale was 2 nm.

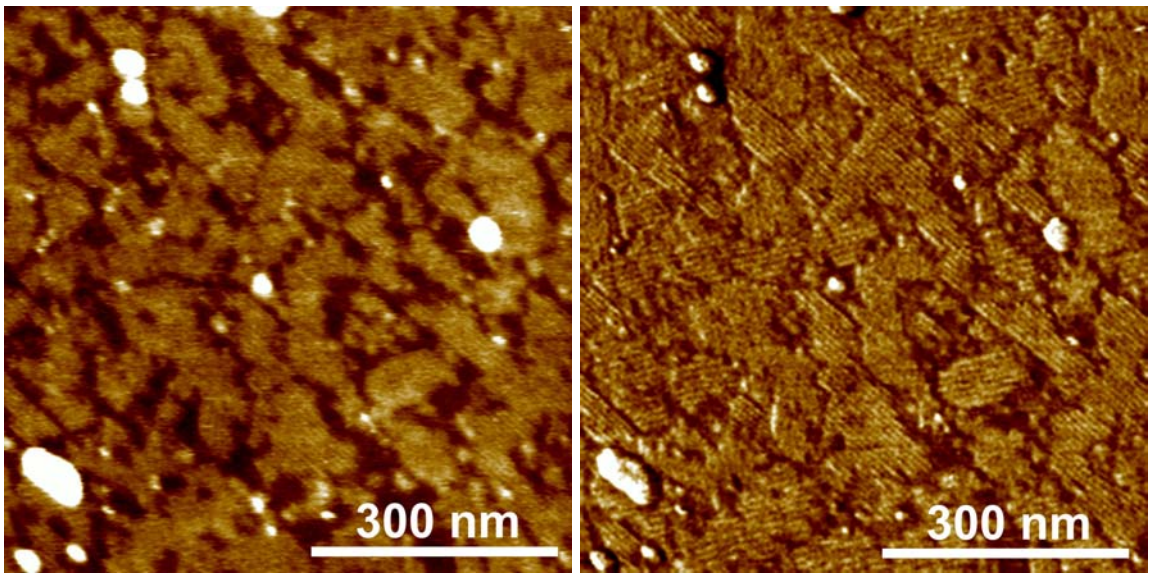

Figure F3. AFM images of a chloroform solution of **1** and **3** at a ratio of α = 0.5 spin-coated onto HOPG: Height image (left) and phase image (right). The z-scale for all images was 2 nm.

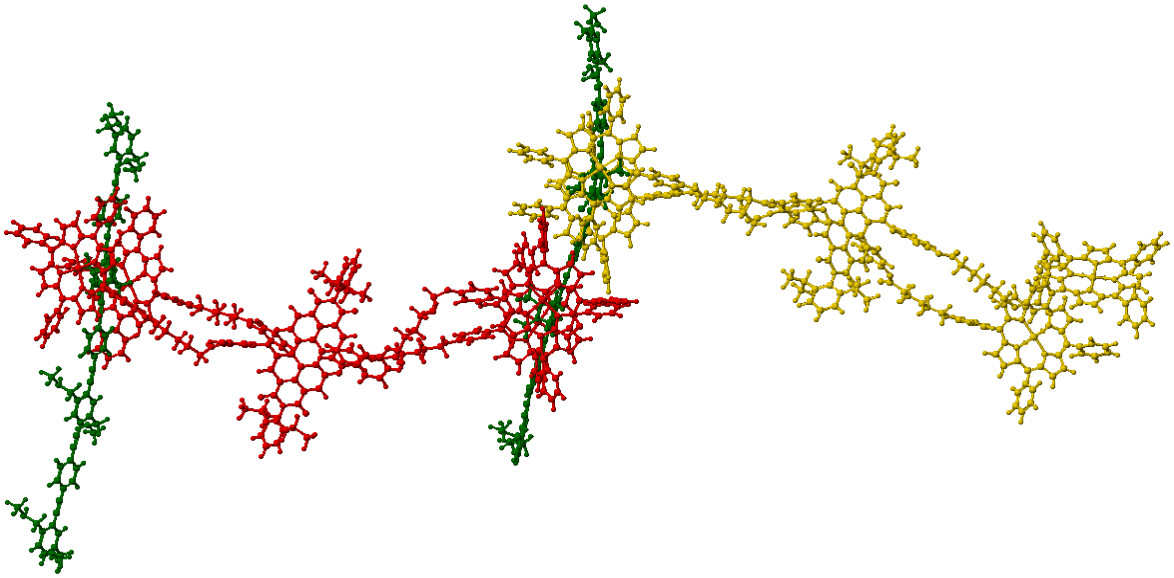

Figure F4. Optimized structure for cross-linking of two polymer strands of **3** by **1**. The structure was optimized by MM3 force field using Cache Quantum Cache Workspace 5.0. Molecules of cross-linker **1** that form a sandwich complex with polymers are highlighted in red and yellow, and the polymer strands are shown in green.

F.2 Self-Assembly of Linear π-Conjugated Polymer 3 and Supramolecular Cross-Linker 1

The self-assembly of **1** and **3** was further investigated by constant host titration in chloroform using UV/Vis spectroscopy. The concentrations of polymer **3** employed in these experiments reflect the concentrations of one repeating unit of **3** and was determined by the absorption of a solution of **3** in chloroform at 403 nm.[17] The spectral changes of cross-linker **1** upon succesive addition of a solution of polymer **3** are shown in Figure F5.

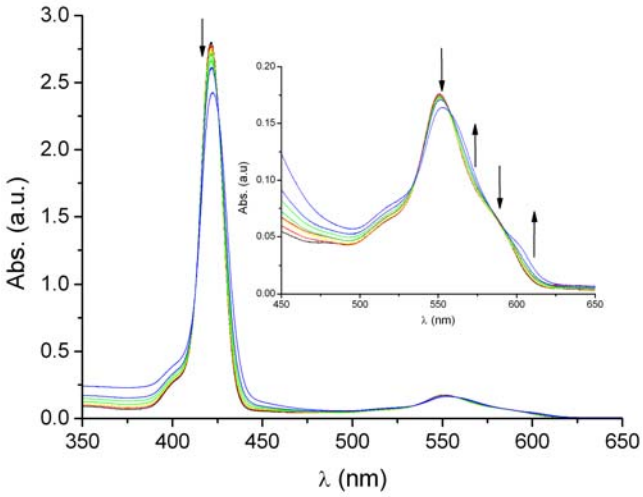

Figure F5. UV/Vis spectra of zinc porphyrin/perylene bisimide **1** (8.2 x 10^{-6} M) upon addition of polymer **3** (7.5 x 10^{-5} M) in $CHCl_3$ at 23 °C. Inset: Expanded view of the Q-band region. Arrows indicate changes upon addition of **3**.

For the Soret band (422 nm) a decrease of the intensity was observed upon addition of polymer **3** to a solution of **1**. The Q-band region (450-650 nm) revealed the characteristic decrease of the band at 550 nm and an increase of the absorption at 580 nm and 605 nm indicating the formation of a complex between the zinc porphyrin units of **1** and the amino functionalities of polymer **3**. Unfortunately, even at a 9-fold excess of amine binding sites of polymer **3** no saturation of the binding sites of **1** was achieved. This experimental limitation is due to the highly dilute conditions owing to the low solubility of polymer **3** in chloroform.

Absorption spectra were measured at a lower concentration of **1** and larger excess of polymer **3** (see Figure F6).[F1] After subtraction of the absorption spectrum of the polymer, the spectrum obtained for a 200-fold excess of the binding units of polymer **3** with respect to the binding units of **1** revealed the binding of the amine-functionalities of polymer **3** (Figure F6) to **1**. The Soret band was bathochromically shifted by 5 nm and in the Q-band region (450-650 nm) new bands were observed at 580 nm and 605 nm

indicative for the formation of complex between **1** and **3**. A binding constant could not be determined due to the limited solubility of polymer **3**.

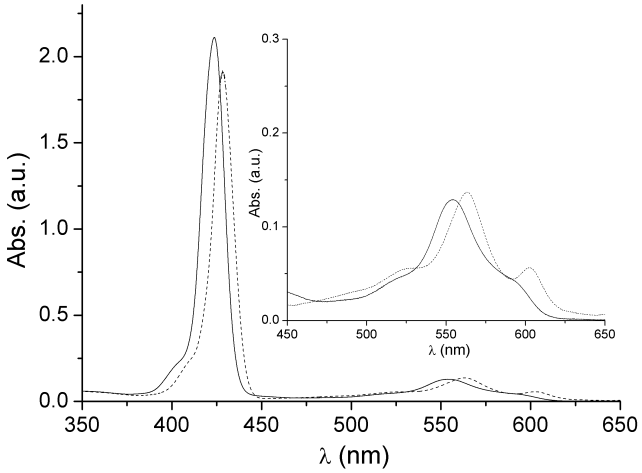

Figure F6. UV/Vis absorption spectra of **1** (1.2 x 10^{-6} M) in chloroform (solid line) and corrected absorption spectra of **1** in the presence of a 200-fold excess of the repeating unit of **3** (dashed line). Inset: Expanded view of the Q-band region.

Experimental

The titration experiments were carried out on a Perkin Elmer Lamda 950 at ambient conditions. A solution of zinc porphyrin/perylene bisimide **1** in chloroform with a concentration of 8.2 x 10^{-5} M was prepared (solution A). A portion of solution A was diluted with chloroform by a factor of 10 which was then used as host solution with a concentration of 8.2 x 10^{-6} M of **1**. Another portion of solution A was diluted with the polymer stock solution (7.99 x 10^{-5} M determined by UV/Vis spectroscopy) in chloroform directly obtain after deprotection of boc-groups by a factor of 10 and this solution was used as the guest solution with a concentration of polymer **3** of 7.2 x 10^{-5} M and **1** of 8.2 x 10^{-6} M. The solutions were prepared the evening before the experiments were performed.

To 8.2 x 10^{-6} M solution of **1** in chloroform in a 0.2 cm quartz cuvette at 23 °C were added via a microliter syringe 10 µl aliquots of a solution of polymer **3** (7.2 x 10^{-5} M) and **1** (8.2 x 10^{-6} M). After each addition, a UV/Vis spectrum was recorded.

F.3 Additional Notes

F1 Attempt to perform titration experiments at this concentration failed because the necessary amounts (excess) of polymer **3** could not be dissolved due to the limited solubility of polymer **3**. In this case no change of the absorption was observed up to a 20-fold excess of **3**. Kinetic effects were excluded by time dependent measurements (not shown).

Curriculum Vitae

Peter Osswald

Date of birth: November 11th, 1977
in Laupheim, Germany
single; no children
nationality: german

UNIVERSITY EDUCATION

since Oct. 2002	Dissertation Institut für Organische Chemie, Universität Würzburg, Germany; supervisor: Prof. Dr. Frank Würthner
Sept. 2002	Diploma (corresponds to master's degree)
March 2002 - Sept. 2002	Diploma Thesis Abteilung für Organische Chemie II, Universität Ulm; supervisor: Prof. Dr. Frank Würthner *„Synthese von Oligoethylenglycol-substituierten 1,6,7,12-Tetraphenoxy-Perylenbisimiden“*
Feb. 2002	Diploma examination
Oct. 1997	started studies at the Universität Ulm, Germany

SCHOLASTIC EDUCATION

Sept. 1988 – June 1997	Gymnasium, Laupheim, Germany (corresponds to high school); Abitur (corresponds to A-levels)
Sept. 1984 – July 1988	Grundschule Wain, Germany (primary school)

List of Publications:

“Palladium Complexes with Bidentate P,N Ligands: Synthesis, Characterization and Application in Ethene Oligomerization.”
G. Müller, M. Klinga, P. Osswald, M. Leskelae, B. Rieger
Zeitschrift für Naturforschung, B **2002**, *57*, 803-809.

“Tetrachloro-Substituted Perylene Bisimide Dyes as Promising n-Type Organic Semiconductors: Studies on Structural, Electrochemical and Charge Transport Properties.”
Z. Chen, M. G. Debije, T. Debaerdemaeker, P. Osswald, F. Würthner
ChemPhysChem **2004**, *5*, 137-140.

“Supramolecular p-n-Heterojunctions by Co-Self-Organization of Oligo(*p*-phenylene Vinylene) and Perylene Bisimide Dyes.”
F. Würthner, Z. Chen, F. J. M. Hoeben, P. Osswald, C.-C. You, P. Jonkheijm, J. von Herrikhuyzen, A. P. H. J. Schenning, P. P. A. M. van der Schoot, E. W. Meijer, E. H. A. Beckers, S. C. J. Meskers, R. A. J. Janssen
J. Am. Chem. Soc. **2004**, *126*, 10611-10618.
.
“Perylene Bisimide Based Macrocycles: Effective Probes for the Assessment of Conformational Effects on Optical Properties.”
P. Osswald, D. Leusser, D. Stalke, F. Würthner
Angew. Chem. **2005**, *117*, 254-257; *Angew. Chem. Int. Ed.* **2005**, *44,* 250-253.

“Synthesis, Optical and Electrochemical Properties of Core-Fluorinated Perylene Bisimides.”
F. Würthner, P. Osswald, R. Schmidt, T. E. Kaiser, H. Mansikkamäki, M. Könemann
Org. Lett. **2006**, *8*, 3765-3768.

“The Importance of Nanoscopic Ordering on the Kinetics of Photoinduced Charge Transfer in Aggregated π-Conjugated Hydrogen-Bonded Donor-Acceptor Systems.”
E. H. A. Beckers, Z. Chen, S. C. J. Meskers, P. Jonkheijm, A. P. H. J. Schenning, X.-Q. Li, P. Osswald, F. Würthner, R. A. J. Janssen
J. Phys. Chem. **2006**, *110*, 16967-16978.

“Perylene Bisimide Atropisomers: Synthesis, Resolution, and Stereochemical Assignment.”
P. Osswald, M. Reichert, G. Bringmann, F. Würthner
J. Org. Chem., accepted for publication.